The Quaternary stratigraphy of the Gods and Yakaw rivers area, northeastern Manitoba

by

Luka Nickolas Mesich

A thesis

presented to the University of Waterloo

in fulfilment of the

thesis requirement for the degree of

Master of Science

in

Earth Sciences

Waterloo, Ontario, Canada, 2025

© Luka Nickolas Mesich 2025

Author's Declaration

I hereby declare that I am the sole author of this thesis. This is a true copy of the thesis, including any required final revisions, as accepted by my examiners.

I understand that my thesis may be made electronically available to the public.

Abstract

Reconstructing the spatiotemporal dynamics of past glaciations provides a long-term perspective that is essential to understanding how Earth systems respond to climate change over different timescales. While most ice sheet reconstructions focus on the last glaciation, incorporating stratigraphic records from older glaciations enhances our understanding of past glacial-interglacial cycles. The western Hudson Bay Lowland (HBL) in northeastern Manitoba preserves thick Quaternary sediment sequences (20–70+ m) spanning multiple glacial-interglacial cycles, influenced by two major ice spreading centers of the Laurentide Ice Sheet (the Keewatin dome to the northwest and the Quebec-Labrador dome to the east).

This study revisits the Quaternary stratigraphy along the Gods and Yakaw rivers in the western HBL using contemporary techniques, including a detailed, multi-parameter approach to characterize tills, combining field observations, paleo-ice flow indicators (till fabric analysis, lodged boulder striations), and till composition (matrix geochemistry, clast-lithology counts). For this thesis, a hybrid lithostratigraphic-allostratigraphic approach was employed across ten sections to reconstruct local glacial dynamics and establish an updated stratigraphic framework.

Results confirm a complex, laterally variable stratigraphy. The revised framework includes 21 delineated stratigraphic units: 15 tills correlated using primarily paleo-ice flow indicators and stratigraphic position, and 6 sorted sediment units defined by allostratigraphy. Several key findings emerge from this framework, including: (1) A more detailed reconstruction of local glacial dynamics, (2) recognition of at least 4 sub-till sorted sediment units interpreted as ice-free intervals, and (3) a relative stratigraphy that extends the Quaternary record in the region, possibly back to MIS 12 or even older. Sediment provenance and ice-flow indicator analysis suggest that older tills (units 1t–11t) were dominantly sourced from a Quebec-Labrador dome, while younger tills (units 13t–20t) exhibit more complex signatures. This shift between units 11t and 13t may reflect changes in paleo-ice sheet configuration, bedrock availability to glacial erosion, or entrainment of pre-existing sediment. Although some till units appear superficially similar, they are interpreted as discrete tills deposited during separate ice-flow phases rather than products of glaciotectonic stacking. An alternative explanation invoking glaciotectonism is considered; however, variability of paleo-ice flow indicators, the absence of pervasive deformation structures, and a regional context unfavourable to large-scale glaciotectonism opposes this interpretation.

These findings have broad implications for both ice sheet modeling and mineral exploration. In ice sheet modeling, incorporating records from older glacial-interglacial cycles provides key constraints to long-term ice sheet reconstructions, improving understanding of ice sheet response to climate change, which leads to better predictions of future changes. In mineral exploration, understanding glacial dynamics in thick-drift regions helps establish dispersal directions and sediment provenance, which may either 1) improve the interpretation of indicator mineral source, or 2) confirm a long history of inheritance and overprinting that requires the development of new techniques.

Acknowledgements

First and foremost, I would like to thank my co-supervisors, Dr. Martin Ross and Dr. Michelle Gauthier, for their consistent and thoughtful feedback and support every step of the way over the past two years. Their excellent guidance was essential to both this thesis and my career as a Quaternary geologist. I also thank my committee members, Dr. Brian Kendall and Dr. Chris Yakymchuk, for contributing crucial advice and review over the course of this thesis.

Many thanks are given to Tyler Hodder, Julia Hathaway, and Dr. Eric Grunsky, who have contributed to this thesis invaluably, both in the field and/or during the arduous stages of data analysis.

I would also like to thank the University of Waterloo, the Manitoba Geological Survey, and Natural Resources Canada for providing the resources, planning, and funding to allow me to do this work. It is truly a privilege to be able to conduct a field study in such a remote and unique part of the world. This research project was funded by Natural Resource Canada's GEM-GeoNorth program through a Research Affiliate Program, by an Ontario Graduate Scholarship (OGS), and by a Natural Sciences and Engineering Research Council of Canada (NSERC) Canada Graduate Scholarship (CGS).

Finally, I would like to thank my partner, my family, and my friends for being a rock-solid support system for me throughout my Master's experience. I would not have been able to do this without you.

Table of Contents

Author's Declaration ii
Abstract iii
Acknowledgements v
List of Figures xi
List of Tables xv
List of Abbreviations xvi
Chapter 1: Introduction 1
1.1 Scientific rationale 1
1.2 Study area and geological setting 3
1.2.1 Study area 3
1.2.2 Regional physiography 5
1.2.2.1 Deglacial-postglacial erosion 5
1.2.3 Bedrock geology 6
1.2.4 Quaternary geology 6
1.2.4.1 Continental glacial dynamics 6
1.2.4.2 Deglaciation of the western HBL following the LGM 8
1.3 Previous work on the Quaternary stratigraphy of the western HBL 9
1.3.1 Netterville's investigation of the Gods River area 11
1.3.2 Regional investigations and the four-till framework 12
1.3.3 Limitations of earlier investigations 15
1.3.4 Implementing a detailed, multi-parameter approach 15
1.4 Knowledge gaps 17
1.5 Thesis objectives 18
1.6 Thesis structure 18
Chapter 2: Methodology 19
2.1 Introduction 19
2.2 Field data collection 19
2.2.1 Stratigraphic logging 19
2.2.2 Sorted sediment 21
2.2.3 Ice-flow data collection 22
2.2.4 Till sampling 23
2.2.5 Compilation 25

2.3 Till-composition analysis 25
2.3.1 Distal bedrock source regions of tracer lithologies 25
2.3.2 Clast-lithology counts 27
2.3.2.1 K-means clustering 30
2.3.3 Matrix geochemistry 31
2.3.3.1 Principal component analysis 31
2.3.4 Till-composition considerations 33
2.4 Stratigraphic approach 34
2.4.1 Stratigraphic beds 34
2.4.1.1 Till beds 34
2.4.1.2 Nonglacial sediment beds 35
2.4.2 Till bed correlations and till units 35
2.4.2.1 Degree of diagenetic alteration 36
2.4.2.2 Interpreted paleo-ice flow 36
2.4.3 Sub-till sorted sediment correlations 38
2.4.4 Definition of stratigraphic terms and classifications 38
2.5 Conclusion 39
Chapter 3: Quaternary stratigraphy and paleo-ice flow indicators 40
3.1 Introduction 40
3.2 Methodology 40
3.3 Results 40
3.3.1 Tills 41
3.3.1.1 Colour 43
3.3.1.2 Grain size distribution 44
3.3.1.3 Degree of diagenetic alteration 45
3.3.1.4 Paleo-ice flow indicators 47
3.3.1.5 Clast-lithology counts 47
3.3.1.6 Total carbonate 49
3.3.2 Nonglacial sediment 50
3.3.2.1 Postglacial sediment 50
3.3.2.2 Sub-till sorted sediment 50
3.3.3 Stratigraphic sections 52
3.3.3.1 Section 115-23-002, Gods River 53
3.3.3.2 Section 115-23-003, Yakaw River 60

3.3.3.3 Section 115-23-004, Gods River 67
3.3.3.4 Section 115-23-005, Gods River 75
3.3.3.5 Section 115-23-006, Yakaw River 86
3.3.3.6 Section 115-23-007, Gods River 92
3.3.3.7 Section 115-23-008, Gods River 108
3.3.3.8 Section 115-23-009, Gods River 114
3.4 Discussion 124
3.4.1 Reworked and discontinuous till beds 125
3.4.2 Multiple, discordant sub-till sorted sediments 126
3.4.3 Postglacial sequence 127
3.5 Conclusions 127
Chapter 4: Till composition analysis 128
4.1 Introduction 128
4.2 Methodology 128
4.3 Results 128
4.3.1 Clast-lithology counts 128
4.3.1.1 Clast-lithology counts: K-means clustering 129
4.3.2 Till-matrix geochemistry 136
4.3.2.1 Geochemical data exploration 136
4.3.2.2 Principal component analysis 137
4.4 Discussion 141
4.4.1 Evidence of inheritance and overprinting in till composition 142
4.4.2 Geochemical signature for till samples associated with anoxic deposits 143
4.5 Conclusions 146
Chapter 5: Local stratigraphic framework 147
5.1 Introduction 147
5.2 Methodology 147
5.3 Results 147
5.3.1 Stratigraphic framework 147
5.3.1.1 Unit 1t: NW ice-flow 150
5.3.1.2 Unit 2t: SW ice-flow 150
5.3.1.3 Unit 3t: W ice-flow 150
5.3.1.4 Unit 4s: Heterogeneous sediments 150
5.3.1.5 Unit 5t: S ice-flow 151

5.3.1.6 Unit 6t: SSW–WSW ice-flow 151
5.3.1.7 Unit 7s: Heterogeneous sediments 152
5.3.1.8 Unit 8t: SW ice-flow 152
5.3.1.9 Unit 9t: WNW–NNW ice-flow 152
5.3.1.10 Unit 10t: W–WNW ice-flow 153
5.3.1.11 Unit 11t: SW ice-flow 153
5.3.1.12 Unit 12s: Heterogeneous sediments 153
5.3.1.13 Unit 13t: WSW–W ice-flow 154
5.3.1.14 Unit 14t: S–SSW ice-flow 154
5.3.1.15 Unit 15t: WNW–NW or ESE–SE ice-flow 155
5.3.1.16 Unit 16t: S–SW ice-flow 155
5.3.1.17 Unit 17s: Proglacial sediments 156
5.3.1.18 Unit 18t: SW–W ice-flow 156
5.3.1.19 Unit 19s: Heterogeneous sediments 156
5.3.1.20 Unit 20t: Young till, variable ice-flow 157
5.3.1.21 Unit 21s: Postglacial sediments 157
5.4 Discussion 158
5.4.1 A fragmented stratigraphic record 161
5.4.1.1 An alternative stratigraphic placement of section 23-005 beds 162
5.4.2 Till units: discrete glacial events or glaciotectonic stacking? 163
5.4.3 Interpreted provenance of till units 164
5.4.3.1 Units 1t–11t: strong HBB provenance signal, Q-L influence 164
5.4.3.2 Units 13t–18t: a major decrease of HBB-sourced detritus, unclear provenance 164
5.4.4 Comparison with previous studies 168
5.5 Conclusions 170
Chapter 6: Conclusions and further work 171
6.1 Research summary and contributions 171
6.2 Recommendations for future research 173
References 175
Appendix A – Related publications 186
Appendix B – Section and sample data 187
Appendix C – Till-matrix geochemistry data 197
Appendix D – Till-matrix geochemistry data: Quality assurance and quality control 198
Ca/Mg method 198

Partial digestion 200
Fusion digestion 212
Appendix E – Clast-lithology counts 224
Tabulated counts 224
Pictures of sorted clast counts 245
Appendix F – Radiocarbon dating 424
Appendix G – Paleo-ice flow measurements 425
Appendix H – Stratigraphic columns for 2019 and 2022 sections 505
Sections 112-19-628 and 112-629 505
Section 112-22-200 505
Section 112-22-201 506
Appendix I – Till composition analysis 507
Clast-lithology clustering 507
Till-matrix geochemistry 507
Appendix J – Till unit data 510

List of Figures

Figure 1.1: The spatial extent of the Hudson Bay Lowlands (HBL; light brown) and the study area. […] 2
Figure 1.2: The study area and neighbouring recent studies (Gillam study area, Kaskattama highland study area), with a digital elevation model […] 4
Figure 1.3: Both major ice-spreading centers (Keewatin sector, Quebec-Labrador sector) of the LIS advanced across the western HBL during the last glacial cycle […] 8
Figure 1.4: Location of the 2023 field sites and previously studied sections in the study area (outlined in red on the inset map) in northeastern Manitoba. […] 10
Figure 2.1: An example of an investigated site (115-23-009) in the 2023 field season. […] 20
Figure 2.2: An overview of ice-flow data collection and analysis […] 23
Figure 2.3: Till sample 115-23-007-D05, including (A) a 2-3 kg bag collected for grain size, clast lithology, and geochemical analysis, and (B) an 11.4 L pail collected for indicator-mineral analysis. 24
Figure 2.4: Regional bedrock geology domains of central Canada, and distinct clast lithologies observed in the study area. […] 26
Figure 2.5: An example of clast-lithology identification and categorization. […] 28
Figure 3.1: Examples of massive till with well-developed blocky soil structure and oxidation staining along joint faces. […] 41
Figure 3.2: Examples of sorted sediments within till beds […] 42
Figure 3.3: Till matrix grain size ternary diagram for 2023 samples, coloured by grain size category. […] 44
Figure 3.4: Examples of different degrees of diagenetic alteration in till beds with similar texture […] 46
Figure 3.5: The distribution of each major clast-lithology group […] 48
Figure 3.6: Cumulative distribution of total carbonate from the fine-grained matrix of till samples […] 49
Figure 3.7: Overview of section 115-23-005 […] 51
Figure 3.8: Simplified stratigraphy of sections from the study area […] 52
Figure 3.9: Overview of section 115-23-002, viewed towards the northwest. 53
Figure 3.10: Stratigraphic log of section 115-23-002. […] 54
Figure 3.11: Summary of till sample data for section 115-23-002. […] 55
Figure 3.12: (A) Very dark grey-brown till of Bed 2-A. (B) Dark grey-brown till of Bed 2-B. 56
Figure 3.13: [115-23-002 Photos #1] 57
Figure 3.14: [115-23-002 Photos #2] 58
Figure 3.15: [115-23-002 Photos #3] 59
Figure 3.16: Overview of section 115-23-003, viewed towards the south. 60
Figure 3.17: Stratigraphic log of section 115-23-003. […] 61
Figure 3.18: Summary of till sample data for section 115-23-003. […] 62
Figure 3.19: [115-23-003 Photos #1] 63
Figure 3.20: [115-23-003 Photos #2] 64

Figure 3.21: [115-23-003 Photos #3]....65
Figure 3.22: Overview of section 115-23-004, which is situated only ~100 m from section 115-23-002. View is towards the north. 67
Figure 3.23: Stratigraphic log and simplified till sample data for section 115-23-004. […]....68
Figure 3.24: Stratigraphic log for Exposure-1 of Section 115-23-004. […]....70
Figure 3.25: The stratigraphic sequence at Exposure-1 of Section 115-23-004 […]....71
Figure 3.26: Stratigraphic log for Exposure-2 of Section 115-23-004. […]....72
Figure 3.27: The stratigraphic sequence at Exposure-2 of Section 115-23-004 [...]....73
Figure 3.28: The blue-grey till of Bed 4-B underlies the dark grey brown diamict of Bed 4-C. 74
Figure 3.29: Overview of section 115-23-005, viewed towards the northeast. 75
Figure 3.30: Stratigraphic log of section 115-23-005. […] 76
Figure 3.31: Summary of till sample data for section 115-23-005. […]....77
Figure 3.32: Stratigraphic log for Exposure-1 of Section 115-23-005. […]....78
Figure 3.33: The stratigraphic sequence at Exposure-1 of Section 115-23-005 […]....79
Figure 3.34: Stratigraphic log for Exposure-2 of Section 115-23-005. […]....80
Figure 3.35: The stratigraphic sequence at Exposure-2 of Section 115-23-005. […]....81
Figure 3.36: Stratigraphic log for Exposure-3 of Section 115-23-005. […]....82
Figure 3.37: The stratigraphic sequence of Bed 5-B at Exposure-3 of Section 115-23-005. […]....83
Figure 3.38: [115-23-005 Photos #1]....84
Figure 3.39: [115-23-005 Photos #2]....85
Figure 3.40: Overview of section 115-23-006, viewed towards the northwest. 86
Figure 3.41: Stratigraphic log of section 115-23-006. […] 87
Figure 3.42: Summary of till sample data for section 115-23-006. […]....88
Figure 3.43: [115-23-006 Photos #1]....88
Figure 3.44: [115-23-006 Photos #2]....90
Figure 3.45: [115-23-006 Photos #3]....91
Figure 3.46: Overview of section 115-23-007, viewed towards the north....92
Figure 3.47: Stratigraphic log of section 115-23-007. […] 93
Figure 3.48: Summary of till sample data for section 115-23-007. […]....94
Figure 3.49: Stratigraphic log for Exposure-1 of Section 115-23-007. […]....95
Figure 3.50: The stratigraphic sequence at Exposure-1 of Section 115-23-007 […]....95
Figure 3.51: [115-23-007 Photos #1]....96
Figure 3.52: Stratigraphic log for Exposure-3 of Section 115-23-007. […]....97
Figure 3.53: The stratigraphic sequence at Exposure-3 of Section 115-23-007 […]....98
Figure 3.54: Stratigraphic log for Exposure-4 of Section 115-23-007. […]....99
Figure 3.55: The stratigraphic sequence at Exposure-4 of Section 115-23-007. 100
Figure 3.56: Stratigraphic log for Exposure-5 of Section 115-23-007. […]....101

Figure 3.57: The stratigraphic sequence at Exposure-5 of Section 115-23-007. 102
Figure 3.58: [115-23-007 Photos #2]....103
Figure 3.59: Stratigraphic log for Exposure-2 of Section 115-23-007. […]....104
Figure 3.60: The stratigraphic sequence at Exposure-2 of Section 115-23-007 […]....105
Figure 3.61: [115-23-007 Photos #3]....106
Figure 3.62: Overview of section 115-23-008, viewed towards the west.....108
Figure 3.63: Stratigraphic log of section 115-23-008. […] 109
Figure 3.64: Summary of till sample data for section 115-23-008. […]....110
Figure 3.65: [115-23-008 Photos #1]....111
Figure 3.66: [115-23-008 Photos #2]....112
Figure 3.67: [115-23-008 Photos #3]....113
Figure 3.68: Overview of section 115-23-009, viewed towards the northeast. 114
Figure 3.69: Stratigraphic log of section 115-23-009. […] 115
Figure 3.70: Summary of till sample data for section 115-23-009. […]....116
Figure 3.71: [115-23-009 Photos #1]....117
Figure 3.72: Stratigraphic log for Exposure-1 of Section 115-23-009. […]....118
Figure 3.73: The stratigraphic sequence at Exposure-1 of Section 115-23-009 […]....119
Figure 3.74: [115-23-009 Photos #2]....120
Figure 3.75: [115-23-009 Photos #3]....121
Figure 3.76: [115-23-009 Photos #4]....122
Figure 3.77: [115-23-009 Photos #5]....123
Figure 3.78: Simplified stratigraphy of sections from the study area, with paleo-ice flow indicators, till sub-beds based on laboratory data, and tentative correlations […]....124
Figure 4.1: Normalized clast-lithology proportion ternary diagram for 2019, 2022, and 2023 samples collected in the Gods River area. […]....129
Figure 4.2: K-means clustering applied to normalized clast-lithology proportions.....130
Figure 4.3: Clustered bar chart of clast-lithology clusters and their associated ice-flow direction. 132
Figure 4.4: Clast-lithology clusters overlaying the simplified stratigraphic sections from the study area. […]....133
Figure 4.5: QQ plots of select trace elements for till samples and a grab sample of sub-till sorted sediment from section 23-004 […] 136
Figure 4.6: Element loadings for each principal component of the selected element assemblage. […]....138
Figure 4.7: Till samples plotted on a ternary grain size chart, coloured by PC1 score (left) and PC2 score (right). […] 138
Figure 4.8: Till samples plotted on a ternary clast-lithology plot, coloured by PC1 score (left) and PC2 score (right). […]....139
Figure 4.9: PC2 scores overlaying the simplified stratigraphic sections from the study area. […]....140

Figure 4.10: Clast-lithology clusters and PC2 scores overlaying the simplified stratigraphic sections from the study area, with several updated ice-flow direction interpretations. […] 141
Figure 4.11: Summed Z-scores of elements associated with deposits formed in an anoxic environment (Ba, Rb, V) are overlain on the simplified stratigraphic sections from the study area. […] 144
Figure 5.1: Stratigraphic units shown on the simplified stratigraphic sections from the study area. 148
Figure 5.2: Boxplots of till parameters of each till unit […] 149
Figure 5.3: Delineated units of the study area displayed on a stratigraphic cross-section. […] 160

List of Tables

Table 1.1: Summary of the regional glacial history of northern and central Manitoba […].....14
Table 2.1: Major lithology classes and their associated detailed lithology classes.....29
Table 2.2: Calculated standard deviation values for each parameter, defined as the thresholds for significant changes. Data from all till samples are used in these calculations.....35
Table 2.3: Percentile-based categorical terms used to describe clast lithology proportionality.....38
Table 3.1: Observed Munsell colours of till samples from the 2023 field season. 43
Table 3.2: The number of till beds and samples that exhibit the different degrees of blocky soil structure and oxidation along joints, from the 2023 field season. 45
Table 4.1: Normalized clast-lithology proportions by cluster. 130
Table 4.2: Observations of distinctive lithologies by cluster. 131
Table 4.3: Summary of clast-lithology clusters. […] 135
Table 4.4: Coefficients of determination (R^2) showing the strength of relationships between individual element concentrations and clast-lithology proportions. […].....137
Table 5.1: Summary and tentative Marine Isotope Stage estimates of units from relative stratigraphy. 159
Table 5.2: Assigned units for beds of section 23-005, with an alternative assignment based on an approach focused more on till composition. 162
Table 5.3: Presence and average proportion of select tracer lithologies (Dubawnt Supergroup and oolitic jasper clasts) by unit. […] 166

List of Abbreviations

CLR	centered-log ratio
GR	granitoid rocks
HBB	Hudson Bay Basin
HBIS	Hudson Bay Ice Saddle
HBL	Hudson Bay Lowlands
ICP-MS	inductively coupled plasma mass spectrometry
LGM	Last Glacial Maximum
LIS	Laurentide Ice Sheet
MGS	Manitoba Geologic Survey
MIS	Marine Isotope Stage
OSL	optically-stimulated luminescence
PC	principal component
PCA	principal component analysis
Q-L	Quebec-Labrador
QA/QC	quality assurance and quality control
QQ	quantile-quantile
SRC	Saskatchewan Research Council
UGG	undifferentiated greenstone and greywackes

Chapter 1: Introduction

1.1 Scientific rationale

During the Quaternary glaciations, the waxing and waning of paleo-ice sheets profoundly altered landscapes through subglacial processes and caused global fluctuations in Earth's hydrological cycle and climate patterns (Batchelor et al., 2019; Dalton et al., 2022). The geological record left behind offers a valuable means to reconstruct the glacial and nonglacial history of affected regions, providing crucial insights into the long-term behaviour of ice sheets (Batchelor et al., 2019; Gowan et al., 2021; Pico, 2022; Dalton et al., 2022). This long-term perspective is essential for understanding how Earth systems respond to climate change and how landscapes evolve over different time scales.

Reconstructions of the Last Glacial Maximum (LGM) often rely on surface landforms and ice margin retreat chronologies (e.g., Margold et al., 2018; Dalton et al., 2020; 2022). In contrast, studies of older glacial events must rely heavily on stratigraphic evidence. Stratigraphic studies have therefore provided most of the insights into the extent and character of older glacial and interglacial events in Canada (e.g., McDonald and Shilts, 1971; Karrow, 1974; Monaghan and Larson, 1986; Evans and Campbell, 1995; Norris et al., 2018; Evans et al., 2021). However, these stratigraphic studies are constrained by the availability, preservation, and accessibility of natural exposures. As a result, most research has focused on the outer limits of paleo-ice sheets, where thicker deposits are more likely to be preserved and accessible. This is especially true in North America, where inner regions of former ice sheets are often thin or lack clear evidence of older glacial-interglacial cycles (e.g., Ó Cofaigh et al., 2013, Rice et al., 2024) and may be less accessible.

An important exception is the Hudson Bay Lowlands (HBL), a low-lying wetland underlain by the Hudson Bay sedimentary basin (Figure 1.1; Dredge and Dyke, 2020). The HBL contains large (~20–220 m; cf. Hodder and Gauthier, 2021), well-preserved sedimentary successions with deposits dating back to Marine Isotope Stage (MIS) 5 (130–71 ka; Skinner, 1973; Thorleifson et al., 1993; Dalton et al., 2018; Gao et al, 2020), MIS 7 (243–191 ka; Nielsen et al., 1986; Hodder et al., 2024b), or even the early Quaternary (>0.773 Ma; Su, 2022). Natural river-cut exposures in the HBL offer valuable insights into these understudied older glacial and interglacial events. As such, the HBL provides a rare opportunity to investigate the long-term glacial dynamics and ice-sheet configurations in an inner core region that is otherwise difficult to study. This Quaternary record at the center of former North American ice sheets is particularly significant, as it documents phases of severe ice volume reduction with climates cooler than

present day (interstadial) or complete deglaciation with climates analogous to present day (interglacial; Gauthier et al., 2021).



Figure 1.1: The spatial extent of the Hudson Bay Lowlands (HBL; light brown) and the study area. The blue dashed line marks extent of the North American Ice Sheet Complex during the LGM, including the Laurentide Ice Sheet (LIS) which covered the study area; isochron shapefile (22-ka optimal) retrieved from Dalton et al. (2023).

Early attempts to characterize the glacial history of the western HBL often overlooked the complex spatial and temporal variability of the region's Quaternary deposits, grouping sedimentary units of seemingly similar characteristics across large distances (e.g., McDonald, 1969; Klassen, 1986; Nielsen et al., 1986). More recent efforts have adopted a multi-parameter approach, incorporating methodologies such as till-led frameworks, clast-lithology counts, till-matrix geochemistry, and paleo-ice flow indicators (e.g., Hodder et al., 2017; Wang, 2018; Gauthier et al., 2019; Hodder et al., 2024a; 2024b; Gauthier et al., *in review*). These studies have highlighted the limitations of earlier stratigraphic correlations and prompted a comprehensive reassessment of the regional Quaternary reconstructions.

Aligned with these recent efforts, the primary goal of this research is to apply a multi-parameter approach to improve our understanding of the Quaternary history and till provenance in the Gods River area in the western HBL. This area contains four discerned till units and at least three pre-Holocene sorted sediment

units, one of which is organic-bearing (Netterville, 1974). Integrating a revised Gods River stratigraphy with nearby frameworks from Kaskattama (Hodder et al., 2024a; 2024b) and Gillam (Gauthier et al., *in review*) will provide essential long-term geological constraints for ice sheet models aiming to reconstruct the evolution of the LIS (cf. Gowan et al., 2021). Additionally, improved understanding of regions with shifting ice flows and multiple spreading center influences may help identify bedrock sources of indicator minerals of economic interest (McClenaghan et al., 2023).

1.2 Study area and geological setting

1.2.1 Study area

The study area lies in the western HBL, centered around Gods River just southeast of its confluence with Hayes River, and includes nearby study sites along Hayes River, Little Hayes Creek, Yakaw River, and Twin Creeks (Figure 1.2). This remote area is situated approximately between the town of Gillam, the First Nations community of Shamattawa, and the historic settlement of York Factory.

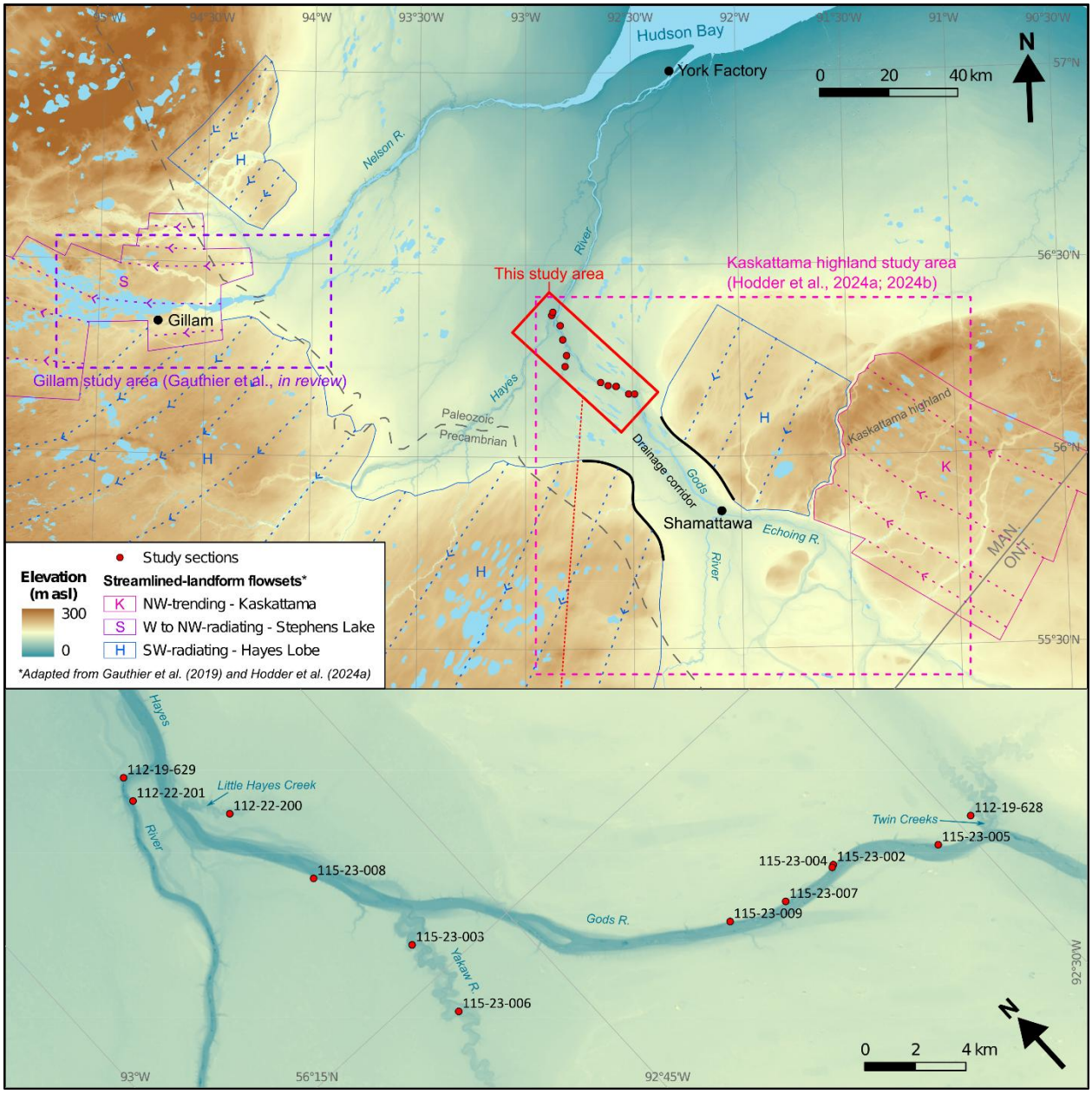


Figure 1.2: The study area and neighbouring recent studies (Gillam study area, Kaskattama highland study area), with a digital elevation model showing nearby topographic features, including the Kaskattama highland and a major drainage corridor (30 m resolution, Earth Observation Research Center and Japanese Aerospace Exploration Agency, 2022). Streamlined landform flowsets are depicted, including those associated with the Hayes Lobe, Stephens Lake sublobe, and the Kaskattama flowset. The approximate boundary between Paleozoic (Hudson Bay Basin) and Precambrian (Canadian Shield) bedrock is also shown.

1.2.2 Regional physiography

The regional physiography of the HBL is predominantly flat (decrease of ~0.7 m/km towards Hudson Bay), except for deep incisions (~30–50 m) by large rivers (e.g., Hayes River, Gods River), and shallower channels (~10–30 m) made by meandering tributaries (e.g., Yakaw River, Little Hayes Creek, Twin Creeks). Wetlands, including extensive bogs, fens, and permafrost peatlands dominate the landscape of the HBL (Abraham and Keddy, 2005).

Despite the generally uniform physiography of the HBL, considerable variability exists beneath the surface, particularly in the thickness and distribution of Quaternary sediments. Near the study area, Netterville (1974) describes a river cut section (Section 2, about 14 km upstream of Twin Creeks) along Gods River with 21.5 m of Quaternary sediments above bedrock, whereas an exploration drillhole by BHP Billiton Diamonds Inc. indicated a Quaternary thickness of 89.2–91.2 m in the study area (Bilben, 2005). However, the total thickness of Quaternary sediments in this region remains largely unknown, as bedrock outcrops are rare and drillhole data is sparse (Hodder and Gauthier, 2021).

The regional study area was last glaciated by the southwest-trending Hayes Lobe (Dredge and Cowan, 1989; Gauthier et al., 2019), the imprint of which was eroded from the study area (see section 1.2.2.1 below; Figure 1.2). Glacial sediments are overlain primarily by glaciomarine sediments and peat (Klassen and Netterville, 1978), which obscure most surface glacial geomorphology.

1.2.2.1 Deglacial-postglacial erosion

A prominent feature of the regional area is a broad erosional drainage corridor (~20 km wide; Figure 1.2), formed as an outlet from Lake Agassiz during the Holocene (Dredge, 1983). This drainage corridor separates the Kaskattama highland (~50 km to the east of the study area) and elevated terrain associated with the Canadian Shield to the south. Here, the elevational change between the corridor's base (~80–100 m asl) and surrounding highlands (~130–150 m asl), represents erosion of ~45–60 m of the stratigraphic record near Shamattawa (Hodder et al., 2024b).

The base of this erosional corridor widens towards the northwest, encompassing the study area (Figure 1.2). Here, elevations at the top of the river cuts reach ~80 m asl on the southeast side and ~60–70 m asl on the northwest side. When compared to the nearest highlands (~120–150 m asl, ~10 km to the east), these elevations suggest potential erosion of at least ~40 m in the southeast and ~50–60 m in the northwest.

1.2.3 Bedrock geology

The study area is situated over the flat-lying Paleozoic Hudson Bay Basin (HBB), about 20 km northeast of its boundary with the Precambrian shield (Figure 1.2). HBB rocks primarily contain calcareous sandstone, limestone, dolostone (Nicolas and Armstrong, 2017). However, much about the geometry and extent of strata in the HBB Paleozoic sequence is unknown due to limited drillholes and bedrock exposures in the western HBL (cf. Nicolas and Armstrong, 2017; Hodder and Gauthier, 2021). For example, black shale with a probable Cretaceous age was recovered from a single drillhole in the Kaskattama highland (KK1; McCracken, 2014; Nicolas and Armstrong, 2017), overlying the Severn River Formation in an area where bedrock is otherwise expected to be either the Attawapiskat or the Ekwan River formations. The HBB unconformably overlies and is surrounded by the Precambrian shield, which primarily consists of a variety of felsic rocks (e.g., granite, granodiorite, diorite, tonalite, felsic gneiss, syenite; Rinne, 2020). Greenstone belts consisting of metasedimentary and metavolcanic rocks are also scattered across the Precambrian shield, including the Fox River Belt, which is situated about 40 km to the south of the study area (Rinne, 2020).

1.2.4 Quaternary geology

HBB bedrock in the study area is overlain by a particularly thick blanket of glacial and nonglacial Quaternary sediments, deposited over at least three glacial cycles (Dredge and McMartin, 2011; Gauthier et al., 2019), that are laterally and stratigraphically variable (e.g., Netterville, 1974, Klassen, 1986). Postglacial deposits commonly cap sections throughout the western HBL, including sediments deposited by Glacial Lake Agassiz, the Tyrrell Sea, and fluvial systems following marine regression (Dredge and McMartin, 2011). Sub-till nonglacial sorted sediments (i.e., sediments deposited in an interglacial or interstadial), although discontinuous, are relatively common in the depositional record of the western HBL (Netterville, 1974; Nielsen et al., 1986; Dredge et al., 1990; Roy, 1998, Dalton et al., 2016). Sub-till sorted sediments, containing organics with nonfinite radiocarbon ages (i.e., an age beyond the limit of radiocarbon dating), have been interpreted as nonglacial deposits (Dredge et al., 1990). Stratigraphic records investigated by previous studies in the western HBL have shown at least two separate ice-free phases (Nielsen et al., 1986; Roy, 1998; Dredge and McMartin, 2011).

1.2.4.1 Continental glacial dynamics

During the last glacial cycle, the western HBL was situated in between and was influenced by two paleo-ice spreading centers of the LIS: the Keewatin to the northwest, and the Quebec-Labrador (Q-L) to the east-northeast (Shilts et al., 1979; Prest, 1990; Figure 1.3). During the evolution of the LIS (and likely previous iterations), the position and orientation of these domes shifted over time, resulting in down-ice

shifts in ice-flow direction. The Keewatin dome shifted several times during the last glacial cycle, each phase resulting in either subtle or major changes in emanating ice-flow directions (McMartin and Henderson, 2004). The Q-L dome migrated northwards during the last glacial cycle, causing a counter-clockwise shift in paleo-ice flow direction recorded to the east of Hudson and James Bay (Parent et al., 1995; Veillette et al., 1999; 2017). The western HBL, therefore, experienced dynamic and potentially competing ice flows which shifted in dominance at different stages of LIS evolution (Dredge and McMartin, 2011).

Additionally, considerable uncertainty remains regarding the evolution of these ice divides, particularly how their migration influenced ice-flow patterns across the western HBL and the relative timing of these flows. Furthermore, existing knowledge is primarily based on available bedrock striae and surface landform orientations (e.g., Boulton and Clark, 1990; Parent et al., 1995; Veillette et al., 1999; McMartin and Henderson, 2004, Veillette et al., 2017), methods that primarily reflect conditions from the most recent glaciation. Therefore, configurations and evolution of the LIS during the last glaciation may not accurately represent the evolution of ice-sheets during previous glaciations.

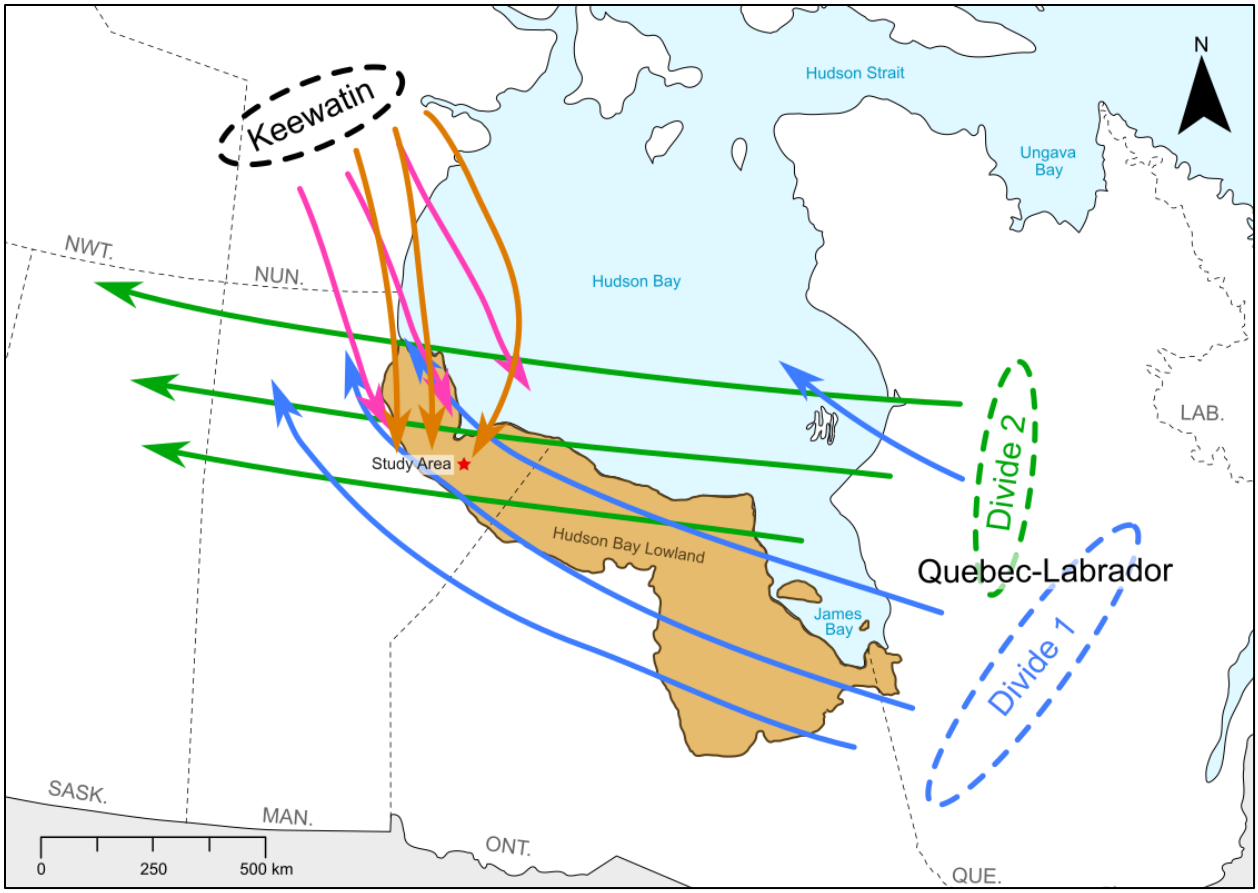


Figure 1.3: Both major ice-spreading centers (Keewatin sector, Quebec-Labrador sector) of the LIS advanced across the western HBL during the last glacial cycle (approximate ice-flow directions depicted by arrows). Note the northward migration of the Quebec-Labrador ice divide over time (Parent et al., 1995; Veillette et al., 1999; 2017).

1.2.4.2 Deglaciation of the western HBL following the LGM

Following the LGM, deglaciation in the region began at around 9450-9530 BP based on freshwater shell radiocarbon ages (Gauthier et al., 2020). Proglacial Lake Agassiz formed as deglaciation progressed, impounded by the SW margin of the Hudson Bay Ice Saddle (HBIS; Teller and Leverington, 2004; Gauthier et al., 2020). Periodic subglacial 'leaking' of Lake Agassiz occurred through the HBIS to the NE, preceding the incursion of the Tyrrell Sea, and subsequent collapse of the HBIS between 8.57 ± 0.28 and 8.11 ± 0.19 ka BP (Gauthier et al., 2020).

1.3 Previous work on the Quaternary stratigraphy of the western HBL

Tyrrell (1916) marks the first substantial investigation of the Quaternary stratigraphy of river cuts in the western HBL, including the Nelson, Hayes, and Gods rivers (known at the time as the Shamattawa River). Here was the first observation of organic-bearing sub-till sorted sediments along Gods River, as well as the highly laterally variable nature of the stratigraphy.

The area was not revisited until Operation Winisk, a reconnaissance-level survey initiated in 1967 by the Geological Survey of Canada to better understand the geology of the HBL (Figure 1.4; Craig, 1969; McDonald, 1969). McDonald (1969) created an initial stratigraphic framework, which included at least three till units and a sub-till nonglacial unit assumed to be correlative across the HBL.

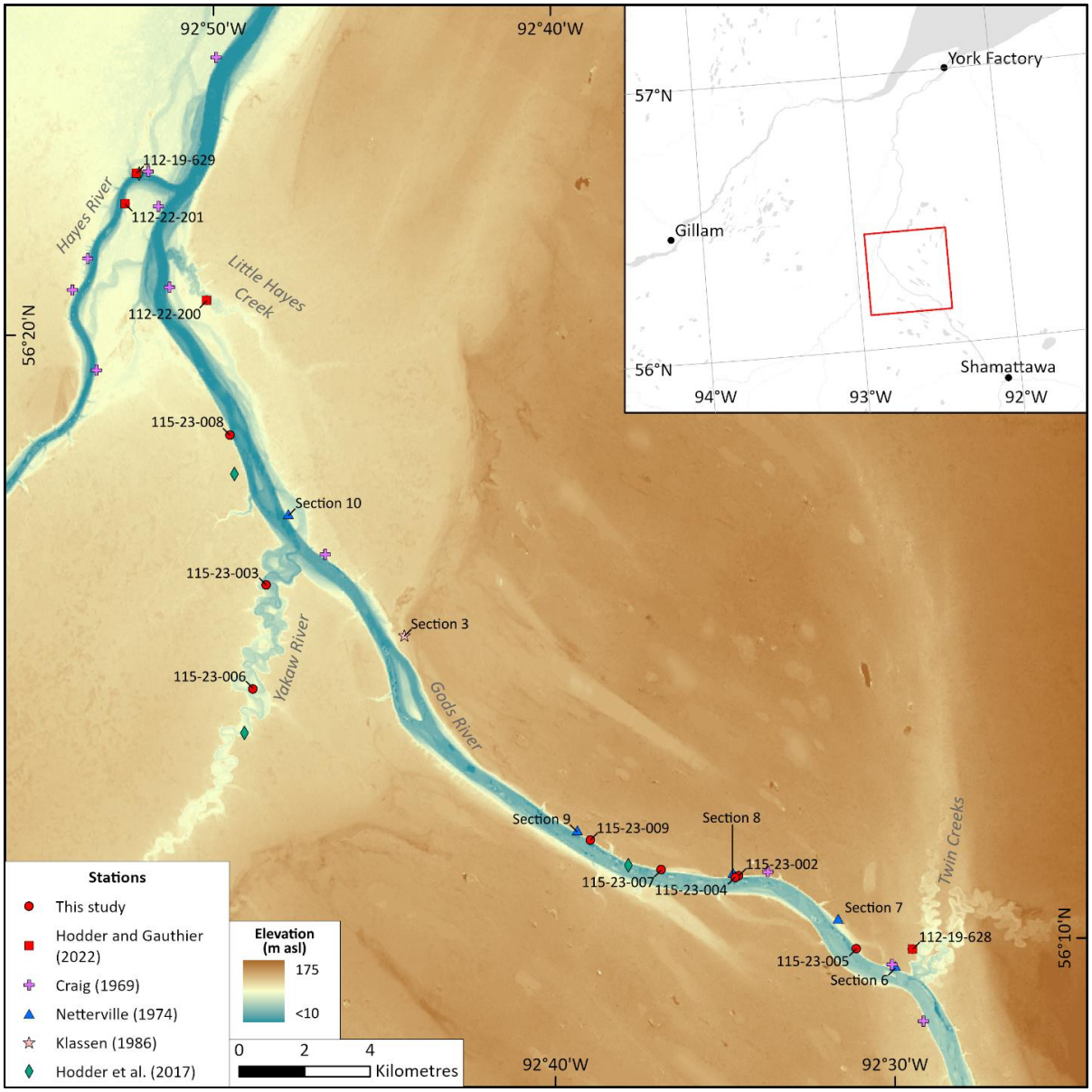


Figure 1.4: Location of the 2023 field sites and previously studied sections in the study area (outlined in red on the inset map) in northeastern Manitoba. Field sites used for this study are in red. Background hillshade image was generated from a digital elevation model (30 m resolution, Earth Observation Research Center and Japanese Aerospace Exploration Agency, 2022).

1.3.1 Netterville's investigation of the Gods River area

Netterville (1974) was the first detailed investigation of the Quaternary stratigraphy of sections along Gods River and was a substantial improvement on the regional stratigraphic framework from Operation Winisk, as a more focused study is crucial to appreciate the fragmented nature of the stratigraphy. This study involved the investigation of 26 exposures and produced 10 representative sections, 5 of which lay within the study area (Sections 6–10; Figure 1.4).

Netterville (1974) used a multitude of techniques, including analysis of glacial and nonglacial beds, to establish its stratigraphic framework. Till-fabric analysis was conducted, where the orientation of long-axis of at least 50 clasts from 3–4 locations was measured from each till unit across multiple sections, totaling 150 clasts per unit. A total of 28 till samples were analyzed for grain-size using sieves, and the calcite and dolomite percentages of the fine-grained matrix (44–63 microns) were obtained via the Chittick method. A total of 28 sub-till organic-rich silt samples were also collected for paleoecological investigation via palynomorph (pollen) counting.

Using these techniques, Netterville (1974) delineated four till units (Till A–D), three sub-till sorted sediment units (Gods River sediments, Twin Creeks sediments, and an unnamed sediment unit), and the Tyrrell Sea sediments associated with marine deposition following deglaciation in the region. Till units were roughly differentiated by Munsell colour, texture, and degree of jointing and oxidation. Ultimately though, the till units were based on their stratigraphic position relative to sub-till sorted sediments units, as their characteristics were undiagnostic and varied. Each defined till unit is separated by sorted sediments, including an undated, organic-bearing interglacial unit (referred to as Gods River sediments) between Till A and B, interpreted to represent the last interglacial episode and thus correlated to the Missinaibi Fm of the southeastern HBL. Twin Creeks sediments, between Till B and C, are devoid of organics and are interpreted to be deposited by glacial meltwater. Twin Creeks sediments are correlated with Friday Creek sediments of the southeastern HBL based on stratigraphic position and lack of organics.

Problematically, the analytical work on till units defined by Netterville (1974) was conducted after descriptive work and field identification based primarily on stratigraphic position, creating a sub-optimal 'unit-first' approach. This approach limits the ability to revise correlations based on analytical data and overly relies on initial qualitative observations. Issues arise particularly from assumptions regarding the consistent presence and stratigraphic order of sorted sediment beds, which complicates correlations across sections, especially when sub-till sorted sediment beds are absent. Consequently, this often results in ambiguity, with many till beds assigned multiple possible units. This approach also impacts data

presentation; sample data and paleo-ice flow measurements are grouped by unit and lack depth or locational data. For example, till-fabric data from multiple locations are combined into single rose diagram per unit, which is problematic when done after the correlation and unit assignment rather than being used to do the correlation. In addition, it is known that ice flow directions during a single ice flow phase may span a certain range across a region and may also shift over time during the deposition of a single till sheet. Therefore, the analytical data presented in Netterville (1974) are unfortunately unusable for inclusion in this study.

1.3.2 Regional investigations and the four-till framework

In investigations along the Nelson River near Gillam, Nielsen et al. (1986) established a four-till stratigraphic framework that served as the foundation for subsequent studies in the western HBL. The Sundance Till, the oldest till unit observed in the area, is underlain by bedrock at the Sundance section, and is separated from an overlying till by sorted sediments or an interpreted paleosol and minor organic sediments. Measured paleo-ice flow indicators from the Sundance Till indicate a southeast flow direction, while underlying bedrock striae record an earlier, west-southwest paleo-ice flow. The Sundance Till is distinctive in its properties, as well; compared to overlying tills, it is much sandier (45% sand, 45% silt and 10% clay) and richer in Precambrian clasts with an inferred northwest provenance (~55% Precambrian, ~45% Paleozoic carbonate; Dredge and McMartin, 2011).

The Amery Till overlies the Sundance Till, with an interpreted southwest to west paleo-ice flow, and a siltier and more carbonate-rich composition indicating sediment sourced from the HBB. The Nelson River Sediments often serve as a key ‘marker bed’ for stratigraphic correlations between sections and are correlated with each other primarily based on elevation and stratigraphic position if organics are not present.

Overlying the Amery Till at seven sites are the Nelson River Sediments, a nonglacial unit with a range of sedimentological characteristics, including thinly bedded sand, silt, and clay, occasional dropstones, and visible organic material (woody and compressed peat) at the Henday and Limestone sections (Nielsen et al., 1986). The Nelson River Sediments are correlated to the Gods River Sediment from Netterville (1974) and the Missinaibi Fm from Skinner (1973), and therefore also interpreted as Sangamonian in age, or correlative to MIS 5.

Nielsen et al. (1986) distinguished two tills that overly the Nelson River Sediments: the Long Spruce Till, and the Sky Pilot Till. Although they are similar in texture and composition to each other and to the Amery Till, they differ based on colour; the Long Spruce Till is light olive grey, while the Sky Pilot Till is pale yellowish brown. The Long Spruce Till was interpreted to be deposited by west paleo-ice flow

based on composition. Nielsen et al. (1986) also note a range of greywacke clast conent (interpreted as east-sourced omars) within the Long Spruce Till (23% in two samples, compared to the average of 5%), implying variability within the provenance of grey tills overlying Nelson River Sediments. The Sky Pilot Till, meanwhile, is interpreted as being deposited by a shifting ice-flow, including west- and southwest-flowing ice based on till fabrics and drumlin orientations. The Sky Pilot Till, too, shows some variability; along the Limestone spillway, soft light-brown till with 5% greywackes overlies a more compact and fissile brown till with about 20% greywackes. Additionally, Nielsen et al. (1986) note a variable texture within Sky Pilot Till samples. These variations imply complexity within the till beds assigned to the Sky Pilot Till.

Overlying the Long Spruce and Sky Pilot tills are the Henday sediments, a unit that encompasses several facies, including glaciofluvial, diamicton, till, and subaqueous debris flows (cf. Nielsen et al., 1986). Henday sediments are then overlain by glaciolacustrine and glaciomarine sediments, deposited by glacial Lake Agassiz and the Tyrrell Sea, respectively.

Additionally, Klassen (1986) in a regional study involving sections along the Gods, Hayes, and Nelson rivers, attempted to correlate the framework developed by Nielsen et al. (1986) to sites along Gods River, including one in the study area (Section 3; see Figure 1.4). Klassen (1986) observed the Gods River sediments described by Netterville (1974) at sites along Gods River and correlated them to the Nelson River sediments as part of the regional framework. This correlation is, again, primarily due to both beds being the uppermost sub-till sorted sediment bed containing organics. Klassen (1986) also correlated the till underlying the Gods River sediments to the Amery Till.

Dredge and McMartin (2011) summarize the regional glacial history of northern and central Manitoba based on a compilation of stratigraphic sections available at the time, with additional evidence from bedrock striae (Table 1.1).

Table 1.1: Summary of the regional glacial history of northern and central Manitoba (Dredge and McMartin, 2011).

Event	Interpreted age	Marine isotope stage(s)	Summary of description	Associated unit(s)	Evidence
9	Deglaciation	MIS 1	Northward Keewatin ice dome shift; eastward Quebec-Labrador ice dome shift	Glaciolacustrine sediments from glacial Lake Agassiz, Tyrrell Sea sediments	Presence of glaciolacustrine and marine deposits at/near surface
8	Late Wisconsinan, deglaciation	MIS 2-4	Eastward Keewatin ice dome shift; shifting ice flow patterns, deglaciation, small glacial readvances	-	Striae, till fabrics
7	Main-late Wisconsinan	MIS 2-4	Shifts in ice flow (W and SW); westward confluence shift of ice-spreading centers	Wigwam Creek Formation (Long Spruce Till, Sky Pilot Till)	Till composition, till fabrics
6	Early-main Wisconsinan	MIS 2-4	Southeastward ice flow	-	Cross-cutting striae, Dubawnt erratics at the base of the Long Spruce till
5	Sangamon	MIS 5	Interglacial	Nelson River Sediments, Gods River Sediments	Sub-till organic-bearing sorted sediment, nonfinite radiocarbon dates, ~121 ka optical dates
4	Illinoian	MIS 6	Westward ice flow	Amery Till	Till composition, lodged boulders, till fabrics
3	Pre-Sangamon	MIS 7 or older	Interglacial	-	Paleosol development above Sundance till
2	-	-	Southeastward ice flow	Sundance Till	Till composition, till fabrics, crag and tail features, Dubawnt erratics
1	-	-	Westward ice flow	-	Omars contained by the lowest tills, bedrock striae below Sundance till

1.3.3 Limitations of earlier investigations

Early attempts at a Quaternary stratigraphic framework in the HBL focused largely on sorted sediment 'marker beds' and stratigraphic position, with some secondary focus on till appearance in the field and some clast fabrics. These studies tended to assume organic-rich sorted sediment beds were laterally continuous units across the HBL (e.g., Skinner, 1973; Klassen, 1986; Thorleifson et al., 1993; Dredge and McMartin, 2011). In the Gods River area, sub-till organic-bearing unit (Gods River sediments) are often interpreted as Sangamonian in age (e.g., Netterville, 1974, Klassen, 1986), simply because they are the uppermost organic-bearing units (Dredge and McMartin, 2011).

The idea that all organic-rich sorted sediment beds are correlative was challenged by several studies. Two separate ice-free phases were inferred from amino acid data, termed the Bell Sea and the Prest Sea (Andrews et al., 1983; Wyatt, 1990; Thorleifson et al., 1993). Furthermore, these organic-bearing sediments were found to be laterally discontinuous and can transition to organic-barren beds of variable facies and interpreted depositional environments (cf. Gauthier et al., 2019, Dalton et al., 2016). Therefore, caution must be taken when correlating these beds without age constraints. Further, recent optical age estimates on some of these uppermost sub-till sorted sediments have assigned them to MIS 5, MIS 7, or possibly older stages (cf. Hodder et al., 2023; Gauthier et al., 2024; Hodder et al., 2024a). This includes the MIS 7 'Echoing River sediments', which are the only organic-bearing sediments at a section east of Shamattawa, ~60 km from the study area (Hodder et al., 2024b). Therefore, correlation between so-called 'marker beds' should only be done after comprehensive geochronologic and paleoenvironmental analyses.

Furthermore, previous regional correlations that include the Gods River area often fail to consider the regional physiography and elevation differences between study areas. Specifically, the erosional corridor developed by Lake Agassiz drainage is often overlooked which, as previously stated, likely accounts for erosion of ~40–60 m of the stratigraphic record in the study area (see section 1.2.2.1). The preserved stratigraphic record in the Gods River area may therefore contain much older sediments than the surrounding, higher-elevation areas (e.g., Gillam, Kaskattama; Figure 1.2).

1.3.4 Implementing a detailed, multi-parameter approach

Previous stratigraphic frameworks named regional tills in the HBL assuming they are laterally extensive and homogeneous (Nielsen et al., 1986). However, till beds in the area are difficult to correlate across sections due to their fragmented nature and internal heterogeneity (Gauthier et al., 2019; Hodder and Gauthier, 2022). Each till bed varies laterally in characteristics such as colour, texture, blockiness, degree of oxidation, clast fabric, till matrix geochemistry, and clast lithologies in such a way that a simple approach at correlation is unlikely to produce a reliable stratigraphic framework. Therefore, the four-till

stratigraphic framework that was developed for the HBL using few criteria (e.g. colour, texture) that are now known to vary laterally within the same bed poorly represents the spatiotemporal complexities of the stratigraphic record of western HBL, including its discordant and fragmented nature, and is why a detailed, multi-parameter approach has been suggested to avoid such oversimplifications (Gauthier et al., 2019; 2024).

The work of Hodder et al. (2017) represents a compilation of stratigraphic data collected in a regional-scale till survey conducted by the Manitoba Geologic Survey (MGS) in 2001 and 2002 (Nielsen, 2001; 2002), including 4 sections within the study area. Further fieldwork conducted by the MGS in 2019 and 2022 involves 3 stratigraphic sections near the confluence of the Hayes and Gods rivers (112-19-629, 112-22-200, 112-22-201), published in Hodder and Gauthier (2022), and includes an unpublished stratigraphic section (112-19-628) along Twin Creeks (Figure 1.4).

Work conducted in Hodder et al. (2017) represents the first of such a detailed, multi-parameter approach to Quaternary stratigraphic sections within the western HBL (Figure 1.4), incorporating methodologies such as till clast fabric analysis, clast-lithology counts, till-matrix geochemistry (reported but not analyzed and interpreted), and indicator mineral analysis. Samples were collected from till beds every 2 or 3 m intervals, facilitating the ability to study changes of till properties within a field-defined bed. Additionally, this study was the first to abstain from correlating to regional till sheets within the field, allowing for more nuanced correlations which combined field data and laboratory analysis.

Since Hodder et al. (2017), efforts to characterize the fragmented Quaternary stratigraphy of the western HBL have adopted a hybrid lithostratigraphy-allostratigraphy approach to correlate sediment units (e.g., Hodder et al., 2024a; 2024b; Gauthier et al., *in review*). In this approach, lithostratigraphy is applied to correlate till units, which serve as bounding surfaces for allostratigraphic sub-till sorted sediment units.

1.4 Knowledge gaps

Recent detailed investigations of Quaternary stratigraphy have significantly advanced our understanding of glacial and interglacial cycles, paleo-ice flow dynamics, and till provenance across the western HBL (e.g., Hodder et al., 2024a; 2024b; Gauthier et al., *in review*). Although numerous regional and reconnaissance-scale studies have included the Gods River area, the last detailed local-scale investigation — Netterville (1974) — likely did not fully capture the area's complexity. As a result, substantial knowledge gaps remain, limiting interpretations of broader regional and continental-scale Quaternary history.

Earlier stratigraphic frameworks that include the Gods River area (e.g., Netterville, 1974, Klassen, 1986) suggest the presence of four main till units. However, recent revisions in nearby Kaskattama and Gillam areas (Hodder et al., 2024a; 2024b; Gauthier et al., *in review*) reveal greater stratigraphic complexity, raising questions about both the number of till units and the number of glacial-interglacial cycles preserved in this region. This complexity also casts doubt on the correlation and interpreted age of interglacial sediments, namely, the organic-rich Gods River Sediments. These sediments were previously correlated primarily based on apparent stratigraphic position, without accounting for late- to post-glacial erosion of ~40–60 m of sediment. Given this erosion and the discontinuous nature of units in the western HBL, the Gods River sediments may not only be fragmented, but could also record multiple interglacial episodes, with some beds being potentially older than previously thought (i.e., older than MIS 5).

The provenance of tills in the study area also remains uncertain. A key question is which major spreading center — Keewatin or Quebec-Labrador (Q-L) — predominantly influenced the composition of local tills through time. Was the Q-L influence dominant, as observed in the Kaskattama highlands? Or did a Keewatin-sourced ice-flow extend into the study area, as seen in the Gillam area? If so, during which glacial event(s)? Additional gaps include limited understanding of how ice-flow dynamics evolved throughout successive glaciations, particularly whether shifts in ice-flow direction were repeated across different glaciations, and whether separate ice flows with similar orientations produced comparable till compositions.

1.5 Thesis objectives

This research seeks to further develop the Quaternary stratigraphy of the Gods and Yakaw rivers area within the western HBL of Manitoba, Canada. This study area potentially records three or more glaciations and includes at least one organic-rich nonglacial unit of unknown age. Importantly, it is located between two other recent revisions of Quaternary stratigraphy in the western HBL (Kaskattama and Gillam) and will hence contribute to understanding the long-term evolution of the Laurentide ice sheet(s). More specifically, the thesis objectives are to:

1) Unravel the local Quaternary stratigraphy using a hybrid lithostratigraphic-allostratigraphic approach, which includes:

    • A detailed, multi-parameter characterization of tills and paleo-ice flow data in the context of a long and fragmented Quaternary record with multiple glacial-interglacial cycles

    • An investigation of the possible local relationship between paleo-ice flow and till composition

2) Compare the local Quaternary stratigraphy to previous studies (i.e., Netterville, 1974, Dredge and McMartin, 2011) and their regional glacial dynamics reconstruction

1.6 Thesis structure

Chapter 1 presents the scientific rationale for the research, introduces the study area and its geological setting, reviews previous research on the Quaternary stratigraphy of the western HBL, and finally, states the objectives. Chapter 2 overviews the methods and analytical approaches used throughout this thesis. Chapter 3 presents detailed descriptions of the Quaternary stratigraphy of sections investigated in this study, including sedimentological characteristics and measured paleo-ice flow indicators and their interpretations. Chapter 4 applies compositional analysis on tills to interpret provenance and compare their characteristics. Chapter 5 constructs the interpreted Quaternary stratigraphic framework of the Gods River area by correlating units using a combination of results from Chapter 3 and 4 and discusses broad provenance regions of till units. Chapter 6 discusses conclusions and future work.

Chapter 2: Methodology

2.1 Introduction

The following sections outline the techniques used to unravel the local Quaternary stratigraphy by constructing a detailed, multi-parameter stratigraphic framework. Field work was conducted to collect foundational stratigraphic data, including detailed sections descriptions, sample collection, and paleo-ice flow indicator measurements. Till samples were analyzed for Munsell colour, grain size distribution, paleo-ice flow indicators, matrix geochemistry, and clast lithology; these laboratory data were used to further delineate till beds. The compositional data of till samples was then analyzed, with multivariate analysis performed on clast-lithology counts and till-matrix geochemistry to facilitate the interpretation of sediment provenance and to support stratigraphic correlations. Sediment beds were then correlated using a combination of lithostratigraphy and allostratigraphy to construct a local stratigraphic framework.

2.2 Field data collection

Helicopter-assisted field work was completed in August 2023 over the course of a two-week period, targeting river cuts along the Gods and Yakaw rivers with minimal vegetation cover. Quaternary stratigraphy was studied at 8 sections within the study area, where various observations, samples and measurements were gathered at each section (Figure 1.2). The 6 sections situated on Gods River and the two sections along the Yakaw Rivers expose 20–45 m and 20–30 m of Quaternary sediments, respectively. Bedrock contacts with overlying Quaternary sediments were not observed at any site.

2.2.1 Stratigraphic logging

At each section, overlying slumped materials (colluvium) were first cleared with shovels, where possible, to expose a continuous stratigraphy that was then documented in detail (Figure 2.1). Sediment beds and stratigraphic contacts were described, photographed, and thicknesses were recorded, similar to protocols from recent studies in the area (e.g., Hodder and Gauthier, 2022). Several obstacles, such as excessive colluvium, hazardous slope angles, or seeping water at the base of sections hindered or prevented the collection of observations and/or samples in a simple straight vertical fashion (see Figure 2.1).

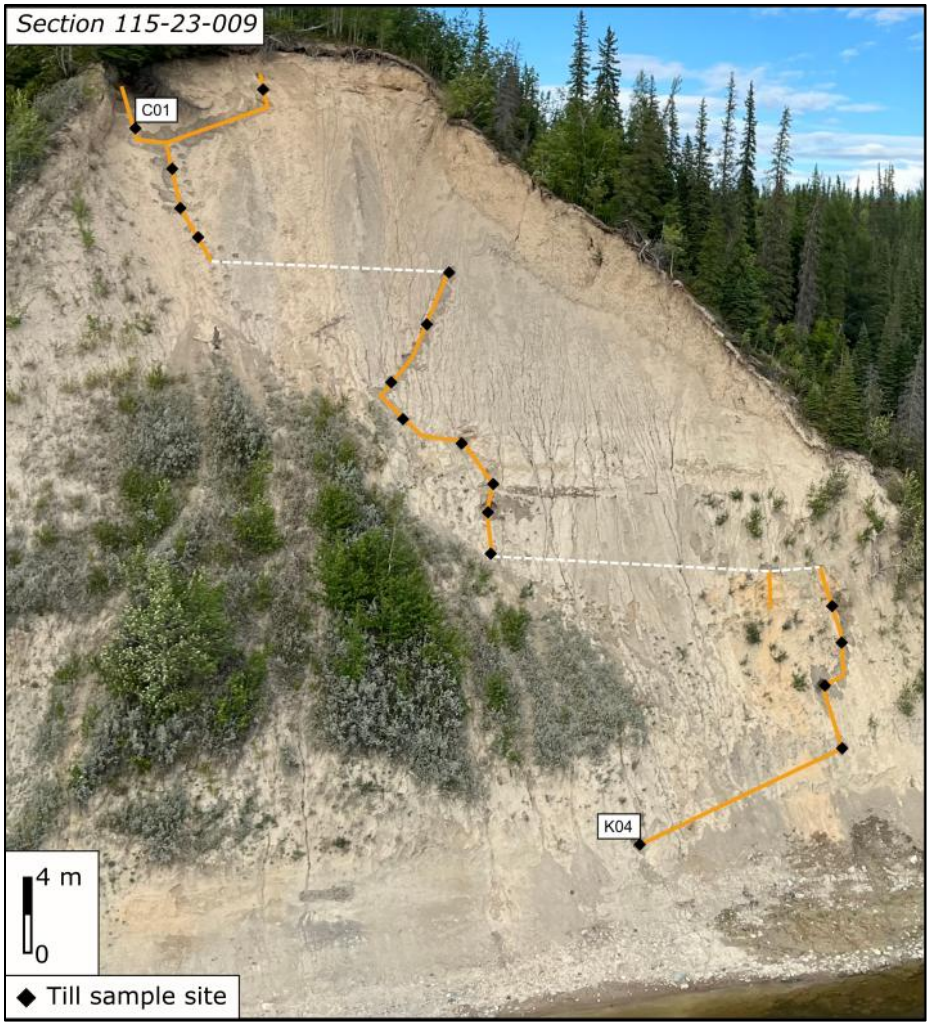


Figure 2.1: An example of an investigated site (115-23-009) in the 2023 field season. This site exposes an extensive record of glacial and nonglacial Quaternary sediments (~44 m), which are covered by varying amounts of colluvium. The approximate path of investigated sediments is shown in orange, and lateral correlations are shown by a dashed white line. Sample locations are approximate.

Diamict beds are initially assessed to determine if they meet diagnostic criteria for till, such as the presence of angular to subrounded, striated, and faceted clasts of mixed lithology, as well as a massive, poorly sorted, and consolidated matrix, along with a consistent clast fabric and lateral continuity (Evans et al., 2006; Evans and Benn, 2021). If these criteria are satisfied, the diamict bed is interpreted as glaciogenic and referred to as a till bed thereafter. Furthermore, till beds lacking folding or faulting and with high consolidation are interpreted as subglacial traction till, as these characteristics are indicative of subglacial deposition, where sediment is entrained, abraded, and compacted under ice pressure (Evans et al., 2006).

Till beds were preliminarily distinguished from one another based on their sedimentological characteristics, visible contacts and relative stratigraphic position at each section (discussed further in section 2.4.1). This initial framework, although refined later with additional lab data, allowed for local correlations between tills in such a discontinuous and patchy geologic setting, where units laterally appear and disappear on the tens of meters-scale. Descriptions of diamict beds included colour, matrix grain size, estimated gravel-sized clast percentage, sedimentary structures, degree of over-consolidation, degree of 'blocky' structure, degree of oxidation along joints, and the nature of upper and lower contacts. Certain field-based observations, such as colour and matrix grain size, were later confirmed or revised by laboratory analysis.

2.2.2 Sorted sediment

Sub-till organic-bearing sorted sediments, observed at many studied sections, can provide useful insights for both paleoenvironment characterization and geochronological constraints (cf. Gauthier et al., 2021). Sub-till organic-bearing sorted sediments were sampled for pollen and non-pollen palynomorphs. A total of 63 samples from five sections were submitted for analysis by collaborators at the Department of Earth Sciences, University of Toronto (Toronto, Ontario). There, species are to be identified and counted for paleoclimate interpretation. Additionally, wood samples found in one sub-till nonglacial unit (115-23-005-Ex2) were partially identified by Rodolphe D. Fecteau and Associates (Dundas, Ontario).

Dating nonglacial sediments in the HBL has historically been challenging, due to either limitations with geochronological methods (e.g., nonfinite radiocarbon ages) or the limited availability of suitable material needed for techniques such as optically-stimulated luminescence (OSL) dating and $^{230}Th/^{234}U$ dating (Dalton et al., 2016). As such, samples were taken when certain criteria were met. Marine shells or shell fragments, when available, were sampled for radiocarbon dating when there was reason to believe it could be dated (<50 ka), with a preference for paired, unbroken shells in marine sediments to ensure samples are in situ. Such marine shells or shell fragments were collected from 2 sections (115-23-003, 115-23-006) and submitted to the Radiocarbon Laboratory at the University of Ottawa (Ottawa, Ontario) to establish radiocarbon ages. Here, these ages are used to confirm either a) upper marine sediments were deposited during the Holocene, or b) shell fragments are old and transported. One additional sample of wood fragments from a sub-till sorted sediment package was submitted to confirm pre-Holocene deposition (from 115-23-005). Bedded nonglacial sands, when available, were sampled for OSL dating. Suitable sediments were found at 2 sections (115-23-005, 115-23-009) and were each sampled twice at different depths for submission to the University of the Fraser Valley Luminescence dating laboratory

(Abbotsford, British Columbia) for dating. These OSL samples and their results fall outside the scope of this thesis and are therefore not further discussed herein.

2.2.3 Ice-flow data collection

Indicators of ice flow orientation during till deposition were measured at each section at multiple depths. The orientation of elongated clasts in subglacial traction till were measured in the field and were analyzed using stereonets and the orientation tensor method (Allmendinger et al., 2011). This process, commonly referred to as either clast-fabric or till-fabric analysis, can be used to infer paleo-ice flow orientation, given that elongated clasts tend to align to the main shear direction at the time of deposition (Hicock et al., 1996). The trend and plunge of around 20-40 acceptable clasts were measured at each till fabric site (Figure 2.2A), the lower range due to time constraints. An acceptable clast is one with an A:B axis (length) ratio >1.5:1 (Hicock et al., 1996), an A-axis plunge <70°, a B-axis plunge <60° (Holmes, 1941), and without rotation interference from other clasts due to direct contact with (or in close proximity with) a significantly larger clast (Andrews and Smith, 1969). Till fabric data was then plotted on stereonets and the eigenvectors and eigenvalues were calculated using Python script (Figure 2.2B). Paleo-ice flow orientation was then inferred from the principal eigenvector based on its strength (if its normalized eigenvalue is >0.54) and a visual inspection of fabric shape or modality (Hicock et al., 1996). Here, fabric modality is only used for paleo-ice flow orientation, as the above criteria for acceptable clasts (the exclusion of steeply plunging clasts) render data unusable for process interpretation. This inferred paleo-ice flow orientation is initially left as bi-directional, since plunge is not consistently related to ice-flow direction (Andrews and Smith, 1969; Gauthier et al., 2019). Another paleo-ice flow indicator is the presence of in-situ lodged cobbles or boulders with parallel striations on their upper surfaces (Figure 2.2C). These striations are interpreted as evidence of the ice flow direction associated with the overlying till, given a bullet-shaped form with a smoothed stoss side and a plucked lee side (McMartin and Paulen, 2009). Clast-fabric measurements, along with their statistics and interpretations, are presented in Appendix G.

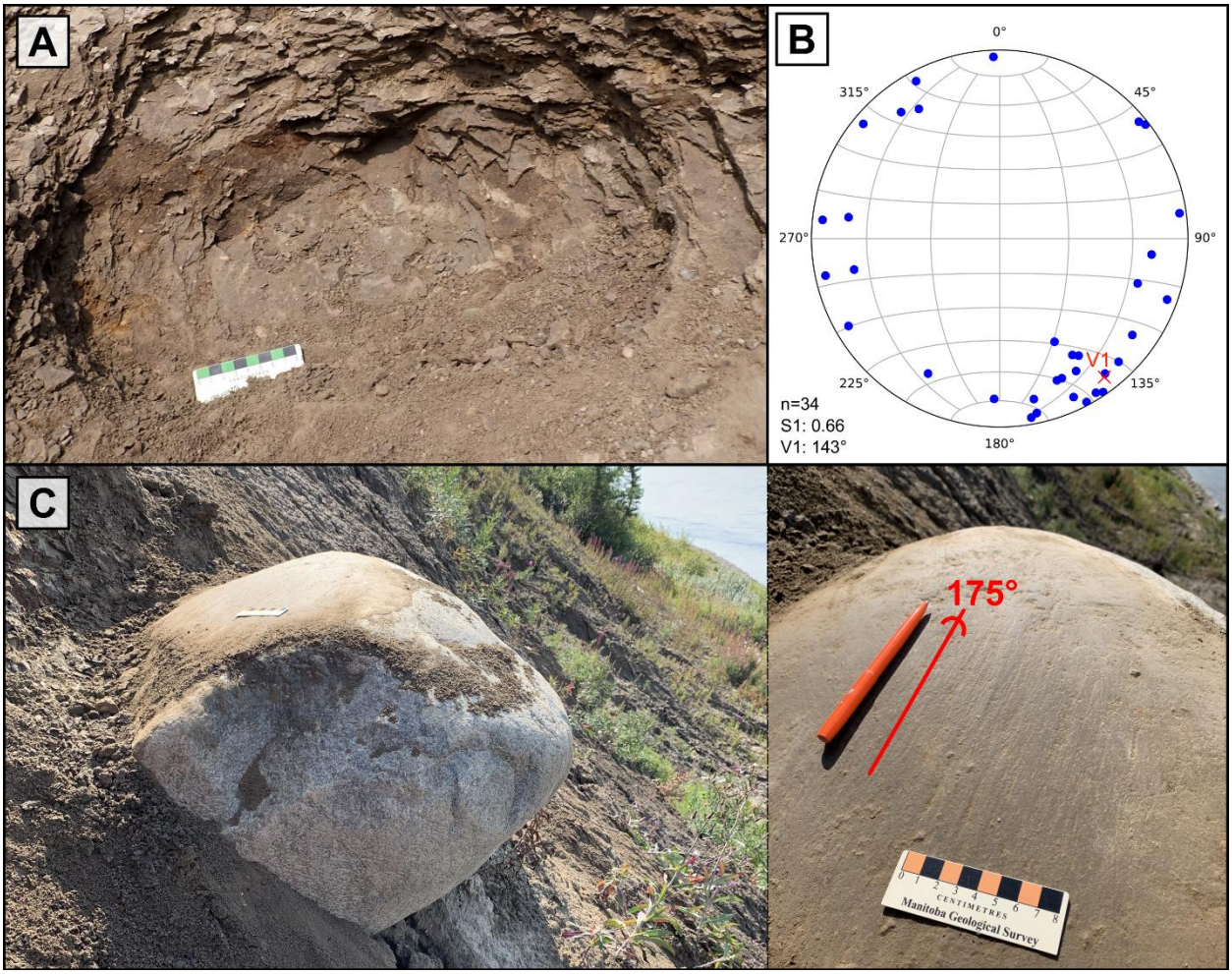


Figure 2.2: An overview of ice-flow data collection and analysis, including (A) a till-fabric site (sample 115-23-009-D07), (B) collected till fabric data from 115-23-009-D07 plotted on a stereonet (with principal eigenvector (V1) in spherical coordinates, normalized eigenvalue (S1), and number of measurements (n) noted), and (C) an in-situ lodged boulder with parallel striations trending 175°, part of a boulder pavement below sample 115-23-005-B05.

2.2.4 Till sampling

Each till unit was sampled using unpainted shovels at 2–3 m vertical intervals, if thickness permitted, avoiding contamination from outside sediments and vegetation. A total of 100 till samples, each weighing 2–3 kg (Figure 2.2), were taken from the project area for analysis. This includes 84 taken in 2023, joining 8 samples collected in 2022 from two sections and 8 samples in 2019 from two sections (one of which is unpublished; Hodder and Gauthier, 2022). The 2023 till samples were split for archiving purposes at the MGS Midland Sample and Core Library in Winnipeg, Manitoba. Till samples were then assessed for damp colouring using a Munsell chart (Munsell Color–X-Rite, Incorporated, 2015).

Till samples were then analyzed for grain size and matrix geochemistry (<63 µm size fraction) at Saskatchewan Research Council (SRC) Geoanalytical Laboratories in Saskatoon, Saskatchewan. At SRC, the sand-size fraction was determined by sieve analysis, while the silt- and clay-size fraction was determined by pipette method. Specifically, an aliquot of <2 mm sample material was transferred to a flask and an aliquot of Calgon™ was added. Deionized water was added to the flask, and the flask was shaken until the contents were thoroughly mixed. The contents of the flask (<2 mm size fraction) were sieved through a 63 µm mesh screen into a graduated cylinder to separate the sand-size fraction. From the remaining <63 µm size fraction in the graduated cylinder, an aliquot of the sample was immediately removed. A second aliquot (of clay) was removed from the cylinder after a certain period of time (the time period is dependent on the ambient room temperature). The sieved sand and aliquots of sample material were dried and re-weighed. Calculations were performed to determine the percentage of sand, silt and clay in the sample based on the total weight. An SRC standard was prepared and inserted into the group every 19 samples, and replicate samples were inserted at the end of every other 19-sample group, to monitor analytical accuracy and precision.

An additional 11.4 L till sample was collected using shovels for indicator-mineral analysis at 33 sample sites (Figure 2.3), preferentially sampling at the base of till units for uniformity/consistency of sample location and to minimize the risk of sampling supraglacial melt-out material. These samples were submitted to Overburden Drilling Management Limited in Ottawa, Ontario for indicator-mineral analyses in collaboration with the Geological Survey of Canada.



Figure 2.3: Till sample 115-23-007-D05, including (A) a 2-3 kg bag collected for grain size, clast lithology, and geochemical analysis, and (B) an 11.4 L pail collected for indicator-mineral analysis.

2.2.5 Compilation

Similar fieldwork was conducted at an additional four sections in the field area (Hodder et al., 2017; Hodder and Gauthier, 2022; Hodder et al., 2024a). The data from these four sections collected in the 2019 and 2022 field seasons (112-19-628, 112-19-629, 112-22-200, 112-22-201) will be incorporated into this study and include stratigraphic, sedimentological, grain size, ice-flow indicator, clast lithology, and matrix geochemistry datasets (when comparable across years).

2.3 Till-composition analysis

Till composition (e.g., clast-lithology counts, indicator minerals, till-matrix geochemistry) has been used extensively in provenance studies for mineral exploration, to determine up-ice bedrock source regions and map sediment dispersal patterns (e.g., McClenaghan et al., 2002; Grunsky, 2010; McMartin et al., 2016; Lipp et al., 2020; 2021; Rice et al. 2024). Ideally, the proportions of clast lithologies within till samples (i.e., clast-lithology counts, or pebble lithology counts), which are inferred to reflect spatially distinct, up-ice bedrock sources, provide critical evidence for net ice flow direction (Dredge and McMartin, 2011; Gauthier et al., 2019; McClenaghan et al., 2023). Likewise, till-matrix geochemistry can give key insights to provenance by using elemental assemblages as proxies for up-ice bedrock sources (cf. McClenaghan et al., 2023).

Multivariate techniques were used to reduce the dimensionality of the data and cluster till samples with similar compositional signatures. The objectives of clustering samples are to (1) use clast-lithology proportions and till matrix geochemistry (as a proxy for lithology) for provenance insights, and to (2) aid in till bed correlations (see section 2.4.2). Here, principal component analysis (PCA) and k-means clustering were used, as they have been successfully employed elsewhere to help determine sediment provenance: either PCA alone (e.g., McMartin et al., 2016; Lipp et al., 2020; 2021) or PCA in combination with k-means clustering (e.g., Grunsky, 2010; Rice et al., 2024).

2.3.1 Distal bedrock source regions of tracer lithologies

Clast lithologies associated with distinctive, spatially restricted bedrock sources (i.e., tracer lithologies) are important indicators of ice flow direction and till provenance. In the HBL, the key tracer lithologies are distally-sourced and are useful to distinguish northwestern and eastern till provenance (Dredge and McMartin, 2011).

Tracer lithologies indicating northwest provenance include purple porphyritic rhyolites with sanidine phenocrysts from the Pitz Fm (Figure 2.4E) and red volcanic rocks with phlogopite phenocrysts (minettes) from the Christopher Island Fm, both of which are from the Paleoproterozoic Dubawnt Supergroup located ~900 km northwest of the study area in mainland Nunavut (Rainbird et al., 2003).

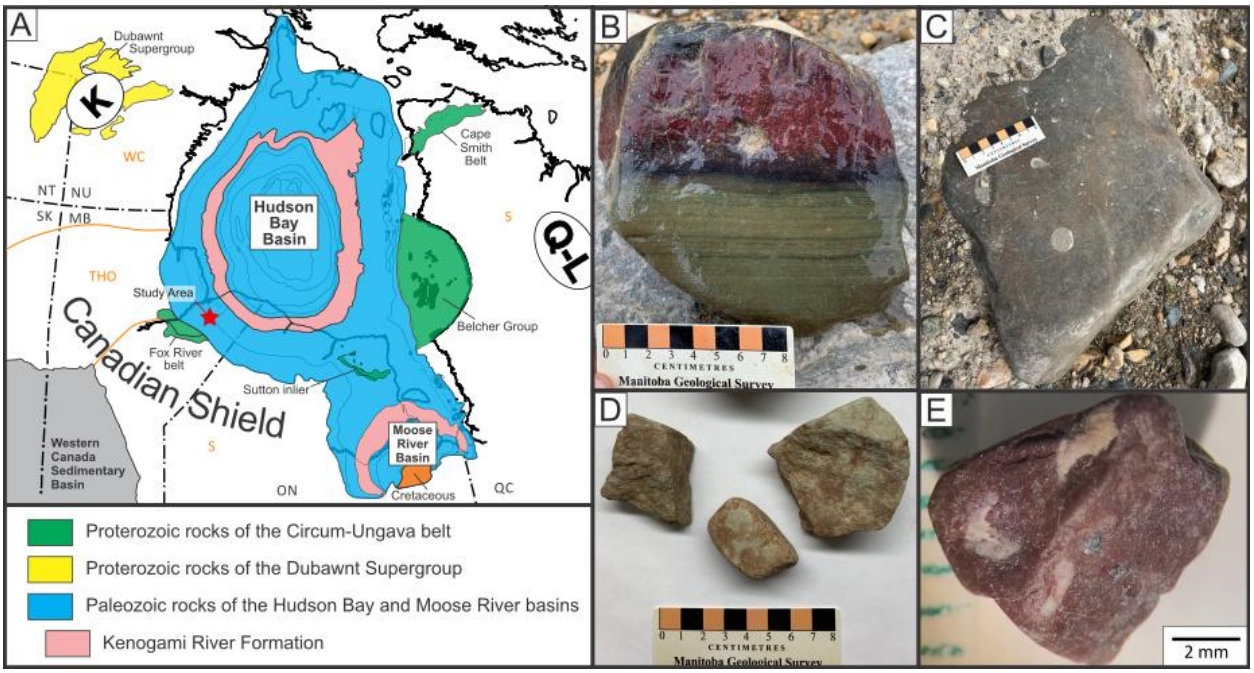


Figure 2.4: Regional bedrock geology domains of central Canada, and distinct clast lithologies observed in the study area. (A) bedrock geology modified from Wheeler et al. (1996). Bedrock sources of distinctive erratics include the Dubawnt Supergroup, the Belcher Group/Sutton inlier, the Cape Smith belt, the Fox River belt, the Hudson Bay Basin (HBB), and the Moose River Basin. The position of the Keewatin (K) and Quebec-Labrador (Q-L) ice-spreading centers during deglaciation following the LGM are also shown, as per Dalton et al. (2023). Figure is modified from Hodder et al. (2024b); (B) a cobble-sized hand sample of oolitic jasper in contact with argillites from the Kipalu Fm (Jackson, 2013), found in the study area, and sourced from the Belcher Group. (C) a boulder-sized example of an Omarolluk Fm clast (omar) with its distinctive calcareous concretions, found in the study area, sourced from the Belcher Group. (D) pebble- and cobble-sized hand samples of Kenogami River Fm clasts, sourced from the HBB. (E) a pebble-sized example of a Pitz Fm clast, sourced from the Dubawnt Supergroup. Photos B, D, and E courtesy of Tyler Hodder. Other abbreviations: WC, Western Churchill; THO, Trans-Hudson Orogen; S, Superior.

Tracer lithologies known to be sourced from the east include dark siliceous greywackes with light calcareous concretions from the Omarolluk Fm (also known as omars; Figure 2.4C; Prest et al., 2000) and oolitic jasper from the Kipalu Fm (Figure 2.4B), both of which are from the Paleoproterozoic Belcher Group on the eastern side of Hudson Bay (~800 km east of the study area; Jackson, 2013). Alternatively, oolitic jasper is also found in the Sutton Inlier, situated ~500 km east-southeast of the study area (Stott et al., 2010).

The Proterozoic Fox River and Cape Smith belts (situated ~30 km to the southwest and ~1000 km northeast of the study area, respectively) are comprised of metasedimentary and metavolcanic rocks (Rinne, 2020; St-Onge et al., 1989), which may contribute fined-grained dark clasts to the till, thus introducing potential confusion regarding omar identification (see below). Furthermore, red sedimentary clasts (including pink to red carbonate, red fine-grained sandstone, red siltstone; Figure 2.4D) may be sourced from the Silurian Kenogami River Fm in the HBB (Gao et al., 2020).

Most tracer lithologies in the HBL can be confidently identified in smaller size fractions (2-4 mm or 4-8 mm) for the purpose of clast-lithology counts (see section 2.3.2 below). However, the identification of omars (Figure 2.4C) in these size fractions is particularly challenging due to their resemblance to fine-grained rocks from Archean or Proterozoic greenstone belts, especially when their distinctive concretions are absent (Prest et al., 2000; Hodder et al., 2017; Hodder and Kelley, 2018; Gauthier et al., 2019). For this reason, omars must be first recognized in the field in larger size fractions (cobbles and boulders) where their diagnostic features are visible, before dark fine-grained rocks in smaller size fractions can be even partially attributed to this lithology. While this approach is valuable, it introduces uncertainty regarding the exact proportion of omars in the smaller size fractions (discussed further below).

2.3.2 Clast-lithology counts

Here, the clast lithology of small gravel-sized fractions (2–4 mm and 4–8 mm, separated by sieving) of till samples (n=100) were categorized and counted by the author (Figure 2.5), following common practices from other recent studies in the region (Hodder and Kelley, 2018; Gauthier et al., 2019, 2024, Hodder et al., 2024a). For each till sample, a minimum of 250–300 clasts were obtained from the 2–8 mm size fraction (Bridgland, 1986). Samples were split using a laboratory sample splitter to mitigate biases associated with hand-picking clasts from a larger sample population. Clast lithologies were then identified by microscopy and sorted into detailed categories (e.g., carbonate, quartzite, chert, metavolcanic, sulfides, etc.) that also include the specific tracer lithologies (see section 2.3.1 above).



Figure 2.5: An example of clast-lithology identification and categorization. Clasts are from the 4–8 mm size fraction of sample 115-23-002-D02.

For provenance analysis, detailed categories were then grouped, when applicable, to make three major lithology classes reflecting regional bedrock geology: Hudson Bay Basin (HBB), granitoid rocks (GR), and undifferentiated greenstone and greywackes (UGG; Table 2.1). Count percentage is used as opposed to weight percentage, as recommended by Bridgland (1986). The count percentage of each major class is calculated by dividing its count by the sum of the counts of all three classes, normalized to reflect the major geologic terranes of interest. Meanwhile, tracer lithologies present in clast-lithology counts are expressed as a count percentage of the total counted sum of the 2–8 mm size fraction.

Table 2.1: Major lithology classes and their associated detailed lithology classes.

Major lithology class	**Detailed lithology class**
Hudson Bay Basin (HBB)	Grey, tan, white carbonate
	Pink carbonate
	Chert
	Shell fragment
	Paleozoic fossil
	Fine-grained red sandstone (Kenogami Formation)
Granitoid rocks (GR)	Granitoid
	Exotic granitoid
	Amphibolite, gabbro
Undifferentiated greenstone and greywackes (UGG)	

Additionally, a centered-log ratio (CLR) transformation was applied to the normalized proportions for the purposes of clustering (see section 2.3.2.1 below). This step is required to transform data from dependent (i.e., all elements summing to a constant) and positive to independent variables that range from negative to positive (Grunsky, 2010).

HBB clasts, often accounting for a majority of clast counts in the HBL, may be sourced locally or from elsewhere within the HBB (Figure 2.4) and include carbonates, chert, shell fragments, Paleozoic fossils, and fine- grained red sandstone from the Kenogami Fm. As such, HBB clasts are not diagnostic of any particular paleo-ice flow direction.

The GR category, including primarily granitoid clasts as well as amphibolites and gabbros, are either sourced from NW (Churchill Province) or SE (Superior Province; Figure 2.4). However, there is an average background concentration of ~10% granitoid clasts within till in the HBL (Shilts, 1980), indicating this category is unreliable as a provenance indicator at low concentrations. Higher proportions of GR rocks in clast counts are generally assumed to be indicative of a NW provenance due to closer proximity of the Churchill Province in that direction.

Due to the difficulty in identifying omars in smaller size fractions (see section 2.3.1), many studies interested in omars for till provenance analysis have opted to lump dark, fine-grained clasts under a broader UGG category (e.g., Hodder et al., 2017; Hodder and Kelley, 2018; Gauthier et al., 2019; Hodder and Gauthier, 2022; Hodder et al., 2024a; 2024b). Interpreting elevated UGG proportions as indicative of increased omar content therefore requires additional lines of evidence. Hodder et al. (2024b)

demonstrated that elevated UGG concentration is associated with an eastern provenance in multiple stratigraphic units (units 3 and 6). This interpretation was based on corresponding detrital hornblende $^{40}Ar/^{39}Ar$ ages indicative of clasts derived from the Superior Province, an ice-flow history that crosses over the Belcher Group and Sutton inlier, and the presence of numerous oolitic jasper clasts. Given the proximity of the Gods River area to the study area examined by Hodder et al. (2024b; Figure 1.2), the UGG category has the potential to distinguish NW versus SE provenance. However, its applicability remains uncertain, particularly if the tills in the current study area were deposited during different glaciations under different ice sector configurations.

Additionally, a possible local bedrock high and Precambrian rock exposure of the Fox River Belt underneath the Kaskattama highlands has been proposed (Hodder et al., 2024b), which would serve as another source of Precambrian clasts (including GR clasts and/or UGGs) from the SE to E.

Broadly speaking in northern Manitoba, southeast to south-trending paleo-ice flows accompanied by Precambrian shield-derived till and/or Dubawnt erratics suggest Keewatin sector provenance, while west to northwest-trending paleo-ice flows and till derived from Paleozoic carbonates and/or erratics of an eastern provenance indicate ice flow from the Quebec-Labrador sector (Dredge and McMartin, 2011). However, this generalization may not hold true in the Gods River area, as a) ice flows emanating from either sector pass over Paleozoic carbonate bedrock, b) later ice flows entrain or modify pre-existing till sheets (i.e., inheritance and overprinting; Gauthier et al., 2019), and c) the exact configuration and spatiotemporal dynamics of pre-LGM continental ice sheets is not necessarily the same as that of the LIS during the last glaciation.

2.3.2.1 K-means clustering

To enhance stratigraphic interpretation of clast-lithology counts results, k-means clustering is applied to CLR-transformed clast-lithology proportions (after applying closure to 100%) to group till samples with similar compositional signatures. This was done by using the sci-kit learn package in Python (Pedregosa et al., 2011). K-means clustering is an unsupervised machine learning technique which aims to partition samples into a specified number of distinct clusters, functioning by iteratively minimizing variance within clusters and maximizing variance between clusters (Grunsky, 2010). The number of clusters can either be assigned manually using contextual knowledge, or by techniques like the ‘elbow’ method. Choosing the most suitable number of clusters is an iterative process, as it can be first used as an exploratory tool yielding insights that improve contextual knowledge. The resulting clusters indicate groupings of similar signature, which lends itself to exploring the relationship between till composition and paleo-ice flow direction, till provenance interpretations, and stratigraphic comparisons between or within sections.

Finally, important assumptions of the above clustering methods are that clusters are spherical, convex, and isotropic, which may not be the case with real compositional data.

2.3.3 Matrix geochemistry

The fine-grained matrix of 2023 till samples (n=84; <0.063 mm size fraction) was separated by sieving and splitting for a range of digestions and geochemical analyses at SRC. Aqua regia digestion (3:1 HCl:HNO3), a partial digestion method, and lithium metaborate fusion, a near total digestion method, were performed on samples which were then analyzed using inductively coupled plasma mass spectrometry (ICP-MS). As lithium metaborate fusion is more representative of the total sample geochemistry, it has been commonly used to determine provenance and thus will be the primary elemental suite investigated for till provenance analysis (McClenaghan et al., 2023). A total of 58 elements were analyzed using near total digestion. Additionally, the weight percentages of calcium, magnesium, and total carbonate were determined through HCl digestion.

Quality assurance and quality control (QA/QC) methods include calculating the percent relative standard deviation (using lab duplicates) and percent relative difference (using standards) to determine analytical precision and accuracy, respectively, as described by Piercey (2014; see Appendix D). Precision biplots were also created to visually show imprecise data, set at a 20% level of precision above or below the 1:1 line. Elements that do not meet QA/QC standards set out in Piercey (2014) via these methods were not used for further analysis.

Exploration of geochemical data included histograms, univariate quantile-quantile plots, and boxplots to identify anomalies and investigate the overall data structure and variance. Erroneous outliers, commonly removed at this stage (cf. Grunsky, 2010), were not positively identified. Bivariate plots were generated to assess correlations between major clast lithology classes (HBB, GR, UGG) and individual elements, with R^2 values calculated. Although a correlation of ±0.5 usually indicates a significant relationship (Reimann et al., 2008I), no such correlations were found. Therefore, weaker correlations (R^2 values $\sim\geq$ 0.25) were considered potentially meaningful. Elements showing such correlations with clast lithology were included in the element assemblage used for PCA as potential indicators of bedrock provenance.

2.3.3.1 Principal component analysis

Geochemical data is compositional by nature and therefore needs to be transformed to be used in multivariate analysis techniques such as PCA due to the closure problem explained above. First, a CLR transformation was applied to transform data from dependent and positive to independent variables that

range from negative to positive. Data was then standardized to unit variance, to ensure PCA captures geochemically meaningful differences rather than variable scale.

PCA was then performed on the geochemical dataset using the scikit-learn package in Python (Pedregosa et al., 2011). The purpose of PCA is to reduce the dimensionality of the dataset into a more manageable form while retaining relevant information (Grunsky, 2010). Essentially, PCA operates by identifying covarying elements and expressing them as principal components (PCs), ordered by importance in explaining variance, where individual samples can be described by a small number of PC scores instead of numerous element concentrations.

Additionally, reducing the elements used in PCA to key variables which explain most of the variance in the dataset increases interpretability and reduces initial data dimensionality to limit any issues associated with high dimensionality and low sample size (Grunsky, *personal communication,* 2024). Reducing the input elements to just the major elements (e.g., Al, Ca, K, Mg, Na, etc.; also referred to as major oxides), has previously proven to be helpful in interpreting sediment provenance (e.g., Lipp et al., 2020; Rice et al., 2024; Hodder et al., 2024b). These elements are major constituents of common rock-forming minerals and may therefore reflect the bulk composition of source lithologies, in addition to other surficial processes affecting these elements (e.g., grain size sorting, weathering). Additionally, Hodder et al., 2024b demonstrated a link between PCs and major clast lithology classes using a modified major element assemblage that included select minor and trace elements (Al, Ca, K, Mg, Mn, Na, Fe, Rb, Zr, and the sum of light rare earth elements [La, Ce, Pr, Nd, Sm, Eu]). Here, certain elements are interpreted to be indicative of provenance (Shield-rich: Al, Fe, Rb; Paleozoic-rich: Ca, Mg, Mn; UGG-rich: Na, Zr). Therefore, major elements (with appropriate QA/QC results) were selected for use as an appropriate sub-composition as input for PCA, along with previously identified elements correlative to clast lithology.

Once the sub-composition was established, the optimal number of PCs is determined by the ‘elbow’ method applied to scree plots, with a preference for PCs to account for near 95% of the total variance in the dataset. With regards to geochemical data, PCs are expected to represent geological processes which can explain covariance in the dataset (e.g., sediment derived from different bedrock lithology, post-depositional processes, differential grain size; Grunsky, 2010). As such, special care must be taken to ensure PCs are specifically related to provenance. K-means clustering (see section 2.3.2.1) will be used on PCA results if two or more PCs can be confidently attributed to differential provenance.

2.3.4 Till-composition considerations

When attempting to determine till provenance from compositional data, several interacting factors complicate interpretations. The topography, structure, and lithological properties (e.g., roughness, hardness, fissility) of subglacial bedrock directly influences the availability of primary material for glacial erosion and subsequent entrainment (Phillips et al., 2010). The effects of bedrock topography are particularly significant in areas with thick sediment cover like the western HBL; bedrock highs with thin or patchy sediment cover may be more continuous sources of detritus, while bedrock lows may be buried beneath pre-existing sediments and protected from glacial erosion (Hodder and Gauthier, 2017; McClenaghan et al., 2023). Although bedrock was not observed to outcrop in the study area, bedrock topography has implications for up-ice source regions. High-elevation bedrock with thin sediment cover may have been continuously eroded throughout multiple glaciations, while buried, low-elevation bedrock may have only been available for erosion by the oldest glaciation and may be only present in the till composition of overlying tills due to re-entrainment of underlying tills (inheritance).

The burial of bedrock by pre-existing sediment also highlights the challenge of overprinting and inheritance in regions of thick drift with multiple generations of till sheets or other pre-existing materials (cf. Trommelen et al., 2013). In such areas, pre-existing till sheets may contribute material with a contrasting provenance signal to that of primary material, diluting or obscuring the signal of bedrock erosion and transport associated with the current ice flow. Overprinting and inheritance are especially relevant when considering the multi-generational palimpsest dispersal in the western HBL (Gauthier et al., 2019); for example, pre-existing materials reflective of a Keewatin-sourced flow may be entrained by a subsequent W-ice flow and deposited alongside material transported from the east. This concept also applies to ice-flow shifts associated with a migrating ice divide (e.g., Rice et al., 2024). To account for these complexities, provenance interpretations using clast-lithology counts and till-matrix geochemistry must carefully consider the stratigraphic and glaciological history of the region, including potential sources of inherited materials and the impacts of multi-generational dispersal.

2.4 Stratigraphic approach

A hybrid lithostratigraphic-allostratigraphic approach is employed to correlate informal stratigraphic units in the study area, similar to recent studies in the HBL (e.g., Hodder et al., 2024a; 2024b; Gauthier et al., *in review*). The North American Stratigraphic Code (North American Commission on Stratigraphic Nomenclature, 2021) advises defining informal units when the extent and significance of the units outside the study area are uncertain, or when innovative techniques are used in their definition. Here, informal till units are defined through a multi-parameter lithostratigraphic approach (discussed further in section 2.4.2).

2.4.1 Stratigraphic beds

2.4.1.1 Till beds

Till beds are initially differentiated in the field based on sedimentological characteristics (e.g., qualitative grain size distribution, colour, degree of oxidation along joints, consolidation, and sedimentary structures) within identified bounding surfaces, and according to their stratigraphic position. Till beds are named by their section reference (number) and the bed position, starting from the base (letter). For example, Bed 2-A is the bottommost bed at section 112-23-002.

The beds are then further subdivided, or their boundaries more precisely defined, using a combination of measured paleo-ice flow indicators (e.g., clast fabrics and striated lodged boulders) and analytical laboratory data (e.g., quantitative <2 mm grain size distribution, total carbonate from till-matrix geochemistry, and till-clast lithology). Significant changes observed within a field-defined till bed provide grounds for subdividing a till bed further, although do not necessarily mean sediments were deposited during a separate glaciation. Here, priority is placed on paleo-ice flow over other parameters, due to its robustness compared to other parameters, which may be less consistent across a unit (discussed further in section 2.4.2). A change in interpreted ice-flow direction of ≥~90°, or a change of ≥~45°, supported by strong till-fabrics and additional evidence (i.e., significant changes in other qualitative or quantitative parameters) would justify a subdivision. Additionally, if significant changes to multiple parameters are observed within a bidirectional till bed, a subdivision would also be justified, due to the ambiguity of the paleo-ice flow indicators. Table 2.2 presents the mean and standard deviation values for each parameter across all till samples, which serve as the threshold for determining significant changes in quantitative parameters. Till beds defined in the field that are subdivided in this way are denoted by sub-beds (e.g., till bed 6-B contains sub-beds 6-B-1 and 6-B-2, which differ by paleo-ice flow direction and clast lithology).

Table 2.2: Calculated standard deviation values for each parameter, defined as the thresholds for significant changes. Data from all till samples are used in these calculations.

Parameter		**Mean**	**Standard deviation (σ)**	**Significant change threshold (±1σ)**
Total carbonate (wt. %)		41.3	5.3	±5.3
<2 mm grain size distribution (wt. %)	Sand	29.1	5.8	±5.8
	Silt	50.0	5.5	±5.5
	Clay	20.9	7.5	±7.5
Clast count proportion (ct. %)	HBB	76.2	6.0	±6.0
	GR	14.8	4.8	±4.8
	UGG	8.9	4.3	±4.3

2.4.1.2 Nonglacial sediment beds

Nonglacial sediment beds are lumped into a single bed when similar lithofacies suggests a similar depositional environment (e.g., similar processes and energy levels) and therefore a facies association can be made. Lumping lithofacies simplifies site stratigraphy and site-to-site comparisons when allostratigraphy is used for correlations (see section 2.4.3). At the same time, the detailed lithostratigraphy is preserved; when multiple lithofacies are grouped to create a single bed, each lithofacies is denoted as a sub-bed (e.g., bed 3-H contains lithofacies 3-H-1, lithofacies 3-H-2, and lithofacies 3-H-3; see section 3.3.3.2). Similarly, when interstratified lithofacies reflect depositional cyclicity, a facies sequence is defined, and the lithofacies are lumped accordingly into a higher rank (e.g., lithofacies sequence 3-E-1; see section 3.3.3.2).

2.4.2 Till bed correlations and till units

Once stratigraphic beds are assigned for a single section, till beds are correlated using lithostratigraphy to adjacent sections and then across the study area to establish local till units. The correlation of these beds is based on several factors, including the degree of diagenetic alteration (consolidation, oxidation development along joint faces), the interpreted ice-flow direction during deposition, and relative stratigraphic position. Parameters pertaining to till composition (till-matrix geochemistry, clast lithology) are used to further substantiate correlations. Here, the delineated till units are provisionally defined as deposits from the same glacial event, although multiple till units may be from within the same broader glaciation. The stratigraphic context of surrounding sections may also improve unit assignment, and therefore interpreted contacts may be drawn within beds delineated in the field if it is consistent with the

surrounding framework and patterns in till parameters. Furthermore, multiple beds at a single section may be grouped into a single unit, provided they are consistent with the stratigraphic context of surrounding sections.

2.4.2.1 Degree of diagenetic alteration

In glaciated regions, the degree of sediment consolidation indicates the maximum effective pressure (i.e., cryostatic pressure minus subglacial water pressure) experienced by the sediment, as consolidation and development of joint faces is due to pressure-induced rearrangement of grains and dewatering (degree of blocky soil structure) due to overburden pressure (cf. Bjørlykke, 2014). Sediments retain most of their high bulk density (low voids ratio e; e= volume of voids divided by volume of solids) after cryostatic pressure has been removed, reflecting the maximum overburden pressure they experienced (Tulaczyk et al., 2000). Older tills are more likely to have experienced higher maximum overconsolidation at one point during one or more glaciations following their deposition. In addition, old tills tend to be characterized by oxidation staining and the presence of other neo-minerals, which indicate long-term water-mineral interactions in the subsurface. In some cases, early partial cementation may have occurred as well. Altogether, till stiffness, bulk density and presence of visible diagenetic alteration indicate the relative age of sediments and can be used to correlate certain beds regionally, assuming 1) similar grain size distributions between sediments, and 2) similar maximum effective pressure across the areas being compared.

2.4.2.2 Interpreted paleo-ice flow

Multi-phase palimpsest dispersal patterns, common in inner core regions of the LIS, further complicate correlations (cf. Trommelen et al., 2013), as ice may entrain and redeposit pre-existing sediment that was originally deposited during an earlier ice-flow event with a different provenance. For example, a till sheet with elevated greywacke clast concentration, deposited by westward flow from a Q-L ice spreading center, could be entrained and redeposited by southeast flow from the Keewatin dome, resulting in a mismatch between interpreted ice-flow direction and expected till composition. Ice sheets can also incorporate underlying proglacial or interglacial sediments, which also alter till composition. Therefore, correlations between till beds in this thick-drift inner-core study area are preferentially guided by interpreted paleo-ice flow direction and relative stratigraphic position, and less so by till composition.

Unimodal clast fabrics are interpreted to reflect a single dominant ice-flow direction, while spread fabrics suggest temporal variability in stress or minor directional shifts during deposition. Bimodal clast fabrics may indicate partial preservation of older orientations following a shift in ice flow and remobilization of

till during a subsequent ice flow phase, or the inclusion of transverse clasts that roll along their b-axis (Andrews and Smith, 1969). As such, unimodal or sub-unimodal clast fabrics are only used for confident paleo-ice flow interpretation, with special consideration given to bimodal fabrics based on their stratigraphic context. When determining ice-flow direction from bi-directional clast-fabric orientations, regional dynamics and till composition provide essential context given the unreliability of fabric plunge as an indicator (Andrews and Smith, 1969; Gauthier et al., 2019). A key constraint on ice-flow interpretations of till fabrics is that other regional indicators in the western HBL show no evidence of ice flow trending north, northeast, or east (cf. Gauthier et al., 2019). Consequently, any observed bi-directional till fabrics involving these directions are assumed to reflect south, southwest or west ice-flow directions instead. Southeast- or northwest- trending ice-flow indicators are more difficult to interpret, however, since both directions have been identified in northern Manitoba (Gauthier et al., 2019, Hodder et al. 2024b). Therefore, till fabrics showing preferred southeast-northwest orientations are initially left as bi-directional for the purposes of correlations. After till units are constructed, an interpretation of either southeast or northwest ice-flow direction may be given based on observable repeated trends in ice-flow sequences and/or till composition.

Despite extensive mixing in areas of thick drift, till composition may still reflect broad provenance regions to some extent, aiding in the differentiation of these southeast-northwest paleo-ice flow indicators. For example, a high proportion (i.e., greater than 3rd quartile; see section 2.4.4 below) of granitoid clasts may indicate a northwestern source from the Precambrian shield rocks of the Churchill Province (Figure 2.4). In contrast, a high proportion of UGG clasts could point to an east–southeast source (if a reasonable association is made; see section 2.3.2). The presence of tracer lithologies (see section 2.3.1) within samples can give further insights into the broad, continental provenance of till, and may help support directional interpretations. The presence of oolitic jasper, sourced from the east, may support a west–northwest paleo-ice flow direction, while the presence of Dubawnt Supergroup rocks, sourced from the northwest, may support a southeast paleo-ice flow direction. Although the presence of glacial erratics alone may not indicate southeast versus northwest paleo-ice flow direction, as both can be present within a single till sample, they could be used to support other evidence (e.g., a high proportion of UGG clasts coupled with oolitic jasper clasts would support an eastern provenance). These compositional shifts provide additional context to interpret ice flow directions based on regional bedrock geology, helping to delineate provenance areas and refine interpretations of ice-flow phases.

2.4.3 Sub-till sorted sediment correlations

Till units, once established, serve as bounding surfaces for the allostratigraphic correlation of sub-till sorted sediment packages. Allostratigraphy is essential due to the fragmented nature of Quaternary sediments in the HBL, where unconformities are frequent and depositional environments of sub-till sorted sediments from the same time period can differ greatly between sections (Gauthier et al., 2021). Furthermore, allostratigraphy is crucial to assign relative ages to sub-till sorted sediments since multiple nonglacial units are recognized in the region (Nielsen et al., 1986; Dredge and McMartin, 2011).

2.4.4 Definition of stratigraphic terms and classifications

Several quantitative parameters have been classified for readability in the detailed descriptions of stratigraphic sections, including total carbonate content, till matrix texture, and clast-lithology counts. The total carbonate content of the fine-grained matrix in till samples (see section 2.3.3) is categorized into groups based on populations identified within the distribution of the carbonate content. Till matrix texture (<2 mm size fraction) is described from smallest concentration to largest concentration and is considered significant only if >15% (e.g., a matrix with 20% sand, 30% silt, and 50% clay would be described as a sandy-silty-clay matrix, while a matrix with 50% sand, 40% silt, and 10% clay would be described as a silty-sand matrix). Clast lithology results included within stratigraphic writing include terms for each major lithology category based on percentiles to provide relative context to each result (Table 2.3). If a descriptive term for a major lithology category is not present in writing, it is moderate.

Table 2.3: Percentile-based categorical terms used to describe clast lithology proportionality.

Categorical term for clast-lithology	**Percentile range**
Very low	<5th percentile
Low	5th–25th percentile
Moderate	25th–75th percentile
High	75th–95th percentile
Very high	>95th percentile

2.5 Conclusion

In summary, this chapter has outlined the methods used to investigate the Quaternary stratigraphy of the study area and the composition of collected till samples. Fieldwork provided essential stratigraphic and sedimentological information, and laboratory analysis provided additional parameters to further delineate stratigraphic beds. Clustering techniques were utilized on till compositional data to group samples, supporting correlations across sections and provenance interpretations. Sediment beds were correlated to construct a stratigraphic framework using a hybrid lithostratigraphy-allostratigraphy approach. These methods were applied to create a robust and detailed multi-parameter Quaternary stratigraphic framework, from which interpretations can be made about the Quaternary history, till provenance, and ice-flow dynamics of the study area. The results of these analyses are presented in the following three chapters.

Chapter 3: Quaternary stratigraphy and paleo-ice flow indicators

3.1 Introduction

This chapter focuses on the results of field-based Quaternary investigations of eight sections in the study area investigated in the 2023 field season, including six along the Gods River and two along the Yakaw River (Figure 1.2). This includes observations on sedimentological characteristics (e.g., colour, texture, degree of diagenetic alteration), paleo-ice flow indicators (till fabrics, lodged boulders), and the stratigraphic sequence at individual sections. These field-based observations act as a crucial first step towards unravelling the complex Quaternary stratigraphy of the study area.

3.2 Methodology

Field data was collected in the study area, including the documentation of stratigraphic sections (section 2.2.1), the collection of sorted-sediment samples (section 2.2.2), paleo-ice flow indicator measurements from till (section 2.2.3), and till samples (section 2.2.4). This stratigraphic data was then compiled with other nearby sections documented with similar methodology (section 2.2.5).

Afterwards, sediment beds originally defined in the field were further refined through laboratory work (section 2.3.1). Till beds were further subdivided (see section 2.4.1.1) based on results from paleo-ice flow indicator data such as till clast fabric (section 2.2.3), as well as from till matrix texture (<2 mm size fraction; section 2.2.4), fine till-matrix geochemistry (specifically, total carbonate in weight percentage; section 2.3.3), and clast lithology counts (section 2.2.2).

3.3 Results

Quaternary sediments observed along the Gods and Yakaw rivers consist of postglacial sediments overlying thick sequences of tills and nonglacial sediments. Postglacial sediments include glaciolacustrine, marine, and fluvial deposits, typically around 3 m thick, although locally thin at times (~0.3 m at two sections). Diamict beds interpreted as till (see section 2.2.1) vary significantly in thickness (0.2–19.5 m) but are generally thick (~5–10 m). Sub-till sorted sediments interpreted as nonglacial deposits also exhibit a range in thickness, reaching up to 6.2 m in some places, and absent in others. It is important to note that selected sections often were in areas with minimal slumping, thereby introducing a bias towards locations with thick beds of till, which generally forms more stable cliff exposures compared to sorted sediments. In the following sub-sections, the general sedimentology of tills and nonglacial sediments are described, followed by a detailed description of the stratigraphy of each individual section.

3.3.1 Tills

Till beds encountered in the study area are most often matrix-supported, overconsolidated, and often exhibit well-developed blocky soil structure and oxidation along joints (Figure 3.1). Isolated deformed lenses or beds of sorted sediment are occasionally observed within till beds (Figure 3.2). Till beds observed are generally massive and no glaciotectonic features were observed to supplement or contradict ice-flow interpretations. Tills were also observed to occasionally contain transported and broken marine fossils, mineralized concretions, wood fragments, and black shale clasts.

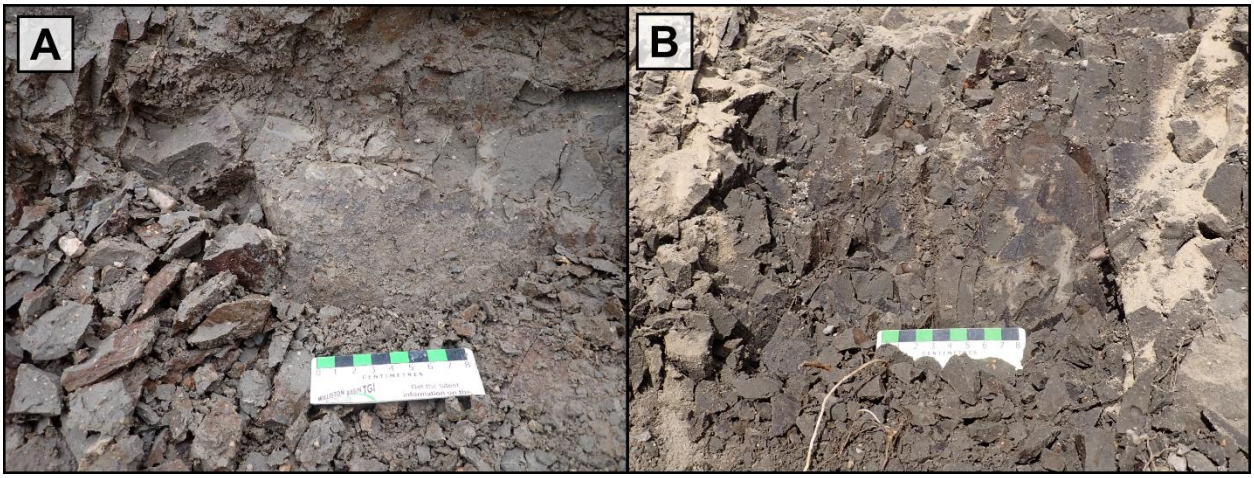


Figure 3.1: Examples of massive till with well-developed blocky soil structure and oxidation staining along joint faces. (A) Till Bed 6-B at 8.4 m depth. (B) Till Bed 9-A at 40.3 m depth.

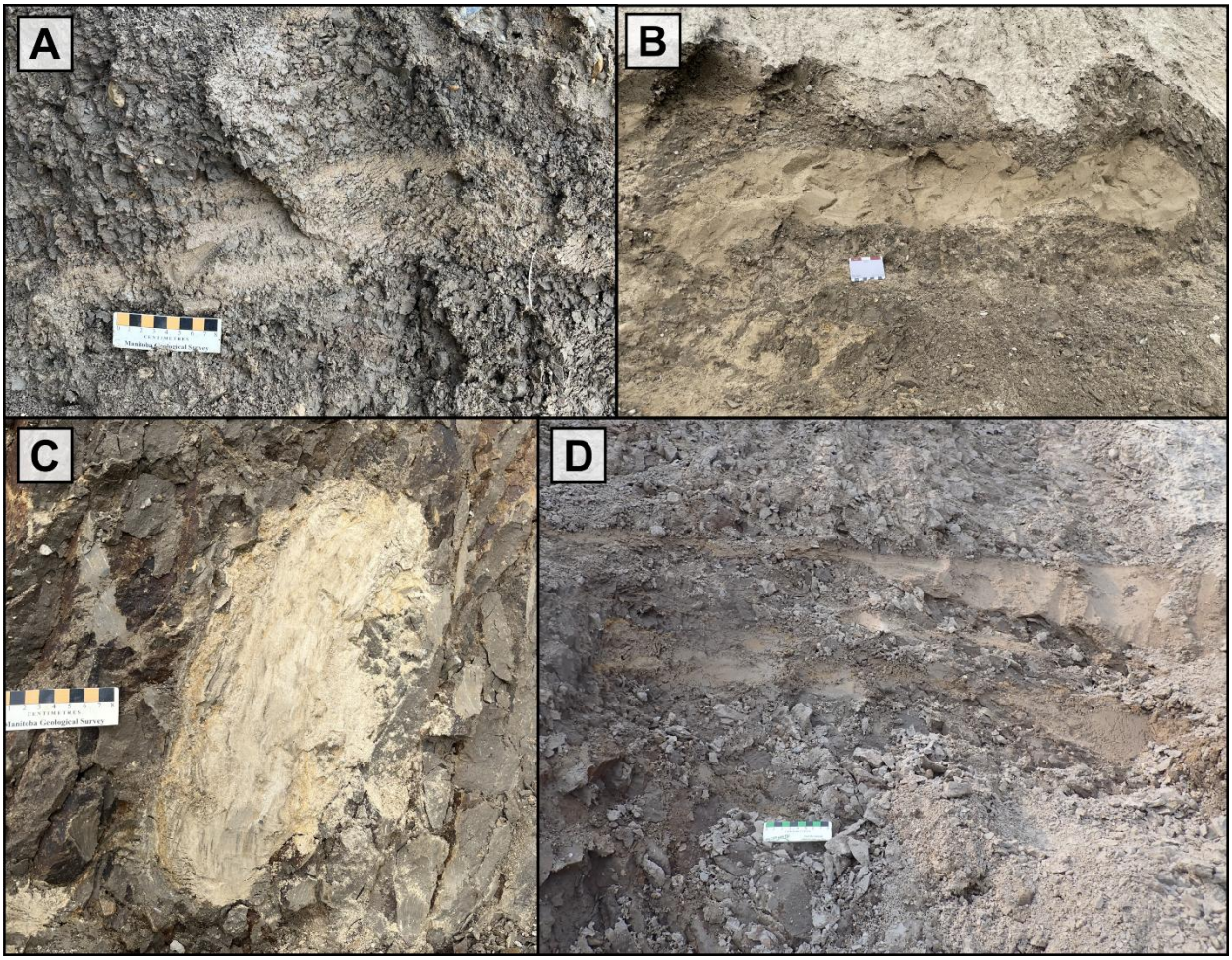


Figure 3.2: Examples of sorted sediments within till beds, including (A) a sand-silt lens within Bed 5-E at 4 m depth, (B) a tube-like lens within Bed 2-D at 12 m depth, consisting of very well sorted fine sand, (C) rotated laminated rip-up sand clast at 16 m depth within Bed 7-G, and (D) discontinuous sand beds at 13 m depth within Bed 8-A.

3.3.1.1 Colour

Till colours observed in the field predominantly consist of grey brown and olive brown hues, with lesser proportions of dark grey, brown, and yellow brown hues (Table 3.1). Within individual sections, till colours are typically darker at the base of sections and become lighter upsection. Considerable colour changes are also observed within till beds; some beds exhibit two or three distinct colours. These variations often represent gradational changes that were not immediately apparent upon initial field observations.

Table 3.1: Observed Munsell colours of till samples from the 2023 field season.

Munsell colour	**No. of samples**
Dark grey brown	27
Olive brown	19
Very dark grey brown	14
Dark olive brown	5
Brown	3
Light olive brown	2
Light yellow brown	2
Very dark grey	2
Dark grey	1
Dark yellow brown	1
Grey brown	1
Yellow brown	1

3.3.1.2 Grain size distribution

The grain size distribution of the 2023 till samples (<2 mm size fraction) predominantly consists of higher proportions of silt, with lower proportions of sand and clay (average distribution: 29% sand, 49% silt, 22% clay). The majority of samples have a clayey sandy silt matrix (see section 2.4.4) with a notable smaller population (n=4) of silty clay to sandy silty clay samples that deviate from the larger group (Figure 3.3). This smaller population corresponds to samples from Beds 4-B, 2-B, and 5-A, which are the lowermost till sample from each of their respective sections.

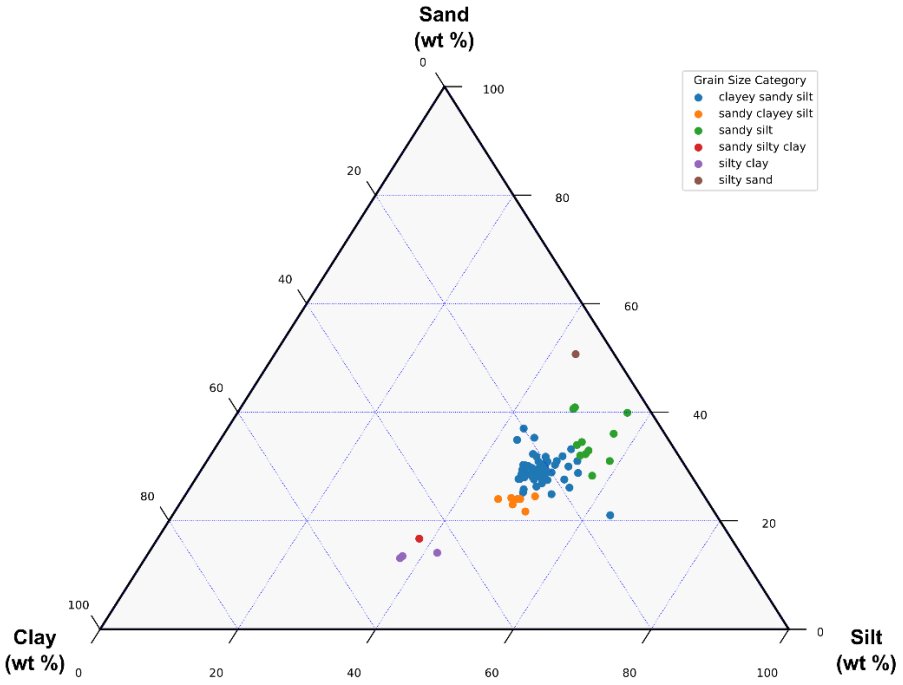


Figure 3.3: Till matrix grain size ternary diagram for 2023 samples, coloured by grain size category. Abbreviation: wt %, weight percentage.

3.3.1.3 Degree of diagenetic alteration

Observed tills differ notably in their degree of overconsolidation and diagenetic alteration (i.e., degree of blocky soil structure and oxidation along joint faces; see section 2.4.2.1), although most till beds exhibit a well-developed blocky soil structure and oxidation staining along joint faces (Table 3.2). Here, "blocky soil structure" refers to the size of blocks that break off from the sediment bed, which is controlled by the spacing between joint faces; this spacing is interpreted to result from the removal of cryostatic pressure during glacial retreat. Tills range from being loose and crumbly to having a weakly-developed blocky soil structure (~<3 cm blocks) or a well-developed blocky soil structure (~>3 cm blocks; Figure 3.4). Their degree of diagenetic alteration generally aligns with their stratigraphic position given similar matrix textures; looser, less oxidized tills overlie tills with larger blocks and more developed oxidation along joint faces.

Table 3.2: The number of till beds and samples that exhibit the different degrees of blocky soil structure and oxidation along joints, from the 2023 field season.

		No. of beds	**No. of samples**
Degree of blocky soil structure	Loose, crumbly	4	3
	Weakly-developed blocky structure (~<3 cm blocks)	6	8
	Well-developed blocky structure (~>3 cm blocks)	24	73
Degree of oxidation along joints	No oxidation	5	5
	Minor oxidation	6	5
	Major oxidation	23	73



Figure 3.4: Examples of different degrees of diagenetic alteration in till beds with similar texture, including (A) loose, crumbly till with no oxidation stains (sample 200-A01 from Bed 200-E), (B) till with weakly-developed blocky structure and minor oxidation development along joint faces (sample 008-B01 from Bed 8-D), and (C) till with well-developed blocky structure and major oxidation development along joint faces (sample 008-F01 from Bed 8-A).

3.3.1.4 Paleo-ice flow indicators

During the 2023 field season, the orientation of elongated clasts was measured at 54 till sample locations for the purpose of till clast fabric analysis. One additional till-fabric was conducted at a site where the corresponding till sample was lost (sample 007-D08). Additionally, in-situ lodged cobbles or boulders with parallel striations on their upper surfaces were found at or below 5 till-sample sites and were measured for paleo-ice flow. Of the till-fabric analyses, one was deemed weak (S1<0.54) but usable for paleo-ice flow direction interpretation (sample 008-F03), and five were weak and unusable (samples 002-C01, 002-D02, 003-D01, 007-D07, 009-E01; Appendix G, Table 3). Dominant interpreted ice-flow directions include SW (n=18) and NW-SE (n=15), with lesser amounts of indications of W (n=7), WNW-ESE (n=7), S (n=6), SSW (n=5), WSW (n=5), and NNW-SSE (n=3).

Notably, remarkable variability in interpreted paleo-ice flow direction exists within field-defined till beds at single sections. For example, within section 7-G, till fabrics indicate direction of shear shifted from W to S, then from S to NNW or SSE. As a result of these intra-bed variations, 12 subdivisions have been made within field-defined beds to better represent the complex record. Specifically, 4 subdivisions have been made based exclusively on a possible >90° change in ice-flow direction, and 8 subdivisions have been made based on a >45° change supported by significant changes in other till parameters.

3.3.1.5 Clast-lithology counts

Although a more comprehensive analysis of till composition is presented in Chapter 4, clast-lithology counts are occasionally used in this chapter to assist in subdividing till beds (see section 2.4.1.1). To this end, clast-lithology proportions are incorporated into the stratigraphic descriptions, expressed as 1) closed proportions of the three major clast-lithology groups, and 2) descriptive terms representing percentile-based categories (as defined in section 2.4.4) for relative comparisons. The distribution of each major clast-lithology group across these categories is shown in Figure 3.5.

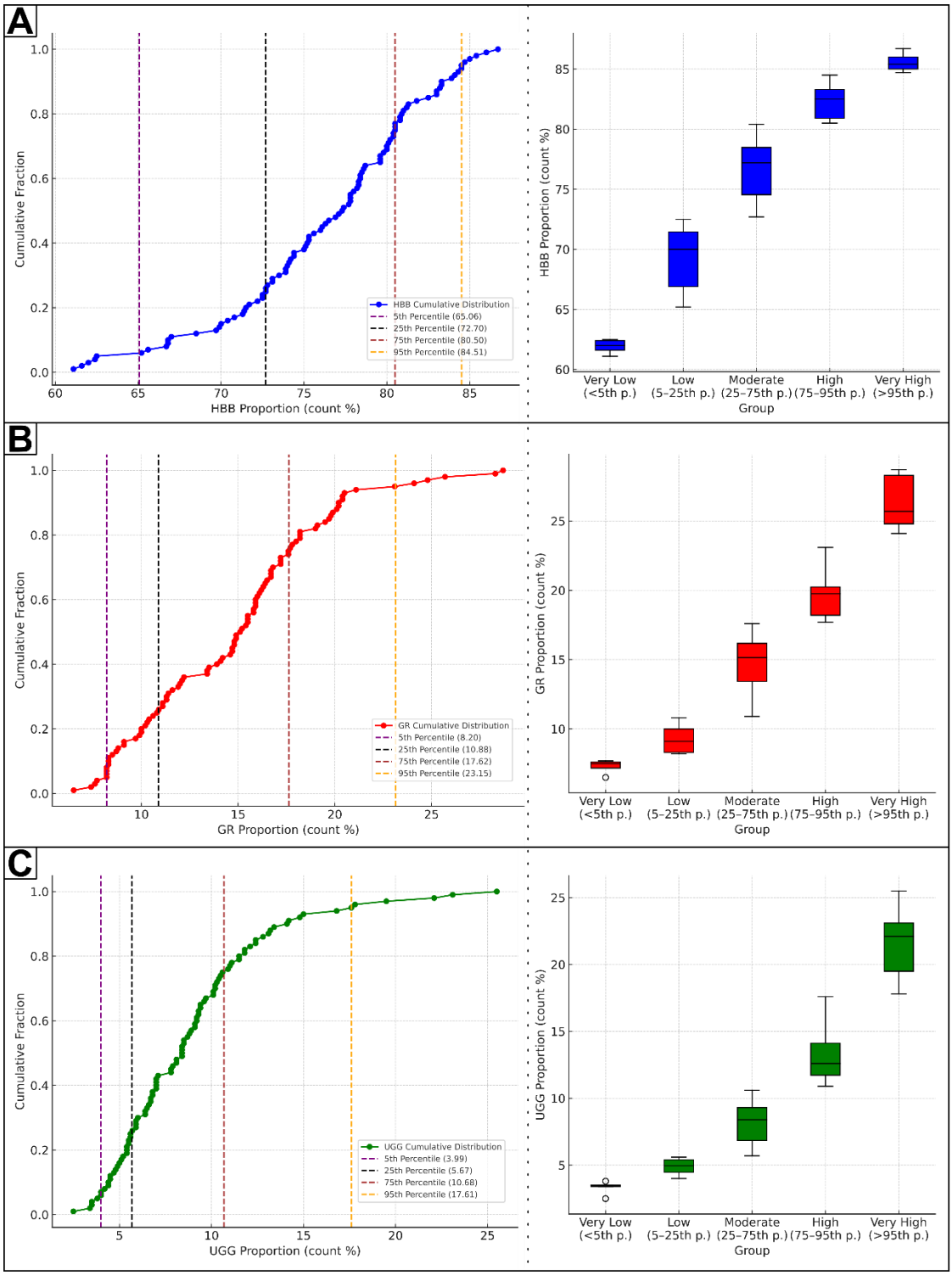


Figure 3.5: The distribution of each major clast-lithology group, including (A) HBB clasts, (B) GR clasts, and (C) UGG clasts. Left panels show the cumulative distribution with percentiles, while right panels present boxplots of each percentile-based group. Abbreviations: p., percentile; HBB, Hudson Bay Basin rocks; GR, granitoid rocks; UGG, undifferentiated greenstone and greywackes.

3.3.1.6 Total carbonate

The total carbonate content of the fine-grained matrix in till samples ranges from 23.4–50.3% and a cumulative distribution plot shows three separate populations (Figure 3.6). To capture the sub-populations, the terms defined to describe the total carbonate content in the descriptions of stratigraphic sections include *weakly calcareous* (<36.5%), *moderately calcareous* (36.5–46.5%), and *highly calcareous* (>46.5%). The majority of samples are moderately calcareous (n=67), with fewer classified as weakly calcareous (n=15) or highly calcareous (n=18).

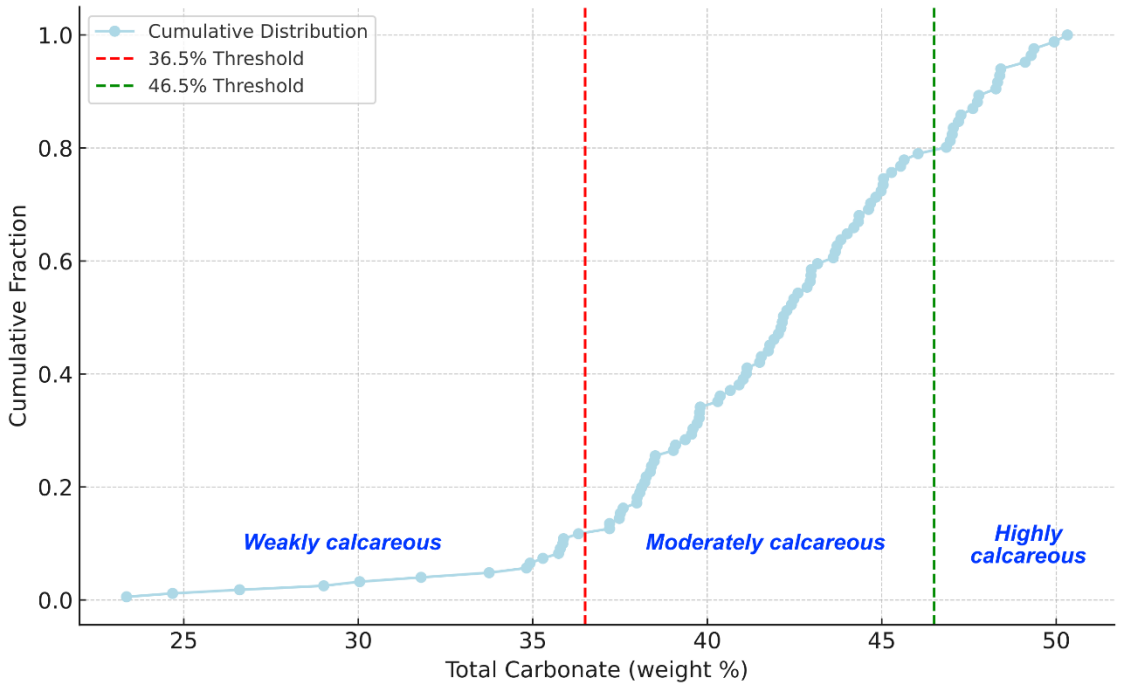


Figure 3.6: Cumulative distribution of total carbonate from the fine-grained matrix of till samples, including distinct sub-populations (labelled in blue).

3.3.2 Nonglacial sediment

Sorted-sediment beds, although not the focus of this thesis, provide key constraints for the relative age of till units. Specifically, the sedimentological characteristics of nonglacial deposits offer insights into paleoclimatic conditions that followed or preceded glaciations, thereby helping establish minimum climatic stage estimates within the relative stratigraphy. The subsections below outline the two main categories of nonglacial sediments: postglacial sediments that cap stratigraphic sequences, and sub-till sorted sediments that record earlier nonglacial phases or events.

3.3.2.1 Postglacial sediment

The uppermost sorted sediment bed(s) at each section are interpreted as postglacial. Although age dating techniques or paleo-environmental analysis have not been applied consistently to confirm a postglacial age, their ubiquity in the western HBL (see section 1.2.4) generally allows a reasonable postglacial interpretation. Postglacial sediments were identified at all examined sections, with interpreted depositional environments varying from glaciolacustrine, marine, and fluvial. Among the examined sections, section 115-23-006 provides perhaps the most complete record of the transition from glacial to modern depositional environments (section 3.3.3.6). This sequence likely captures the depositional progression from glaciolacustrine (associated with glacial Lake Agassiz) to postglacial marine (Tyrrell Sea), to fluvial.

3.3.2.2 Sub-till sorted sediment

Sub-till sorted sediment packages are substantially variable in both their sedimentological characteristics and interpreted depositional environment. This variability is evident even within the same stratigraphic bed when observed at different exposures (Figure 3.7). Additionally, some packages contain organic material (e.g., wood fragments, matted organics, or charcoal) while others are devoid of any visible organics. Across all studied sections, three organic-bearing sub-till sorted sediment packages were identified (beds 5-B, 7-A, and 9-C), and one sub-till sorted sediment package containing heavily oxidized and cemented gravel (Bed 7-C). An additional 10 beds may be subglacial or nonglacial (beds 2-C, 3-B, 3-C, 3-E, 3-F, 5-D, 7-F, 8-B, 8-E, 9-E).

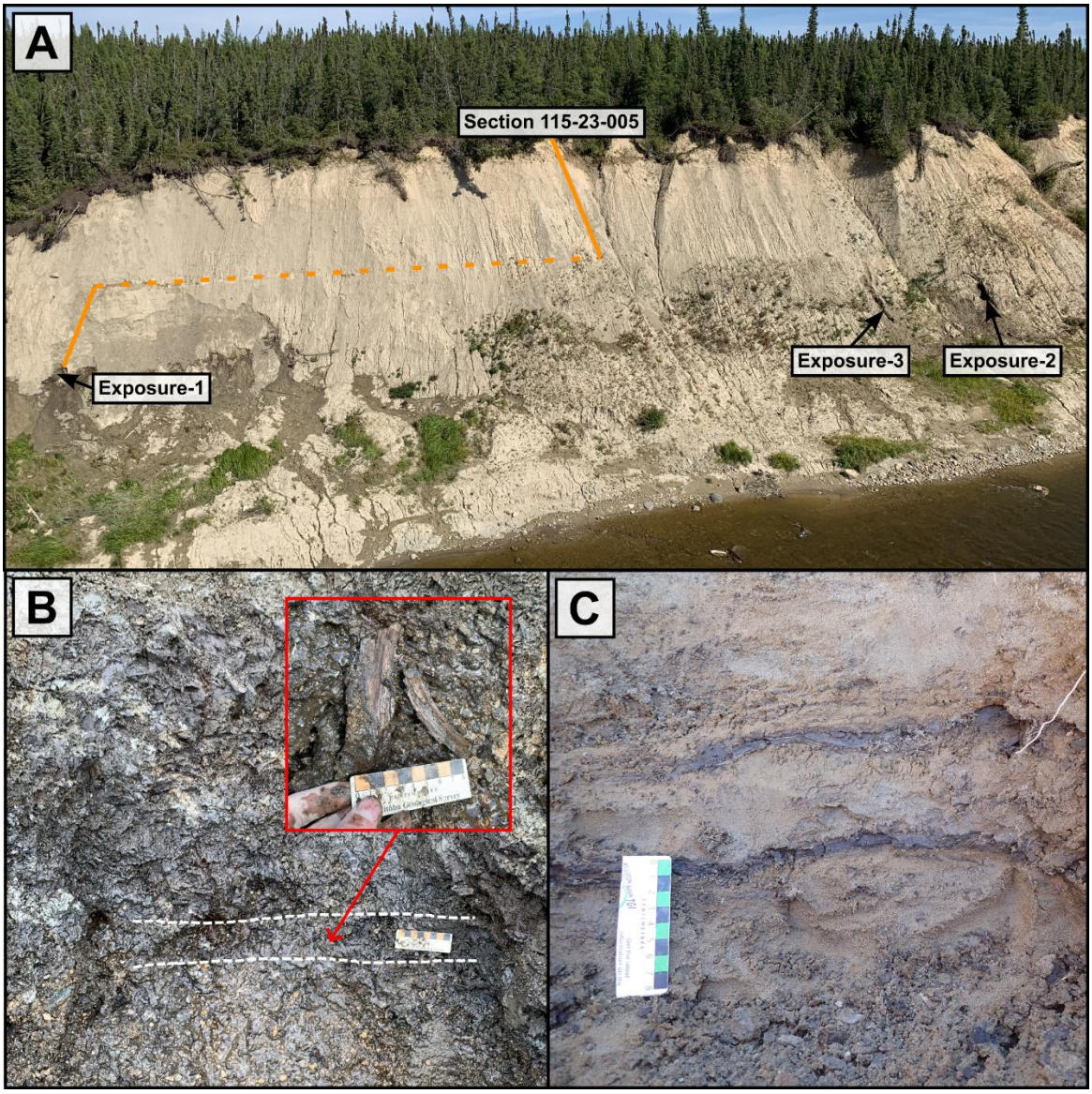


Figure 3.7: (A) Overview of section 115-23-005, with three exposures of organic-bearing sub-till sorted sediment packages belonging to Bed 5-B. (B) A layer of matted plant materials (white outline) between gravel and silt beds at Exposure-1. (C) Two thin beds of organic-rich silt within the horizontally bedded sand of Exposure-3.

3.3.3 Stratigraphic sections

Herein, the 8 sections visited in the 2023 field season are documented in detail (115-23-002–115-23-009; Figure 3.8). Documentation for sections examined in 2019 and 2022 is provided in Appendix H.

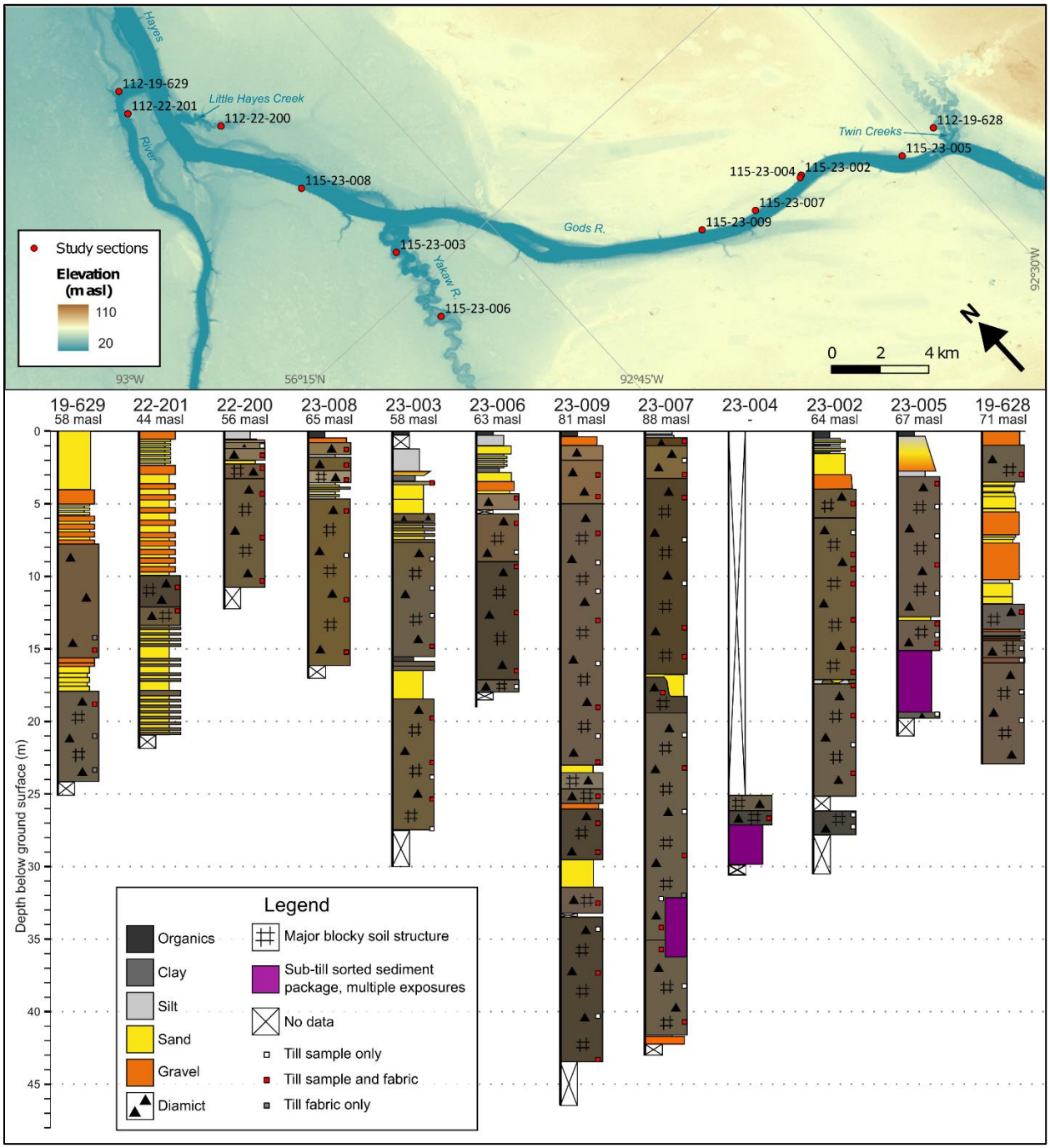


Figure 3.8: Simplified stratigraphy of sections from the study area, including those visited during the 2019 (xxx-19-xxx), 2022 (xxx-22-xxx), and 2023 (xxx-23-xxx) field seasons. Till sample and till fabric analysis locations are also shown.

3.3.3.1 Section 115-23-002, Gods River

At site 115-23-002 along Gods River (Figure 3.8), a 28-meter-thick sequence of sediments was exposed along a 20-meter stretch of the east-facing side of a gully (Figure 3.9). This gully is carved into the northern cut bank of the Gods River. A total of 7 stratigraphic beds were identified in the field based on visible contacts and internal characteristics. Four of these beds are diamicts interpreted as till, two are sorted sediment beds, and one is a mixture of sorted sediment and diamict (Figure 3.10). Across the 5 till beds and sub-beds, 14 samples were collected (Figure 3.11).



Figure 3.9: Overview of section 115-23-002, viewed towards the northwest.

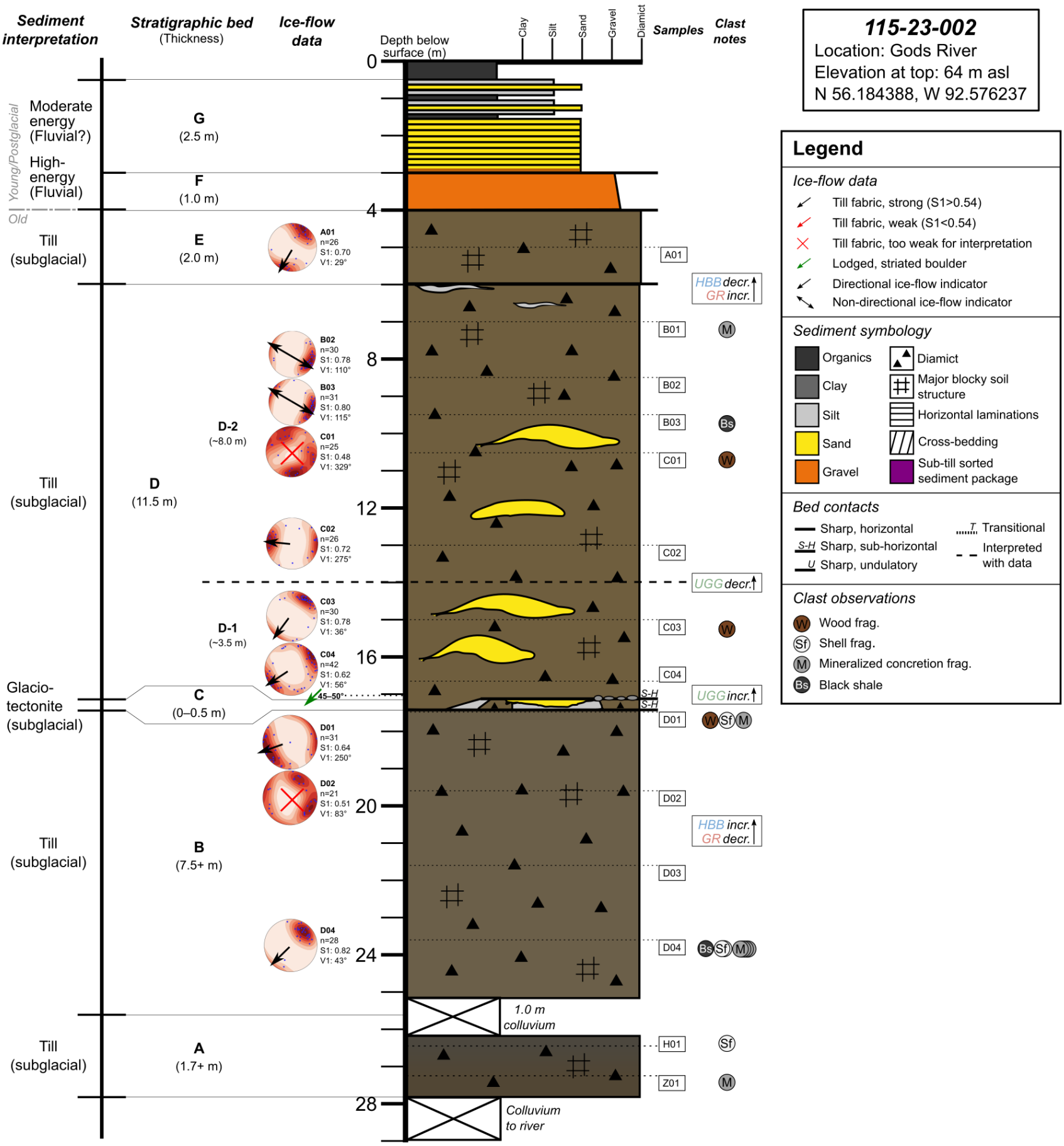


Figure 3.10: Stratigraphic log of section 115-23-002. Diamict beds are coloured by their sampled Munsell colour. Abbreviations: asl, above sea level; frag., fragment; HBB, Hudson Bay Basin; GR, granitoid; UGG, undifferentiated greenstone and greywacke.

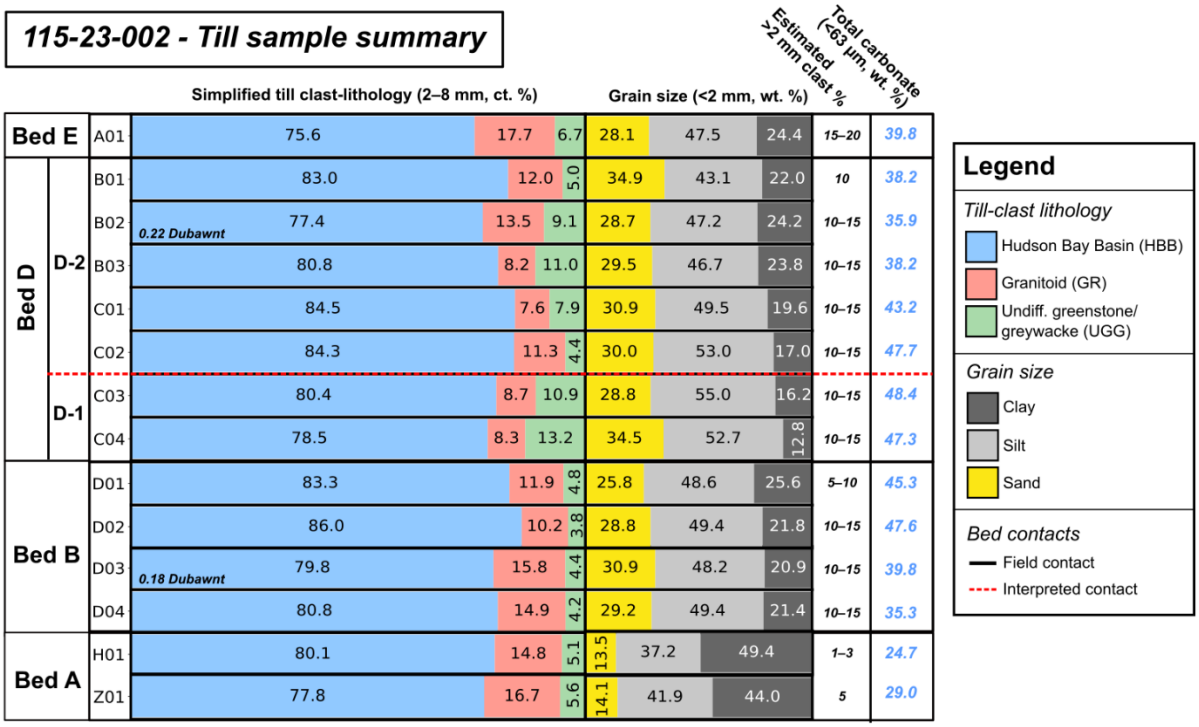


Figure 3.11: Summary of till sample data for section 115-23-002. Abbreviations: ct., count, wt., weight.

Bed 2-A is a massive diamict, at least 1.7 m thick, that is very dark grey-brown (2.5Y 3/2) to very dark grey (2.5Y 3/1) in colour (Figure 3.12A). Bed 2-A is highly overconsolidated, has a weakly calcareous and silty-clay to clayey silt matrix, and has a well-developed blocky structure with oxidation along joints. The bed contains 1–5% striated and/or faceted clasts of granule- to pebble size and has a detectable smell of sulphur. Bed 2-A clasts have low UGG (Z01, H01: 77.8–80.1% HBB, 14.8–16.7% GR, 5.1–5.6% UGG; Appendix E, Table 5). Bed 2-A is interpreted as subglacial traction till.

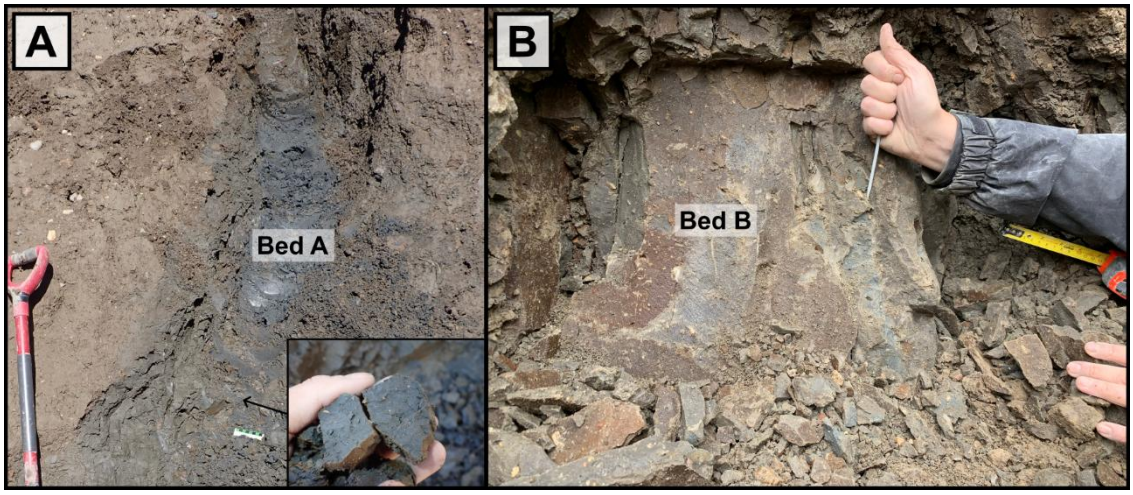


Figure 3.12: (A) Very dark grey-brown till of Bed 2-A. (B) Dark grey-brown till of Bed 2-B.

Bed 2-B is a massive dark grey-brown diamict (2.5Y 4/2; Figure 3.12B), at least 7.5 m thick, that is highly overconsolidated, has variably calcareous clayey sandy-silt matrix, a well-developed blocky structure with oxidation along joints, and contains 10–15% striated and/or faceted clasts of granule to pebble size. Three clast fabrics were measured from Bed 2-B and are interpreted to record a shift in the direction of shear from SW to WSW over time (223°, 250°, Appendix G, Table 3). Bed 2-B clasts have moderate to very high HBB, moderate to low GR, and low to very low UGG (D04–D01 (n=4): 79.8–86.0% HBB, 10.2–15.8% GR, 3.8–4.8% UGG; Appendix E, Table 5). About halfway up Bed 2-B (between D03 and D02), there is a notable 6.2% increase in HBB concentration, and a 5.6% decrease in GR concentration (Figure 3.11). Bed 2-B is interpreted as subglacial traction till. Bed 2-B overlies Bed 2-A, however, the contact was covered by colluvium and thus not observed.

Bed 2-C consists of a very poorly sorted heterogeneous mélange of silt, sand, clasts, and diamict (Figure 3.13), from 0–0.5 m thick. Clasts are subangular to subrounded and granule- to large pebble-sized. Subhorizontal, deformed layers of diamict and silt are present in the upper ~0.2 m of Bed 2-C. Bed 2-C is interpreted as a glaciotectonite, representing reworking and deformation of pre-existing sediment under subglacial conditions. When present, Bed 2-C overlies Bed 2-B with a sharp subhorizontal contact.

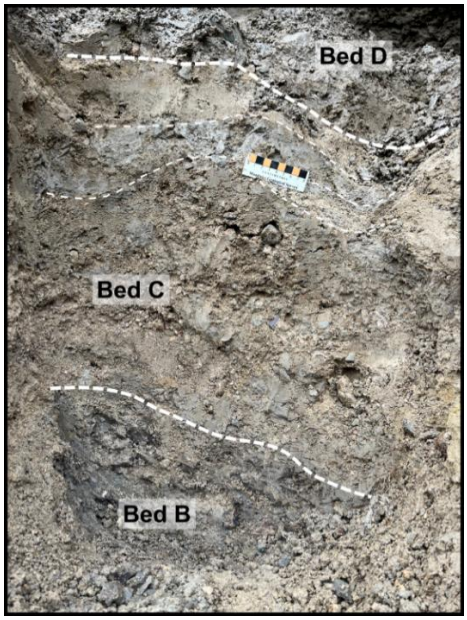


Figure 3.13: Mélange of sorted sediment and diamict of Bed 3-C. Contacts with Bed 2-B (lower) and 2-D (upper) are outlined by a thick dotted line. Deformed layers in the upper portion of the bed are outlined in a thin dotted line.

Bed 2-D is a massive olive-brown diamict (2.5Y 4/3; Figure 3.14B), about 11.5 m thick, that is highly overconsolidated, and changes upsection from a highly calcareous sandy-silt matrix to a moderately calcareous clayey sandy-silt matrix. Bed 2-D has a well-developed blocky structure with oxidation along joints and contains 10–15% striated and/or faceted clasts of granule to pebble size. At the base of Bed 2-D, there is a clast lag, consisting of subangular to subrounded pebbles to small boulders. At 1.5 m and 2.5 m above the base of Bed 2-D, there are two deformed, very well-sorted fine sand lenses 5–50 cm thick. At about 5.0 m above the base of Bed 2-D, there is a 20 cm thick, tube-like, very well sorted fine sand lens (Figure 3.14C). At about 6.5 m above the base of Bed 2-D, there is a poorly sorted fine to medium sand lens with granules, which coarsens upsection to moderately sorted medium sand with disseminated pebbles (Figure 3.14D). There are also two massive, red-brown coarse silt lenses near the upper contact of Bed 2-D (Figure 3.14E). Five unimodal clast fabrics were measured from Bed 2-D and are interpreted to indicate a shift in the direction of shear from SW to W–ESE-WNW during deposition (236°, 216°; 275°, 115-295°, 110-290°, Appendix G, Table 3). The orientations of four clasts from the clast lag were measured, all of which with a-axes oriented SW, with one flat-topped cobble with parallel striations that were oriented S (45–50°, 168°, Appendix G, Table 2). Due to this interpreted change in ice-flow direction, Bed 2-D is separated into Bed 2-D-1 (~3.5 m thick, SW fabric) and Bed 2-D-2 (~8.0 m thick, W–ESE-WNW fabric). This subdivision is supported by a significant change in composition between samples on either side of the interpreted contact; the Bed 2-D-1 sample contains 10.9% UGG clasts, while the Bed 2-D-2 sample contains only 4.4% UGG clasts (a 6.5% decrease; Figure 3.11). More precisely,

Bed 2-D-1 clasts have low GR and high UGG (C04, C03: 78.5–80.4% HBB, 8.3–8.7% GR, 10.9–13.2% UGG; Appendix E, Table 5), while Bed 2-D-2 clasts have moderate to high HBB, moderate to very low GR, and low to high UGG (C02–B01 (n=5): 77.4–84.5% HBB, 7.6–13.5% GR, 4.4–11.0% UGG; Appendix E, Table 5). Also, there is an 8.4% increase in UGG concentration from Bed 2-B (below) to the base of Bed 2-D-1 (Figure 3.11). Bed 2-D is interpreted as subglacial traction till. Bed 2-D overlies Bed 2-C and 2-B with a sharp subhorizontal contact at the clast lag (Figure 3.14A).

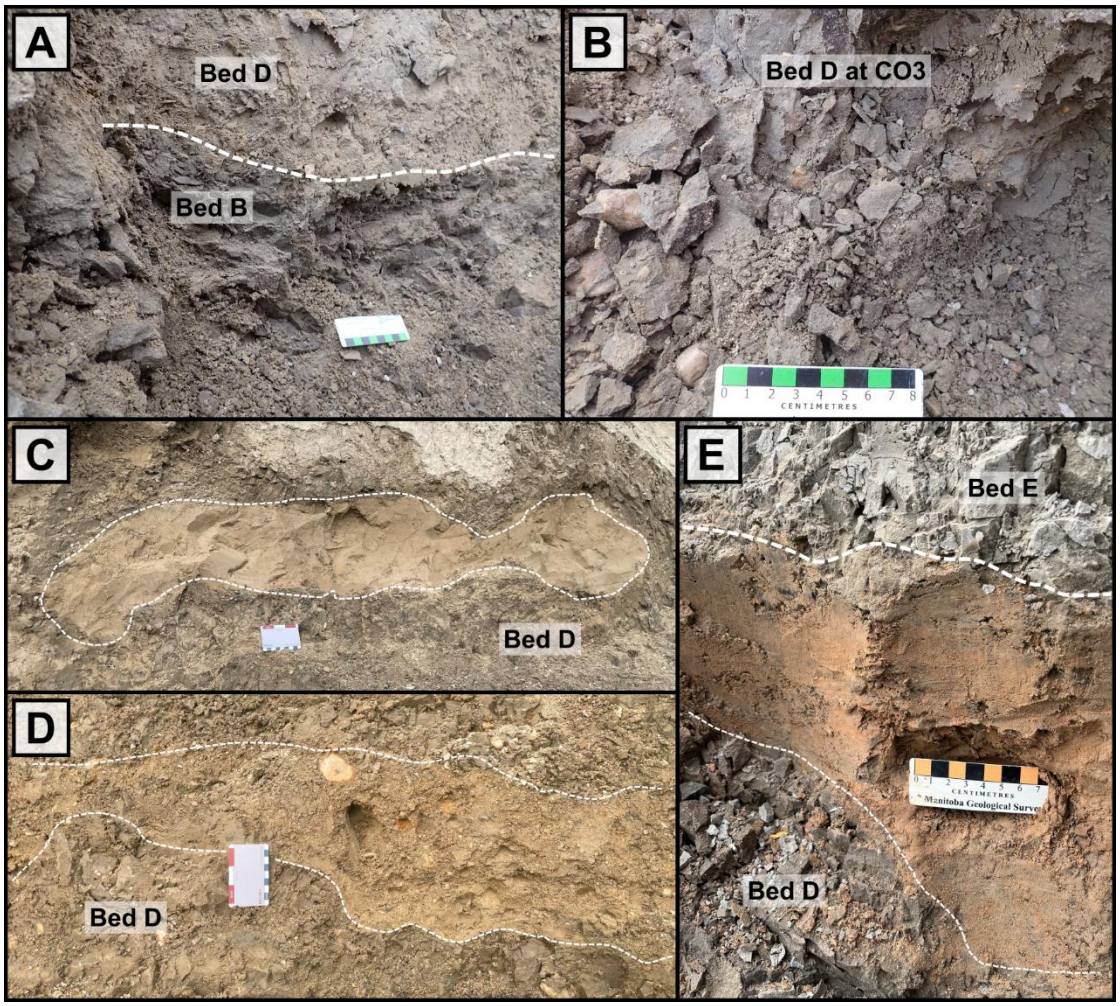


Figure 3.14: (A) Bed 2-B sharply overlying Bed 2-B with a sub-horizontal contact. (B) Olive-brown till of Bed 2-D. (C) Tube-shaped lens within Bed 2-D containing well-sorted very fine sand. (D) Poorly sorted sand lens within Bed 2-D. (E) One of two red-brown silt lenses near and at the upper contact of Bed 2-D with Bed 2-E.

Bed 2-E is a massive olive-brown diamict (2.5Y 4/3; Figure 3.15A), 2.0 m thick, that is highly overconsolidated, has a moderately calcareous clayey sandy-silt matrix, has a well-developed blocky structure with minor oxidation along joints, and contains 15–20% striated and/or faceted clasts of granule to pebble size. One spread unimodal clast fabric was measured from Bed 2-E and is interpreted to indicate

shear stress was SSW, (209°, Appendix G, Table 3). Bed 2-E clasts have high GR (A01: 75.6% HBB, 17.7% GR, 6.7% UGG; Appendix E, Table 5). There is a 7.4% decrease in HBB concentration from Bed 2-D-2 (below) to the base of Bed 2-E, and a 5.7% increase in GR concentration (Figure 3.11). Bed 2-E is interpreted as subglacial traction till. Bed 2-E overlies Bed 2-D with a sharp horizontal contact.

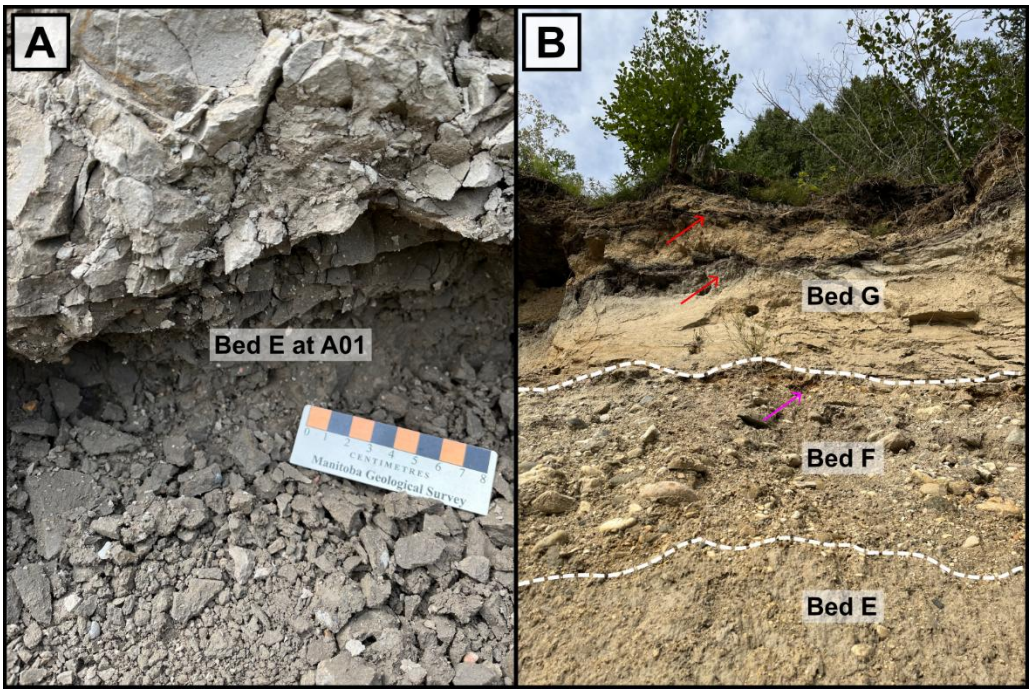


Figure 3.15: (A) Olive-brown till of Bed 2-E. (B) Beds 2-E, -F, and -G. The magenta arrow points to oxidation within the top 3 cm of Bed 2-F, while the red arrows point to the two paleosols found in Bed 2-G.

Bed 2-F consists of moderately sorted sandy gravel that roughly fines upwards (Figure 3.15B). Bed 2-F contains subrounded clasts that are granule- to boulder-sized, with small pebble-sized clasts most prevalent. The uppermost 3 cm of gravel is oxidized. Bed 2-F is interpreted as a post-glacial, high-energy fluvial deposit, based on the subrounded shape of clasts, moderate sorting, and fining-upwards sequence. Bed 2-F overlies Bed 2-E with a sharp horizontal contact.

Bed 2-G consists of laminated silt and sand (Figure 3.15B), inaccessible due to safety concerns. Bed 2-G includes two paleosols, likely caused by modern slumping. Bed 2-G, is tentatively interpreted as a post-glacial fluvial deposit due to its stratigraphic position above Bed 2-F. Bed 2-G overlies Bed 2-F with a sharp horizontal contact, and Bed 2-G is overlain by modern peat.

3.3.3.2 Section 115-23-003, Yakaw River

This 30-m-high section extends about 50 m along the south side of the Yakaw River, to the west of a gully (Figure 3.16). It contains 10 stratigraphic beds: 3 are diamicts interpreted as till, 2 are diamicts interbedded with sorted sediments, and 5 are sorted sediments (Figure 3.17). Across the 3 till beds and sub-beds, 10 samples were collected (Figure 3.18).



Figure 3.16: Overview of section 115-23-003, viewed towards the south.

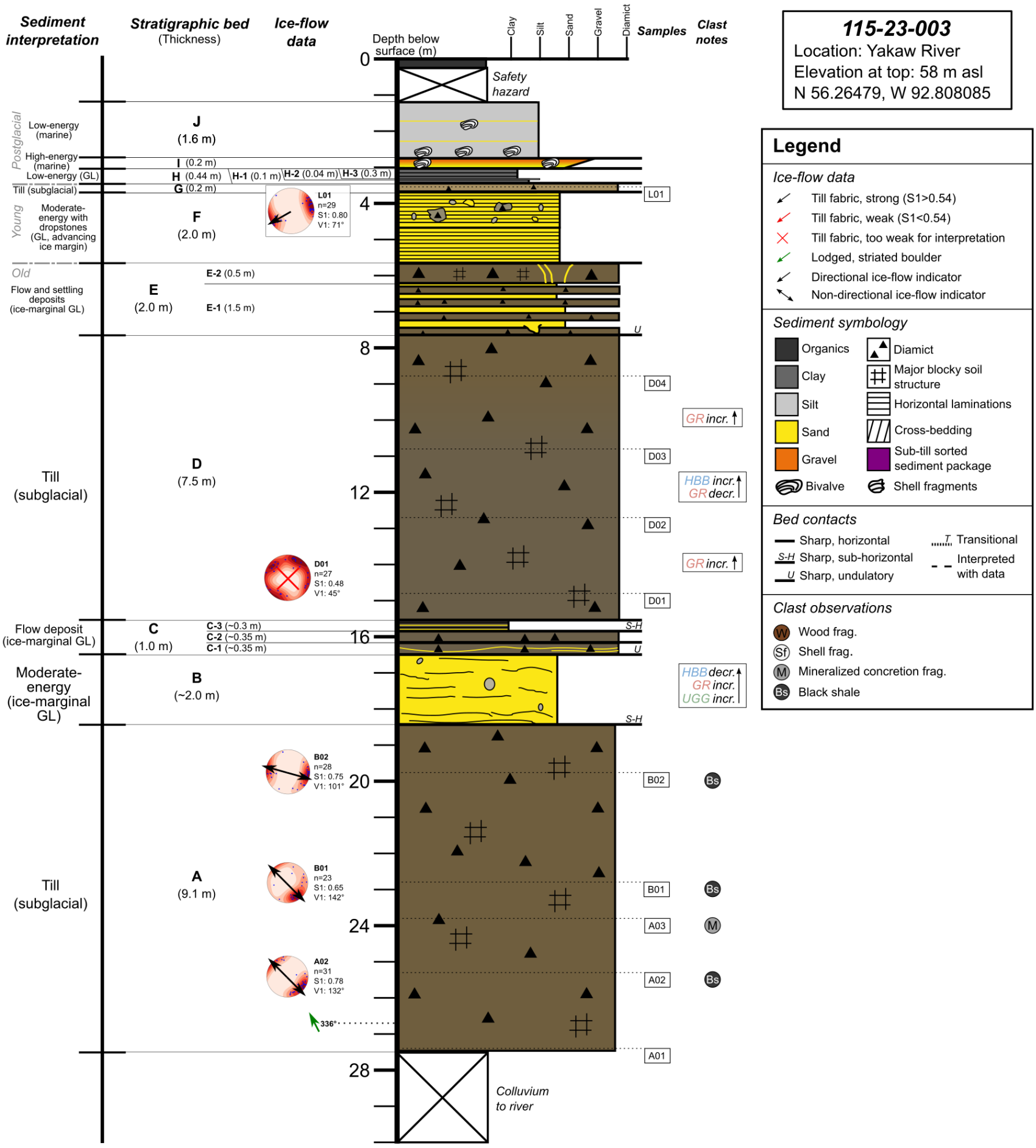


Figure 3.17: Stratigraphic log of section 115-23-003. Diamict beds are coloured by their sampled Munsell colour. Abbreviations: asl, above sea level; frag., fragment; GL, glaciolacustrine; HBB, Hudson Bay Basin; GR, granitoid; UGG, undifferentiated greenstone and greywacke.

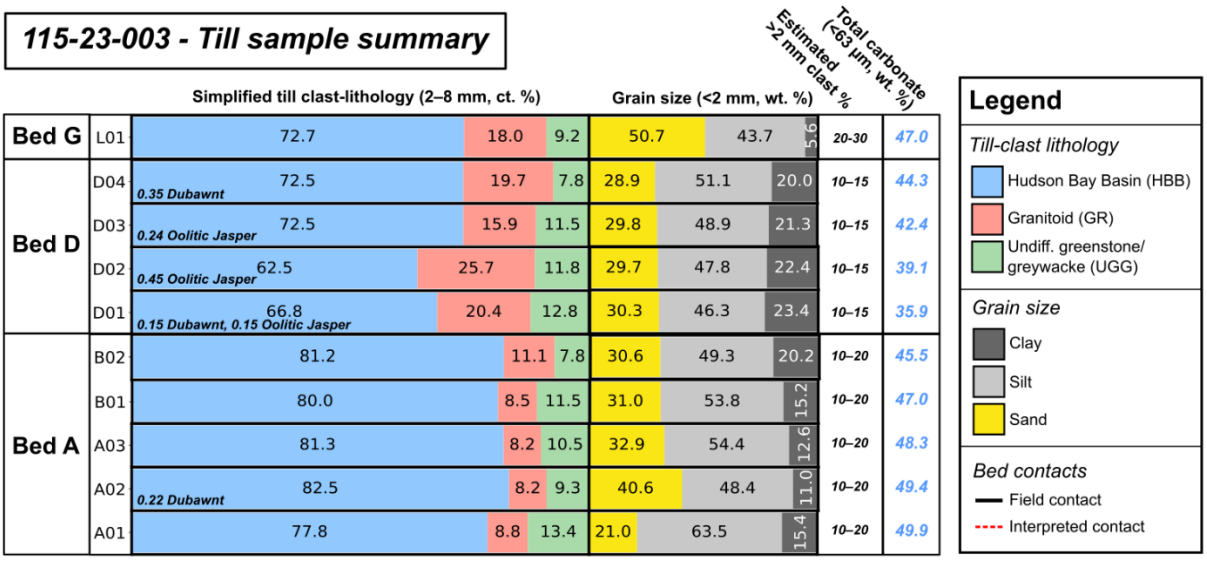


Figure 3.18: Summary of till sample data for section 115-23-003. Abbreviations: ct., count, wt., weight.

The lowermost Bed 3-A is a massive olive-brown (2.5Y 4/3) diamict (Figure 3.19A), at least 9.1 m thick, that is highly overconsolidated and has a moderately to highly calcareous clayey sandy-silt to sandy-silt matrix. Bed 3-A has a well-developed blocky structure with oxidation along joints and contains 10–20% clasts that are granule- to medium cobble-sized and striated and/or faceted. Three spread-unimodal clast fabrics and striae on one lodged boulder were measured from Bed 3-A and are interpreted to indicate shear stress was initially SSE-NNW, changing to SE-NW over time, and then changing to ESE-WNW (156-336°, 132-312°, 142-322°, and 101-281°, Appendix G, Table 3, Table 2). Bed 3-A clasts have moderate to high HBB, low GR, and moderate to high UGG (A01–B02 (n=5): 77.8–82.5% HBB, 8.2–11.1% GR, 7.8–13.4% UGG; Appendix E, Table 5). Bed 3-A is interpreted as subglacial traction till.

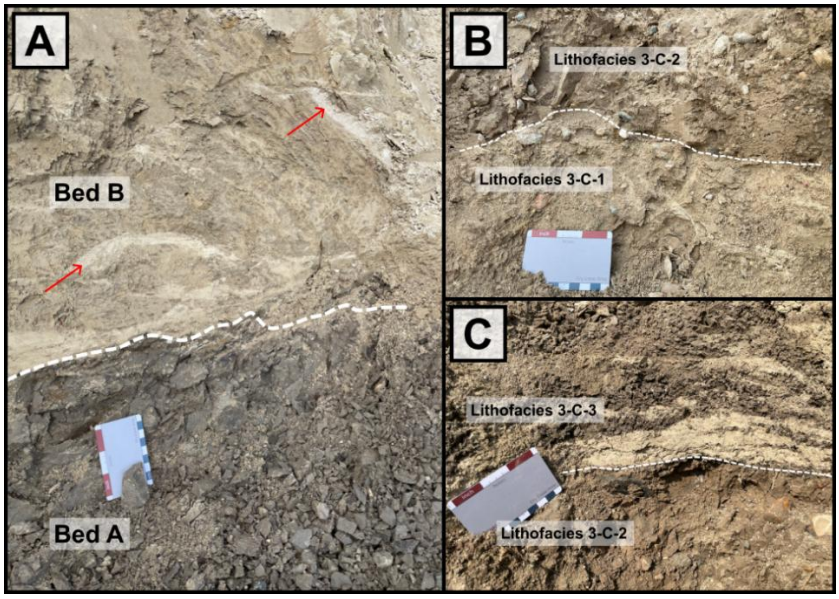


Figure 3.19: (A) Bed 3-B sharply overlying Bed 3-A with a sub-horizontal contact. Red arrows indicate crude laminations. (B) Massive diamict of lithofacies 3-C-2 overlying laminated diamict of lithofacies 3-C-1. (C) Laminated clay and sand of lithofacies 3-C-3 overlying lithofacies 3-C-2.

Bed 3-B consists of 2.35 m of massive to crudely laminated silt to very fine sand (Figure 3.19A), where sub-horizontal bedding is defined by textural changes. There are 1–3% isolated small pebble to granule-sized clasts, with rare cobble-sized clasts, and wisps of oxidation staining throughout. The laminations and scattered larger clasts suggest that Bed 3-B was deposited in an ice-contact (marginal) glaciolacustrine environment, with laminations likely recording seasonal changes while the larger clasts are interpreted to be 'dropstones' released from floating icebergs. Bed 3-B overlies Bed 3-A, with a sharp sub-horizontal contact.

Bed 3-C (Figure 3.19B, C), 1.0 m thick, consists of about 0.35 m of diamict laminated with sand (lithofacies 3-C-1), sharply overlain by about 0.35 m of massive diamict (lithofacies 3-C-2), which is then sharply overlain by 0.3 m of laminated dark brown clay with deformed sand laminations (lithofacies 3-C-3). The diamict, sand, and clay of Bed 3-C suggest ice-contact (marginal) glaciolacustrine deposition. Bed 3-C overlies Bed 3-B with a sharp undulatory contact.

Bed 3-D is a massive diamict (Figure 3.20A), 7.5 m thick, which ranges in colour from dark grey-brown (2.5Y 4/2) to olive-brown (2.5Y 4/3). Bed 3-D is highly overconsolidated, has a moderately calcareous clayey silty-sand matrix, has a well-developed blocky structure with oxidation along joints, and contains 10–15% striated and/or faceted clasts that are granule- to small pebble-sized. One spread bimodal clast fabric was measured from Bed 3-D, though due to a lack of clasts and significant spread, a shear-stress direction could not be determined. Here, the two dominant clast orientations are NE-SW and ESE-WNW.

Bed 3-D clasts have low to very low HBB, moderate to very high GR, and moderate to high UGG (D01–D04 (n=4): 62.5–72.5% HBB, 15.9–25.7% GR, 7.8–12.8% UGG; Appendix E, Table 5). Notably, there is a sharp decrease in GR clast proportions upsection, corresponding to an increase in HBB clasts (D02: 62.5% HBB, 25.7% GR; D03: 72.5% HBB, 15.9% GR; Figure 3.18). Also, there are notable increases in GR clast concentration from D01 to D02 (5.3%) and from D03 to D04 (4.8%; Figure 3.18). Oolitic jasper and Dubawnt erratics are both present in Bed 3-D. Additionally, there is a 14.4% decrease in HBB concentration, 9.3% increase in GR concentration, and 5.0% increase in UGG concentration from Bed 3-A (below) to the base of Bed 3-D (Figure 3.18). Bed 3-D is interpreted as subglacial traction till. Bed 3-D overlies Bed 3-C, with a sharp horizontal contact.

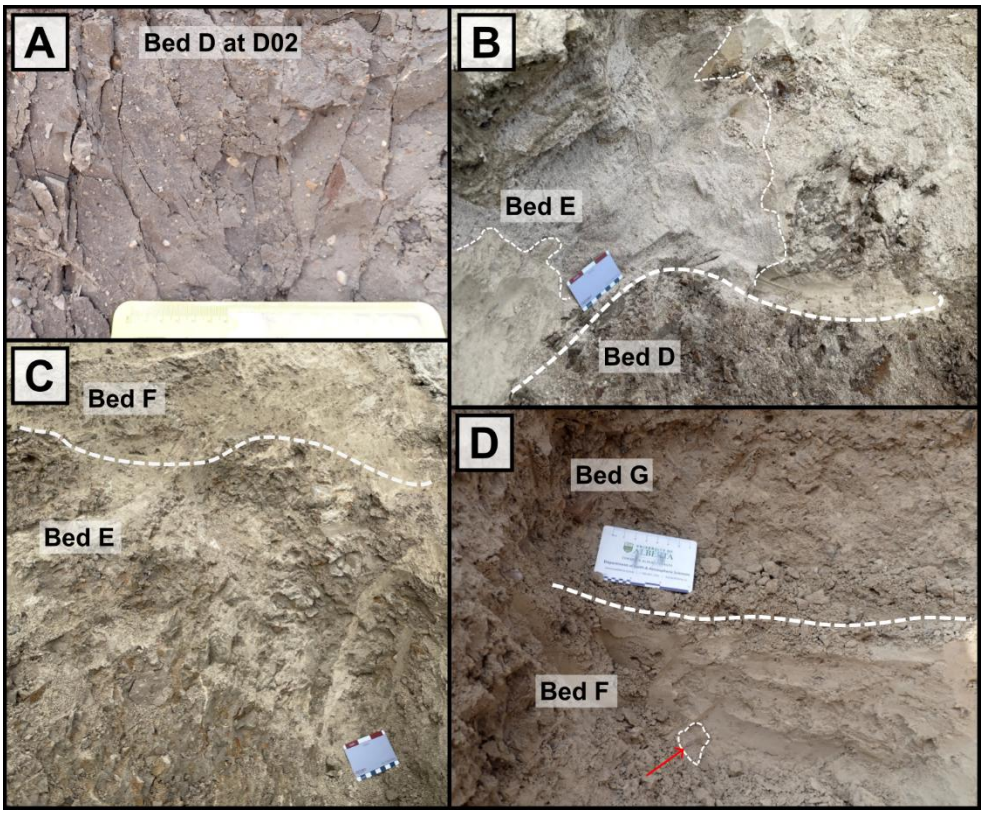


Figure 3.20: (A) Dark grey-brown till of Bed 3-D. (B) Bed 3-D till overlain by interstratified silt to sand and diamict layers of Bed 3-E. The cross-cutting coarse sand lens is also outlined. (C) Bed 3-E diamict with infilled fractures overlain by laminated sand and silt of Bed 3-F. (D) Bed 3-F, with an inclusion of coarse sand (red arrow), overlain by Bed 3-G till.

Bed 3-E (Figure 3.20B, C), 2.0 m thick, consists of 1.5 m of interstratified silt to very fine sand and diamict layers (lithofacies 3-E-1) overlain by 0.5 m of diamict (lithofacies 3-E-2). The bottom 1.0 m of layers of lithofacies 3-E-1 are notably more silty and stiffer than the overlying 0.5 m. There is an irregularly shaped lens of coarse sand cross-cutting the very fine sand with an irregular contact. Lithofacies 3-E-1 overlies Bed 3-D with a sharp, undulatory contact. Lithofacies 3-E-2 diamict is

massive, dark brown, highly overconsolidated, has a well-developed blocky structure with oxidation along joints, and contains steeply inclined silt-filled fractures. The alternating sand and diamict layers of Bed 3-E are interpreted to indicate periodic subaqueous slurries interrupting glaciolacustrine sedimentation.

Bed 3-F consists of 2.0 m of laminated, yellow-brown very fine sand to silt (Figure 3.20C, D), with 1–3% pebble-sized clasts that are subangular to subrounded. The upper 1.0 m contains small inclusions of both diamict and coarse sand. Bed 3-F is interpreted as a glaciolacustrine deposit, shifting from ice-distal to ice-proximal upsection indicative of an advancing ice margin. Bed 3-F overlies Bed 3-E, with a sharp horizontal contact.

Bed 3-G is a massive light yellow-brown (2.5Y 6/4) diamict (Figure 3.20D, Figure 3.21A), 0.2 m thick, that is overconsolidated, crumbly, and has a highly calcareous silty-sand matrix. Bed 3-G contains 20–30% clasts that are granule- to small pebble-sized and striated and/or faceted. One spread-unimodal clast fabric was measured from Bed 3-G and is interpreted to indicate shear stress during deposition was WSW (251°, Appendix G, Table 3). Bed 3-G clasts have high GR (L01: 72.7% HBB, 18.0% GR, 9.2% UGG; Appendix E, Table 5). Bed 3-G is interpreted as subglacial traction till. Bed 3-G overlies Bed 3-F, with a sharp horizontal contact.

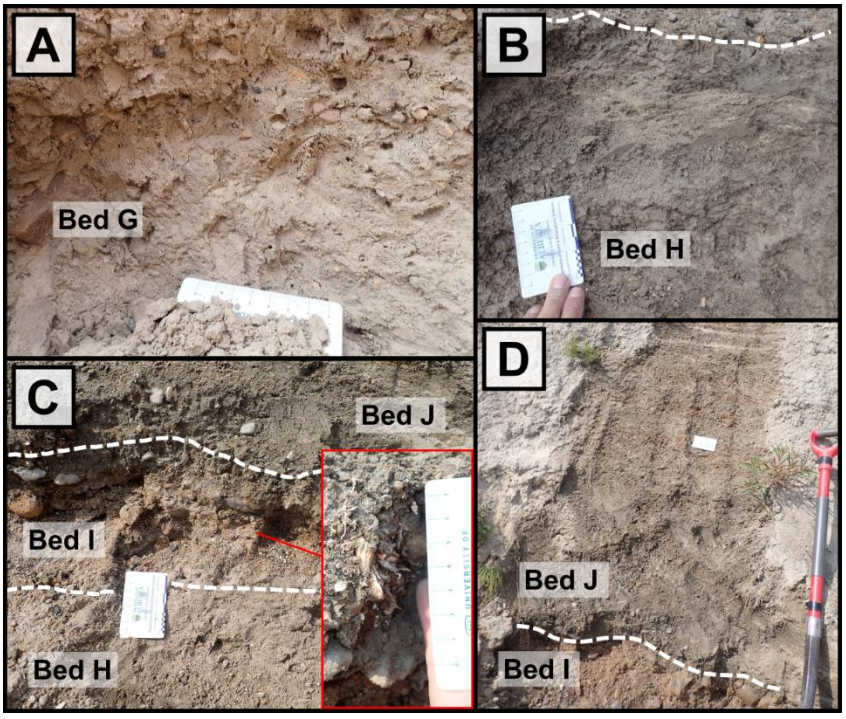


Figure 3.21: (A) Crumbly, yellow-brown till of Bed 3-G. (B) Laminated silt and clay of Bed 3-H. (C) Sand and gravel of Bed 3-I, containing bivalve shells (red). (D) Massive brown silt of Bed 3-J, containing some fine sand laminations.

Bed 3-H (Figure 3.21B), 0.44 m thick, consists of 0.1 m of massive silty clay (lithofacies 3-H-1), overlain by 0.04 m of contorted silt (lithofacies 3-H-2), which is then overlain by 0.3 m of laminated silt and clay (lithofacies 3-H-3). Lithofacies 3-H-1 contains about 10% pebble-sized clasts and sharply overlies Bed 3-G with a horizontal contact. Lithofacies 3-H-2 sharply overlies lithofacies 3-H-1 horizontally. Lithofacies 3-H-3 is thinly laminated (1–3 mm) and overlies lithofacies 3-H-2 with a sharp horizontal contact. Bed 3-H is interpreted as a deep-water glaciolacustrine deposit.

Bed 3-I (Figure 3.21C), 0.2 m thick, consists of 0.1 m of moderately sorted medium sand with 15% pebble-sized clasts, conformably overlain by 0.1 m of moderately sorted very coarse sand with 30–40% pebble-sized clasts. Both beds contained *Hiatella arctica* and *Mya truncata* in growth position. The sampled paired *Hiatella arctica* returned a conventional radiocarbon age of 7700 ± 25 ^{14}C years BP (UOC-23328; Appendix F). Bed 3-I is interpreted as a postglacial marine deposit (Tyrrell Sea sediments). Bed 3-I overlies Bed 3-H, with a sharp horizontal contact.

The uppermost observed Bed 3-J is a massive brown silt (Figure 3.21D), 1.6 m thick, that contains a few fine sand laminations and rare *Hiatella arctica*. The lowermost 0.1 m of Bed 3-J contains 20% pebble-sized clasts and common shells (including *Hiatella arctica* specimens, other clams, and barnacles). Bed 3-J is interpreted as a postglacial marine deposit formed in an offshore marine environment. Bed 3-J overlies Bed 3-I, with a sharp horizontal contact.

About 1.0 m of sediments lie between Bed 3-J and the overlying modern peat, which were inaccessible due to safety concerns.

3.3.3.3 Section 115-23-004, Gods River

At section 115-23-004 along Gods River, approximately 4.5 m of sediments were exposed at the base of the northern cut bank, across two exposures located ~15 m apart, designated as Exposure-1 and Exposure-2 (Figure 3.22). Section 115-23-004 is only ~100 m southwest of section 115-23-002 yet exposes sub-till sediments not observed at 002 (presumably covered by colluvium). This site contains 3 stratigraphic beds: 2 diamicts interpreted as till (of which, one sample was taken), and 1 sub-till sorted sediment package (Figure 3.23).

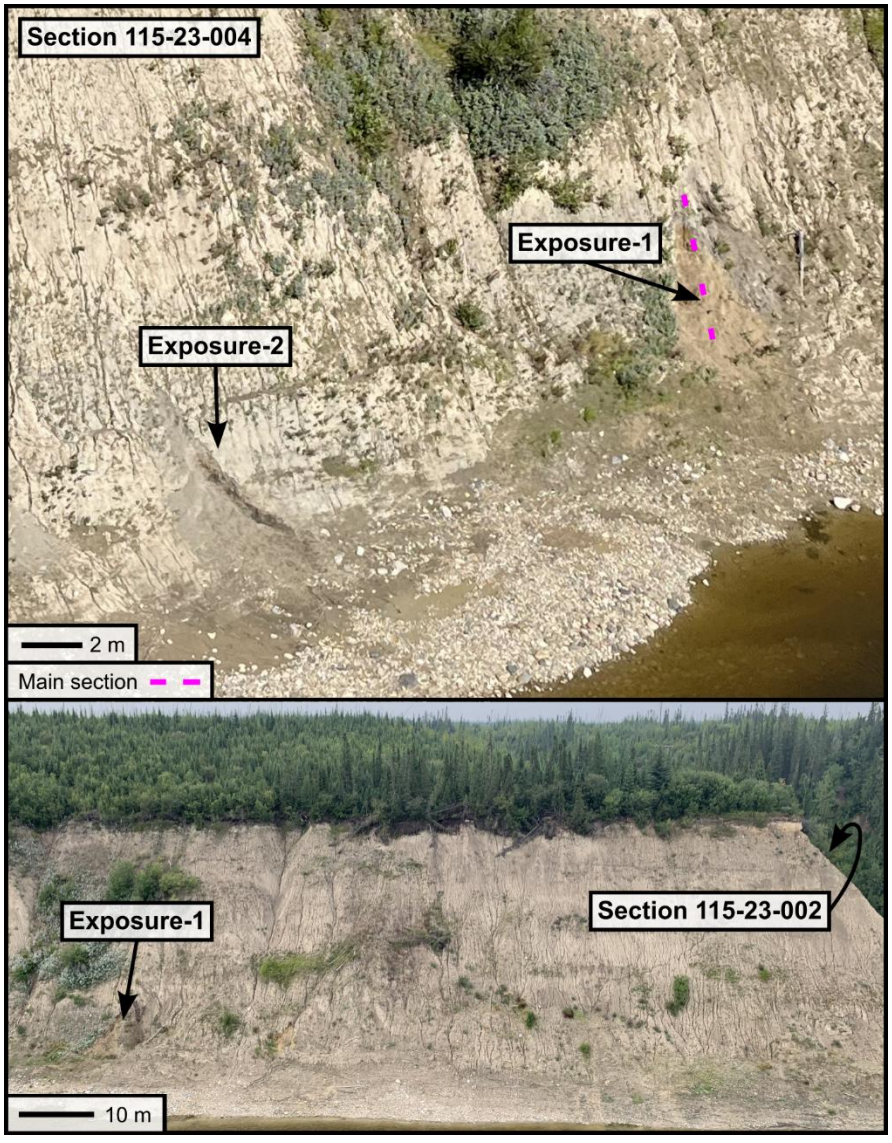


Figure 3.22: Overview of section 115-23-004, which is situated only ~100 m from section 115-23-002. View is towards the north.

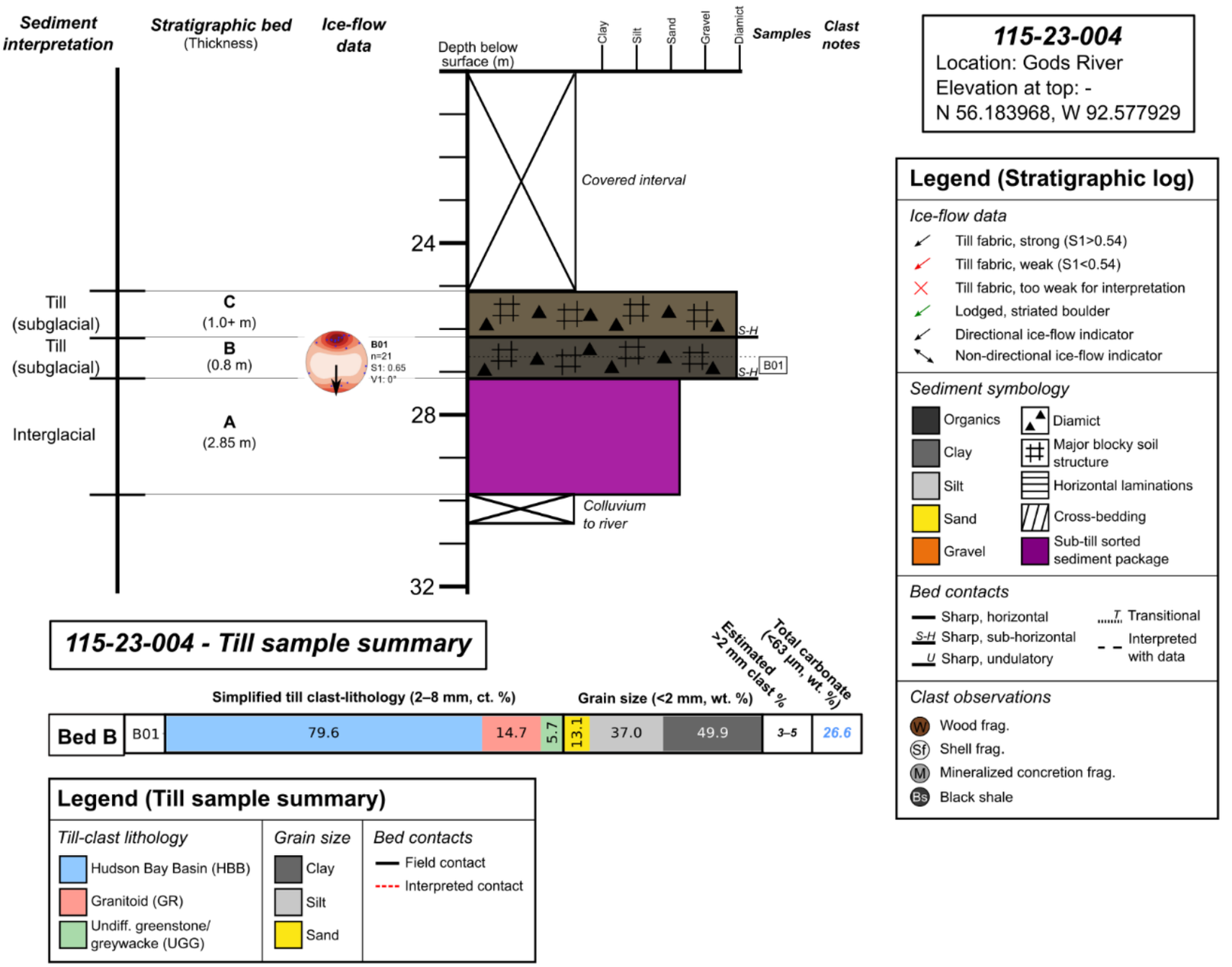


Figure 3.23: Stratigraphic log and simplified till sample data for section 115-23-004. Diamict beds are coloured by their sampled Munsell colour. Abbreviations: asl, above sea level; frag., fragment; HBB, Hudson Bay Basin; GR, granitoid; UGG, undifferentiated greenstone and greywacke.

The lowermost Bed 4-A is a sub-till sorted sediment package, exposed in two places along the section (Exposure-1 and Exposure-2). The correlation is based on their shared upper contact with Bed 4-B. Bed 4-A is interpreted as a lacustrine or marine deposit, including intervals formed under anoxic conditions, as suggested by the blue-gray (gleyed) silty clay of lithofacies 4-A-2-1. Furthermore, Bed 4-A is interpreted to be deposited at the onset of a glaciation, with evidence of an advancing ice margin indicated by the mixture of diamict and sand (lithofacies 4-A-1-6; see below).

At Exposure-1 (Figure 3.24: stratigraphic log; Figure 3.25: photos), Bed 4-A consists of at least 2.85 m of sediment across six lithofacies. It begins with at least 0.1 m of massive, dark brown silt (lithofacies 4-A-1-1). This is sharply overlain by 0.2 m of massive, fine to medium sand (lithofacies 4-A-1-2). Above this lies 0.4 m of medium sand and silt with inclined bedding (lithofacies 4-A-1-3) with a sharp contact. Overlying this is 1.1 m of massive, dark brown silt (lithofacies 4-A-1-4), which is highly overconsolidated, has a well-developed blocky structure with oxidation along joints, and contains minor, laterally discontinuous medium sand lenses less than 1 cm thick. Lithofacies 4-A-1-3 transitions into lithofacies 4-A-1-4. It is followed by 0.6 m of horizontally bedded medium sand and silt (lithofacies 4-A-1-5), where silt beds become less prominent and thinner upsection, while sand beds become more prominent and thicker; sand beds are approximately 1 cm thick at the base and up to 8 cm thick at the top. Finally, 0.45 m of mixed diamict and medium sand with no clear bedding (lithofacies 4-A-1-6) overlies lithofacies 4-A-1-5, with a transitional contact.

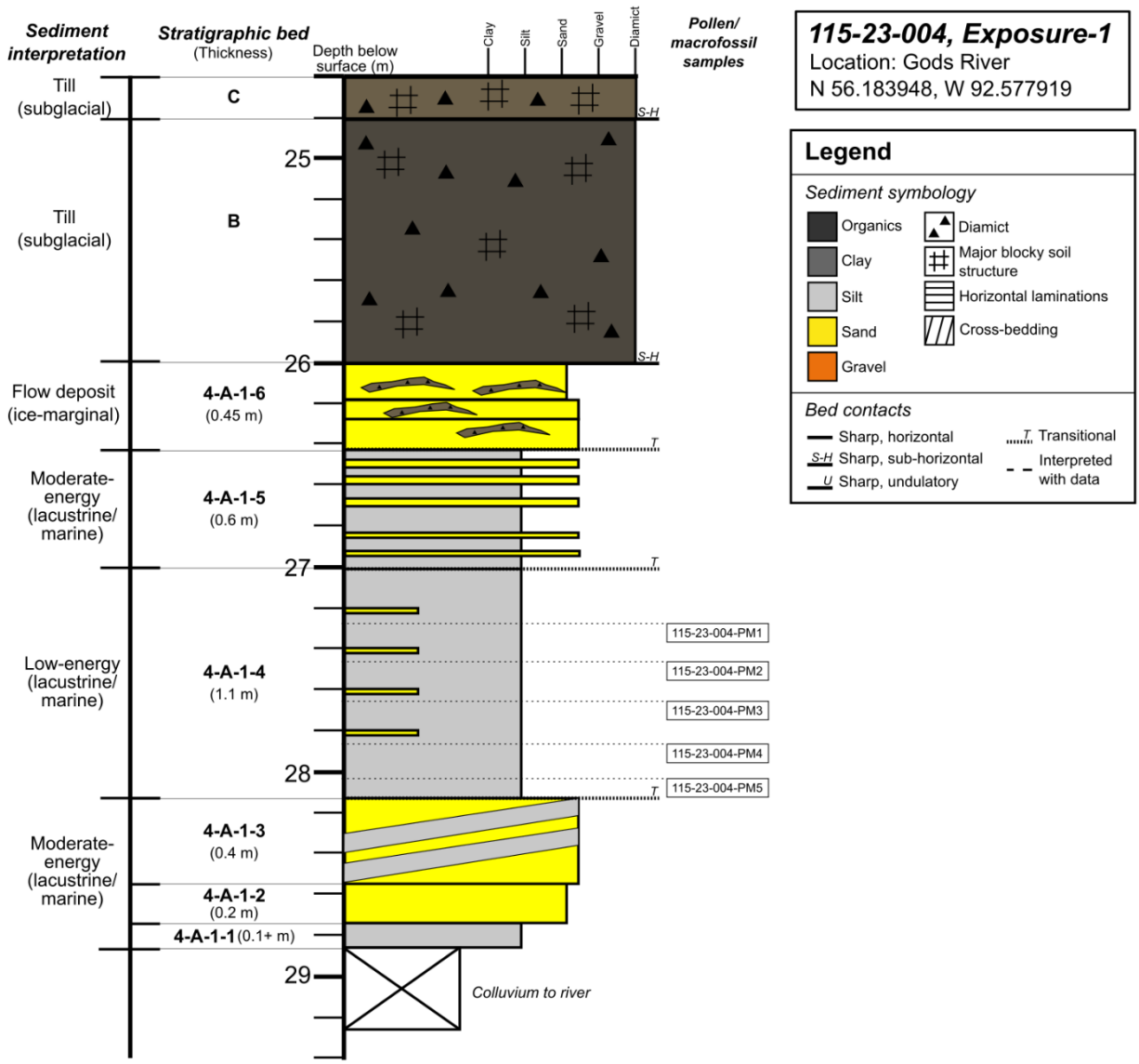


Figure 3.24: Stratigraphic log for Exposure-1 of Section 115-23-004. Diamict beds are coloured by their sampled Munsell colour.

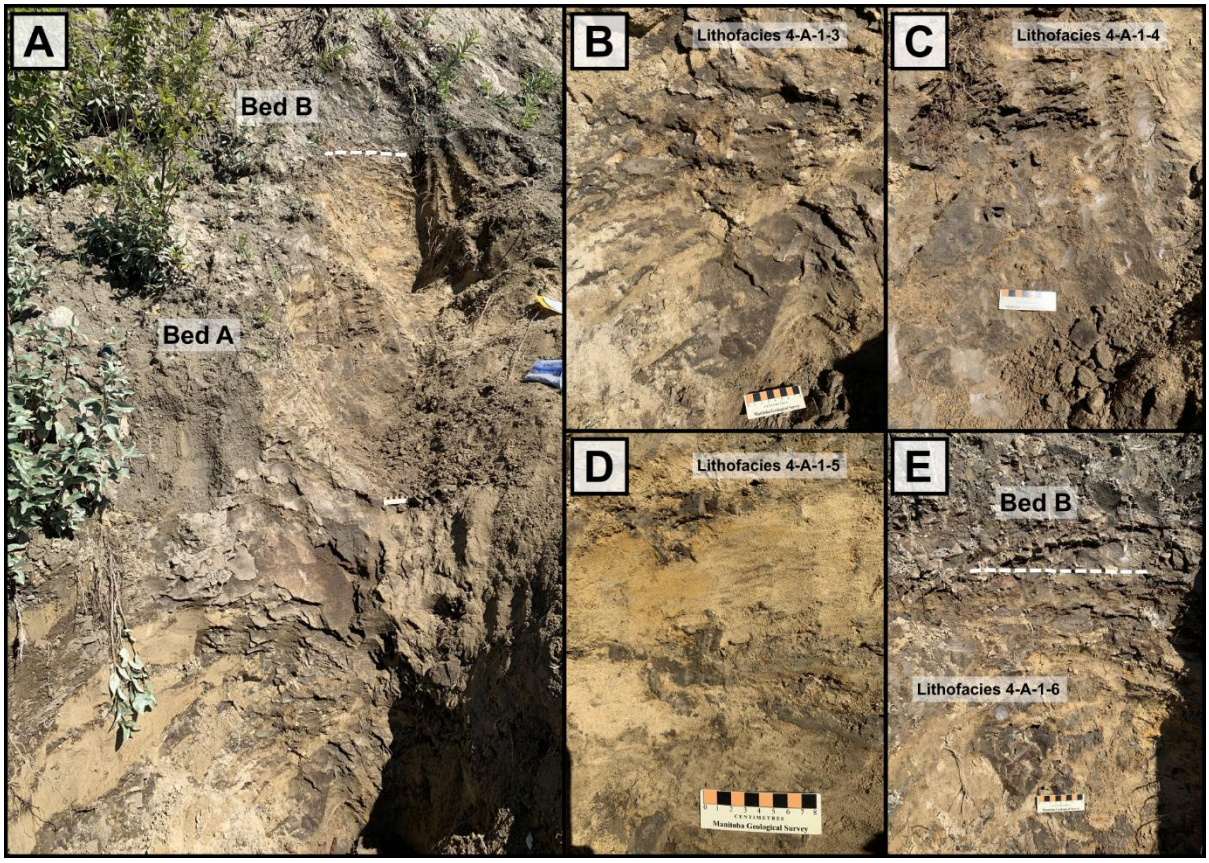


Figure 3.25: The stratigraphic sequence at Exposure-1 of Section 115-23-004, including: (A) Overview of Exposure-1; (B) sand and silt with inclined bedding of lithofacies 4-A-1-3; (C) massive, dark brown silt of lithofacies 4-A-1-4; (D) horizontally bedded sand and silt of lithofacies 4-A-1-5; and (E) mixed diamict and sand of lithofacies 4-A-1-6, underlying Bed 4-B.

At Exposure-2 (Figure 3.26: stratigraphic log; Figure 3.27: photos), Bed 4-A consists of at least 2.4 m of sediment across 2 lithofacies. It begins with at least 2.0 m of massive, blue-gray (gleyed) silty clay (lithofacies 4-A-2-1), which is highly overconsolidated, has a well-developed blocky structure with oxidation along joints, and contains no clasts. Four samples were collected from Bed 4-A for paleomagnetic analysis. The results show normal polarity, indicating that these sediments likely postdate the Brunhes-Matuyama reversal (Mazzaferro, 2025). This is sharply overlain by 0.4 m of massive, dark brown silt (lithofacies 4-A-2-2), which is also highly overconsolidated, has a well-developed blocky structure with oxidation along joints, and contains no clasts.

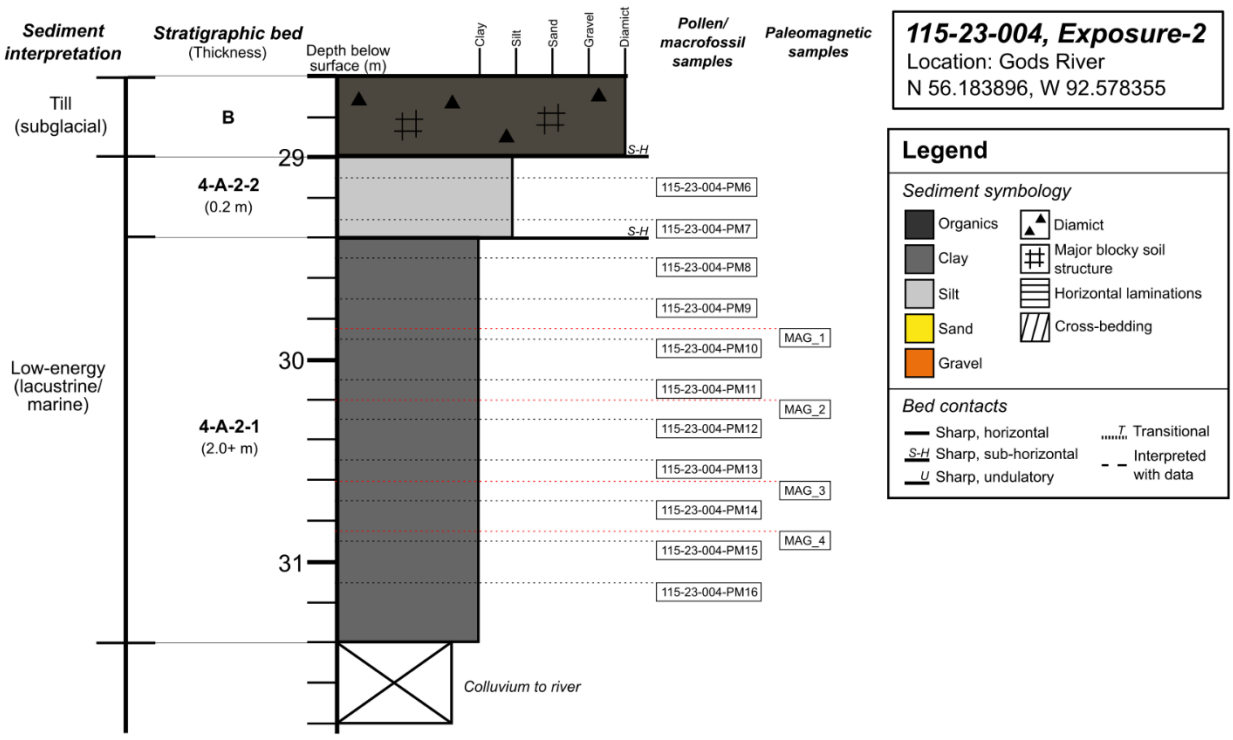


Figure 3.26: Stratigraphic log for Exposure-2 of Section 115-23-004. Diamict beds are coloured by their sampled Munsell colour.

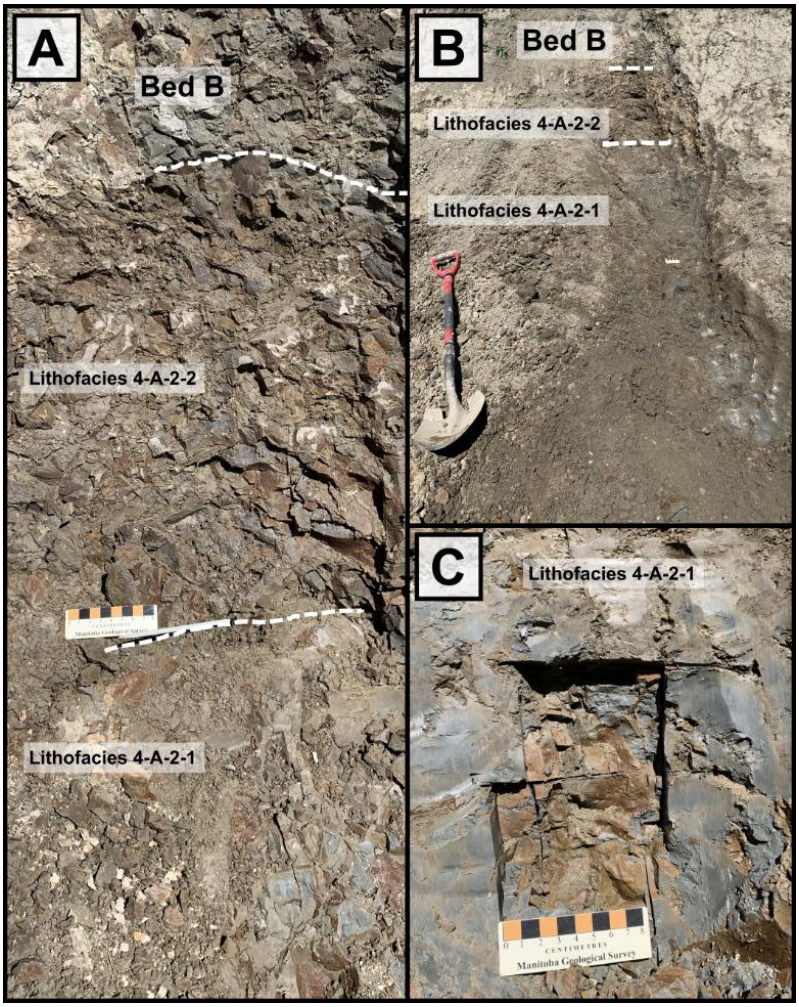


Figure 3.27: The stratigraphic sequence at Exposure-2 of Section 115-23-004, including: (A) Close-up of beds 4-A and 4-B; (B) overview of Exposure-2; and (C) blue-grey clay of lithofacies 4-A-2-1, sampled for paleomagnetic analysis.

Bed 4-B is a massive very dark grey (2.5Y 3/1) diamict with a blue-grey appearance (Figure 3.28) that is 0.8 m thick, highly overconsolidated, has a weakly calcareous silty-clay matrix, has a well-developed blocky structure with oxidation along joints, contains 3–5% striated and/or faceted clasts that are granule- to large pebble-sized, and smells of sulphur. One unimodal clast fabric was measured from Bed 4-B and are interpreted to indicate shear stress was S (180°, Appendix G, Table 3). Bed 4-B clasts have moderate concentrations of all three simplified lithology categories (B01: 79.6% HBB, 14.7% GR, 5.7% UGG; Appendix E, Table 5). Bed 4-B is interpreted as subglacial traction till. Bed 4-B overlies Bed 4-A, with a sharp sub-horizontal contact.

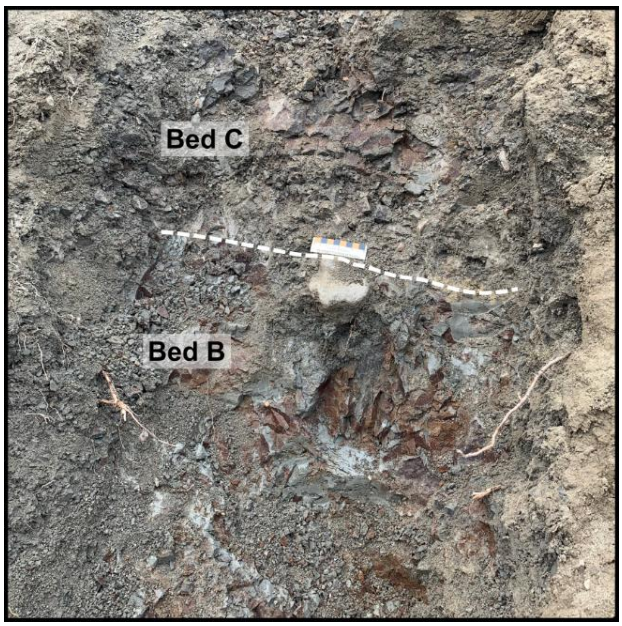


Figure 3.28: The blue-grey till of Bed 4-B underlies the dark grey brown diamict of Bed 4-C.

Bed 4-C is a massive dark grey brown diamict (Figure 3.28), at least 1.0 m thick, that is highly overconsolidated, has a well-developed blocky structure with oxidation along joints, and contains 10–15% striated and/or faceted clasts that are granule- to pebble-sized clasts. Bed 4-C is interpreted as subglacial traction till. Bed 4-C overlies Bed 4-B, with a sharp sub-horizontal contact.

3.3.3.4 Section 115-23-005, Gods River

This 20-m-high section (Figure 3.29) extends about 100 m along a northern cut bank of the Gods River. It contains 7 stratigraphic beds: 3 diamicts interpreted as till, 3 sorted sediments, and 1 sub-till sorted sediment package (Figure 3.30). Across the 4 till beds and sub-beds, 9 samples were collected (Figure 3.31).

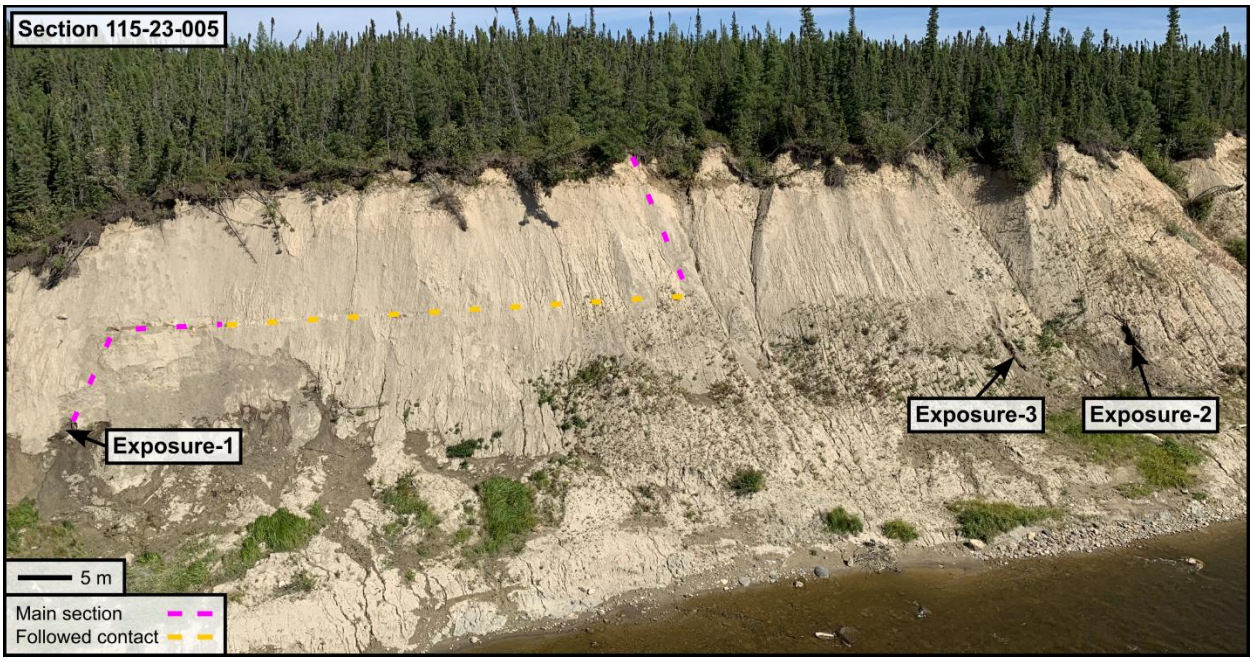


Figure 3.29: Overview of section 115-23-005, viewed towards the northeast.

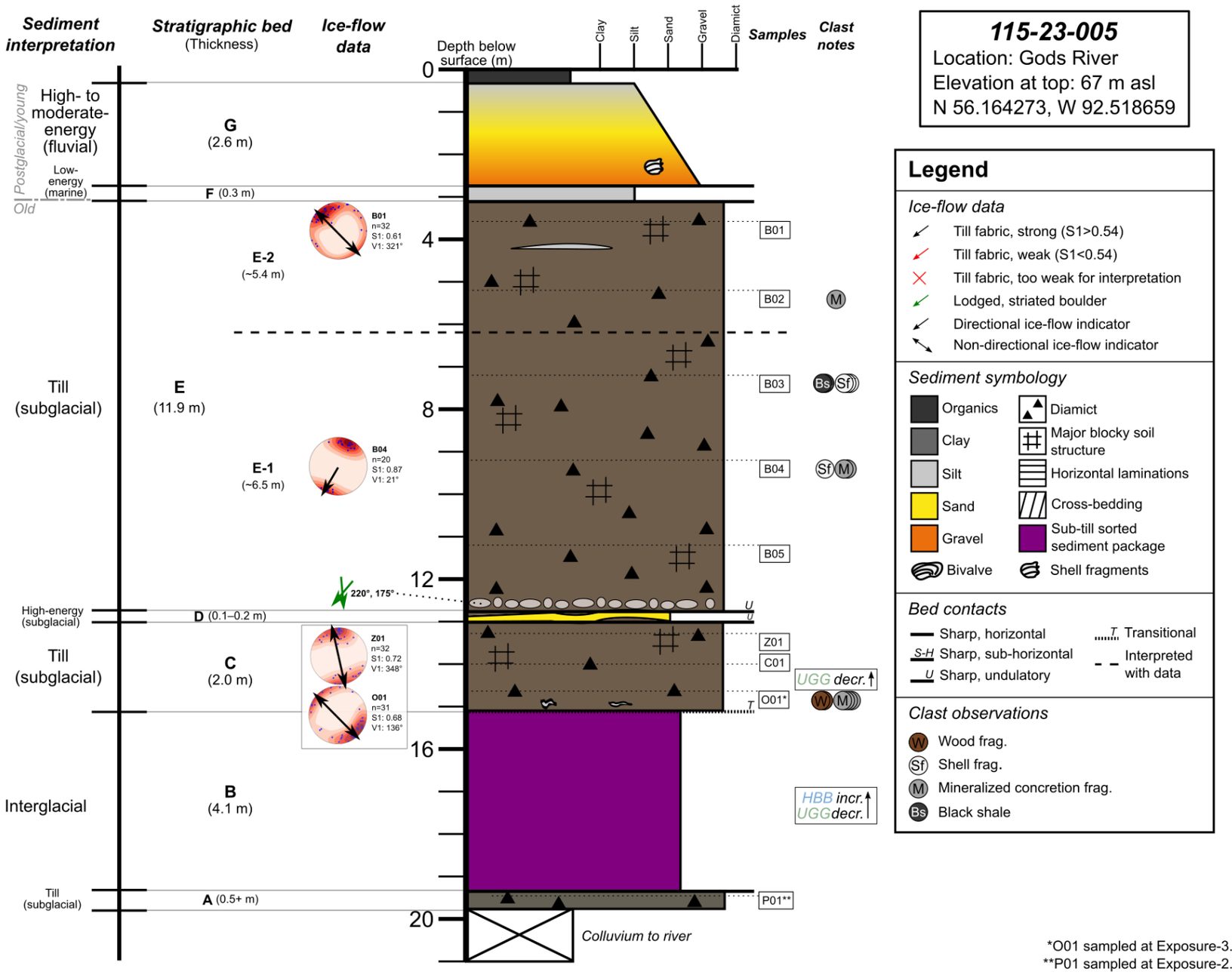


Figure 3.30: Stratigraphic log of section 115-23-005. Diamict beds are coloured by their sampled Munsell colour. Abbreviations: asl, above sea level; frag., fragment; HBB, Hudson Bay Basin; GR, granitoid; UGG, undifferentiated greenstone and greywacke.

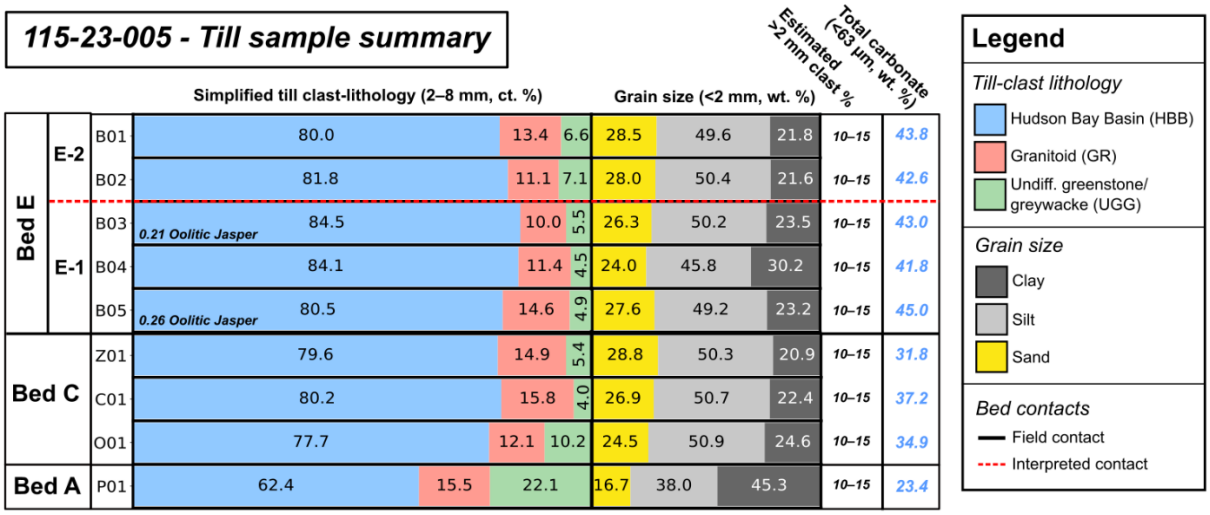


Figure 3.31: Summary of till sample data for section 115-23-005. Abbreviations: ct., count, wt., weight.

The lowermost Bed 5-A is a massive dark grey (5Y 4/1) diamict, at least 0.5 m thick, that is highly overconsolidated, has a weakly calcareous sandy silty-clay matrix, has a weakly-developed blocky structure with minor oxidation along joints, and contains 10–15% striated and/or faceted clasts that are granule- to small pebble-sized. Bed 5-A clasts have very low HBB and very high GR (P01: 62.4% HBB, 15.5% GR, 22.1% UGG; Appendix E, Table 5). Bed 5-A is interpreted as subglacial traction till.

Bed 5-B consists of sub-till sorted sediments across three exposures, designated as Exposure-1, Exposure-2, and Exposure-3, correlated based on their shared upper contact with Bed 5-C. The presence of organics in sub-till Bed 5-B indicates deposition in an interglacial. Bed 5-B overlies Bed 5-A with a sharp horizontal contact at each exposure.

At Exposure-1 (Figure 3.32: stratigraphic log; Figure 3.33: photos), Bed 5-B consists of 0.75 m of sediment across 3 lithofacies. It begins with 0.4 m of organic-bearing, poorly sorted gravel (lithofacies 5-B-1-1), which contains granule- to large pebble-sized clasts and large wood fragments up to 15 cm long. Overlying this is 0.05 m of matted organics (lithofacies 5-B-1-2), composed of compressed plant material including large wood pieces up to 20 cm in length. Finally, above the organics is 0.3 m of blue-grey silt (lithofacies 5-B-1-3), containing about 3% granule- to large pebble-sized clasts, as well as organic-rich lenses and minor diamict inclusions. All contacts are sharp and horizontal.

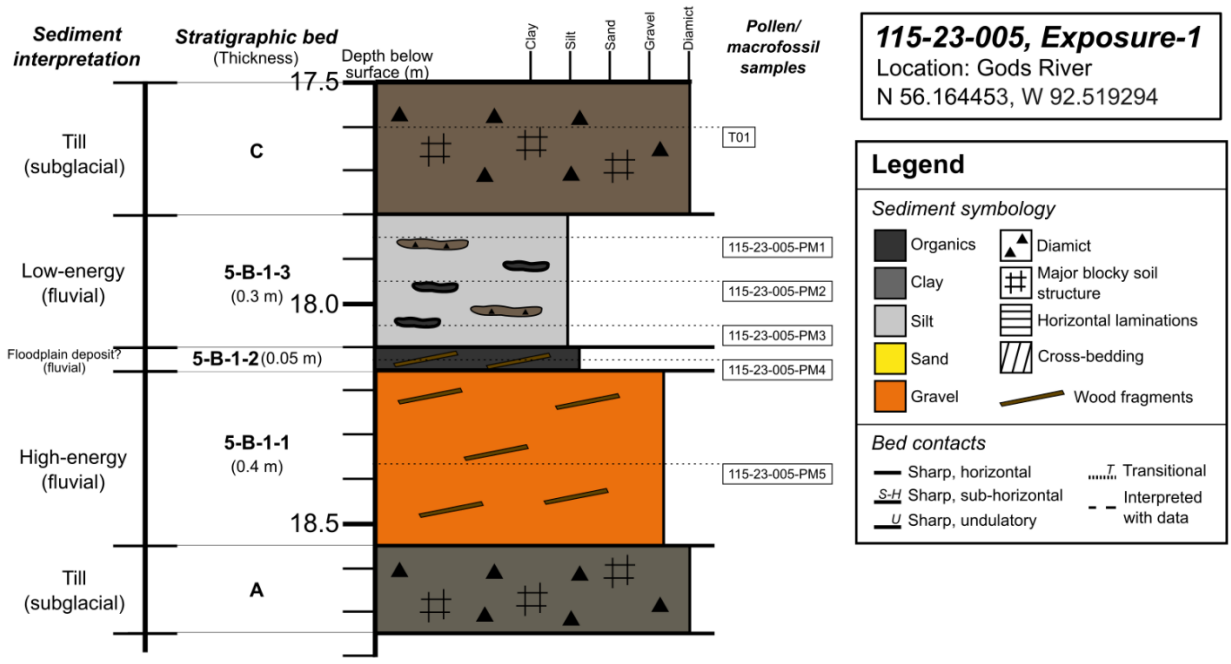


Figure 3.32: Stratigraphic log for Exposure-1 of Section 115-23-005. Diamict beds are coloured by their sampled Munsell colour.

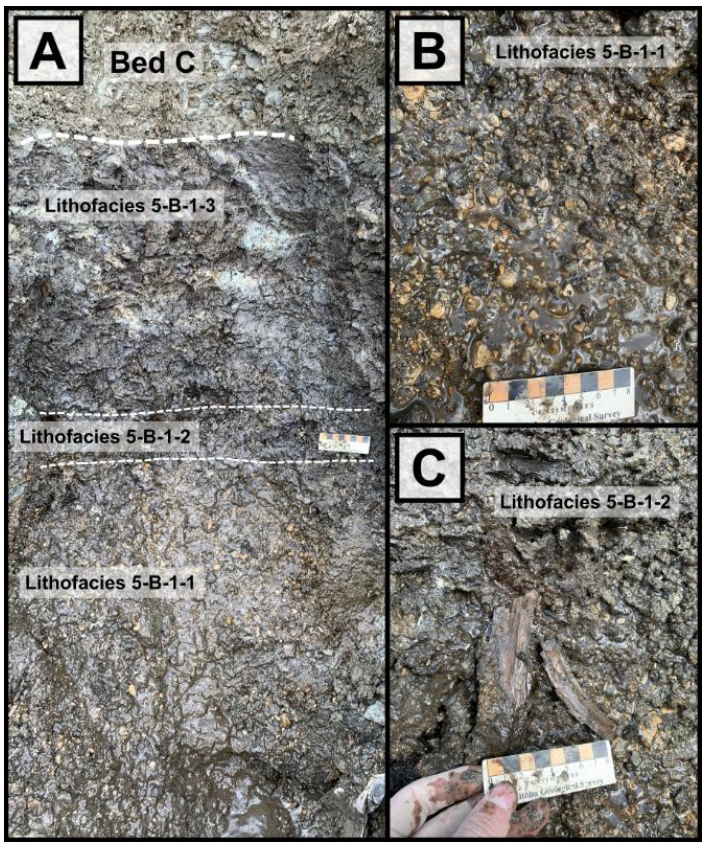


Figure 3.33: (A) The stratigraphic sequence at Exposure-1 of Section 115-23-005, including organic-bearing gravel (5-B-1-1), matted organics (5-B-1-2), and blue-grey silt (5-B-1-3). (B) Seeping gravel of lithofacies 5-B-1-1. (C) A 10 cm-long wood fragment extracted from lithofacies 5-B-1-2.

At Exposure-2 (Figure 3.34: stratigraphic log; Figure 3.35: photos), Bed 5-B consists of 2.4 m of sediment across 7 lithofacies. It begins with 0.05 m of poorly sorted, blue-grey gravel (lithofacies 5-B-2-1), predominantly composed of carbonate clasts in a fine to medium sand matrix. This is overlain by 0.4 m of organic-rich, moderately sorted silty fine sand with weak horizontal bedding (lithofacies 5-B-2-2). Above this is 0.15 m of poorly sorted sandy gravel (lithofacies 5-B-2-3), matrix- to clast-supported and containing granule- to large pebble-sized clasts with wood fragments. Next is 0.1 m of massive brown silt (lithofacies 5-B-2-4), followed by 0.15 m of additional sandy gravel (lithofacies 5-B-2-5), also matrix- to clast-supported and rich in coarse clasts and wood. Overlying this is 1.05 m of moderately to well-sorted, horizontal sand laminations (lithofacies 5-B-2-6), interbedded with organic-rich laminae. This interval contains minor normal faults, and a large transported coniferous log greater than 50 cm long and 30–40 cm wide, dated at >45500 ^{14}C years BP (conventional; UOC-26756; Appendix F). Finally, 0.5 m of highly overconsolidated blue-grey diamict (lithofacies 5-B-2-7) caps the exposure. This diamict has a

clayey-silt matrix, minor oxidation along joints, and contains ~5% carbonate clasts and some organic-bearing lenses. All contacts are sharp and horizontal.

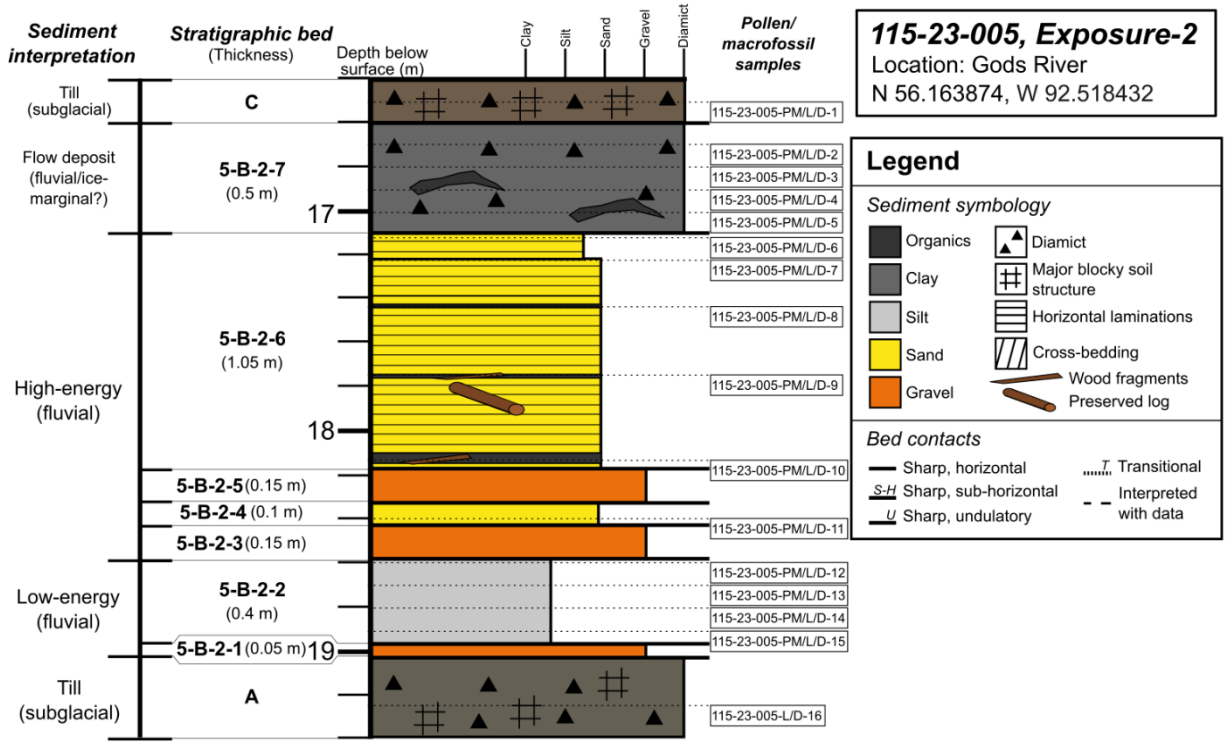


Figure 3.34: Stratigraphic log for Exposure-2 of Section 115-23-005. Diamict beds are coloured by their sampled Munsell colour, except for lithofacies 5-B-2-7 (not sampled but observed to be blue-gray).

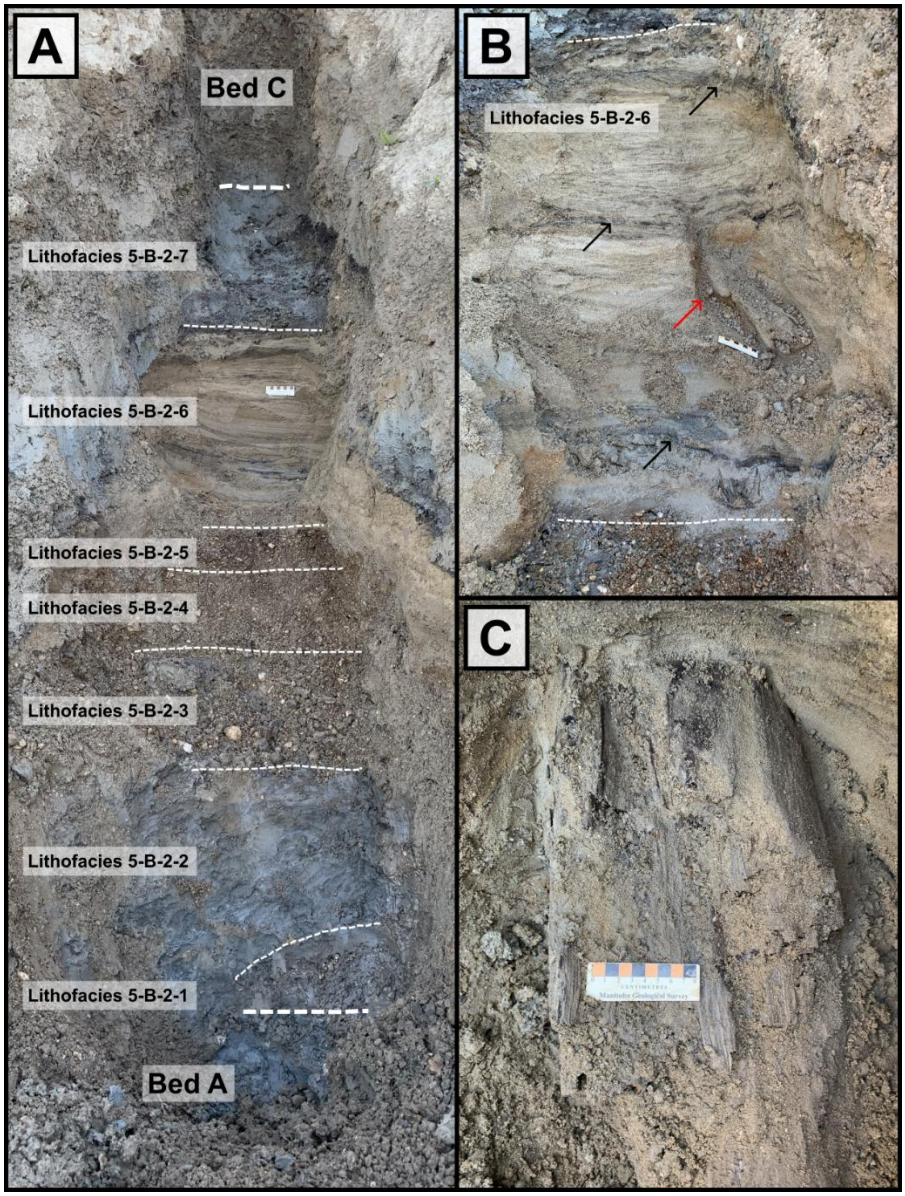


Figure 3.35: (A) The stratigraphic sequence at Exposure-2 of Section 115-23-005. (B) Horizontally bedded sand of lithofacies 5-B-2-6, containing organic-rich layers (black arrows) and a large coniferous log (red arrow, enlarged in (C)).

At Exposure-3 (Figure 3.36: stratigraphic log; Figure 3.37: photos), Bed 5-B consists of 3.5 m of sediment across 6 lithofacies. It begins with 0.4 m of compact, blue-grey clay (lithofacies 5-B-3-1) containing minor oxidation and 1% small pebbles. This is followed by 0.2 m of poorly sorted gravel (lithofacies 5-B-3-2) with pebble-sized clasts and wood fragments in a fine to very coarse sand matrix. Above this is 0.25 m of massive, organic-rich silt (lithofacies 5-B-3-3), which contains finger-thick twigs near its base. This is overlain by 0.8 m of poorly sorted gravel (lithofacies 5-B-3-4) with similar composition and two thin wood mats located at 0.25 m and 0.65 m from the top. Above the gravel lies

1.25 m of horizontally bedded fine to medium sand (lithofacies 5-B-3-5), containing minor organic-rich silt laminations. The thickness of individual sand beds decreases upward, from 7–15 cm at the base to 3–5 cm at the top. Capping this sequence is 1.2 m of massive, organic-rich dark brown silt (lithofacies 5-B-3-6), which contains rare wood fragments and twigs near the top. All contacts are sharp and horizontal.

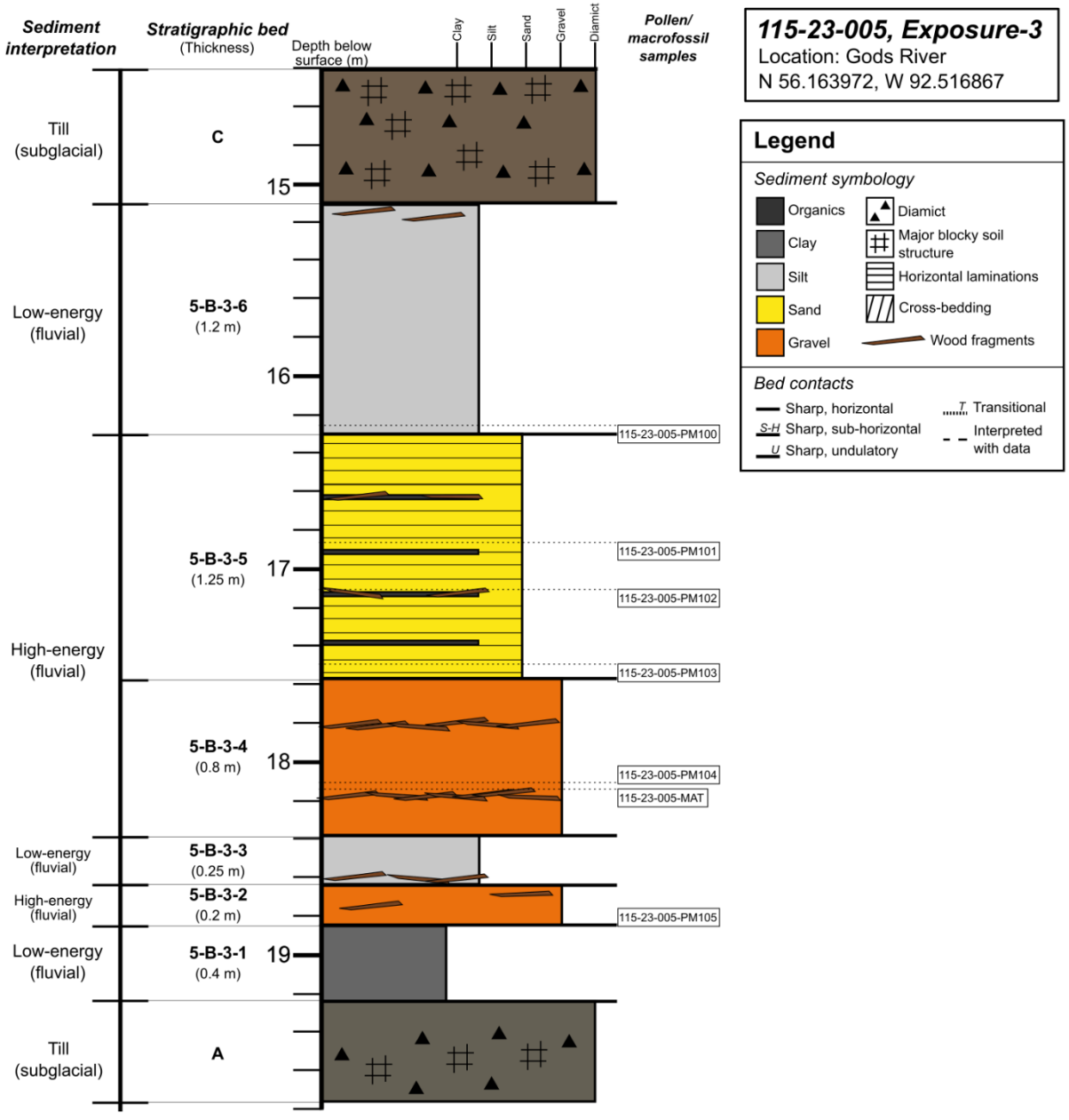


Figure 3.36: Stratigraphic log for Exposure-3 of Section 115-23-005. Diamict beds are coloured by their sampled Munsell colour.

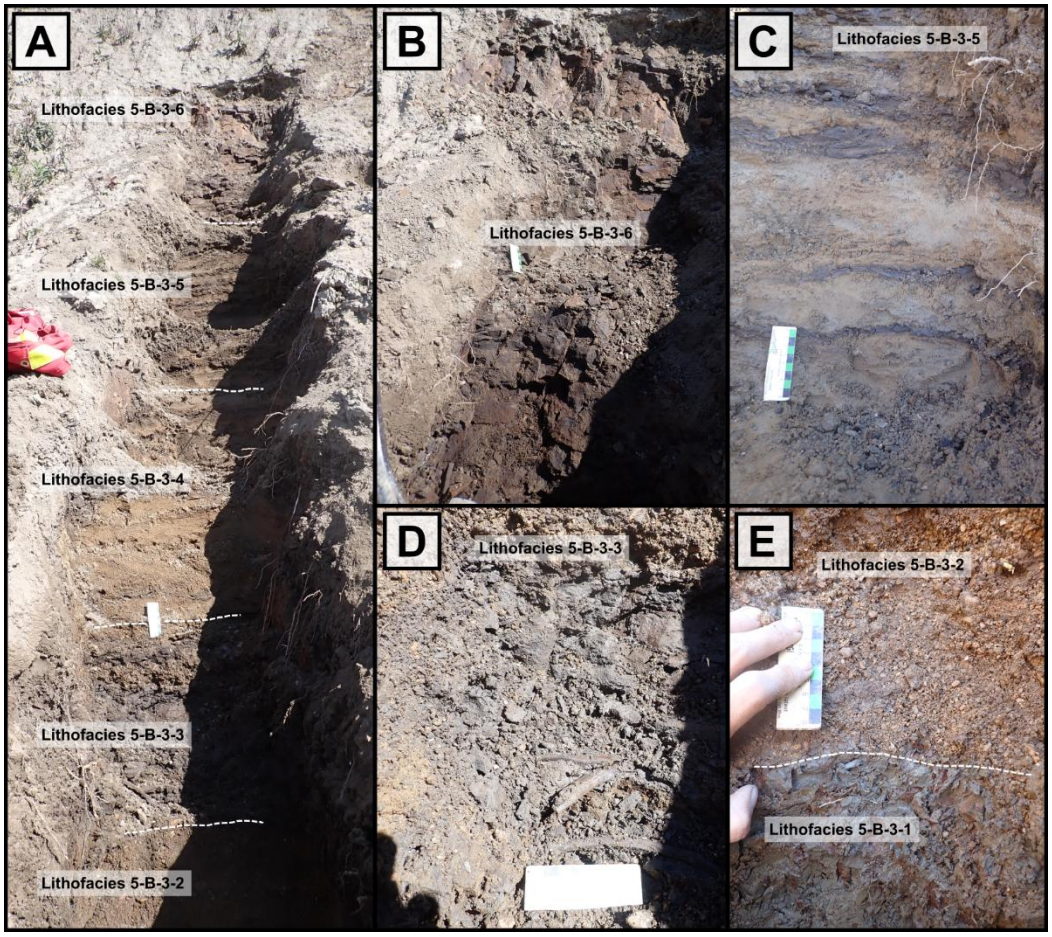


Figure 3.37: (A) The stratigraphic sequence of Bed 5-B at Exposure-3 of Section 115-23-005. (B) Massive, organic-rich brown silt of lithofacies 5-B-3-6. (C) Horizontally interbedded sand and organic silt of lithofacies 5-B-3-5. (D) Massive, organic-rich silt of lithofacies 5-B-3-3, containing wood fragments. (E) Gravel of lithofacies 5-B-3-2 overlies the blue-grey clay of lithofacies 5-B-3-1.

Bed 5-C is a massive diamict (Figure 3.38A, B), 2.0 m thick, that ranges in colour from very dark grey brown (10YR 3/2) to grey brown (10YR 4/2), is highly overconsolidated, has a weakly to moderately calcareous sandy clayey-silt to clayey sandy-silt matrix, has a well-developed blocky structure with oxidation along joints, and contains 10–15% striated and/or faceted subangular to subrounded clasts that are granule- to small cobble-sized. Two spread-unimodal clast fabrics were measured from Bed 5-C and are interpreted to indicate shear stress was SSE-NNW to SE-NW (168-348°, 136-316°, Appendix G, Table 3). Bed 5-C clasts have low to moderate UGG (O01–Z01 (n=3): 77.7–80.2% HBB, 12.1–15.8% GR, 4.0–10.2% UGG; Appendix E, Table 5). Notably, there is a decrease in UGG clast concentration from O01 to C01 (6.2%; Figure 3.31). Additionally, there is a 15.3% increase in HBB concentration and an 11.9% decrease in UGG concentration from Bed 5-A (below) to the base of Bed 5-C (Figure 3.31).

Bed 5-C is interpreted as subglacial traction till. Bed 5-C overlies Bed 5-B, with a transitional contact, about 5 cm, with some rip-up clasts of underlying silt and wood fragments at its base.

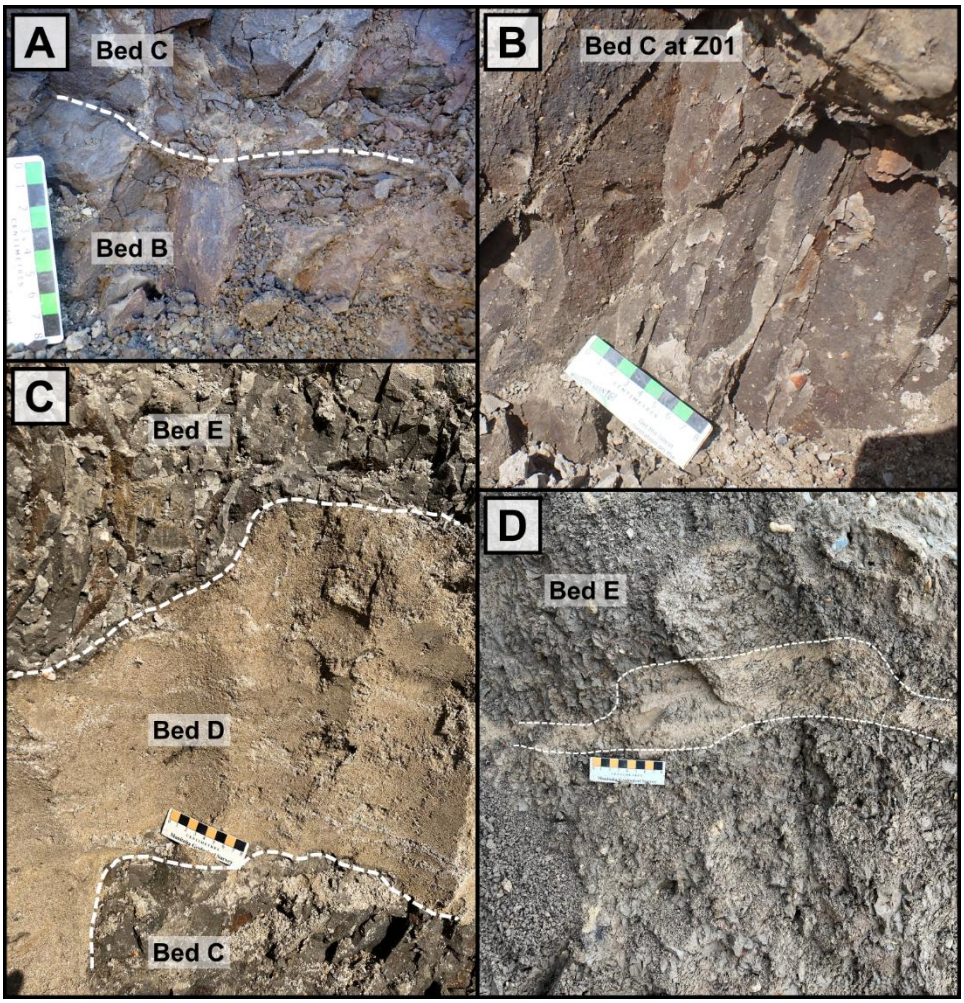


Figure 3.38: (A) Bed 5-C till overlying Bed 5-B silt at Exposure-3. (B) Gray brown till of Bed 5-C. (C) Massive coarse to medium sand of Bed 5-D, with undulatory contacts to overlying and underlying beds. (D) Gray brown till of Bed 5-E with a tan sand-silt lens (outlined).

Bed 5-D consists of 0.1–0.2 m of massive, medium to coarse sand (Figure 3.38C). Bed 5-D is interpreted as a subglacial deposit. Bed 5-D overlies Bed 5-C, with a sharp, undulatory lower contact.

Bed 5-E is a massive gray brown (10YR 4/2) diamict (Figure 3.38C, D), 11.9 m thick, that is highly overconsolidated, has a moderately calcareous sandy clayey-silt to clayey sandy-silt matrix, has a well-developed blocky structure with oxidation along joints. Bed 5-E contains 10–15% striated and/or faceted clasts that are granule- to small cobble-sized. Bed 5-E contains a boulder bed 0.2 m above its base, consisting of cobble- to boulder-sized clasts. Bed 5-E also contains a sandy silt lens, 3 cm thick, 1 m below its upper contact. Paleo-ice flow indicators measured from Bed 5-E suggest a shifting shear stress

during deposition. One spread unimodal clast fabric and the orientation of two lodged boulders were measured from Bed 5-E, are interpreted to indicate shear stress was SSW (201°, 220°, 175°, Appendix G, Table 3, Table 2). Another spread unimodal clast fabric is interpreted to indicate shear stress changed to SE-NW upsection (141-321°, Appendix G, Table 3). As such, Bed 5-E is separated into Bed 5-E-1 (~6.5 m thick, SSW fabric) and Bed 5-E-2 (~5.4 m thick, SE-NW fabric) based on the possibility of a 120° change in interpreted ice-flow direction. Bed 5-E-1 clasts have moderate to high HBB, moderate to low GR, and low UGG (B05–B03 (n=3): 80.5–84.5% HBB, 10.0–14.6% GR, 4.5–5.5% UGG; Appendix E, Table 5) with some oolitic jasper clasts present. Bed 5-E-2 clasts have moderate to high HBB (B02, B01: 80.0–81.8% HBB, 11.1–13.4% GR, 6.6–7.1% UGG; Appendix E, Table 5). Bed 5-E is interpreted as subglacial traction till. Bed 5-E overlies Bed 5-D, with a sharp undulatory lower contact.

Bed 5-F consists of alternating-coloured layers of silt, including red-brown, gray, and brown layers (Figure 3.39A). Bed 5-F is interpreted as a post-glacial marine deposit. Bed 5-F overlies Bed 5-E, with a sharp horizontal contact.

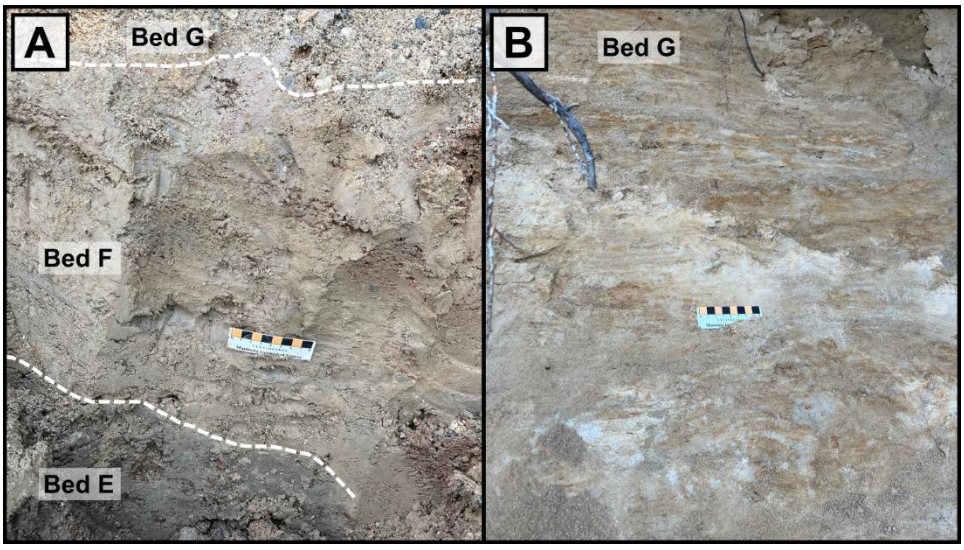


Figure 3.39: (A) Bed 5-G gravel overlies the multicoloured silt of Bed 5-F, which in turn overlies Bed 5-E till. (B) Texturally bedded coarse sand to silty sand of bed 5-G.

Bed 5-G consists of texturally bedded silty-sand to coarse sand and gravel that is fining upwards (Figure 3.39B). The lowermost 0.2 m of Bed 5-G is a layer of poorly sorted sandy gravel, containing granule-medium sized cobbles and rare shell fragments. Bed 5-G overlies Bed 5-F, with a sharp horizontal contact. Bed 5-G is interpreted as a fluvial channel deposit based on the moderate sorting and fining-upwards sequence. Bed 5-G is overlain by modern peat.

3.3.3.5 Section 115-23-006, Yakaw River

This 18-m-high section (Figure 3.40) extends about 25 m along a northern cut bank of the meandering Yakaw River. It contains 8 stratigraphic beds: 4 are diamicts interpreted as till, and 4 are sorted sediments (Figure 3.41). Across the 5 till beds and sub-beds, 7 samples were collected (Figure 3.42).

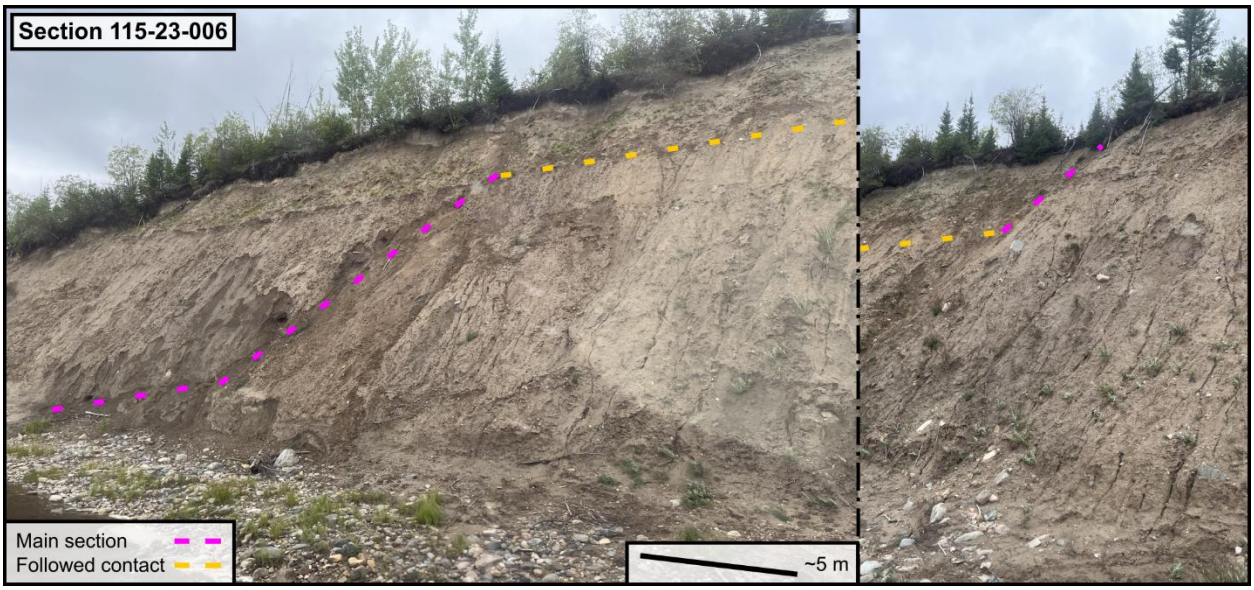


Figure 3.40: Overview of section 115-23-006, viewed towards the northwest.

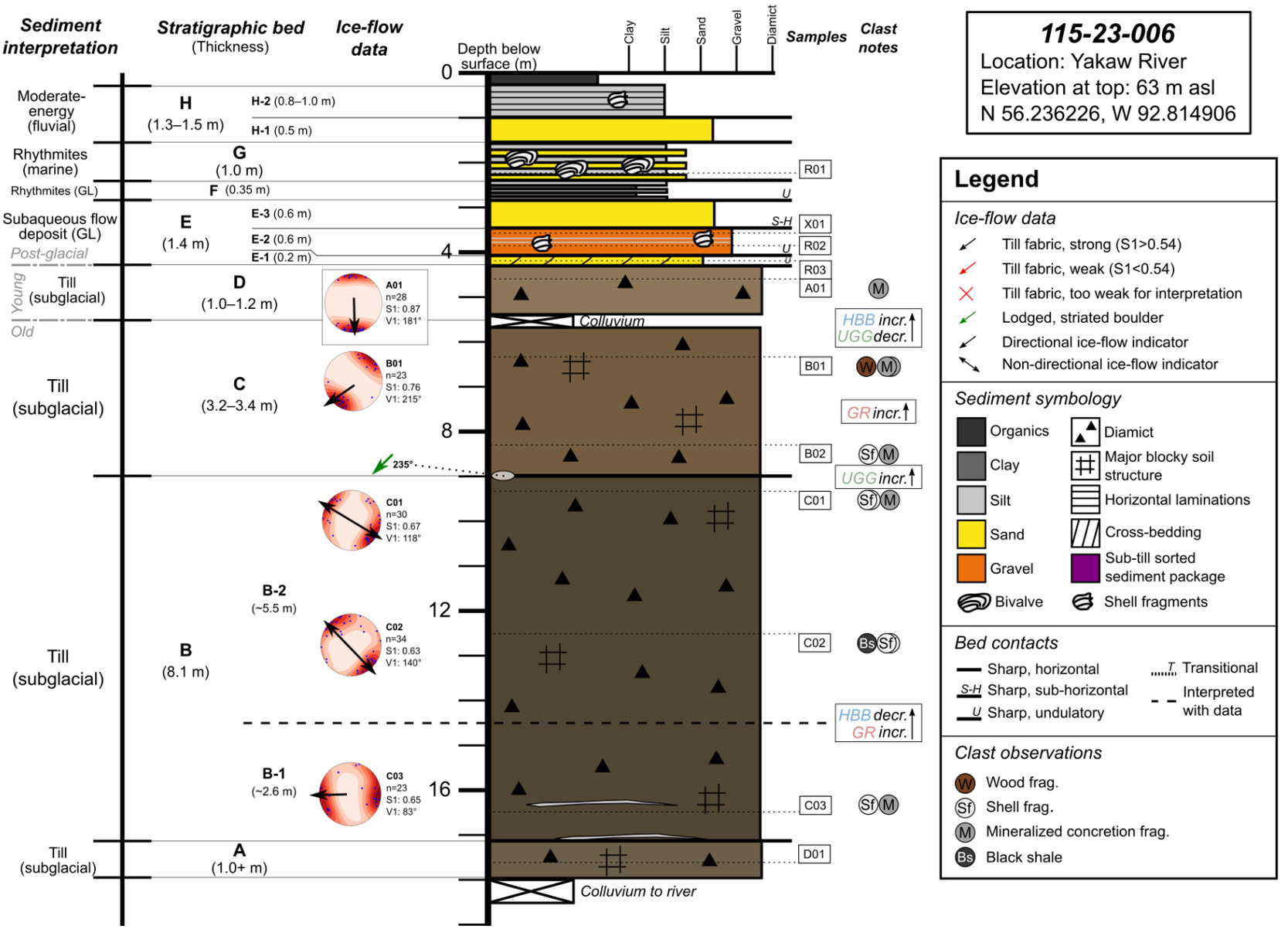


Figure 3.41: Stratigraphic log of section 115-23-006. Diamict beds are coloured by their sampled Munsell colour. Abbreviations: asl, above sea level; frag., fragment; GL, glaciolacustrine; HBB, Hudson Bay Basin; GR, granitoid; UGG, undifferentiated greenstone and greywacke.

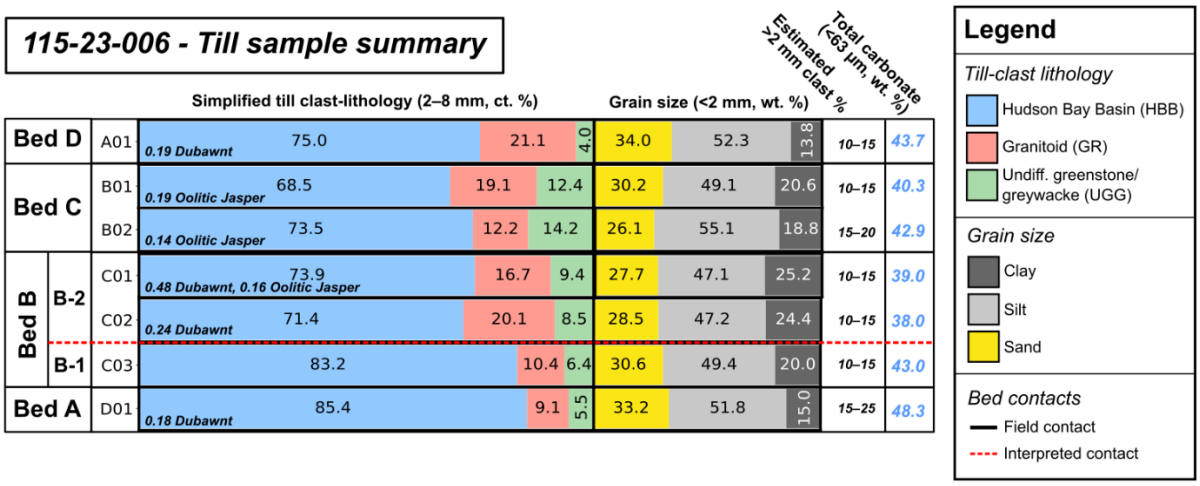


Figure 3.42: Summary of till sample data for section 115-23-006. Abbreviations: ct., count, wt., weight.

The lowermost Bed 6-A is a massive dark grey-brown (2.5Y 4/2) diamict (Figure 3.43A), at least 1.0 m thick, that is highly overconsolidated, has a highly calcareous clayey silty-sand matrix, has a well-developed blocky structure with oxidation along joints, and contains 15–25% striated and/or faceted clasts that are granule- to small pebble-sized. Bed 6-A clasts have very high HBB, low GR, and low UGG (D01: 85.4% HBB, 9.1% GR, 5.5% UGG; Appendix E, Table 5). Bed 6-A is interpreted as subglacial traction till.

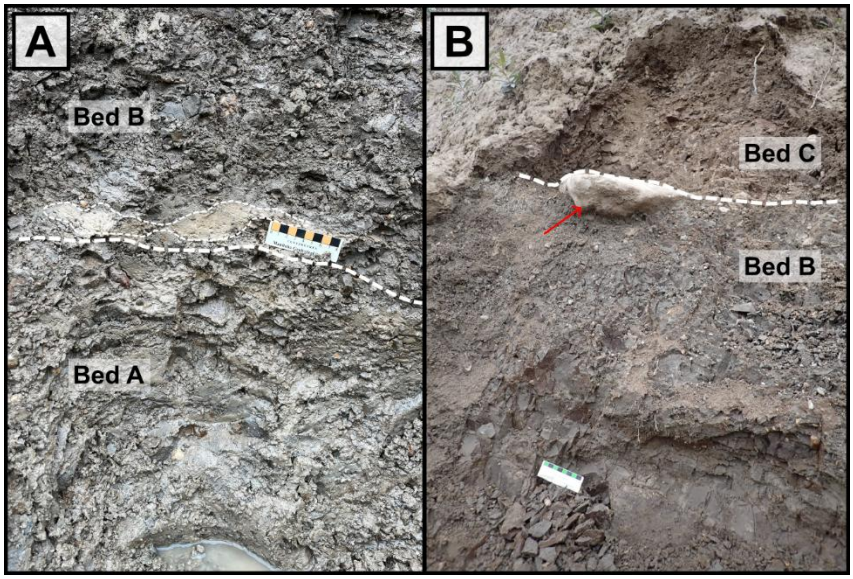


Figure 3.43: (A) Wet and seeping dark grey brown till of Bed 6-A, overlain by very dark grey brown till of Bed 6-B (which includes a tan silt lens, outlined). (B) Bed 6-B is overlain by brown till of Bed 6-C, with a striated lodged boulder at the contact (red arrow).

Bed 6-B is a massive very dark grey-brown (2.5Y 3/2) diamict (Figure 3.43A, B), 8.1 m thick, that is highly overconsolidated, has a moderately calcareous clayey silty-sand matrix, has a well-developed blocky structure with oxidation along joints, and contains 10–15% striated and/or faceted clasts that are granule- to small boulder-sized, with small pebble-sized clasts most prevalent. Bed 6-B also contains a massive, tan silt lens with sandy gravel near its base, from 17.0–17.1 m. A similar tan silt lens is found at about 16.3 m. Three spread unimodal clast fabrics were measured from Bed 6-B and are interpreted to indicate shear stress was initially W and shifted to approximately SE-NW over time (263°, 140-320°, 118-298°, Appendix G, Table 3). As such, Bed 6-B is separated into Bed 6-B-1 (~2.6 m thick, W fabric) and Bed 6-B-2 (~5.5 m thick, SE-NW fabric). This subdivision is strongly supported by significant changes in clast lithology (11.8% decrease in HBB, 9.7% increase in GR; Figure 3.42). Specifically, Bed 6-B-1 clasts have high HBB, low GR (C03: 83.2% HBB, 10.4% GR, 6.4% UGG) and no Dubawnt erratics, while Bed 6-B-2 clasts have moderate to low HBB, moderate to high GR, and high UGG (C02, C01: 71.4–73.9% HBB, 16.7–20.1% GR, 8.5–9.4% UGG), and Dubawnt erratics present (0.24–0.48%; Appendix E, Table 5). Bed 6-B is interpreted as subglacial traction till. Bed 6-B overlies Bed 6-A, with a sharp sub-horizontal contact.

Bed 6-C is a massive brown (10YR 4/3) diamict (Figure 3.43B), 3.2–3.4 m thick, that is highly overconsolidated, has a moderately calcareous clayey sandy-silt matrix, has a well-developed blocky structure with oxidation along joints, and contains 10-20% striated and/or faceted subangular to subrounded clasts that are granule- to small pebble-sized. One spread-unimodal clast fabric and striae on one lodged boulder were measured from Bed 6-C and are interpreted to indicate shear stress was SW (215°, 235°, Appendix G, Table 3, Table 2). Bed 6-C clasts have moderate to low HBB, moderate to high GR, and high UGG (B02, B01: 68.5–73.5% HBB, 12.2–19.1% GR, 12.4–14.2% UGG; Appendix E, Table 5). Notably, there is a 6.9% increase in GR concentration upsection within Bed 6-C (Figure 3.42). Additionally, there is a 4.8% increase in UGG concentration from Bed 6-B (below) to the base of Bed 6-C (Figure 3.42). Bed 6-C is interpreted as subglacial traction till. Bed 6-C overlies Bed 6-B, with a sharp horizontal contact.

Bed 6-D is a massive brown (10YR 5/3) diamict (Figure 3.44A), 1.0–1.2 m thick, that is overconsolidated, has a moderately calcareous sandy-silt matrix, has a weakly-developed blocky structure with minor oxidation along joints, and contains 10-15% striated and/or faceted subangular to subrounded clasts that are granule- to small pebble-sized. One spread-unimodal clast fabric was measured from Bed 6-D and is interpreted to indicate shear stress was S (181°, Appendix G, Table 3). Bed 6-D clasts have high GR and low UGG (A01: 75.0% HBB, 21.1% GR, 4.0% UGG; Appendix E, Table 5). There is a 6.5% increase in HBB concentration from Bed 6-C (below) to the base of Bed 8-D, and an 8.4% decrease

in UGG concentration (Figure 3.42). Bed 6-D is interpreted as subglacial traction till. Bed 6-D overlies Bed 6-C, the exact nature of the contact obscured due to colluvium cover.

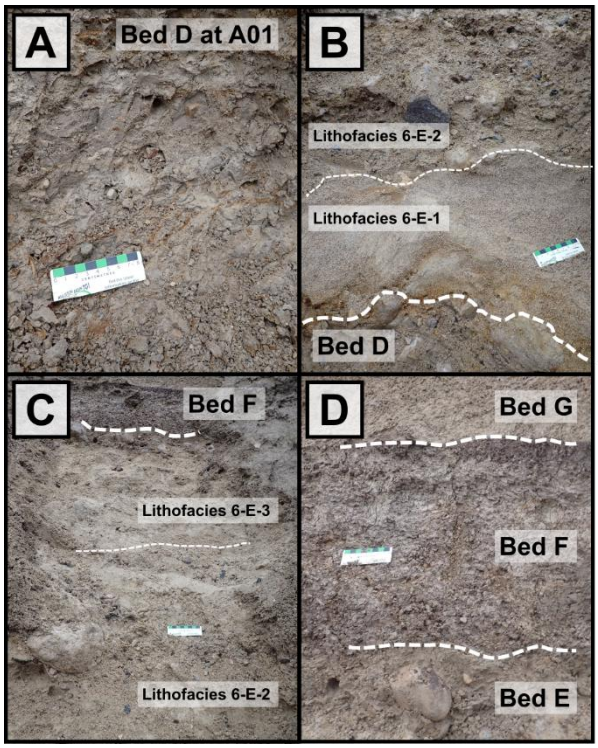


Figure 3.44: (A) Brown till of Bed 6-D. (B) Bed 6-D is overlain by bedded coarse sand of lithofacies 6-E-1, which is then overlain by medium to poorly sorted sandy gravel of lithofacies 6-E-2. (C) Medium to poorly sorted gravelly sand of lithofacies 6-E-3 overlies lithofacies 6-E-2. (D) Interbedded clay and silt of Bed 6-F.

Bed 6-E (Figure 3.44B, C), 1.4 m thick, consists of 0.2 m of very well sorted, horizontal to cross-bedded coarse sand (lithofacies 6-E-1), overlain by 0.6 m of poorly sorted, yellow-brown sandy gravel (lithofacies 6-E-2), which is then overlain by 0.6 m of medium to poorly sorted, yellow-brown gravelly sand (lithofacies 6-E-3). Lithofacies 6-E-1 contains a few fine sand laminae and no visible organics, and overlies Bed 6-D, with a sharp undulatory contact. Lithofacies 6-E-2 contains about 40% granule- to large cobble-sized clasts, with small pebble-sized clasts most prevalent, and some silty beds throughout. Two broken and transported shell fragments were documented within lithofacies 6-E-2. One 3×5 mm shell fragment was sampled for radiocarbon dating, which returned a conventional age of >47 100 ^{14}C years BP (UOC-23330, Appendix F). Lithofacies 6-E-2 overlies Bed 6-E-1, with a sharp undulating contact. Lithofacies 6-E-3 contains 20–30% subangular to rounded granule- to medium cobble-sized clasts, some of which are faceted, and a very fine to medium-sand, tan matrix. No visible organics were found within lithofacies 6-E-3. Lithofacies 6-E-3 overlies lithofacies 6-E-2, with a sharp sub-horizontal contact. Bed 6-

E is interpreted as an ice-marginal subaqueous deposit, perhaps formed near the grounding line of a retreating ice sheet.

Bed 6-F consists of 0.35 m of red-brown clay interbedded with tan silt (Figure 3.44D). Horizontal beds are 1–3 mm thick. No visible organics were found within Bed 6-F. Bed 6-F is interpreted as rhythmites, formed in a deep-water glaciolacustrine deposit. Bed 6-F overlies Bed 6-E, with a sharp undulatory contact.

Bed 6-G consists of 1.0 m of interstratified brown silt and fine sand (Figure 3.45), commonly containing *Hiatella arctica* and *Portlandia arctica* paired valves in growth position. One *Hiatella arctica* was sampled for radiocarbon dating, which returned a conventional age of 7490 ± 25 ^{14}C years BP (UOC-23329, Appendix F). Bed 6-G is interpreted as rhythmites deposited in a post-glacial marine environment (Tyrrell Sea). Bed 6-G overlies Bed 6-F, with a sharp horizontal contact.

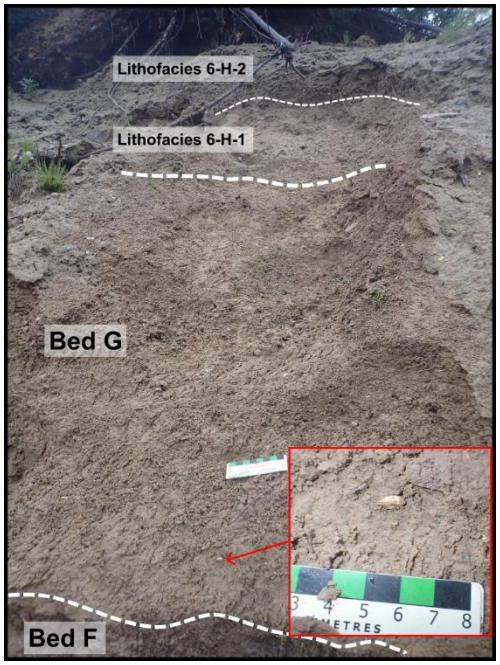


Figure 3.45: Interstratified silt and sand of Bed 6-G contains paired marine clam valves in growth position (red). Bed 6-G is overlain by gravelly sand (6-H-1) and silt (6-H-2) of Bed 6-H.

Bed 6-H (Figure 3.45), 1.3–1.5 m thick, consists of 0.5 m of gravelly sand (lithofacies 6-H-1), overlain by 0.8–1.0 m of grey-brown, laminated to massive silt with rare pebbles and shell fragments (lithofacies 6-H-2). Lithofacies 6-H-1 contains about 20% sub-rounded to rounded pebble- to cobble-sized clasts with marine shells. Bed 6-H-1 overlies Bed 6-G, with a sharp horizontal contact. Lithofacies 6-H-2 overlies lithofacies 6-H-1 with a sharp horizontal contact. Bed 6-H is interpreted as a post-glacial fluvial deposit. Bed 6-H is overlain by modern peat.

3.3.3.6 Section 115-23-007, Gods River

This 42-m-high section (Figure 3.46) extends about 100 m along a northern cut bank of Gods River. It contains 12 stratigraphic beds: 8 diamicts interpreted as till, 3 sub-till sorted sediment packages, and 1 sorted sediment (Figure 3.47). Across the 8 till beds and sub-beds, 18 samples were collected (Figure 3.48).

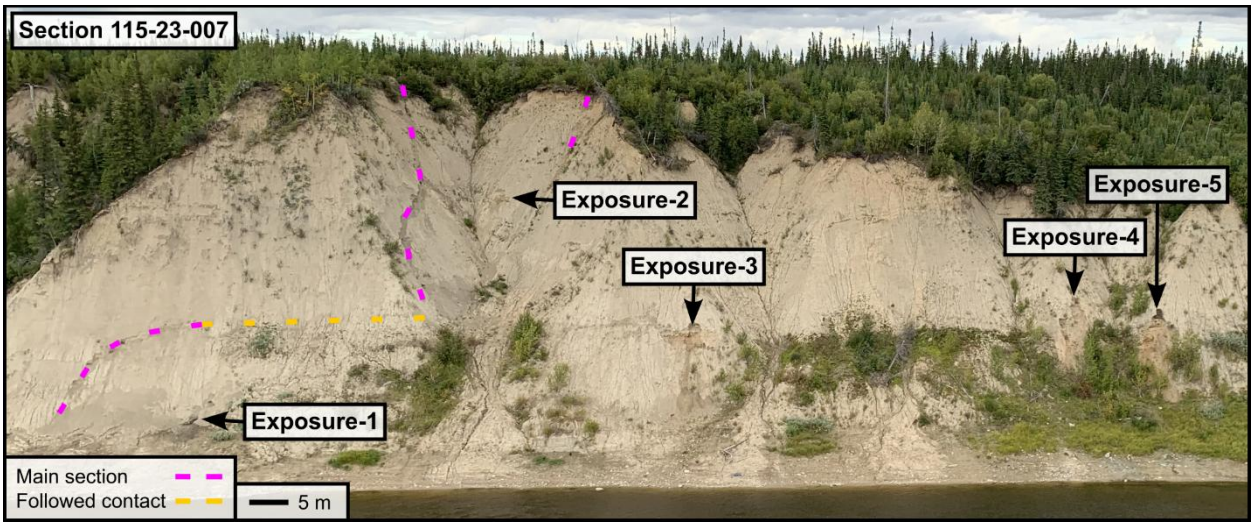


Figure 3.46: Overview of section 115-23-007, viewed towards the north.

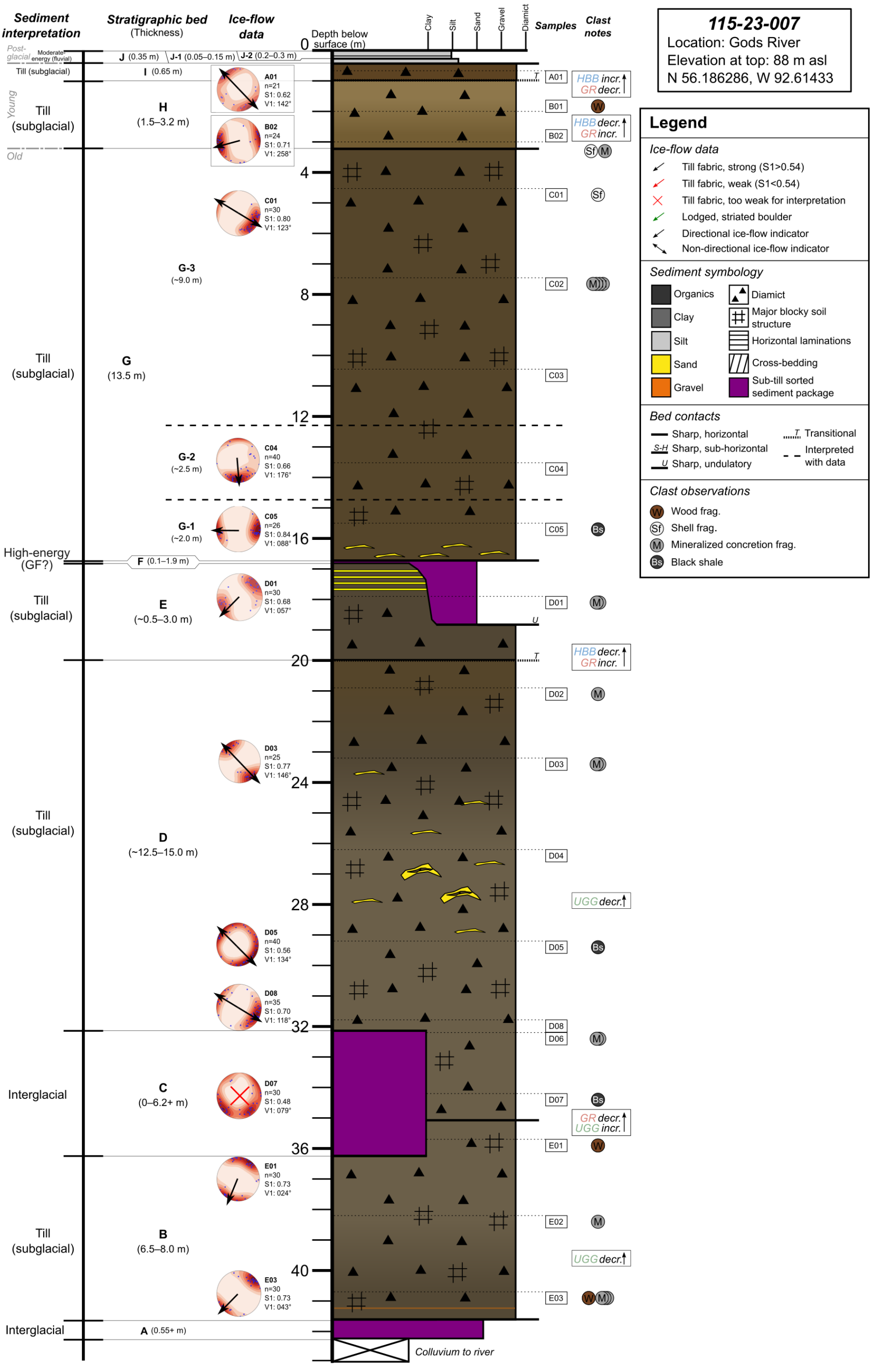


Figure 3.47: Stratigraphic log of section 115-23-007. Diamict beds are coloured by their sampled Munsell colour. Abbreviations: asl, above sea level; frag., fragment; GF, glaciofluvial; HBB, Hudson Bay Basin; GR, granitoid; UGG, undifferentiated greenstone and greywacke.

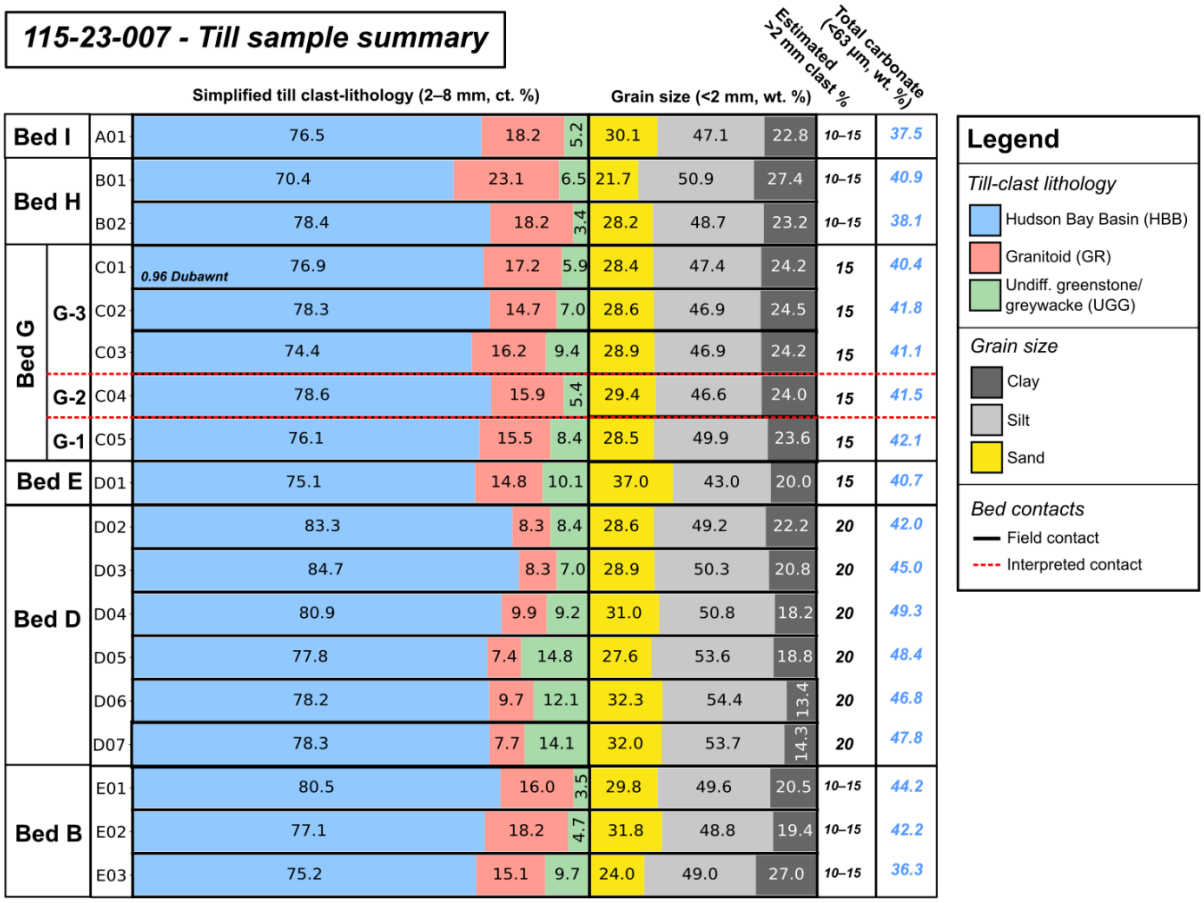


Figure 3.48: Summary of till sample data for section 115-23-007. Abbreviations: ct., count, wt., weight.

The lowermost Bed 7-A consists of a sub-till sorted sediment package with one investigated exposure (Exposure-1). At Exposure-1 (Figure 3.49: stratigraphic log; Figure 3.50: photos), Bed 7-A consists of at least 0.55 m of sediments divided into 2 lithofacies. The lower lithofacies (7-A-1-1) comprises at least 0.5 m of poorly sorted, blue-gray sandy gravel containing subangular to subrounded granule- to pebble-sized clasts and shell fragments in a sandy matrix. Overlying this is 0.01–0.05 m of organic-bearing, laminated silt (lithofacies 7-A-1-2), which is dark grey to black in colour and sharply overlies lithofacies 7-A-1-1. The presence of organics in sub-till Bed 7-A indicates deposition in an interglacial.

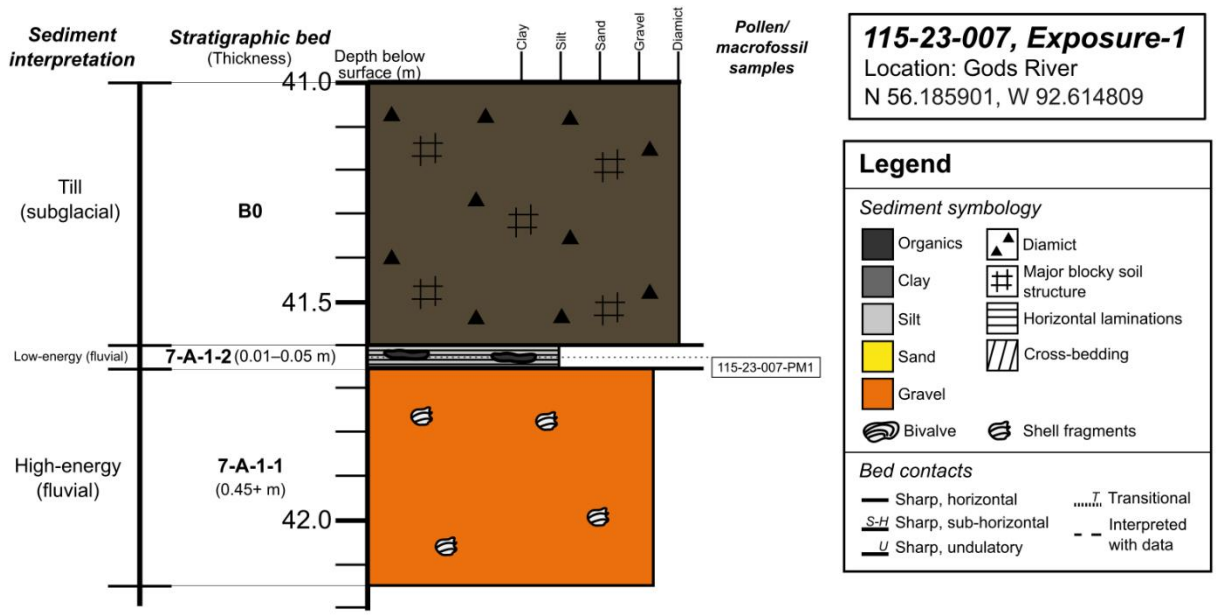


Figure 3.49: Stratigraphic log for Exposure-1 of Section 115-23-007. The diamict bed is coloured by its sampled Munsell colour.

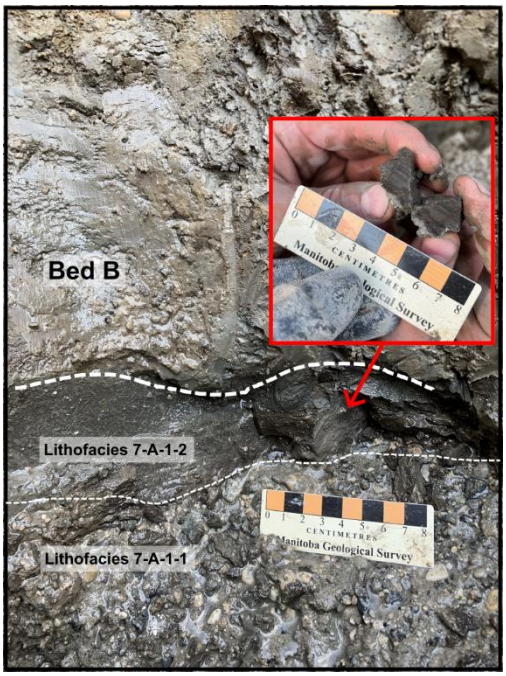


Figure 3.50: The stratigraphic sequence at Exposure-1 of Section 115-23-007, including poorly sorted gravel (7-A-1-1) and organic-bearing laminated silt (7-A-1-2) underlying Bed 7-B diamict.

Bed 7-B is a massive diamict (Figure 3.50, Figure 3.51A, B), 6.5–8.0 m thick, which lightens in colour upsection from very dark grey-brown (2.5Y 3/2) to dark grey-brown (2.5Y 4/2), and changes in texture upsection from sandy clayey-silt to clayey sandy-silt. Bed 7-B is highly overconsolidated, has a

moderately calcareous matrix, a well-developed blocky structure with oxidation along joints, and contains 10–15% striated and/or faceted clasts that are granule- to pebble-sized. Near the bottom of Bed 7-B there is a thin (~5 cm) layer of orange-brown diamict. Two spread unimodal clast fabrics were measured from Bed 7-B and are interpreted to indicate shear stress was SW to SSW (223°, 204°, Appendix G, Table 3). Bed 7-B till clasts have moderate to high GR and moderate to very low UGG (E03–E01 (n=3): 75.2–80.5% HBB, 15.1–18.2% GR, 3.5–9.7% UGG; Appendix E, Table 5). Notably, there is a 5.0% decrease in UGG concentration upsection within Bed 7-B (from E03 to E02; Figure 3.48). Bed 7-B is interpreted as subglacial traction till. Bed 7-B overlies Bed 7-A, with a sharp horizontal contact.

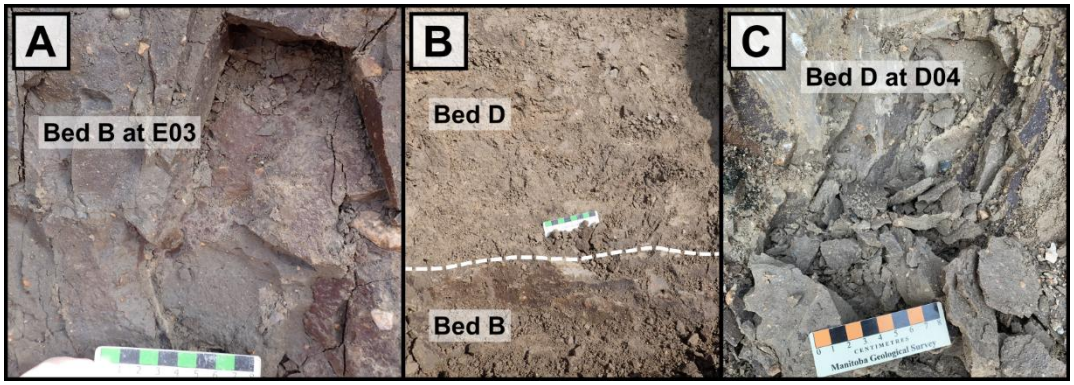


Figure 3.51: (A) Very dark grey brown till of Bed 7-B. (B) Bed 7-D sharply overlies Bed 7-B where Bed 7-C is not present. (C) Dark grey brown till of Bed 7-D.

Bed 7-C, 0–6.2+ m thick, consists of sorted sediments (Exposure-3, Exposure-4, and Exposure-5), correlated based on their shared upper contact of Bed 7-D. Bed 7-C is interpreted to be deposited during an ice-free phase.

At Exposure-3 (Figure 3.52: stratigraphic log; Figure 3.53: photo), Bed 7-C is 1.4 m thick and consists of 3 lithofacies. It begins with approximately 0.8 m of poorly sorted, matrix-supported sandy gravel (lithofacies 7-C-3-1) that includes rip-up clasts of diamict. Lithofacies 7-C-3-1 overlies Bed 7-B with a sharp undulatory contact. Overlying this is about 0.2 m of heavily oxidized and cemented gravel (lithofacies 7-C-3-2), consisting of pebbles, cobbles, and boulders with extensive clay alteration. Heavily weathered, crumbly granite cobbles are common, while others preserve striations. This layer varies laterally, with oxidation decreasing with depth. Lithofacies 7-C-3-2 overlies lithofacies 7-C-3-1 with a transitional contact. Capping the sequence is 0.4 m of horizontally bedded sand and gravel (lithofacies 7-C-3-3), with 15–35% granule- to small pebble-sized clasts supported by a coarse sand matrix. This lithofacies includes round clay clasts, shell fragments, and diamict rip-up clasts, along with some medium to coarse sand beds. Lithofacies 7-C-3-3 overlies lithofacies 7-C-3-2 with a sharp undulatory contact.

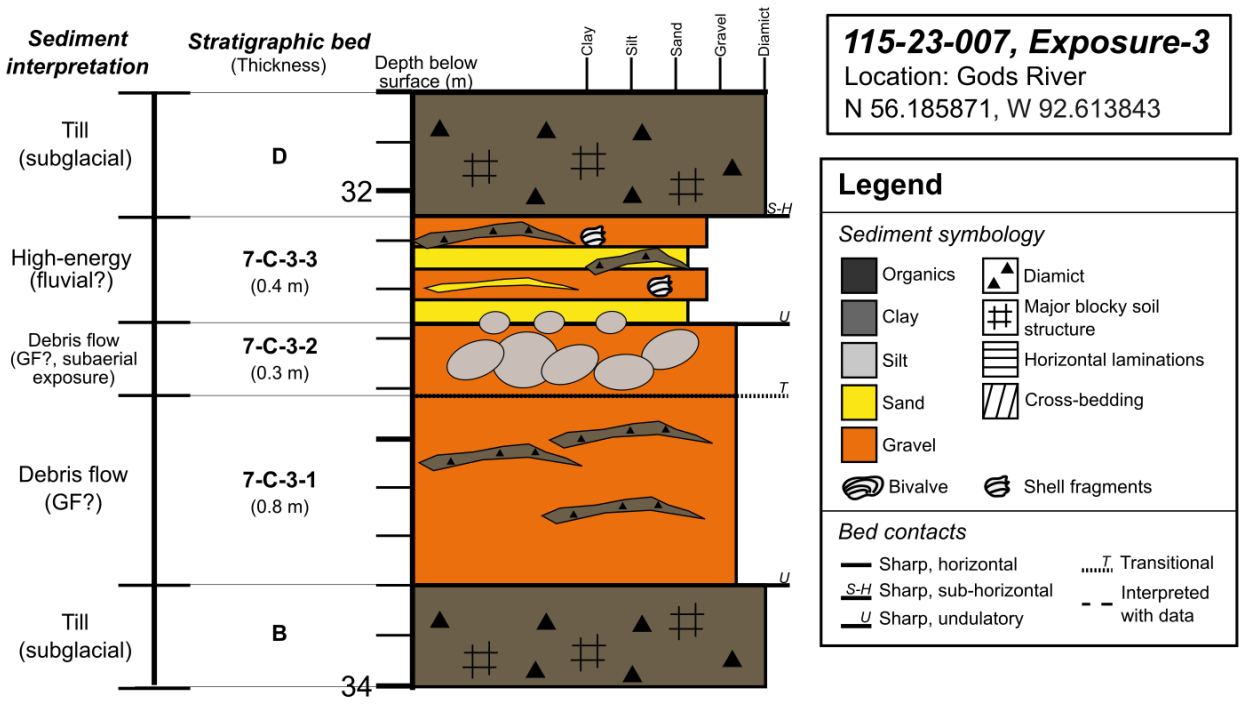


Figure 3.52: Stratigraphic log for Exposure-3 of Section 115-23-007. Diamict beds are coloured by their sampled Munsell colour.

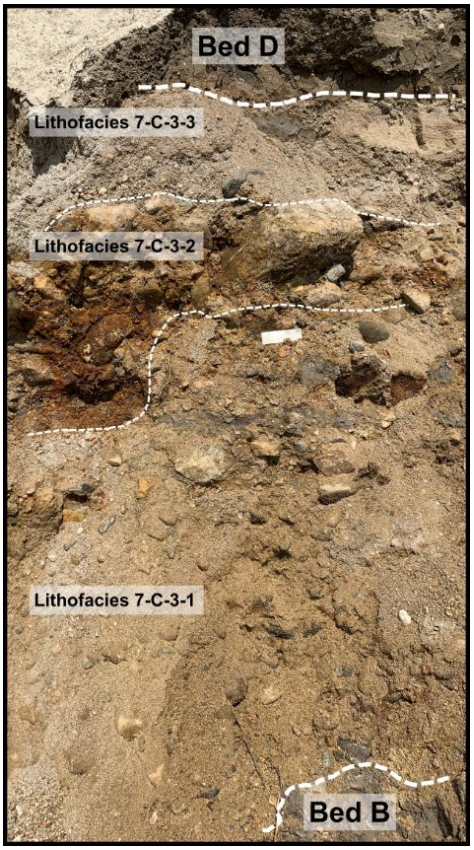


Figure 3.53: The stratigraphic sequence at Exposure-3 of Section 115-23-007, including sandy gravel (7-C-3-1), cemented and heavily oxidized sandy gravel (7-C-3-2), and interbedded sand and gravel (7-C-3-3).

At Exposure-4 (Figure 3.54: stratigraphic log; Figure 3.55: photos), Bed 7-C is at least 4.1 m thick and consists of 7 lithofacies. It begins with at least 0.4 m of horizontally bedded medium to fine sand (7-C-4-1). Above this is 0.7 m of poorly sorted, matrix-supported gravelly sand (7-C-4-2) with angular to subrounded clasts and occasional diamict rip-up clasts. The uppermost 0.2 m contains two layers of cobble- to boulder-sized clasts. Next is 0.7 m of horizontally to cross-bedded fine sand (7-C-4-3) with occasional granule beds, shell fragments, and rip-up clasts of diamict. Overlying this is 0.1–0.5 m of moderately sorted gravel (7-C-4-4), which fines upward from pebble-sized to granule-sized clasts and contains rare boulders and a few diamict lenses. The next lithofacies (7-C-4-5) is 1.0 m thick and composed of moderately sorted, coarse to medium sand with textural bedding and occasional diamict lenses. This is followed by 1.1 m of poorly sorted sandy gravel (7-C-4-6), with small granule- to small pebble-sized clasts, some diamict lenses, and a basal gravel bed of subangular to subrounded pebble- to cobble-sized clasts. At the top is 0.2 m of texturally bedded coarse silt and medium sand (7-C-4-7), with oxidation in the uppermost 2 mm and scattered staining throughout. All contacts are sharp and horizontal.

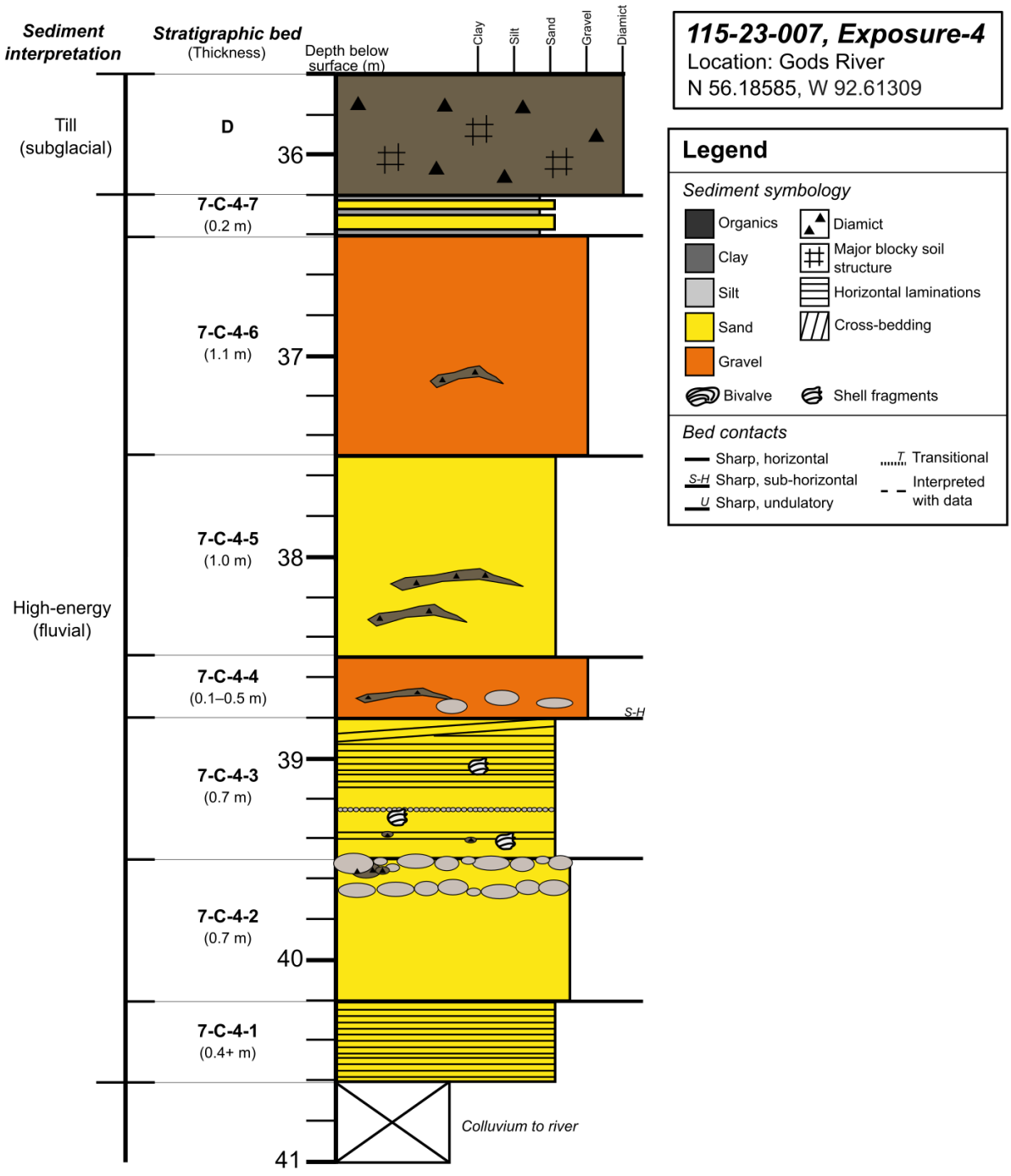


Figure 3.54: Stratigraphic log for Exposure-4 of Section 115-23-007. Diamict beds are coloured by their sampled Munsell colour.

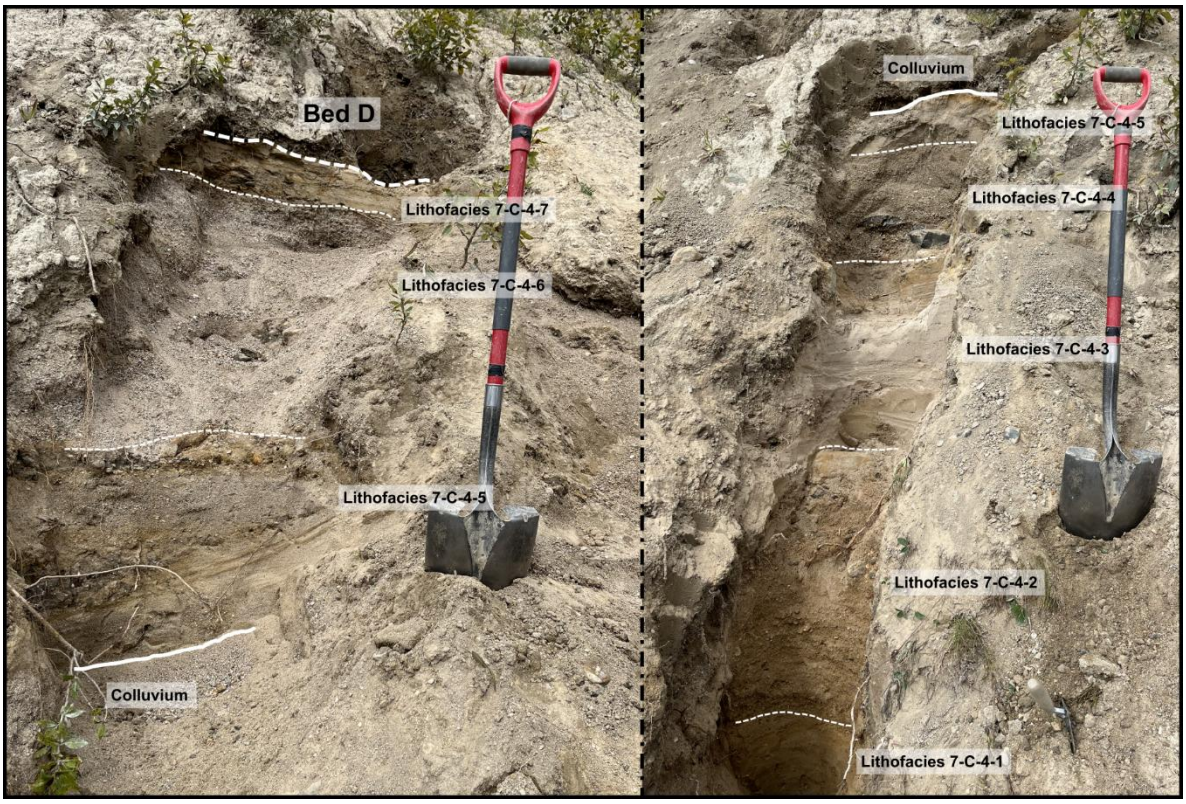


Figure 3.55: The stratigraphic sequence at Exposure-4 of Section 115-23-007.

At Exposure-5 (Figure 3.56: stratigraphic log; Figure 3.57: photos), Bed 7-C is 5.7 m thick, and consists of 7 lithofacies. The sequence begins with 1.9 m of horizontally bedded sand and gravel (7-C-5-1), with beds 10–20 cm thick and moderately to well sorted. Shell fragments are common, including some up to 6 mm and a complete valve found in the lowermost 30 cm. This is overlain by 0.2 m of horizontally bedded sand and gravel (7-C-5-2), with thinner, 3–5 cm beds. Above this is 0.2 m of cross-bedded coarse sand (7-C-5-3), with shell fragments and granule beds. Following this is 0.5 m of texturally bedded fine sand and silty fine sand (7-C-5-4), with beds 1–2 cm thick. Above this is 0.2 m of horizontally bedded silt (7-C-5-5), containing minor 1–2 cm thick beds of clay and sand. Next is 0.5 m of well-sorted coarse sand (7-C-5-6), with pockets of cobbles and boulders. Capping the section is 0.7 m of massive blue clay (7-C-5-7), which includes a 5 cm thick horizontal brown silt bed and a 2 cm thick horizontal bed of orange medium sand. All contacts are sharp and horizontal.

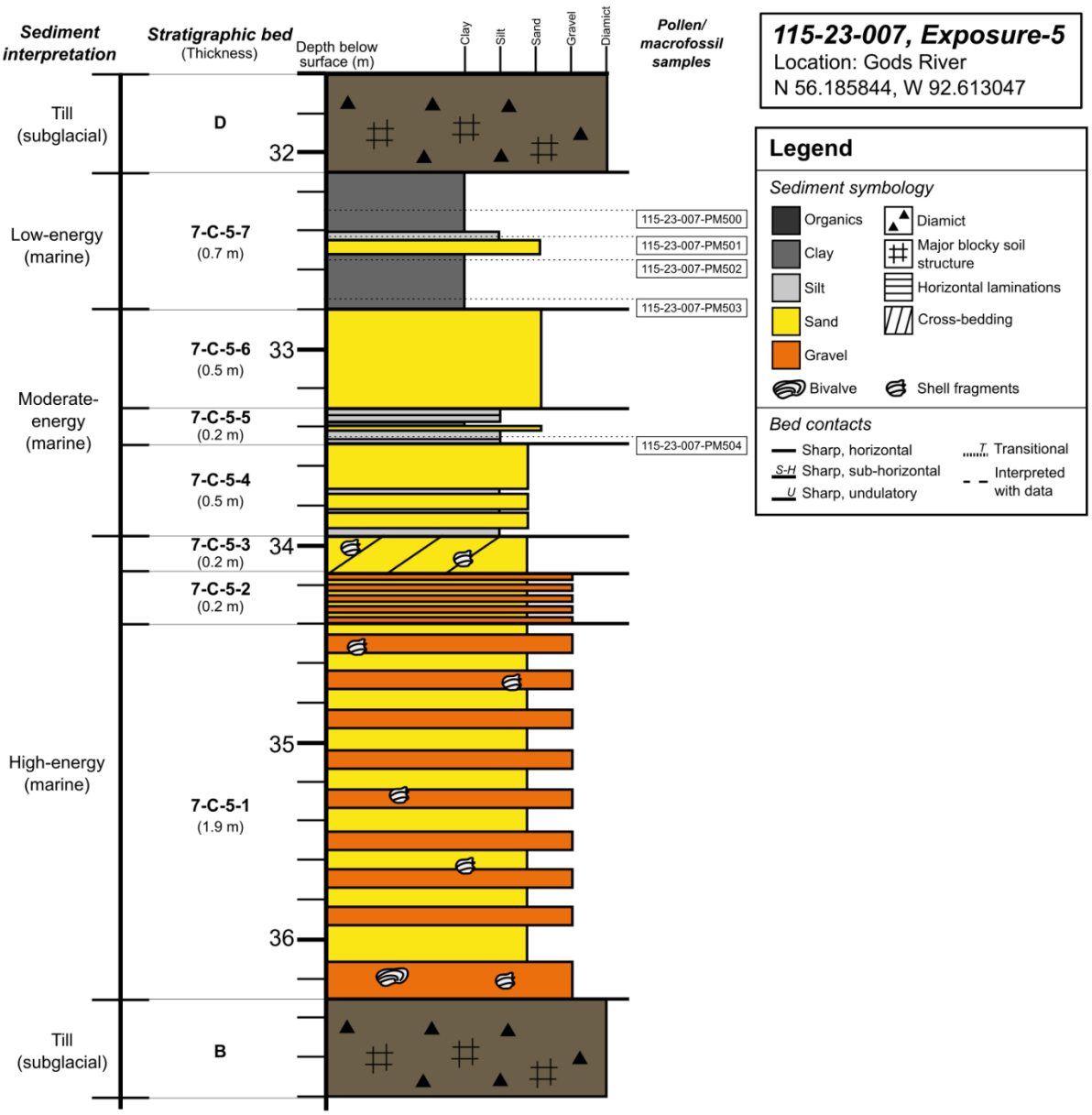


Figure 3.56: Stratigraphic log for Exposure-5 of Section 115-23-007. Diamict beds are coloured by their sampled Munsell colour.

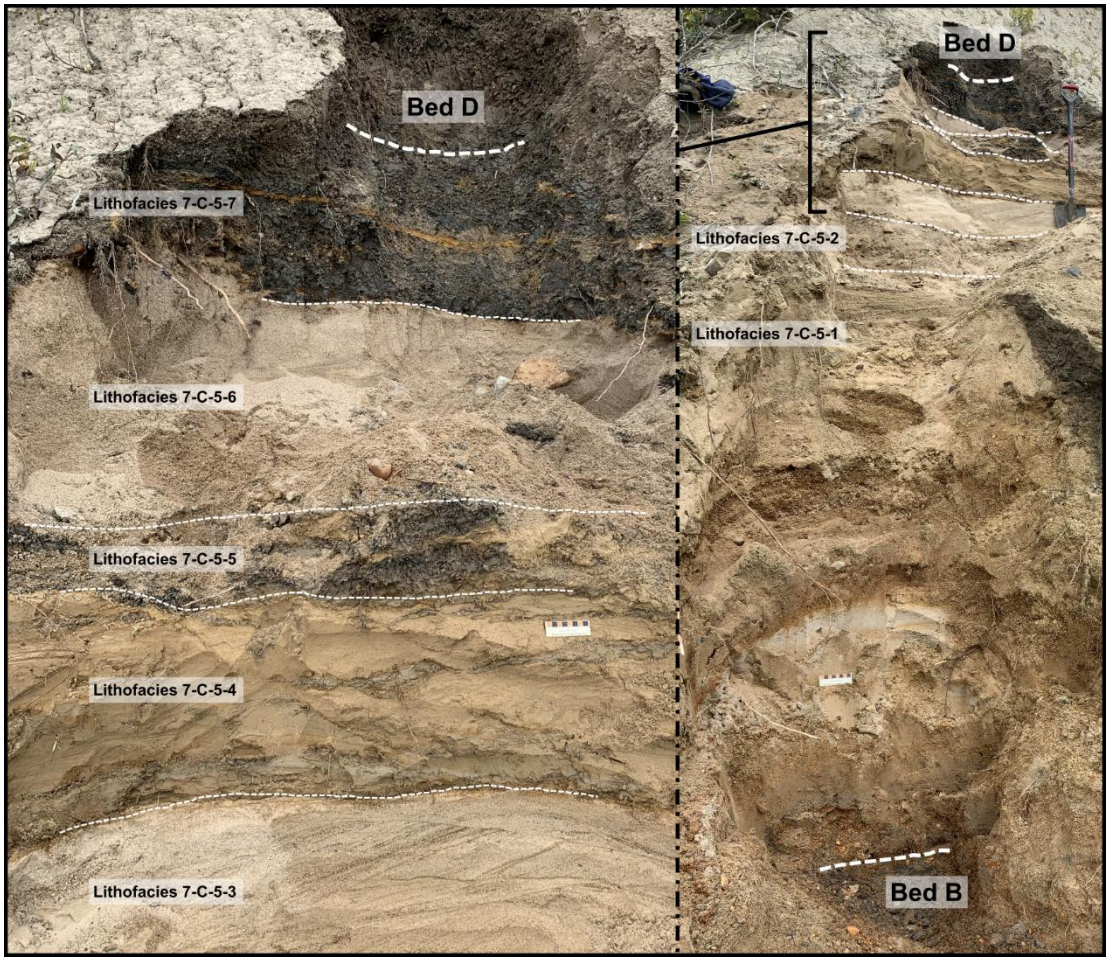


Figure 3.57: The stratigraphic sequence at Exposure-5 of Section 115-23-007.

Bed 7-D is a massive diamict (Figure 3.51B, C), about 12.5–15.0 m thick, which ranges in colour from dark gray brown (2.5Y 4/2) to dark olive brown (2.5Y 3/3) and very dark gray brown (2.5Y 3/2). Bed 7-D has a moderately to highly calcareous and sandy silt to clayey sandy-silt matrix that is highly overconsolidated, has a well-developed blocky structure with oxidation along joints, and contains about 15% striated and/or faceted clasts. Three spread unimodal clast fabrics were measured from Bed 7-D and are interpreted to indicate shear stress changed upsection from ESE-WNW to SE-NW (118-298°, 134-314°, 146-326°, Appendix G, Table 3). Bed 7-D clast lithologies are variable and include a 5.6% decrease in UGG concentration upsection (from D05 to D04; Figure 3.48). In the lower part, clasts have moderate HBB, low to very low GR, and high UGG (D07–D05 (n=3): 77.8–78.3% HBB, 7.4–9.7% GR, 12.1–14.8% UGG; Appendix E, Table 5). In the upper part, clasts have high to very high HBB, low GR, and moderate UGG (D04–D02 (n=3): 80.9–84.7% HBB, 8.3–9.9% GR, 7.0–9.2% UGG; Appendix E, Table 5). Strikingly, there is a 10.6% increase in UGG from Bed 7-B (below) to the base of Bed 7-D, and an 8.4% decrease in GR concentration (Figure 3.48). Bed 7-D is interpreted as subglacial traction till. Bed 7-

D overlies both Bed 7-C and Bed 7-B due to the lateral variability of Bed 7-C, with sharp horizontal contacts at both beds.

Bed 7-E is a massive, very dark grey brown (2.5Y 3/2) diamict (Figure 3.58), about 0.5–3.0 m thick, that is highly overconsolidated, has a moderately calcareous clayey sandy-silt matrix, has a well-developed blocky texture with oxidation along joints, and contains about 15% striated and/or faceted clasts. The uppermost 1.0 m of Bed 7-E contains sub-horizontal contorted fine to medium sand beds. One spread unimodal clast fabric was measured from Bed 7-E and is interpreted to indicate shear stress was SW (237°, Appendix G, Table 3). Bed 7-E clasts have moderate concentrations of all three simplified lithology categories (D01: 75.1% HBB, 14.8% GR, 10.1% UGG; Appendix E, Table 5), associated with a 6.5% increase in GR from the top of Bed 7-D, and an 8.2% decrease in HBB concentration (Figure 3.48). Bed 7-E is interpreted as subglacial traction till. Bed 7-E overlies Bed 7-D with a transitional contact.



Figure 3.58: Very dark grey brown till of Bed 7-E, containing sub-horizontal sand beds.

Bed 7-F consists of laterally variable sand, correlated locally across a gully. Along the main section, Bed 7-F is 0.1 m thick and consists of massive medium sand, with a sharp horizontal contact overlying Bed 7-E. At Exposure-2 (Figure 3.59: stratigraphic log; Figure 3.60: photos), Bed 7-F is about 1.4 m thick and consists of 3 lithofacies. It begins with 0.3–0.8 m of medium sand (lithofacies 7-F-2-1), which is well sorted and contains deformed horizontal bedding, minor coarse sand lenses, and some oxidation. Above this is 0.6 m of medium to fine sand (lithofacies 7-F-2-2), also well sorted, with sub-horizontal textural bedding and rare silt beds. Capping the sequence is 0.5 m of well-sorted, horizontally bedded fine sand (lithofacies 7-F-2-3). All contacts are sharp and sub-horizontal. Bed 7-F is tentatively interpreted as being deposited in a glaciofluvial environment during a phase of relative warming.

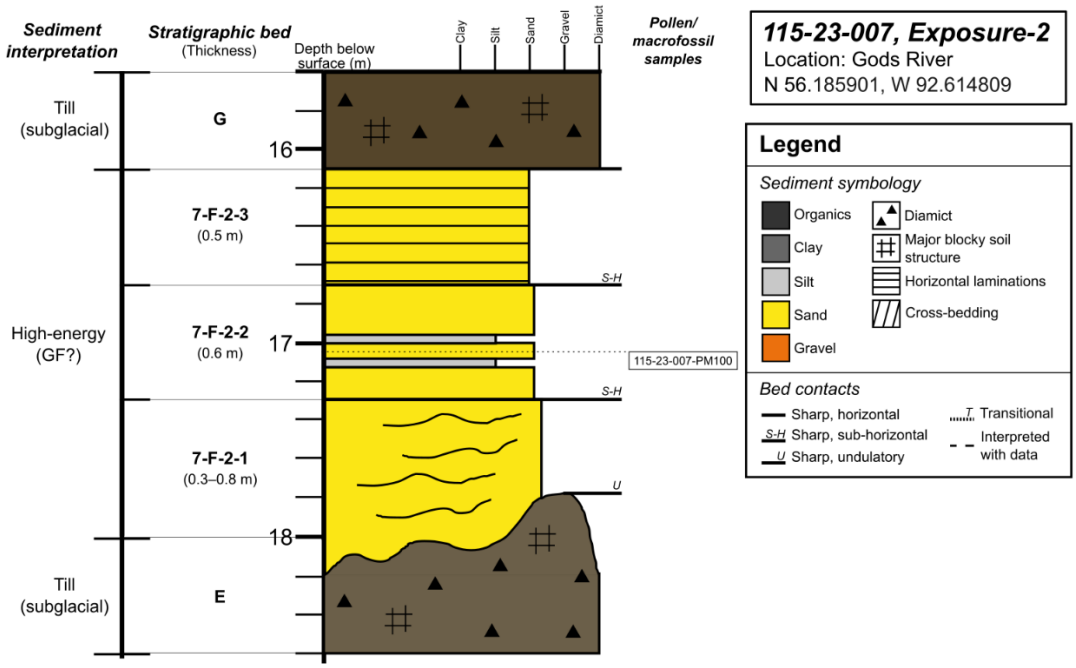


Figure 3.59: Stratigraphic log for Exposure-2 of Section 115-23-007. Diamict beds are coloured by their sampled Munsell colour. Abbreviations: GF, glaciofluvial.

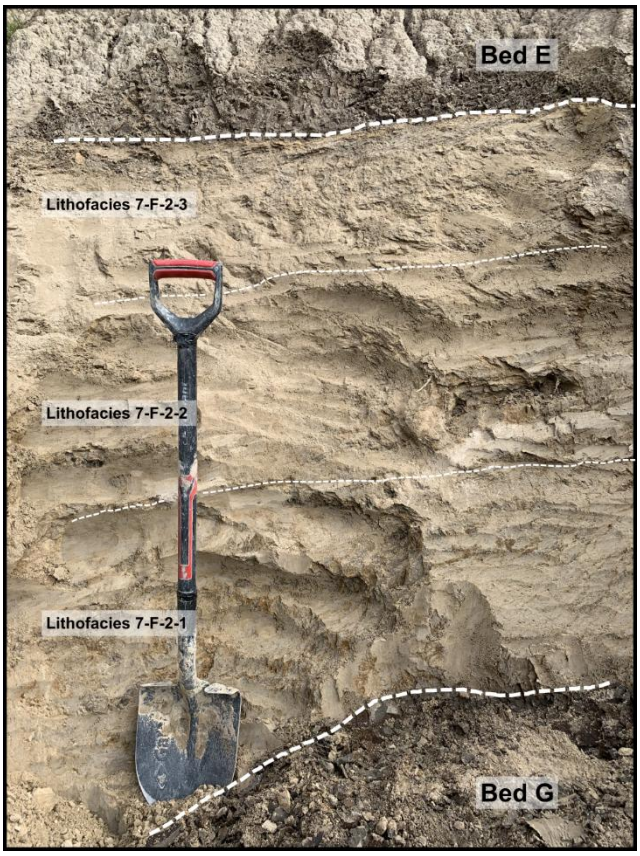


Figure 3.60: The stratigraphic sequence at Exposure-2 of Section 115-23-007, including medium sand (7-F-2-1), medium to fine sand with silt beds (7-F-2-2), and horizontally bedded fine sand (7-F-2-3).

Bed 7-G is a massive, dark olive brown (2.5Y 3/3) diamict (Figure 3.61A, B), 13.5 m thick, that is highly overconsolidated, has a moderately calcareous clayey sandy-silt matrix, has a well-developed blocky structure with oxidation along joints, and contains about 15% striated and/or faceted clasts. Spread unimodal clast fabrics measured from Bed 7-G suggest a shifting shear stress over time (Appendix G, Table 3). As such, Bed 7-G, originally logged as one bed, has been further separated into three sub-beds based on significant changes in paleo-ice flow direction, including at the base Bed 7-G-1 (~2.0 m thick, W fabric; 268°), Bed 7-G-2 (~2.5 m thick, S fabric; 176°), and Bed 7-G-3 (~9.0 m thick, ESE-WNW fabric, 118-298°). The subdivision between Beds 7-G-1 and 7-G-2 is based on a 92° change in interpreted ice-flow direction. Bed 7-G-1 clasts have moderate concentrations of all three simplified lithology categories (C05: 76.1% HBB, 15.5% GR, 8.4% UGG), and Bed 7-G-2 clasts have low UGG (C04: 78.6% HBB, 15.9% GR, 5.4% UGG; Appendix E, Table 5). The subdivision between Beds 7-G-2 and 7-G-3 is based on a significant change in paleo-ice flow direction (53° or 127°). Bed 7-G-3 clasts have moderate concentrations of all three simplified lithology categories (C03–C01 (n=3): 74.4–78.3% HBB, 14.7–17.2% GR, 5.9–9.4% UGG; Appendix E, Table 5). There is an elevated proportion of Dubawnt erratics in

the uppermost sample C01 (0.96%; Figure 3.48). The bottommost 1.0 m of Bed 7-G contains moderately sorted, medium to coarse sand lenses and rip-up clasts of sand, that increase in frequency towards the lower contact. Bed 7-G is interpreted as subglacial traction till. Bed 7-G overlies Bed 7-F, with a sharp horizontal contact.

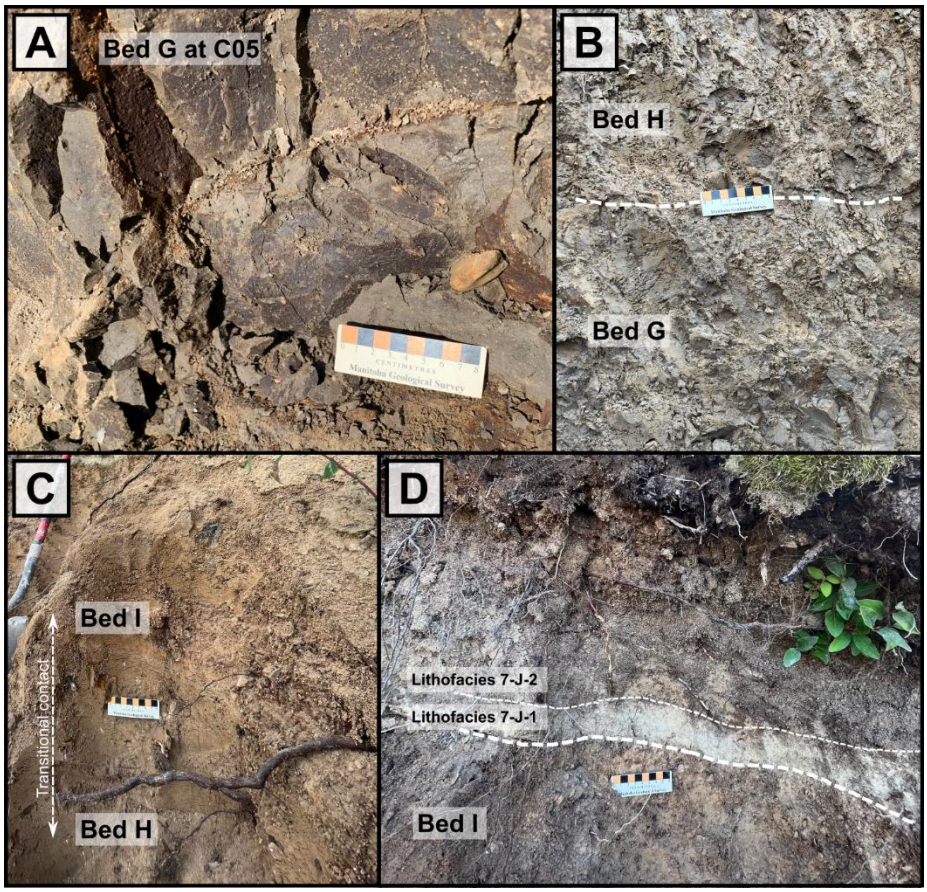


Figure 3.61: (A) Dark olive brown till of Bed 7-G. (B) Olive brown till of Bed 7-H overlies the slightly darker Bed 7-G. (C) Bed 7-H transitions into the dark grey brown till of Bed 7-I. (D) Beige sandy silt (lithofacies 7-J-1) and brown silt (lithofacies 7-J-2) overlie Bed 7-I.

Bed 7-H is a massive diamict (Figure 3.61B, C), 1.5–3.2 m thick, which ranges in colour from olive brown (2.5Y 4/4) to light olive brown (2.5Y 5/4), and ranges in matrix texture from sandy clayey-silt to clayey sandy-silt. Bed 7-H is moderately calcareous, noncompact to overconsolidated, has a weakly-developed blocky structure with no oxidation along joints, and contains 10–15% striated and/or faceted clasts that are granule- to cobble-sized. One spread unimodal clast fabric was measured from Bed 7-H and is interpreted to indicate shear stress was ENE-WNW (78-258°, Appendix G, Table 3). Bed 7-H clasts have moderate to low HBB, high GR, and moderate to very low UGG (B02, B01: 70.4–78.4% HBB, 18.2–23.1% GR, 3.4–6.5% UGG; Appendix E, Table 5). There is a notable 8.0% decrease in HBB

concentrations upsection, and a 4.9% increase in GR concentrations (Figure 3.48). Bed 7-H is interpreted as subglacial traction till. Bed 7-H overlies Bed 7-G, with a sharp horizontal contact.

Bed 7-I is a massive dark grey brown (10YR 3/4) diamict (Figure 3.61C, D), 0.65 m thick, that is noncompact, has a moderately calcareous clayey sandy-silt matrix, does not have a blocky structure, and contains 10–15% striated and/or faceted clasts that are granule- to medium pebble-sized. One spread unimodal clast fabric was measured from Bed 7-I and is interpreted to indicate shear stress was SE-NW (142-322°, Appendix G, Table 3). Bed 7-I clasts have high GR and low UGG (A01: 76.5% HBB, 18.2% GR, 5.2% UGG; Appendix E, Table 5). There is a 6.1% increase in HBB from Bed 7-H (below) to the base of Bed 7-I, and a 4.9% decrease in GR concentration (Figure 3.48). Bed 7-I is interpreted as subglacial traction till. Bed 7-I has a transitional lower contact with Bed 7-H, defined primarily by a colour change.

Bed 7-J (Figure 3.61D), 0.35 m thick, consists of 0.05–0.15 m of massive beige sandy silt (lithofacies 7-J-1), overlain by 0.2–0.3 m of massive brown silt (lithofacies 7-J-2). Lithofacies 7-J-2 has weak laminations in its lowermost 5 cm and contains rare subangular to rounded clasts that are granule- to large-pebble sized. Lithofacies 7-J-1 overlies Bed 7-I, with a sharp horizontal contact. Lithofacies 7-J-2 overlies lithofacies 7-J-1, with a sharp horizontal contact. Bed 7-J is interpreted as a postglacial fluvial deposit.

3.3.3.7 Section 115-23-008, Gods River

This 16-m-high section (Figure 3.62) extends about 10 m along the west side of the Gods River. The Quaternary sediments here have been recently exposed in the headscarp of a retrogressive thaw slump (sometime after 2018). It contains 9 stratigraphic beds: 5 diamicts interpreted as till, 3 sorted sediments, and 1 diamict interpreted as till associated with sorted sediments (Figure 3.63). Across the 6 till beds and sub-beds, 7 samples were collected (Figure 3.64).



Figure 3.62: Overview of section 115-23-008, viewed towards the west.

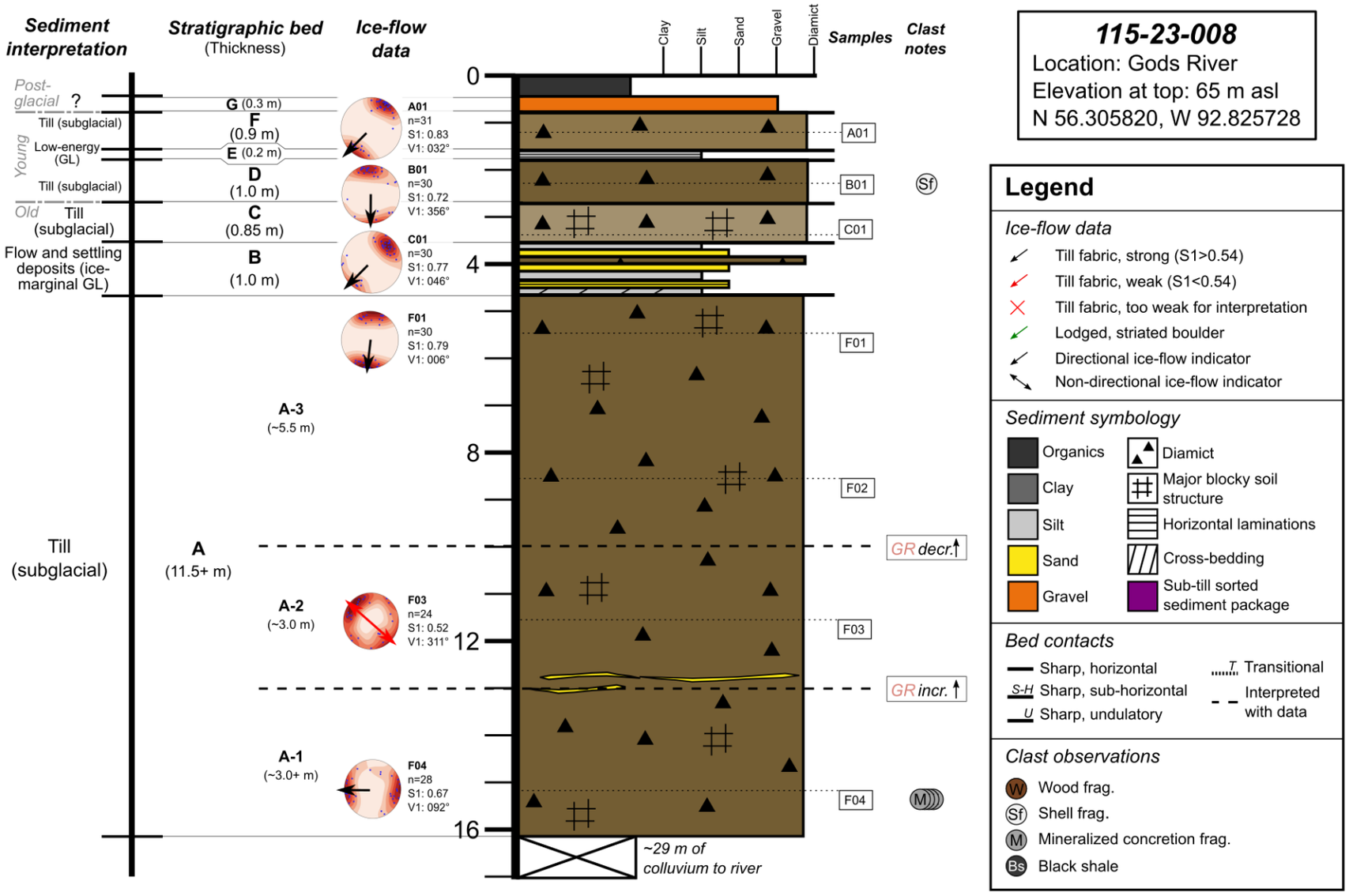


Figure 3.63: Stratigraphic log of section 115-23-008. Diamict beds are coloured by their sampled Munsell colour. Abbreviations: asl, above sea level; frag., fragment; GL, glaciolacustrine; HBB, Hudson Bay Basin; GR, granitoid; UGG, undifferentiated greenstone and greywacke.

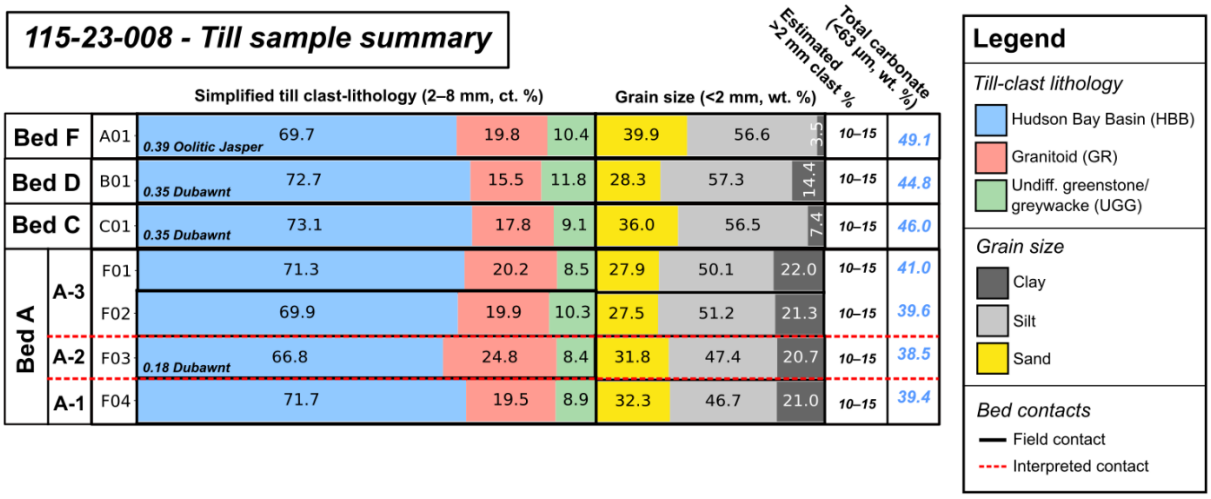


Figure 3.64: Summary of till sample data for section 115-23-008. Abbreviations: ct., count, wt., weight.

The lowermost Bed 8-A is a massive olive-brown (2.5Y 4/4) diamict (Figure 3.65A, B, C), at least 11.5 m thick, that is highly overconsolidated and has a moderately calcareous clayey sandy-silt matrix. Bed 8-A has a well-developed blocky structure with oxidation along joints and contains 10–15% clasts that are granule- to small pebble-sized and striated and/or faceted. Bed 8-A contains discontinuous sand lenses from 12.6–13.1 m (Figure 3.65A) and is gleyed near the top contact. Clast fabrics measured from Bed 8-A suggest a shifting shear stress over time (Appendix G, Table 3). As such, Bed 8-A, originally logged as one bed, has been further separated into three sub-beds based on significant changes in paleo-ice flow direction and/or composition, including at the base of Bed 8-A-1 (~3.0+ m thick, W fabric, 272°), Bed 8-A-2 (~3.0 m thick, SE-NW fabric; 131-311°), and Bed 8-A-3 (~5.5 m thick, S fabric, 186°). The subdivision between Beds 8-A-1 and 8-A-2 is based on the possibility of a 141° change in interpreted ice-flow direction and supported by a significant change in clast lithology (a 5.3% increase in GR concentration; Figure 3.64). Bed 8-A-1 clasts have low HBB and high GR (F04: 71.7% HBB, 19.5% GR, 8.9% UGG), while Bed 8-A-2 clasts have low HBB and very high GR (F03: 66.8% HBB, 24.8% GR, 8.4% UGG; Appendix E, Table 5). Further upsection, the subdivision between Beds 8-A-2 and 8-A-3 is based on the 125° or 55° change in interpreted ice-flow direction and again supported by a significant change in clast lithology (4.9% decrease in GR concentration; Figure 3.64). The interpreted contact between the two sub-beds is tentatively placed due to the compositional and textural similarity of samples F02 and F01. Bed 8-A-3 clasts have low HBB and high GR (F02, F01: 69.9–71.3% HBB, 19.9–20.2% GR, 8.5–10.3% UGG; Appendix E, Table 5). Bed 8-A is interpreted as subglacial traction till.

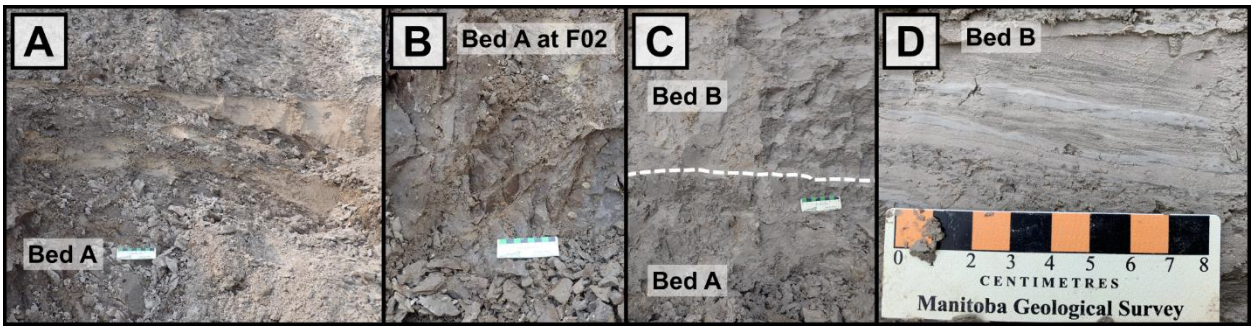


Figure 3.65: (A) Discontinuous sand lenses of Bed 8-A. (B) Olive-brown till of Bed 8-A. (C) Bed 8-A is overlain by laminated silt of Bed 8-B. (D) Interbedded silt and fine sand exhibits micro-faulting within Bed 8-B.

Bed 8-B consists of 1.0 m of laminated to interbedded silt and fine sand (Figure 3.65C, D), containing diamict beds that increase in thickness and abundance upsection. Laminations are horizontal to cross-bedded and micro-faulting is observed within the laminations (Figure 3.65D). Bed 8-B is interpreted as an ice-proximal glaciolacustrine deposit. Bed 8-B overlies Bed 8-A with a sharp horizontal contact.

Bed 8-C is a massive light-yellow brown (2.5Y 6/3) diamict (Figure 3.66A, B, C), 0.85 m thick, that is highly overconsolidated, has a moderately calcareous sandy-silt matrix, has a well-developed blocky structure with oxidation along joints, and contains 5–10% striated and/or faceted subangular to subrounded clasts that are granule- to small pebble-sized. One unimodal clast fabric was measured from Bed 8-C and is interpreted to indicate shear stress was SW (226°, Appendix G, Table 3). Bed 8-C clasts have high GR (C01: 73.1% HBB, 17.8% GR, 9.1% UGG; Appendix E, Table 5). Bed 8-C is interpreted as subglacial traction till. Bed 8-C overlies Bed 8-B, with a sharp horizontal contact.

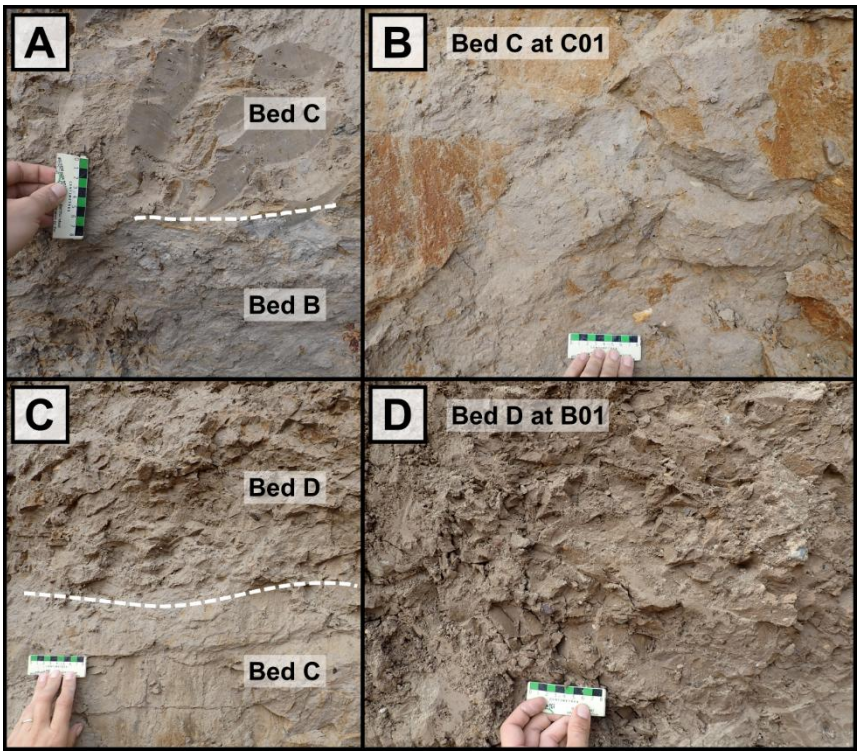


Figure 3.66: (A) Bed 8-B contact with overlying Bed 8-C till. (B) Light yellow-brown till of Bed 8-C. (C) Bed 8-C contact with overlying Bed 8-D till. (D) Olive-brown till of Bed 8-D.

Bed 8-D is a massive olive brown (2.5Y 4/4) diamict (Figure 3.66C, D), 1.0 m thick, that is highly overconsolidated, has a moderately calcareous sandy-silt matrix, has a weakly-developed blocky structure with minor oxidation along joints, and contains 10-15% striated and/or faceted subangular to subrounded clasts that are granule- to medium pebble-sized. Bed 8-D contains a few tan silt stringers which are 1–6 cm thick and extend horizontally 0.9–1.5 m. One spread unimodal clast fabric was measured from Bed 8-D and is interpreted to indicate shear stress was S (176°, Appendix G, Table 3). Bed 8-D till clasts have high UGG (B01: 72.7% HBB, 15.5% GR, 11.8% UGG; Appendix E, Table 5). Bed 8-D is interpreted as subglacial traction till. Bed 8-D overlies Bed 8-C, with a sharp horizontal contact.

Bed 8-E consists of 0.1–0.3 m of laminated yellow-brown silt (Figure 3.67A, B), with 1–3% subrounded, small pebble-sized clasts. Bed 8-E is interpreted as a glaciolacustrine deposit. Bed 8-E overlies Bed 8-D, with a sharp horizontal contact.

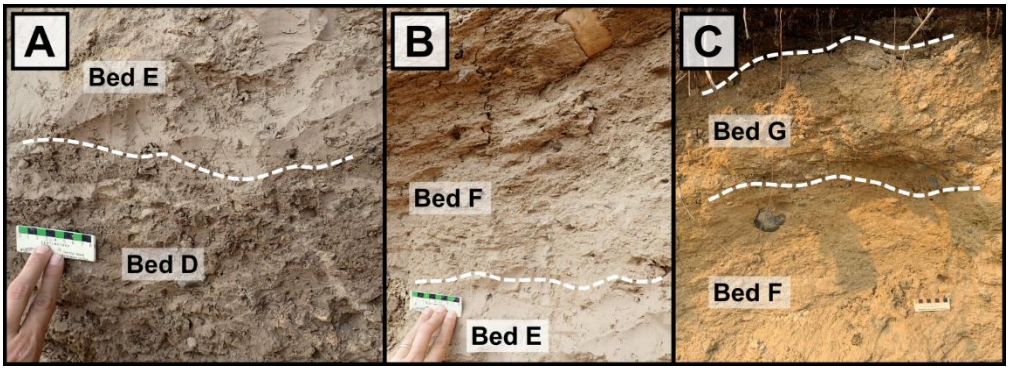


Figure 3.67: (A) Laminated yellow-brown silt of Bed 8-E overlying Bed 8-D till. (B) Light olive brown till of Bed 8-F overlying Bed 8-E. (C) Sandy gravel of Bed 8-G caps the stratigraphic sequence of Section 115-23-008.

Bed 8-F is a massive light olive brown (2.5Y 5/4) diamict (Figure 3.67B, C), 0.9 m thick, that is noncompact, has a highly calcareous sandy-silt matrix, and contains 10–15% striated and/or faceted subangular to subrounded clasts. One unimodal clast fabric was measured from Bed 8-F and is interpreted to indicate shear stress was NE-SW (32-212°, Appendix G, Table 3). Bed 8-F till clasts have low HBB and high GR (A01: 69.7% HBB, 19.8% GR, 10.4% UGG; Appendix E, Table 5). Bed 8-F is interpreted as subglacial traction till. Bed 8-F overlies Bed 8-E, with a sharp horizontal contact.

Bed 8-G consists of about 0.3 m of sandy gravel (Figure 3.67C), interbedded with the underlying diamict of Bed 8-F, that was inaccessible due to safety concerns. Bed 8-G is interpreted as a postglacial deposit (likely either fluvial or marine). Bed 8-G is overlain by modern peat.

3.3.3.8 Section 115-23-009, Gods River

This 44-m-high section (Figure 3.68) extends about 50 m along a northern cut bank of Gods River. It contains 10 stratigraphic beds: 7 diamicts interpreted as till and 3 sorted sediment beds (Figure 3.69). Across the 12 till beds and sub-beds, 18 samples were collected (Figure 3.70).

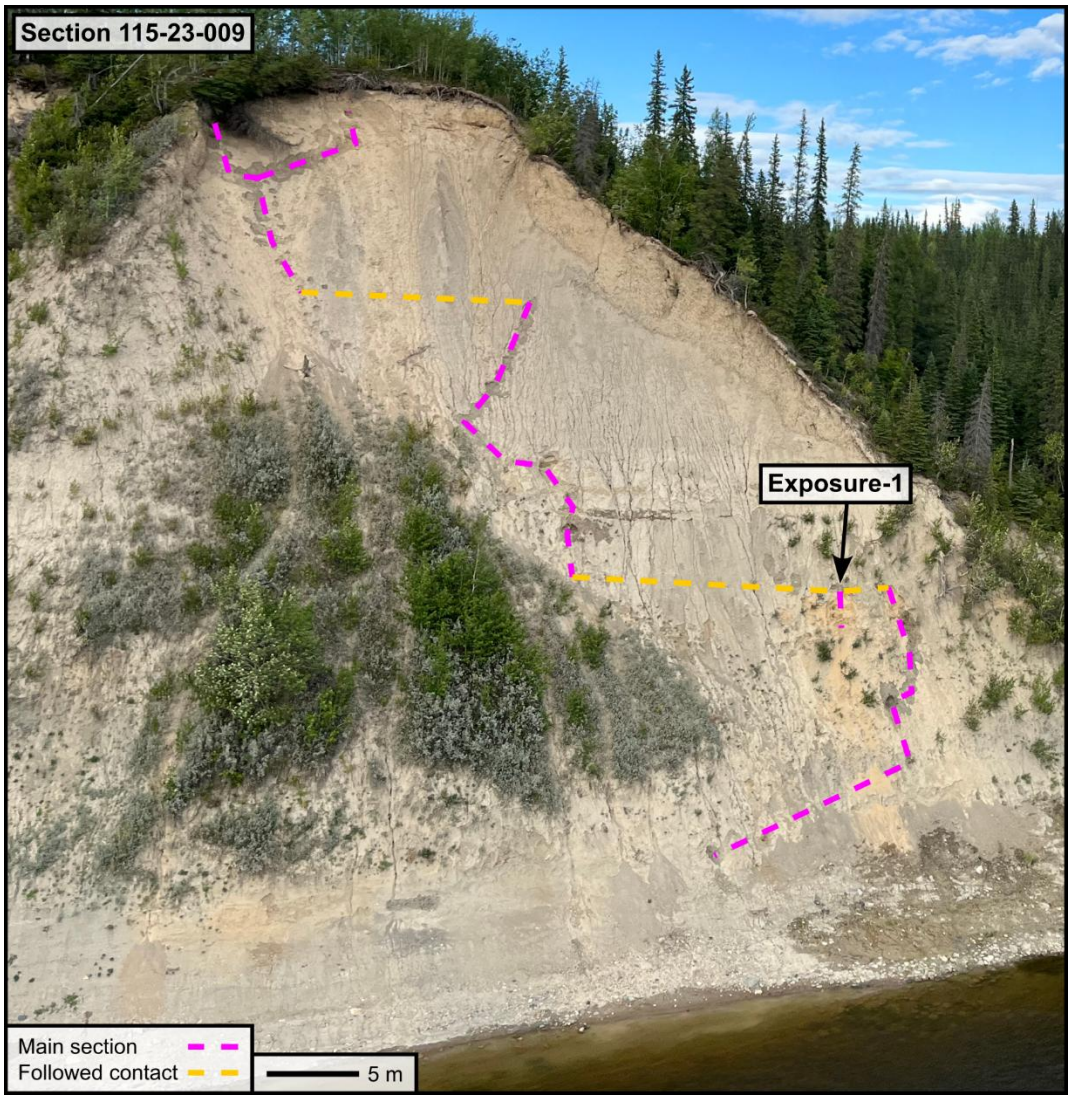


Figure 3.68: Overview of section 115-23-009, viewed towards the northeast.

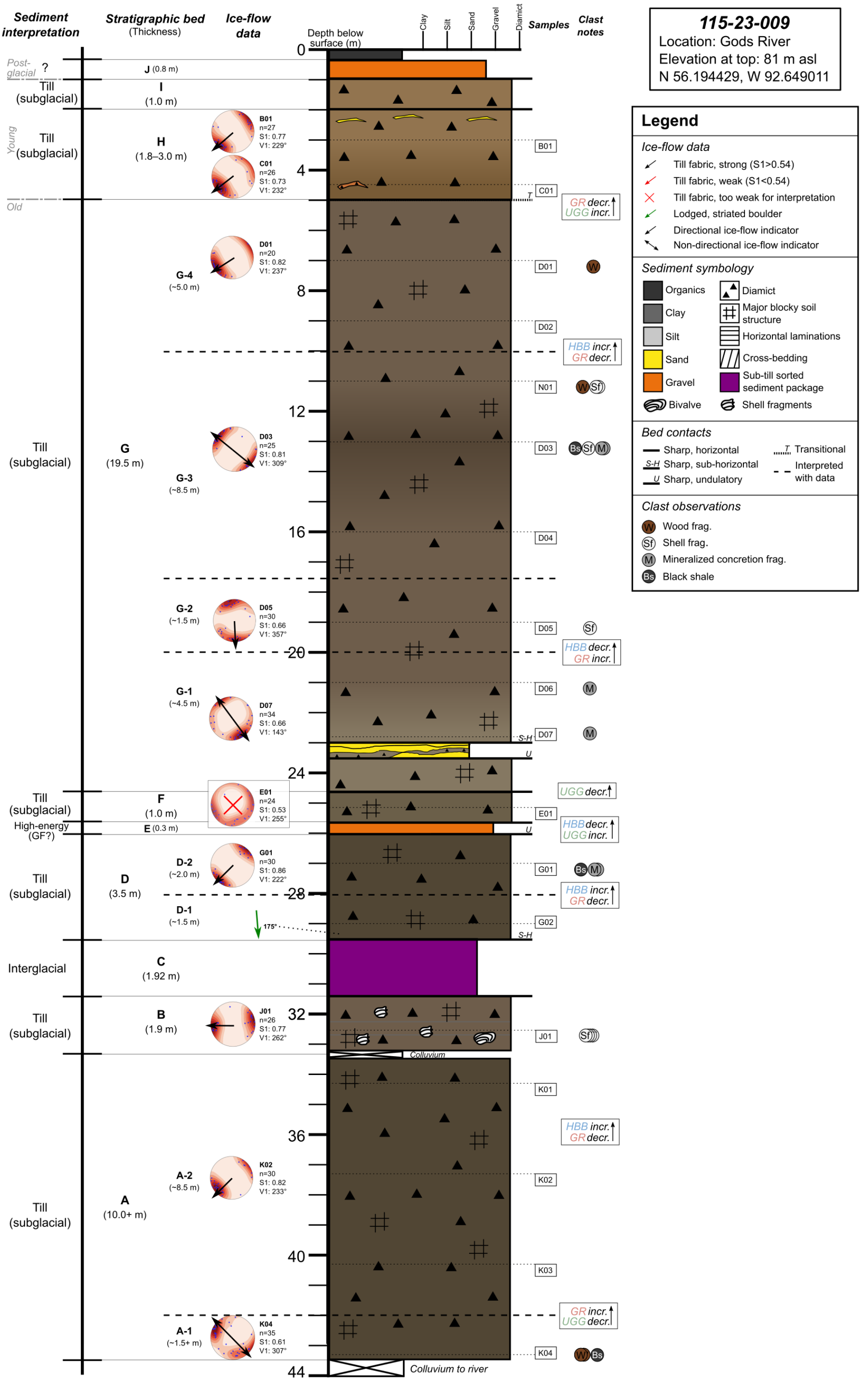


Figure 3.69: Stratigraphic log of section 115-23-009. Diamict beds are coloured by their sampled Munsell colour. Abbreviations: asl, above sea level; frag., fragment; GF, glaciofluvial; HBB, Hudson Bay Basin; GR, granitoid; UGG, undifferentiated greenstone and greywacke.

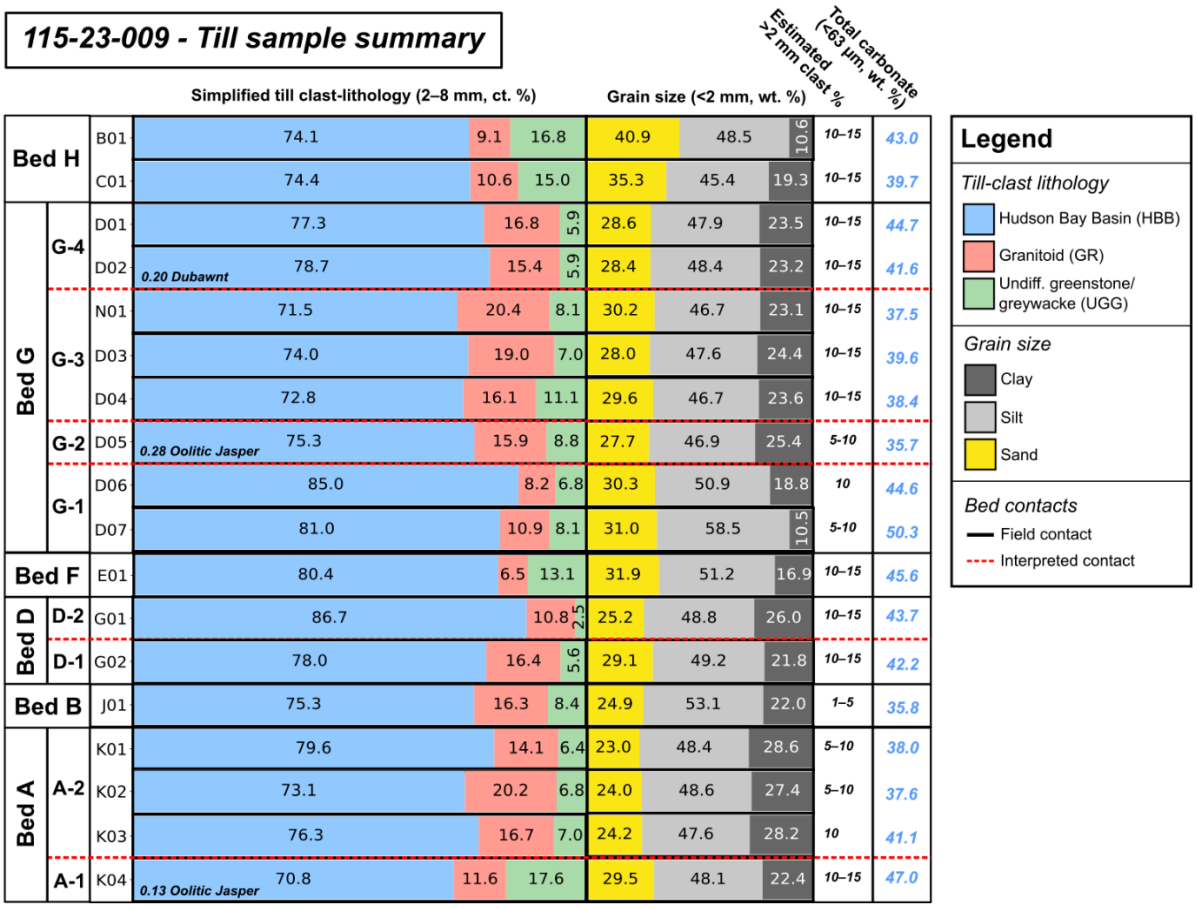


Figure 3.70: Summary of till sample data for section 115-23-009. Abbreviations: ct., count, wt., weight.

The lowermost Bed 9-A is a massive, very dark grey brown (2.5Y 3/2) diamict (Figure 3.71A, B), at least 10.0 m thick, that is highly overconsolidated, has a well-developed blocky structure with oxidation along joints, has a matrix that changes upsection from a highly calcareous clayey sandy-silt matrix that contains 10–15% clasts, to a moderately calcareous sandy clayey-silt matrix containing 5–10% clasts. Notably, till at sample K04 was considerably harder than all other tills observed in the study area, making fabric measurement and sample collection difficult. Clasts are striated and/or faceted, and mostly of granule size. Two spread unimodal clast fabrics measured from Bed 9-A suggest the shear stress direction shifted from SE-NW to SW (127-307°; 233°; Appendix G, Table 3). As such, Bed 9-A has been separated into Bed 9-A-1 (~1.5+ m thick, NW-SE fabric) and Bed 9-A-2 (~8.5 m thick, SW fabric) based on a significant (74°) change in paleo-ice flow direction. This subdivision is supported by significant changes in composition (5.1% increase in GR, 10.6% decrease in UGG, 4.9% increase in total carbonate upsection; Figure 3.70), which also marks the location of the interpreted contact. To elaborate, Bed 9-A-1 clasts show low HBB and high UGG (K04: 70.8% HBB, 11.6% GR, 17.6% UGG), while Bed 9-A-2

clasts have moderate concentrations of all three simplified lithology categories, apart from one sample with a high GR concentration (K03–K01 (n=3): 73.1–79.6% HBB, 14.1–20.2% GR, 6.4–7.0% UGG; Appendix E, Table 5). There is a notable 6.1% decrease in GR concentration upsection after this high-GR sample (from K02 to K01), accompanied by a 6.5% increase in HBB concentration (Figure 3.70). Bed 9-A is interpreted as subglacial traction till.

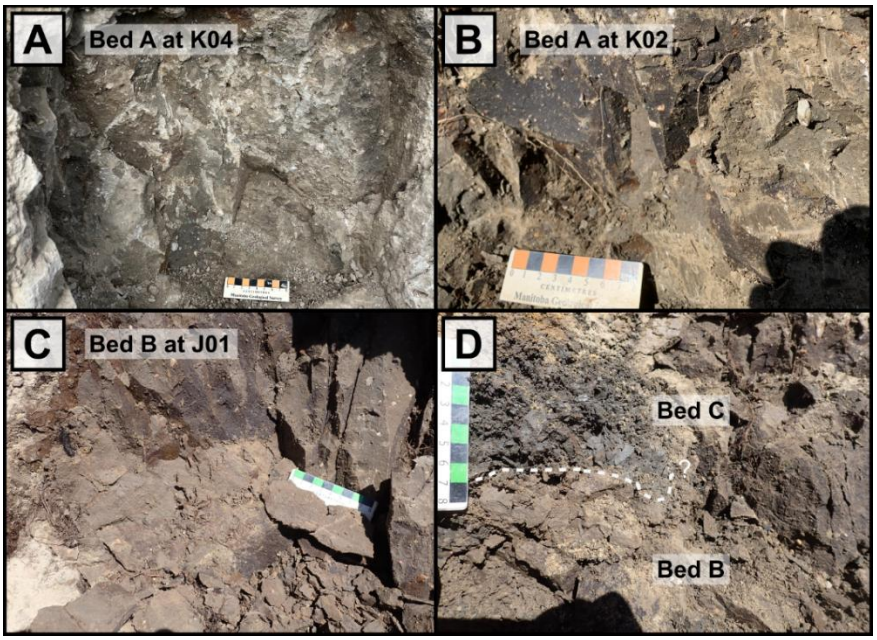


Figure 3.71: (A) Very dark grey brown till of Bed 9-A at K04 and (B) K02. (C) Dark grey brown till of bed 9-B. (D) Sorted sediment of Bed 9-C overlies Bed 9-B till with a sharp undulatory contact that pinches out.

Bed 9-B is a massive dark grey brown (10YR 4/2) diamict (Figure 3.71C, D), 1.9 m thick, that is highly overconsolidated and has a moderately calcareous clayey sandy-silt matrix, has a well-developed blocky structure with oxidation along joints, and contains 1–5% clasts of granule- to small pebble size that are striated and/or faceted. Bed 9-B contains two 0.5 cm thick clay seams and a clay bleb. At least four marine shell fragments were found, 1–2 cm wide, and one whole *Macoma* sp. valve. One spread-unimodal clast fabric was measured from Bed 9-B and is interpreted to indicate shear stress was W (262°, Appendix G, Table 3). Bed 9-B clasts have moderate concentrations of all three simplified lithology categories (J01: 75.3% HBB, 16.3% GR, 8.4% UGG; Appendix E, Table 5). Bed 9-B is interpreted as subglacial traction till. Bed 9-B overlies Bed 9-A, its exact contact hidden by colluvium cover.

Bed 9-C is a sub-till sorted sediment package with one exposure (Exposure-1). At Exposure-1 (Figure 3.72: stratigraphic log; Figure 3.73: photos), Bed 9-C is 2.0 m thick and consists of four lithofacies. At the base is 0.5 m of interbedded medium to coarse sand and silt to very fine sand (lithofacies 9-C-1-1). The uppermost sand layer contains minor beds of very coarse sand and granules along with shell fragments,

while the basal sand layer includes pockets of moderately sorted very coarse sand with shell fragments and charcoal near its base. Lithofacies 9-C-1-1 overlies Bed 9-B with a sharp undulatory contact. This is overlain by 0.04–0.15 m of poorly sorted gravel (lithofacies 9-C-1-2), which consists of 40% granule- to small pebble-sized clasts, some preserving striations on their lower surfaces, in a medium sand matrix. Shell fragments (1–3 mm) and silt laminae are also present near the top of this layer. Lithofacies 9-C-1-2 overlies lithofacies 9-C-1-1, with a sharp undulatory contact. Above this lies 1.3 m of very well sorted medium sand (lithofacies 9-C-1-3), featuring wavy to inclined bedding with rippled cross-laminations and a single silt bed located 0.4 m from the base. Lithofacies 9-C-1-3 overlies lithofacies 9-C-1-2 with a sharp undulatory contact. Capping the section is up to 0.2 m of horizontal to cross-bedded fine sand and silt (lithofacies 9-C-1-4), which overlies the previous layer with a sharp undulatory contact at an incline that pinches out (Figure 3.71D). The presence of charcoal in sub-till Bed 9-C indicates deposition in an interglacial.

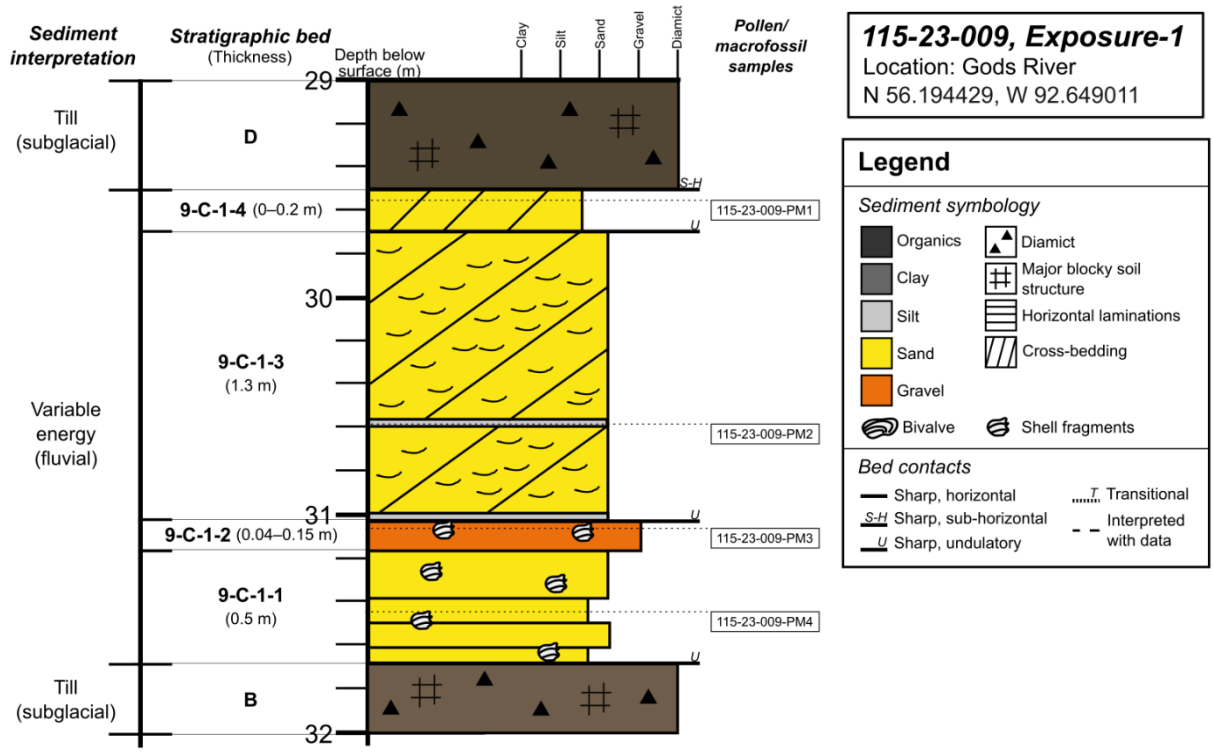


Figure 3.72: Stratigraphic log for Exposure-1 of Section 115-23-009. The diamict bed is coloured by its sampled Munsell colour.

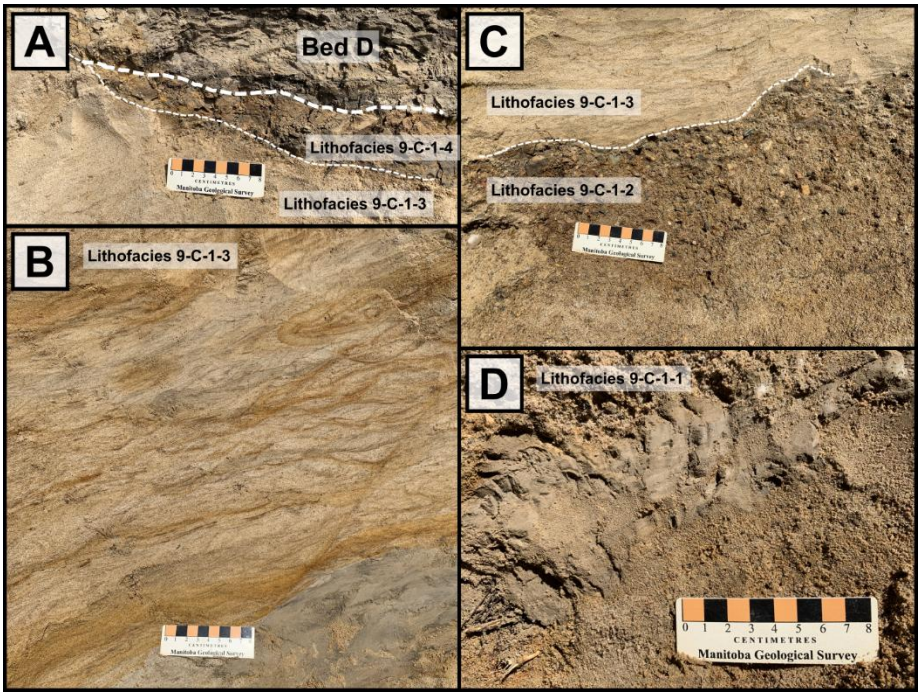


Figure 3.73: The stratigraphic sequence at Exposure-1 of Section 115-23-009, including: (A) Laminated sand and silt (lithofacies 9-C-1-4) overlying medium sand (lithofacies 9-C-1-3). (B) Inclined ripple cross-laminations in lithofacies 9-C-1-3. (C) Poorly sorted gravel (lithofacies 9-C-1-4) and its contact with the overlying sand (lithofacies 9-C-1-3). (D) Interbedded medium to coarse sand and silt to very fine sand (lithofacies 9-C-1-1).

Bed 9-D is a massive, very dark grey brown (2.5Y 3/2) diamict (Figure 3.74A, B), 3.5 m thick, that is highly overconsolidated and has a moderately calcareous clayey sandy-silt matrix, has a well-developed blocky structure with oxidation along joints, and contains 10–15% clasts that are striated and/or faceted. Paleo-ice flow indicators measured from Bed 9-D suggest a changing shear stress over time. The orientation was measured from one striated, lodged boulder within the bottom half of Bed 9-D and is interpreted to indicate shear stress was oriented S (175°, Appendix G, Table 2). One spread unimodal clast fabric was measured from the upper half of Bed 9-D and is interpreted to indicate shear stress was SW (222°, Appendix G, Table 3). As such, Bed 9-D has been separated into Bed 9-D-1 (~1.5 m thick, S fabric) and Bed 9-D-2 (~2.0 m thick, SW fabric) based on a significant change in paleo-ice flow direction. This subdivision is supported by significant changes in composition from G02 to G01 (8.7% increase in HBB, 5.6% decrease in GR upsection; Figure 3.70). Specifically, Bed 9-D-1 has low UGG (G02: 78.0% HBB, 16.4% GR, 5.6% UGG), and Bed 9-D-2 has very high HBB, low GR, and very low UGG (G01: 86.7% HBB, 10.8% GR, 2.5% UGG; Appendix E, Table 5). Bed 9-D is interpreted as subglacial traction till. Bed 9-D overlies Bed 9-C, with a sharp sub-horizontal contact.

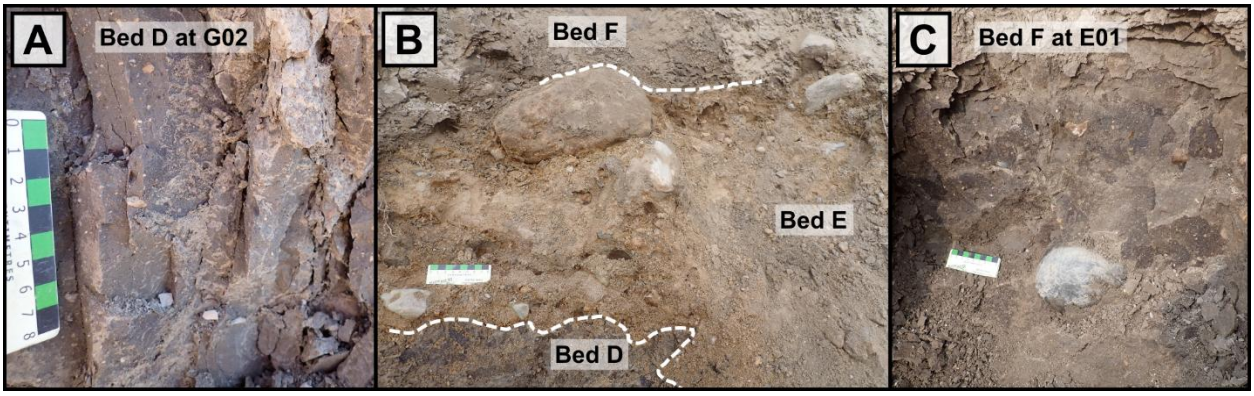


Figure 3.74: (A) Very dark grey brown till of Bed 9-D. (B) Poorly sorted gravel of Bed 9-E surrounded by till beds 9-D and 9-F. (C) Dark grey brown till of Bed 9-C.

Bed 9-E is a poorly sorted gravel (Figure 3.74B), 0.3 m thick, consisting of 20–50% granule- to small pebble-sized clasts that are sub-angular to sub-rounded and faceted, within a silt to medium sand matrix. Bed 9-E also contains some diamict lenses. Bed 9-E is tentatively interpreted as a glaciofluvial deposit. Bed 9-E overlies Bed 9-D with a sharp undulatory contact.

Bed 9-F is a massive, dark grey brown (2.5Y 4/2) diamict (Figure 3.74B, C, Figure 3.75A), 1.0 m thick, that is highly overconsolidated and has a moderately calcareous clayey sandy-silt matrix, has a well-developed blocky structure with oxidation along joints, and contains 10–15% clasts that are granule- to small cobble-sized, sub-angular to sub-rounded, and striated and/or faceted. One spread bimodal clast fabric was measured from Bed 9-F, though due to a lack of clasts and significant spread, a shear-stress direction could not be determined. Bed 9-F clasts have very low GR, and high UGG (E01: 80.4% HBB, 6.5% GR, 13.1% UGG; Appendix E, Table 5). There is a 6.3% decrease in HBB concentration from Bed 9-D (below) to the base of Bed 9-F, and a 10.6% increase in UGG concentration (Figure 3.70). Bed 9-F is interpreted as subglacial traction till. Bed 9-F overlies Bed 9-E with a sharp horizontal contact.

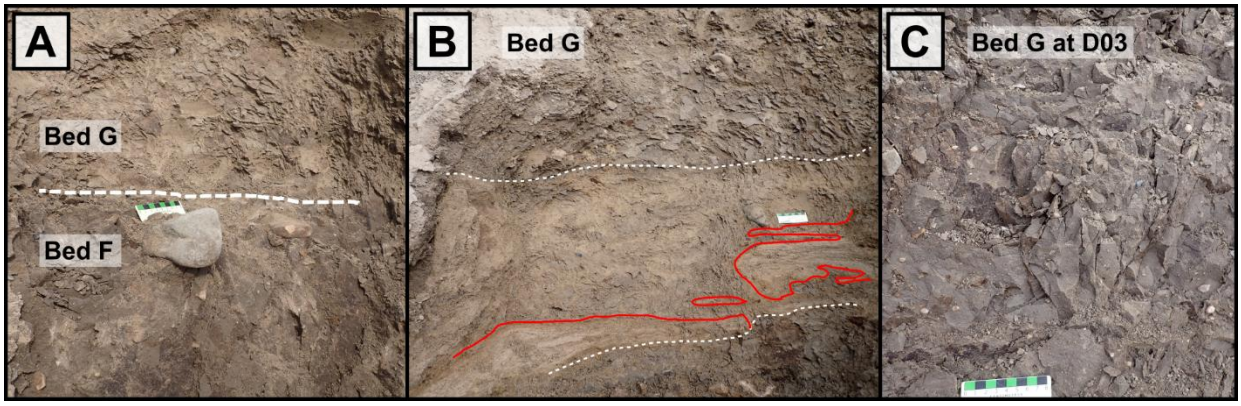


Figure 3.75: (A) Grey-brown till of bed 9-G overlies Bed 9-F till. (B) Contorted beds of diamict and sand within Bed 9-G. White outlines the extent of the feature, and red outlines a distinguishable bed with laminations that show evidence of intrusion from the underlying diamict. (C) The till of Bed 9-G is very dark grey-brown at D03.

Bed 9-G is a massive diamict (Figure 3.75), about 19.5 m thick, with variable colour, mostly dark grey-brown (10YR 4/2), with samples that are also grey-brown (2.5Y 5/2) and very dark grey-brown (10YR 3/2). Bed 9-G is highly overconsolidated and has a moderately to highly calcareous clayey sandy-silt matrix and well-developed blocky structure with oxidation along joints. In the bottommost 7.0 m, Bed 9-G contains 5–10% sub-angular to sub-rounded striated and/or faceted clasts that are of granule- to small pebble size, while in the uppermost 9.5 m, Bed 9-G contains 10–15% striated and/or faceted clasts of granule- to medium pebble size. Spread unimodal clast fabrics measured from Bed 9-G suggest a shifting shear stress over time (Appendix G, Table 3). As such, Bed 9-G, originally logged as one bed, has been further separated into four sub-beds based on significant changes in paleo-ice flow direction and/or composition, including at the base of Bed 9-G-1 (~4.5 m thick, SE-NW fabric; 143-323°), Bed 9-G-2 (~1.5 m thick, S fabric; 177°), Bed 9-G-3 (~8.5 m thick, SE-NW fabric; 129-309°), and Bed 9-G-4 (~5.0 m thick, SW fabric; 237°). The subdivision between Beds 9-G-1 and 9-G-2 is based on the possibility of a 152° change in interpreted ice-flow direction and supported by significant changes in composition (9.7% decrease in HBB, 7.7% increase in GR, 8.9% decrease in total carbonate; Figure 3.70). Specifically, Bed 9-G-1 clasts have high to very high HBB, moderate to low GR (D07, D06: 81.0–85.0% HBB, 8.2–10.9% GR, 6.8–8.1% UGG), and Bed 9-G-2 clasts have moderate concentrations of all three simplified lithology categories (D05: 75.3% HBB, 15.9% GR, 8.8% UGG; Appendix E, Table 5). The subdivision between Beds 9-G-2 and 9-G-3 is based on a significant change in paleo-ice flow direction (48° or 132°). Bed 9-G-3 clasts have moderate to low HBB, moderate to high GR, moderate to high UGG (D04–N01 (n=3): 71.5–74.0% HBB, 16.1–20.4% GR, 7.0–11.1% UGG; Appendix E, Table 5). The subdivision between Beds 9-G-3 and 9-G-4 is based on a significant change in paleo-ice flow direction (69° or 108°) and supported by changes in clast lithology at the interpreted contact (7.2% increase in HBB, 5.0% decrease

in GR; Figure 3.70). Bed 9-G-4 clasts have moderate concentrations of all three simplified lithology categories (D02, D01: 77.3–78.7% HBB, 15.4–16.8% GR, 5.9% UGG; Appendix E, Table 5). Additionally, there is a 5.0% decrease in UGG concentration from Bed 9-F (below) to the base of Bed 9-G (Figure 3.70). Bed 9-G contains about 0.5 m of contorted beds of sandy diamict, medium sand, and coarse sand that exhibit intrusion features of the underlying diamict (Figure 3.75B). Bed 9-G is interpreted as subglacial traction till. Bed 9-G overlies Bed 9-F with a sharp sub-horizontal contact.

Bed 9-H is a massive diamict (Figure 3.76), 1.8–3.0 m thick, that changes in colour from dark yellow brown (10YR 4/4) to yellow brown (10YR 5/4) upsection, and ranges in matrix texture from a clayey sandy-silt matrix to a sandy-silt matrix. Bed 9-H has a moderately calcareous matrix, is overconsolidated, has a weakly-developed blocky structure with minor to no oxidation along joints, and contains 10–15% striated and/or faceted clasts that are sub-angular to sub-rounded and of granule- to pebble size. Bed 9-H contains a red diamict lens 0.5 m above its lower contact (Figure 3.76B), and sand lenses in the uppermost 0.5 m (Figure 3.76C). Two spread unimodal clast fabrics were measured from Bed 9-H and are interpreted to indicate shear stress was SW (232°, 229°, Appendix G, Table 3). Bed 9-H clasts have low GR and high UGG (C01, B01: 74.1–74.4% HBB, 9.1–10.6% GR, 15.0–16.8% UGG; Appendix E, Table 5). There is a 6.2% decrease in GR concentration from Bed 9-G (below) to the base of Bed 9-H, and a 9.1% increase in UGG concentration (Figure 3.70). Bed 9-H is interpreted as subglacial traction till. Bed 9-H overlies Bed 9-G, its contact transitional to sharp and sub-horizontal (Figure 3.76A).

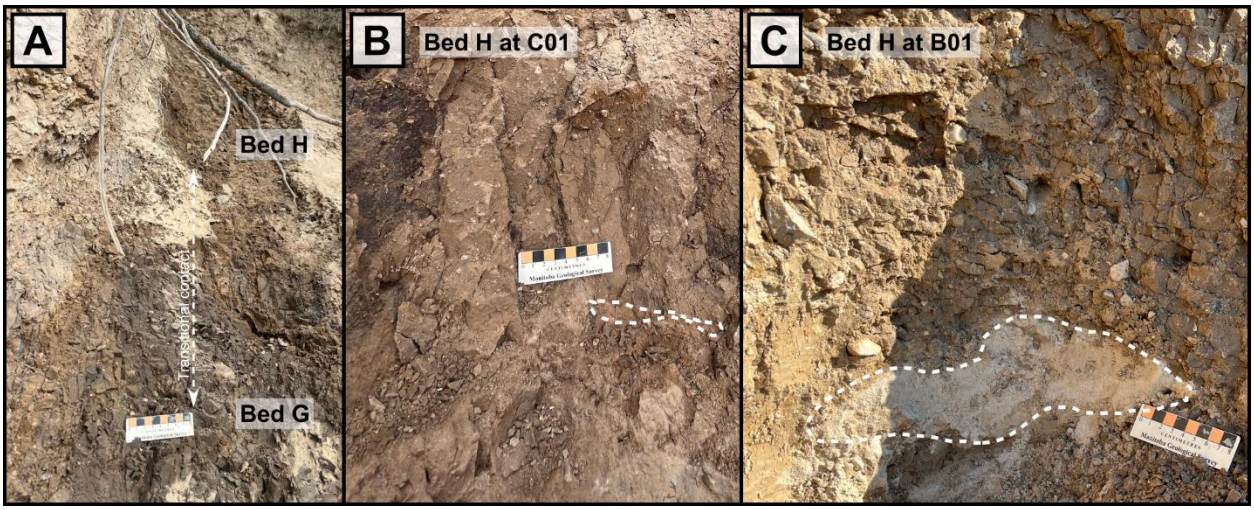


Figure 3.76: (A) A transitional contact is observed between till beds 9-G and 9-H. (B) Dark yellow brown till of Bed 9-H. A small red diamict lens is outlined in white. (C) Yellow brown till of Bed 9-H. A sand lens is outlined in white.

Bed 9-I is a massive, crumbly yellow brown diamict (Figure 3.77) about 1.0 m thick, which was inaccessible due to safety hazards. Bed 9-I is interpreted as subglacial traction till. Bed 9-I overlies Bed 9-H with a sharp horizontal contact.

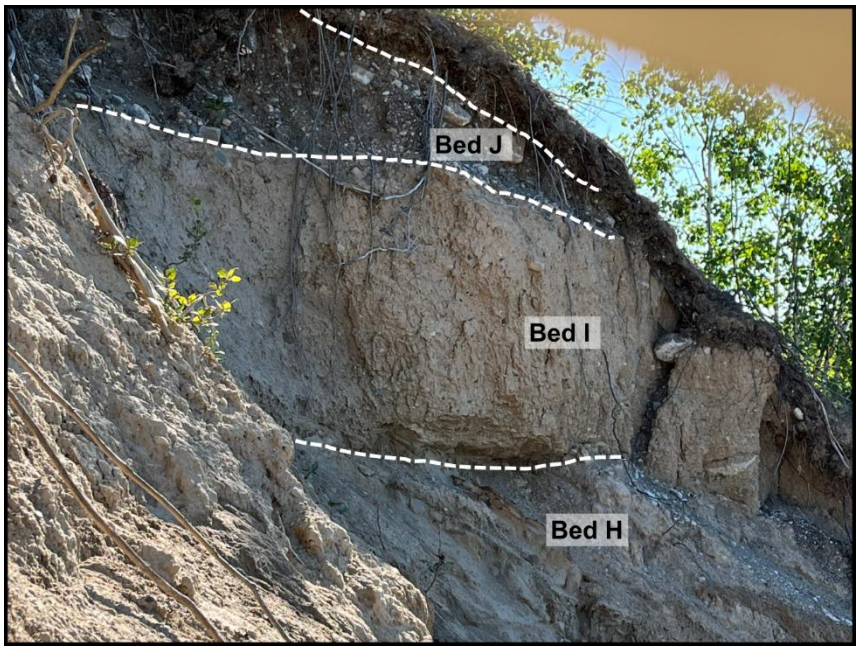


Figure 3.77: Beds 9-H, 9-I, and 9-J, observed from a distance. Bed 9-I is approximately 1 m thick.

Bed 9-J is a sandy gravel (Figure 3.77), about 0.8 m thick, inaccessible due to safety hazards, that overlies Bed 9-I with a sharp horizontal contact. Bed 9-J is tentatively interpreted as a postglacial deposit and is overlain by modern peat.

3.4 Discussion

The studied sections in the Gods River area reveal a complex stratigraphic architecture of tills with unique combinations of stratigraphic position, interpreted ice-flow direction, and sedimentological properties (Figure 3.78). No single site preserves a complete stratigraphic record, so correlations between sites are key in deciphering the local Quaternary history and relative ice-flow chronology.

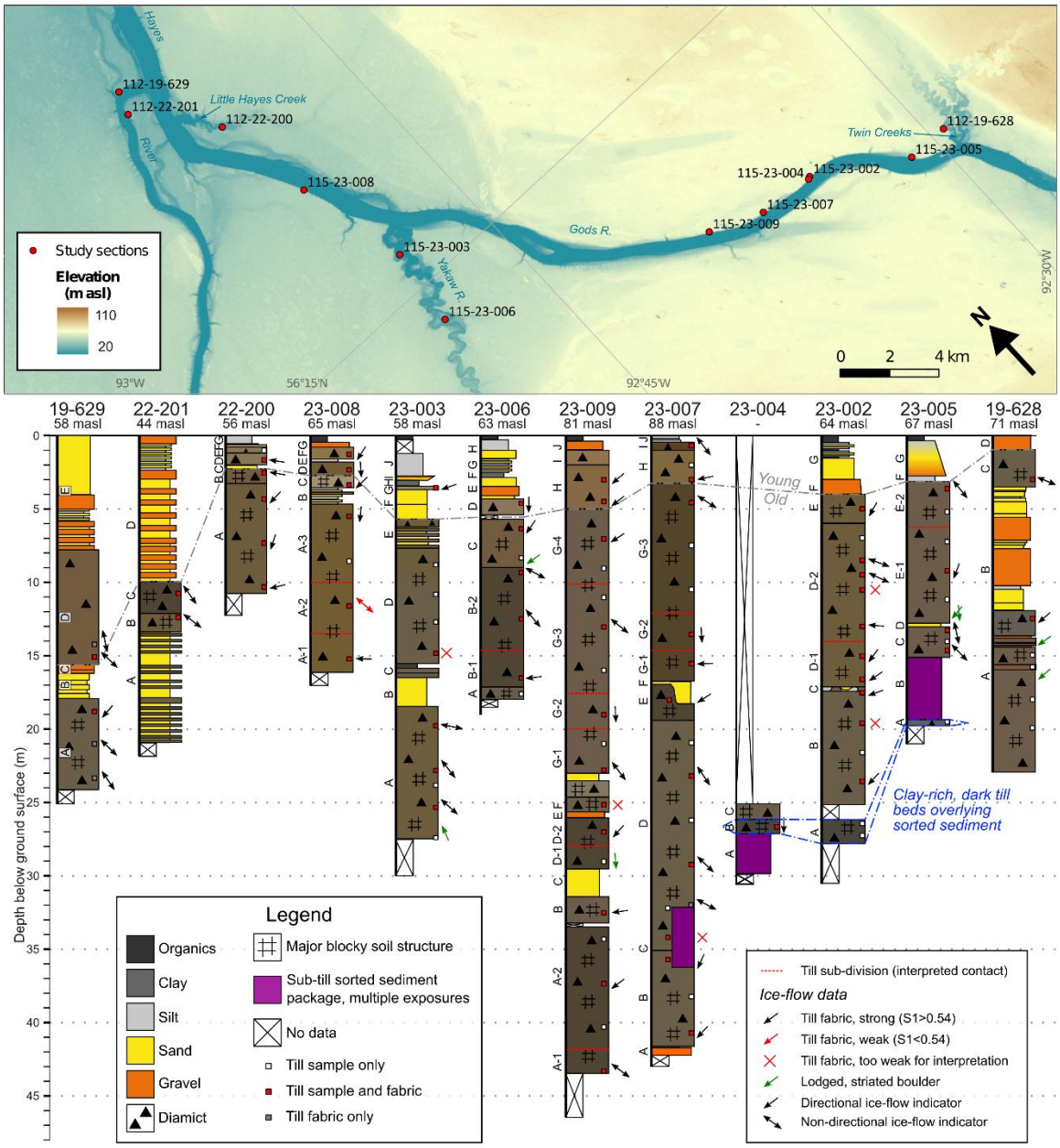


Figure 3.78: Simplified stratigraphy of sections from the study area, with paleo-ice flow indicators, till sub-beds based on laboratory data, and tentative correlations (including a division between upper 'young' till beds versus 'older' ones in gray, and clay-rich, dark till beds overlying sorted sediment in blue).

At this stage, preliminary correlations can be made based on certain observed till characteristics, including texture and degree of diagenetic alteration. The uppermost till beds of sections are often loose and crumbly, or with weakly-developed blocky soil structure, in stark contrast to underlying till beds with a well-developed blocky soil structure. Such upper till beds (8-D, 8-F, 3-G, 6-D, 9-H, 9-I, 7-H, 7-I) are tentatively correlated on this basis, and interpreted to be deposited during a younger glaciation than underlying tills (Figure 3.78). These upper till beds are tentatively assigned to the last glaciation. Additionally, several till beds overlying sub-till sorted sediments (4-B, 2-B, 5-A) are tentatively correlated based on their similar clay-rich texture (see the sub-population in section 3.3.1.2) and dark colour, which likely reflects incorporation of underlying fine-grained material deposited under anoxic conditions (Figure 3.78).

Western sections (23-008, 23-003, 23-006; Figure 3.78) are also distinguishable from eastern sections (23-009, 23-007, 23-004, 23-002, 23-005) from preliminary till composition results: western sections reveal till beds with very high GR clast proportions for the study area, while eastern sections tend to have higher proportions of HBB clasts. Additionally, more extensive eastern sections (23-009, 23-007) record a high number of till beds and sub-beds (n=12 and n=8, respectively), reflecting a complex ice-flow history between different interpreted ice-flow directions.

Dominant interpreted ice-flow directions include SW and NW-SE (see section 3.3.1.4), with many NW-SE, WNW-ESE, and NNW-SSE interpreted ice-flow directions still maintaining an uncertain ice-flow direction. Till beds associated with NW-SE ice-flows may be able to be discerned by till composition analysis in the next chapter, which focuses on better understanding till provenance.

3.4.1 Reworked and discontinuous till beds

Till beds, defined in the field based on traceable contacts and lateral correlations, not only have variable properties between sections (e.g., interpreted ice-flow direction, colour, texture, degree of diagenetic alteration), but they are also internally heterogenous. Notably, several till beds exhibit dramatic shifts in interpreted ice-flow direction yet are not accompanied by a change in till composition (e.g., clast lithology, total carbonate). For instance, Bed 7-G exhibits 2 interpreted shifts in ice-flow direction, one of which is approximately 90°, yet clast lithologies remain generally similar. To account for complexities within till beds, 12 subdivisions were made (interpreted contacts), based on shifts in ice-flow direction and accompanying changes in till properties.

Additionally, till samples share relatively similar textural and compositional properties. Most till samples exhibit grain size distributions clustered around a clayey sandy silt matrix, with four exceptions exhibiting a higher clay content (likely due to incorporation of underlying clay-rich sub-till sorted sediments). The

proportionality of clast lithologies is also generally consistent across till samples (albeit with important variations discussed further in Chapter 4): carbonate clasts derived from the HBB consistently dominate clast-lithology counts, while GR and UGG proportions are more variable.

The lack of strong changes in till properties with major changes in ice-flow direction, paired with a generally coherent distribution of grain size and clast lithology, suggests that many tills represent overprinted or inherited material rather than entirely new sediment packages deposited by each glaciation. This supports interpretations of the western HBL as a mosaic of variably reworked subglacial sediments shaped by palimpsest ice-flow histories (Trommelen et al., 2013).

These findings indicate that the previous, 4-till stratigraphic frameworks applied to this area (Netterville, 1974; Dredge et al., 2011) do not properly characterize observed variability in ice-flow direction and more subtle compositional changes within and between tills. Other recent studies in the HBL have also observed similar stratigraphic complexity (e.g., Hodder et al. 2024b). Despite this complexity, ice-flow direction remains a valuable tool for correlations, which is where till composition analysis may facilitate discerning NW versus SE provenance, as demonstrated in recent studies (Hodder et al., 2024b).

3.4.2 Multiple, discordant sub-till sorted sediments

Sub-till sorted sediment packages are primarily interpreted as either fluvial or marine in origin, although exposures grouped within the same package do not always share the same depositional interpretation. For example, in Bed 7-C at section 115-23-007, Exposures 4 and 5 (located ~10 m apart) show contrasting stratigraphic sequences and are interpreted as fluvial and marine, respectively. At this same section, two sub-till sorted sediment packages (beds 7-A and 7-C) are interpreted to reflect ice-free conditions, representing two separate interglaciations based on their stratigraphic positions (i.e., relative to their bounding till beds). This is the first documented case in the HBL where multiple interglacial sorted sediment packages are observed within a single stratigraphic succession at one site. Lateral heterogeneity and multiple exposures within just this one section further exemplify the need for caution when interpreting ages of sub-till sorted sediments.

3.4.3 Postglacial sequence

The postglacial succession consists, in upwards order, of glaciolacustrine, then marine, and then fluvial sediments. This observed sequence agrees with the current conceptual model of deglaciation in the western HBL (i.e., glacial Lake Agassiz followed by Tyrrell Sea; see section 1.2.4.2). Whole shells sampled from postglacial marine sediments returned radiocarbon ages of 7700 ± 25 and 7490 ± 25 ^{14}C years BP, similar to others obtained from Tyrrell Sea sediments (c.f. Gauthier et al., 2020). One dated shell fragment from within postglacial gravels yielded non-finite radiocarbon ages and is therefore interpreted as allochthonous and originating from older marine deposits that predate the Tyrrell Sea.

3.5 Conclusions

This chapter presented the results of field-based stratigraphic investigations in the study area, including sedimentological observations, measurement and interpretation of paleo-ice flow indicators, and a revision of stratigraphic sequences at individual sections. A total of 62 till beds and sub-till sorted sediment beds were recorded and sampled in detail, and substantial changes were observed between vertical exposures and within tills. Tentative correlations were made between tills with similar sedimentological characteristics, including uppermost till beds interpreted as younger, and clay-rich tills overlying sorted sediment. Till beds, although recording dramatic changes in ice-flow direction variably paired with changes in till properties, also exhibit evidence of inheritance and overprinting. Sub-till sorted sediment beds were observed in many exposures, at times at multiple stratigraphic positions within the same section and with laterally variable depositional environments. The observed postglacial sequence and radiocarbon ages in the uppermost sediments, when present, align with the expected transition from glacial Lake Agassiz to the Tyrrell Sea, and subsequent glacioisostatic uplift.

The work presented in this chapter represents a crucial first step in unravelling the complex Quaternary stratigraphy of the study area, as these observations provide the foundational context for further analysis. Chapter 4 builds on these observations by analyzing till composition to support later stratigraphic correlations and investigate the possible relationship between paleo-ice flow direction and till composition, with particular interest in discerning provenance for tills associated with a NW-SE interpreted ice-flow direction.

Chapter 4: Till composition analysis

4.1 Introduction

This chapter discusses the results of lab-based compositional analysis of till samples, with a focus on clast-lithology counts and till-matrix geochemistry. Here, till-composition analysis is used to explore the relationship between till composition and paleo-ice flow direction to better understand till provenance and mixing from different bedrock source regions. Patterns in till composition within and between sections are secondarily used to contribute to stratigraphic correlations.

4.2 Methodology

Till samples collected during stratigraphic investigations of the study area were analyzed for clast-lithology counts (2–8 mm size fraction; section 2.3.2) and matrix geochemistry (<0.063 mm size fraction; section 2.3.3). When possible, this data was then compiled with other till samples from nearby sections analyzed with similar methodology (section 2.2.5). K-means clustering was used on clast-lithology counts (section 2.3.2.1), and PCA was used to reduce dimensionality in the matrix geochemistry dataset, and to interpret principal components as proxies for provenance driving the observed variance (section 2.3.3.1).

4.3 Results

4.3.1 Clast-lithology counts

Tabulated clast-lithology results are provided in Appendix E, and the normalized proportions are visualized in stratigraphic order in 'Till sample summary' figures of section 3.3.3 and subsections therein. Although clast-lithology counts were addressed briefly in their stratigraphic context in Chapter 3, the following results represent a more integrated approach to analyzing till composition.

Clast-lithology counts were conducted and tabulated for samples collected in 2022 and 2023 and compiled with data from samples collected in 2019 (n=100 samples total). In general, there is a dominant proportion of HBB clasts, with lesser amounts of GR and UGG (normalized average: 76.2% HBB, 14.8% GR, 8.9% UGG). When plotted as normalized proportions on a ternary diagram (Figure 4.1), clast-lithology counts form a moderately dispersed distribution without strong outliers and display an arcuate trend that forms a compositional continuum between GR-rich and UGG-rich endmembers.

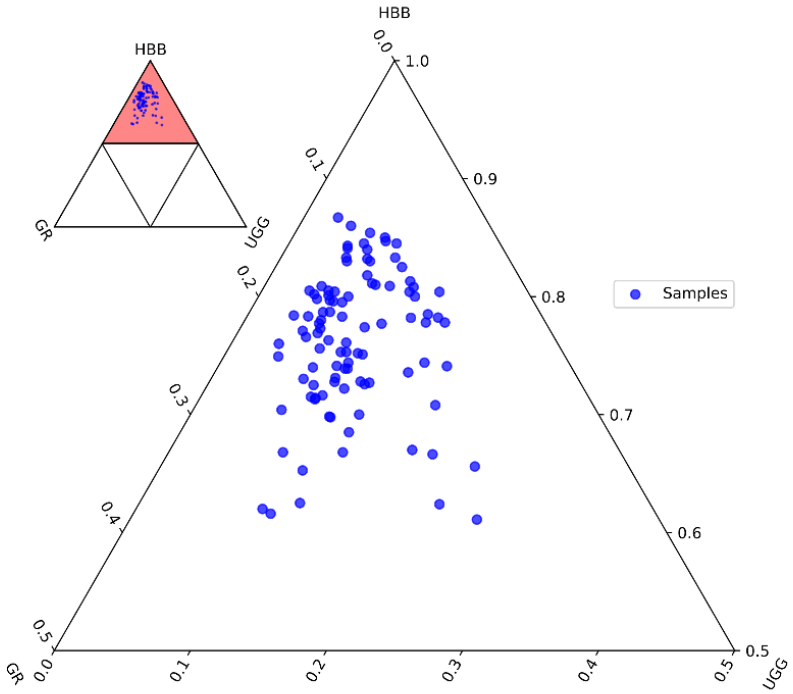


Figure 4.1: Normalized clast-lithology proportion ternary diagram for 2019, 2022, and 2023 samples collected in the Gods River area. Abbreviations: HBB, Hudson Bay Basin; GR, granitoid rocks; UGG, undifferentiated greenstone and greywacke.

Tracer lithologies indicative of spatially-constrained bedrock source regions were also observed in the clast lithology counts in trace amounts. Observed tracer lithologies include oolitic jasper, porphyritic rhyolites (Pitz Fm), red minettes (Christopher Island Fm), and red carbonates, sandstones, and siltstones (Kenogami River Fm). Additionally, other distinct clasts observed include shell fragments, black shale clasts, mineralized sulphide fragments, and wood fragments. These clasts are relatively uncommon, observed in only 18% of samples on average, and typically comprise less than 0.50% of the total clast count. One notable exception is the Kenogami River Fm clasts, which are more frequent and tend to have higher proportions when present, although still quite low (average when present: 0.79%).

4.3.1.1 Clast-lithology counts: K-means clustering

First, a centered log ratio transformation was applied to the normalized clast-lithology proportions (see section 2.3.2). K-means clustering was then applied, and five clusters were selected as the best fit based on the elbow method and ease of interpretability (Appendix I, Figure 1). The five K-means clusters follow the arcuate trend observed in the data, although their boundaries are indistinct along the continuum (Figure 4.2). For each cluster, the proportions of major clast categories and observations of distinctive clast-lithologies of clusters are presented in Table 4.1 and Table 4.2, respectively.

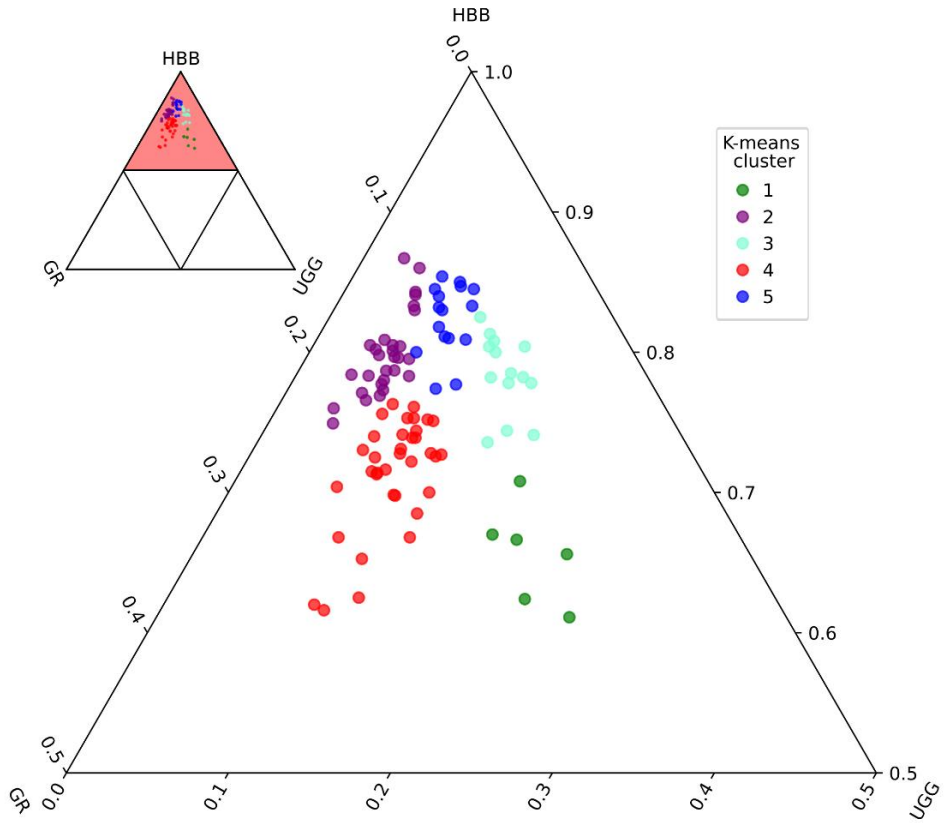


Figure 4.2: K-means clustering applied to normalized clast-lithology proportions.

Table 4.1: Normalized clast-lithology proportions by cluster.

Cluster	No. of samples	HBB clasts (ct %)		GR clasts (ct %)		UGG clasts (ct %)	
		Range	*Average*	*Range*	*Average*	*Range*	*Average*
1	6	61.1–70.8	66	11.3–15.5	13	17.6–25.5	21
2	29	75.0–86.7	80	10.2–21.1	15	2.5–7.0	5
3	14	73.5–82.5	78	6.5–12.2	9	9.3–16.8	13
4	35	61.6–76.3	71	14.8–28.7	19	6.5–12.8	9
5	16	77.4–85.4	82	7.6–13.5	10	5.5–10.2	7

Table 4.2: Observations of distinctive lithologies by cluster.

Cluster	No. of samples	Shell fragment (% of samples)	Kenogami River Fm (% of samples)	Dubawnt Supergroup (% of samples)	Oolitic jasper (% of samples)	Shale (% of samples)	Mineralized sulfide concretions (% of samples)	Wood fragment (% of samples)
1	6	0	67	17	33	17	0	17
2	29	17	24	14	3	3	38	7
3	14	0	43	7	7	36	21	7
4	35	20	51	20	26	6	17	11
5	16	12	38	12	6	12	44	6

Cluster 1 is characterized by the highest proportion (>95th percentile) of UGG clasts, HBB clasts in the 1st–17th percentile, and GR clasts in the 29th–54th percentile. Distinctive lithologies more prevalent in Cluster 1 samples include Kenogami River Fm (67% of samples) and oolitic jasper (33%), with no observations of shell fragments or sulphides. Cluster 1 samples are associated with a NW-SE (3 samples), WNW-ESE (1 sample) or SW (1 sample) interpreted paleo-ice flow orientation (Figure 4.3). Cluster 1 is associated with till that exhibits both well-developed and weakly-developed blocky soil structure, with or without oxidation along joint faces. Cluster 1 tills are in five sections throughout the study area (Figure 4.4). As oolitic jasper is likely sourced from ESE–E of the study area, and UGG clasts are likely sourced from E–ENE of the study area (see section 2.3.1), eastern till provenance with interpreted NW and W ice-flow directions is most likely. The one cluster 1 sample associated with SW-trending ice (section 19-629; Appendix H) is at odds with this interpretation but could represent isolated compositional inheritance from the underlying tills with NW-trending fabrics.

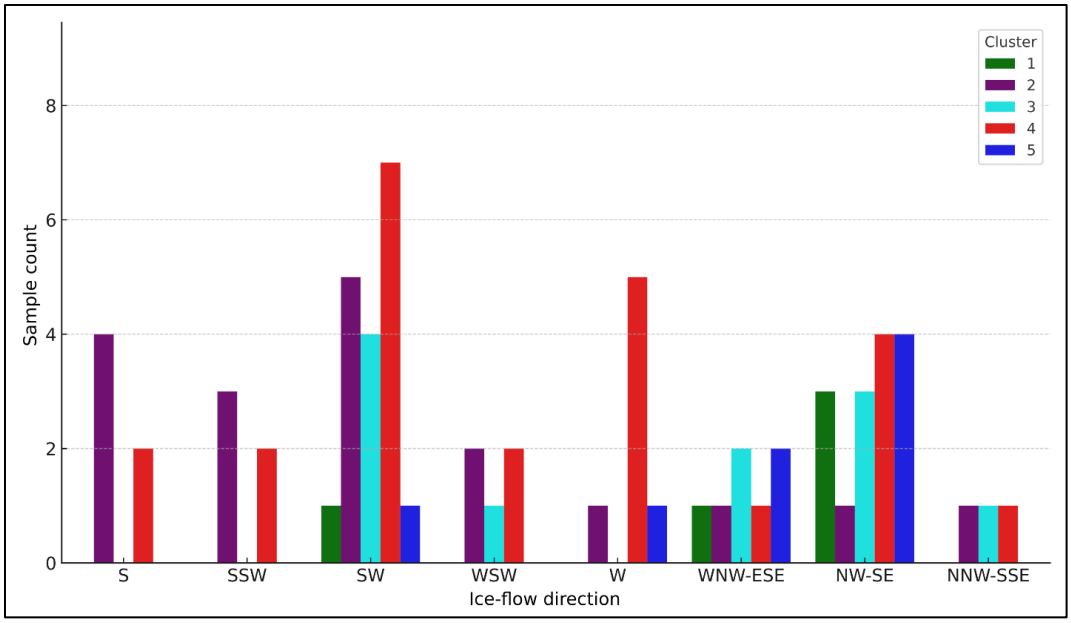


Figure 4.3: Clustered bar chart of clast-lithology clusters and their associated ice-flow direction.

Cluster 2 is characterized by UGG clasts in the 1st–40th percentile, HBB clasts in the 38th–100th percentile, and GR clasts in the 21st–94th percentile. Distinctive lithologies more prevalent in Cluster 2 samples include sulphides (38% of samples) and Kenogami River Fm (24%). Cluster 2 samples are associated with all paleo-ice flow directions but are more common in samples associated with S–WSW directions. Cluster 2 is associated with till that exhibits both well-developed and weakly-developed blocky soil structure, with or without oxidation along joint faces. Cluster 2 samples are mostly situated within eastern sections of the study area (Figure 4.4). S–WSW paleo-ice flow directions and a lack of UGGs suggest a N–ENE till provenance, with variable influence from HBB carbonates and, to the north, from Churchill granitoid source bedrock (Figure 2.4).

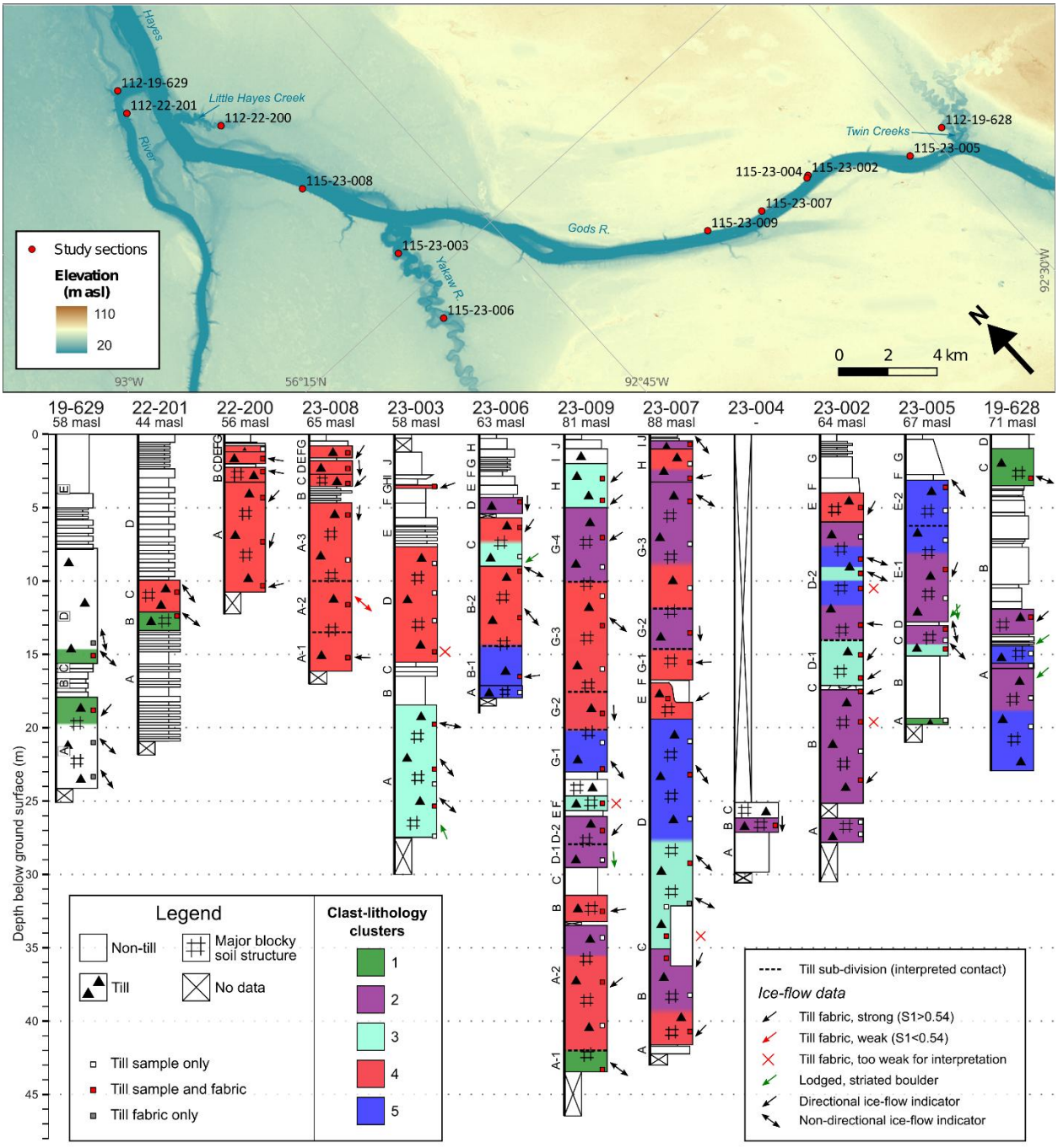


Figure 4.4: Clast-lithology clusters overlaying the simplified stratigraphic sections from the study area. Till samples and/or beds without data are left uncoloured.

Cluster 3 is characterized by GR clasts in the 1st–36th percentile, UGG clasts in the 62nd–94th percentile, and HBB clasts in the 30th–85th percentile. Distinctive lithologies more prevalent in Cluster 3 samples include Kenogami River Fm (43% of samples) and shale (36%), with no observations of shell fragments. Cluster 3 is associated with SW (4 samples), NW-SE (3 samples), WNW-ESE (2 samples), and WSW (1

sample) flows and with tills that exhibit well-developed blocky soil structure and oxidation along joint faces. Cluster 3 samples are more common in the eastern two-thirds of the study area (Figure 4.4). SW and WNW-ESE–NW-SE ice-flow directions, the presence of shale clasts, and near-background levels of GR clasts (~10%) suggest a NE and E till provenance with variable contribution from carbonate and UGG source bedrocks and minor input from shale bedrock. Shale clasts present are likely derived from unmapped shale bedrock in the HBB, such as the Cretaceous shale unit found in drillhole KK1 (see section 1.2.3), which was drilled ~100 km east of the study area.

Cluster 4 is characterized by GR clasts in the 46th–100th percentile, UGG clasts in the 33rd–86th percentile, and HBB clasts in the 2nd–46th percentile. Distinctive lithologies more prevalent in Cluster 4 samples include Kenogami River Fm (51% of samples) and oolitic jasper (26%). Additionally, Cluster 4 has the highest frequency of Dubawnt appearances (20%). Cluster 4 is associated with all paleo-ice flow directions, though more commonly associated with SW (7 samples), W (5 samples), and NW-SE (4 samples) interpreted ice-flow directions. Cluster 4 is associated with tills that exhibit both loose or blocky soil structure, with or without oxidation along joint faces. Samples classified as cluster 4 are more common on the western side of the study area, especially in sections 112-22-200 and 115-23-008, where each till sample belongs to cluster 4 (Figure 4.4). Cluster 4 exhibits a contradictory mix of properties, possibly due to inheritance: SW, W, and NW-SE interpreted ice-flow directions are paired with a moderate to very high proportions of GR clasts, Dubawnt clasts, and oolitic jasper clasts. Unexpectedly, westward ice-flows are associated with a very high proportion of GR clasts (200-C03), and southward-interpreted ice-flows have oolitic jasper clasts present (009-D05). Therefore, it is difficult to interpret a broad provenance that encompasses this group alone; more detail is needed to interpret the provenance of cluster 4 samples.

Cluster 5 is characterized by HBB clasts in the 51st–98th percentile, UGG clasts in the 22nd–71st percentile, and GR clasts in the 3rd–39th percentile. Distinctive lithologies more prevalent in Cluster 5 samples include sulphides (44% of samples) and Kenogami River Fm (38%). Cluster 5 is often associated with a NW-SE (4 samples) or WNW-ESE (2 samples) interpreted ice-flow direction, although some cluster 5 tills are interpreted to have been deposited by SW and W-trending ice-flows (1 sample each). Cluster 5 is associated with till that exhibits well-developed blocky soil structure, with oxidation along joint faces, and are more common on the eastern side of the study area (Figure 4.4). WNW-ESE–NW-SE ice-flow directions, high proportions of HBB clasts, and near-background levels of GR clasts (~10%) suggest a SE–ESE till provenance with high influence from HBB bedrock.

The properties and associations of clast-lithology clusters and their till provenance interpretations are summarized in Table 4.3 below. No clear associations were observed between clast-lithology clusters and grain size distribution.

Table 4.3: Summary of clast-lithology clusters. Abbreviation: pctl. = percentile.

Cluster	Relative clast lithology clast proportion			Most frequent distinctive lithologies	Associated ice-flow directions	Interpreted provenance
	HBB	GR	UGG			
1	1st–17th pctl.	29th–54th pctl.	95th–100th pctl.	Kenogami, jasper	NW-SE (60%), WNW-ESE (20%), SW (20%)	E
2	38th–100th pctl.	21st–94th pctl.	1st–40th pctl.	Sulphides, Kenogami	S–WSW (77%), W (7%), WNW-ESE (7%), NNW-SSE (7%)	N–ENE
3	30th–85th pctl.	1st–36th pctl.	62nd–94th pctl.	Kenogami, shale	SW (50%), NW-SE (38%), WNW-ESE (25%), WSW (12%)	NE and E
4	2nd–46th pctl.	46th–100th pctl.	33rd–86th pctl.	Kenogami, jasper (highest Dubawnt)	SW (29%), W (21%), NW-SE (17%), S (8%), SSW (8%), WSW (8%), WNW-ESE (4%), NNW-SSE (4%)	?
5	51st–98th pctl.	3rd–39th pctl.	22nd–71st pctl.	Sulphides, Kenogami	NW-SE (50%), WNW-ESE (25%), W (13%), SW (13%)	SE–ESE

4.3.2 Till-matrix geochemistry

Till-matrix geochemistry data (lithium metaborate fusion, ICP-MS) from the 2022 and 2023 field seasons (n=8 and n=84, respectively) were compiled, as both datasets were analyzed using the same laboratory, techniques, and detection limits. Data from the 2019 field season (n=8) were excluded from quantitative analysis due to the significant differences in detection limits and analytical methods, as well as the small sample size which would make leveling unfeasible. Data was then pre-processed: censored values were imputed using half of the lower limit of detection for each element, a centered log ratio transformation was applied, and the data was standardized (detailed further in Appendix I).

4.3.2.1 Geochemical data exploration

Clay-rich till beds overlying sorted sediment beds (a tentative correlation discussed previously in section 3.4) are expected to exhibit a trace element signature similar to that of the underlying material. This includes proportions of V, Ba, and Rb that are elevated to that of other tills, as observed in the single grab sample collected from the underlying silty clay interpreted to be deposited under anoxic conditions (004-EXP2-MARINE). Quantile-quantile (QQ) plots of these select trace elements reveal that samples from the previously identified till beds are indeed elevated (002-H01, 002-Z01, 004-B01, 005-P01; Figure 4.5). Surprisingly, several other till samples show similar geochemical signatures (002-B02, 009-D04, 009-D05, 009-N01). These 8 geochemically unique samples have been excluded from PCA to maximize the potential for principal components to represent processes related to provenance, rather than other processes like incorporation of underlying sediment.

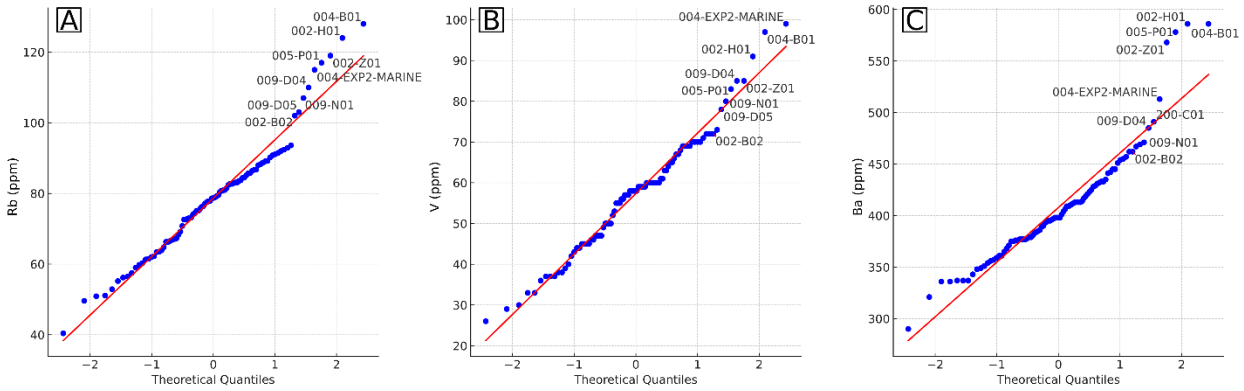


Figure 4.5: QQ plots of select trace elements for till samples and a grab sample of sub-till sorted sediment from section 23-004 (004-EXP2-MARINE), including: (A) Rb, (B) V, and (C) Ba. Elevated samples are labelled.

Before PCA was conducted, relationships between individual elements and major clast-lithology classes were explored. Possible relationships (R^2 value ≥ 0.25) are presented below in Table 4.4. Several expected relationships were very weak or not observed (HBB and Mg: $R^2 = 0.03$; HBB and Total carb: $R^2 = 0.11$; GR and summed rare earth elements [∑REEs: Nd + Sm + Eu+ Gd + Er + Y + Yb]: $R^2 = 0.04$). Due to the possible relationship between Th and GR, Th was considered for PCA as an indicator of granitoid contribution. Despite this weak univariate relationship, Th may still contribute meaningfully to geochemical trends linked to granitoid input in the multivariate context of PCA, especially if Th covaries with other elements commonly associated with granitoids (e.g., Na, Si). Ba was excluded from PCA due to the previously observed association with sorted sediment beds, which could confuse provenance interpretations.

Table 4.4: Coefficients of determination (R^2) showing the strength of relationships between individual element concentrations and clast-lithology proportions. Only $R^2 \geq 0.25$ are shown.

	HBB (ct%)	**GR (ct%)**	**UGG (ct%)**
CaO (%)	0.28		
Ba (ppm)		0.31	
Th (ppm)		0.25	
SiO_2 (%)		0.29	
Na_2O (%)		0.32	0.25

4.3.2.2 Principal component analysis

The element assemblage chosen for analysis includes major elements (Al, Ca, Fe, K, Mg, Na, Si, Ti) and Th (discussed in the previous subsection). Mn and P were not used due to QAQC issues (Appendix I). For the selected element assemblage, the optimal number of principal components was determined to be 2 based on the elbow method (Appendix I, Figure 3). Here, the first two principal components explain 77.2% of the variance of the dataset. Element loadings for these principal components are presented in Figure 4.6.

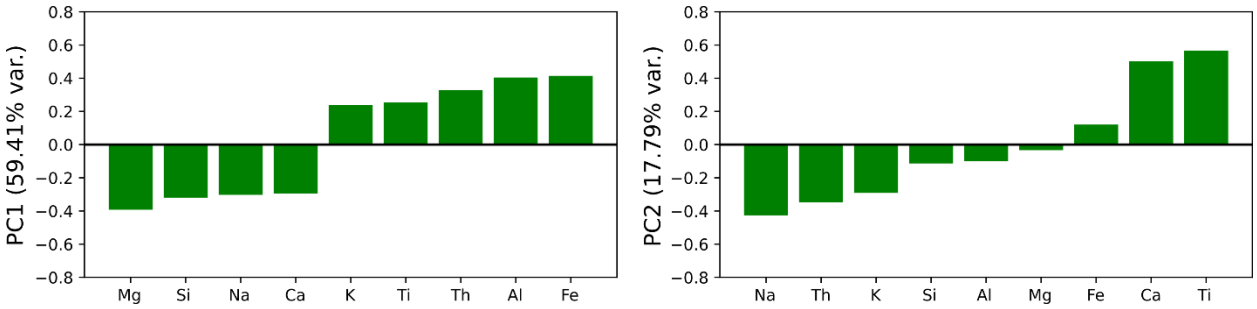


Figure 4.6: Element loadings for each principal component of the selected element assemblage. var. = explained variance.

Matrix texture appears to reflect a large component of PC1 based on the loadings (Si and Na are paired with Ca and Mg, which is unexpected for a provenance signal), particularly the clay content within the analyzed <63 µm fraction (Figure 4.7). High PC1 scores indicate greater proportions of elements typically associated with clay minerals (Fe, Al, K), while low PC1 scores suggest greater proportions of elements associated with coarser materials, such as carbonates (Ca, Mg), quartz (Si), and sodium feldspars (Na), which are more abundant in the silt- and sand-sized fractions.

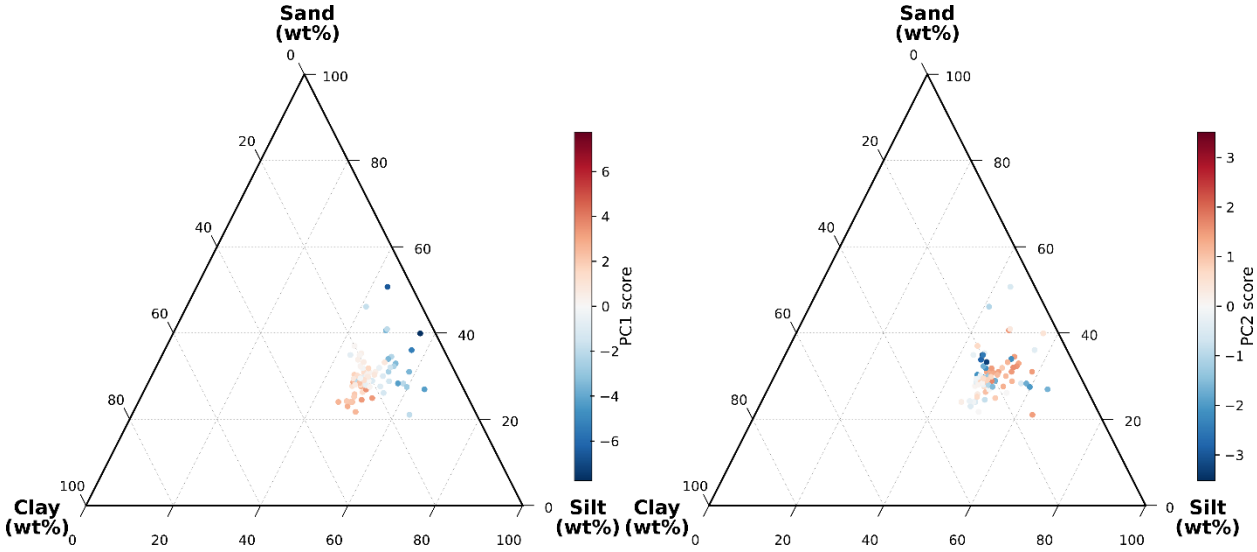


Figure 4.7: Till samples plotted on a ternary grain size chart, coloured by PC1 score (left) and PC2 score (right). The continuous gradation of PC1 scores displayed suggests matrix texture (specifically clay content) is associated with the covariance explained by PC1. Abbreviation: wt%, weight percentage.

PC2 appears to broadly reflect clast lithology, specifically lithologies sourced from the HBB versus non-HBB lithologies. High PC2 scores suggest a higher proportion of Ca, associated with carbonates from the HBB. Meanwhile, low PC2 scores suggest a higher proportion of elements associated with granitoids or greywackes (Th, Na, Si, K, Al). The relationship between PC2 and clast-lithology is demonstrated in Figure 4.8 below. The loading of Fe and Ti is unexpectedly associated with Ca, when considering a simple carbonate versus igneous/siliciclastic geochemical signature. This association may reflect contributions from Fe-bearing carbonates or incorporations of fines from shale sources in the HBB, though it may also result from a covariance effect rather than a direct mineralogical signal.

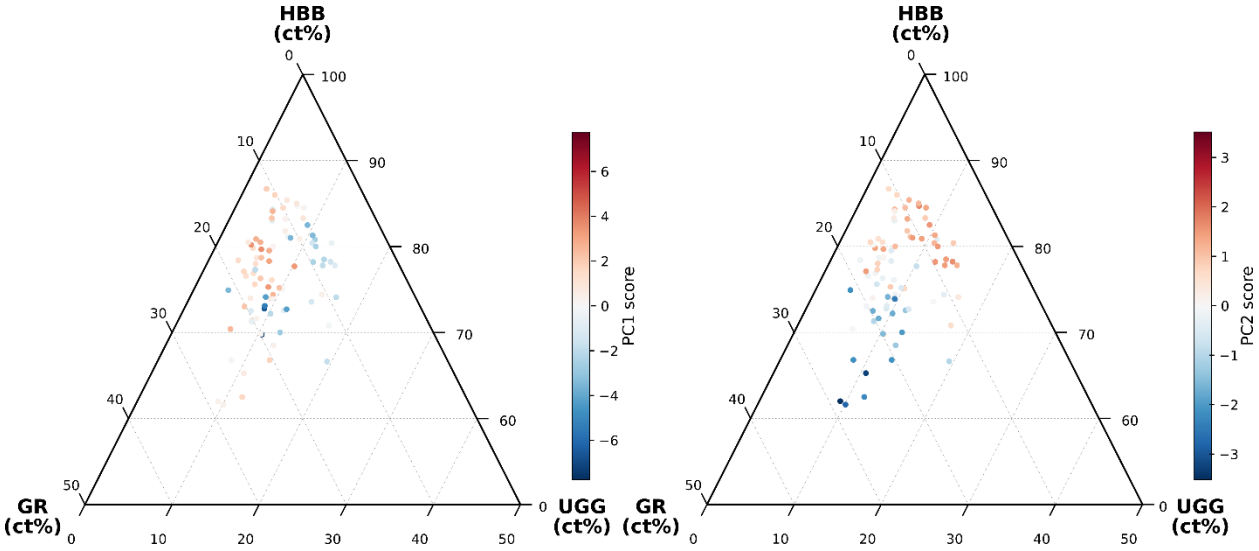


Figure 4.8: Till samples plotted on a ternary clast-lithology plot, coloured by PC1 score (left) and PC2 score (right). The continuous gradation of PC2 scores displayed suggests clast lithology (specifically HBB content) is associated with the covariance explained by PC2. Abbreviations: HBB, Hudson Bay Basin; GR, granitoid rocks; UGG, undifferentiated greenstone and greywacke; ct%, count percentage.

Since matrix texture accounts for much of the variance explained by PC1, it cannot be reliably used to infer provenance. As a result, clustering techniques (e.g., k-means clustering) are of limited value in this case, as not all PCs are related to bedrock provenance. Assuming at least a moderate relationship between the provenance of the till matrix and that of larger clasts, and that PC2 is more clearly related to clast lithologies, PC2 is used to investigate geochemical patterns related to till provenance.

Plotting PC2 scores stratigraphically (Figure 4.9) shows clear distinctions between positive (red), negative (blue), and near-zero scores (grey). First, strongly negative scores (low HBB contribution) are observed in samples from western sections (22-201–23-006). Also, sections often transition from positive to negative/near-zero scores upsection (e.g., 23-003, 23-007), representing a shift in provenance from HBB sources to an influx of non-HBB sources. This transition is also observed within till beds, either

across sub-beds previously established (e.g., 23-006: sub-bed 6-B-1 to 6-B-2, 23-009: sub-bed 9-G-1 to 9-G-2/3) and within sub-bed 2-D-2 at section 23-002. This transition from positive to negative/near-zero scores is notably lacking in section 23-005. Finally, negative scores are uncommon near the bottom of sections, although they are present (e.g., 9-A-2, 7-B, 5-C). This could represent one or more older ice-flow events depositing sediment from non-HBB sources.

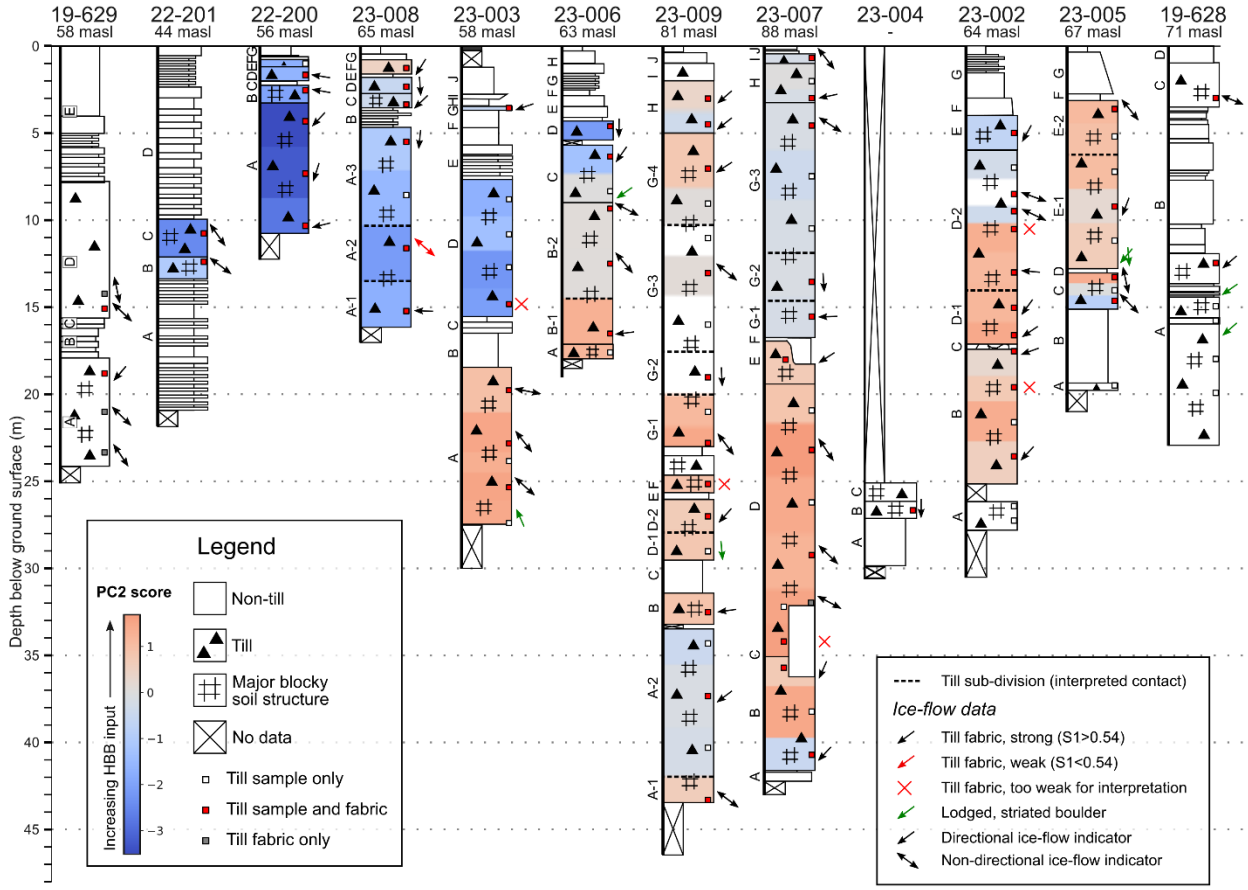


Figure 4.9: PC2 scores overlaying the simplified stratigraphic sections from the study area. Till samples and/or beds without data are left uncoloured, including the 8 samples associated with a reducing geochemical signature (see section 4.3.2.1).

4.4 Discussion

Comparing CL clusters and PC2 score results show many similarities spatially and stratigraphically (Figure 4.10). Western sections tend to have elevated GR clast content (CL cluster 4) and contribution from non-HBB sources (strongly negative PC2 scores), seemingly separate from eastern sections. CL clusters and PC2 scores both show a transition from HBB input to non-HBB/GR input upsection (sections 23-003, 23-006, 23-009, and 23-007): CL clusters 5 and 3 transition to 2 and 4, while PC2 scores transition from positive to negative. PC2 scores seem to show this transition more consistently, especially in section 23-002, where PC2 scores capture a transition that was undetected by a major change in clast-lithology count (and therefore not divided by sub-beds).

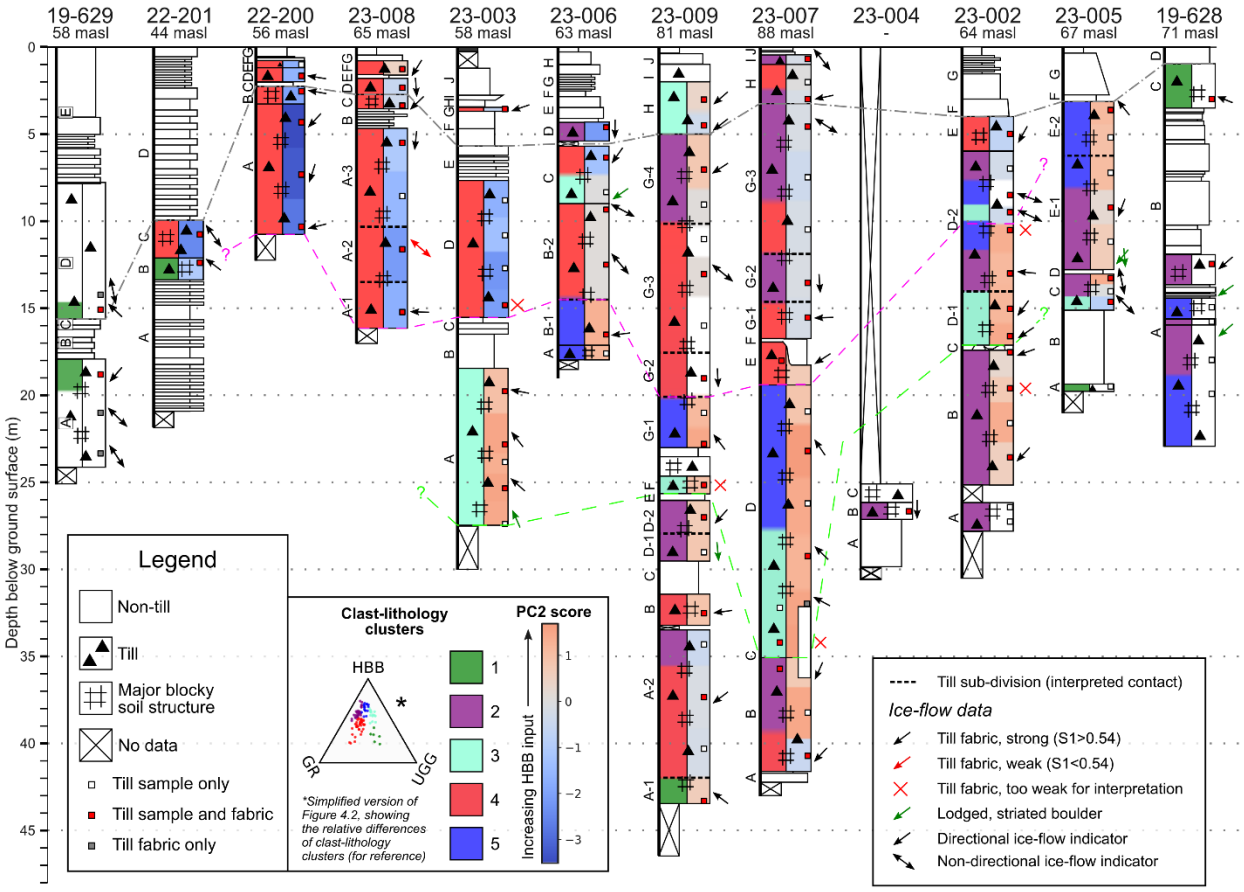


Figure 4.10: Clast-lithology clusters and PC2 scores overlaying the simplified stratigraphic sections from the study area, with several updated ice-flow direction interpretations. Additional preliminary correlations based on these results are shown as dashed lines (magenta and lime green). Till samples and/or beds without data are left uncoloured. Abbreviations: Abbreviations: HBB, Hudson Bay Basin; GR, granitoid rocks; UGG, undifferentiated greenstone and greywacke

At this stage, till samples previously associated with bi-directional interpreted ice-flow directions (NW-SE, WNW-ESE, and NNW-SSE) are interpreted as NW, WNW, and NNW, if: a) they belong to CL cluster 1 (eastern-interpreted provenance with very high UGG and oolitic jasper), or b) they belong to CL cluster 3 or 5 (eastern-interpreted provenance) and have a corroboratory positive PC2 score. Other bi-directional interpreted ice-flow directions are indeterminate due to complications with inheritance and overprinting (discussed in the following section).

Additional stratigraphic correlations can be made based on this updated understanding of till provenance. The first correlative contact (magenta line, Figure 4.10) is drawn at the previously discussed transition between HBB input to non-HBB/GR input, which represents a change in ice-flow direction from W–NW to a variable ice-flow direction (W or SW or indeterminate NW-SE). Another correlative contact (lime green line, Figure 4.10) can be drawn underneath these tills with elevated HBB input. Underlying these tills are sorted sediment packages, which are in turn underlain by tills belonging to CL cluster 2 and associated with a SW–WSW interpreted ice-flow direction.

4.4.1 Evidence of inheritance and overprinting in till composition

A high degree of mixing and gradational changes is evident in the till composition, both within till beds and between sections. This is reflected in the broad compositional similarities among most till samples and unexpected, seemingly inconsistent till composition and ice-flow direction pairs.

The distribution of clast-lithology proportions forms an arc-like continuum (Figure 4.1), with GR- and UGG-rich samples at opposite ends, and HBB-rich samples concentrated in the middle. This continuum suggests inheritance and overprinting of GR and UGG sources, with predominant contribution from local HBB bedrock. The inverse relationship between GR and UGG proportions is also notable, as samples with low HBB rarely exhibit balanced proportions of GR and UGG, which indicates some mutual exclusivity between these sources.

Additionally, many till samples have unexpected pairings between till composition and interpreted ice-flow direction. CL cluster 4 suggests a northern provenance (high granitoid content, Dubawnt erratics) yet associated till fabrics predominately indicate SW and W ice-flow directions (Figure 4.3). Even in clearer trends, these unexpected pairings exist: CL cluster 1 (eastern provenance) has a till sample associated with a SW ice-flow direction, and CL cluster 2 (N–ENE provenance) has a till sample associated with a westward ice-flow direction.

However, mixing is not consistent throughout the study area; some variability exists between sections, especially in clast lithology. CL clusters 2 and 5, which are enriched in HBB clasts, are absent in western sections yet common in eastern sections. These clusters represent intermediate compositions along the GR-UGG continuum, bridging the endmember groups (Figure 4.2). Their presence only in the east may suggest that till beds in eastern sections either underwent a higher degree of mixing or accumulated more HBB-sourced detritus from SW-flowing lobes, while those in the western sections are more reflective of non-HBB endmember compositions.

4.4.2 Geochemical signature for till samples associated with anoxic deposits

One key observation is the connection of specific till samples with a geochemical signature indicative of inheritance of sediments deposited under anoxic conditions. Specifically, elevated concentrations of Rb, V, and Ba are observed in four clay-rich samples with a blue-gray (gleyed) appearance that overlie sorted sediments (samples from beds 4-B, 2-A and 5-A; Figure 4.11).

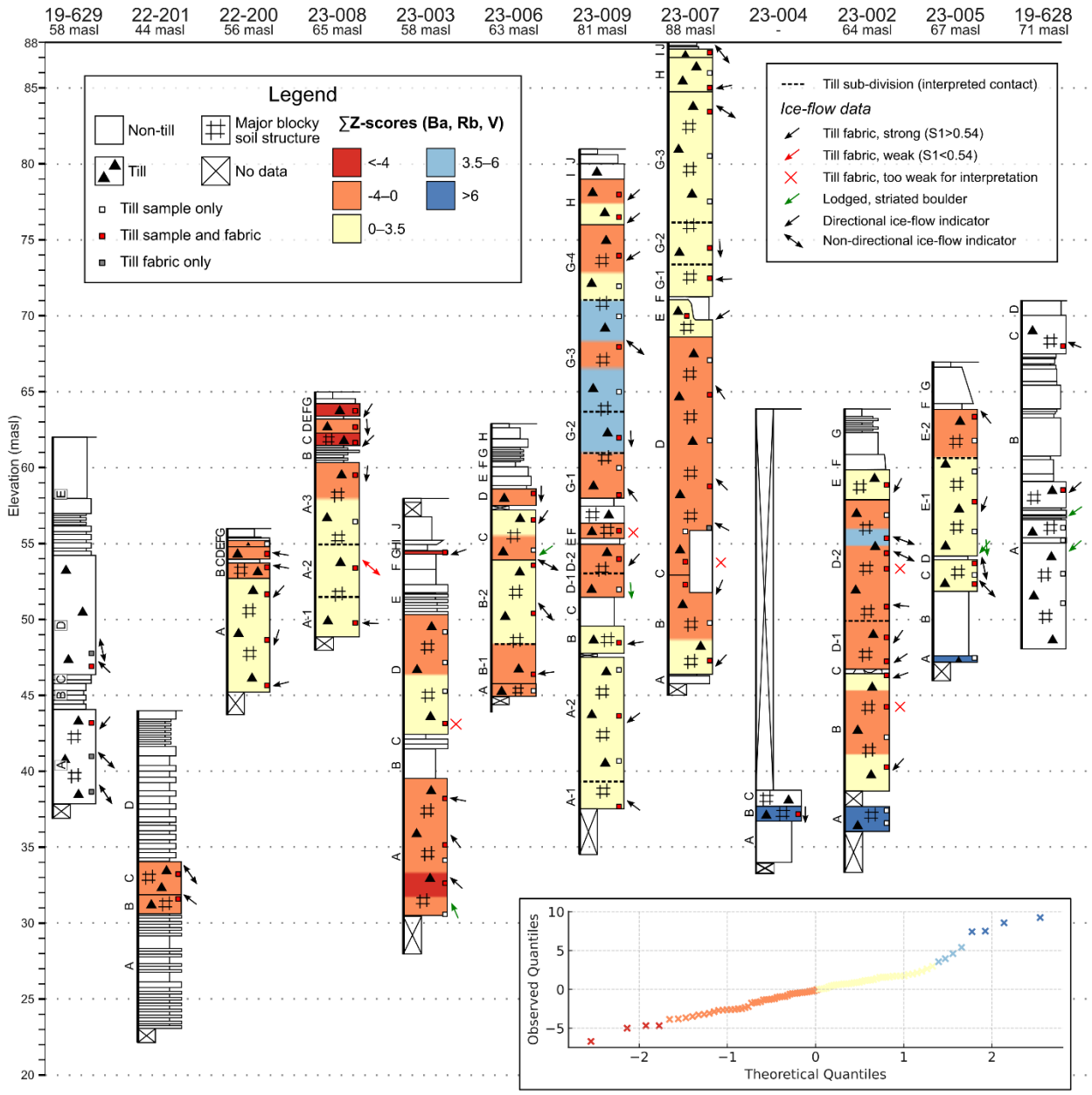


Figure 4.11: Summed Z-scores of elements associated with deposits formed in an anoxic environment (Ba, Rb, V) are overlain on the simplified stratigraphic sections from the study area. Till samples and/or beds without data are left uncoloured.

This geochemical signature may reflect a combination of terrigenous input, grain size sorting, and anoxic conditions associated with deposition in an epicontinental marine or lacustrine environment. Rb commonly follows K in both igneous and sedimentary rocks (Rose et al., 1983) and likely reflects terrigenous input of fine-grained felsic or clay minerals (K-feldspar, muscovite, kaolinite, etc.). Ba is also commonly linked to felsic rocks (Rose et al., 1983) and may be linked to grain size if it is adsorbed onto clay minerals or precipitated as fine barite. Elevated Ba could therefore indicate diagenetic barite formation under sulfate-reducing (anoxic) conditions, which is more plausible in this high-latitude epicontinental setting than biogenic cycling typically associated with high-productivity marine environments (Hendy, 2010; Henkel et al., 2012). Vanadium, being redox-sensitive, could indicate anoxic conditions where it is adsorbed onto organic matter or sulfides (Breit and Wanty, 1991; Algeo and Rowe, 2012). However plausible, the connection between this geochemical signature and a definitive marine or lacustrine signature remains tentative, since only one gleyed silty clay sample was collected for reference. Furthermore, common elemental proxies for paleosalinity, which could support a marine interpretation, are not available due to limited analytes and complicating effects of significant carbonate content (preventing interpretations based on Sr/Ba ratios; cf. Wei and Algeo, 2020 and references therein).

Interestingly, four other samples (from sub-beds 2-D-2, 9-G-2 and 9-G-3) exhibit a similar geochemical signature, yet these samples are not stratigraphically associated with sorted sediments (Figure 4.11). Therefore, the distinct geochemical signature of these samples may reflect inheritance of anoxic deposits, possibly from an up-ice interglacial deposit. Sample 002-B02 was retrieved at an elevation just ~3.5 m above the interglacial package at section 23-005 (bed 5-B) and has a similar interpreted paleo-ice flow direction to the overlying till bed 5-C (002-B02: 290°; 005-O01: 316°). This could suggest that the geochemical signature present may be due to inheritance of the same interglacial that deposited bed 5-B. Samples from bed 9-G-2 and 9-G-3, however, were retrieved from a much higher elevation (~6–14 m) than the closest marine deposit (bed 7-C). Additionally, till sub-bed 9-G-3 has an uncertain (NW-SE) associated ice-flow direction, in contrast to till bed 7-D (NW), which overlies bed 7-C.

The exact source (anoxic deposit) remains uncertain. However, PC2 scores provide additional insights suggesting a possible unobserved anoxic deposit. The four samples with a marine signature are positioned at or above the transition from positive to negative/near-zero PC2 scores, marking a shift in till composition that is interpreted to record two glaciations (Figure 4.9). The anoxic deposit signal in the four till samples above that transition could thus represent inheritance from interglacial marine or lacustrine sediments that are missing between the two contrasting tills. Given the fragmented nature of sediments in the western HBL, it is therefore possible that a stratigraphically-higher interglacial bed exists yet is likely unexposed in visited sections.

4.5 Conclusions

Till compositional analysis confirms that the net composition tills in the study area are both fragmented and result from a combination of overprinting and inheritance, reflecting repeated erosion-transport-deposition cycles involving remobilization of pre-existing sediment mixed with newly produced sediment and variable provenance. This complexity caused by overprinting and inheritance is evident in the broad spread observed in grain size and unexpected pairings between interpreted ice-flow direction and till composition.

Despite overprinting and inheritance, certain clast-lithology clusters broadly correlate with interpreted paleo ice-flow directions and can be used to infer provenance. Till samples with GR proportions near the ~10% background level (clusters 1, 3, and 5) are associated mainly with NW, W, and SW ice-flow directions, and therefore likely reflect transport from the northeast, east, or southeast, with GR input primarily from recycled material. In contrast, CL clusters 2 and 4 are more complex: their elevated GR content paired with Dubawnt clasts are expected to reflect increased sediment input from the northwest, yet the lack of clear correlations with ice-flow indicators weakens a direct provenance link. Instead, the compositional signature of CL clusters 2 and 4 may reflect re-entrainment of northwest-derived sediment that was subsequently mixed with till transported from other directions, obscuring a simple directional relationship.

PC2 scores, which reveal the influence of HBB-sourced rocks on till-matrix geochemistry, are consistent with findings from CL clusters, and elucidate stratigraphic patterns that are perhaps unclear with clast-lithology alone. Specifically, PC2 scores capture an upsection transition from positive to negative scores (representing a decrease in HBB influence on matrix geochemistry), which is a pattern seen at 5 sections throughout the study area. Univariate analysis (of Rb, V, and Ba) reveals eight till samples with a geochemical signature indicative of inheritance of anoxic sediments. Out of these samples, four are not associated with a sub-till sorted sediment package but instead lie at the aforementioned transition between positive and negative PC2 scores, suggesting the presence of an unexposed interglacial package, possibly deposited between this transition.

Together, clast lithologies and matrix geochemistry provide sufficient information about till provenance to make further preliminary correlations. This includes correlative contacts between 1) positive and negative PC2 scores (paired with decreases in HBB clasts), and 2) between CL cluster 2 (overlain by sorted sediments) and CL cluster 3 in several instances (sections 23-009, 23-007, and 23-002). The findings presented in this chapter will be integrated with stratigraphic context in Chapter 5 to further develop local stratigraphic correlations.

Chapter 5: Local stratigraphic framework

5.1 Introduction

This chapter proposes the updated stratigraphic framework for the study area and discusses the implications of this framework for the local long-term Quaternary history. The till units are discussed in detail, including their interpreted broad bedrock provenance regions and relative glacial sequences.

5.2 Methodology

Till beds and sub-beds are correlated to form units based on lithostratigraphy (section 2.4.2). These lithostratigraphic correlations consider findings from previous chapters, including stratigraphic position, bed contacts (observed and interpreted), degree of diagenetic alteration, clast lithology, matrix geochemistry, and especially, interpreted paleo-ice flow direction. After till units are delineated, sub-till sorted sediment beds are correlated to form units based on relative age using allostratigraphy (section 2.4.3).

5.3 Results

5.3.1 Stratigraphic framework

The stratigraphic framework for the 12 investigated sections is presented in the following subsections, starting with the stratigraphically oldest unit. Each unit number is denoted as till or sorted sediment using a modifier ('t' or 's', respectively). In total, 21 units are recognized, representing at least 15 ice-flow events and 6 sorted sediment packages (including 3–4 ice-free phases, 1–2 proglacial deposits and Holocene sorted sediments; Figure 5.1). Till-composition parameters related to provenance (clast lithology proportions and PC2 score) of units are presented in Figure 5.2. Detailed parameter summaries for each unit are presented in Appendix J.

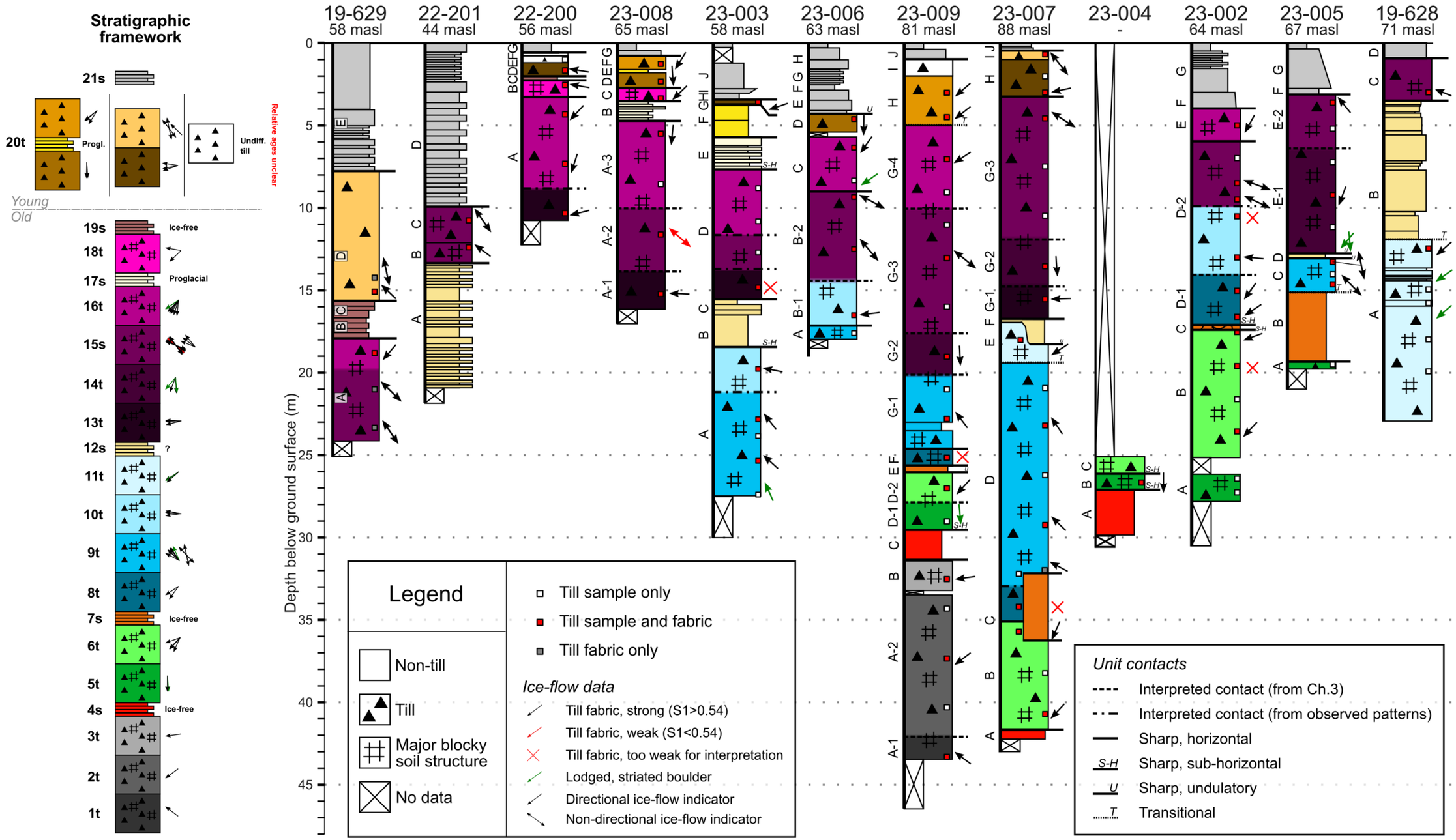


Figure 5.1: Stratigraphic units shown on the simplified stratigraphic sections from the study area.

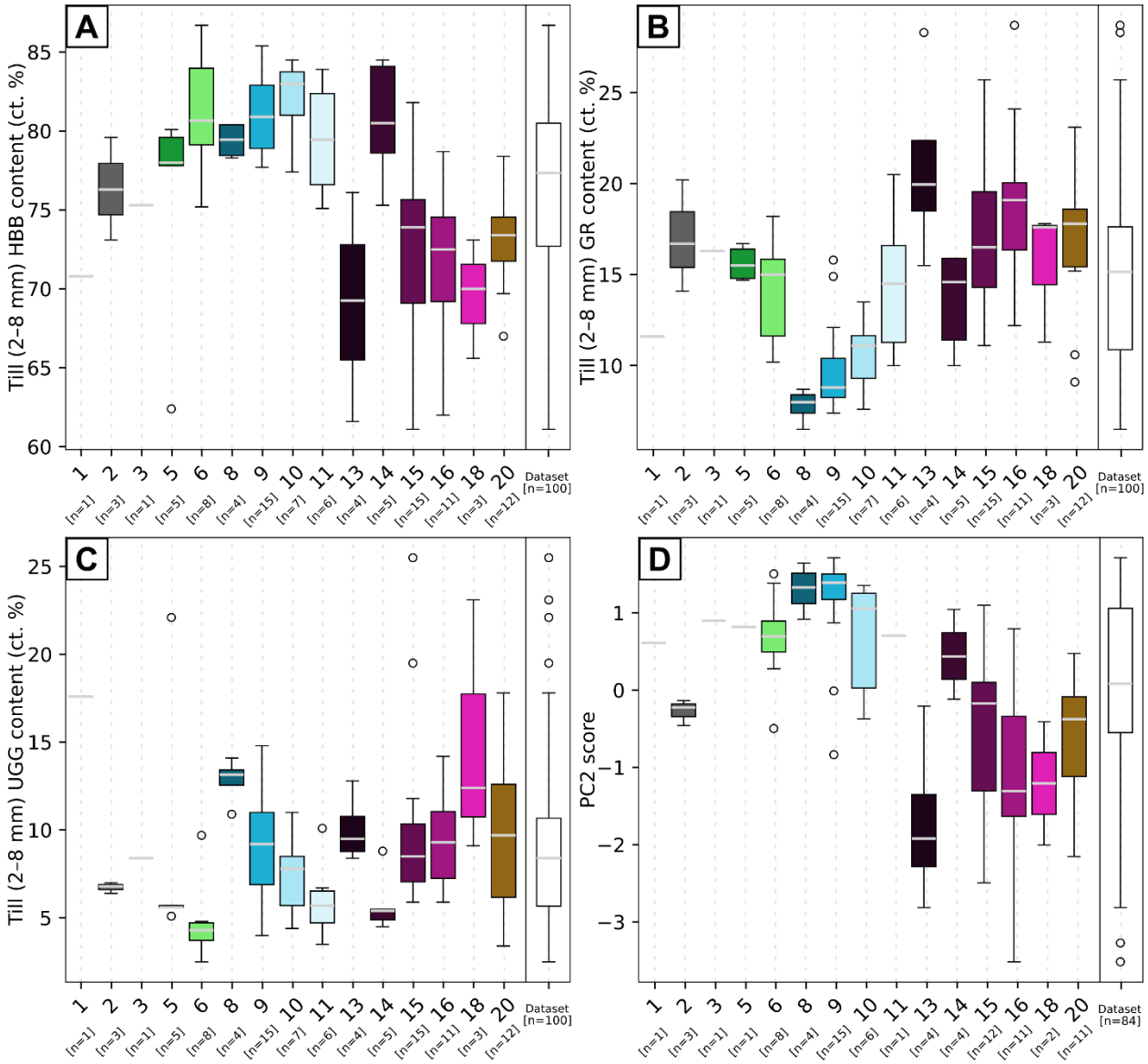


Figure 5.2: Boxplots of till parameters of each till unit ('t' modifier is dropped from unit names for brevity), including: (A) HBB clast proportion; (B) GR clast proportion; (C) UGG clast proportion; and (D) PC2 score of till-matrix geochemistry (select elemental assemblage). Abbreviations: GR, granitoid; HBB, Hudson Bay Basin; UGG, undifferentiated greenstone and greywacke; ct. %, normalized count percentage; PC2, principal component 2.

5.3.1.1 Unit 1t: NW ice-flow

Unit 1t (1 till sample, 1 fabric) is identified at just one section (23-009). Unit 1t is very dark grey brown in colour, is highly overconsolidated with well-developed blocky structure, and has well-developed oxidation rinds on joint surfaces. The one sample contains a relatively low proportion of HBB clasts and a high proportion of UGG clasts (HBB: 17th percentile, GR: 32nd, UGG: 95th) yet has a highly calcareous matrix and positive PC2 score, which indicate input from HBB source rocks. Unit 1t is interpreted to have been deposited by a NW ice-flow (307°) based on one unimodal clast fabric and till composition indicative of eastern provenance (see section 4.4). The lower contact of Unit 1t was not observed.

5.3.1.2 Unit 2t: SW ice-flow

Unit 2t (3 till samples, 1 fabric) is identified at just one section (23-009). Unit 2t is very dark grey brown in colour, is highly overconsolidated with well-developed blocky structure, and has well-developed oxidation rinds on joint surfaces. Samples generally contain relatively moderate proportions in all major categories, except one sample with high GR (HBB: 28–66th percentile, GR: 41–90th, UGG: 31–41st). Unit 2t also has a moderately calcareous matrix and negative PC2 scores, which indicates input from non-HBB source rocks. Unit 2t is interpreted to have been deposited by a SW ice-flow (233°) based on one unimodal clast fabric. The lower contact with Unit 1t is gradational and based on a change in ice-flow direction upsection (74°) and supported by clast lithology (5.1% increase in GR, 10.6% decrease in UGG), total carbonate (4.9% increase), and PC2 score (0.8 decrease; from positive to negative).

5.3.1.3 Unit 3t: W ice-flow

Unit 3t (1 till sample, 1 fabric) is identified at just one section (23-009). Unit 3t is dark grey brown in colour, is highly overconsolidated with well-developed blocky structure, and has well-developed oxidation rinds on joint surfaces. The one sample contains relatively moderate proportions in all major categories (HBB: 42nd percentile, GR: 64th, UGG: 50th). Unit 3t also has a weakly calcareous matrix but a positive PC2 score, which indicates mixed input from HBB and non-HBB source rocks. Unit 3t is interpreted to have been deposited by a W ice-flow (262°) based on one unimodal clast fabric. The lower contact with Unit 2t was not observed due to colluvium, however, there is a change in PC2 score from negative to positive from Units 2 to 3 (1.4 increase).

5.3.1.4 Unit 4s: Heterogeneous sediments

Unit 4s is identified at three sections (23-004, 23-007, 23-009) and encompasses four sub-till sorted sediment exposures (23-004: Exposure-1, Exposure-2; 23-007: Exposure-1; 23-009: Exposure-1). Unit 4s is defined by its bounding surfaces with unit 3t and 5t (allostratigraphy). Unit 4s is laterally

heterogeneous and discontinuous, consisting of well to poorly sorted sand, silt, gravel, and overconsolidated silty clay, with common features such as cross-laminations, inclined bedding, shell fragments, charcoal, and organic-rich laminae. These characteristics indicate deposition in a range of environments including marine/lacustrine, fluvial, and ice-marginal settings, and collectively represent one or more ice-free intervals. Unit 4s is likely deposited after the Brunhes-Matuyama reversal (~781 ka) based on paleomagnetic analysis from sampled sediment (see section 3.3.3.3). The lower contact with Unit 3t was only observed at section 23-009, where it is sharp and undulatory.

5.3.1.5 Unit 5t: S ice-flow

Unit 5t (5 till samples, 1 fabric, 1 striated boulder) is identified at four sections (23-002, 23-004, 23-005, 23-009), and is correlated based on interpreted S ice-flow directions and stratigraphic position (Figure 5.1), and supported by similar clast-lithology proportions (Figure 5.2). Unit 5t is dark grey, very dark grey, or very dark grey brown in colour, is highly overconsolidated with well-developed blocky structure, and has well-developed oxidation rinds on joint surfaces. Samples vary in clast-lithology: they generally contain relatively moderate proportions in all major categories, except one sample with high UGG (HBB: 4–71st percentile, GR: 44–68th, UGG: 17–98th). Unit 5t also has a weakly or moderately calcareous matrix and positive PC2 scores, indicating mixed input from HBB and non-HBB source rocks. Unit 5t is interpreted to have been deposited by a S ice-flow (175–180°) based on one unimodal clast fabric and one lodged and striated boulder. The lower contact with Unit 4s was only observed at sections 23-004 and 23-009, where it is sharp and sub-horizontal.

5.3.1.6 Unit 6t: SSW–WSW ice-flow

Unit 6t (8 till samples, 5 fabrics) is identified at four sections (23-002, 23-004, 23-007, 23-009), and is correlated based on interpreted SSW–WSW ice-flow directions and stratigraphic position (Figure 5.1), and supported by similar clast-lithology and PC2 scores (Figure 5.2). Unit 6t is dark grey brown or very dark grey brown in colour, is highly overconsolidated with well-developed blocky structure, and has well-developed oxidation rinds on joint surfaces. Samples vary in clast-lithology but generally have relatively high proportions of HBB and low proportions of UGG clasts (HBB: 40–100th percentile, GR: 21–80th, UGG: 1–67th). Unit 6t also has a variably calcareous matrix and typically positive PC2 scores, which indicates input from HBB source rocks. Unit 6t is interpreted to have been deposited by a SSW–WSW ice-flow (204–250°) based on five unimodal clast fabrics. The lower contact with Unit 5t is sharp (23-004) to gradational (23-009) and may be accompanied by a change in till-clast composition (23-009), though no such change is observed in 23-002. At 23-007, the lower contact of Unit 6t is instead with Unit 4s, where it is sharp and horizontal.

5.3.1.7 Unit 7s: Heterogeneous sediments

Unit 7s is identified at four sections (23-002, 23-005, 23-007, 23-009) and encompasses eight sub-till sorted sediment exposures (23-002: Bed 2-C; 23-005: Exposure-1, Exposure-2, Exposure-3; 23-007: Exposure-3, Exposure-4, Exposure-5; 23-009: Bed 9-E). Unit 7s is defined by its bounding surfaces with units 6t and 8t (allostratigraphy). Unit 7s is laterally heterogeneous and discontinuous, consisting of poorly to moderately sorted sands, gravels, silts, and clays, with common features such as horizontal and cross-bedding, shell fragments, diamict rip-up clasts, organic-rich layers, and large wood fragments. These characteristics indicate deposition in a range of environments including marine, fluvial, and ice-marginal settings, with localized evidence of subglacial reworking and deformation, and collectively represent one or more ice-free intervals. The lower contact with Unit 6t is sharp and undulatory (23-009), horizontal (23-007) or sub-horizontal (23-002). At 23-005, the lower contact of Unit 7s is instead with Unit 5t, where it is sharp and horizontal.

5.3.1.8 Unit 8t: SW ice-flow

Unit 8t (4 till samples, 2 fabrics) is identified at three sections (23-002, 23-007, 23-009), and is correlated based on interpreted SW ice-flow directions and stratigraphic position (Figure 5.1), and supported by similar clast-lithology and PC2 scores (Figure 5.2). Unit 8t is dark grey brown or olive brown in colour, is highly overconsolidated with well-developed blocky structure, and has well-developed oxidation rinds on joint surfaces. Samples have relatively high proportions of UGG and low proportions of GR clasts (HBB: 58–74th percentile, GR: 1–13th, UGG: 76–90th). From units 6t to 8t, there is a significant increase in UGG clasts upsection, which is observed at all sections. Unit 8t also has a moderately to highly calcareous matrix and positive PC2 scores, which indicates input from HBB source rocks. Unit 8t is interpreted to have been deposited by a SW ice-flow (216–236°) based on two unimodal clast fabrics. The lower contact with Unit 7s is sharp (23-007, 23-009) to sub-horizontal (23-002).

5.3.1.9 Unit 9t: WNW–NNW ice-flow

Unit 9t (15 till samples, 8 fabrics, 1 striated boulder) is identified at five sections (23-003, 23-005, 23-006, 23-007, 23-009), and is correlated based on interpreted WNW–NNW ice-flow directions and stratigraphic position (Figure 5.1), and supported by similar clast-lithology and PC2 scores (Figure 5.2). Unit 9t is commonly dark grey brown or olive brown in colour, is highly overconsolidated with well-developed blocky structure, and has well-developed oxidation rinds on joint surfaces. Samples generally have relatively high proportions of HBB and low proportions of GR clasts (HBB: 52–98th percentile, GR: 2–57th, UGG: 6–92nd). Unit 9t also has a variably calcareous matrix and typically positive PC2 scores, which indicates input from HBB source rocks. Unit 9t is interpreted to have been deposited by a WNW–

NNW ice-flow (298–336°) based on one lodged striated boulder and eight unimodal clast fabrics, six of which were associated with samples interpreted to be of eastern provenance (see section 4.4). The lower contact with Unit 8t is sharp and horizontal (23-009) to gradational (23-007) and may be accompanied by a change in till-clast composition (23-009; UGG decrease upsection). At 23-005, the lower contact of Unit 9t is instead with Unit 7s, where it is transitional.

5.3.1.10 Unit 10t: W–WNW ice-flow

Unit 10t (4 till samples, 3 fabrics) is identified at three sections (23-002, 23-003, 23-006), and is correlated based on interpreted W–WNW ice-flow directions and stratigraphic position (Figure 5.1), and supported by similar clast-lithology and PC2 scores (Figure 5.2). Unit 10t is olive brown or very dark grey brown in colour, is highly overconsolidated with well-developed blocky structure, and has well-developed oxidation rinds on joint surfaces. Samples generally have relatively high proportions of HBB and low proportions of GR clasts (HBB: 51–95th percentile, GR: 3–39th, UGG: 9–77th). Unit 10t also has a moderately to highly calcareous matrix and typically positive PC2 scores, which indicates input from HBB source rocks. Unit 10t is interpreted to have been deposited by a W–WNW ice-flow (263–295°) based on three unimodal clast fabrics. The lower contact with Unit 9t is sharp and horizontal (23-006) to gradational (23-003). At 23-002, the lower contact of Unit 10t is instead with Unit 8t, where it is gradational and accompanied by a decrease in UGG clast content upsection.

5.3.1.11 Unit 11t: SW ice-flow

Unit 11t (7 till samples, 2 fabrics, 2 striated boulders) is identified at two sections (23-007, 19-628) and is correlated based on interpreted SW ice-flow directions and stratigraphic position (Figure 5.1). Unit 11t is typically dark grey brown in colour, is highly overconsolidated with well-developed blocky structure, and has well-developed oxidation rinds on joint surfaces. Samples vary in clast-lithology (HBB: 39–91st percentile, GR: 19–93rd, UGG: 3–69th). Unit 11t also has a weakly to moderately calcareous matrix, and the one sample analyzed by PCA has a positive PC2 score, indicating mixed input from HBB and non-HBB source rocks. Unit 11t is interpreted to have been deposited by a SW ice-flow (229–238°) based on two unimodal clast fabrics and two lodged, striated boulders. The lower contact with Unit 10t is transitional (23-007) and is accompanied by a significant change in till-clast composition upsection (decrease in HBB, increase in GR clasts).

5.3.1.12 Unit 12s: Heterogeneous sediments

Unit 12s is identified at five sections (19-628, 22-201, 23-003, 23-005, 23-007) and encompasses five sub-till sorted sediment exposures (19-628: Bed B; 22-201: Bed A; 23-003: Beds 3-B and 3-C; 23-005:

Bed 5-D; 23-007: Bed 7-F). Unit 12s is defined by its bounding surfaces with units 11t and 13t (allostratigraphy). Unit 12s is laterally heterogeneous and discontinuous, consisting of sorted and interbedded sediments, including massive to laminated silt, sand, and clay, with scattered dropstones, laminated diamict, oxidation stains, and local diamict interbeds. These characteristics suggest deposition in ice-contact glaciolacustrine and glaciofluvial environments during at least one phase of relative warming or partial deglaciation, with localized subglacial reworking. Although no direct evidence of ice-free conditions was observed in Unit 12s, the anoxic deposit signal in till samples when this unit is absent but expected to be situated (see section 4.4.2) may suggest that ice-free conditions may have occurred but were not preserved in the stratigraphic record. The lower contact with Unit 11t is sharp and undulatory (23-007) or transitional (19-629). The lower contact of Unit 12s is also observed to be sharp and sub-horizontal with Unit 10t (23-003), or sharp and undulatory with Unit 9t (23-005).

5.3.1.13 Unit 13t: WSW–W ice-flow

Unit 13t (4 till samples, 3 fabrics) is identified at four sections (22-200, 23-003, 23-007, 23-008), and is correlated based on interpreted WSW–W ice-flow directions and stratigraphic position (Figure 5.1), and supported by similar clast-lithology and PC2 scores (Figure 5.2). Unit 13t is olive brown, dark grey brown, or dark olive brown in colour, is highly overconsolidated with well-developed blocky structure, and has well-developed oxidation rinds on joint surfaces. Samples generally have relatively higher proportions of GR and UGG, and lower proportions of HBB (HBB: 2–45th percentile, GR: 54–99th, UGG: 50–86th). Unit 13t also has a weakly to moderately calcareous matrix and negative PC2 scores, which indicates input from non-HBB source rocks. Unit 13t is interpreted to have been deposited by a WSW–W ice-flow (256–272°) based on three unimodal clast fabrics. The lower contact with Unit 12s is sharp and horizontal (23-003, 23-007) and may be accompanied by a significant change in till-clast composition upsection from Unit 11t (decrease in HBB, increase in GR and UGG clasts; 23-003).

5.3.1.14 Unit 14t: S–SSW ice-flow

Unit 14t (5 till samples, 3 fabrics, 2 striated boulders) is identified at three sections (23-005, 23-007, 23-009) and is correlated based on interpreted S–SSW ice-flow directions and stratigraphic position (Figure 5.1). Unit 14t is dark grey brown or dark olive brown in colour, is highly overconsolidated with well-developed blocky structure, and has well-developed oxidation rinds on joint surfaces. Samples vary in clast-lithology but typically have relatively higher proportions of HBB (HBB: 41–95th percentile, GR: 19–59th, UGG: 11–56th). Unit 14t also has a weakly to moderately calcareous matrix and both positive and negative PC2 scores, indicating variable input from HBB and non-HBB sources. Unit 14t is interpreted to have been deposited by a S–SSW ice-flow (176–201°) based on three unimodal clast fabrics and two

lodged, striated boulders. The lower contact with Unit 13t is transitional (23-007). The lower contact of Unit 14t is also observed to be sharp and undulatory with Unit 12s (23-005), or transitional with Unit 9t (23-009) and accompanied by a significant change in till-composition upsection (HBB decrease, GR increase).

5.3.1.15 Unit 15t: WNW–NW or ESE–SE ice-flow

Unit 15t (18 till samples, 13 fabrics) is identified at ten sections (19-628, 19-629, 22-201, 23-002, 23-003, 23-005, 23-006, 23-007, 23-008, 23-009), and is correlated based on interpreted WNW–NW or ESE–SE ice-flow directions and stratigraphic position (Figure 5.1), and supported by similar clast-lithology and PC2 scores (Figure 5.2). Unit 15t varies in colour (most commonly dark grey brown), is highly overconsolidated with well-developed blocky structure, and has well-developed oxidation rinds on joint surfaces. Samples vary in clast-lithology but generally have relatively higher proportions of GR and UGG clasts (HBB: 1–84th percentile, GR: 27–98th, UGG: 28–100th). Unit 15t also has a weakly to moderately calcareous matrix and typically negative PC2 scores, which indicates input from non-HBB source rocks. Unit 15t is interpreted to have been deposited by either a WNW–NW (292–325°) or ESE–SE (118–145°) ice-flow based on 13 unimodal clast fabrics. The lower contact with Unit 14t is transitional (23-005, 23-007, 23-009). The lower contact of Unit 15t is also observed to be transitional with Unit 13t (23-003, 23-008) and accompanied by a significant increase in GR clasts upsection, or sharp and horizontal with Unit 12s (19-628, 22-201), or transitional with Unit 10t (23-002, 23-006) and may be accompanied by a significant change in till-composition upsection (HBB decrease, GR increase; 23-006).

5.3.1.16 Unit 16t: S–SW ice-flow

Unit 16t (12 till samples, 7 fabrics, 1 striated boulder) is identified at seven sections (19-629, 22-200, 23-002, 23-003, 23-006, 23-008, 23-009), and is correlated based on S–SW interpreted ice-flow directions and stratigraphic position (Figure 5.1), and supported by similar clast-lithology and PC2 scores (Figure 5.2). Unit 16t is olive brown, dark grey brown, or brown in colour, is highly overconsolidated with well-developed blocky structure, and has well-developed oxidation rinds on joint surfaces. Samples vary in clast-lithology but generally have relatively higher proportions of GR and UGG clasts (HBB: 3–64th percentile, GR: 29–100th, UGG: 28–99th). Unit 16t also has a weakly to moderately calcareous matrix and typically negative PC2 scores, which indicates input from non-HBB source rocks. Unit 16t is interpreted to have been deposited by a S–SW ice-flow (186–237°) based on seven unimodal clast fabrics and one lodged, striated boulder. The lower contact with Unit 15t is transitional (19-629, 23-003, 23-008, 23-009) to sharp and horizontal (23-002, 23-006). At 22-200, the lower contact is instead with Unit 13t, where it is transitional.

5.3.1.17 Unit 17s: Proglacial sediments

Unit 17s is identified at two sections (23-003, 23-008) and encompasses two sub-till sorted sediment exposures (23-003: Bed 3-E; 23-008: Bed 8-B). Unit 17s is defined by its bounding surfaces with units 16t and 18t (allostratigraphy). Unit 17s is laterally heterogeneous and discontinuous, consisting of interbedded and laminated fine sand, silt, and diamict, with features such as micro-faulting and inclined silt-filled fractures. These characteristics suggest deposition in ice-contact glaciolacustrine environment during at least one phase of relative warming or partial deglaciation. The lower contact with Unit 16t is sharp and horizontal (23-008) or sub-horizontal (23-003).

5.3.1.18 Unit 18t: SW–W ice-flow

Unit 18t (2 till samples, 2 fabrics) is identified at two sections (22-200, 23-008) and is correlated based on its lighter colour and stratigraphic position (Figure 5.1). Unit 18t is brown or light yellow brown in colour, is highly overconsolidated with well-developed blocky structure, and has well-developed oxidation rinds on joint surfaces. Samples generally have relatively higher proportions of GR clasts (HBB: 15–29th percentile, GR: 74–77th, UGG: 58–85th). Unit 18t also has a moderately calcareous matrix and negative PC2 scores, which indicates input from non-HBB source rocks. Unit 18t is interpreted to have been deposited by a SW–W ice-flow (226–280°) based on two unimodal clast fabrics. The lower contact is sharp and horizontal with Unit 17s (23-008) or Unit 16t (22-200).

5.3.1.19 Unit 19s: Heterogeneous sediments

Unit 19s is identified at two sections (19-629, 22-200) and encompasses two sub-till sorted sediment exposures (19-629: Beds B and C; 22-200: Bed C). Unit 19s is defined by its bounding surfaces with units 18t and 20t (allostratigraphy). Unit 19s is laterally heterogeneous and discontinuous, consisting of moderately to well-sorted, fine to coarse sands and sandy gravels, with thin bedding, shell fragments, matrix-supported granule- to pebble-sized clasts, and localized diamict interbeds and lenses. These characteristics predominantly indicate deposition in ice-marginal glaciofluvial/fluvial settings, with possible marine sediment contribution, and collectively represent one or more phases of relative warming or partial deglaciation. Although no direct evidence of ice-free conditions was observed in Unit 19s, its stratigraphic position between till units with noticeably different degrees of diagenetic alteration and therefore different relative age (units 18t and 20t; see section 2.4.2.1) likely suggests that ice-free conditions may have occurred but were not preserved in the stratigraphic record. The lower contact is sharp and horizontal with Unit 18t (23-002) or Unit 16t (19-629).

5.3.1.20 Unit 20t: Young till, variable ice-flow

Unit 20t (12 till samples, 11 fabrics) is identified at seven sections (19-629, 22-200, 23-003, 23-006, 23-007, 23-008, 23-009) and is correlated based on a relatively lower degree of diagenetic alteration, lighter colour, and stratigraphic position (Figure 5.1). Unit 20t tills are typically light olive brown, olive brown, or brown in colour. Unit 20t tills are overconsolidated, are either loose or have weakly-developed blocky structure, and either exhibit absent or weakly-developed oxidation rinds on joint surfaces. Till samples vary greatly in clast-lithology but generally have relatively lower proportions of HBB clasts (HBB: 11–61st percentile, GR: 15–95th, UGG: 2–96th). Unit 20t tills also have a moderately to highly calcareous matrix but typically negative PC2 scores, which indicates mixed input from HBB and non-HBB source rocks. Unit 20t tills are interpreted to have been deposited by younger ice-flows of variable direction (SE–NW; 142–322°) based on 11 unimodal fabrics. Unit 20t also includes sub-till sorted sediments interpreted as glaciolacustrine (observed at 23-003, 23-008). The lower contact with Unit 19s is sharp and horizontal (19-629, 22-200, 23-003). The lower contact of Unit 20t is also observed to be sharp and horizontal with Unit 18t (23-008), Unit 17s (23-003), and Unit 15t (23-007), or transitional with Unit 16t (23-009).

5.3.1.21 Unit 21s: Postglacial sediments

Unit 21s is identified at all sections except 23-004. As previously discussed in section 3.4.3, Unit 21s encompasses glaciolacustrine, marine, and fluvial sediments deposited after the last glaciation. The lower contact of Unit 21s is sharp and horizontal with Unit 20t (19-629, 22-200, 23-003, 23-006, 23-007, 23-008, 23-008), Unit 16t (23-002), or Unit 15t (19-628, 22-201, 23-005).

5.4 Discussion

Using a hybrid lithostratigraphy-allostratigraphy approach, the constructed framework reveals 21 units for the Gods and Yakaw rivers area, including 15 till units and 6 sorted sediment units (summarized in Table 5.1). Each till unit has a unique combination of stratigraphic position and interpreted ice-flow direction, representing separate glacial events. Among the 5 sub-till sorted sediment units, two (4s and 7s) are identified to represent ice-free deposition (organic-bearing), two (12s and 19s) are inferred to reflect ice-free deposition based on other proxies (see Table 5.1), and one (17s) is interpreted as representing deposition during a phase of relative warming. A scaled cross-section (with vertical exaggeration) of the framework is presented in Figure 5.3.

Table 5.1: Summary and tentative Marine Isotope Stage estimates of units from relative stratigraphy.

Unit	Climatic phase	Ice-flow direction(s), if applicable	Tentative MIS estimate
21s	Ice-free	-	1
20t	Glacial	Younger ice-flows, variable direction (see Figure 5.1)	2–4
19s	Relative warming, interpreted as ice-free*	-	5
18t	Glacial		6
17s	Relative warming	-	
16t	Glacial		
15t	Glacial		
14t	Glacial		
13t	Glacial		
12s	Relative warming, interpreted as ice-free†	-	7
11t	Glacial		8
10t	Glacial		
9t	Glacial		
8t	Glacial		
7s	Ice-free	-	9
6t	Glacial		10
5t	Glacial		
4s	Ice-free	-	11
3t	Glacial		12+
2t	Glacial		
1t	Glacial		

*Based on a shift in degree of diagenetic alteration (see section 5.3.1.19). †Based on a geochemical signature suggesting incorporation of anoxic sediments and supported by a shift in till composition (see section (5.3.1.12).

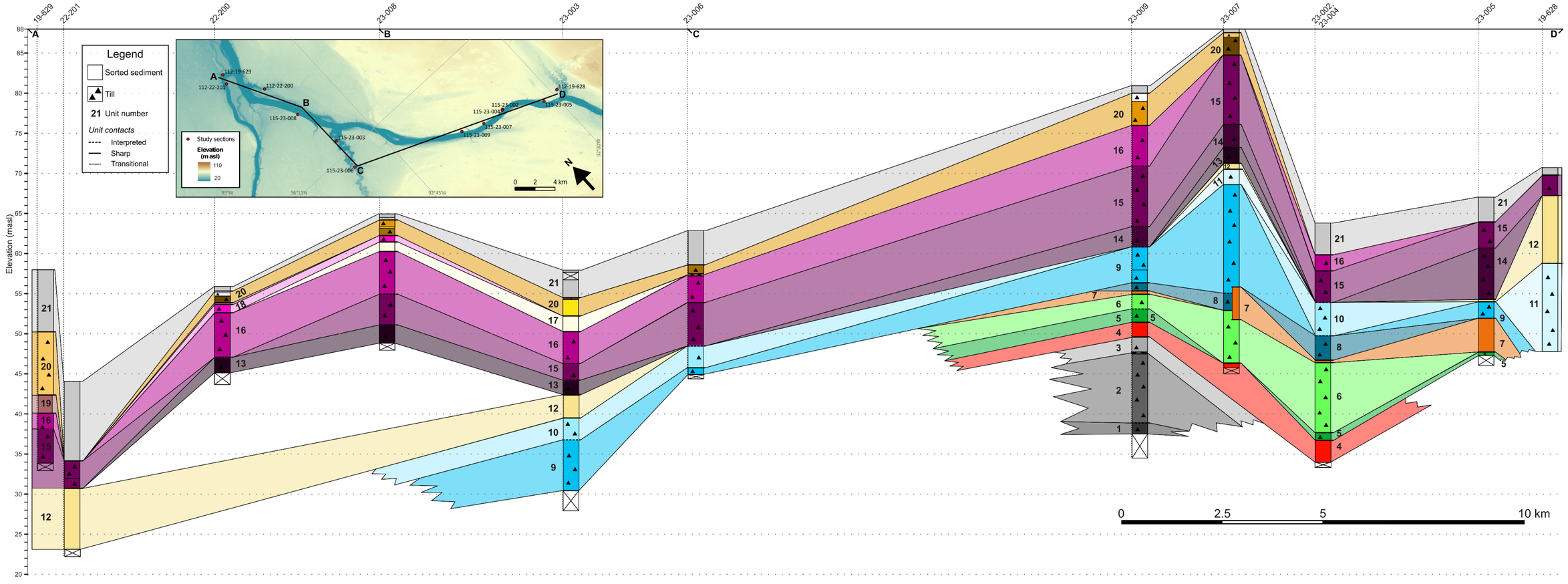


Figure 5.3: Delineated units of the study area displayed on a stratigraphic cross-section. Unit modifiers ('t' and 's') are dropped from unit names for brevity. Interpolated areas are displayed at 50% opacity.

Although geochronological and paleoenvironmental data is limited, minimum climatic stages can be estimated from this framework using relative stratigraphy (Table 5.1). Here, sub-till sorted sediment units identified/interpreted as ice-free phases are used as climatic brackets, and till units between them are assumed to belong to the same glacial stage. However, without paleoenvironment characterization and geochronological constraints (see section 2.2.2), these assignments remain as minimum estimates and should be revisited as new data becomes available.

Assigning minimum age estimates based on relative stratigraphy places the oldest preserved deposits in the study area at MIS 12, and the oldest interglacial at MIS 11. This would be consistent with earlier suspicions that the Gods and Yakaw rivers area preserves a much older stratigraphy than previously recognized, based on uncertain interglacial ages and possible removal of ~50 m of sediment during development of the observed drainage corridor (see section 1.3.3).

5.4.1 A fragmented stratigraphic record

The revised framework highlights the discontinuous nature of Quaternary sediments in the study area. In particular, the preservation of individual units is often limited, particularly for lower units (1t–3t), Unit 20t, and sub-till sorted sediment units (4s, 7s, 12s, 17s, 19s). The scarcity of units 1t–3t is likely due to their depth and the lack of sufficiently deep stratigraphic exposures. Unit 20t is thin and fragmented, likely due to erosion associated with the observed erosional corridor (see section 1.2.2.1). Sorted sediment units are either naturally thinner, more erodible, or deposited in more of a patchwork than till units (see section 1.3.3). Even units that are relatively laterally continuous (e.g., units 9t and 16t) are not preserved at all sections (Figure 5.3). Additionally, it is important to note that no individual section preserves the full stratigraphic sequence; even the most complete section (23-009) is missing 7 units, while other sections are commonly missing 10 or more units (Figure 5.3).

Given this fragmented nature, unit correlations required numerous case-by-case judgements. While every effort was made to choose the most reasonable and internally consistent interpretations, poorly aligned or contradictory parameters prevented conclusive correlations at times. These interpretive challenges highlight the complexity of reconstructing glacial histories in regions with fragmented and discontinuous stratigraphy like the western HBL.

5.4.1.1 An alternative stratigraphic placement of section 23-005 beds

One particularly challenging correlation involves the placement of beds from section 23-005 within the local stratigraphic framework. Correlating tills of shorter sections, such as 23-005, is especially difficult as their limited vertical extent captures only a portion of the full stratigraphic sequence and includes a limited number of paleo-ice flow indicators to aid interpretation. Since correlations prioritize interpreted ice-flow directions, section 23-005 beds were assigned to units 5t, 7s, 9t, 12s, 14t, 15t, and 21s (Figure 5.1).

An alternative correlation approach is to prioritize till composition in instances where multiple correlation scenarios are possible based on ice-flow direction. Here, till beds 5-E-1 and 5-E-2 show clast-lithology compositions and PC2 scores more consistent with tills below Unit 12s (CL cluster 5, positive PC2 score; Figure 4.10). Reassigning these beds to units 8t and 9t would shift the underlying beds accordingly (Table 5.2).

Table 5.2: Assigned units for beds of section 23-005, with an alternative assignment based on an approach focused more on till composition.

Section 23-005 bed	**Assigned units**	**Alternative units**
G	21s	21s
F	21s	21s
E-2	15t	9t
E-1	14t	8t
D	12s	7s
C	9t	?
B	7s	4s
A	5t	1t? (Similar clast lithology)

While this alternative unit assignment results in a stronger alignment of till composition (clast-lithology, PC2 score), there are several trade-offs with this alternative unit assignment. First, it disrupts the correlation of the bottommost tills of section 23-002, 23-004, and 23-005, which had been previously grouped based on similar colour, texture, and till-matrix geochemistry (see sections 3.4, 4.4.2). Second, it also introduces an additional interpreted ice-flow direction within the interval between units 4s and 7s, complicating the ice-flow record further with only one instance of this ice-flow direction. Therefore, despite the compositional agreement in the alternative approach, the original assignments based on ice-flow direction and other supporting parameters remain preferable.

5.4.2 Till units: discrete glacial events or glaciotectonic stacking?

It is important to note that although till units are provisionally interpreted as products of separate glacial events (i.e., at least separate ice-flow phases, not necessarily separate glaciations; see section 2.4.2), it is possible that multiple units represent glaciotectonically thrust-stacked tills deposited during a single glacial event (e.g., Evans et al., 2021). Distinguishing between these scenarios is particularly challenging due to absent geomorphological features and large-scale glaciotectonic features within sections (e.g., bedrock rafting, folds, thrusts), which are commonly the basis of glaciotectonic interpretations in other studies (e.g., Evans, 2000, Henricksen et al., 2001, Evans et al., 2021). Additionally, glaciotectonically stacked tills generally form in ice-marginal settings (cf. Hart and Boulton, 1991), but interpreting tills in the study area, a core region of the Laurentide Ice Sheet, as ice-marginal is challenging in vertical sections unless there is a recognizable stratigraphic sequence consistent with an ice margin advance and/or retreat.

In general, tills are interpreted as the product of distinct glacial events when they display unimodal clast fabric orientations that differ from adjacent units, indicating primary deposition by separate ice flow phases. In contrast, glaciotectonic stacking typically results in tills with weakly developed fabrics due to deformation, or consistent orientations across stacked units, reflecting either complete reworking (e.g., Evans, 2000), or simple stacking of similar till sheets (e.g., Evans et al., 2021). Although steeply plunging clasts were excluded from fabric analysis (see section 2.2.3), which may partially limit assessment of fabric strength, the observed differences in orientation patterns between tills remain robust and provide meaningful constraints on depositional versus glaciotectonic origins. Furthermore, as most tills are massive, deformation patterns are particularly hard to recognize, and the simplest interpretation of such tills is that they reflect primary deposition (Evans et al., 2006). Finally, ice-marginal settings formed during glacial maxima, such as along the southern or northwestern margins of the LIS, likely exerted significantly greater compressional, thrusting forces than those formed during the initial growth phases of ice sheets in core regions like the western HBL, or during the late stages of a much smaller LIS surrounded by large bodies of water. The ice marginal settings in the western HBL are thus not considered favorable to large scale glaciotectonism as interpreted in southern and central Alberta (Evans, Phillips, and Atkinson, 2021) and in the Smoking Hills area of the Northwest Territories (Evans et al., 2021).

Therefore, most till units are interpreted to represent separate depositional events, based primarily on their distinct ice-flow directions, the unimodality and strength of their fabrics, the lack of observed glaciotectonic deformation structures, and the regional position of the western HBL within the ice sheet. Future paleoenvironmental or geochronological techniques may confirm or deny this interpretation.

5.4.3 Interpreted provenance of till units

The following section discusses the likely bedrock provenance of sediment in each till unit and the relative influence of paleo-ice spreading centers. Units 1t to 11t exhibit strong compositional and directional evidence for sediment sourced from the HBB or bedrock to the east and are therefore interpreted to primarily reflect influence from a Q-L ice-spreading sector. In contrast, units 13t to 18t display a more complex set of compositional data and directional indicators, complicating provenance interpretations and suggesting possible contributions from both Q-L and Keewatin sources. Unit 20t is not included in this discussion, as provenance interpretations are uncertain due to variable compositional data (samples span all CL clusters, and range from positive to negative PC2 scores) and sparse, thin stratigraphic exposures.

5.4.3.1 Units 1t–11t: strong HBB provenance signal, Q-L influence

The till composition of units 1t to 11t is primarily characterized by strong signals of HBB and/or UGG influence (Figure 5.2), paired with predominantly NW, W, and SW interpreted ice-flow directions (Figure 5.1). These parameters suggest sediment was sourced from local or eastern bedrock, consistent with ice emanating from a Q-L paleo-ice-spreading center. Although Unit 5t exhibits southward interpreted ice-flow indicators, no major associated shifts in till composition are observed. This suggests there was no significant transition from Q–L to Keewatin influence at that time. Therefore, units 1t–11t are interpreted to reflect deposition by Q–L-sourced ice-flows, which may have been curvilinear (NW), direct (W–SW), or from a prior HBIS (SW).

5.4.3.2 Units 13t–18t: a major decrease of HBB-sourced detritus, unclear provenance

A striking shift in till composition is observed across Unit 12s, marked by an upsection increase in GR and UGG clast proportions and a corresponding decrease in HBB clasts and PC2 scores (magenta line in Figure 4.10, Figure 5.2). This compositional change can reflect a major influx of shield-sourced detritus or a reduction in available HBB-sourced sediment. Regardless of the cause, this shift from units 1t–11t to 13t–18t represents the most drastic change in till composition observed in the local stratigraphic record.

If this shift represents diminished HBB-sourced sediment, it may reflect the burial of up-ice HBB bedrock, rendering it less accessible to erosion by later glaciations (discussed in section 2.3.4). In

contrast, shield-derived lithologies may have remained more available. This is consistent with expected differences in bedrock erodibility; softer and more fissile carbonates of the HBB would be prone to glacial erosion, which could have led to the development of topographic lows that were infilled and buried, while resistant shield bedrock would remain nearer to surface and available as primary material.

If the shift is not caused by diminished HBB bedrock availability, this change in till composition appears inconsistent with the interpreted westward ice-flow direction of Unit 13t. An eastern-sourced till would be expected to exhibit strong HBB input paired with limited GR input, since the nearest mapped granitoid bedrock to the east lie some 900 km away, to the east of Hudson Bay (Figure 2.4). If the westward ice-flow interpretation is indeed correct, then the elevated GR content in Unit 13t must originate either from either unmapped or now-buried topographic highs of shield bedrock, distal eastern transport, or from the entrainment of pre-existing sediments.

However, Unit 13t is compositionally distinct from other tills with a similar interpreted ice-flow direction (units 3t and 10t), which show a till composition much more reflective of HBB source rock (high HBB clasts, positive PC2 score; Figure 5.3) than Unit 13t. If this discrepancy is not due to a reduction in HBB bedrock availability, it may cast doubt on the previous assumption that eastward ice-flows are generally absent in the western HBL (see section 2.4.2.2). Alternatively, Unit 13t may instead represent an eastward ice-flow, which introduced sediment enriched in GR and UGG following the interpreted ice-free interval represented by Unit 12s.

This interpretation of an eastward ice-flow is supported by spatial patterns, as upper till beds assigned to units 13t–16t exhibit notable compositional differences between northwestern sections (22-201, 22-200, 23-008, 23-003, 23-006) and southeastern sections (23-009, 23-007, 23-002; Figure 4.10). Northwestern tills are on average more granitoid-rich (GR: 19.5%; HBB: 70.1%; PC2 score: -1.26) than southeastern tills (GR: 16.7%, HBB: 75.8%; PC2 score: -0.08). This trend may reflect a gradual shift in till composition down-ice, from more shield-derived, granitoid-rich sources in the northwest to more incorporation of local, HBB sources in the southeast. Here, ice flowing south/southeast/eastward may have initially eroded exposed granitoid bedrock at the ice-bed interface, incorporating shield-derived detritus. As ice advanced farther across the HBL, this granitoid signal likely became more diluted due to a) a transition from exposed to buried subglacial bedrock, either by sediment deposition and cover or the erosion of topographic highs; and/or b) progressive entrainment of pre-existing surficial sediments compositionally higher in HBB material (as indicated by underlying tills).

The increase in tracer lithologies across this divide is also of note, as both Dubawnt Supergroup and oolitic jasper clasts noticeably increase from units 1t–11t to 13t–18t (Table 5.3). This may reflect the low

proportion of HBB clasts in units 13t–18t, which permit a greater relative representation of non-HBB lithologies. However, variation in NW-sourced versus E-sourced tracer lithologies is observed among units 13t–18t, suggesting a provenance signal: the presence and proportion of Dubawnt clasts is highest in Unit 15t (WNW–NW or ESE–SE ice-flow), while oolitic jasper is highest in units 14t and 16t (S–SSW and S–SW ice-flow, respectively). This suggests tracer lithologies are not randomly distributed but instead relate to ice-flow direction. In particular, the association of high Dubawnt clast content with Unit 15t supports a NW provenance interpretation, while oolitic jasper in units 14t and 16t supports an eastern provenance interpretation.

Table 5.3: Presence and average proportion of select tracer lithologies (Dubawnt Supergroup and oolitic jasper clasts) by unit. Summary rows are in gray, and elevated presences discussed are bolded.

Till unit(s)	Dubawnt Supergroup clasts		Oolitic jasper clasts	
	Proportion of non-zero samples [%]	**Average value among non-zero samples (count %)**	**Proportion of non-zero samples [%]**	**Average value among non-zero samples (count %)**
1	0/1 [0%]	-	1/1 [100%]	0.13
2	0/3 [0%]	-	0/3 [0%]	-
3	0/1 [0%]	-	0/1 [0%]	-
5	0/5 [0%]	-	0/5 [0%]	-
6	1/8 [12.5%]	0.18	0/8 [0%]	-
8	0/4 [0%]	-	0/4 [0%]	-
9	2/15 [13.3%]	0.2	0/15 [0%]	-
10	1/7 [14.3%]	0.22	0/7 [0%]	-
11	0/6 [0%]	-	0/6 [0%]	-
1–11	4/50 [8.0%]	0.2	1/50 [2.0%]	0.13
13	1/4 [25%]	0.15	1/4 [25%]	0.15
14	0/5 [0%]	-	**3/5 [60%]**	0.25
15	**5/15 [33.3%]**	0.41	2/15 [13.3%]	0.31
16	2/12 [16.7%]	0.28	**5/12 [41.7%]**	0.22
18	1/2 [50%]	0.35	0/2 [0%]	-
13–18	9/38 [23.7%]	0.34	11/38 [28.9%]	0.24
20	2/12 [16.7%]	0.27	2/12 [16.7%]	0.29

The provenance of detritus responsible for the till composition shift across Unit 12s remains unclear. If the shift cannot be reasonably explained by eastern sources or by re-entrainment of older sediment, it raises broader implications for the configuration of ice-sheets at the time. An eastward ice-flow associated with Unit 13t would imply ice-flow emanating from a Keewatin ice-spreading sector, where ice-flow is either curvilinear from a Keewatin dome to the northwest, or linear from one situated farther south than that of the LGM. Keewatin-derived ice-flows would explain the observed spatial gradient in till composition and suggest that Unit 15t's ambiguous NW-SE fabrics instead reflect SE ice-flows, supported by high GR and Dubawnt clast proportions.

However, a Keewatin-sourced interpretation is challenged by the elevated presence of UGG and oolitic jasper clasts in units 13t–18t, which are expected to be sourced from the east. These properties led to several Unit 15t samples being assigned an interpreted NW ice-flow direction (section 4.4), which cannot be overlooked.

In summary, the stark compositional contrast between units 1t–11t and 13t–18t likely reflects changes in sediment availability and transport and/or a reconfiguration of paleo-ice sheet spreading centers. However, disentangling the relative influence of Keewatin versus Q-L ice-spreading sectors on units 13t–18t remains challenging with till composition and ice-flow data alone.

5.4.4 Comparison with previous studies

As discussed in section 1.3.1, Netterville (1974) recognized four till units and three sub-till sorted sediment units, one of which was interpreted as an interglacial unit presumed to be correlative across the local area. The age of these four tills and other sub-till sorted sediments are anchored by this interglacial unit and correlated primarily on the basis of stratigraphic position. Netterville (1974) tentatively extended this correlation to the southeastern HBL in northern Ontario (Skinner, 1974), based on similar apparent stratigraphic positions, again using interglacial sediments as an anchor. This approach rested on several assumptions, including: 1) sub-till sediments are locally correlative based solely on observed stratigraphic position, 2) interglacial sediments represent the most recent interglacial, and 3) sub-till sediments are correlative at regional to continental scales.

The work presented here questions each of these assumptions. Using a detailed, multi-parameter lithostratigraphic approach to correlate till units, combined with allostratigraphy to correlate sub-till sorted sediments, 15 till units and 5 sub-till sorted sediment units are delineated, four of which are interpreted as ice-free deposits. A key parameter used for differentiating till units is interpreted ice-flow direction, which reveals a more complex sequence of ice-flow phases and directional shifts than previously recognized. This contrasts with earlier interpretations of ice-flow history, which contain conflicting directional evidence within units that likely contain multiple ice-flow events (Netterville, 1974; Klassen, 1986). Additionally, whereas prior frameworks and compilations assigned the interglacial deposit in the area to the Sangamonian (i.e., MIS 5; Netterville, 1974; Klassen, 1986; Dredge and McMartin, 2011), this revised framework reassigns the oldest ice-free deposit to at least MIS 11. This demonstrates that sub-till sorted sediments in the study area are indeed more numerous and fragmented than previously assumed and should not be treated as a single correlative unit or used as a marker bed with a sure stratigraphic position.

When compared with the regional synthesis of the Quaternary stratigraphy of northern and central Manitoba assembled in Dredge and McMartin (2011; see Table 1.1), these findings indicate that the synthesis is oversimplified in the number and sequence of ice-flow phases, and limited in the temporal extent of preserved deposits. Here, direct connections are difficult because the presented synthesis is based on assumptions questioned in this study. However, the local record established here would extend the Quaternary history much further back in time than previously inferred; while the synthesis places the oldest interglacial in the region at presumably MIS 7, the revised framework presented here extends it to at least MIS 11.

Another notable observation from the comparison to the summary presented in Dredge and McMartin (2011) is the apparent absence of a distinct Keewatin-sourced till in the study area, despite the study area's long record of Quaternary history. In studies of the Gillam area, the Sundance Till (interpreted as Keewatin-sourced) is recognized based on several characteristics recognizable in the field (sandy texture, GR-rich, contains Dubawnt clasts, associated with SE ice-flow indicators; see section 1.3.2 and Table 1.1). Although several units (5t, 9t, 14t, 15t, 16t) indicate ice-flow directions consistent with a Keewatin source (SE–S), they do not exhibit the distinctive sandy texture or GR-rich clast proportions of Keewatin-sourced tills like the Sundance Till.

However, the Gillam area lies much closer to the Precambrian-Paleozoic boundary than this study area (see Figure 1.2). Therefore, any SE- or S-directed ice-flows arriving at this study area would have travelled farther over the HBB, allowing more opportunity for modification of an original Keewatin signature through input or concentration of HBB-derived material (e.g., direct bedrock erosion, incorporation of pre-existing HBB-rich sediments, comminution of HBB clasts) than in the Gillam area (cf. Gauthier et al., 2019). As a result, Keewatin-sourced tills in this study area may be substantially diluted in their original signal.

If any till from this revised framework has a possible connection to a Keewatin-sourced till, even in a modified or diluted form, Unit 15t may be the most plausible candidate. Unit 15t generally contains a higher percentile of GR clasts, a matrix composition indicative of non-HBB source rock input (section 5.3.1.15), the highest Dubawnt clast content (Table 5.3), and possibly an ESE–SE ice-flow direction (discussed in section 5.4.3.2). Nonetheless, uncertainty persists about a true Keewatin sourced till in the study area and this could be explained by one of the following reasons: a) one was not preserved locally; b) it predates the oldest observed deposits; or c) one is present only in a diluted form, possibly represented by unit 15t.

5.5 Conclusions

The revised framework presented in this chapter represents a substantial advancement to the local stratigraphy presented in Netterville (1974), which recognized only four tills and a single interglacial unit. In contrast, this framework delineates up to 15 till units and 5 sub-till sorted sediment units, four of which are interpreted as ice-free deposits. Each till unit has a distinct combination of stratigraphic position and interpreted ice-flow direction, revealing a more complex history of ice-flow phases and directional shifts than previously established. Finally, the framework reassigns the oldest preserved deposits in the study area to MIS 12, and the oldest interglacial unit to MIS 11. These estimated climatic stages are substantially older than previous interpretations, which tentatively assign the oldest till to be at least MIS 6, and the oldest interglacial to MIS 5. Such an increase in stratigraphic resolution is the result of a multi-parameter approach, integrating ice-flow directional indicators, sedimentology, clast composition, and matrix geochemistry to resolve subtle but significant changes within the glacial record.

This stratigraphic framework is consistent across most sections, despite local complexities and several units with sparse exposures. While some uncertainties remain, particularly in correlating tills in shorter sections or in the absence of ice-flow indicators, the revised framework more accurately reflects the fragmented and discontinuous nature of the western HBL stratigraphy, where some units are thin, patchy, or entirely absent in certain sections.

Provenance interpretations suggest that tills from units 1t–11t predominantly reflect eastern input from ice-flows emanating from a Q-L ice-spreading sector, whereas contradicting parameters from till units 13t–18t suggest possible contributions from both Q-L and Keewatin sources. The transition from units 1t–11t to 13t–20t marks the most pronounced and consistently observed shift in till composition in the study area, characterized by a major decrease in HBB-derived sediment and an increase in shield-sourced material. This change may reflect either a reduction in the availability of HBB bedrock for glacial erosion or a reconfiguration of paleo-ice sheet spreading centers.

Chapter 6: Conclusions and further work

6.1 Research summary and contributions

This research revisits the Quaternary stratigraphy and till provenance of the Gods and Yakaw rivers area in the western HBL, a core region within the LIS influenced from multiple ice-spreading centers (Keewatin and Quebec-Labrador domes; Shilts et al., 1979; Prest, 1990). Unlike many other inner-core regions, this area preserves a thick yet laterally discontinuous record of sediment spanning multiple glacial-interglacial cycles (Dredge and McMartin, 2011; Gauthier et al., 2019), making it a rare archive for investigations of older and understudied Quaternary events. This study area's position within a broad erosional drainage corridor further increases the likelihood of preserving a stratigraphic record of older glacial-interglacial cycles.

Although this area was previously investigated in Netterville (1974), ongoing work in the western HBL using a detailed, multi-parameter approach that combines lithostratigraphy and allostratigraphy (Hodder et al., 2024a; 2024b; Gauthier et al., *in review*) has revealed a more complex and fragmented stratigraphy than previously recognized. Earlier studies, including Netterville (1974), produced a framework based primarily on stratigraphic position, assuming laterally continuous sorted sediment beds, with limited integration of analytical data when correlating units. Subsequent regional frameworks (Klassen, 1986; Dredge and McMartin, 2011) used similar assumptions when incorporating the framework outlined in Netterville (1974), without addressing the implications of the erosional corridor for regional correlations, or the potential for laterally discontinuous units.

As a result, several uncertainties remained prior to this work: the total number of units and the number of preserved glacial-interglacial cycles remained unclear; both the age and correlation of organic-bearing sediments were unresolved, with the possibility that they represent multiple interglacial episodes and may be considerably older than previously assumed; and ice-flow dynamics and till provenance had never been addressed for this area, including the relative influence and timing of ice flows emanating from the Keewatin versus Quebec-Labrador ice-spreading sectors.

The first thesis objective directly addressed the bulk of these knowledge gaps, by unravelling the Quaternary stratigraphy of the region using this hybrid lithostratigraphic-allostratigraphic approach, supported by a detailed, multi-parameter characterization of tills and paleo-ice flow indicators. This work resulted in a revised Quaternary framework that delineates 21 units, including 15 till units and 6 sorted sediment units. Relative stratigraphic relationships, combined with interpretations of ice-free conditions represented by certain sub-till sorted sediments, indicate that at least five glacial-interglacial cycles are recorded, with most sub-till sorted sediments older than previously assumed. The 15 till units document a complex sequence of ice-flow events, each defined by a unique combination of interpreted ice-flow direction, stratigraphic position, and other till properties (e.g., compaction, clast-lithology, matrix geochemistry).

As part of the first objective, the relationship between paleo-ice flow direction and till composition was investigated to better understand till provenance. This was completed by comparing compositional data (k-means clustering of clast-lithology counts, PCA on matrix geochemistry) to ice-flow indicator data. This analysis revealed that samples with GR proportions near the ~10% background level (CL clusters 1, 3, and 5) are predominantly associated with NW-, W-, and SW-directed ice flows, suggesting transport from the northeast, east, or southeast. In contrast, elevated GR clast proportions in CL clusters 2 and 4 have an uncertain provenance. Overall, units 1t–11t appear to be primarily influenced by the Quebec-Labrador sector, while units 13t–18t likely reflect mixed influence from both the Keewatin and Quebec-Labrador ice-spreading centers.

Finally, the revised Quaternary stratigraphy was compared to previous studies and their regional glacial dynamics reconstruction. Earlier frameworks, such as Netterville (1974), recognized only four tills and three sub-till sorted sediment units, with ages and correlations anchored to a single interglacial deposit. Contrastingly, the revised framework presented here recognizes 15 tills and 5 sub-till sorted sediment units, four of which are interpreted as ice-free. This comparison also reveals that: sub-till sediments are more numerous and fragmented than previously recognized; that interpreted ice-flow directions reveal a more complex sequence of phases and directional shifts; and the oldest ice-free deposit observed in the area is assigned to MIS 11 or older, instead of MIS 5. Comparison with the regional synthesis of Dredge and McMartin (2011) further indicates that the stratigraphy preserved in the Gods and Yakaw rivers area is especially old for the western HBL. This comparison also reveals the apparent absence of a distinct Keewatin-sourced till in the study area, with unit 15t being a possible, albeit diluted, candidate.

In summary, this research provides a refined, higher-resolution stratigraphic framework for an inner-core region of the LIS, extending the recognized Quaternary record in the western HBL back to at least MIS 12 based on relative stratigraphic relationships. By applying a detailed, multi-parameter lithostratigraphic-allostratigraphic approach to the particularly complex stratigraphy in this area, tills and sub-till sediments in the Gods and Yakaw river area are shown to be more numerous, discontinuous, and variable than previously recognized, and regional marker beds such as organic-bearing units are demonstrated to be unreliable for correlation without geochronological or paleoenvironmental controls. These results provide new insights into the timing and relative influence of ice-spreading centres over multiple glacial-interglacial cycles, providing critical constraints for ice-sheet modelling. The provenance analysis presented in this thesis also provides valuable insights for mineral exploration in terrains affected by multiple ice-flow sources and/or sediment recycling. More broadly, this research contributes to the understanding of the long-term behaviour of continental ice sheets over multiple glacial-interglacial cycles, providing key insights into how Earth's cryosphere and landscapes respond to climate change across different time scales.

6.2 Recommendations for future research

Several limitations and uncertainties identified in this thesis could be readily addressed in future work. One of the most pressing limitations is the lack of climatic or geochronological constraints on sub-till sorted sediment units (see section 2.2.2). Paleoclimate interpretations from paleoenvironmental techniques may prove useful for either reinforcing unit correlations or refining their interpretations. Geochronological methods (e.g., OSL dating, cosmogenic nuclide dating) would be particularly valuable to test the validity of the minimum climatic stages assigned from relative stratigraphy. Such samples were submitted for analysis but not yet available during the writing of this thesis.

Another considerable limitation is the amount of data available. Despite analyzing 10 sections and 100 till samples, the fragmented nature of the stratigraphy creates uncertainty in certain correlations, especially those involving stratigraphically lower and sparsely exposed units. Investigating additional sections would help test the correlations presented here and refine the ice-flow histories of older tills (e.g., units 1t–3t, 5t–6t), which may only capture part of a glacial phase.

The interpretation of several tills containing geochemical signatures of anoxic sediment incorporation (see section 4.4.2) also remains uncertain. This is due to the limited number of samples from sediments interpreted to be deposited under anoxic conditions, and the absence of paleosalinity proxies. As a result, the climatic interpretation of Unit 12s (and the minimum climatic stages of underlying units) remains tentative. Therefore, it is recommended that future work includes additional sampling of such sediments, and the application of paleosalinity proxies (cf. Wei and Algeo, 2020) to both tills and sorted sediments to test this interpretation.

Certain questions regarding till provenance remains unresolved, including the transport direction of tills with NW-SE fabrics, and the source of the GR clast influx observed within units 13t–18t. Detrital hornblende $^{40}Ar/^{39}Ar$ dating, which has been used previously to help differentiate SE- and NW-sourced tills (Hodder et al., 2024b; see section 2.3.2), may help address these uncertainties.

Finally, the work presented here is well suited for further research that incorporates the Gods and Yakaw rivers area with other study areas within the western HBL. Regional-scale correlations to areas like the Kaskattama highlands (Hodder et al., 2024a; 2024b) and the Gillam area (Gauthier et al., *in review*) are beyond the scope of this thesis but would be valuable for establishing a more comprehensive Quaternary history of the western HBL. Additionally, broader correlations may help delineate tills within Unit 20t, where tills with variable fabrics and compositions are currently lumped together due to their sparse, thin exposures and unclear stratigraphic relationships.

References

Abraham, K. F., and Keddy, C. J. (2005). The Hudson Bay Lowland. In L. H. Fraser & P. A. Keddy (Eds.), *The World's Largest Wetlands: Ecology and Conservation* (pp. 118–148). chapter, Cambridge: Cambridge University Press. https://doi.org/10.1017/CBO9780511542091.005

Algeo, T. J., and Rowe, H. (2012). Paleoceanographic applications of trace-metal concentration data. *Chemical Geology*, *324–325*, 6–18. https://doi.org/10.1016/j.chemgeo.2011.09.002

Allmendinger, R. W., Cardozo, N., and Fisher, D. M. (2011). *Structural Geology Algorithms: Vectors and Tensors* (1st ed.). Cambridge University Press. https://doi.org/10.1017/CBO9780511920202

Andrews, J. T., Shilts, W. W., and Miller, G. H. (1983). Multiple deglaciations of the Hudson Bay Lowlands, Canada, since deposition of the Missinaibi (last interglacial?) Formation; Quaternary Research, v. 19, p. 18-37. https://doi.org/10.1016/0033-5894(83)90025-X

Andrews, J. T., and Smith, D. I. (1969). Statistical analysis of till fabric: Methodology, local and regional variability (with particular reference to the north Yorkshire till cliffs). *Quarterly Journal of the Geological Society*, *125*(1–4), 503–542. https://doi.org/10.1144/gsjgs.125.1.0503

Batchelor, C. L., Margold, M., Krapp, M., Murton, D. K., Dalton, A. S., Gibbard, P. L., Stokes, C. R., Murton, J. B., and Manica, A. (2019). The configuration of Northern Hemisphere ice sheets through the Quaternary. *Nature Communications*, *10*(1), 3713. https://doi.org/10.1038/s41467-019-11601-2

Bilben, S. (2005). MEAP Final Report – Stephens Lake Nickel Project. Exploration Report, BHP Billiton Diamonds Inc.

Bjørlykke, K. (2014). Relationships between depositional environments, burial history and rock properties. Some principal aspects of diagenetic process in sedimentary basins. *Sedimentary Geology*, *301*, 1–14. https://doi.org/10.1016/j.sedgeo.2013.12.002

Boulton, G. S., and Clark, C. D. (1990). A highly mobile Laurentide ice sheet revealed by satellite images of glacial lineations. *Nature*, *346*(6287), 813–817. https://doi.org/10.1038/346813a0

Breit, G. N., and Wanty, R. B. (1991). Vanadium accumulation in carbonaceous rocks: A review of geochemical controls during deposition and diagenesis. *Chemical Geology*, *91*(2), 83–97. https://doi.org/10.1016/0009-2541(91)90083-4

Bridgland, D. R. (Ed.). (1986). *Clast lithological analysis*. Quaternary Research Association.

Craig, B.G. (1969). Late glacial and post-glacial history of the Hudson Bay region; in Earth Science Symposium on Hudson Bay, P.J. Hood (ed.), Geological Survey of Canada, Paper 68-83, p. 63-77.

Dalton, A. S., Dulfer, H. E., Margold, M., Heyman, J., Clague, J. J., Froese, D. G., Gauthier, M. S., Hughes, A. L. C., Jennings, C. E., Norris, S. L., and Stoker, B. J. (2023). Deglaciation of the north American ice sheet complex in calendar years based on a comprehensive database of chronological data: NADI-1. *Quaternary Science Reviews*, *321*, 108345. https://doi.org/10.1016/j.quascirev.2023.108345

Dalton, A. S., Finkelstein, S. A., Barnett, P. J., and Forman, S. L. (2016). Constraining the Late Pleistocene history of the Laurentide Ice Sheet by dating the Missinaibi Formation, Hudson Bay Lowlands, Canada. *Quaternary Science Reviews*, *146*, 288–299. https://doi.org/10.1016/j.quascirev.2016.06.015

Dalton, A. S., Finkelstein, S. A., Barnett, P. J., Väliranta, M., and Forman, S. L. (2018). Late Pleistocene chronology, palaeoecology and stratigraphy at a suite of sites along the Albany River, Hudson Bay Lowlands, Canada. *Palaeogeography, Palaeoclimatology, Palaeoecology*, *492*, 50–63. https://doi.org/10.1016/j.palaeo.2017.12.011

Dalton, A. S., Margold, M., Stokes, C. R., Tarasov, L., Dyke, A. S., et al. (2020). An updated radiocarbon-based ice margin chronology for the last deglaciation of the North American Ice Sheet Complex. *Quaternary Science Reviews*, *234*, 106223. https://doi.org/10.1016/j.quascirev.2020.106223

Dalton, A. S., Stokes, C. R., and Batchelor, C. L. (2022). Evolution of the Laurentide and Innuitian ice sheets prior to the Last Glacial Maximum (115 ka to 25 ka). *Earth-Science Reviews*, *224*, 103875. https://doi.org/10.1016/j.earscirev.2021.103875

Dredge, L.A. (1983). Character and development of northern Lake Agassiz and its relation to Keewatin and Hudsonian ice regimes. In Glacial Lake Agassiz. Geological Association of Canada, Special Paper 26. Edited by J.T. Teller and L. Clayton. pp. 117–131.

Dredge, L. A. and Cowan, W. R. (1989). Quaternary geology of the southwestern Canadian Shield; *in* Quaternary Geology of Canada and Greenland, R. J. Fulton Geological Survey of Canada, Geology of Canada Series, no 1, p. 214-248.

Dredge, L. A., and Dyke, L. D. (2020). Landscapes and Landforms of the Hudson Bay Lowlands. In O. Slaymaker & N. Catto (Eds.), *Landscapes and Landforms of Eastern Canada* (pp. 211–227). Springer International Publishing. https://doi.org/10.1007/978-3-030-35137-3_8

Dredge, L. A., and McMartin, I. (2011). *Glacial stratigraphy of northern and central Manitoba* (No. 600; p. 600). https://doi.org/10.4095/288561

Dredge, L. A., Morgan, A. V., and Nielsen, E. (1990). Sangamon and Pre-Sangamon Interglaciations in the Hudson Bay Lowlands of Manitoba. *Géographie Physique et Quaternaire*, *44*(3), 319–336. https://doi.org/10.7202/032833ar

Earth Observation Research Center and Japanese Aerospace Exploration Agency (2022). ALOS Global Digital Surface Model; Earth Observation Research Center and Japanese Aerospace Exploration Agency, ALOS World 3D - 30m, URL <https://www.eorc.jaxa.jp/ALOS/en/dataset/aw3d30/aw3d30_e.htm> [January 2025].

Evans, D. J. A. (2000). A gravel outwash/deformation till continuum, skalafellsjokull, iceland. *Geografiska Annaler: Series A, Physical Geography*, *82*(4), 499–512. https://doi.org/10.1111/j.0435-3676.2000.00137.x

Evans, D.J.A., and Benn, D.I. (2021). *A practical guide to the study of glacial sediments*. 2nd ed. Quaternary Research Association, London.

Evans, D. J. A., and Campbell, I. A. (1995). Quaternary stratigraphy of the buried valleys of the lower Red Deer River, Alberta, Canada. *Journal of Quaternary Science*, *10*(2), 123–148. https://doi.org/10.1002/jqs.3390100204

Evans, D. J. A., Phillips, E. R., and Atkinson, N. (2021). Glacitectonic rafts and their role in the generation of Quaternary subglacial bedforms and deposits. *Quaternary Research*, *104*, 101–135. https://doi.org/10.1017/qua.2021.11

Evans, D. J. A., Phillips, E. R., Hiemstra, J. F., and Auton, C. A. (2006). Subglacial till: Formation, sedimentary characteristics and classification. *Earth-Science Reviews*, *78*(1–2), 115–176. https://doi.org/10.1016/j.earscirev.2006.04.001

Evans, D. J. A., Smith, I. R., Gosse, J. C., and Galloway, J. M. (2021). Glacial landforms and sediments (landsystem) of the Smoking Hills area, Northwest Territories, Canada: Implications for regional Pliocene – Pleistocene Laurentide Ice Sheet dynamics. *Quaternary Science Reviews*, *262*, 106958. https://doi.org/10.1016/j.quascirev.2021.106958

Gao, C., Huot, S., McDonald, A. M., Crabtree, D. C., and Turton, C. L. (2020). Subtill nonglacial deposits and their climatic implications for the Last Interglacial (MIS 5e), Hudson Bay Lowlands, Canada. *Quaternary Science Reviews*, *248*, 106590. https://doi.org/10.1016/j.quascirev.2020.106590

Gauthier, M. S., Hodder, T. J., Lian, O. B., Finkelstein, S. A., Dalton, A. S., and Paulen, R. C. (2021). *GS2021-8: Stratigraphic, paleoenvironmental and geochronological investigations of intertill nonglacial deposits in northeastern Manitoba (parts of NTS 54B–F, K, L, 64A, H, I)*; in Report of Activities 2021, Manitoba Agriculture and Resource Development, Manitoba Geological Survey, p. 71–76.

Gauthier, M. S., Hodder, T. J., Ross, M., Kelley, S. E., Rochester, A., and McCausland, P. (2019). The subglacial mosaic of the Laurentide Ice Sheet; a study of the interior region of southwestern Hudson Bay. *Quaternary Science Reviews*, *214*, 1–27. https://doi.org/10.1016/j.quascirev.2019.04.015

Gauthier, M. S., Kelley, S. E., and Hodder, T. J. (2020). Lake Agassiz drainage bracketed Holocene Hudson Bay Ice Saddle collapse. *Earth and Planetary Science Letters*, *544*, 116372. https://doi.org/10.1016/j.epsl.2020.116372

Gauthier, M.S., Hodder, T. J., Dalton, A., Lian, O. B., Schaarschmidt, M., Ross, M., Väliranta, M., and Finkelstein, S. (2024). Preservation of probable MIS 7 deglacial and nonglacial deposits near the edge of the Hudson Bay Lowland in Manitoba, Canada. *Canadian Journal of Earth Sciences*, cjes-2024-0019. https://doi.org/10.1139/cjes-2024-0019

Gowan, E. J., Zhang, X., Khosravi, S., Rovere, A., Stocchi, P., Hughes, A. L. C., Gyllencreutz, R., Mangerud, J., Svendsen, J.-I., and Lohmann, G. (2021). A new global ice sheet reconstruction for the past 80 000 years. *Nature Communications*, *12*(1), 1199. https://doi.org/10.1038/s41467-021-21469-w

Grunsky, E. C. (2010). The interpretation of geochemical survey data. *Geochemistry: Exploration, Environment, Analysis*, *10*(1), 27–74. https://doi.org/10.1144/1467-7873/09-210

Hart, J. K., and Boulton, G. S. (1991). The interrelation of glaciotectonic and glaciodepositional processes within the glacial environment. *Quaternary Science Reviews*, *10*(4), 335–350. https://doi.org/10.1016/0277-3791(91)90035-S

Hendy, I. L. (2010). Diagenetic behavior of barite in a coastal upwelling setting. Paleoceanography, 25(4). https://doi.org/10.1029/2009PA001890

Henriksen, M., Mangerud, J., Maslenikova, O., Matiouchkov, A., and Tveranger, J. (2001). Weichselian stratigraphy and glaciotectonic deformation along the lower Pechora River, Arctic Russia. *Global and Planetary Change*, *31*(1–4), 297–319. https://doi.org/10.1016/S0921-8181(01)00126-6

Hicock, S. R., Goff, J. R., Lian, O. B., and Little, E. C. (1996). On the Interpretation of Subglacial Till Fabric. *SEPM Journal of Sedimentary Research*, *Vol. 66*. https://doi.org/10.1306/D4268441-2B26-11D7-8648000102C1865D

Hodder, T. J. and Gauthier, M. S. (2017). Till composition in the Hayes River area, Hudson Bay Lowland, northeast Manitoba; Manitoba Mining and Minerals Convention, Winnipeg, MB, poster.

Hodder, T. J., and Gauthier, M. S. (2021). *GS2021-7: Quaternary stratigraphic and depth to bedrock data compilation for northeastern Manitoba*; in Report of Activities 2021, Manitoba Agriculture and Resource Development, Manitoba Geological Survey, p. 66–70.

Hodder, T. J., and Gauthier, M. S. (2022). *GS2022-12: Quaternary stratigraphic investigations near the confluence of the Hayes and Gods rivers, northeastern Manitoba (part of NTS 54C7)*; in Report of Activities 2022, Manitoba Natural Resources and Northern Development, Manitoba Geological Survey, p. 110–120.

Hodder, T. J., Gauthier, M. S., Kelley, S. E., and Ross, M. (2024a). *Open File OF2024-1: Quaternary site, till composition and ice-flow indicator datasets in the Kaskattama highland area, northeastern Manitoba (parts of NTS 53N, O, 54B, C)*. Manitoba Economic Development, Investment, Trade and Natural Resources, Manitoba Geological Survey, Open File OF2024-1, 20 p., 9 appendices.

Hodder, T. J., Gauthier, M. S., and Nielsen, E. (2017). *Open File OF2017-4: Quaternary stratigraphy and till composition along the Hayes, Gods, Nelson, Fox, Stupart, Yakaw, Angling and Pennycutaway rivers, northeast Manitoba (parts of NTS 53N, 54C, 54D, 54F)*; Manitoba Growth, Enterprise and Trade, Manitoba Geological Survey, Open File OF2017-4, 20 p.

Hodder, T. J., Gauthier, M. S., Ross, M., Kelley, S. E., Lian, O. B., Dalton, A. S., and Finkelstein, S. A. (2024b). Unravelling the fragmented sediment–landform assemblage in an area of thick Quaternary sediment, western Hudson Bay Lowland, Canada. *Canadian Journal of Earth Sciences*, cjes-2024-0018. https://doi.org/10.1139/cjes-2024-0018

Hodder, T. J., Gauthier, M. S., Ross, M., and Lian, O. B. (2023). Was there a nonglacial episode in the western Hudson Bay Lowland during Marine Isotope Stage 3? *Quaternary Research*, *116*, 148–161. https://doi.org/10.1017/qua.2023.35

Hodder, T. J., and Kelley, S. E. (2018). *GS2018-13: Kimberlite-indicator minerals and clast-lithology composition of till, Kaskattama highland region, northeastern Manitoba (parts of NTS 53N, O, 54B, C)*; *in* Report of Activities 2018, Manitoba Growth, Enterprise and Trade, Manitoba Geological Survey, p. 150–165.

Holmes, C. D. (1941). Till fabric. *Geological Society of America Bulletin*, *52*(9), 1299–1354. https://doi.org/10.1130/GSAB-52-1299

Jackson, G. D. (2013). *Geology, Belcher Islands, Nunavut* (No. 4923; p. 4923). https://doi.org/10.4095/292434

Karrow, P. F. (1974). Till Stratigraphy in Parts of Southwestern Ontario. *Geological Society of America Bulletin*, *85*(5), 761. https://doi.org/10.1130/0016-7606(1974)85<761:TSIPOS>2.0.CO;2

Klassen, R. W. (1986). *Surficial geology of north-central Manitoba*. Geological Survey of Canada.

Klassen, R. W. and Netterville, J. A. (1978). Surficial Geology Hayes River, Manitoba: Geological Survey of Canada. Map 2-1978. Scale 1:250 000.

Lipp, A. G., Roberts, G. G., Whittaker, A. C., Gowing, C. J. B., and Fernandes, V. M. (2021). Source Region Geochemistry From Unmixing Downstream Sedimentary Elemental Compositions. *Geochemistry, Geophysics, Geosystems*, *22*(10), e2021GC009838. https://doi.org/10.1029/2021GC009838

Lipp, A. G., Shorttle, O., Syvret, F., and Roberts, G. G. (2020). Major Element Composition of Sediments in Terms of Weathering and Provenance: Implications for Crustal Recycling. *Geochemistry, Geophysics, Geosystems*, *21*(6), e2019GC008758. https://doi.org/10.1029/2019GC008758

Margold, M., Stokes, C. R., and Clark, C. D. (2018). Reconciling records of ice streaming and ice margin retreat to produce a palaeogeographic reconstruction of the deglaciation of the Laurentide Ice Sheet. *Quaternary Science Reviews*, *189*, 1–30. https://doi.org/10.1016/j.quascirev.2018.03.013

Mazzaferro, A. G. M. (2025). *Paleomagnetism and Sedimentology of a Marine Unit Within Manitoba's Quaternary Stratigraphy.* (Unpublished honours thesis). University of Waterloo.

McClenaghan, M. B., Paulen, R. C., Smith, I. R., Rice, J. M., Plouffe, A., McMartin, I., Campbell, J. E., Lehtonen, M., Parsasadr, M., and Beckett-Brown, C. E. (2023). Review of till geochemistry and indicator mineral methods for mineral exploration in glaciated terrain. *Geochemistry: Exploration, Environment, Analysis*, *23*(4), geochem2023-013. https://doi.org/10.1144/geochem2023-013

McClenaghan, M. B., Ward, B. C., Kjarsgaard, I. M., Kjarsgaard, B. A., Kerr, D. E., and Dredge, L. A. (2002). Indicator mineral and till geochemical dispersal patterns associated with the Ranch Lake kimberlite, Lac de Gras region, NWT, Canada. *Geochemistry: Exploration, Environment, Analysis*, *2*(4), 299–319. https://doi.org/10.1144/1467-787302-004

McCracken, A.D. (2014). Report on 10 conodont samples (9 from the Early Silurian, early Llandovery Severn River Formation, 1 barren conodont sample from the Ordovician Red Head Rapids Formation) in the Foran Mining Kaskattama Kimberlite 1 (KK1) core (near Bouchard Lake and Kaskattama River), Hudson Bay Lowland, northeastern Manitoba, submitted in 2014 by Michelle Nicolas (Manitoba Geological Survey), NTS 054B/07, Con. No. 1973; Geological Survey of Canada, Paleontological Report 3-ADM-2014, 9 p.

McDonald, B.C. (1969). Glacial and interglacial stratigraphy, Hudson Bay Lowland; in Earth Science Symposium on Hudson Bay, P.J. Hood (Ed.), Geological Survey of Canada, Paper 68-83, p. 78-99.

McDonald, B. C., and Shilts, W. W. (1971). Quaternary Stratigraphy and Events in Southeastern Quebec. *Geological Society of America Bulletin*, *82*(3), 683. https://doi.org/10.1130/0016-7606(1971)82[683:QSAEIS]2.0.CO;2

McMartin, I., and Henderson, P. J. (2006). Evidence from Keewatin (Central Nunavut) for Paleo-Ice Divide Migration. *Géographie Physique et Quaternaire*, *58*(2–3), 163–186. https://doi.org/10.7202/013137ar

McMartin, I. and Paulen, R.C. (2009). Ice-flow indicators and the importance of ice-flow mapping for drift prospecting. In: R.C. Paulen and I. McMartin (eds.), *Application of Till and Stream Sediment Heavy Mineral and Geochemical Methods to Mineral Exploration in Western and Northern Canada*. Geological Association of Canada, Short Course Notes 18, pp. 153–166.

McMartin, I., Dredge, L. A., Grunsky, E., and Pehrsson, S. (2016). Till Geochemistry in West-Central Manitoba: Interpretation of Provenance and Mineralization Based on Glacial History and Multivariate Data Analysis. *Economic Geology*, *111*(4), 1001–1020. https://doi.org/10.2113/econgeo.111.4.1001

Monaghan, G. W., and Larson, G. J. (1986). Late Wisconsinan drift stratigraphy of the Saginaw Ice Lobe in south-central Michigan. *Geological Society of America Bulletin*, *97*(3), 324. https://doi.org/10.1130/0016-7606(1986)97<324:LWDSOT>2.0.CO;2

Munsell Color–X-Rite, Incorporated. (2015). Munsell Soil Color Book; Pantone LLC, Carlstadt, New Jersey, 42 p.

Netterville, J. A. (1974). *Quaternary Stratigraphy Of The Lower Gods River Region, Hudson Bay Lowlands, Manitoba* (MSc thesis). University of Calgary.

Nicolas, M.P.B. and Armstrong, D.K. (2017). *Update on Paleozoic stratigraphic correlations in the Hudson Bay Lowland, northeastern Manitoba and northern Ontario*; in Report of Activities 2017, Manitoba Growth, Enterprise and Trade, Manitoba Geological Survey, p. 133–147.

Nielsen, E. (2001). *Quaternary Stratigraphy, Till Provenance and Kimberlite Indicator-Mineral Surveys along the Lower Hayes River*; in Report of Activities 2001, Manitoba Industry, Trade and Mines, Manitoba Geological Survey, p. 121-125.

Nielsen, E. (2002). *Quaternary Stratigraphy and Ice-flow History Along the Lower Nelson, Hayes, Gods and Pennycutaway Rivers and Implications for Diamond Exploration in Northeastern Manitoba*; *in* Report of Activities 2002, Manitoba Industry, Trade and Mines, Manitoba Geological Survey, p. 209-215.

Nielsen, E., Morgan, A. V., Morgan, A., Mott, R. J., Rutter, N. W., and Causse, C. (1986). Stratigraphy, paleoecology, and glacial history of the Gillam area, Manitoba. *Canadian Journal of Earth Sciences*, *23*(11), 1641–1661. https://doi.org/10.1139/e86-153

Norris, S. L., Evans, D. J. A., and Cofaigh, C. Ó. (2018). Geomorphology and till architecture of terrestrial palaeo-ice streams of the southwest Laurentide Ice Sheet: A borehole stratigraphic approach. *Quaternary Science Reviews*, *186*, 186–214. https://doi.org/10.1016/j.quascirev.2017.12.018

North American Commission on Stratigraphic Nomenclature. (2021). *Stratigraphy*, 18(3): 153–204. https://doi.org/10.29041/strat.18.3.01

Ó Cofaigh, C., Stokes, C. R., Lian, O. B., Clark, C. D., and Tulacyzk, S. (2013). Formation of mega-scale glacial lineations on the Dubawnt Lake Ice Stream bed: 2. Sedimentology and stratigraphy. *Quaternary Science Reviews*, *77*, 210–227. https://doi.org/10.1016/j.quascirev.2013.06.028

Parent, M., Paradis, S. J., and Boisvert, É. (1995). Ice-flow patterns and glacial transport in the eastern Hudson Bay region: Implications for the late Quaternary dynamics of the Laurentide Ice Sheet. *Canadian Journal of Earth Sciences*, *32*(12), 2057–2070. https://doi.org/10.1139/e95-159

Pedregosa, F., Varoquaux, G., Gramfort, A., Michel, V., Thirion, B., Grisel, O., Blondel, M., Prettenhofer, P., Weiss, R., Dubourg, V., Vanderplas, J., Passos, A., Cournapeau, D., Brucher, M., Perrot, M., and Duchesnay, E. (2011). Scikit-learn: Machine learning in Python. *Journal of Machine Learning Research, 12*, 2825–2830.

Phillips, E., Everest, J., and Diaz-Doce, D. (2010). Bedrock controls on subglacial landform distribution and geomorphological processes: Evidence from the Late Devensian Irish Sea Ice Stream. *Sedimentary Geology*, *232*(3–4), 98–118. https://doi.org/10.1016/j.sedgeo.2009.11.004

Pico, T. (2022). Toward New and Independent Constraints on Global Mean Sea-Level Highstands During the Last Glaciation (Marine Isotope Stage 3, 5a, and 5c). *Paleoceanography and Paleoclimatology*, *37*(12), e2022PA004560. https://doi.org/10.1029/2022PA004560

Piercey, S. J. (2014). Modern Analytical Facilities 2. A Review of Quality Assurance and Quality Control (QA/QC) Procedures for Lithogeochemical Data. *Geoscience Canada*, *41*(1), 75. https://doi.org/10.12789/geocanj.2014.41.035

Prest, V. K. (1990). Laurentide Ice-Flow Patterns: A Historical Review, and Implications of the Dispersal of Belcher Islands Erratics. *Géographie Physique et Quaternaire*, *44*(2), 113–136. https://doi.org/10.7202/032812ar

Prest, V. K., Donaldson, J. A., and Mooers, H. D. (2000). The Omar Story: The Role of Omars in Assessing Glacial History of West-Central North America. *Géographie Physique et Quaternaire*, *54*(3), 257–270. https://doi.org/10.7202/005654ar

Rainbird, R. H., Hadlari, T., Aspler, L. B., Donaldson, J. A., LeCheminant, A. N., and Peterson, T. D. (2003). Sequence stratigraphy and evolution of the Paleoproterozoic intracontinental Baker Lake and Thelon basins, western Churchill Province, Nunavut, Canada. *Precambrian Research*, *125*(1–2), 21–53. https://doi.org/10.1016/S0301-9268(03)00076-7

Reimann, C., Filzmoser, P., Garrett, R. G., and Dutter, R. (2008). *Statistical Data Analysis Explained: Applied Environmental Statistics with R* (1st ed.). Wiley. https://doi.org/10.1002/9780470987605

Rice, J. M., Ross, M., Campbell, H. E., Paulen, R. C., and McClenaghan, M. B. (2024). Net evolution of subglacial sediment transport in the Quebec–Labrador sector of the Laurentide Ice Sheet. *Canadian Journal of Earth Sciences*, *61*(4), 524–542. https://doi.org/10.1139/cjes-2023-0050

Rinne, M. 2020. Bedrock geology of the Fox River belt, Manitoba, (parts of NTS 53M–O, 54B, D), Manitoba Agriculture and Resource Development, Manitoba Geological Survey. OF2020-4, 2 maps at 1:525 000 scale, 1 map at 1:250 000 scale and 1 map at 1:50 000 scale.

Rose, A. W., Hawkes, H. E., and Webb, J. S. (1983). *Geochemistry in mineral exploration* (2nd ed.). Academic Press.

Roy, M. (1998). *Pleistocene stratigraphy of the lower Nelson River area—Implications for the evolution of the Hudson Bay Lowland of Manitoba, Canada*. (MSc thesis). University of Quebec.

Shilts, W. W. (1980). Flow patterns in the central North American ice sheet. *Nature*, *286*(5770), 213–218. https://doi.org/10.1038/286213a0

Shilts, W. W., Cunningham, C. M., and Kaszycki, C. A. (1979). Keewatin Ice Sheet—Re-evaluation of the traditional concept of the Laurentide Ice Sheet. *Geology*, *7*(11), 537. https://doi.org/10.1130/0091-7613(1979)7<537:KISOTT>2.0.CO;2

Skinner, R. G. (1973). *Quaternary stratigraphy of the Moose River Basin, Ontario* (No. 225; p. 225). https://doi.org/10.4095/100702

St-Onge, M.R., Lucas, S.B., Scott, D.J., and Begin, N.J. (1989). *Evidence for the development of oceanic crust and for continental rifting in the tectonostratigraphy of the Early Proterozoic Cape Smith Belt*. Geosci. Canada 16, 119–122.

Stott, G.M., Buse, S., Davis, D.W., and Hamilton, M.A. (2010). The Sutton inliers – a Paleoproterozoic succession in the Hudson Bay Lowland; in Summary of Field Work and Other Activities 2010, Ontario Geological Survey, Open File Report 6260: 19-1–19-14.

Su, Y. (2022). *Using Paleomagnetism to Date Quaternary Sediments in the Hudson Bay Lowlands, Northeastern Manitoba*. (Unpublished honours thesis). University of Waterloo.

Teller, J. T., and Leverington, D. W. (2004). Glacial Lake Agassiz: A 5000 yr history of change and its relationship to the 18O record of Greenland. *Geological Society of America Bulletin*. https://doi.org/10.1130/B25316.1

Thorleifson, L. H., Wyatt, P. H., and Warman, T. A. (1993). *Quaternary stratigraphy of the Severn and Winisk drainage basins, northern Ontario* (No. 442; p. 442). https://doi.org/10.4095/183911

Trommelen, M. S., Ross, M., and Campbell, J. E. (2013). Inherited clast dispersal patterns: Implications for palaeoglaciology of the SE Keewatin Sector of the Laurentide Ice Sheet. *Boreas*, *42*(3), 693–713. https://doi.org/10.1111/j.1502-3885.2012.00308.x

Tulaczyk, S., Kamb, W. B., and Engelhardt, H. F. (2000). Basal mechanics of Ice Stream B, west Antarctica: 1. Till mechanics. *Journal of Geophysical Research: Solid Earth*, *105*(B1), 463–481. https://doi.org/10.1029/1999JB900329

Tyrrell, J. (1916). *Notes on the Geology of Nelson and Hayes Rivers, vol. 10*.

Veillette, J. J., Dyke, A. S., and Roy, M. (1999). Ice-flow evolution of the Labrador Sector of the Laurentide Ice Sheet: A review, with new evidence from northern Quebec. *Quaternary Science Reviews*, *18,* 8–9. https://doi.org/10.1016/S0277-3791(98)00076-6

Veillette, J. J., Roy, M., Paulen, R. C., Ménard, M., and St-Jacques, G. (2017). Uncovering the hidden part of a large ice stream of the Laurentide Ice Sheet, northern Ontario, Canada. *Quaternary Science Reviews*, *155*, 136–158. https://doi.org/10.1016/j.quascirev.2016.11.008

Wang, Y. (2018). *Statistical analysis of till geochemistry in the Nelson River area, northeastern Manitoba: Implications for Quaternary glacial stratigraphy*. (MSc thesis). University of Waterloo.

Wei, W., and Algeo, T. J. (2020). Elemental proxies for paleosalinity analysis of ancient shales and mudrocks. *Geochimica et Cosmochimica Acta*, *287*, 341–366. https://doi.org/10.1016/j.gca.2019.06.034

Wheeler, J. O., Hoffman, P. F., Card, K. D., Davidson, A., Sanford, B. V., Okulitch, A. V., and Roest, W. R. (1996). *Geological map of Canada* (No. 1860A; p. 1860A). https://doi.org/10.4095/208175

Wyatt, P. H. (1990). Amino acid evidence indicating two or more ages of pre-Holocene nonglacial deposits in Hudson Bay Lowland, Northern Ontario; Geographie Physique et Quaternaire, v. 44, no. 3, p. 389-393. https://doi.org/10.7202/032838ar

Appendix A – Related publications

Mesich, L. N., Gauthier, M. S. and Hodder, T. J. (2024). *Till geochemistry from eight sections near the confluence of the Hayes and Gods rivers, northeastern Manitoba (parts of NTS 54C2, 7)*; Manitoba Economic Development, Investment, Trade and Natural Resources, Manitoba Geological Survey, Data Repository Item DRI2024002, Microsoft® Excel® file.

Mesich, N., Gauthier, M. S., Hodder, T. J., Hathaway, J., Schaarschmidt, M., Lian, O.B. and Ross, M. (2023). *Quaternary stratigraphic investigations along the Gods and Yakaw rivers, northeastern Manitoba (parts of NTS 54C2, 7)*; in Report of Activities 2023, Manitoba Economic Development, Investment, Trade and Natural Resources, Manitoba Geological Survey, p. 120–123.

Gauthier, M. S., Mesich, L. N. and Hodder, T. J. (2024). *Till heavy mineral analysis (gold, MMSIM, visual KIM) from eight sections near the confluence of the Hayes and Gods rivers, northeastern Manitoba (parts of NTS 54C2, 7)*; Manitoba Economic Development, Investment, Trade and Natural Resources, Manitoba Geological Survey, Data Repository Item DRI2024001, Microsoft® Excel® file.

Appendix B – Section and sample data

Table 1: Section metadata, including those from previous studies.

Station ID	Latitude	Longitude	Surface elevation (m asl)	Depth to bedrock (m)	Minimum Quaternary thickness (m)	Field year(s)	Data used[1]	References
115-23-002	56.1844	-92.5762	64	-	29.0	2023	Geochem; Lithology; Texture; Fabric	Mesich et al., 2023
115-23-003	56.2648	-92.8081	58	-	30.0	2023	Geochem; Lithology; Texture; Fabric	Mesich et al., 2023
115-23-004	56.1840	-92.5779	-	-	29.0	2023	Geochem; Lithology; Texture; Fabric	Mesich et al., 2023
115-23-005	56.1643	-92.5187	67	-	20.0	2023	Geochem; Lithology; Texture; Fabric	Mesich et al., 2023
115-23-006	56.2362	-92.8149	63	-	17.4	2023	Geochem; Lithology; Texture; Fabric	Mesich et al., 2023
115-23-007	56.1863	-92.6143	88	-	42.2	2023	Geochem; Lithology; Texture; Fabric	Mesich et al., 2023
115-23-008	56.3058	-92.8257	65	-	45.0	2023	Geochem; Lithology; Texture; Fabric	Mesich et al., 2023
115-23-009	56.1944	-92.6490	81	-	47.0	2023	Geochem; Lithology; Texture; Fabric	Mesich et al., 2023
112-22-200	56.3428	-92.8372	56	-	12.2	2022	Geochem; Lithology; Texture; Fabric	Hodder and Gauthier, 2022
112-22-201	56.3694	-92.8772	44	-	32.0	2022	Geochem; Lithology; Texture; Fabric	Hodder and Gauthier, 2022
112-19-628	56.1646	-92.4909	71	-	23.0	2019	Lithology; Texture; Fabric	Hodder et al., 2024
112-19-629	56.3777	-92.8717	58	-	24.0	2019	Lithology; Texture; Fabric	Hodder and Gauthier, 2022; Hodder et al., 2024
Section 15 (I)	56.3776	-92.8703	-	-	38.0*	2002	Lithology; Texture; Fabric	Nielsen, 2002; Hodder et al., 2017
Section 20 (N)	56.2952	-92.8236	-	-	32.0*	2002	Lithology; Texture; Fabric	Nielsen, 2002; Hodder et al., 2017
Section 21 (O)	56.1884	-92.6310	-	-	42.0*	2002	Lithology; Texture; Fabric	Nielsen, 2002; Hodder et al., 2017
Section 23 (Q)	56.2235	-92.8202	-	-	20.0*	2002	Lithology; Texture; Fabric	Nielsen, 2002; Hodder et al., 2017
Section 3	56.1500	-92.4500	76	-	32.2	1971-1973	-	Klassen, 1986
NET-6	56.1596	-92.4995	-	-	21.2	1972-1973	-	Netterville, 1974
NET-7	56.1726	-92.5274	-	-	22.1	1972-1973	-	Netterville, 1974
NET-8	56.1854	-92.5789	-	-	28.3	1972-1973	-	Netterville, 1974
NET-9	56.1973	-92.6554	-	-	20.0	1972-1973	-	Netterville, 1974
NET-10	56.2843	-92.7971	-	-	16.6	1972-1973	-	Netterville, 1974

[1] Abbreviations: Geochem, till-matrix (<63 µm size fraction) geochemical analysis (Ca/Mg method, partial, and fusion); Lithology, clast-lithology counts; Fabric, clast fabric analysis; Lithology, clast-lithology counts; Texture, till-matrix (<2 mm size fraction) grain size analysis. *Likely overestimated (cf. Hodder and Gauthier, 2022).

Table 2: Till sample metadata, including those from previous studies.

Sample Site ID	Station ID	Latitude	Longitude	Depth from (m bgs)	Depth to (m bgs)	Material	Purpose[1]
115-23-002-A01	115-23-002	56.1844	-92.5762	4.45	4.55	Till	Geochem; Lithology; Texture; Fabric
115-23-002-B01	115-23-002	56.1844	-92.5762	6.45	6.55	Till	Geochem; Lithology; Texture
115-23-002-B02	115-23-002	56.1844	-92.5762	7.95	8.05	Till	Geochem; Lithology; Texture; Fabric
115-23-002-B03	115-23-002	56.1844	-92.5762	8.95	9.05	Till	Geochem; Lithology; Texture; IM; Fabric
115-23-002-C01	115-23-002	56.1844	-92.5762	9.95	10.05	Till	Geochem; Lithology; Texture; Fabric
115-23-002-C02	115-23-002	56.1844	-92.5762	12.45	12.55	Till	Geochem; Lithology; Texture; IM; Fabric
115-23-002-C03	115-23-002	56.1844	-92.5762	14.45	14.55	Till	Geochem; Lithology; Texture; Fabric
115-23-002-C04	115-23-002	56.1844	-92.5762	16.15	16.25	Till	Geochem; Lithology; Texture; IM; Fabric
115-23-002-D01	115-23-002	56.1844	-92.5762	17.35	17.45	Till	Geochem; Lithology; Texture; IM; Fabric
115-23-002-D02	115-23-002	56.1844	-92.5762	19.55	19.65	Till	Geochem; Lithology; Texture; Fabric
115-23-002-D03	115-23-002	56.1844	-92.5762	21.55	21.65	Till	Geochem; Lithology; Texture
115-23-002-D04	115-23-002	56.1844	-92.5762	23.55	23.65	Till	Geochem; Lithology; Texture; IM; Fabric
115-23-002-H01	115-23-002	56.1844	-92.5762	26.45	26.55	Till	Geochem; Lithology; Texture
115-23-002-Z01	115-23-002	56.1844	-92.5762	27.25	27.35	Till	Geochem; Lithology; Texture
115-23-003-A01	115-23-003	56.2648	-92.8081	27.4	27.5	Till	Geochem; Lithology; Texture
115-23-003-A02	115-23-003	56.2648	-92.8081	25.2	25.3	Till	Geochem; Lithology; Texture; IM; Fabric
115-23-003-A03	115-23-003	56.2648	-92.8081	23.8	23.9	Till	Geochem; Lithology; Texture
115-23-003-B01	115-23-003	56.2648	-92.8081	22.8	22.9	Till	Geochem; Lithology; Texture; IM; Fabric
115-23-003-B02	115-23-003	56.2648	-92.8081	19.8	19.9	Till	Geochem; Lithology; Texture; IM; Fabric
115-23-003-D01	115-23-003	56.2648	-92.8081	14.8	14.9	Till	Geochem; Lithology; Texture; IM; Fabric
115-23-003-D02	115-23-003	56.2648	-92.8081	12.8	12.9	Till	Geochem; Lithology; Texture
115-23-003-D03	115-23-003	56.2648	-92.8081	10.8	10.9	Till	Geochem; Lithology; Texture
115-23-003-D04	115-23-003	56.2648	-92.8081	8.8	8.9	Till	Geochem; Lithology; Texture; IM
115-23-003-L01	115-23-003	56.2648	-92.8081	3.25	3.35	Till	Geochem; Lithology; Texture; Fabric
115-23-004-B01	115-23-004	56.1840	-92.5779	25.25	25.35	Till	Geochem; Lithology; Texture; Fabric
115-23-005-B01	115-23-005	56.1643	-92.5187	3.55	3.65	Till	Geochem; Lithology; Texture; IM; Fabric
115-23-005-B02	115-23-005	56.1643	-92.5187	5.05	5.15	Till	Geochem; Lithology; Texture
115-23-005-B03	115-23-005	56.1643	-92.5187	7.05	7.15	Till	Geochem; Lithology; Texture
115-23-005-B04	115-23-005	56.1643	-92.5187	9.05	9.15	Till	Geochem; Lithology; Texture; IM; Fabric
115-23-005-B05	115-23-005	56.1643	-92.5187	11.05	11.15	Till	Geochem; Lithology; Texture
115-23-005-C01	115-23-005	56.1643	-92.5187	13.95	14.05	Till	Geochem; Lithology; Texture
115-23-005-O01	115-23-005	56.1639	-92.5186	15	15.1	Till	Geochem; Lithology; Texture; Fabric
115-23-005-P01	115-23-005	56.1639	-92.5186	19	19.3	Till	Geochem; Lithology; Texture
115-23-005-Z01	115-23-005	56.1643	-92.5187	13.25	13.35	Till	Geochem; Lithology; Texture; Fabric
115-23-006-A01	115-23-006	56.2362	-92.8149	4.7	4.8	Till	Geochem; Lithology; Texture; IM; Fabric
115-23-006-B01	115-23-006	56.2362	-92.8149	6.25	6.35	Till	Geochem; Lithology; Texture; Fabric
115-23-006-B02	115-23-006	56.2362	-92.8149	8.15	8.25	Till	Geochem; Lithology; Texture; IM
115-23-006-C01	115-23-006	56.2362	-92.8149	9.25	9.35	Till	Geochem; Lithology; Texture; IM; Fabric

115-23-006-C02	115-23-006	56.2362	-92.8149	12.45	12.55	Till	Geochem; Lithology; Texture; Fabric
115-23-006-C03	115-23-006	56.2362	-92.8149	16.45	16.55	Till	Geochem; Lithology; Texture; IM; Fabric
115-23-006-D01	115-23-006	56.2362	-92.8149	17.55	17.65	Till	Geochem; Lithology; Texture; IM
115-23-007-A01	115-23-007_Exposure2	56.1863	-92.6145	0.65	0.75	Till	Geochem; Lithology; Texture; Fabric
115-23-007-B01	115-23-007_Exposure2	56.1863	-92.6145	1.95	2.05	Till	Geochem; Lithology; Texture
115-23-007-B02	115-23-007_Exposure2	56.1863	-92.6145	2.95	3.05	Till	Geochem; Lithology; Texture; IM; Fabric
115-23-007-C01	115-23-007_Exposure1	56.1863	-92.6143	4.5	4.6	Till	Geochem; Lithology; Texture; IM; Fabric
115-23-007-C02	115-23-007_Exposure1	56.1863	-92.6143	7.5	7.6	Till	Geochem; Lithology; Texture
115-23-007-C03	115-23-007_Exposure1	56.1863	-92.6143	10.5	10.6	Till	Geochem; Lithology; Texture
115-23-007-C04	115-23-007_Exposure1	56.1863	-92.6143	13.5	13.6	Till	Geochem; Lithology; Texture; IM; Fabric
115-23-007-C05	115-23-007_Exposure1	56.1863	-92.6143	15.5	15.6	Till	Geochem; Lithology; Texture; Fabric
115-23-007-D01	115-23-007_Exposure1	56.1863	-92.6143	17.9	18	Till	Geochem; Lithology; Texture; IM; Fabric
115-23-007-D02	115-23-007_Exposure1	56.1863	-92.6143	20.9	21	Till	Geochem; Lithology; Texture
115-23-007-D03	115-23-007_Exposure1	56.1863	-92.6143	23.1	23.2	Till	Geochem; Lithology; Texture; IM; Fabric
115-23-007-D04	115-23-007_Exposure1	56.1863	-92.6143	26.1	26.2	Till	Geochem; Lithology; Texture
115-23-007-D05	115-23-007_Exposure1	56.1863	-92.6143	29.1	29.2	Till	Geochem; Lithology; Texture; Fabric
115-23-007-D06	115-23-007_Exposure1	56.1863	-92.6143	32.1	32.2	Till	Geochem; Lithology; Texture
115-23-007-D07	115-23-007_Exposure1	56.1863	-92.6143	34.1	34.2	Till	Geochem; Lithology; Texture; IM; Fabric
115-23-007-D08	115-23-007_Interglacial_3	56.1859	-92.6138	31.0	31.1	Till	Fabric
115-23-007-E01	115-23-007_Exposure1	56.1863	-92.6143	35.6	35.7	Till	Geochem; Lithology; Texture; Fabric
115-23-007-E02	115-23-007_Exposure1	56.1863	-92.6143	38.1	38.2	Till	Geochem; Lithology; Texture
115-23-007-E03	115-23-007_Exposure1	56.1863	-92.6143	40.6	40.7	Till	Geochem; Lithology; Texture; IM; Fabric
115-23-008-A01	115-23-008	56.3058	-92.8257	1.1	1.2	Till	Geochem; Lithology; Texture; Fabric
115-23-008-B01	115-23-008	56.3058	-92.8257	2.25	2.35	Till	Geochem; Lithology; Texture; IM; Fabric
115-23-008-C01	115-23-008	56.3058	-92.8257	3.35	3.45	Till	Geochem; Lithology; Texture; IM; Fabric
115-23-008-F01	115-23-008	56.3058	-92.8257	5.45	5.55	Till	Geochem; Lithology; Texture; IM; Fabric
115-23-008-F02	115-23-008	56.3058	-92.8257	8.45	8.55	Till	Geochem; Lithology; Texture
115-23-008-F03	115-23-008	56.3058	-92.8257	11.45	11.55	Till	Geochem; Lithology; Texture; IM; Fabric
115-23-008-F04	115-23-008	56.3058	-92.8257	15.1	15.2	Till	Geochem; Lithology; Texture; IM; Fabric
115-23-009-B01	115-23-009	56.1944	-92.6490	2.9	3.1	Till	Geochem; Lithology; Texture; Fabric
115-23-009-C01	115-23-009	56.1944	-92.6490	4.45	4.55	Till	Geochem; Lithology; Texture; Fabric
115-23-009-D01	115-23-009	56.1944	-92.6490	6.95	7.05	Till	Geochem; Lithology; Texture; Fabric
115-23-009-D02	115-23-009	56.1944	-92.6490	8.95	9.05	Till	Geochem; Lithology; Texture
115-23-009-D03	115-23-009	56.1944	-92.6490	12.95	13.05	Till	Geochem; Lithology; Texture; Fabric
115-23-009-D04	115-23-009	56.1944	-92.6490	15.95	16.05	Till	Geochem; Lithology; Texture
115-23-009-D05	115-23-009	56.1944	-92.6490	18.95	19.05	Till	Geochem; Lithology; Texture; Fabric
115-23-009-D06	115-23-009	56.1944	-92.6490	20.95	21.05	Till	Geochem; Lithology; Texture
115-23-009-D07	115-23-009	56.1944	-92.6490	22.75	22.85	Till	Geochem; Lithology; Texture; IM; Fabric
115-23-009-E01	115-23-009	56.1944	-92.6490	25.05	25.15	Till	Geochem; Lithology; Texture; Fabric
115-23-009-G01	115-23-009	56.1944	-92.6490	26.9	27	Till	Geochem; Lithology; Texture; IM; Fabric
115-23-009-G02	115-23-009	56.1944	-92.6490	28.9	29	Till	Geochem; Lithology; Texture
115-23-009-J01	115-23-009	56.1944	-92.6490	32.4	32.5	Till	Geochem; Lithology; Texture; Fabric

115-23-009-K01	115-23-009	56.1944	-92.6490	34.25	34.35	Till	Geochem; Lithology; Texture
115-23-009-K02	115-23-009	56.1944	-92.6490	37.25	37.35	Till	Geochem; Lithology; Texture; IM; Fabric
115-23-009-K03	115-23-009	56.1944	-92.6490	40.25	40.35	Till	Geochem; Lithology; Texture; Fabric
115-23-009-K04	115-23-009	56.1944	-92.6490	43.25	43.45	Till	Geochem; Lithology; Texture; IM
115-23-009-N01	115-23-009	56.1944	-92.6490	10.95	11.05	Till	Geochem; Lithology; Texture
112-22-200-A01	112-22-200	56.3428	-92.8372	0.9	1	Till	
112-22-200-A02	112-22-200	56.3428	-92.8372	1.5	1.6	Till	
112-22-200-B01	112-22-200	56.3428	-92.8372	2.5	2.6	Till	
112-22-200-C01	112-22-200	56.3428	-92.8372	4.2	4.3	Till	
112-22-200-C02	112-22-200	56.3428	-92.8372	7.2	7.3	Till	
112-22-200-C03	112-22-200	56.3428	-92.8372	10.2	10.3	Till	
112-22-201-A01	112-22-201	56.3694	-92.8772	10.8	10.9	Till	
112-22-201-B01	112-22-201	56.3694	-92.8772	12.6	12.7	Till	
112-19-628-B01	112-19-628	56.1646	-92.4909	3	3.1	Till	Geochem; Lithology; Texture; Fabric
112-19-628-D01	112-19-628	56.1646	-92.4909	12.4	12.5	Till	Geochem; Lithology; Texture; Fabric
112-19-628-D02	112-19-628	56.1646	-92.4909	15	15.1	Till	Geochem; Lithology; Texture
112-19-628-D03	112-19-628	56.1646	-92.4909	15.8	15.9	Till	Geochem; Lithology; Texture
112-19-628-D04	112-19-628	56.1646	-92.4909	18	18.1	Till	Geochem; Lithology; Texture
112-19-628-D05	112-19-628	56.1646	-92.4909	20	20.1	Till	Geochem; Lithology; Texture
W9765	112-19-629	56.3777	-92.8717			Till	Fabric
112-19-629-A01	112-19-629	56.3777	-92.8717	14	14.6	Till	Geochem; Lithology; Texture; Fabric
112-19-629-C01	112-19-629	56.3777	-92.8717	15.7	15.8	Till	Geochem; Lithology; Texture; Fabric
W9769	112-19-629	56.3777	-92.8717			Till	Fabric
W9771	112-19-629	56.3777	-92.8717			Till	Fabric
W9763	Section 15 (I)	56.3776	-92.8703	20		Till	
W9764	Section 15 (I)	56.3776	-92.8703	22		Till	
W9765	Section 15 (I)	56.3776	-92.8703	24		Till	
W9766	Section 15 (I)	56.3776	-92.8703	26		Till	
W9767	Section 15 (I)	56.3776	-92.8703	28.1		Till	
W9768	Section 15 (I)	56.3776	-92.8703	30		Till	
W9769	Section 15 (I)	56.3776	-92.8703	32		Till	
W9770	Section 15 (I)	56.3776	-92.8703	34		Till	
W9771	Section 15 (I)	56.3776	-92.8703	36		Till	
W9772	Section 15 (I)	56.3776	-92.8703	38		Till	
W9813	Section 20 (N)	56.2952	-92.8236	16		Till	
W9814	Section 20 (N)	56.2952	-92.8236	18		Till	
W9815	Section 20 (N)	56.2952	-92.8236	20		Till	
W9816	Section 20 (N)	56.2952	-92.8236	22		Till	
W9817	Section 20 (N)	56.2952	-92.8236	24		Till	
W9818	Section 20 (N)	56.2952	-92.8236	26		Till	
W9819	Section 20 (N)	56.2952	-92.8236	28		Till	
W9820	Section 20 (N)	56.2952	-92.8236	30		Till	

W9821	Section 20 (N)	56.2952	-92.8236	32		Till	
W9823	Section 21 (O)	56.1884	-92.6310	23		Till	
W9824	Section 21 (O)	56.1884	-92.6310	24		Till	
W9825	Section 21 (O)	56.1884	-92.6310	26		Till	
W9826	Section 21 (O)	56.1884	-92.6310	28		Till	
W9827	Section 21 (O)	56.1884	-92.6310	30		Till	
W9828	Section 21 (O)	56.1884	-92.6310	32		Till	
W9829	Section 21 (O)	56.1884	-92.6310	34		Till	
W9830	Section 21 (O)	56.1884	-92.6310	38		Till	
W9831	Section 21 (O)	56.1884	-92.6310	40		Till	
W9832	Section 21 (O)	56.1884	-92.6310	42		Till	
W9842	Section 23 (Q)	56.2235	-92.8202	8.2		Till	
W9843	Section 23 (Q)	56.2235	-92.8202	10		Till	
W9844	Section 23 (Q)	56.2235	-92.8202	12		Till	
W9845	Section 23 (Q)	56.2235	-92.8202	14		Till	
W9846	Section 23 (Q)	56.2235	-92.8202	16		Till	
W9847	Section 23 (Q)	56.2235	-92.8202	18		Till	

[1] Abbreviations: Geochem, till-matrix (<63 µm size fraction) geochemical analysis (Ca/Mg method, partial, and fusion); Lithology, clast-lithology counts; Fabric, clast fabric analysis; IM, indicator mineral analysis (visible gold, kimberlite-indicator minerals, magmatic or metamorphosed massive-sulphide-indicator minerals); Texture, till-matrix (<2 mm size fraction) grain size analysis.

Table 3: Sample metadata for other materials, including those from previous studies.

Sample Site ID	Station ID	Latitude	Longitude	Depth from (m bgs)	Depth to (m bgs)	Material	Purpose[1]
115-23-005-Grav3	115-23-005_Interglacial1	56.1645	-92.5193	18.3		Gravel	Lithology
115-23-006-X01	115-23-006	56.2362	-92.8149	3.5	3.6	Gravel	Lithology
115-23-007-Grav1	115-23-007_Interglacial_3	56.1859	-92.6138	32.2		Gravel	Lithology
115-23-007-Grav2	115-23-007_Interglacial_3	56.1859	-92.6138	33.2		Gravel	Lithology

[1] Abbreviation: Lithology, clast-lithology counts.

Table 4: Physical properties of till and gravel samples, including those from previous studies.

Sample ID	State	Munsell code	Munsell colour	Field clast percentage (%)	Relative density	Blocky texture	Joint staining	Sand (%)	Silt (%)	Clay (%)	Matrix texture[1]
115-23-002-A01	moist	2.5Y4/3	olive brown	15-20	compact	major	minor	28	48	24	clayey sandy silt
115-23-002-B01	moist	2.5Y4/3	olive brown	10	very compact	major	yes	35	43	22	clayey sandy silt
115-23-002-B02	moist	2.5Y4/3	olive brown	10-15	very compact	major	yes	29	47	24	clayey sandy silt
115-23-002-B03	moist	2.5Y4/3	olive brown	10-15	very compact	major	yes	30	47	24	clayey sandy silt
115-23-002-C01	moist	2.5Y4/3	olive brown	10-15	very compact	major	yes	31	50	20	clayey sandy silt
115-23-002-C02	moist	2.5Y4/3	olive brown	10-15	very compact	major	yes	30	53	17	clayey sandy silt
115-23-002-C03	moist	2.5Y4/3	olive brown	10-15	very compact	major	yes	29	55	16	clayey sandy silt
115-23-002-C04	moist	2.5Y4/3	olive brown	10-15	very compact	major	yes	34	53	13	sandy silt
115-23-002-D01	moist	2.5Y4/2	dark grey brown	5-10	very compact	major	yes	26	49	26	clayey sandy silt
115-23-002-D02	moist	2.5Y4/2	dark grey brown	10-15	very compact	major	yes	29	49	22	clayey sandy silt
115-23-002-D03	moist	2.5Y4/2	dark grey brown	10-15	very compact	major	yes	31	48	21	clayey sandy silt
115-23-002-D04	moist	2.5Y3/2	very dark grey brown	10-15	very compact	major	yes	29	49	21	clayey sandy silt
115-23-002-H01	gleyed	5Y3/1	very dark grey	1-3	moderate	minor	minor	14	37	49	clayey silt
115-23-002-Z01	gleyed	2.5Y3/2	very dark grey brown	5	very compact	major	yes	14	42	44	silty clay
115-23-003-A01	moist	2.5Y4/3	olive brown	10-20	very compact	major	yes	21	64	15	clayey sandy silt
115-23-003-A02	moist	2.5Y4/3	olive brown	10-20	very compact	major	yes	41	48	11	sandy silt
115-23-003-A03	moist	2.5Y4/3	olive brown	10-20	very compact	major	yes	33	54	13	sandy silt
115-23-003-B01	moist	2.5Y4/3	olive brown	10-20	very compact	major	yes	31	54	15	clayey sandy silt
115-23-003-B02	moist	2.5Y4/3	olive brown	10-20	very compact	major	yes	31	49	20	clayey sandy silt
115-23-003-D01	moist	2.5Y4/2	dark grey brown	10-15	very compact	major	yes	30	46	23	clayey sandy silt
115-23-003-D02	moist	2.5Y4/2	dark grey brown	10-15	very compact	major	yes	30	48	22	clayey sandy silt
115-23-003-D03	moist	2.5Y4/2	dark grey brown	10-15	very compact	major	yes	30	49	21	clayey sandy silt
115-23-003-D04	moist	2.5Y4/3	olive brown	10-15	very compact	major	yes	29	51	20	clayey sandy silt
115-23-003-L01	moist	2.5Y6/4	light yellow brown	20-30	compact	minor	no	51	44	6	silty sand
115-23-004-B01	moist	2.5Y3/1	very dark grey	3-5	compact	major	yes	13	37	50	silty clay
115-23-005-B01	moist	10YR4/2	dark grey brown	10-15	compact	minor	minor	28	50	22	clayey sandy silt
115-23-005-B02	moist	10YR4/2	dark grey brown	10-15	compact	minor	minor	28	50	22	clayey sandy silt

115-23-005-B03	moist	10YR4/2	dark grey brown	10-15	compact	major	yes	26	50	24	clayey sandy silt
115-23-005-B04	moist	10YR4/2	dark grey brown	10-15	compact	major	yes	24	46	30	sandy clayey silt
115-23-005-B05	moist	10YR4/2	dark grey brown	10-15	compact	major	yes	28	49	23	clayey sandy silt
115-23-005-C01	moist	10YR4/2	dark grey brown	10-15	compact	major	yes	27	51	22	clayey sandy silt
115-23-005-O01	moist	10YR3/2	very dark grey brown	10-15	compact	major	yes	24	51	25	sandy clayey silt
115-23-005-Grav3		-	-		loose	-	-				
115-23-005-P01	gleyed	5Y4/1	dark grey	10-15	compact	?	?	17	38	45	sandy silty clay
115-23-005-Z01	moist	10YR4/2	dark grey brown	10-15	compact	major	yes	29	50	21	clayey sandy silt
115-23-006-A01	moist	10YR5/3	brown	10-15	compact	minor	minor	34	52	14	sandy silt
115-23-006-B01	moist	10YR4/3	brown	10-15	very compact	major	yes	30	49	21	clayey sandy silt
115-23-006-B02	moist	10YR4/3	brown	15-20	very compact	major	yes	26	55	19	clayey sandy silt
115-23-006-C01	moist	2.5Y3/2	very dark grey brown	10-15	very compact	major	yes	28	47	25	clayey sandy silt
115-23-006-C02	moist	2.5Y3/2	very dark grey brown	10-15	very compact	major	yes	28	47	24	clayey sandy silt
115-23-006-C03	moist	2.5Y3/2	very dark grey brown	10-15	very compact	major	yes	31	49	20	clayey sandy silt
115-23-006-D01	moist	2.5Y4/2	dark grey brown	15-25	very compact	major	yes	33	52	15	clayey sandy silt
115-23-006-X01	moist	-	-	40	loose	-	-				
115-23-007-A01	moist	10YR3/4	dark grey brown	10-15	noncompact	no	no	30	47	23	clayey sandy silt
115-23-007-B01	moist	2.5Y5/4	light olive brown	10-15	noncompact	minor	no	22	51	27	sandy clayey silt
115-23-007-B02	moist	2.5Y4/4	olive brown	10-15	compact	minor	no	28	49	23	clayey sandy silt
115-23-007-C01	moist	2.5Y3/3	dark olive brown	15	very compact	major	yes	28	47	24	clayey sandy silt
115-23-007-C02	moist	2.5Y3/3	dark olive brown	15	very compact	major	yes	29	47	24	clayey sandy silt
115-23-007-C03	moist	2.5Y3/3	dark olive brown	15	very compact	major	yes	29	47	24	clayey sandy silt
115-23-007-C04	moist	2.5Y3/3	dark olive brown	15	very compact	major	yes	29	47	24	clayey sandy silt
115-23-007-C05	moist	2.5Y3/3	dark olive brown	15	very compact	major	yes	28	50	24	clayey sandy silt
115-23-007-D01	moist	2.5Y3/2	very dark grey brown	10-15	very compact	major	yes	37	43	20	clayey sandy silt
115-23-007-D02	moist	2.5Y3/3	dark olive brown	15	very compact	major	yes	29	49	22	clayey sandy silt
115-23-007-D03	moist	2.5Y3/2	very dark grey brown	15	very compact	major	yes	29	50	21	clayey sandy silt
115-23-007-D04	moist	2.5Y4/2	dark grey brown	15	very compact	major	yes	31	51	18	clayey sandy silt
115-23-007-D05	moist	2.5Y4/2	dark grey brown	15	very compact	major	yes	28	54	19	clayey sandy silt
115-23-007-D06	moist	2.5Y4/2	dark grey brown	15	very compact	major	yes	32	54	13	sandy silt

115-23-007-Grav1					loose						
115-23-007-Grav2					loose						
115-23-007-D07	moist	2.5Y4/2	dark grey brown	15	very compact	major	yes	32	54	14	sandy silt
115-23-007-D08											
115-23-007-E01	moist	2.5Y4/2	dark grey brown	10-15	very compact	major	yes	30	50	20	clayey sandy silt
115-23-007-E02	moist	2.5Y4/2	dark grey brown	10-15	very compact	major	yes	32	49	19	clayey sandy silt
115-23-007-E03	moist	2.5Y3/2	very dark grey brown	10-15	very compact	major	yes	24	49	27	sandy clayey silt
115-23-008-A01	moist	2.5Y5/4	light olive brown	10-15	noncompact	no	no	40	57	4	sandy silt
115-23-008-B01	moist	2.5Y4/4	olive brown	10-15	compact	minor	yes	28	57	14	sandy silt
115-23-008-C01	moist	2.5Y6/3	light yellow brown	10-15	very compact	major	yes	36	56	7	sandy silt
115-23-008-F01	moist	2.5Y4/4	olive brown	10-15	very compact	major	yes	28	50	22	clayey sandy silt
115-23-008-F02	moist	2.5Y4/4	olive brown	10-15	very compact	major	yes	28	51	21	clayey sandy silt
115-23-008-F03	moist	2.5Y4/4	olive brown	10-15	very compact	major	yes	32	47	21	clayey sandy silt
115-23-008-F04	moist	2.5Y4/4	olive brown	10-15	very compact	major	yes	32	47	21	clayey sandy silt
115-23-009-B01	moist	10YR5/4	yellow brown	10-15	compact	major	minor	41	48	11	sandy silt
115-23-009-C01	moist	10YR4/4	dark yellow brown	10-15	compact	major	minor	35	45	19	clayey sandy silt
115-23-009-D01	moist	10YR4/2	dark grey brown	10-15	very compact	major	yes	29	48	24	clayey sandy silt
115-23-009-D02	moist	10YR4/2	dark grey brown	10-15	very compact	major	yes	28	48	23	clayey sandy silt
115-23-009-D03	moist	10YR3/2	very dark grey brown	10-15	very compact	major	yes	28	48	24	clayey sandy silt
115-23-009-D04	moist	10YR4/2	dark grey brown	10-15	very compact	major	yes	30	47	24	clayey sandy silt
115-23-009-D05	moist	10YR4/2	dark grey brown	5-10	very compact	major	yes	28	47	25	clayey sandy silt
115-23-009-D06	moist	10YR4/2	dark grey brown	10	very compact	major	yes	30	51	19	clayey sandy silt
115-23-009-D07	moist	2.5Y5/2	grey brown	5-10	very compact	major	yes	31	58	10	sandy silt
115-23-009-E01	moist	2.5Y4/2	dark grey brown	10-15	very compact	major	yes	32	51	17	clayey sandy silt
115-23-009-G01	moist	2.5Y3/2	very dark grey brown	10-15	very compact	major	yes	25	49	26	clayey sandy silt
115-23-009-G02	moist	2.5Y3/2	very dark grey brown	10-15	very compact	major	yes	29	49	22	clayey sandy silt
115-23-009-J01	moist	10YR4/2	dark grey brown	1-5	very compact	major	yes	25	53	22	clayey sandy silt
115-23-009-K01	moist	2.5Y3/2	very dark grey brown	5-10	very compact	major	yes	23	48	29	sandy clayey silt
115-23-009-K02	moist	2.5Y3/2	very dark grey brown	5-10	very compact	major	yes	24	49	27	sandy clayey silt
115-23-009-K03	moist	2.5Y3/2	very dark grey brown	10	very compact	major	yes	24	48	28	sandy clayey silt

115-23-009-K04	dry	2.5Y3/2	very dark grey brown	10-15	very compact	major	yes	30	48	22	clayey sandy silt
115-23-009-N01	moist	10YR4/2	dark grey brown	10-15	very compact	major	yes	30	47	23	clayey sandy silt
112-22-200-A01		2.5Y5/3	light olive brown					28	59	13	sandy silt
112-22-200-A02		2.5Y5/3	light olive brown					27	64	9	sandy silt
112-22-200-B01		10YR4/3	brown					27	60	13	sandy silt
112-22-200-C01		2.5Y4/3	olive brown					35	45	20	clayey sandy silt
112-22-200-C02		2.5Y4/3	olive brown					33	47	20	clayey sandy silt
112-22-200-C03		2.5Y4/3	olive brown					34	45	21	clayey sandy silt
112-22-201-A01		2.5Y3/2	very dark grayish brown					35	45	20	clayey sandy silt
112-22-201-B01		2.5Y4/3	olive brown					46	41	13	silty sand
112-19-628-B01		2.5Y 4/1	dark grey								
112-19-628-D01		10YR 4/1	dark grey								
112-19-628-D02		10YR 4/2	dark greyish brown								
112-19-628-D03		5YR 4/4	reddish brown								
112-19-628-D04		10YR 4/2	dark greyish brown								
112-19-628-D05		10YR 4/2	dark greyish brown								
W9765											
112-19-629-A01		10YR 4/3	brown								
112-19-629-C01		10YR 4/2	dark greyish brown								
W9769											
W9771											
W9763		10YR 4/3	brown								
W9764		10YR 4/2	dark grayish brown								
W9765		2.5Y 4/4	olive brown								
W9766		10YR 4/3	brown								
W9767		2.5Y 4/4	olive brown								
W9768		10YR 4/2	dark grayish brown								
W9769		10YR 4/3	brown								
W9770		10YR 4/3	brown								
W9771		10YR 4/3	brown								

W9772		10YR 4/2	dark grayish brown							
W9813		10YR 4/3	brown							
W9814		10YR 4/3	brown							
W9815		10YR 4/3	brown							
W9816		10YR 4/2	dark grayish brown							
W9817		2.5Y 4/2	dark grayish brown							
W9818		2.5Y 4/2	dark grayish brown							
W9819		2.5Y 4/2	dark grayish brown							
W9820		10YR 4/2	dark grayish brown							
W9821		10YR 4/2	dark grayish brown							
W9822		-	-							
W9823		10YR 4/2	dark grayish brown							
W9824		10YR 4/2	dark grayish brown							
W9825		10YR 4/2	dark grayish brown							
W9826		10YR 4/2	dark grayish brown							
W9827		10YR 4/2	dark grayish brown							
W9828		2.5Y 3/2	brown							
W9829		10YR 2/2	very dark brown							
W9830		5Y 3/2	dark olive gray							
W9831		5Y 4/1	dark gray							
W9832		5Y 4/1	dark gray							
W9842		2.5Y 4/4	olive brown							
W9843		10YR 4/2	dark grayish brown							
W9844		10YR 4/2	dark grayish brown							
W9845		10YR 4/2	dark grayish brown							
W9846		10YR 4/2	dark grayish brown							
W9847		10YR 4/2	dark grayish brown							
[1] Texture is described from smallest concentration to largest concentration; significant only if >15%.										

Appendix C – Till-matrix geochemistry data

All till-matrix geochemistry data used in this thesis can be found as a data repository item on the Manitoba Geological Survey website. Samples from 2023 can be found in DRI2024002 (found on https://gov.mb.ca/iem/info/libmin/2024pubs.html, last accessed 2025-04-09), and samples from 2022 can be found in DRI2023008 (found on https://gov.mb.ca/iem/info/libmin/2023pubs.html, last accessed 2025-06-03).

Appendix D – Till-matrix geochemistry data: Quality assurance and quality control

Ca/Mg method

Lab repeats: Precision biplots

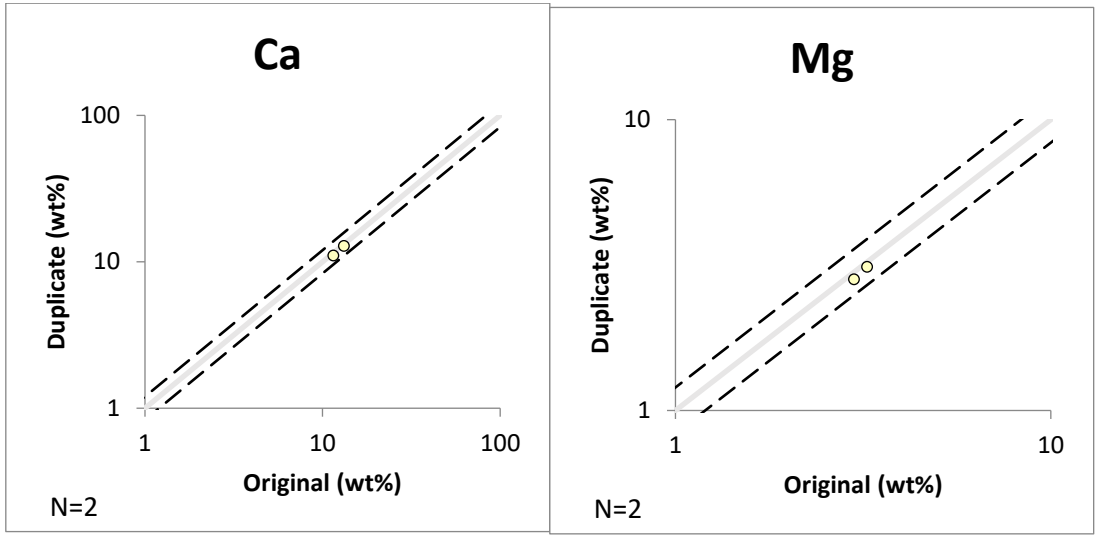


Figure 1: Precision biplots for lab duplicates of till-matrix (<63 µm size-fraction) geochemistry of total carbonate content by Ca/Mg method. Control lines (dashed black) are set at a 20% level of precision above or below the 1:1 line (grey).

Reference materials: %RSD

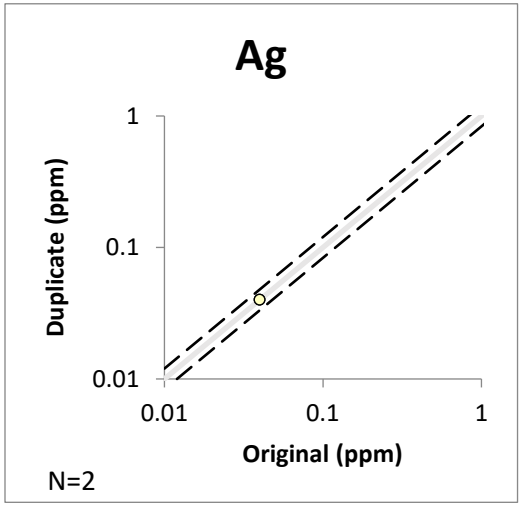
Table 1: %RSD for till-matrix (<63 µm size-fraction) geochemistry of total carbonate content by Ca/Mg method.

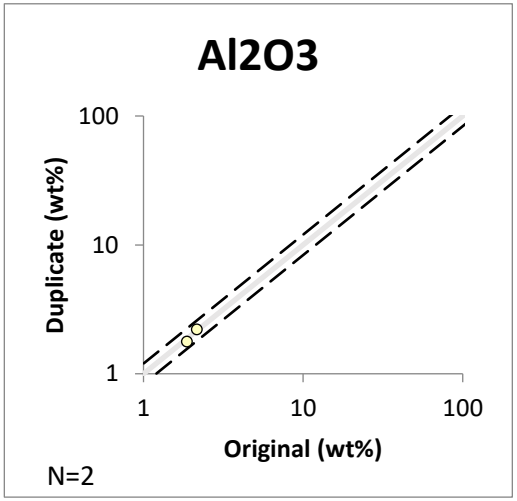
Sample ID	Ca (wt%)	Mg (wt%)
115-23-002-B04	0.42	0.32
115-23-005-A01	0.42	0.32
115-23-007-A02	0.40	0.30
115-23-009-A02	0.43	0.32
%RSD	**3.01**	**3.17**

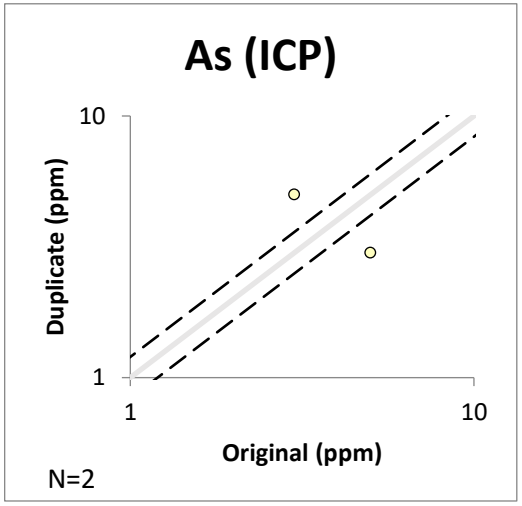
%RSD = measure of precision (0-3%, excellent; 3-7% is very good to good; 7-10% is good; >10% not precise) [Piercey, 2014]

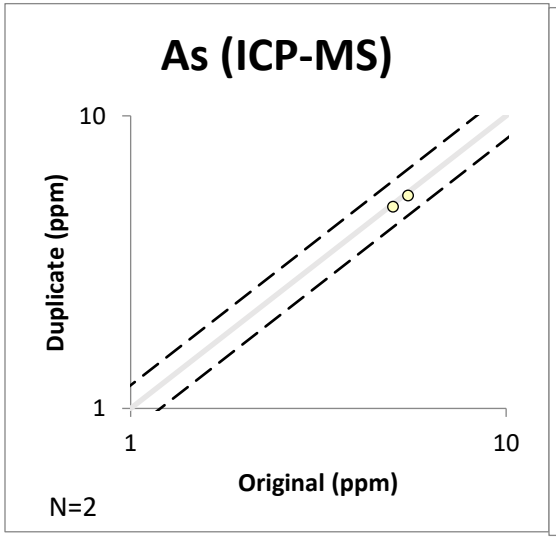
Partial digestion

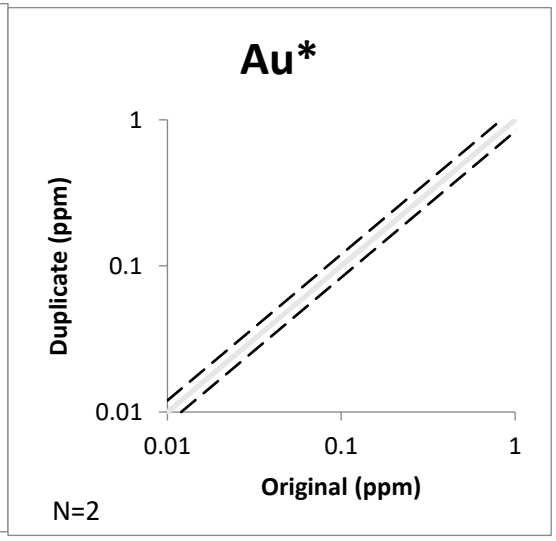
Lab repeats: Precision biplots

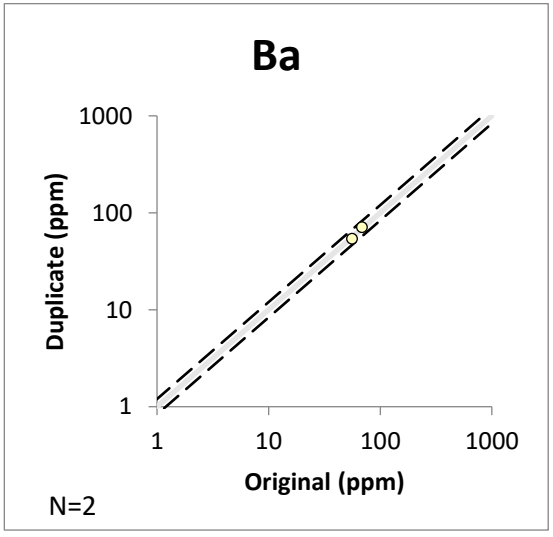


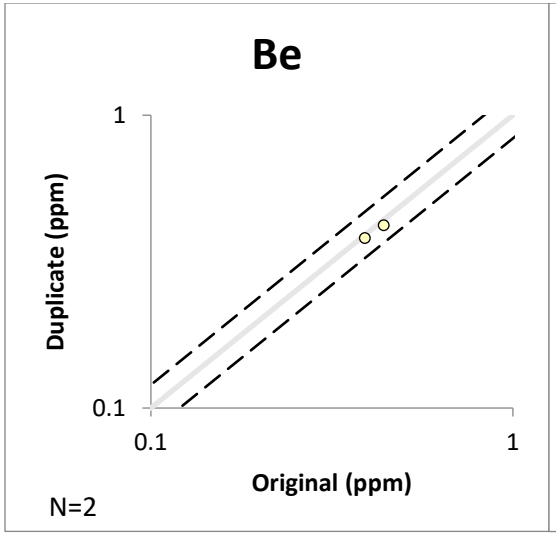


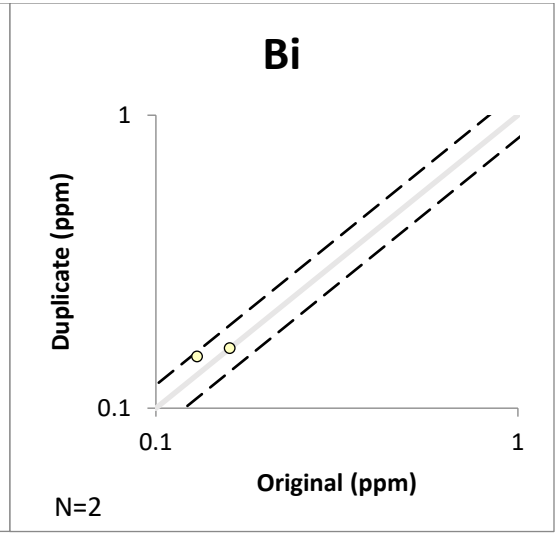


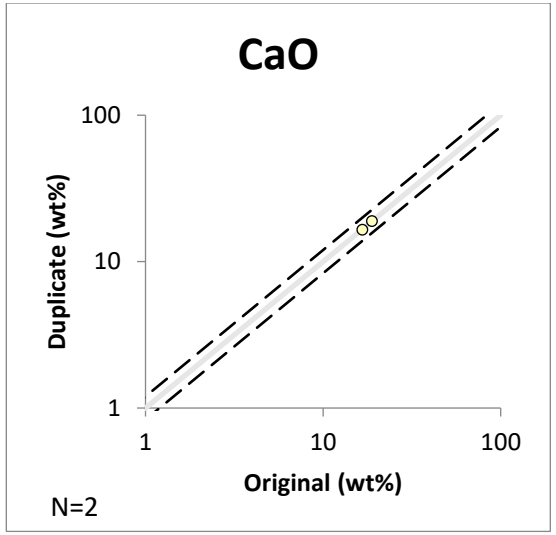


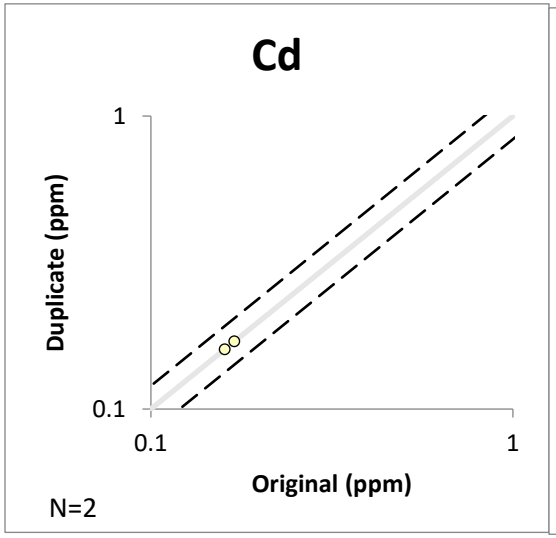


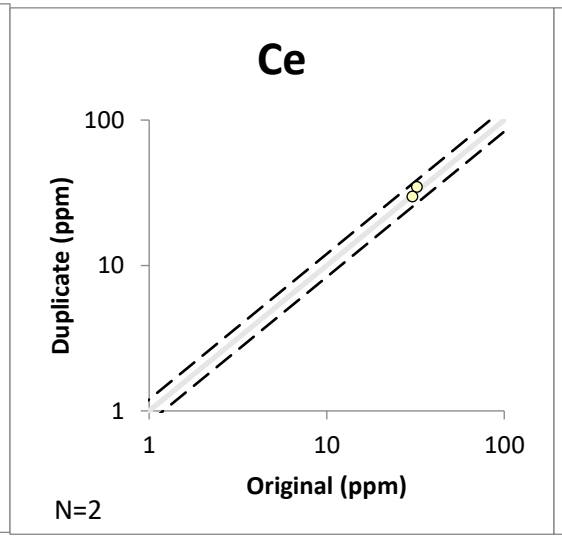


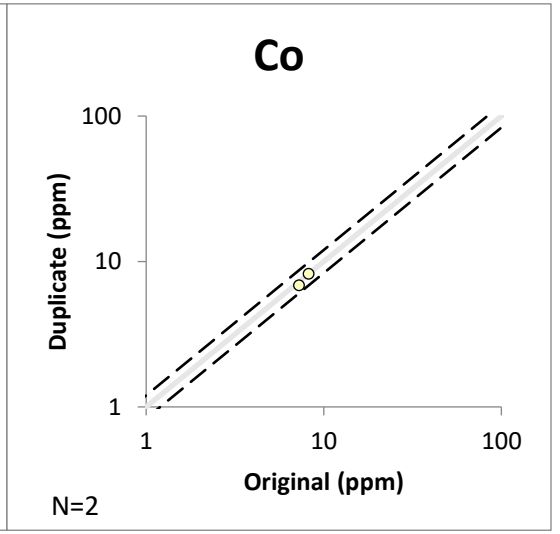

Be
Duplicate (ppm)
1
0.1
0.1
1
Original (ppm)
N=2

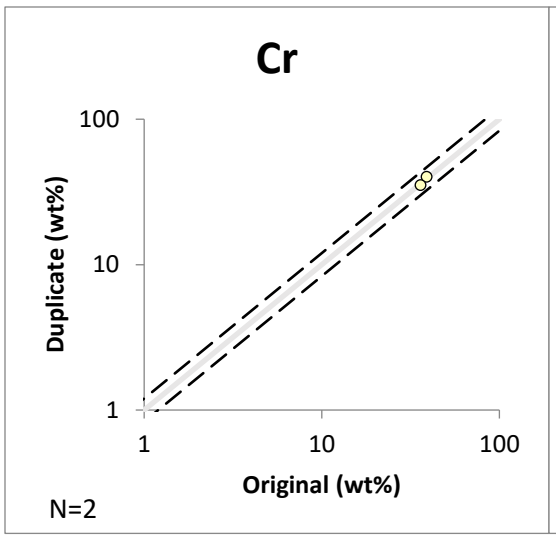

Bi
Duplicate (ppm)
1
0.1
0.1
1
Original (ppm)
N=2

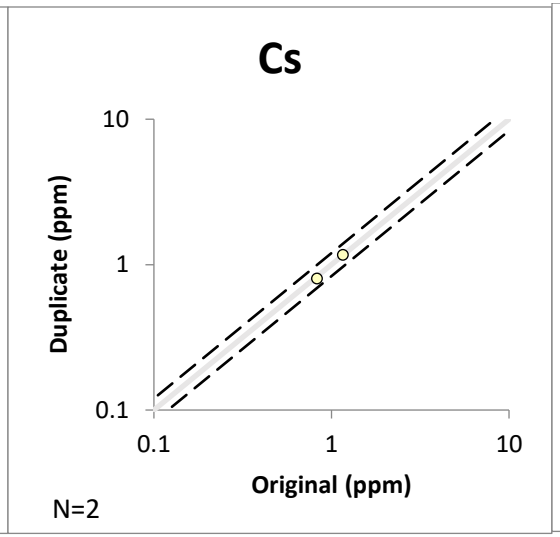

CaO
Duplicate (wt%)
100
10
1
1
10
100
Original (wt%)
N=2

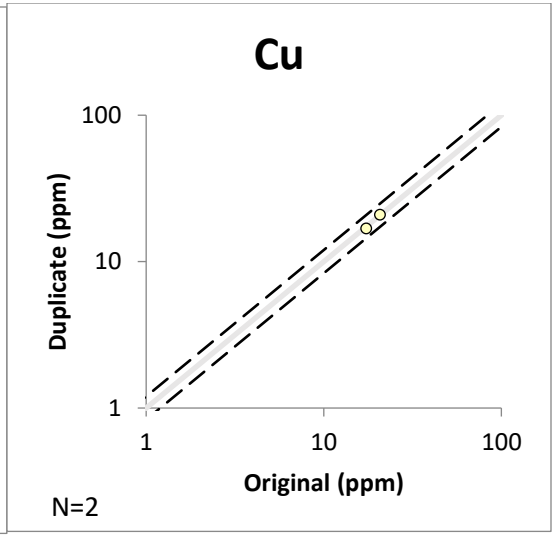

Cd
Duplicate (ppm)
1
0.1
0.1
1
Original (ppm)
N=2

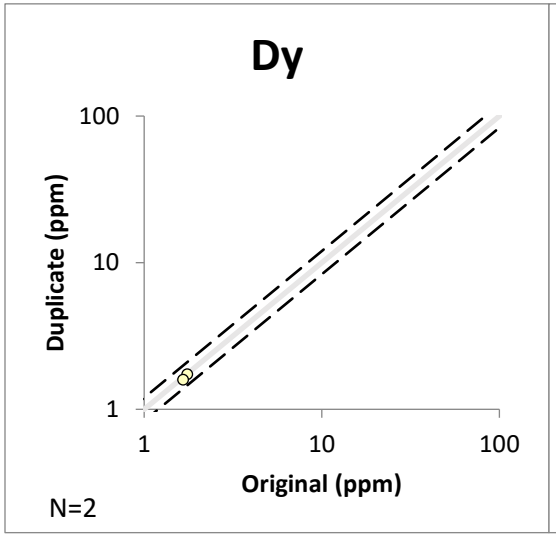

Ce
Duplicate (ppm)
100
10
1
1
10
100
Original (ppm)
N=2

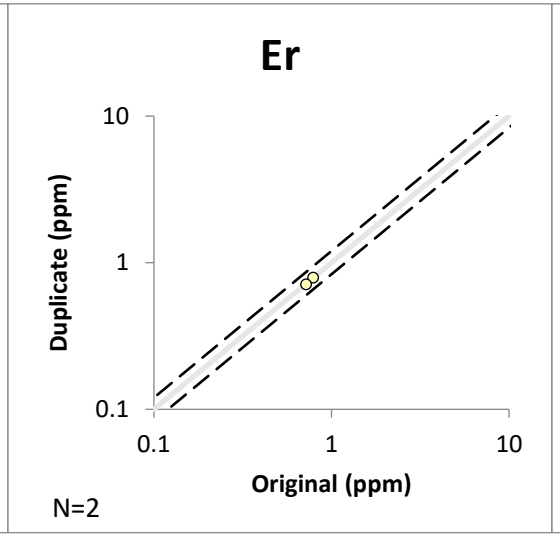

Co
Duplicate (ppm)
100
10
1
1
10
100
Original (ppm)
N=2

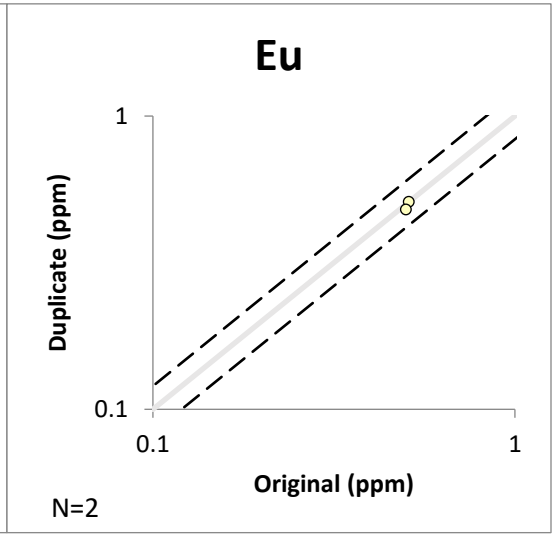

Cr
100
10
1
Duplicate (wt%)
1
10
100
Original (wt%)
N=2

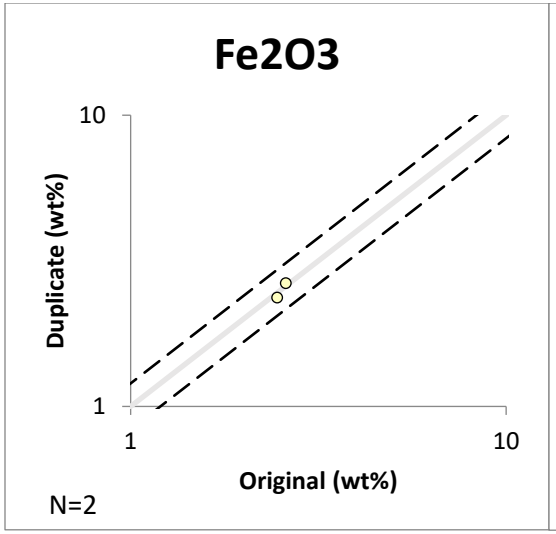

Cs
10
1
0.1
Duplicate (ppm)
0.1
1
10
Original (ppm)
N=2

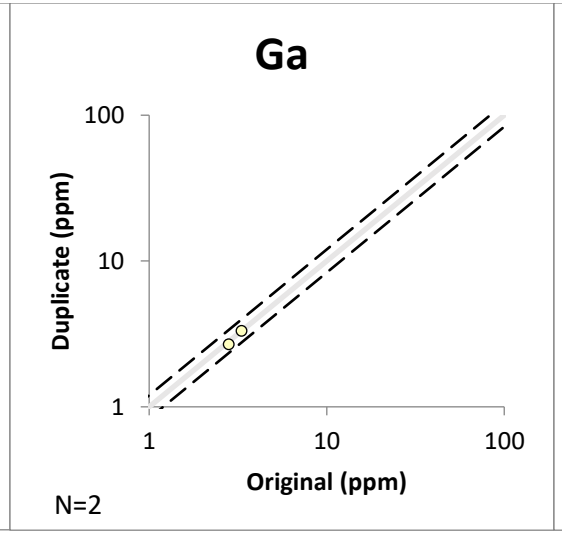

Cu
100
10
1
Duplicate (ppm)
1
10
100
Original (ppm)
N=2

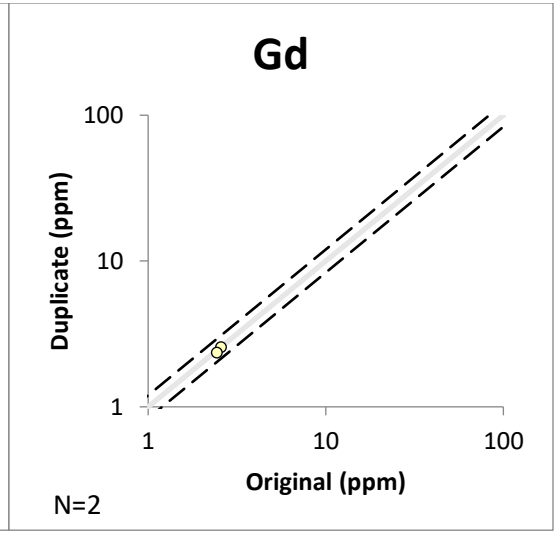

Dy
100
10
1
Duplicate (ppm)
1
10
100
Original (ppm)
N=2

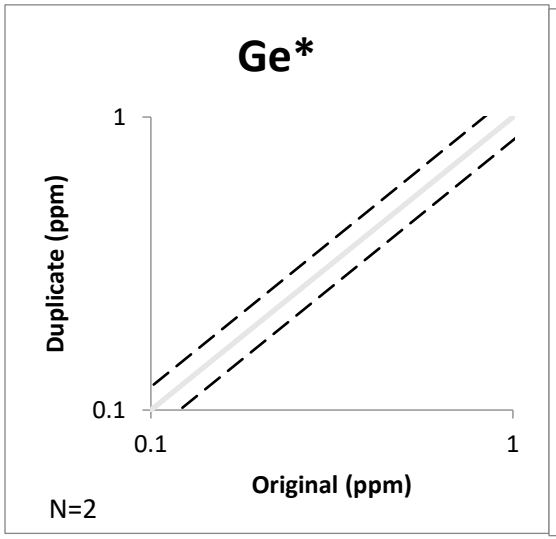

Er
10
1
0.1
Duplicate (ppm)
0.1
1
10
Original (ppm)
N=2

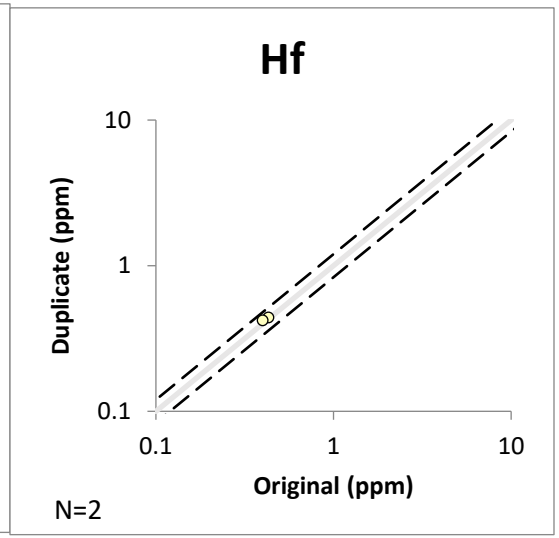

Eu
1
0.1
Duplicate (ppm)
0.1
1
Original (ppm)
N=2

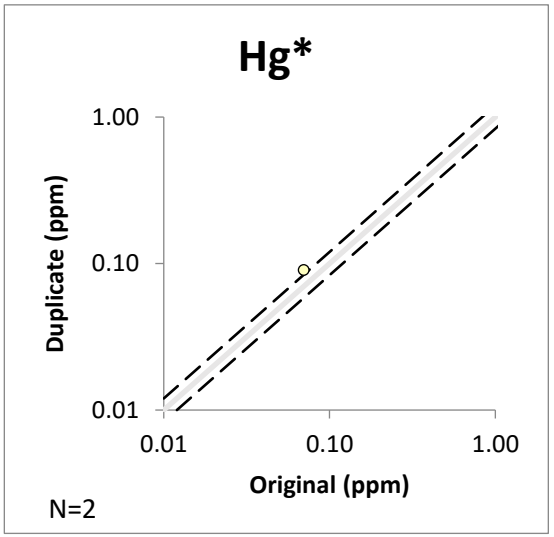

Fe2O3
10
1
Duplicate (wt%)
1
10
Original (wt%)
N=2

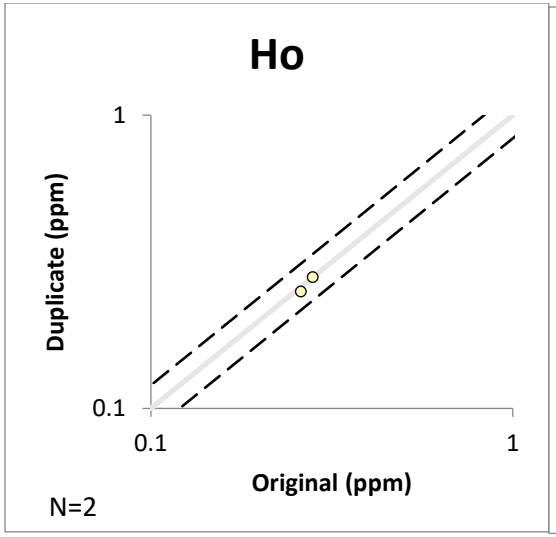

Ga
100
10
1
Duplicate (ppm)
1
10
100
Original (ppm)
N=2

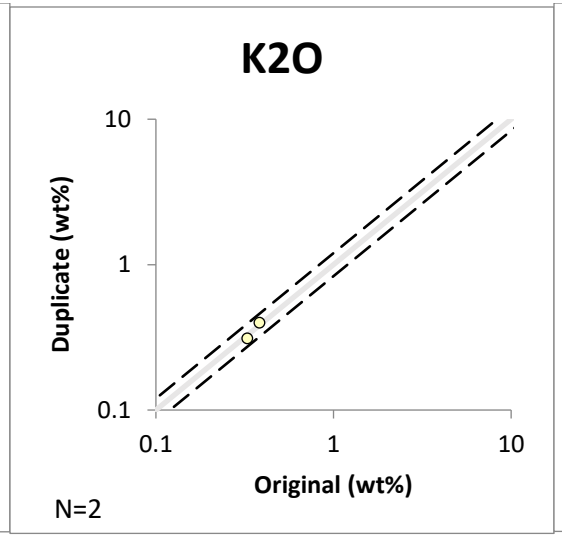

Gd
100
10
1
Duplicate (ppm)
1
10
100
Original (ppm)
N=2

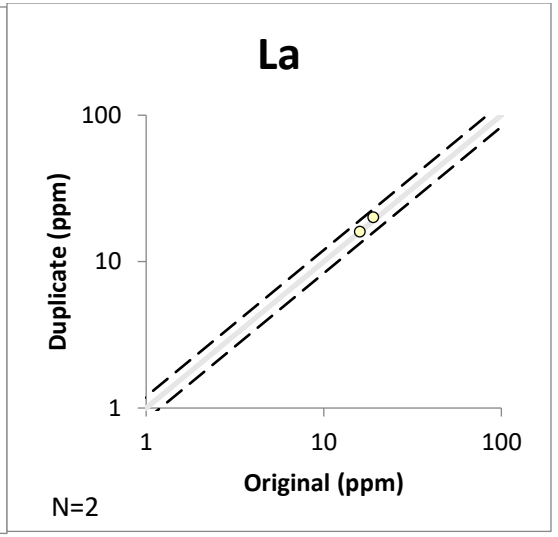

Ge*
1
0.1
Duplicate (ppm)
0.1
1
Original (ppm)
N=2

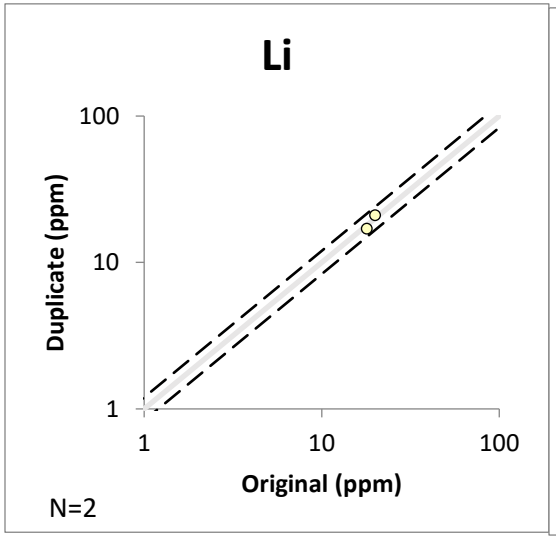

Hf
10
1
0.1
Duplicate (ppm)
0.1
1
10
Original (ppm)
N=2

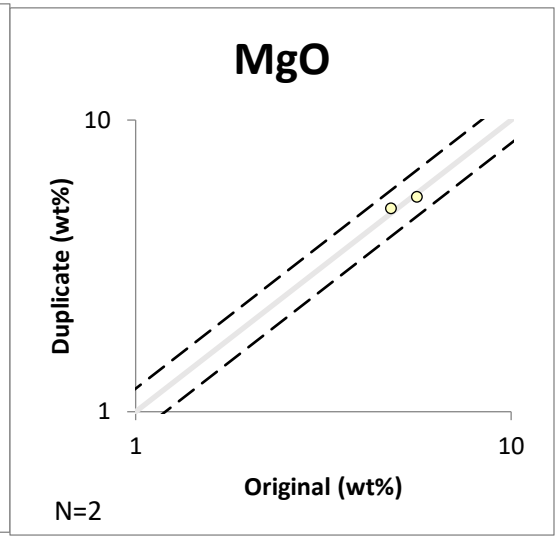

Hg*
1.00
0.10
0.01
Duplicate (ppm)
0.01
0.10
1.00
Original (ppm)
N=2

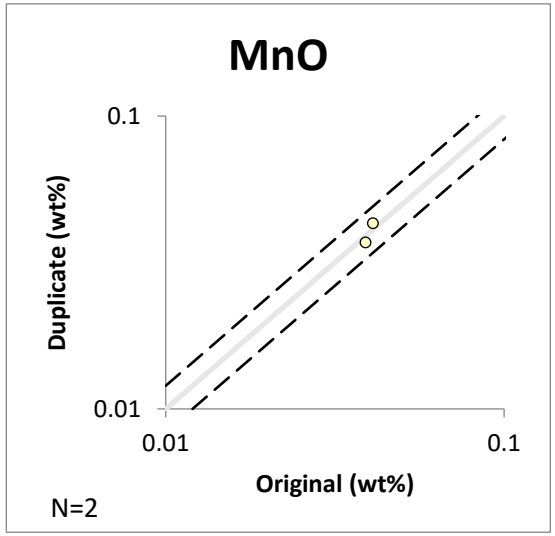

Ho
Duplicate (ppm)
1
0.1
0.1
1
Original (ppm)
N=2

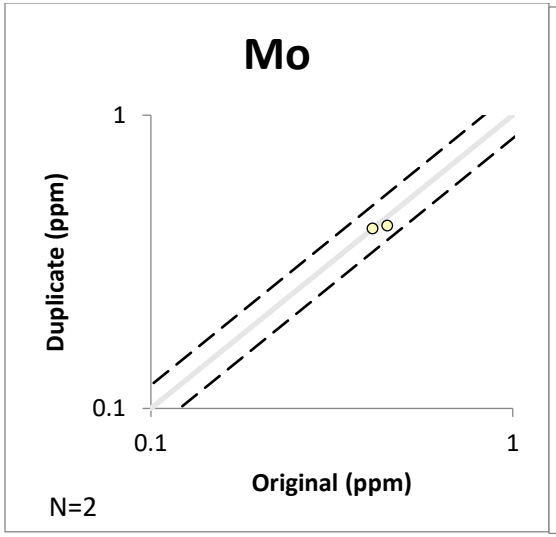

K2O
Duplicate (wt%)
10
1
0.1
0.1
1
10
Original (wt%)
N=2

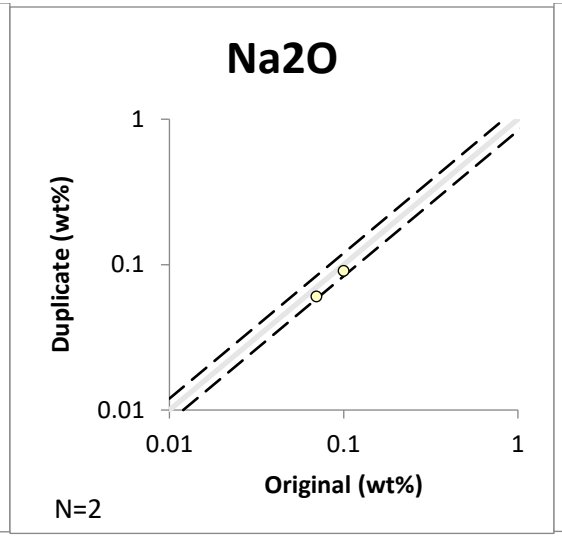

La
Duplicate (ppm)
100
10
1
1
10
100
Original (ppm)
N=2

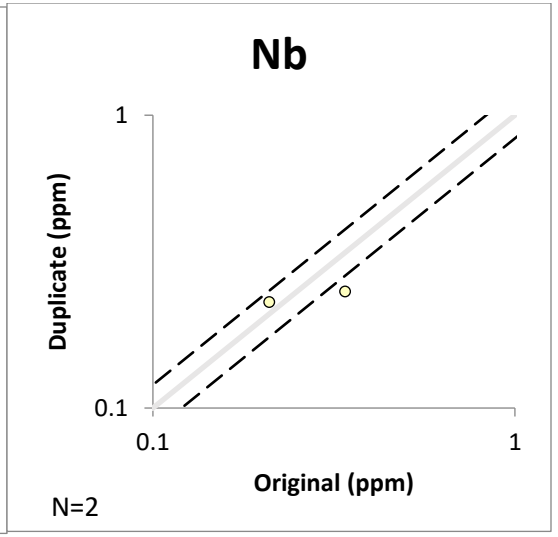

Li
Duplicate (ppm)
100
10
1
1
10
100
Original (ppm)
N=2

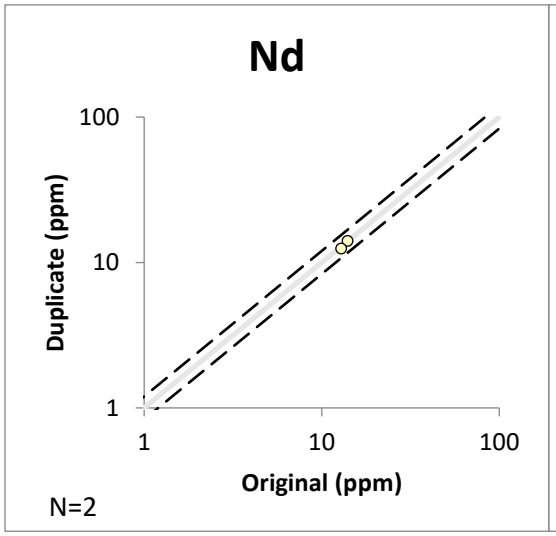

MgO
Duplicate (wt%)
10
1
1
10
Original (wt%)
N=2

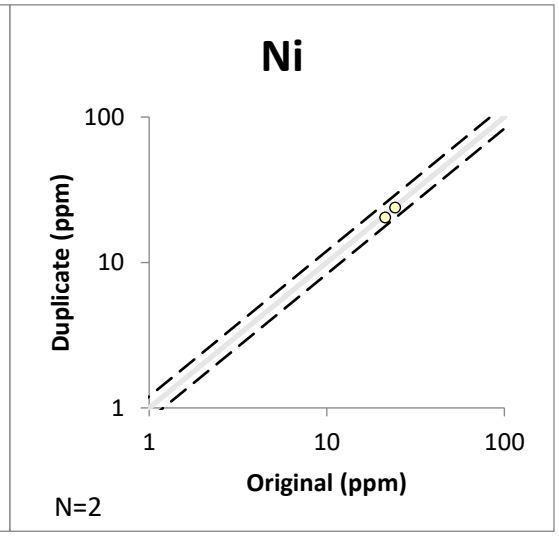

MnO
Duplicate (wt%)
0.1
0.01
0.01
0.1
Original (wt%)
N=2

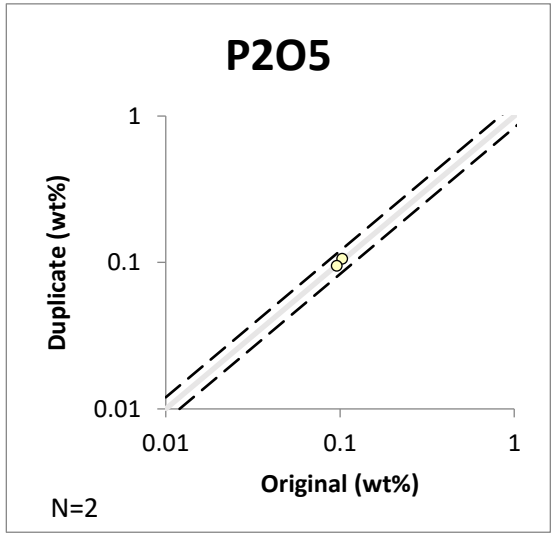

Mo
Duplicate (ppm)
1
0.1
0.1
1
Original (ppm)
N=2

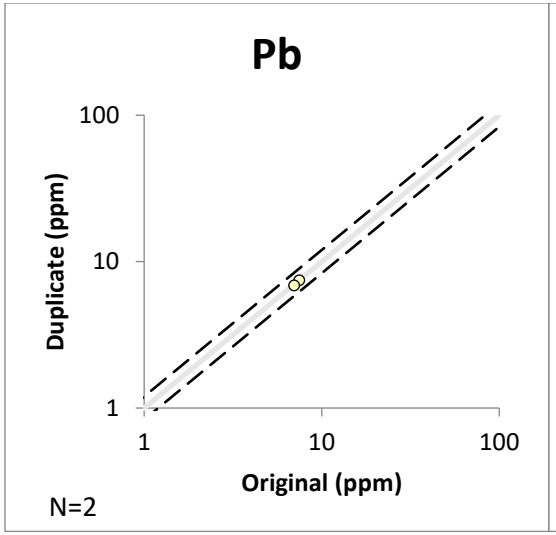

Na2O
Duplicate (wt%)
1
0.1
0.01
0.01
0.1
1
Original (wt%)
N=2

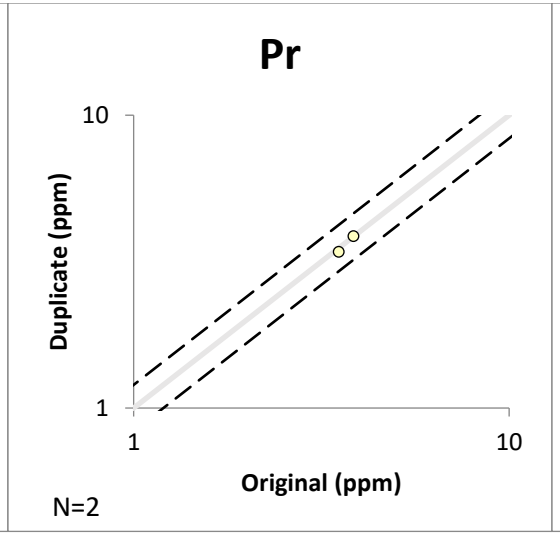

Nb
Duplicate (ppm)
1
0.1
0.1
1
Original (ppm)
N=2

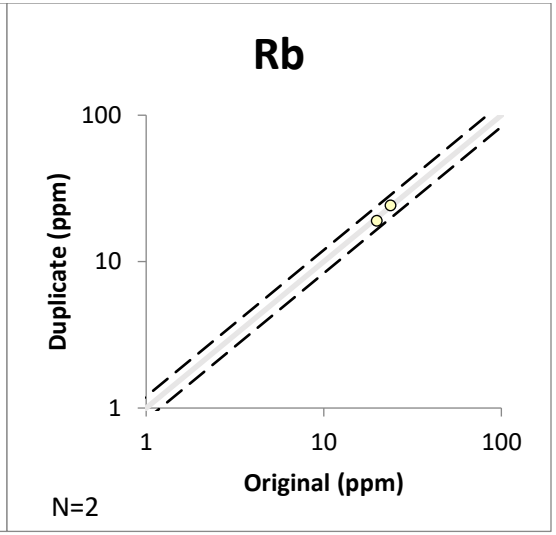

Nd
Duplicate (ppm)
100
10
1
1
10
100
Original (ppm)
N=2

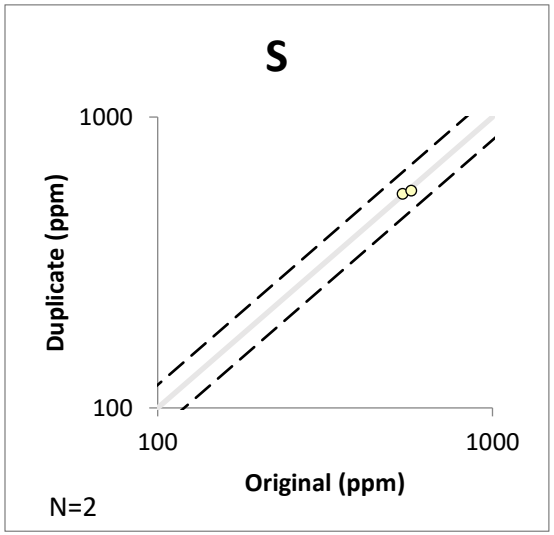

Ni
Duplicate (ppm)
100
10
1
1
10
100
Original (ppm)
N=2

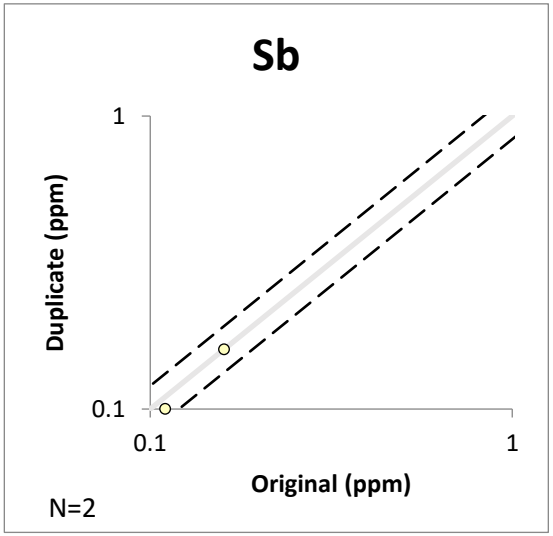

P2O5
Duplicate (wt%)
1
0.1
0.01
0.01
0.1
1
Original (wt%)
N=2

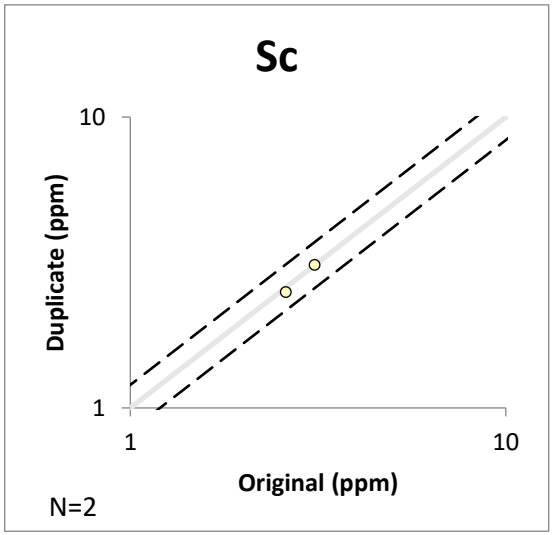

Pb
100
10
1
Duplicate (ppm)
1
10
100
Original (ppm)
N=2

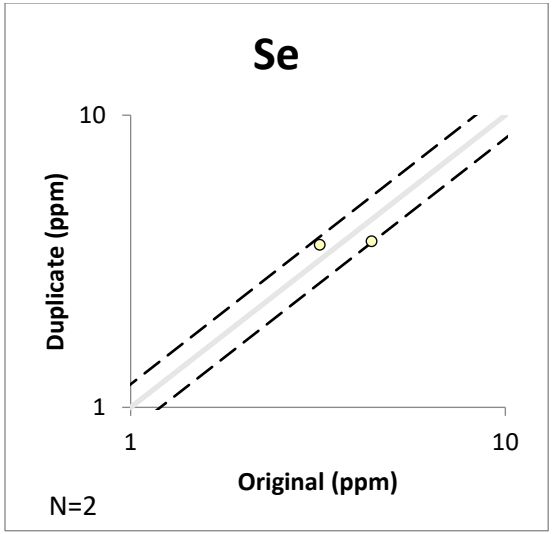

Pr
10
1
Duplicate (ppm)
1
10
Original (ppm)
N=2

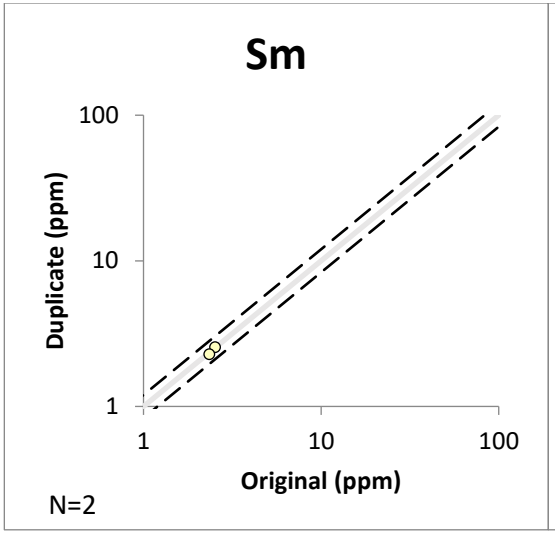

Rb
100
10
1
Duplicate (ppm)
1
10
100
Original (ppm)
N=2

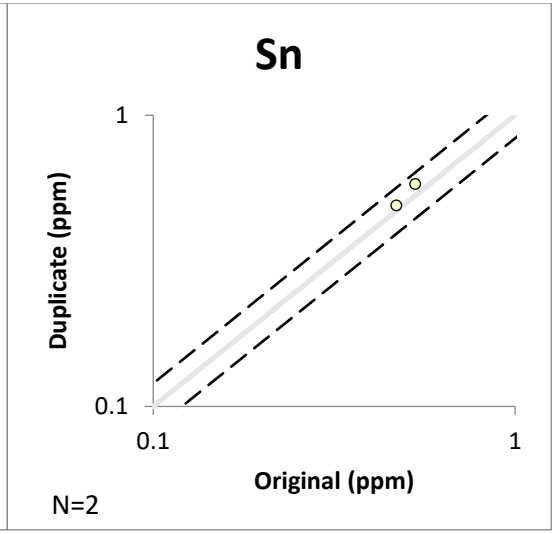

S
1000
100
Duplicate (ppm)
100
1000
Original (ppm)
N=2

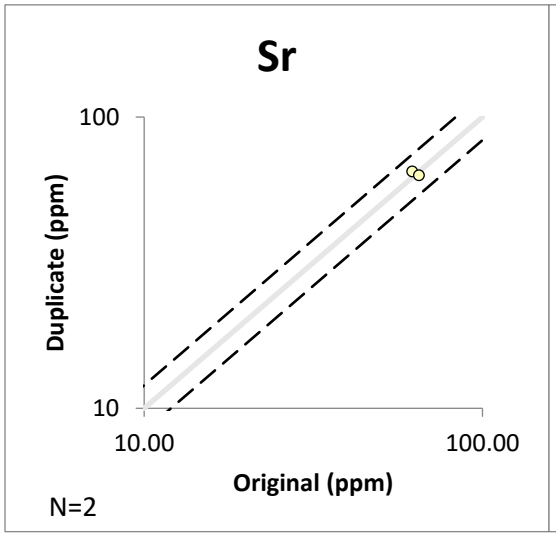

Sb
1
0.1
Duplicate (ppm)
0.1
1
Original (ppm)
N=2

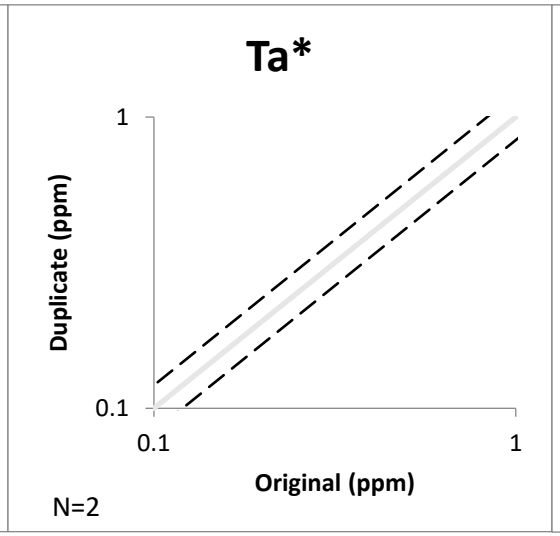

Sc
10
1
Duplicate (ppm)
1
10
Original (ppm)
N=2

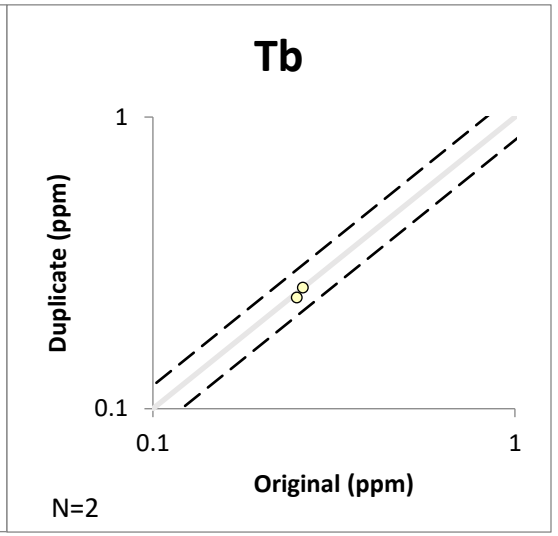

Se
10
1
Duplicate (ppm)
1
10
Original (ppm)
N=2

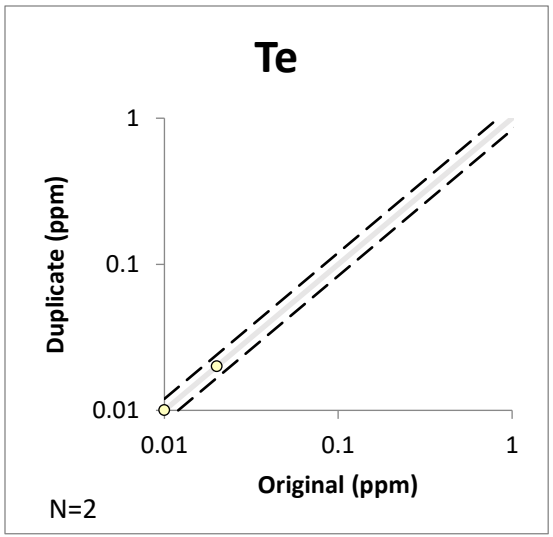

Sm
100
10
1
Duplicate (ppm)
1
10
100
Original (ppm)
N=2

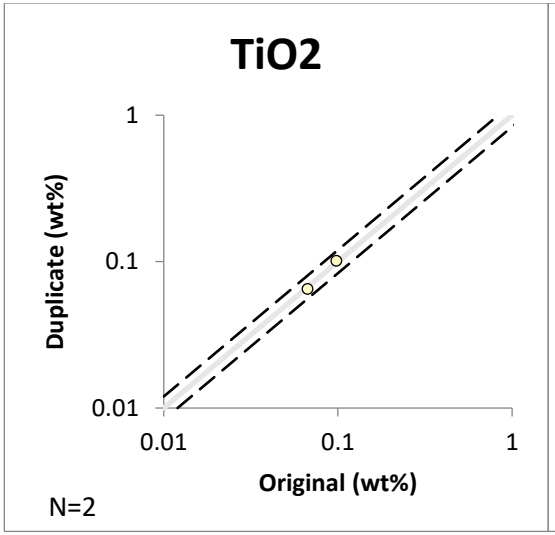

Sn
1
0.1
Duplicate (ppm)
0.1
1
Original (ppm)
N=2

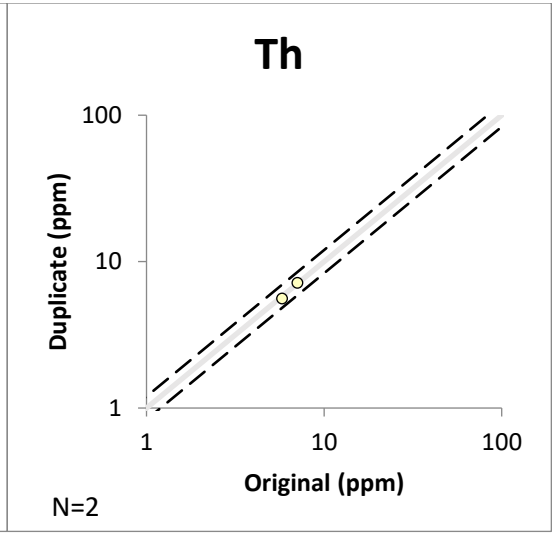

Sr
100
10
Duplicate (ppm)
10.00
100.00
Original (ppm)
N=2

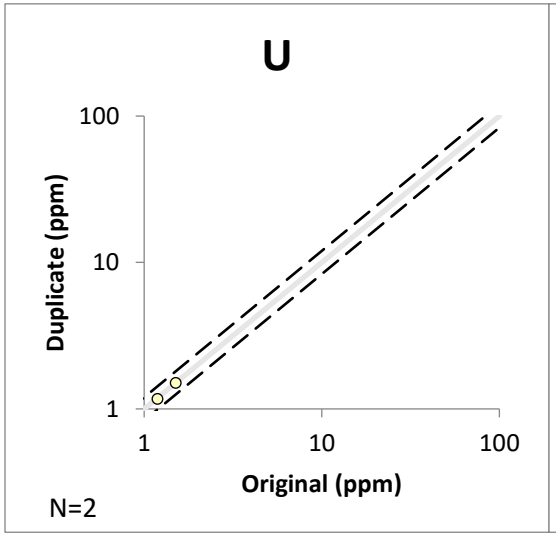

Ta*
1
0.1
Duplicate (ppm)
0.1
1
Original (ppm)
N=2

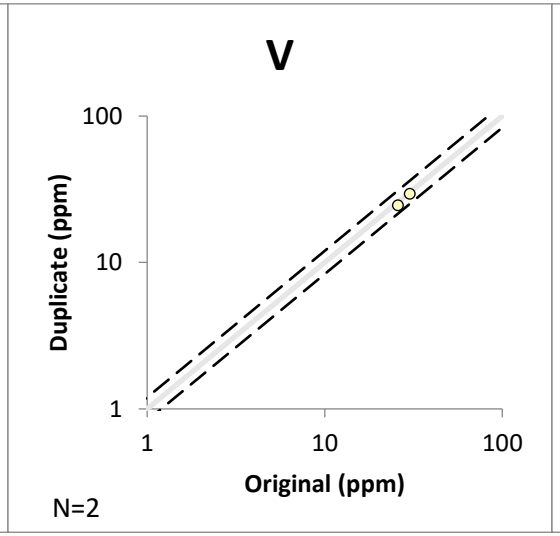

Tb
1
0.1
Duplicate (ppm)
0.1
1
Original (ppm)
N=2

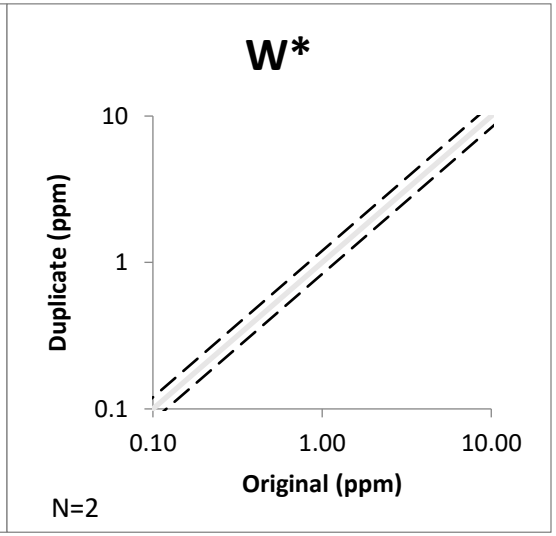

Te
Duplicate (ppm)
1
0.1
0.01
0.01
0.1
1
Original (ppm)
N=2


TiO2
Duplicate (wt%)
1
0.1
0.01
0.01
0.1
1
Original (wt%)
N=2


Th
Duplicate (ppm)
100
10
1
1
10
100
Original (ppm)
N=2


U
Duplicate (ppm)
100
10
1
1
10
100
Original (ppm)
N=2


V
Duplicate (ppm)
100
10
1
1
10
100
Original (ppm)
N=2


W*
Duplicate (ppm)
10
1
0.1
0.10
1.00
10.00
Original (ppm)
N=2

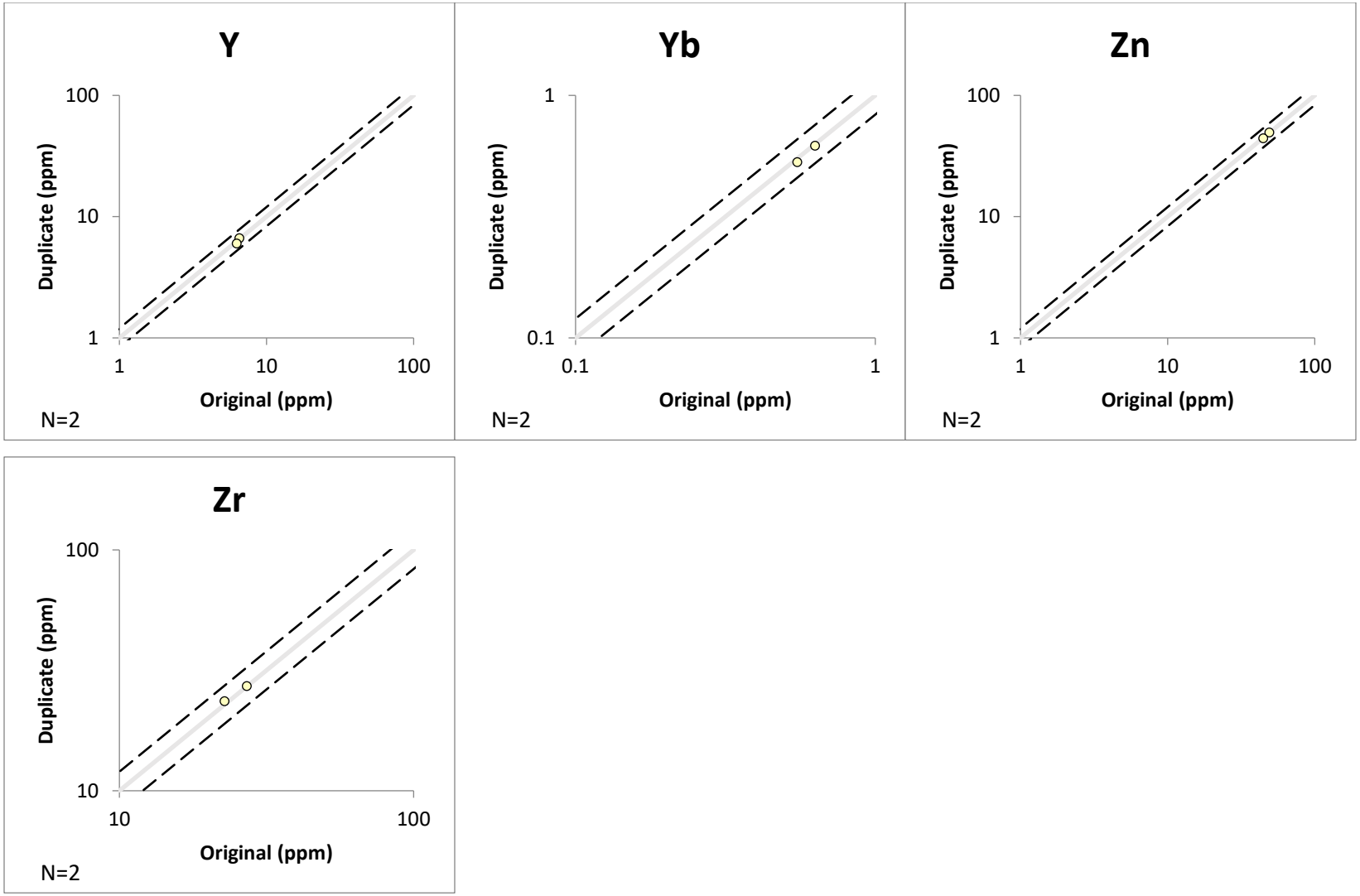


Figure 2: Precision biplots for lab duplicates of till-matrix (<63 µm size-fraction) geochemistry by partial digestion and ICP-MS and ICP analysis. Control lines (dashed black) are set at a 20% level of precision above or below the 1:1 line (grey). * = Data has one or more value below detection limit.

Reference materials: %RSD and %RD

Table 2: %RSD and %RD for till-matrix (<63 μm size-fraction) geochemistry by partial digestion and ICP-MS and ICP analysis.

Sample ID	Ag (ppm)	Al_2O_3 (wt%)	As (ppm, ICP)	As (ppm, ICP-MS)	Au (ppm)	Ba (ppm)	Be (ppm)	Bi (ppm)	CaO (wt%)	Cd (ppm)
MGS standard - OREAS 46	0.03	0.75	1	-	0.001	55	0.17	0.03	0.60	0.04
115-23-002-B04	0.02	1.33	1	2.34	<0.01	49	0.13	0.04	0.92	0.1
115-23-005-A01	0.02	1.35	<1	2.28	<0.01	49	0.14	0.04	0.88	0.08
115-23-007-A02	0.02	1.03	1	2.38	<0.01	37	0.12	0.04	0.68	0.08
115-23-009-A02	0.02	1.40	<1	2.28	<0.01	47	0.12	0.04	0.92	0.06
%RSD	**0.00**	**13.12**	**-**	**2.11**	**-**	**12.63**	**7.51**	**0.00**	**13.52**	**20.41**
%RD	**-20.00**	**70.79**	**-**	**-**	**-**	**-17.27**	**-25.00**	**42.86**	**41.67**	**122.22**

Ce (ppm)	Co (ppm)	Cr (ppm)	Cs (ppm)	Cu (ppm)	Dy (ppm)	Er (ppm)	Eu (ppm)	Fe_2O_3 (wt%)	Ga (ppm)	Gd (ppm)	Ge (ppm)	Hf (ppm)	Hg (ppm)
27.3	5.83	25	0.36	23.4	-	-	-	1.45	2.99	1.64	0.061	-	-
21.1	4.75	26	0.28	24.7	0.9	0.42	0.34	2.09	1.75	1.39	<0.01	0.14	0.1
23.3	4.68	26	0.28	24	0.88	0.41	0.33	2.10	1.74	1.35	<0.01	0.14	0.08
17.7	4.63	20	0.28	24.1	0.91	0.43	0.34	1.58	1.8	1.42	<0.01	0.13	<0.01
22.8	4.55	27	0.28	23.6	0.94	0.45	0.35	2.08	1.84	1.45	<0.01	0.15	<0.01
11.93	**1.81**	**12.94**	**0.00**	**1.89**	**2.75**	**3.99**	**2.40**	**13.00**	**2.61**	**3.05**	**-**	**5.83**	**-**
-22.25	**-20.20**	**-1.00**	**-22.22**	**2.99**	**-**	**-**	**-**	**35.34**	**-40.38**	**-14.48**	**-**	**-**	**-**

Ho (ppm)	K_2O (wt%)	La (ppm)	Li (ppm)	MgO (wt%)	MnO (wt%)	Mo (ppm)	Na_2O (wt%)	Nb (ppm)	Nd (ppm)	Ni (ppm)	P_2O_5 (wt%)	Pb (ppm)	Pr (ppm)
0.2	0.109	16	7	0.46	0.025	0.66	0.08	-	13.20	16.3	0.053	2.02	3.75
0.14	0.123	12	6	0.82	0.033	0.67	0.09	0.16	8	15.7	0.144	2.09	2.16
0.14	0.124	13	6	0.82	0.033	0.66	0.10	0.14	7.86	15.1	0.142	1.98	2.16
0.15	0.093	10	4	0.62	0.025	0.69	0.07	0.16	8.13	15.4	0.109	1.95	2.25
0.15	0.124	13	6	0.84	0.033	0.68	0.10	0.2	8.24	15	0.139	1.94	2.24
3.98	**13.22**	**11.79**	**18.18**	**13.33**	**12.90**	**1.91**	**15.71**	**15.25**	**2.04**	**2.07**	**12.33**	**3.46**	**2.24**
-27.50	**6.42**	**-22.58**	**-18.88**	**68.95**	**24.00**	**2.27**	**16.88**	**-**	**-38.96**	**-6.13**	**151.89**	**-1.49**	**-41.27**

Rb (ppm)	S (ppm)	Sb (ppm)	Sc (ppm)	Se (ppm)	Sm (ppm)	Sn (ppm)	Sr (ppm)	Ta (ppm)	Tb (ppm)	Te (ppm)	Th (ppm)	TiO_2 (wt%)	U (ppm)
6.11	<50	0.07	2.8	<0.20	2.11	0.4	27	-	0.20	-	2.87	0.065	0.43
5.46	51	0.08	1.8	<0.1	1.37	0.33	19	<0.01	0.13	<0.01	1.96	0.102	0.41
5.35	52	0.08	1.7	0.6	1.34	0.33	19	<0.01	0.13	0.01	2.02	0.103	0.44
5.68	40	0.08	1.7	0.1	1.39	0.33	15	<0.01	0.14	<0.01	1.99	0.079	0.4
5.68	53	0.08	1.7	0.8	1.43	0.33	21	<0.01	0.14	<0.01	1.96	0.114	0.4
2.98	**12.36**	**0.00**	**2.90**	**-**	**2.73**	**0.00**	**13.60**	**-**	**4.28**	**-**	**1.45**	**14.78**	**4.59**
-9.29	**-**	**17.65**	**-37.95**	**-**	**-34.48**	**-17.50**	**-31.23**	**-**	**-32.50**	**-**	**-30.92**	**53.08**	**-4.07**

V (ppm)	W (ppm)	Y (ppm)	Yb (ppm)	Zn (ppm)	Zr (ppm)
22.1	0.073	5.06	0.48	20.7	5.66
17.2	<0.1	3.54	0.34	24.7	6.56
16.9	<0.1	3.6	0.34	24.2	6.89
16.6	<0.1	3.7	0.34	24.1	6.67
16.4	<0.1	3.9	0.36	24.3	7.19
2.09	**-**	**4.28**	**2.90**	**1.08**	**4.07**
-24.10	**-**	**-27.17**	**-28.13**	**17.51**	**20.63**

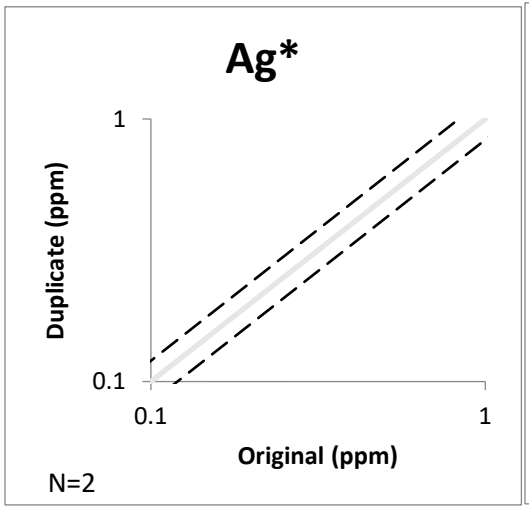
%RSD = measure of precision (0-3%, excellent; 3-7% is very good to good; 7-10% is good; >10% not precise) [Piercey, 2014]

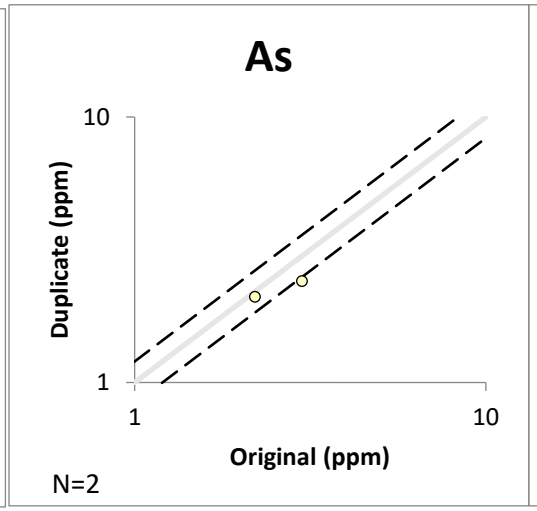
%RD = measure of accuracy (±0-3, excellent; ±3-7% very good; ±7-10% good; >±10% not accurate) [Piercey, 2014]

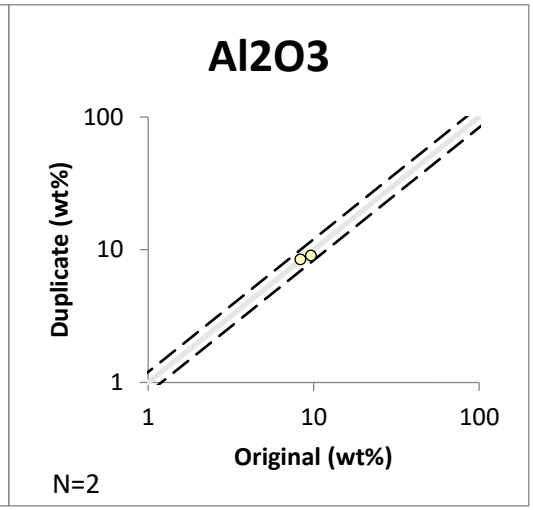
-: Not applicable

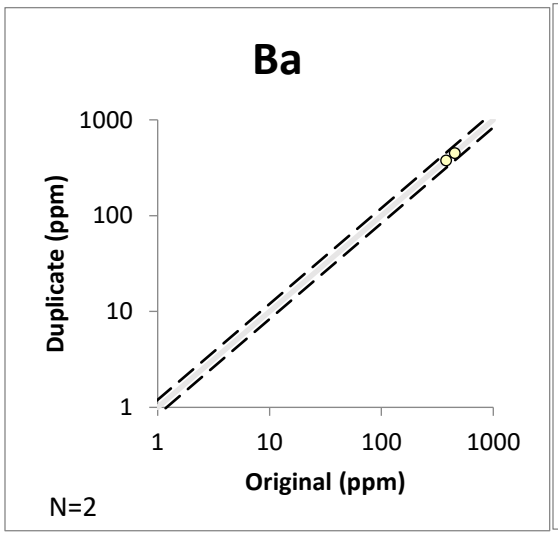
Fusion digestion

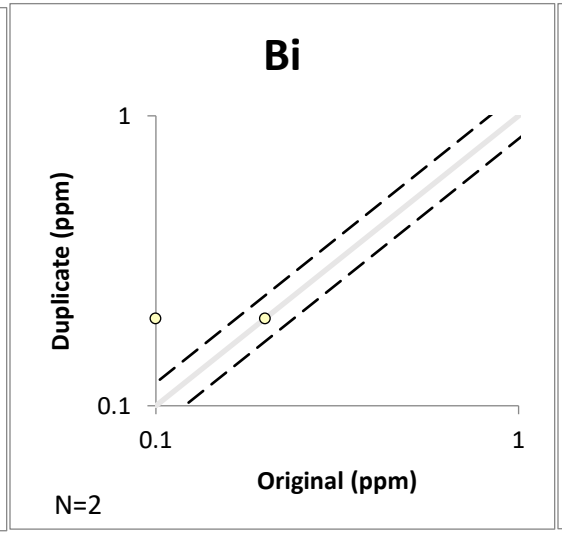
Lab repeats: Precision biplots

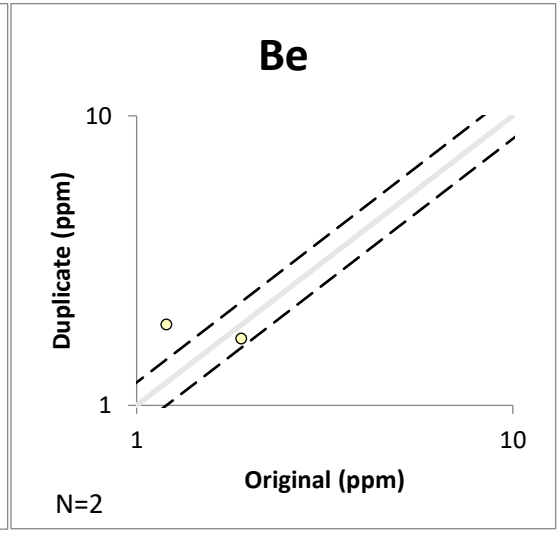


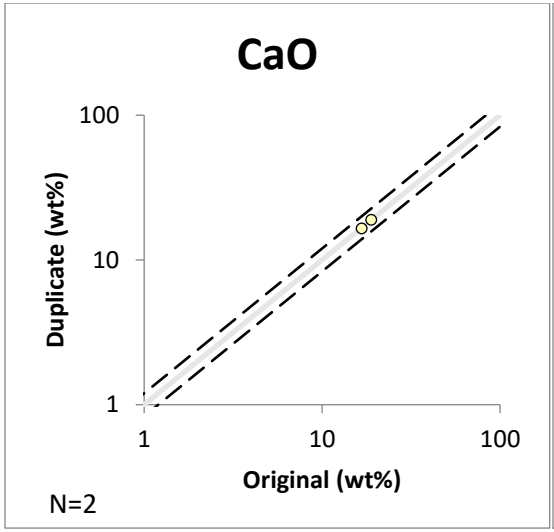


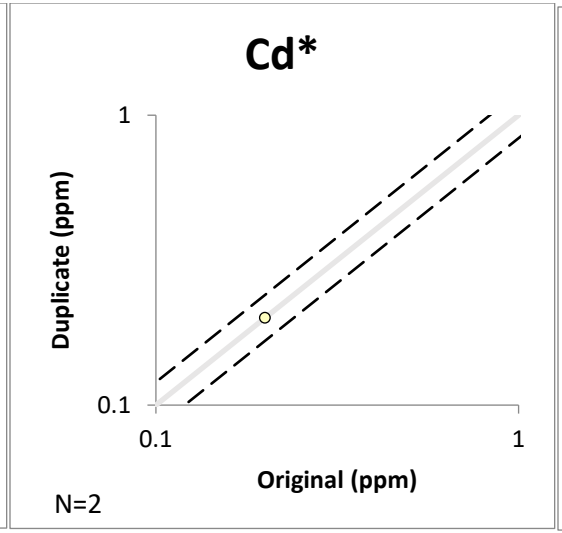


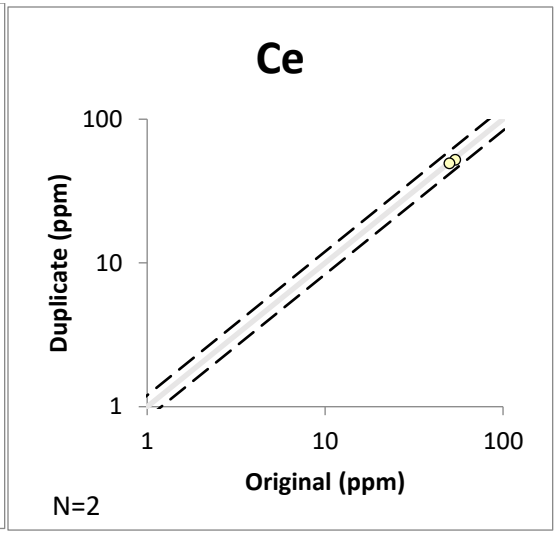


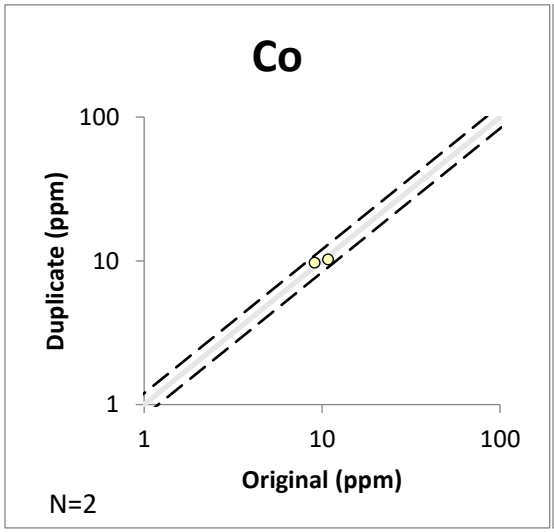


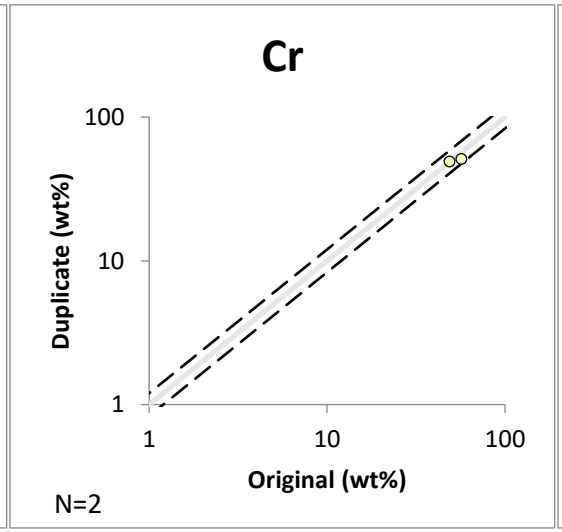


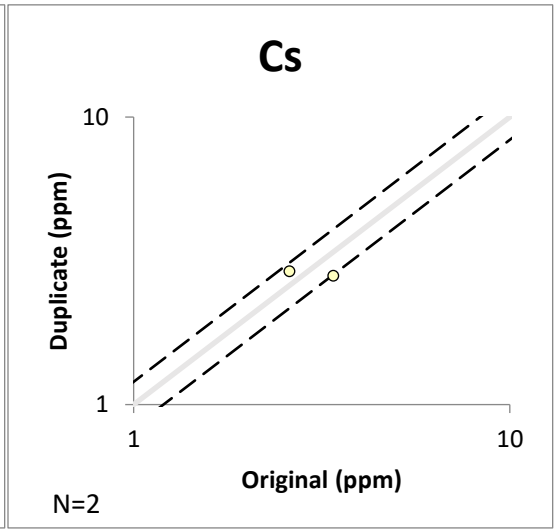

CaO
100
10
1
Duplicate (wt%)
1
10
100
Original (wt%)
N=2

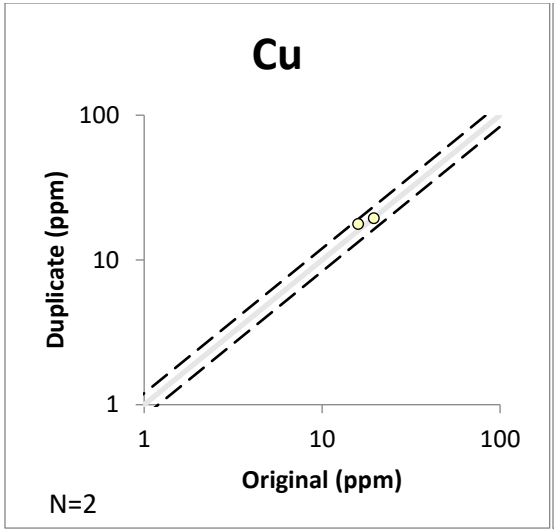

Cd*
1
0.1
Duplicate (ppm)
0.1
1
Original (ppm)
N=2

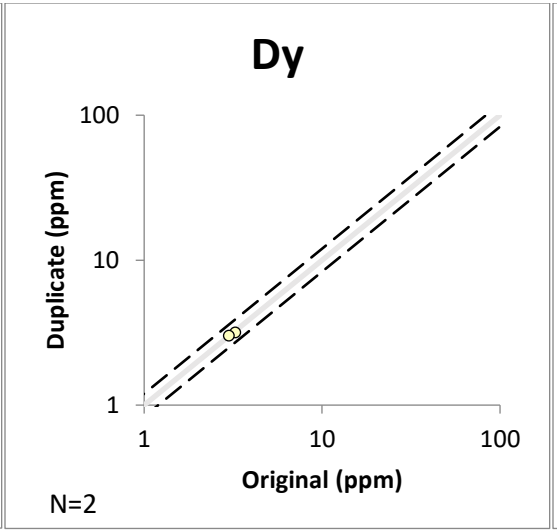

Ce
100
10
1
Duplicate (ppm)
1
10
100
Original (ppm)
N=2

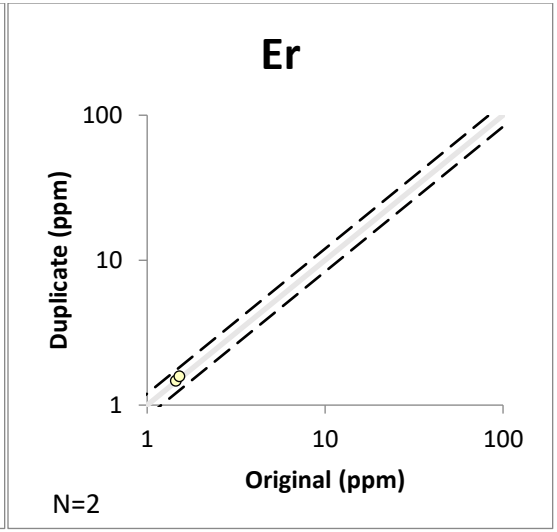

Co
100
10
1
Duplicate (ppm)
1
10
100
Original (ppm)
N=2

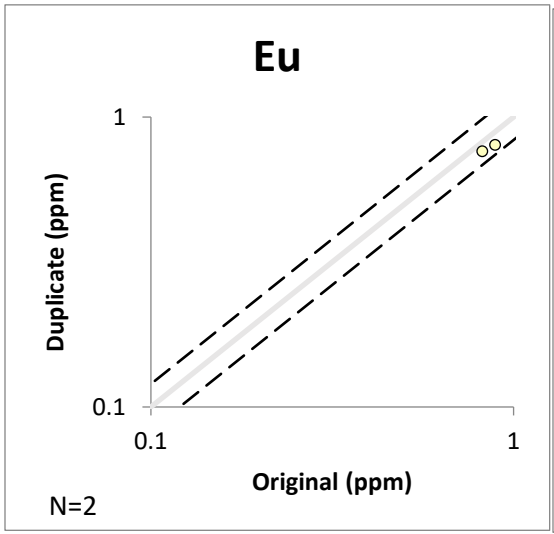

Cr
100
10
1
Duplicate (wt%)
1
10
100
Original (wt%)
N=2

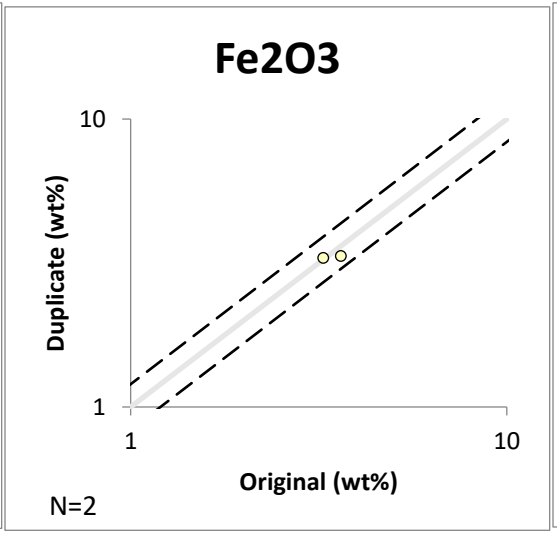

Cs
10
1
Duplicate (ppm)
1
10
Original (ppm)
N=2

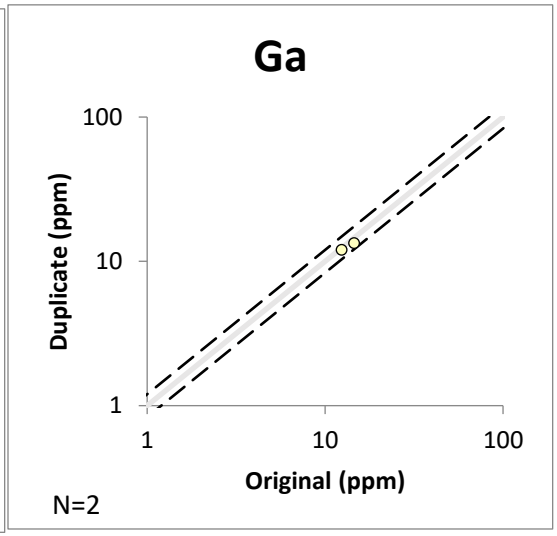

Cu
100
10
1
Duplicate (ppm)
1
10
100
Original (ppm)
N=2

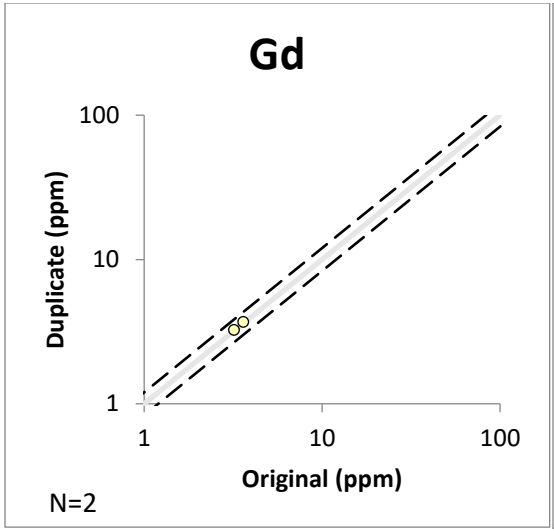

Dy
100
10
1
Duplicate (ppm)
1
10
100
Original (ppm)
N=2

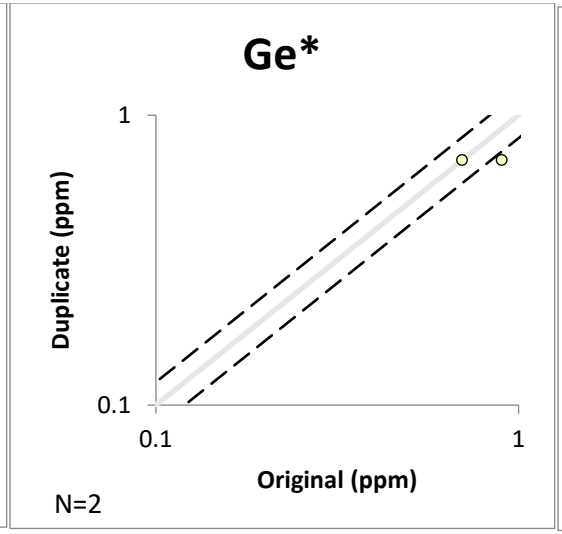

Er
100
10
1
Duplicate (ppm)
1
10
100
Original (ppm)
N=2

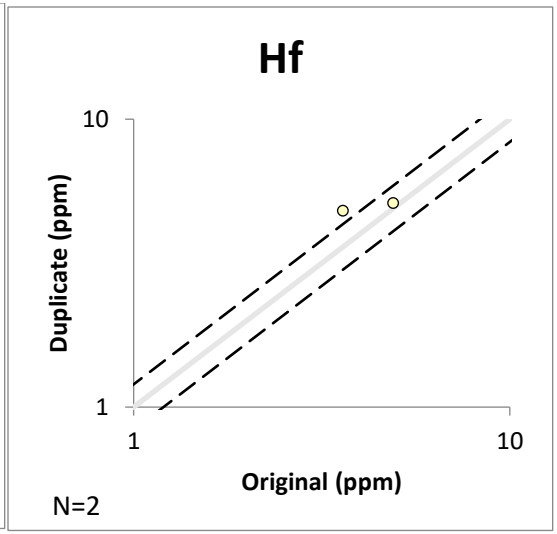

Eu
1
0.1
Duplicate (ppm)
0.1
1
Original (ppm)
N=2

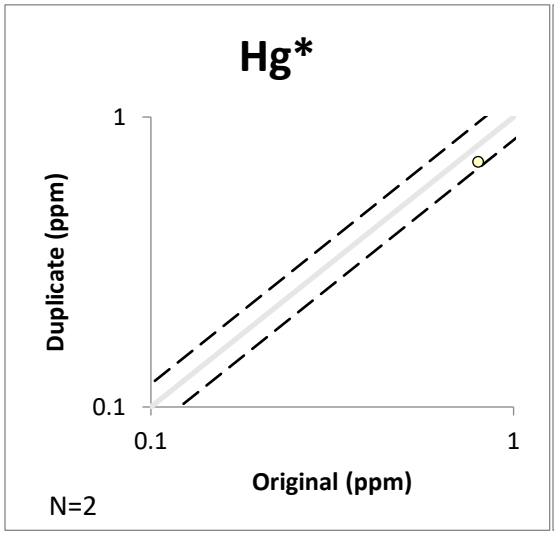

Fe2O3
10
1
Duplicate (wt%)
1
10
Original (wt%)
N=2

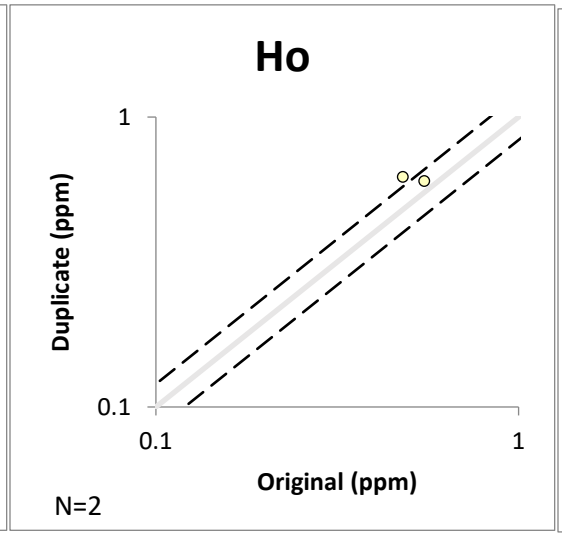

Ga
100
10
1
Duplicate (ppm)
1
10
100
Original (ppm)
N=2

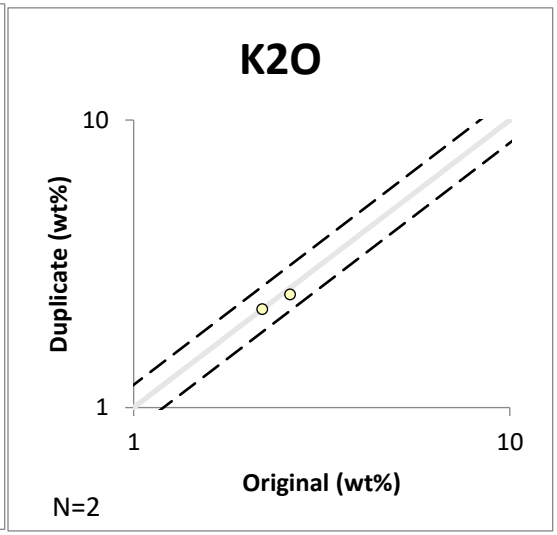

Gd
100
10
1
Duplicate (ppm)
1
10
100
Original (ppm)
N=2

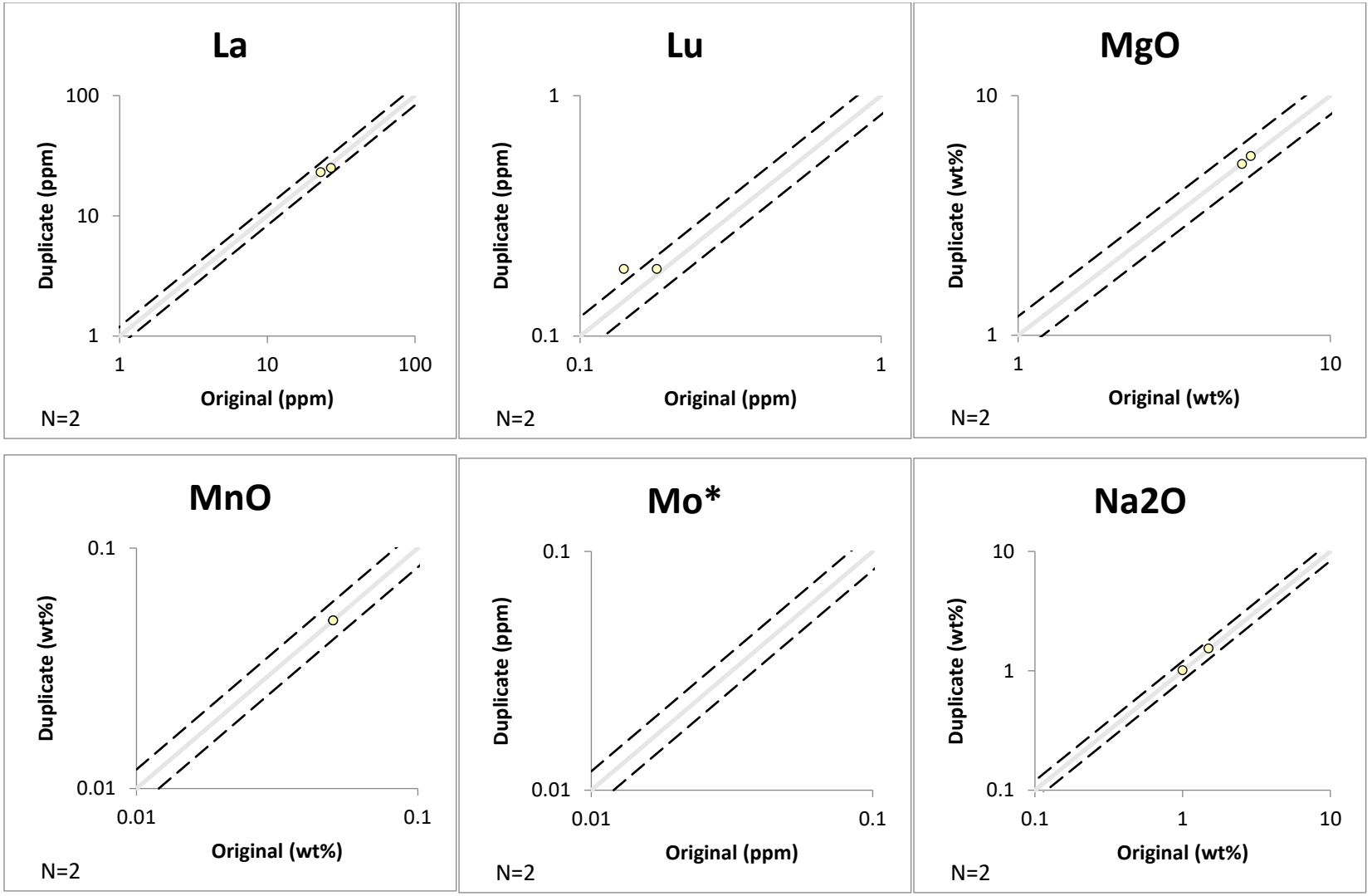

Ge*
1
0.1
Duplicate (ppm)
0.1
1
Original (ppm)
N=2

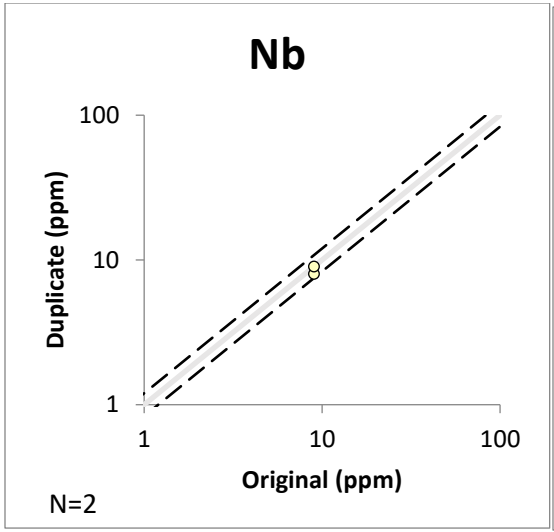

Hf
10
1
Duplicate (ppm)
1
10
Original (ppm)
N=2

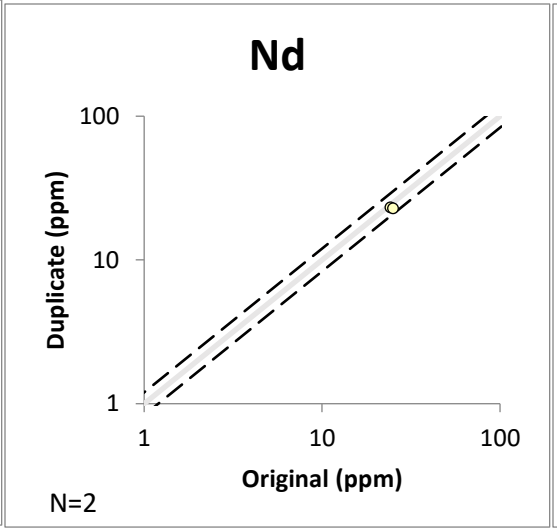

Hg*
1
0.1
Duplicate (ppm)
0.1
1
Original (ppm)
N=2

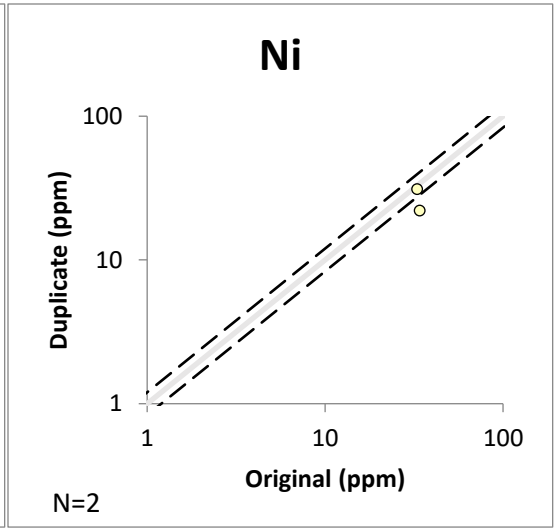

Ho
1
0.1
Duplicate (ppm)
0.1
1
Original (ppm)
N=2

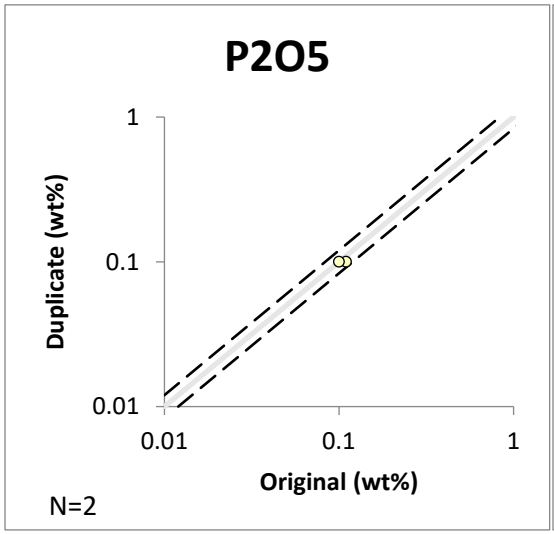

K2O
10
1
Duplicate (wt%)
1
10
Original (wt%)
N=2

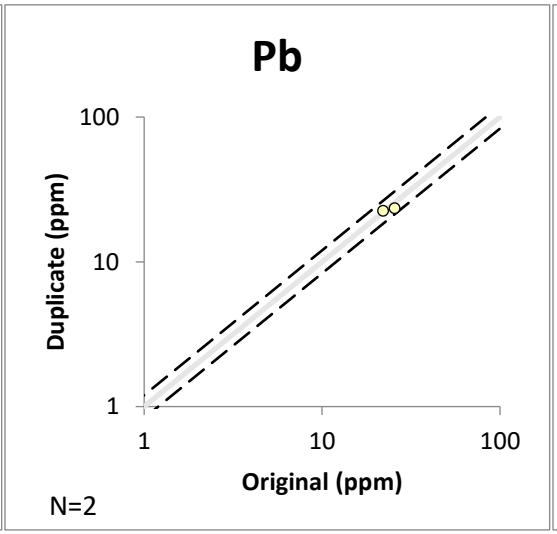

La
100
10
1
Duplicate (ppm)
1
10
100
Original (ppm)
N=2
Lu
1
0.1
Duplicate (ppm)
0.1
1
Original (ppm)
N=2
MgO
10
1
Duplicate (wt%)
1
10
Original (wt%)
N=2
MnO
0.1
0.01
Duplicate (wt%)
0.01
0.1
Original (wt%)
N=2
Mo*
0.1
0.01
Duplicate (ppm)
0.01
0.1
Original (ppm)
N=2
Na2O
10
1
0.1
Duplicate (wt%)
0.1
1
10
Original (wt%)
N=2

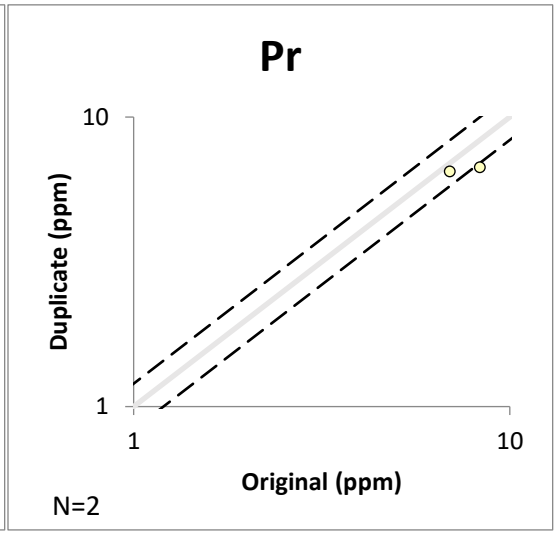

Nb
100
10
1
Duplicate (ppm)
1
10
100
Original (ppm)
N=2

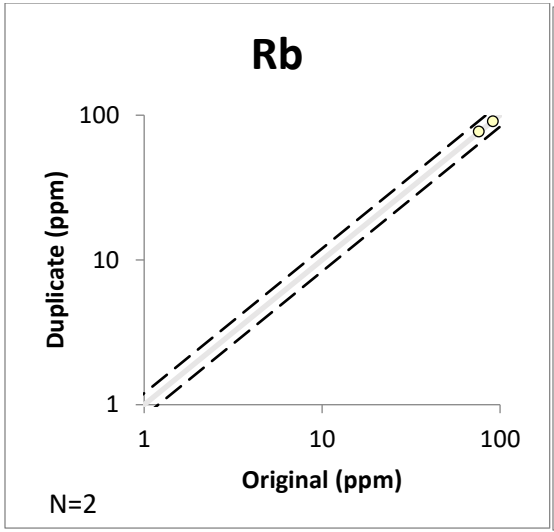

Nd
100
10
1
Duplicate (ppm)
1
10
100
Original (ppm)
N=2

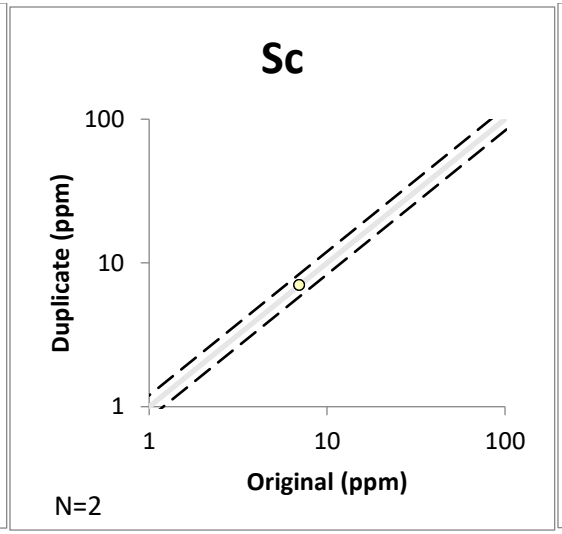

Ni
100
10
1
Duplicate (ppm)
1
10
100
Original (ppm)
N=2

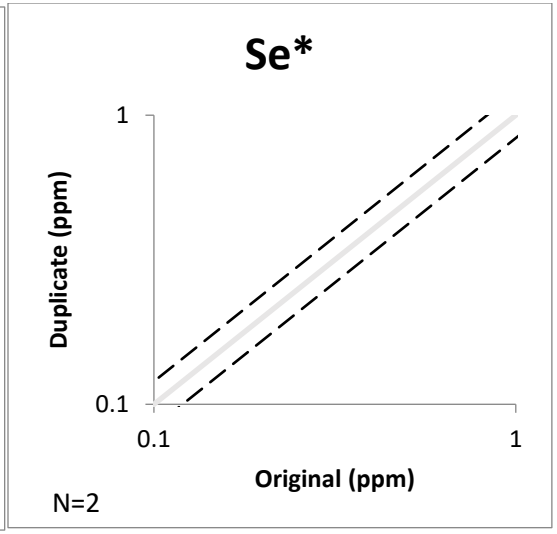

P2O5
1
0.1
0.01
Duplicate (wt%)
0.01
0.1
1
Original (wt%)
N=2

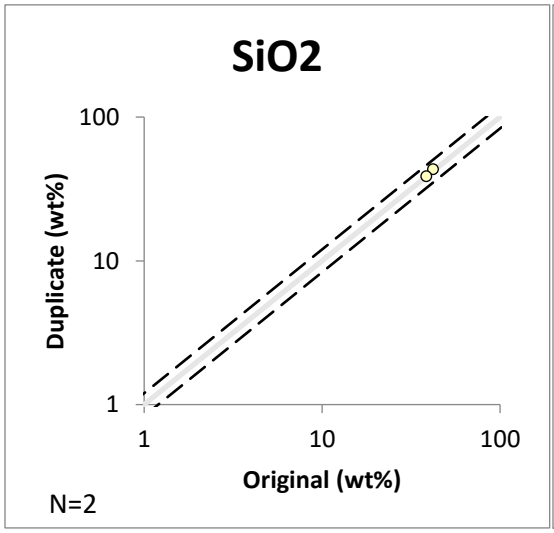

Pb
100
10
1
Duplicate (ppm)
1
10
100
Original (ppm)
N=2

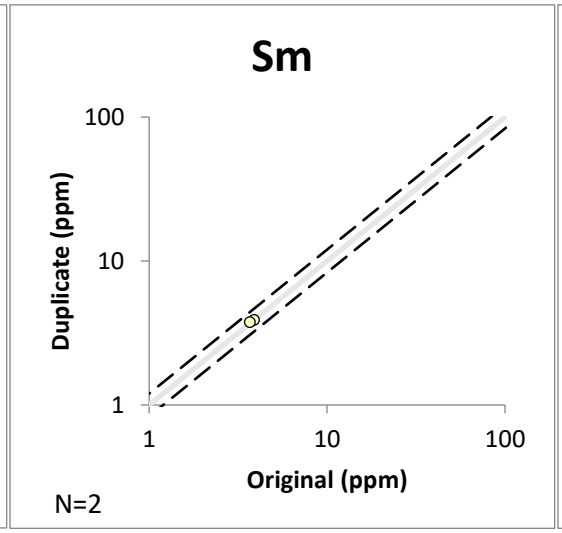

Pr
10
1
Duplicate (ppm)
1
10
Original (ppm)
N=2

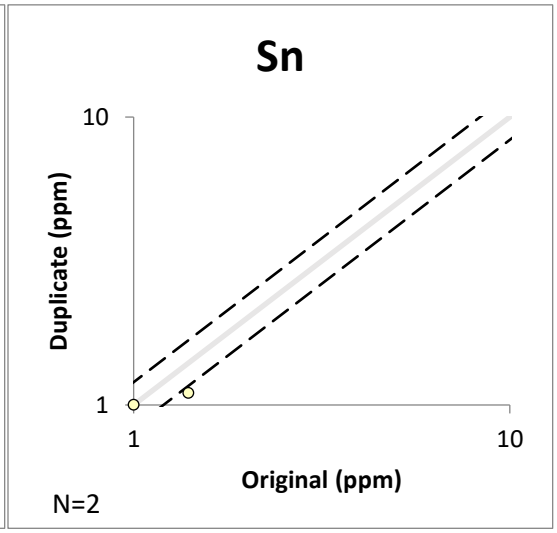

Rb
100
10
1
Duplicate (ppm)
1
10
100
Original (ppm)
N=2

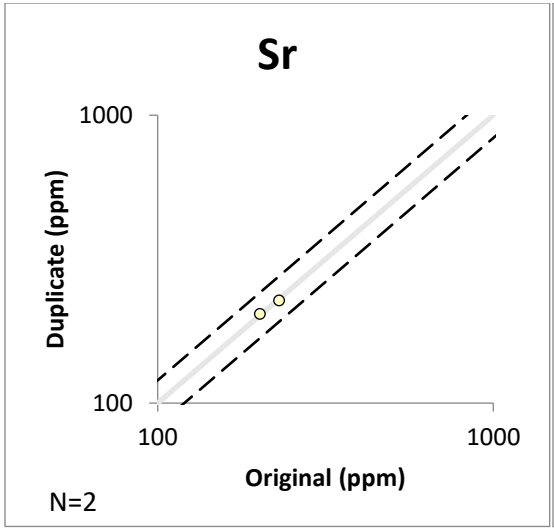

Sc
100
10
1
Duplicate (ppm)
1
10
100
Original (ppm)
N=2

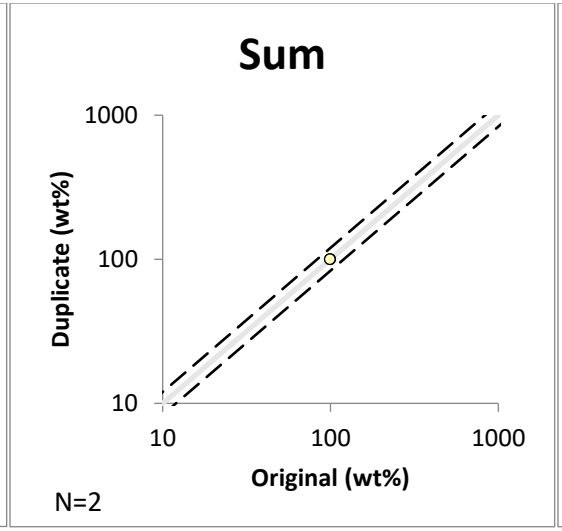

Se*
1
0.1
Duplicate (ppm)
0.1
1
Original (ppm)
N=2

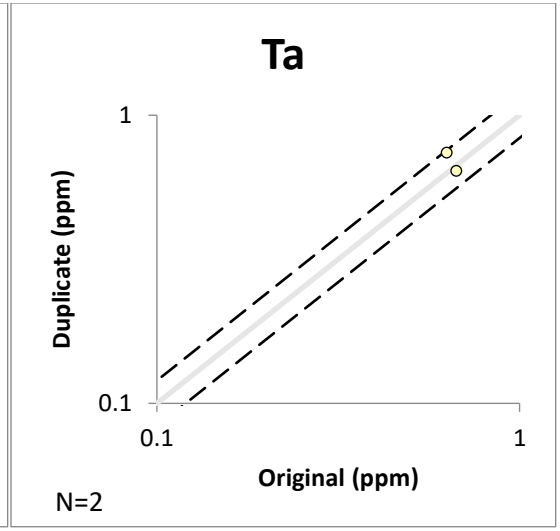

SiO2
100
10
1
Duplicate (wt%)
1
10
100
Original (wt%)
N=2

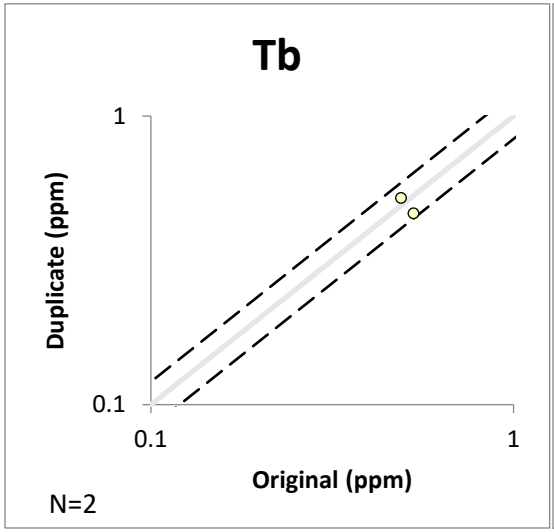

Sm
100
10
1
Duplicate (ppm)
1
10
100
Original (ppm)
N=2

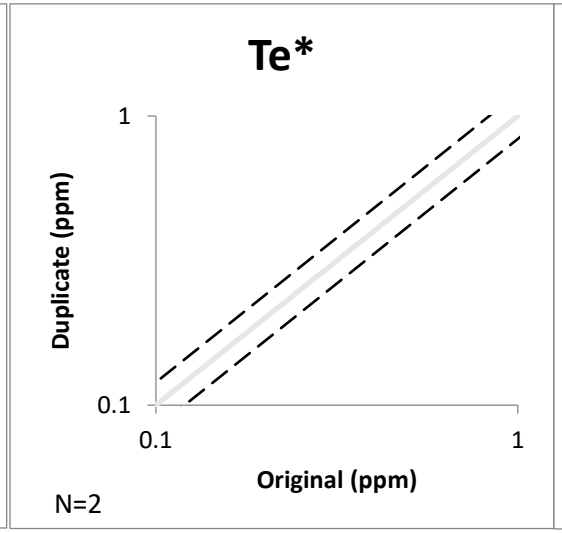

Sn
10
1
Duplicate (ppm)
1
10
Original (ppm)
N=2

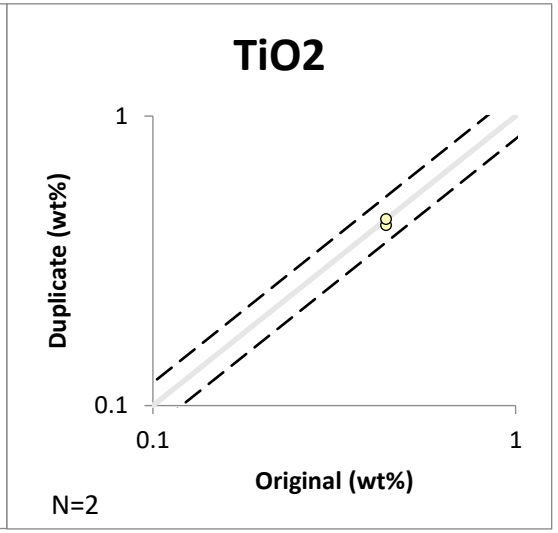

Sr
1000
100
Duplicate (ppm)
100
1000
Original (ppm)
N=2

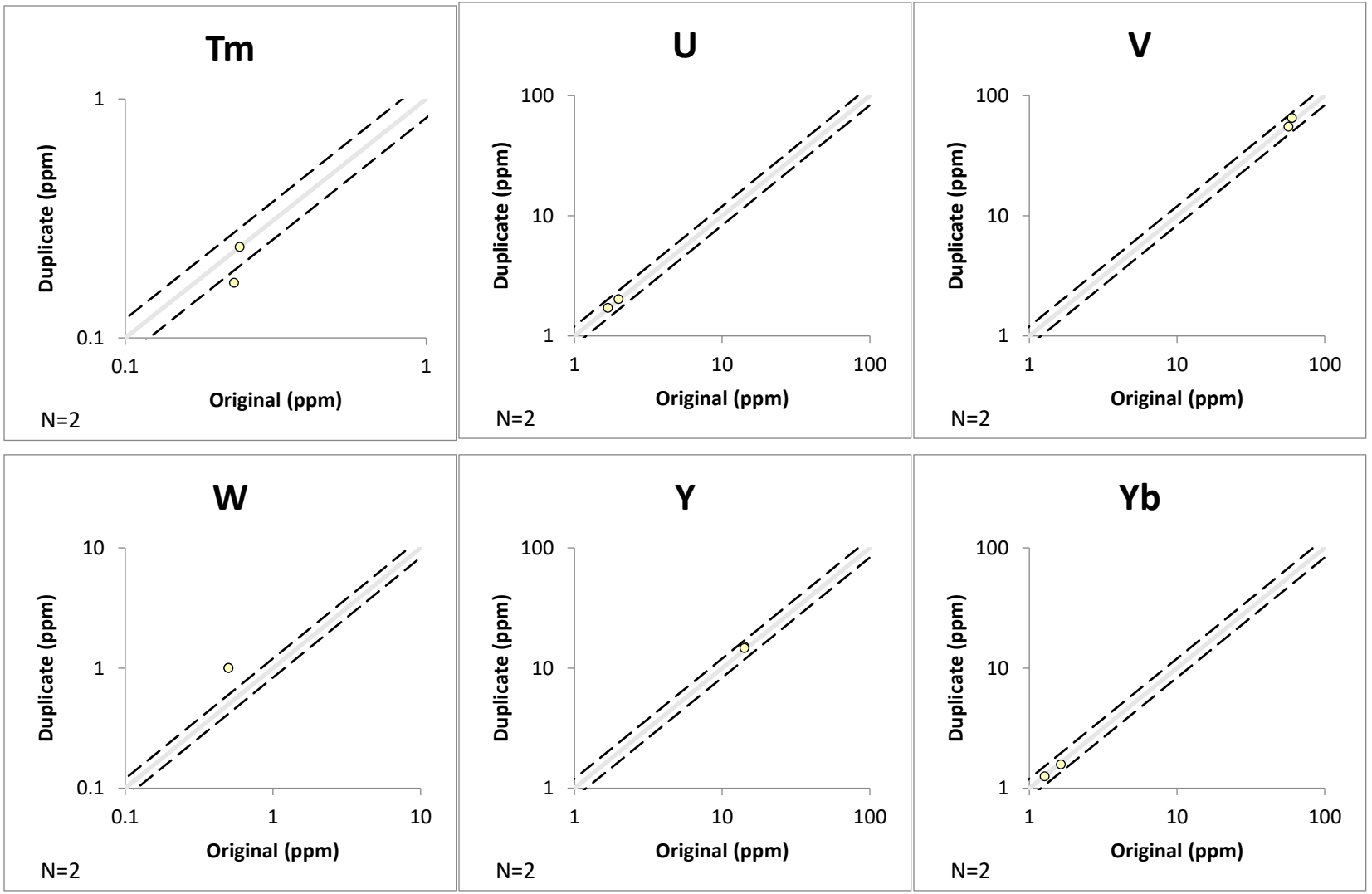

Sum
1000
100
10
Duplicate (wt%)
10
100
1000
Original (wt%)
N=2


Ta
1
0.1
Duplicate (ppm)
0.1
1
Original (ppm)
N=2


Tb
1
0.1
Duplicate (ppm)
0.1
1
Original (ppm)
N=2


Te*
1
0.1
Duplicate (ppm)
0.1
1
Original (ppm)
N=2


TiO2
1
0.1
Duplicate (wt%)
0.1
1
Original (wt%)
N=2


Tm
Duplicate (ppm)
1
0.1
0.1
1
Original (ppm)
N=2
U
Duplicate (ppm)
100
10
1
1
10
100
Original (ppm)
N=2
V
Duplicate (ppm)
100
10
1
1
10
100
Original (ppm)
N=2
W
Duplicate (ppm)
10
1
0.1
0.1
1
10
Original (ppm)
N=2
Y
Duplicate (ppm)
100
10
1
1
10
100
Original (ppm)
N=2
Yb
Duplicate (ppm)
100
10
1
1
10
100
Original (ppm)
N=2

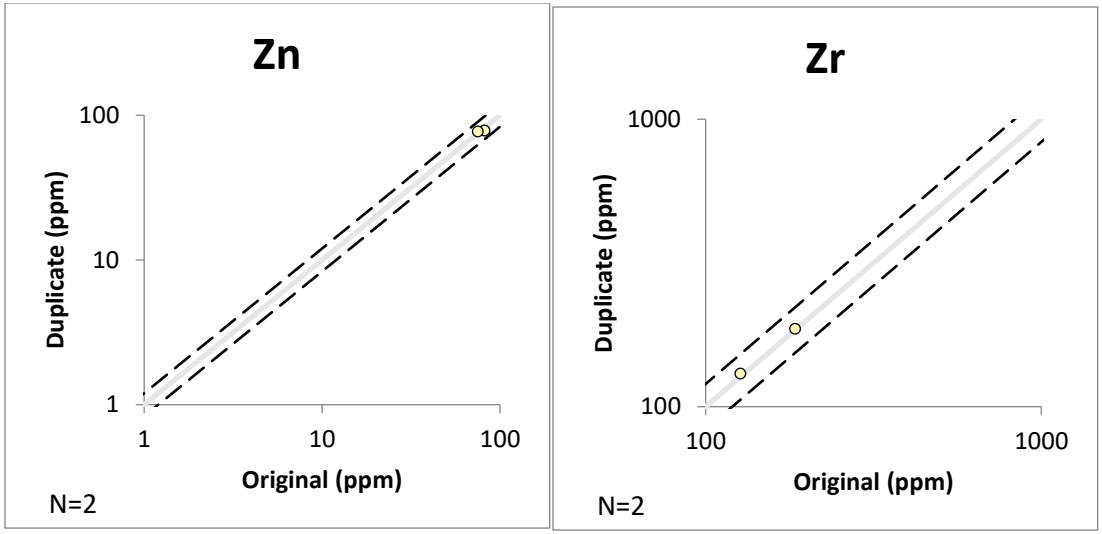


Figure 3: Precision biplots for lab duplicates of till-matrix (<63 µm size-fraction) geochemistry by fusion digestion and ICP-MS and ICP-OES analysis. Control lines (dashed black) are set at a 20% level of precision above or below the 1:1 line (grey). * = Data has one or more value below detection limit.

Reference materials: %RSD and %RD

Table 3: %RSD and %RD for till-matrix (<63 µm size-fraction) geochemistry by fusion digestion and ICP-MS and ICP-OES analysis.

Sample ID	Al_2O_3 (wt%)	CaO (wt%)	Fe_2O_3 (wt%)	K_2O (wt%)	LOI (wt%)	MgO (wt%)	MnO (wt%)	Na_2O (wt%)	P_2O_5 (wt%)
MGS standard - OREAS 46	12.05	3.40	3.79	1.42	-	1.61	0.06	3.49	0.12
115-23-002-B04	11.90	3.58	3.92	1.56	0.90	1.56	0.06	3.66	0.11
115-23-005-A01	12.10	3.59	3.95	1.53	0.90	1.59	0.06	3.59	0.12
115-23-007-A02	12.10	3.66	4.00	1.53	0.80	1.62	0.06	3.58	0.13
115-23-009-A02	12.00	3.64	3.97	1.53	0.90	1.60	0.06	3.60	0.12
%RSD	**0.80**	**1.07**	**0.85**	**0.98**	**5.71**	**1.57**	**0.00**	**1.00**	**6.80**
%RD	**-0.21**	**6.40**	**4.49**	**8.27**	**-**	**-1.09**	**-6.25**	**3.37**	**-1.64**

SiO_2 (wt%)	TiO_2 (wt%)	Total (wt%)	Ag (ppm)	As (ppm)	Ba (ppm)	Be (ppm)	Bi (ppm)	Cd (ppm)	Ce (ppm)	Co (ppm)	Cr (ppm)	Cs (ppm)	Cu (ppm)	Dy (ppm)
72.7	0.37	-	-	-	461.00	0.9	-	-	37.2	9.9	66	0.6	-	2.0
72.3	0.38	99.93	<0.1	0.80	471.00	1.0	<0.1	0	30.0	10.7	63	0.5	24	1.9
72.1	0.38	99.91	<0.1	0.90	476.00	1.1	<0.1	0	32.0	11.1	61	0.6	27	2.5
72.2	0.38	100.06	<0.1	0.80	474.00	1.6	<0.1	<0.1	31.0	10.5	59	0.8	26	2.3
72.1	0.38	99.90	<0.1	1.00	482.00	0.7	<0.1	<0.1	29.0	10.3	61	0.7	25	2.3
0.13	**0.00**	**0.07**	**-**	**10.94**	**0.98**	**34.02**	**-**	**-**	**4.23**	**3.21**	**2.68**	**19.86**	**5.15**	**11.13**
-0.76	**2.15**	**-**	**-**	**-**	**3.20**	**19.57**	**-**	**-**	**-18.01**	**7.25**	**-7.58**	**4.84**	**-**	**11.51**

Er (ppm)	Eu (ppm)	Ga (ppm)	Gd (ppm)	Ge (ppm)	Hf (ppm)	Hg (ppm)	Ho (ppm)	La (ppm)	Lu (ppm)	Mo (ppm)	Nb (ppm)	Nd (ppm)	Ni (ppm)	Pb (ppm)
1.1	0.9	14	2.6	-	4.1	-	0.40	19.7	0.2	<2	5	18.70	30.70	-
1.0	0.9	15	2.6	1.1	3.8	0.50	0.38	14.0	0.2	<0.1	5	17.20	31.0	12.60
1.1	0.9	16	2.8	0.6	4.4	0.50	0.41	16.0	0.1	<0.1	6	18.40	33.0	12.70
1.1	0.8	15	2.8	1.2	4.1	1.00	0.34	15.0	0.2	<0.1	5	17.40	33.0	14.40
1.0	1.0	14	2.5	1.0	4.0	0.80	0.40	14.0	0.2	<0.1	5	17.90	35.0	12.60
7.85	**6.60**	**5.73**	**6.64**	**26.97**	**6.13**	**34.99**	**8.09**	**6.49**	**27.50**	**-**	**9.52**	**3.03**	**4.95**	**6.77**
-6.92	**2.27**	**4.79**	**2.88**	**-**	**-0.85**	**-**	**-4.37**	**-25.13**	**-4.69**	**-**	**-3.14**	**-5.21**	**7.49**	**-**

Pr (ppm)	Rb (ppm)	Sb (ppm)	Sc (ppm)	Se (ppm)	Sm (ppm)	Sn (ppm)	Sr (ppm)	Ta (ppm)	Tb (ppm)	Te (ppm)	Th (ppm)	Tm (ppm)	U (ppm)	V (ppm)
4.8	34	-	9	-	3.3	-	404.00	0.31	0.4	-	3.23	0.16	1	60
4.8	37	1	8	<1	2.8	1	433.00	0.35	0.3	<0.1	2.76	0.18	1	58
5.0	39	<1	9	8.00	3.3	1	445.00	0.30	0.4	0.30	3.39	0.19	1	63
5.0	37	<1	9	5.00	3.6	1	432.00	0.37	0.4	<0.1	2.82	0.19	1	60
4.8	36	2	8	7.00	3.1	1	430.00	0.35	0.4	<0.1	2.90	0.13	1	58
2.30	**2.53**	**-**	**6.79**	**-**	**9.43**	**17.21**	**1.56**	**8.72**	**12.28**	**-**	**9.69**	**16.65**	**16.84**	**3.95**
1.98	**11.42**	**-**	**-7.31**	**-**	**-4.13**	**-**	**7.67**	**10.48**	**3.47**	**-**	**-8.13**	**7.81**	**3.04**	**-0.42**

W (ppm)	Y (ppm)	Yb (ppm)	Zn (ppm)	Zr (ppm)
<1	11.4	1.07	-	159
<1	10.2	1.14	61	127
<1	10.9	1.07	57	138
<1	10.7	1.05	63	142
<1	10.7	0.9	60	138
-	**2.81**	**9.71**	**4.15**	**4.73**
-	**-6.80**	**-2.80**	**-**	**-14.31**

%RSD = measure of precision (0-3%, excellent; 3-7% is very good to good; 7-10% is good; >10% not precise) [Piercey, 2014]

%RD = measure of accuracy (±0-3, excellent; ±3-7% very good; ±7-10% good; >±10% not accurate) [Piercey, 2014]

-: Not applicable

Appendix E – Clast-lithology counts

Tabulated counts

Table 1: Detailed clast-lithology counts for 2022 and 2023 samples (2-4 mm size fraction).

	2-4 mm																							
Sample ID	Grey, tan, white carbonate	Pink carbonate	Chert	Shell fragment	Paleozoic Fossil	Fine-grained red sandstone (Kenoganii Formation)	Quartzite	Quartz	Qtz arenite	Metased	Exotic Sed	Undifferentiated sandstone and siltstone	Undifferentiated greenstone and greywacke	Granitoid	Exotic granitoid	Amphibolite, gabbro	Ironstone	Metavolcanic	Paragneiss	Red or purple volcanic (Duhavent Supergroup)	Oolitic Jasper	Shale	Sulphides	Wood	Sum
115-23-002-A01	230	0	0	0	0	1	2	4	1	2	0	1	19	62	0	1	0	0	0	0	0	0	0	0	323
115-23-002-B01	268	0	0	0	0	0	2	3	0	0	0	0	16	45	2	0	0	2	0	0	0	0	1	0	339
115-23-002-B02	232	2	1	0	0	0	3	2	0	1	1	0	25	43	0	1	0	1	0	1	0	0	0	0	313
115-23-002-B03	399	3	3	0	0	0	3	2	0	4	3	1	59	44	0	0	1	3	0	0	0	0	0	0	525
115-23-002-C01	282	2	3	0	0	0	0	2	0	2	1	5	22	26	0	1	0	2	0	0	0	0	0	1	349
115-23-002-C02	366	4	5	0	1	0	2	5	0	0	1	0	19	55	0	1	0	0	0	0	0	0	0	0	459
115-23-002-C03	287	1	0	0	0	0	2	3	0	0	1	1	34	32	0	1	0	5	0	0	0	0	0	1	368
115-23-002-C04	197	1	1	0	0	0	1	1	0	5	0	0	32	26	1	3	0	4	0	0	0	0	0	0	272
115-23-002-D01	217	2	1	0	0	2	3	2	0	0	1	0	10	30	0	0	0	0	0	0	0	0	0	0	268
115-23-002-D02	321	1	1	0	0	0	4	5	1	0	2	1	13	41	0	1	0	4	0	0	0	0	0	0	395
115-23-002-D03	257	3	1	0	0	0	2	8	0	1	0	1	15	45	1	5	0	2	0	1	0	0	0	0	342
115-23-002-D04	178	2	2	1	1	0	3	1	0	0	0	0	14	39	0	1	0	0	0	0	0	0	1	0	243
115-23-002-H01	243	0	2	1	0	0	3	1	1	3	0	1	16	44	1	2	0	3	0	0	0	0	0	0	321
115-23-002-Z01	209	1	0	0	0	0	0	2	0	2	1	0	14	46	0	3	0	2	0	0	0	0	1	0	281
115-23-003-A01	163	1	0	0	0	0	1	1	0	4	0	1	32	21	0	0	0	1	0	0	0	0	0	0	225
115-23-003-A02	215	0	2	0	0	1	2	0	1	1	1	0	25	18	0	0	0	2	0	0	0	1	0	0	269
115-23-003-A03	225	1	2	0	0	0	1	3	0	2	1	0	30	33	0	0	0	1	0	0	0	0	0	0	299
115-23-003-B01	223	2	1	0	0	2	0	0	0	2	2	0	28	27	0	0	0	1	0	0	0	1	0	0	289
115-23-003-B02	196	2	1	0	0	2	0	1	0	0	0	0	15	29	1	1	0	0	0	0	0	1	0	0	249

115-23-003-D01	184	0	0	0	0	1	3	0	0	3	0	2	34	60	0	2	0	3	0	0	0	0	0	0	292
115-23-003-D02	150	0	0	0	0	0	3	2	0	2	0	1	33	64	3	0	0	1	0	0	1	0	0	0	260
115-23-003-D03	172	0	2	0	0	1	1	5	0	1	0	2	24	49	0	0	0	0	0	0	0	0	0	0	257
115-23-003-D04	202	0	2	0	0	1	6	4	0	2	0	0	16	53	1	0	1	1	1	0	0	0	0	0	290
115-23-003-L01	212	1	1	0	0	0	4	3	1	2	1	3	27	54	1	0	0	2	0	0	1	0	0	0	313
115-23-004-B01	250	0	2	0	0	0	1	1	0	1	1	2	17	46	0	0	0	0	0	0	0	0	0	0	321
115-23-005-B01	233	0	1	0	0	2	1	3	0	0	0	0	13	36	0	1	0	1	0	0	0	0	0	0	291
115-23-005-B02	231	1	1	0	0	0	0	1	0	0	2	2	15	35	0	1	0	0	0	0	0	0	0	0	289
115-23-005-B03	247	0	0	2	0	0	1	2	0	0	1	0	15	35	0	0	0	0	0	0	1	2	0	0	306
115-23-005-B04	219	2	0	1	0	0	1	4	0	1	1	0	8	32	0	0	0	0	0	0	0	0	0	0	269
115-23-005-B05	224	0	0	0	0	0	1	8	0	0	0	0	14	38	0	0	0	2	0	0	1	0	0	0	288
115-23-005-Z01	225	0	5	0	0	0	4	3	0	0	0	0	11	47	0	3	0	1	0	0	0	0	0	0	299
115-23-005-C01	246	0	0	0	0	0	1	4	0	0	1	0	12	49	0	0	1	0	0	0	0	0	0	0	314
115-23-005-O01	212	0	1	0	0	0	0	3	0	0	0	1	27	32	0	1	0	0	0	0	0	0	2	0	279
115-23-005-P01	176	0	2	0	0	0	3	6	1	2	0	1	63	38	0	3	0	6	0	0	0	0	0	0	301
115-23-006-X01	159	0	0	0	0	0	4	2	0	0	2	3	13	34	0	6	0	1	1	0	2	0	0	0	227
115-23-006-A01	186	0	0	0	0	2	2	2	0	1	1	0	8	53	0	1	0	0	0	0	0	0	1	0	257
115-23-006-B01	183	0	0	0	0	0	3	4	0	2	0	1	34	55	0	3	1	2	0	0	1	0	1	1	291
115-23-006-B02	164	4	1	0	0	3	4	2	0	2	0	0	29	26	2	1	0	0	0	0	0	0	0	0	238
115-23-006-C01	172	0	0	0	0	0	0	3	1	1	0	0	23	36	0	2	0	0	0	0	1	0	0	0	239
115-23-006-C02	188	0	0	1	1	0	0	7	0	4	0	0	16	57	0	1	1	1	0	0	0	0	0	0	277
115-23-006-C03	198	1	0	1	1	3	1	1	0	2	0	0	12	22	0	0	0	2	0	0	0	0	1	0	245
115-23-006-D01	238	0	1	0	0	0	5	2	0	2	0	0	19	22	0	1	0	1	0	0	0	0	0	0	291
115-23-007-A01	214	2	0	0	0	0	1	5	0	0	2	1	13	64	0	2	0	4	0	0	0	0	0	0	308
115-23-007-B01	198	1	0	0	0	0	1	4	0	1	0	0	20	66	1	0	0	0	0	0	0	0	0	1	293
115-23-007-B02	219	1	2	1	0	0	2	2	0	5	2	0	10	60	1	3	0	2	0	0	0	0	1	0	311
115-23-007-C01	144	0	0	1	0	0	2	3	0	1	1	0	10	38	0	0	0	1	0	4	0	0	0	0	205
115-23-007-C02	240	0	4	0	0	0	4	3	0	2	1	1	21	45	1	2	0	1	0	0	0	0	1	0	326
115-23-007-C03	225	0	1	0	0	0	1	7	0	2	0	0	29	48	0	1	1	1	0	0	0	0	0	0	316
115-23-007-C04	183	2	2	0	1	0	4	2	0	2	2	0	14	37	0	0	0	3	0	0	0	0	0	0	252

115-23-007-C05	210	0	1	0	0	0	2	5	0	1	0	0	20	41	0	1	0	0	0	0	0	1	0	0	282
115-23-007-D01	191	0	1	0	0	0	2	6	1	1	2	1	24	40	0	0	0	1	0	0	0	0	0	0	270
115-23-007-D02	282	0	0	0	0	0	4	6	0	1	1	0	24	31	0	0	0	1	0	0	0	0	1	0	351
115-23-007-D03	229	0	1	0	0	0	1	1	0	1	0	3	19	23	0	1	0	1	0	0	0	0	1	0	281
115-23-007-D04	226	0	0	0	0	0	0	2	0	0	1	0	27	37	0	0	0	0	0	0	0	0	0	0	293
115-23-007-D05	148	0	0	0	0	0	1	3	0	0	1	0	29	19	0	0	0	0	0	0	0	1	0	0	202
115-23-007-D06	202	0	0	0	0	1	0	0	0	1	0	2	35	26	0	1	0	0	0	0	0	0	2	0	270
115-23-007-D07	205	0	0	0	0	0	0	2	0	1	0	1	35	18	0	0	0	0	0	0	0	1	0	0	263
115-23-007-E01	212	0	3	0	0	1	0	4	0	1	0	3	9	50	0	1	0	0	0	0	0	0	0	1	285
115-23-007-E02	205	0	0	0	0	0	1	6	0	0	1	1	13	52	0	0	0	0	1	0	0	0	1	0	281
115-23-007-E03	235	0	2	0	0	0	4	3	1	0	0	1	29	43	1	2	0	0	0	0	0	0	2	1	324
115-23-007-GRAV1	427	9	1	0	1	0	0	9	0	18	0	0	36	78	0	0	1	4	0	0	0	0	0	0	584
115-23-007-GRAV2	402	0	1	0	1	0	0	8	0	14	0	0	72	77	0	0	13	1	0	0	0	0	0	0	589
115-23-008-A01	166	3	1	0	0	3	3	3	0	2	2	1	26	54	0	3	0	0	0	0	2	0	0	0	269
115-23-008-B01	185	1	0	1	0	0	4	3	1	3	0	2	36	49	2	1	0	3	0	0	0	0	0	0	291
115-23-008-C01	188	0	1	0	0	0	3	3	1	1	1	0	24	53	0	1	0	0	0	1	0	0	0	0	277
115-23-008-F01	182	2	1	0	0	2	1	5	0	3	1	1	18	52	1	2	0	1	0	0	0	0	0	0	272
115-23-008-F02	196	0	0	0	0	2	0	3	0	1	1	1	19	58	0	2	0	0	0	0	1	0	0	0	284
115-23-008-F03	179	0	1	0	0	1	2	6	0	2	1	0	28	68	3	0	1	1	1	0	0	0	0	0	294
115-23-008-F04	189	3	0	0	0	0	3	1	0	1	0	1	25	51	0	4	0	1	0	0	0	0	2	0	281
115-23-009-B01	166	2	0	0	0	0	0	2	0	0	0	0	32	23	0	0	0	0	0	0	0	0	0	0	225
115-23-009-C01	236	1	0	0	0	1	1	2	0	2	0	1	51	43	0	0	0	0	0	0	0	0	0	0	338
115-23-009-D01	252	1	2	0	0	0	4	3	0	0	0	0	19	49	0	5	0	1	1	0	0	0	0	1	338
115-23-009-D02	220	0	1	0	0	0	4	4	0	0	0	0	17	46	0	1	0	0	0	0	0	0	0	0	293
115-23-009-N01	214	0	3	1	0	0	9	3	0	2	0	0	24	71	0	3	0	1	0	0	0	0	0	1	332
115-23-009-D03	199	0	1	1	0	0	6	6	0	6	0	0	22	60	0	1	0	0	0	0	0	1	2	0	305
115-23-009-D04	190	0	1	0	0	0	1	2	0	5	0	1	30	44	0	2	0	0	0	0	0	0	0	0	276
115-23-009-D05	177	1	0	1	1	0	2	4	2	0	0	1	19	40	0	2	0	0	0	0	1	0	0	0	251
115-23-009-D06	280	0	0	0	0	0	3	5	0	0	0	1	22	25	0	2	0	0	0	0	0	0	0	0	338
115-23-009-D07	206	0	1	0	0	2	2	2	0	1	0	0	18	28	0	1	0	0	0	0	0	0	0	0	261

115-23-009-E01	207	0	0	0	0	0	2	1	0	1	1	0	32	22	0	0	0	1	0	0	0	0	0	0	267
115-23-009-G01	223	1	0	0	1	3	1	1	0	0	0	2	6	33	0	1	0	0	0	0	0	1	0	0	273
115-23-009-G02	242	0	1	0	1	0	4	9	0	1	1	0	20	56	0	1	0	3	0	0	0	0	0	0	339
115-23-009-J01	195	0	1	0	0	0	4	7	0	0	2	2	21	50	0	2	0	1	0	0	0	0	0	0	285
115-23-009-K01	221	0	0	0	0	0	3	1	0	0	1	0	17	44	0	2	0	1	0	0	0	0	0	0	290
115-23-009-K02	190	1	0	0	0	0	0	1	0	6	0	0	19	57	0	1	0	0	0	0	0	0	0	0	275
115-23-009-K03	244	0	0	0	0	0	4	3	0	1	1	1	22	59	0	1	0	2	0	0	0	0	0	0	338
115-23-009-K04	262	0	0	0	0	0	4	1	0	4	1	4	62	39	1	5	0	4	0	0	1	0	0	1	389
112-22-200-A01	161	0	0	0	0	1	5	1	0	1	0	0	23	38	1	4	0	0	0	0	0	0	0	0	235
112-22-200-A02	185	3	0	0	0	3	5	1	0	2	0	0	22	48	0	2	0	1	0	0	0	0	0	0	272
112-22-200-B01	225	0	1	0	0	0	2	2	0	4	0	0	45	51	2	2	0	2	0	0	0	0	0	0	336
112-22-200-C01	136	1	0	0	0	6	2	2	0	0	1	0	23	78	2	0	0	0	0	0	0	0	0	0	251
112-22-200-C02	187	1	3	0	0	7	3	1	0	2	0	0	27	72	0	2	0	0	0	0	0	0	0	0	305
112-22-200-C03	179	1	2	0	0	2	4	8	0	0	0	0	31	89	1	4	0	1	1	0	0	0	0	0	323
112-22-201-A01	219	1	0	0	0	3	0	3	0	3	1	0	29	53	0	0	0	0	2	0	0	0	0	0	314
112-22-201-B01	191	5	1	0	0	3	0	0	0	2	3	0	62	49	2	0	0	1	0	1	0	0	0	0	320

Table 2: Detailed clast-lithology counts for 2022 and 2023 samples (4-8 mm size fraction).

	4-8 mm																								
Sample ID	**Grey, tan, white carbonate**	**Pink carbonate**	**Chert**	**Shell fragment**	**Paleozoic Fossil**	**Fine-grained red sandstone (Kenogami Formation)**	**Quartzite**	**Quartz**	**Qtz arenite**	**Metased**	**Exotic Sed**	**Undifferentiated sandstone and siltstone**	**Undifferentiated greenstone and greywacke**	**Granitoid**	**Exotic granitoid**	**Amphibolite, gabbro**	**Ironstone**	**Metavolcanic**	**Paragneiss**	**Red or purple volcanic (Dubawnt Supergroup)**	**Oolitic Jasper**	**Shale**	**Sulphides**	**Wood**	**Sum**
115-23-002-A01	73	0	3	0	0	0	1	0	0	0	0	0	8	9	0	0	0	2	0	0	0	0	0	0	96
115-23-002-B01	114	0	0	0	0	0	1	0	0	1	0	0	7	8	0	0	0	2	0	0	0	0	0	0	133
115-23-002-B02	104	0	0	0	0	0	1	0	0	0	0	0	15	15	0	0	0	0	0	0	0	0	0	0	135
115-23-002-B03	249	4	1	0	0	1	1	1	0	3	5	0	31	20	1	2	0	0	0	0	0	1	0	0	320
115-23-002-C01	121	0	1	0	0	0	0	1	0	0	0	5	16	10	0	0	0	3	0	0	0	0	0	0	157
115-23-002-C02	196	2	0	0	2	0	2	2	0	1	1	1	11	21	0	0	1	0	0	0	0	0	0	0	240
115-23-002-C03	111	0	0	0	0	0	1	1	0	1	0	1	20	10	0	0	0	0	0	0	0	0	0	0	145
115-23-002-C04	207	0	0	0	0	0	3	0	0	0	0	1	36	12	0	1	0	3	0	0	0	0	0	0	263
115-23-002-D01	174	1	0	0	0	3	6	1	0	0	0	0	13	26	1	0	0	0	0	0	0	0	1	0	226
115-23-002-D02	149	0	1	0	0	0	2	0	0	1	0	1	8	14	0	0	0	3	0	0	0	0	0	0	179
115-23-002-D03	155	1	1	0	0	0	3	0	0	1	0	1	8	32	0	0	0	1	0	0	0	0	0	0	203
115-23-002-D04	235	0	3	0	0	0	4	0	0	0	0	1	8	37	1	0	0	1	1	0	0	0	3	0	294
115-23-002-H01	35	0	0	0	0	0	1	0	0	0	0	0	2	5	0	0	0	1	0	0	0	0	0	0	44
115-23-002-Z01	28	0	0	0	0	0	1	1	0	0	0	0	3	2	0	0	0	1	0	0	0	0	0	0	36
115-23-003-A01	154	1	0	0	0	0	1	0	0	4	0	1	23	15	0	0	0	2	0	0	0	0	0	0	201
115-23-003-A02	143	0	2	0	1	0	1	1	0	0	0	0	16	16	1	1	0	1	0	1	0	0	0	0	184
115-23-003-A03	224	2	3	0	0	0	0	0	1	1	1	0	29	13	0	0	0	2	1	0	0	0	1	0	278
115-23-003-B01	237	0	0	0	2	1	1	0	0	3	2	0	39	22	0	1	0	1	0	0	0	0	0	0	309
115-23-003-B02	243	1	2	0	0	1	3	0	0	1	2	3	28	29	0	1	0	3	1	0	0	0	0	0	318
115-23-003-D01	239	1	1	0	0	2	3	1	0	3	1	2	48	65	1	3	0	0	1	1	1	0	0	0	373
115-23-003-D02	113	1	1	0	0	0	1	2	0	0	1	1	17	42	0	0	0	0	0	0	1	0	0	0	180
115-23-003-D03	120	0	1	0	0	0	2	0	0	3	0	1	23	16	0	0	0	0	0	0	1	0	0	0	167
115-23-003-D04	189	0	0	0	0	4	2	0	0	3	1	2	27	50	1	3	0	2	0	2	0	0	0	0	286

115-23-003-L01	139	1	1	0	0	0	0	0	0	0	1	0	18	33	0	0	0	0	0	0	0	0	0	0	193
115-23-004-B01	68	0	0	0	0	0	2	0	0	1	0	0	6	12	0	1	0	2	0	0	0	0	0	0	92
115-23-005-B01	184	1	1	0	2	0	1	0	0	1	1	1	22	33	1	0	0	0	0	0	0	0	0	0	248
115-23-005-B02	100	0	0	0	0	0	0	0	0	0	0	1	14	9	0	0	0	0	0	0	0	0	1	0	125
115-23-005-B03	132	0	0	1	0	0	3	0	0	0	0	1	10	10	0	0	0	4	0	0	0	0	0	0	161
115-23-005-B04	207	1	3	0	0	1	1	0	0	0	1	1	15	26	1	0	0	0	0	0	0	0	2	0	259
115-23-005-B05	73	0	0	0	0	0	2	0	0	0	0	0	4	16	0	0	0	0	0	0	0	0	0	0	95
115-23-005-Z01	79	0	0	0	0	0	1	0	0	1	0	0	10	8	0	0	0	0	0	0	0	0	0	0	99
115-23-005-C01	77	0	0	0	1	0	1	0	0	0	0	0	4	15	0	0	0	0	0	0	0	0	0	0	98
115-23-005-O01	122	0	0	0	0	0	1	0	0	0	0	1	17	18	0	1	0	2	0	0	0	0	2	0	164
115-23-005-P01	39	0	0	0	0	0	4	0	0	2	0	1	14	12	0	1	0	0	0	0	0	0	0	0	73
115-23-006-X01	112	2	0	1	0	0	2	1	0	2	0	3	11	26	0	2	0	0	0	0	0	0	0	0	162
115-23-006-A01	175	4	1	0	1	8	3	0	0	0	0	0	12	50	1	1	0	0	1	1	0	0	0	0	258
115-23-006-B01	158	0	0	0	0	0	3	0	0	0	0	0	28	36	0	1	0	2	1	0	0	0	1	0	230
115-23-006-B02	319	6	2	0	0	7	3	1	2	3	4	2	69	53	1	1	0	0	0	0	1	0	1	0	475
115-23-006-C01	267	6	1	1	1	0	5	3	0	1	0	0	34	60	0	3	0	0	1	3	0	0	1	0	387
115-23-006-C02	86	0	1	0	0	0	4	0	0	3	0	0	17	19	0	1	0	0	0	1	0	0	0	0	132
115-23-006-C03	225	1	1	0	0	1	1	0	0	3	0	0	21	31	1	0	0	0	0	0	0	0	0	0	285
115-23-006-D01	207	1	1	0	0	1	5	0	0	2	2	1	10	22	1	2	0	2	0	1	0	0	0	0	258
115-23-007-A01	120	0	0	0	0	0	0	0	1	2	0	0	10	14	0	0	0	0	0	0	0	0	0	0	147
115-23-007-B01	17	0	0	0	0	0	0	0	0	0	0	1	0	4	0	0	0	0	0	0	0	0	0	0	22
115-23-007-B02	185	4	1	0	0	0	2	0	0	3	0	0	8	31	0	1	0	1	0	0	0	0	0	0	236
115-23-007-C01	233	0	1	0	0	0	4	0	1	3	1	1	19	45	0	2	0	3	0	1	0	0	0	0	314
115-23-007-C02	101	0	1	0	0	0	2	1	1	0	1	1	10	16	0	1	0	0	0	0	0	0	3	0	138
115-23-007-C03	98	1	0	0	0	0	2	0	0	1	4	0	12	22	0	0	0	1	0	0	0	0	0	0	141
115-23-007-C04	224	2	3	0	0	2	1	1	0	5	1	0	15	45	1	2	0	0	0	0	0	0	0	0	302
115-23-007-C05	78	1	0	0	0	0	2	1	0	1	1	1	12	16	0	1	1	1	1	0	0	0	0	0	117
115-23-007-D01	269	0	1	0	0	0	4	1	0	4	0	0	38	46	2	3	0	1	0	0	0	0	2	0	371
115-23-007-D02	141	1	0	0	0	0	4	0	0	0	0	1	19	11	0	0	0	0	0	0	0	0	0	0	177
115-23-007-D03	215	1	1	0	0	0	2	0	0	0	1	1	18	19	0	1	0	2	0	0	0	0	1	0	262

115-23-007-D04	168	0	0	0	0	0	1	0	0	1	0	0	18	11	0	0	0	1	0	0	0	0	0	0	200
115-23-007-D05	177	0	0	0	0	0	3	1	0	0	0	0	33	12	0	0	0	0	0	0	0	1	0	0	227
115-23-007-D06	190	0	1	0	0	0	0	0	0	0	0	0	26	22	0	0	0	0	0	0	0	0	0	0	239
115-23-007-D07	223	1	0	0	0	0	0	0	0	2	0	2	42	24	0	0	0	1	0	0	0	0	0	0	295
115-23-007-E01	125	1	0	0	0	1	0	0	0	0	1	0	6	16	0	1	0	0	0	0	0	0	0	0	151
115-23-007-E02	108	0	1	0	0	0	1	1	0	1	1	0	6	19	0	3	0	0	0	0	0	0	0	0	141
115-23-007-E03	230	0	5	0	0	1	1	0	0	6	1	2	32	48	0	1	0	2	0	0	0	0	1	0	330
115-23-007-GRAV1	121	1	0	0	0	0	1	1	1	3	0	0	27	5	0	0	0	3	0	0	0	0	0	0	163
115-23-007-GRAV2	101	0	1	0	0	0	0	0	0	5	0	0	22	10	0	1	7	2	0	0	0	0	0	0	149
115-23-008-A01	165	1	0	0	1	1	4	2	0	1	3	2	25	37	0	3	0	0	0	0	0	0	0	0	245
115-23-008-B01	204	0	4	0	0	4	1	0	1	1	1	1	29	33	0	0	0	2	0	2	0	0	0	0	283
115-23-008-C01	215	3	1	0	0	2	2	1	2	1	0	0	27	46	0	0	0	1	0	1	0	0	0	0	302
115-23-008-F01	169	2	2	0	0	0	4	0	0	2	0	0	25	42	2	3	0	1	0	0	0	0	0	0	252
115-23-008-F02	128	1	0	0	0	0	1	0	2	0	1	0	29	33	0	0	0	0	0	0	0	0	0	0	195
115-23-008-F03	168	0	1	0	0	0	4	0	1	3	2	0	16	56	2	1	0	0	0	1	0	0	0	0	255
115-23-008-F04	215	0	1	0	0	4	4	1	0	4	1	0	26	56	1	0	0	3	0	0	0	0	1	0	317
115-23-009-B01	260	3	1	0	0	0	5	1	0	1	1	1	66	29	0	1	0	3	0	0	0	0	0	0	372
115-23-009-C01	206	5	2	0	0	0	2	0	0	0	1	1	40	21	0	0	0	3	0	0	0	0	0	0	281
115-23-009-D01	121	1	0	0	0	0	3	0	0	0	0	0	10	27	0	1	0	0	0	0	0	0	0	0	163
115-23-009-D02	152	0	1	0	0	0	3	0	0	0	1	0	11	26	0	0	0	0	0	1	0	0	0	0	195
115-23-009-N01	116	1	0	1	0	0	3	2	0	0	0	2	14	21	0	1	0	0	0	0	0	0	0	0	161
115-23-009-D03	126	0	1	0	0	0	0	0	0	6	0	0	9	22	1	0	0	0	0	0	0	0	0	0	165
115-23-009-D04	102	0	1	0	0	0	4	0	0	1	1	0	15	17	1	1	0	0	0	0	0	0	0	0	143
115-23-009-D05	76	0	0	0	0	0	3	1	0	0	1	0	11	12	0	0	0	1	0	0	0	0	0	0	105
115-23-009-D06	157	0	0	0	1	0	1	0	0	1	0	0	13	15	0	0	0	0	0	0	0	0	1	0	189
115-23-009-D07	197	1	0	0	0	1	1	2	0	2	1	0	23	26	0	0	0	0	0	0	0	0	1	0	255
115-23-009-E01	247	0	0	0	0	0	3	1	0	0	0	1	42	14	0	1	0	1	0	0	0	0	0	0	310
115-23-009-G01	202	4	3	0	2	3	5	3	0	0	0	0	7	20	1	0	0	0	0	0	0	0	2	0	252

115-23-009-G02	174	0	1	0	0	0	2	0	0	1	0	1	10	31	0	0	0	0	0	0	0	0	0	0	220
115-23-009-J01	88	0	2	0	0	0	2	0	0	1	0	0	11	9	0	1	0	0	0	0	0	0	0	0	114
115-23-009-K01	67	0	0	0	0	0	1	0	0	0	0	0	6	5	0	0	0	0	0	0	0	0	0	0	79
115-23-009-K02	196	0	1	0	0	0	3	0	0	1	3	0	17	48	0	1	0	2	0	0	0	0	0	0	272
115-23-009-K03	62	0	0	0	0	0	3	0	0	0	0	0	6	6	0	1	0	0	0	0	0	0	0	0	78
115-23-009-K04	268	0	1	0	0	1	1	1	0	5	0	0	70	39	3	0	0	2	0	0	0	1	0	1	393
112-22-200-A01	128	0	0	0	0	1	6	2	0	0	1	0	18	28	0	0	0	2	0	0	0	0	0	0	186
112-22-200-A02	156	3	0	0	0	0	3	0	0	2	0	0	19	31	0	0	0	2	0	0	0	0	0	0	216
112-22-200-B01	134	2	0	0	0	0	2	0	0	1	0	0	19	36	0	0	0	1	1	0	0	0	0	0	196
112-22-200-C01	117	1	0	0	0	0	3	0	0	2	0	0	16	38	3	0	0	0	0	0	0	0	0	0	180
112-22-200-C02	120	1	0	0	0	0	3	0	0	1	2	0	25	42	2	0	0	0	0	0	0	0	0	0	196
112-22-200-C03	105	0	0	0	0	3	1	0	0	1	0	0	17	37	2	1	0	0	0	0	0	0	0	0	167
112-22-201-A01	127	4	0	0	0	0	3	2	0	5	1	0	17	25	0	1	0	1	0	0	0	0	0	0	186
112-22-201-B01	141	3	1	0	0	1	1	0	0	4	2	1	39	21	0	0	0	1	0	0	0	0	0	0	215

Table 3: Simplified clast-lithology counts for 2022 and 2023 samples (2-8 mm size fraction), including major categories and distinctive lithologies. UGG = Undifferentiated greenstone and greywacke.

	2-8 mm (major categories)					2-8 mm (distinctive lithologies)						
Sample ID	**Hudson Bay Basin**	**Granitoid**	**UGG**	**Other**	**Total Sum**	**Shell fragment**	**Kenogami Fm**	**Dubawnt**	**Oolitic jasper**	**Shale**	**Sulphides**	**Wood**
115-23-002-A01	307	72	27	13	419	0	1	0	0	0	0	0
115-23-002-B01	382	55	23	12	472	0	0	0	0	0	1	0
115-23-002-B02	339	59	40	10	448	0	0	1	0	0	0	0
115-23-002-B03	660	67	90	28	845	0	1	0	0	1	0	0
115-23-002-C01	409	37	38	22	506	0	0	0	0	0	0	1
115-23-002-C02	576	77	30	16	699	0	0	0	0	0	0	0
115-23-002-C03	399	43	54	17	513	0	0	0	0	0	0	1
115-23-002-C04	406	43	68	18	535	0	0	0	0	0	0	0
115-23-002-D01	400	57	23	14	494	0	5	0	0	0	1	0
115-23-002-D02	473	56	21	24	574	0	0	0	0	0	0	0
115-23-002-D03	418	83	23	21	545	0	0	1	0	0	0	0
115-23-002-D04	422	78	22	15	537	1	0	0	0	0	4	0
115-23-002-H01	281	52	18	14	365	1	0	0	0	0	0	0
115-23-002-Z01	238	51	17	11	317	0	0	0	0	0	1	0
115-23-003-A01	319	36	55	16	426	0	0	0	0	0	0	0
115-23-003-A02	364	36	41	12	453	0	1	1	0	1	0	0
115-23-003-A03	457	46	59	15	577	0	0	0	0	0	1	0
115-23-003-B01	468	50	67	13	598	0	3	0	0	1	0	0
115-23-003-B02	448	61	43	15	567	0	3	0	0	1	0	0
115-23-003-D01	428	131	82	24	665	0	3	1	1	0	0	0
115-23-003-D02	265	109	50	16	440	0	0	0	2	0	0	0
115-23-003-D03	296	65	47	16	424	0	1	0	1	0	0	0
115-23-003-D04	398	108	43	27	576	0	5	2	0	0	0	0
115-23-003-L01	355	88	45	18	506	0	0	0	1	0	0	0
115-23-004-B01	320	59	23	11	413	0	0	0	0	0	0	0

115-23-005-B01	424	71	35	9	539	0	2	0	0	0	0	0
115-23-005-B02	333	45	29	7	414	0	0	0	0	0	1	0
115-23-005-B03	382	45	25	15	467	3	0	0	1	2	0	0
115-23-005-B04	434	59	23	12	528	1	1	0	0	0	2	0
115-23-005-B05	297	54	18	14	383	0	0	0	1	0	0	0
115-23-005-Z01	309	58	21	10	398	0	0	0	0	0	0	0
115-23-005-C01	324	64	16	8	412	0	0	0	0	0	0	0
115-23-005-O01	335	52	44	12	443	0	0	0	0	0	4	0
115-23-005-P01	217	54	77	26	374	0	0	0	0	0	0	0
115-23-006-X01	274	68	24	23	389	1	0	0	2	0	0	0
115-23-006-A01	377	106	20	12	515	0	10	1	0	0	1	0
115-23-006-B01	341	95	62	23	521	0	0	0	1	0	2	1
115-23-006-B02	506	84	98	25	713	0	10	0	1	0	1	0
115-23-006-C01	448	101	57	20	626	1	0	3	1	0	1	0
115-23-006-C02	277	78	33	21	409	1	0	1	0	0	0	0
115-23-006-C03	432	54	33	11	530	1	4	0	0	0	1	0
115-23-006-D01	449	48	29	23	549	0	1	1	0	0	0	0
115-23-007-A01	336	80	23	16	455	0	0	0	0	0	0	0
115-23-007-B01	216	71	20	8	315	0	0	0	0	0	0	1
115-23-007-B02	413	96	18	20	547	1	0	0	0	0	1	0
115-23-007-C01	379	85	29	26	519	1	0	5	0	0	0	0
115-23-007-C02	346	65	31	22	464	0	0	0	0	0	4	0
115-23-007-C03	325	71	41	20	457	0	0	0	0	0	0	0
115-23-007-C04	419	85	29	21	554	0	2	0	0	0	0	0
115-23-007-C05	290	59	32	18	399	0	0	0	0	1	0	0
115-23-007-D01	462	91	62	26	641	0	0	0	0	0	2	0
115-23-007-D02	424	42	43	19	528	0	0	0	0	0	1	0
115-23-007-D03	447	44	37	15	543	0	0	0	0	0	2	0
115-23-007-D04	394	48	45	6	493	0	0	0	0	0	0	0
115-23-007-D05	325	31	62	11	429	0	0	0	0	2	0	0

115-23-007-D06	394	49	61	5	509	0	1	0	0	0	2	0
115-23-007-D07	429	42	77	10	558	0	0	0	0	1	0	0
115-23-007-E01	343	68	15	10	436	0	2	0	0	0	0	1
115-23-007-E02	314	74	19	15	422	0	0	0	0	0	1	0
115-23-007-E03	473	95	61	25	654	0	1	0	0	0	3	1
115-23-007-GRAV1	560	83	63	41	747	0	0	0	0	0	0	0
115-23-007-GRAV2	506	88	94	50	738	0	0	0	0	0	0	0
115-23-008-A01	341	97	51	25	514	0	4	0	2	0	0	0
115-23-008-B01	399	85	65	25	574	1	4	2	0	0	0	0
115-23-008-C01	410	100	51	18	579	0	2	2	0	0	0	0
115-23-008-F01	360	102	43	19	524	0	2	0	0	0	0	0
115-23-008-F02	327	93	48	11	479	0	2	0	1	0	0	0
115-23-008-F03	350	130	44	25	549	0	1	1	0	0	0	0
115-23-008-F04	412	112	51	23	598	0	4	0	0	0	3	0
115-23-009-B01	432	53	98	14	597	0	0	0	0	0	0	0
115-23-009-C01	451	64	91	13	619	0	1	0	0	0	0	0
115-23-009-D01	377	82	29	13	501	0	0	0	0	0	0	1
115-23-009-D02	374	73	28	13	488	0	0	1	0	0	0	0
115-23-009-N01	336	96	38	23	493	2	0	0	0	0	0	1
115-23-009-D03	328	84	31	27	470	1	0	0	0	1	2	0
115-23-009-D04	294	65	45	15	419	0	0	0	0	0	0	0
115-23-009-D05	256	54	30	16	356	1	0	0	1	0	0	0
115-23-009-D06	438	42	35	12	527	0	0	0	0	0	1	0
115-23-009-D07	408	55	41	12	516	0	3	0	0	0	1	0
115-23-009-E01	454	37	74	12	577	0	0	0	0	0	0	0
115-23-009-G01	442	55	13	15	525	0	6	0	0	1	2	0
115-23-009-G02	419	88	30	22	559	0	0	0	0	0	0	0
115-23-009-J01	286	62	32	19	399	0	0	0	0	0	0	0

115-23-009-K01	288	51	23	7	369	0	0	0	0	0	0	0
115-23-009-K02	388	107	36	16	547	0	0	0	0	0	0	0
115-23-009-K03	306	67	28	15	416	0	0	0	0	0	0	0
115-23-009-K04	532	87	132	31	782	0	1	0	1	1	0	2
112-22-200-A01	291	71	41	18	421	0	2	0	0	0	0	0
112-22-200-A02	350	81	41	16	488	0	3	0	0	0	0	0
112-22-200-B01	362	91	64	15	532	0	0	0	0	0	0	0
112-22-200-C01	261	121	39	10	431	0	6	0	0	0	0	0
112-22-200-C02	319	118	52	12	501	0	7	0	0	0	0	0
112-22-200-C03	292	134	48	16	490	0	5	0	0	0	0	0
112-22-201-A01	354	79	46	21	500	0	3	0	0	0	0	0
112-22-201-B01	346	72	101	16	535	0	4	1	0	0	0	0

Table 4: Simplified clast-lithology proportions for 2022 and 2023 samples (2-8 mm size fraction), including major categories and distinctive lithologies. UGG = Undifferentiated greenstone and greywacke; ct% = count percentage.

	2-8 mm ct% (major categories)				2-8 mm ct% (distinctive lithologies)						
Sample ID	**Hudson Bay Basin**	**Granitoid**	**UGG**	**Other**	**Shell fragment**	**Kenogami Fm**	**Dubawnt**	**Oolitic jasper**	**Shale**	**Sulphides**	**Wood**
115-23-002-A01	73.3	17.2	6.4	3.1	0.00	0.24	0.00	0.00	0.00	0.00	0.00
115-23-002-B01	80.9	11.7	4.9	2.5	0.00	0.00	0.00	0.00	0.00	0.21	0.00
115-23-002-B02	75.7	13.2	8.9	2.2	0.00	0.00	0.22	0.00	0.00	0.00	0.00
115-23-002-B03	78.1	7.9	10.7	3.3	0.00	0.12	0.00	0.00	0.12	0.00	0.00
115-23-002-C01	80.8	7.3	7.5	4.3	0.00	0.00	0.00	0.00	0.00	0.00	0.20
115-23-002-C02	82.4	11.0	4.3	2.3	0.00	0.00	0.00	0.00	0.00	0.00	0.00
115-23-002-C03	77.8	8.4	10.5	3.3	0.00	0.00	0.00	0.00	0.00	0.00	0.19
115-23-002-C04	75.9	8.0	12.7	3.4	0.00	0.00	0.00	0.00	0.00	0.00	0.00
115-23-002-D01	81.0	11.5	4.7	2.8	0.00	1.01	0.00	0.00	0.00	0.20	0.00
115-23-002-D02	82.4	9.8	3.7	4.2	0.00	0.00	0.00	0.00	0.00	0.00	0.00
115-23-002-D03	76.7	15.2	4.2	3.9	0.00	0.00	0.18	0.00	0.00	0.00	0.00
115-23-002-D04	78.6	14.5	4.1	2.8	0.19	0.00	0.00	0.00	0.00	0.74	0.00
115-23-002-H01	77.0	14.2	4.9	3.8	0.27	0.00	0.00	0.00	0.00	0.00	0.00
115-23-002-Z01	75.1	16.1	5.4	3.5	0.00	0.00	0.00	0.00	0.00	0.32	0.00
115-23-003-A01	74.9	8.5	12.9	3.8	0.00	0.00	0.00	0.00	0.00	0.00	0.00
115-23-003-A02	80.4	7.9	9.1	2.6	0.00	0.22	0.22	0.00	0.22	0.00	0.00
115-23-003-A03	79.2	8.0	10.2	2.6	0.00	0.00	0.00	0.00	0.00	0.17	0.00
115-23-003-B01	78.3	8.4	11.2	2.2	0.00	0.50	0.00	0.00	0.17	0.00	0.00
115-23-003-B02	79.0	10.8	7.6	2.6	0.00	0.53	0.00	0.00	0.18	0.00	0.00
115-23-003-D01	64.4	19.7	12.3	3.6	0.00	0.45	0.15	0.15	0.00	0.00	0.00
115-23-003-D02	60.2	24.8	11.4	3.6	0.00	0.00	0.00	0.45	0.00	0.00	0.00
115-23-003-D03	69.8	15.3	11.1	3.8	0.00	0.24	0.00	0.24	0.00	0.00	0.00
115-23-003-D04	69.1	18.8	7.5	4.7	0.00	0.87	0.35	0.00	0.00	0.00	0.00
115-23-003-L01	70.2	17.4	8.9	3.6	0.00	0.00	0.00	0.20	0.00	0.00	0.00
115-23-004-B01	77.5	14.3	5.6	2.7	0.00	0.00	0.00	0.00	0.00	0.00	0.00
115-23-005-B01	78.7	13.2	6.5	1.7	0.00	0.37	0.00	0.00	0.00	0.00	0.00

115-23-005-B02	80.4	10.9	7.0	1.7	0.00	0.00	0.00	0.00	0.00	0.24	0.00
115-23-005-B03	81.8	9.6	5.4	3.2	0.64	0.00	0.00	0.21	0.43	0.00	0.00
115-23-005-B04	82.2	11.2	4.4	2.3	0.19	0.19	0.00	0.00	0.00	0.38	0.00
115-23-005-B05	77.5	14.1	4.7	3.7	0.00	0.00	0.00	0.26	0.00	0.00	0.00
115-23-005-Z01	77.6	14.6	5.3	2.5	0.00	0.00	0.00	0.00	0.00	0.00	0.00
115-23-005-C01	78.6	15.5	3.9	1.9	0.00	0.00	0.00	0.00	0.00	0.00	0.00
115-23-005-O01	75.6	11.7	9.9	2.7	0.00	0.00	0.00	0.00	0.00	0.90	0.00
115-23-005-P01	58.0	14.4	20.6	7.0	0.00	0.00	0.00	0.00	0.00	0.00	0.00
115-23-006-X01	70.4	17.5	6.2	5.9	0.26	0.00	0.00	0.51	0.00	0.00	0.00
115-23-006-A01	73.2	20.6	3.9	2.3	0.00	1.94	0.19	0.00	0.00	0.19	0.00
115-23-006-B01	65.5	18.2	11.9	4.4	0.00	0.00	0.00	0.19	0.00	0.38	0.19
115-23-006-B02	71.0	11.8	13.7	3.5	0.00	1.40	0.00	0.14	0.00	0.14	0.00
115-23-006-C01	71.6	16.1	9.1	3.2	0.16	0.00	0.48	0.16	0.00	0.16	0.00
115-23-006-C02	67.7	19.1	8.1	5.1	0.24	0.00	0.24	0.00	0.00	0.00	0.00
115-23-006-C03	81.5	10.2	6.2	2.1	0.19	0.75	0.00	0.00	0.00	0.19	0.00
115-23-006-D01	81.8	8.7	5.3	4.2	0.00	0.18	0.18	0.00	0.00	0.00	0.00
115-23-007-A01	73.8	17.6	5.1	3.5	0.00	0.00	0.00	0.00	0.00	0.00	0.00
115-23-007-B01	68.6	22.5	6.3	2.5	0.00	0.00	0.00	0.00	0.00	0.00	0.32
115-23-007-B02	75.5	17.6	3.3	3.7	0.18	0.00	0.00	0.00	0.00	0.18	0.00
115-23-007-C01	73.0	16.4	5.6	5.0	0.19	0.00	0.96	0.00	0.00	0.00	0.00
115-23-007-C02	74.6	14.0	6.7	4.7	0.00	0.00	0.00	0.00	0.00	0.86	0.00
115-23-007-C03	71.1	15.5	9.0	4.4	0.00	0.00	0.00	0.00	0.00	0.00	0.00
115-23-007-C04	75.6	15.3	5.2	3.8	0.00	0.36	0.00	0.00	0.00	0.00	0.00
115-23-007-C05	72.7	14.8	8.0	4.5	0.00	0.00	0.00	0.00	0.25	0.00	0.00
115-23-007-D01	72.1	14.2	9.7	4.1	0.00	0.00	0.00	0.00	0.00	0.31	0.00
115-23-007-D02	80.3	8.0	8.1	3.6	0.00	0.00	0.00	0.00	0.00	0.19	0.00
115-23-007-D03	82.3	8.1	6.8	2.8	0.00	0.00	0.00	0.00	0.00	0.37	0.00
115-23-007-D04	79.9	9.7	9.1	1.2	0.00	0.00	0.00	0.00	0.00	0.00	0.00
115-23-007-D05	75.8	7.2	14.5	2.6	0.00	0.00	0.00	0.00	0.47	0.00	0.00
115-23-007-D06	77.4	9.6	12.0	1.0	0.00	0.20	0.00	0.00	0.00	0.39	0.00

115-23-007-D07	76.9	7.5	13.8	1.8	0.00	0.00	0.00	0.00	0.18	0.00	0.00
115-23-007-E01	78.7	15.6	3.4	2.3	0.00	0.46	0.00	0.00	0.00	0.00	0.23
115-23-007-E02	74.4	17.5	4.5	3.6	0.00	0.00	0.00	0.00	0.00	0.24	0.00
115-23-007-E03	72.3	14.5	9.3	3.8	0.00	0.15	0.00	0.00	0.00	0.46	0.15
115-23-007-GRAV1	75.0	11.1	8.4	5.5	0.00	0.00	0.00	0.00	0.00	0.00	0.00
115-23-007-GRAV2	68.6	11.9	12.7	6.8	0.00	0.00	0.00	0.00	0.00	0.00	0.00
115-23-008-A01	66.3	18.9	9.9	4.9	0.00	0.78	0.00	0.39	0.00	0.00	0.00
115-23-008-B01	69.5	14.8	11.3	4.4	0.17	0.70	0.35	0.00	0.00	0.00	0.00
115-23-008-C01	70.8	17.3	8.8	3.1	0.00	0.35	0.35	0.00	0.00	0.00	0.00
115-23-008-F01	68.7	19.5	8.2	3.6	0.00	0.38	0.00	0.00	0.00	0.00	0.00
115-23-008-F02	68.3	19.4	10.0	2.3	0.00	0.42	0.00	0.21	0.00	0.00	0.00
115-23-008-F03	63.8	23.7	8.0	4.6	0.00	0.18	0.18	0.00	0.00	0.00	0.00
115-23-008-F04	68.9	18.7	8.5	3.8	0.00	0.67	0.00	0.00	0.00	0.50	0.00
115-23-009-B01	72.4	8.9	16.4	2.3	0.00	0.00	0.00	0.00	0.00	0.00	0.00
115-23-009-C01	72.9	10.3	14.7	2.1	0.00	0.16	0.00	0.00	0.00	0.00	0.00
115-23-009-D01	75.2	16.4	5.8	2.6	0.00	0.00	0.00	0.00	0.00	0.00	0.20
115-23-009-D02	76.6	15.0	5.7	2.7	0.00	0.00	0.20	0.00	0.00	0.00	0.00
115-23-009-N01	68.2	19.5	7.7	4.7	0.41	0.00	0.00	0.00	0.00	0.00	0.20
115-23-009-D03	69.8	17.9	6.6	5.7	0.21	0.00	0.00	0.00	0.21	0.43	0.00
115-23-009-D04	70.2	15.5	10.7	3.6	0.00	0.00	0.00	0.00	0.00	0.00	0.00
115-23-009-D05	71.9	15.2	8.4	4.5	0.28	0.00	0.00	0.28	0.00	0.00	0.00
115-23-009-D06	83.1	8.0	6.6	2.3	0.00	0.00	0.00	0.00	0.00	0.19	0.00
115-23-009-D07	79.1	10.7	7.9	2.3	0.00	0.58	0.00	0.00	0.00	0.19	0.00
115-23-009-E01	78.7	6.4	12.8	2.1	0.00	0.00	0.00	0.00	0.00	0.00	0.00
115-23-009-G01	84.2	10.5	2.5	2.9	0.00	1.14	0.00	0.00	0.19	0.38	0.00
115-23-009-G02	75.0	15.7	5.4	3.9	0.00	0.00	0.00	0.00	0.00	0.00	0.00
115-23-009-J01	71.7	15.5	8.0	4.8	0.00	0.00	0.00	0.00	0.00	0.00	0.00
115-23-009-K01	78.0	13.8	6.2	1.9	0.00	0.00	0.00	0.00	0.00	0.00	0.00

115-23-009-K02	70.9	19.6	6.6	2.9	0.00	0.00	0.00	0.00	0.00	0.00	0.00
115-23-009-K03	73.6	16.1	6.7	3.6	0.00	0.00	0.00	0.00	0.00	0.00	0.00
115-23-009-K04	68.0	11.1	16.9	4.0	0.00	0.13	0.00	0.13	0.13	0.00	0.26
112-22-200-A01	69.1	16.9	9.7	4.3	0.00	0.48	0.00	0.00	0.00	0.00	0.00
112-22-200-A02	71.7	16.6	8.4	3.3	0.00	0.61	0.00	0.00	0.00	0.00	0.00
112-22-200-B01	68.0	17.1	12.0	2.8	0.00	0.00	0.00	0.00	0.00	0.00	0.00
112-22-200-C01	60.6	28.1	9.0	2.3	0.00	1.39	0.00	0.00	0.00	0.00	0.00
112-22-200-C02	63.7	23.6	10.4	2.4	0.00	1.40	0.00	0.00	0.00	0.00	0.00
112-22-200-C03	59.6	27.3	9.8	3.3	0.00	1.02	0.00	0.00	0.00	0.00	0.00
112-22-201-A01	70.8	15.8	9.2	4.2	0.00	0.60	0.00	0.00	0.00	0.00	0.00
112-22-201-B01	64.7	13.5	18.9	3.0	0.00	0.75	0.19	0.00	0.00	0.00	0.00
112-19-628-B01	61.1	13.4	25.5	0.0	0.00	0.00	0.00	0.00	0.00	0.00	0.00
112-19-628-D01	77.8	13.7	5.2	3.3	0.00	0.00	0.00	0.00	0.00	0.37	0.00
112-19-628-D02	82.5	10.2	6.6	0.6	0.00	0.83	0.00	0.00	0.00	0.00	0.00
112-19-628-D03	73.1	19.8	3.4	3.7	0.00	8.58	0.00	0.00	0.00	0.00	0.00
112-19-628-D04	76.0	16.7	4.3	3.0	0.00	0.00	0.00	0.00	0.00	0.00	0.00
112-19-628-D05	82.8	9.9	5.9	1.3	0.00	0.00	0.00	0.00	0.00	0.00	0.00
112-19-629-A01	65.9	15.0	17.5	1.7	0.00	0.62	0.00	0.00	0.00	0.00	0.00
112-19-629-C01	64.0	11.0	22.6	2.4	0.00	0.30	0.00	0.30	0.00	0.00	0.00

Table 5: Normalized clast-lithology proportions of major categories for 2022 and 2023 samples (2-8 mm size fraction). UGG = Undifferentiated greenstone and greywacke; ct% = count percentage.

	2-8 mm ct% (major categories, normalized to exclude other clasts)		
Sample ID	**Hudson Bay Basin**	**Granitoid**	**UGG**
115-23-002-A01	75.6	17.7	6.7
115-23-002-B01	83.0	12.0	5.0
115-23-002-B02	77.4	13.5	9.1
115-23-002-B03	80.8	8.2	11.0
115-23-002-C01	84.5	7.6	7.9
115-23-002-C02	84.3	11.3	4.4
115-23-002-C03	80.4	8.7	10.9
115-23-002-C04	78.5	8.3	13.2
115-23-002-D01	83.3	11.9	4.8
115-23-002-D02	86.0	10.2	3.8
115-23-002-D03	79.8	15.8	4.4
115-23-002-D04	80.8	14.9	4.2
115-23-002-H01	80.1	14.8	5.1
115-23-002-Z01	77.8	16.7	5.6
115-23-003-A01	77.8	8.8	13.4
115-23-003-A02	82.5	8.2	9.3
115-23-003-A03	81.3	8.2	10.5
115-23-003-B01	80.0	8.5	11.5
115-23-003-B02	81.2	11.1	7.8
115-23-003-D01	66.8	20.4	12.8
115-23-003-D02	62.5	25.7	11.8
115-23-003-D03	72.5	15.9	11.5
115-23-003-D04	72.5	19.7	7.8

115-23-003-L01	72.7	18.0	9.2
115-23-004-B01	79.6	14.7	5.7
115-23-005-B01	80.0	13.4	6.6
115-23-005-B02	81.8	11.1	7.1
115-23-005-B03	84.5	10.0	5.5
115-23-005-B04	84.1	11.4	4.5
115-23-005-B05	80.5	14.6	4.9
115-23-005-Z01	79.6	14.9	5.4
115-23-005-C01	80.2	15.8	4.0
115-23-005-O01	77.7	12.1	10.2
115-23-005-P01	62.4	15.5	22.1
115-23-006-X01	74.9	18.6	6.6
115-23-006-A01	75.0	21.1	4.0
115-23-006-B01	68.5	19.1	12.4
115-23-006-B02	73.5	12.2	14.2
115-23-006-C01	73.9	16.7	9.4
115-23-006-C02	71.4	20.1	8.5
115-23-006-C03	83.2	10.4	6.4
115-23-006-D01	85.4	9.1	5.5
115-23-007-A01	76.5	18.2	5.2
115-23-007-B01	70.4	23.1	6.5
115-23-007-B02	78.4	18.2	3.4
115-23-007-C01	76.9	17.2	5.9
115-23-007-C02	78.3	14.7	7.0
115-23-007-C03	74.4	16.2	9.4
115-23-007-C04	78.6	15.9	5.4

115-23-007-C05	76.1	15.5	8.4
115-23-007-D01	75.1	14.8	10.1
115-23-007-D02	83.3	8.3	8.4
115-23-007-D03	84.7	8.3	7.0
115-23-007-D04	80.9	9.9	9.2
115-23-007-D05	77.8	7.4	14.8
115-23-007-D06	78.2	9.7	12.1
115-23-007-D07	78.3	7.7	14.1
115-23-007-E01	80.5	16.0	3.5
115-23-007-E02	77.1	18.2	4.7
115-23-007-E03	75.2	15.1	9.7
115-23-007-GRAV1	79.3	11.8	8.9
115-23-007-GRAV2	73.5	12.8	13.7
115-23-008-A01	69.7	19.8	10.4
115-23-008-B01	72.7	15.5	11.8
115-23-008-C01	73.1	17.8	9.1
115-23-008-F01	71.3	20.2	8.5
115-23-008-F02	69.9	19.9	10.3
115-23-008-F03	66.8	24.8	8.4
115-23-008-F04	71.7	19.5	8.9
115-23-009-B01	74.1	9.1	16.8
115-23-009-C01	74.4	10.6	15.0
115-23-009-D01	77.3	16.8	5.9
115-23-009-D02	78.7	15.4	5.9
115-23-009-N01	71.5	20.4	8.1
115-23-009-D03	74.0	19.0	7.0

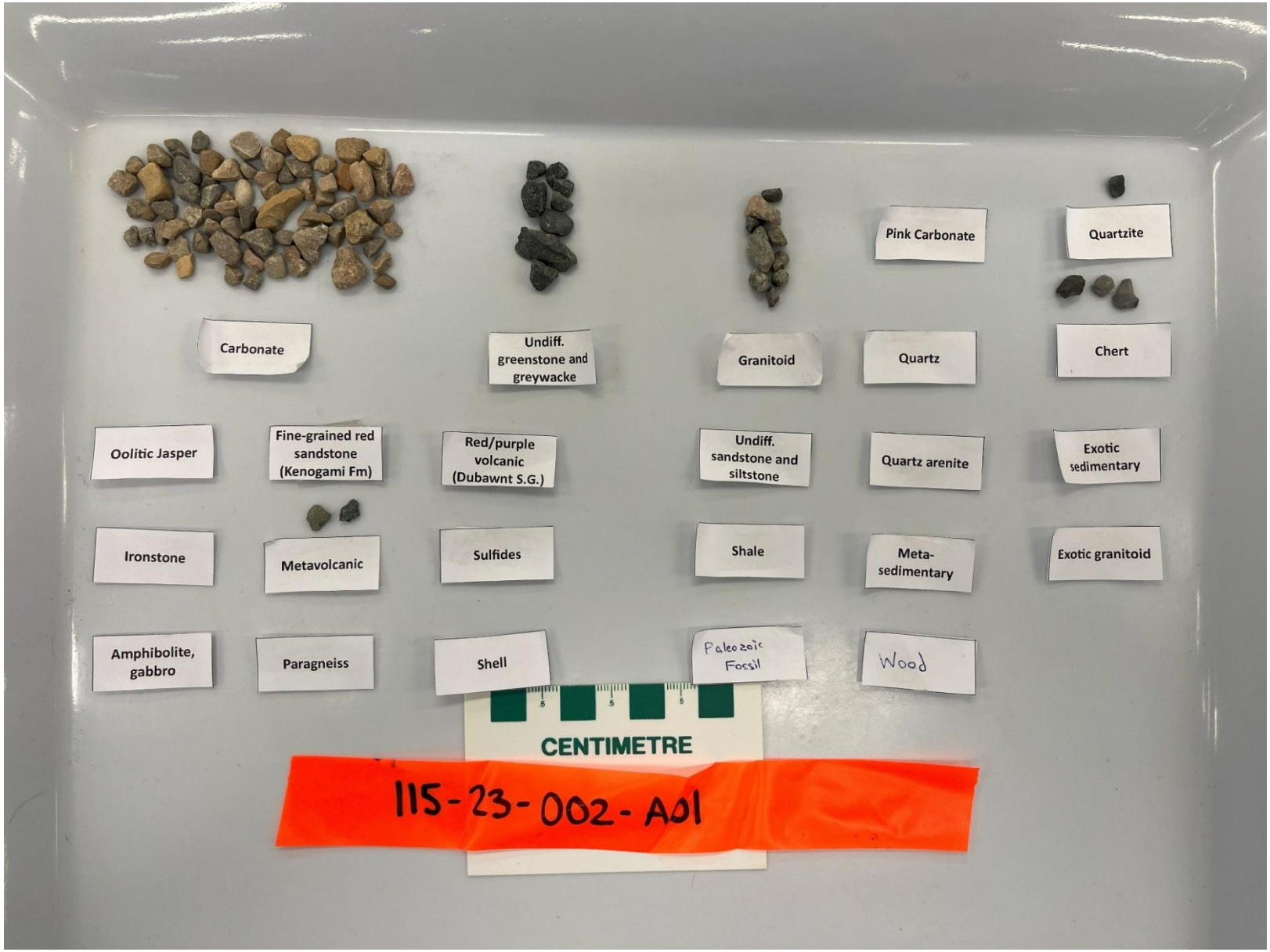
115-23-009-D04	72.8	16.1	11.1
115-23-009-D05	75.3	15.9	8.8
115-23-009-D06	85.0	8.2	6.8
115-23-009-D07	81.0	10.9	8.1
115-23-009-E01	80.4	6.5	13.1
115-23-009-G01	86.7	10.8	2.5
115-23-009-G02	78.0	16.4	5.6
115-23-009-J01	75.3	16.3	8.4
115-23-009-K01	79.6	14.1	6.4
115-23-009-K02	73.1	20.2	6.8
115-23-009-K03	76.3	16.7	7.0
115-23-009-K04	70.8	11.6	17.6
112-22-200-A01	72.2	17.6	10.2
112-22-200-A02	74.2	17.2	8.7
112-22-200-B01	70.0	17.6	12.4
112-22-200-C01	62.0	28.7	9.3
112-22-200-C02	65.2	24.1	10.6
112-22-200-C03	61.6	28.3	10.1
112-22-201-A01	73.9	16.5	9.6
112-22-201-B01	66.7	13.9	19.5
112-19-628-B01	61.1	13.4	25.5
112-19-628-D01	80.5	14.2	5.4
112-19-628-D02	83.0	10.3	6.7
112-19-628-D03	76.0	20.5	3.5
112-19-628-D04	78.4	17.2	4.5
112-19-628-D05	83.9	10.0	6.0

112-19-629-A01	67.0	15.2	17.8
112-19-629-C01	65.6	11.3	23.1

Pictures of sorted clast counts

115-23-002

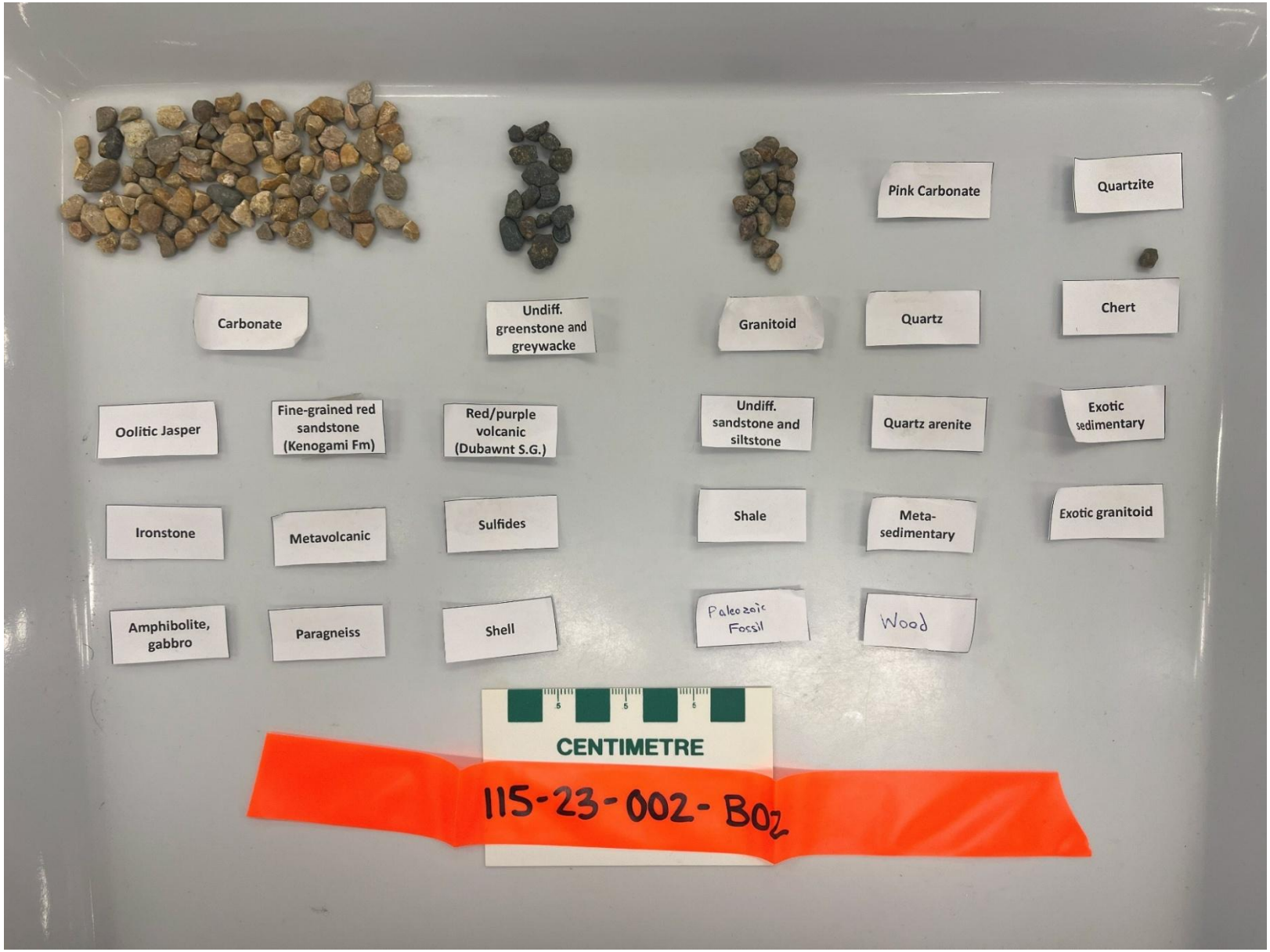



Carbonate
Undiff. greenstone and greywacke
Granitoid
Pink Carbonate
Quartzite
Quartz
Chert
Oolitic Jasper
Fine-grained red sandstone (Kenogami Fm)
Red/purple volcanic (Dubawnt S.G.)
Undiff. sandstone and siltstone
Quartz arenite
Exotic sedimentary
Ironstone
Metavolcanic
Sulfides
Shale
Meta-sedimentary
Exotic granitoid
Amphibolite, gabbro
Paragneiss
Shell
Paleozoic Fossil
Wood
CENTIMETRE
115-23-002-A01


Carbonate
Undiff. greenstone and greywacke
Granitoid
Pink Carbonate
Quartzite
Quartz
Chert
Oolitic Jasper
Fine-grained red sandstone (Kenogami Fm)
Red/purple volcanic (Dubawnt S.G.)
Undiff. sandstone and siltstone
Quartz arenite
Exotic sedimentary
Ironstone
Metavolcanic
Sulfides
Shale
Meta-sedimentary
Exotic granitoid
Amphibolite, gabbro
Paragneiss
Shell
Paleozoic Fossil
Wood
CENTIMETRE
115-23-002-B01


Carbonate
Undiff. greenstone and greywacke
Granitoid
Pink Carbonate
Quartzite
Chert
Quartz
Oolitic Jasper
Fine-grained red sandstone (Kenogami Fm)
Red/purple volcanic (Dubawnt S.G.)
Undiff. sandstone and siltstone
Quartz arenite
Exotic sedimentary
Ironstone
Metavolcanic
Sulfides
Shale
Meta-sedimentary
Exotic granitoid
Amphibolite, gabbro
Paragneiss
Shell
Paleozoic Fossil
Wood
CENTIMETRE
115-23-002-B01


Carbonate
Undiff. greenstone and greywacke
Granitoid
Pink Carbonate
Quartzite
Quartz
Chert
Oolitic Jasper
Fine-grained red sandstone (Kenogami Fm)
Red/purple volcanic (Dubawnt S.G.)
Undiff. sandstone and siltstone
Quartz arenite
Exotic sedimentary
Ironstone
Metavolcanic
Sulfides
Shale
Meta-sedimentary
Exotic granitoid
Amphibolite, gabbro
Paragneiss
Shell
Paleozoic Fossil
Wood
CENTIMETRE
115-23-002-B02


Carbonate
Undiff. greenstone and greywacke
Granitoid
Pink Carbonate
Quartzite
Quartz
Chert
Oolitic Jasper
Fine-grained red sandstone (Kenogami Fm)
Red/purple volcanic (Dubawnt S.G.)
Undiff. sandstone and siltstone
Quartz arenite
Exotic sedimentary
Ironstone
Metavolcanic
Sulfides
Shale
Meta-sedimentary
Exotic granitoid
Amphibolite, gabbro
Paragneiss
Shell
Paleozoic Fossil
Wood
CENTIMETRE
115-23-002-B02


Carbonate
Undiff. greenstone and greywacke
Granitoid
Pink Carbonate
Quartzite
Quartz
Chert
Oolitic Jasper
Fine-grained red sandstone (Kenogami Fm)
Red/purple volcanic (Dubawnt S.G.)
Undiff. sandstone and siltstone
Quartz arenite
Exotic sedimentary
Ironstone
Metavolcanic
Sulfides
Shale
Meta-sedimentary
Exotic granitoid
MGS:Gauthier
115-23-002-B03
2.0-4.0 mm
Amphibolite, gabbro
Paragneiss
Shell
Paleozoic Fossil
Wood
CENTIMETRE


Carbonate
Undiff. greenstone and greywacke
Granitoid
Pink Carbonate
Oolitic Jasper
Fine-grained red sandstone (Kenogami Fm)
Red/purple volcanic (Dubawnt S.G.)
Quartz
Quartzite
Chert
Ironstone
Metavolcanic
Sulfides
Undiff. sandstone and siltstone
Quartz arenite
Exotic sedimentary
MGS:Gauthier
115-23-002-B03
4.0-8.0 mm
Amphibolite, gabbro
Paragneiss
Shell
Shale
Meta-sedimentary
Exotic granitoid
CENTIMETRE


Carbonate
Undiff. greenstone and greywacke
Granitoid
Pink Carbonate
Quartzite
Quartz
Chert
Undiff. sandstone and siltstone
Quartz arenite
Exotic sedimentary
Oolitic Jasper
Fine-grained red sandstone (Kenogami Fm)
Red/purple volcanic (Dubawnt S.G.)
Shale
Meta-sedimentary
Exotic granitoid
Ironstone
Metavolcanic
Sulfides
Paleozoic Fossil
Wood
Amphibolite, gabbro
Paragneiss
Shell
CENTIMETRE
115-23-002-C01


Carbonate
Undiff. greenstone and greywacke
Granitoid
Pink Carbonate
Quartzite
Quartz
Chert
Oolitic Jasper
Fine-grained red sandstone (Kenogami Fm)
Red/purple volcanic (Dubawnt S.G.)
Undiff. sandstone and siltstone
Quartz arenite
Exotic sedimentary
Ironstone
Metavolcanic
Sulfides
Shale
Meta-sedimentary
Exotic granitoid
Amphibolite, gabbro
Paragneiss
Shell
Paleozoic Fossil
Wood
CENTIMETRE
115-23-002-C01

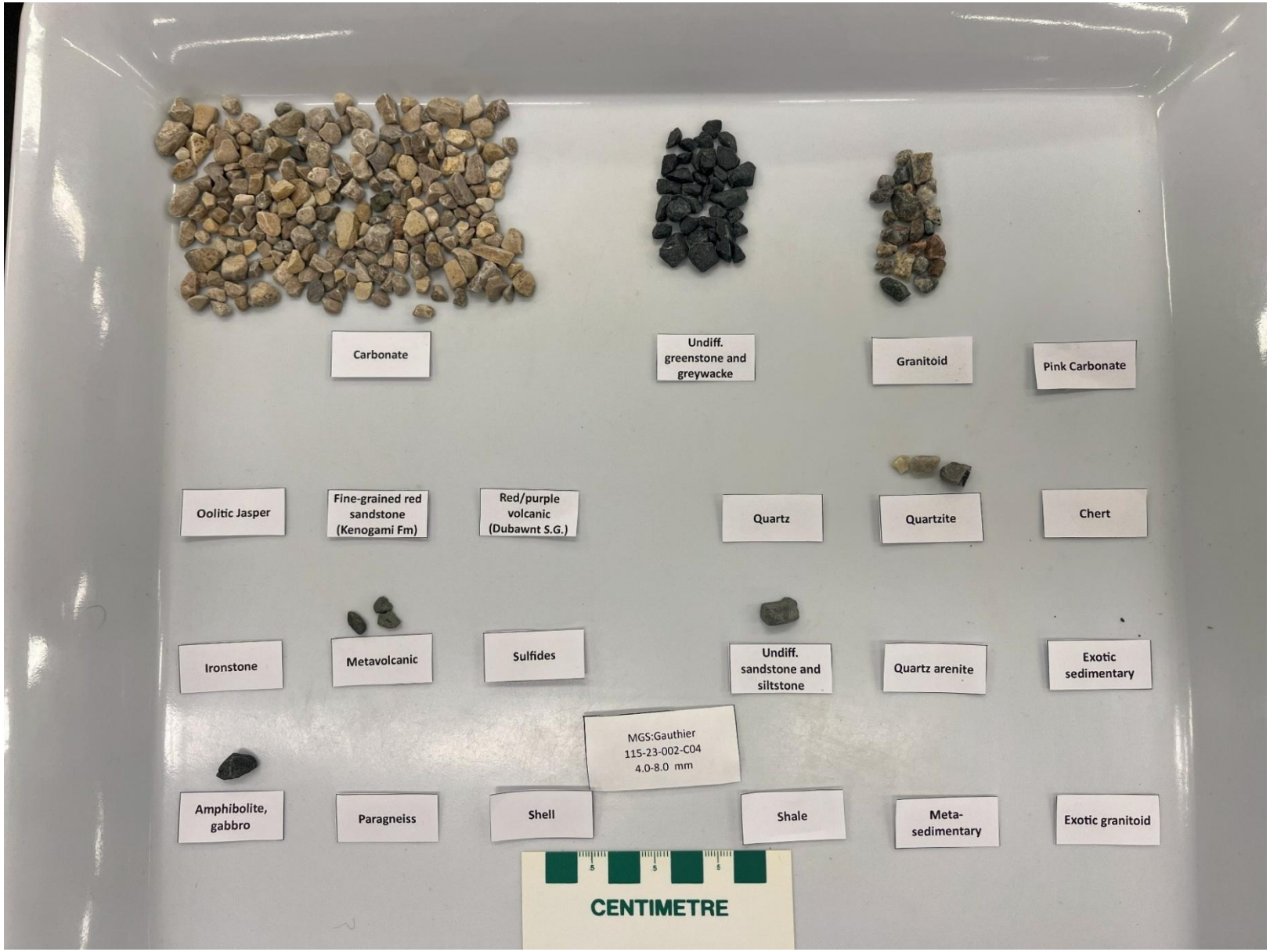

Carbonate
Undiff. greenstone and greywacke
Granitoid
Pink Carbonate
Quartzite
Quartz
Chert
Oolitic Jasper
Fine-grained red sandstone (Kenogami Fm)
Red/purple volcanic (Dubawnt S.G.)
Undiff. sandstone and siltstone
Quartz arenite
Exotic sedimentary
Ironstone
Metavolcanic
Sulfides
Shale
Meta-sedimentary
Exotic granitoid
MGS:Gauthier
115-23-002-C02
2.0-4.0 mm
Amphibolite, gabbro
Paragneiss
Shell
Paleozoic Fossil
Wood
CENTIMETRE


Carbonate
Undiff. greenstone and greywacke
Granitoid
Pink Carbonate
Oolitic Jasper
Fine-grained red sandstone (Kenogami Fm)
Red/purple volcanic (Dubawnt S.G.)
Quartz
Quartzite
Chert
Ironstone
Metavolcanic
Sulfides
Undiff. sandstone and siltstone
Quartz arenite
Exotic sedimentary
MGS:Gauthier
115-23-002-C02
4.0-8.0 mm
Amphibolite, gabbro
Paragneiss
Shell
Shale
Meta-sedimentary
Exotic granitoid
CENTIMETRE
Paleozoic Fossil


Carbonate
Undiff. greenstone and greywacke
Granitoid
Pink Carbonate
Quartzite
Quartz
Chert
Oolitic Jasper
Fine-grained red sandstone (Kenogami Fm)
Red/purple volcanic (Dubawnt S.G.)
Undiff. sandstone and siltstone
Quartz arenite
Exotic sedimentary
Ironstone
Metavolcanic
Sulfides
Shale
Meta-sedimentary
Exotic granitoid
Amphibolite, gabbro
Paragneiss
Shell
Paleozoic Fossil
Wood
CENTIMETRE
115-23-002-C03


Carbonate
Undiff. greenstone and greywacke
Granitoid
Pink Carbonate
Quartzite
Quartz
Chert
Oolitic Jasper
Fine-grained red sandstone (Kenogami Fm)
Red/purple volcanic (Dubawnt S.G.)
Undiff. sandstone and siltstone
Quartz arenite
Exotic sedimentary
Ironstone
Metavolcanic
Sulfides
Shale
Meta-sedimentary
Exotic granitoid
Amphibolite, gabbro
Paragneiss
Shell
Paleozoic Fossil
Wood
CENTIMETRE
115-23-002-C03


Carbonate
Undiff. greenstone and greywacke
Granitoid
Pink Carbonate
Quartzite
Quartz
Chert
Oolitic Jasper
Fine-grained red sandstone (Kenogami Fm)
Red/purple volcanic (Dubawnt S.G.)
Undiff. sandstone and siltstone
Quartz arenite
Exotic sedimentary
Ironstone
Metavolcanic
Sulfides
Shale
Meta-sedimentary
Exotic granitoid
MGS:Gauthier
115-23-002-C04
2.0-4.0 mm
Amphibolite, gabbro
Paragneiss
Shell
Paleozoic Fossil
Wood
CENTIMETRE


Carbonate
Undiff. greenstone and greywacke
Granitoid
Pink Carbonate
Oolitic Jasper
Fine-grained red sandstone (Kenogami Fm)
Red/purple volcanic (Dubawnt S.G.)
Quartz
Quartzite
Chert
Ironstone
Metavolcanic
Sulfides
Undiff. sandstone and siltstone
Quartz arenite
Exotic sedimentary
MGS:Gauthier
115-23-002-C04
4.0-8.0 mm
Amphibolite, gabbro
Paragneiss
Shell
Shale
Meta-sedimentary
Exotic granitoid
CENTIMETRE


Carbonate
Undiff. greenstone and greywacke
Granitoid
Pink Carbonate
Quartzite
Quartz
Chert
Oolitic Jasper
Fine-grained red sandstone (Kenogami Fm)
Red/purple volcanic (Dubawnt S.G.)
Undiff. sandstone and siltstone
Quartz arenite
Exotic sedimentary
Ironstone
Metavolcanic
Sulfides
Shale
Meta-sedimentary
Exotic granitoid
MGS:Gauthier
115-23-002-D01
2.0-4.0 mm
Amphibolite, gabbro
Paragneiss
Shell
Paleozoic Fossil
Wood
CENTIMETRE

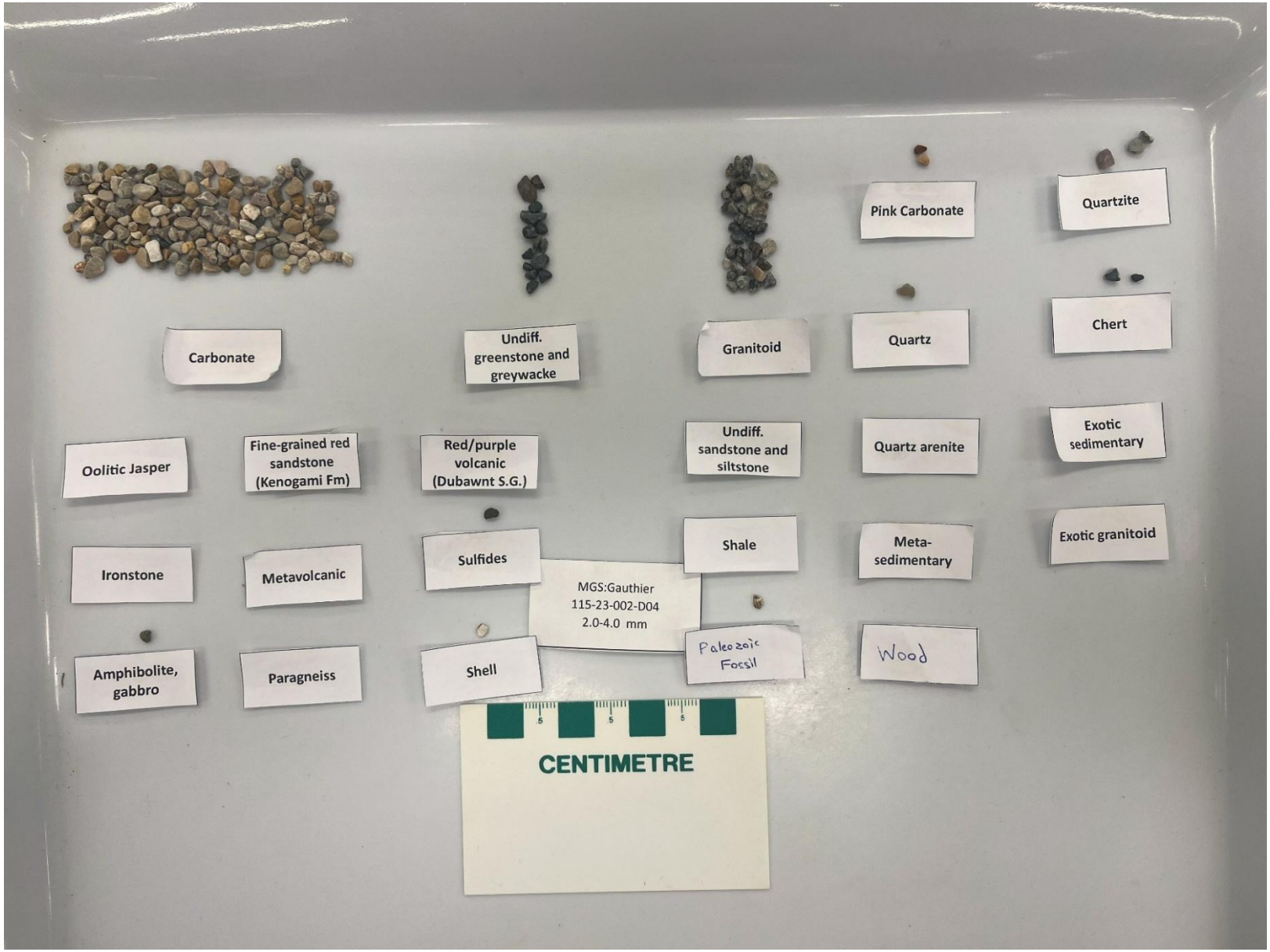

Carbonate
Undiff. greenstone and greywacke
Granitoid
Pink Carbonate
Oolitic Jasper
Fine-grained red sandstone (Kenogami Fm)
Red/purple volcanic (Dubawnt S.G.)
Quartz
Quartzite
Chert
Ironstone
Metavolcanic
Sulfides
Undiff. sandstone and siltstone
Quartz arenite
Exotic sedimentary
MGS:Gauthier
115-23-002-D01
4.0-8.0 mm
Amphibolite, gabbro
Paragneiss
Shell
Shale
Meta-sedimentary
Exotic granitoid


Carbonate
Undiff. greenstone and greywacke
Granitoid
Pink Carbonate
Quartzite
Quartz
Chert
Oolitic Jasper
Fine-grained red sandstone (Kenogami Fm)
Red/purple volcanic (Dubawnt S.G.)
Undiff. sandstone and siltstone
Quartz arenite
Exotic sedimentary
Ironstone
Metavolcanic
Sulfides
Shale
Meta-sedimentary
Exotic granitoid
Amphibolite, gabbro
Paragneiss
Shell
Paleozoic Fossil
Wood
CENTIMETRE
115-23-002-D02

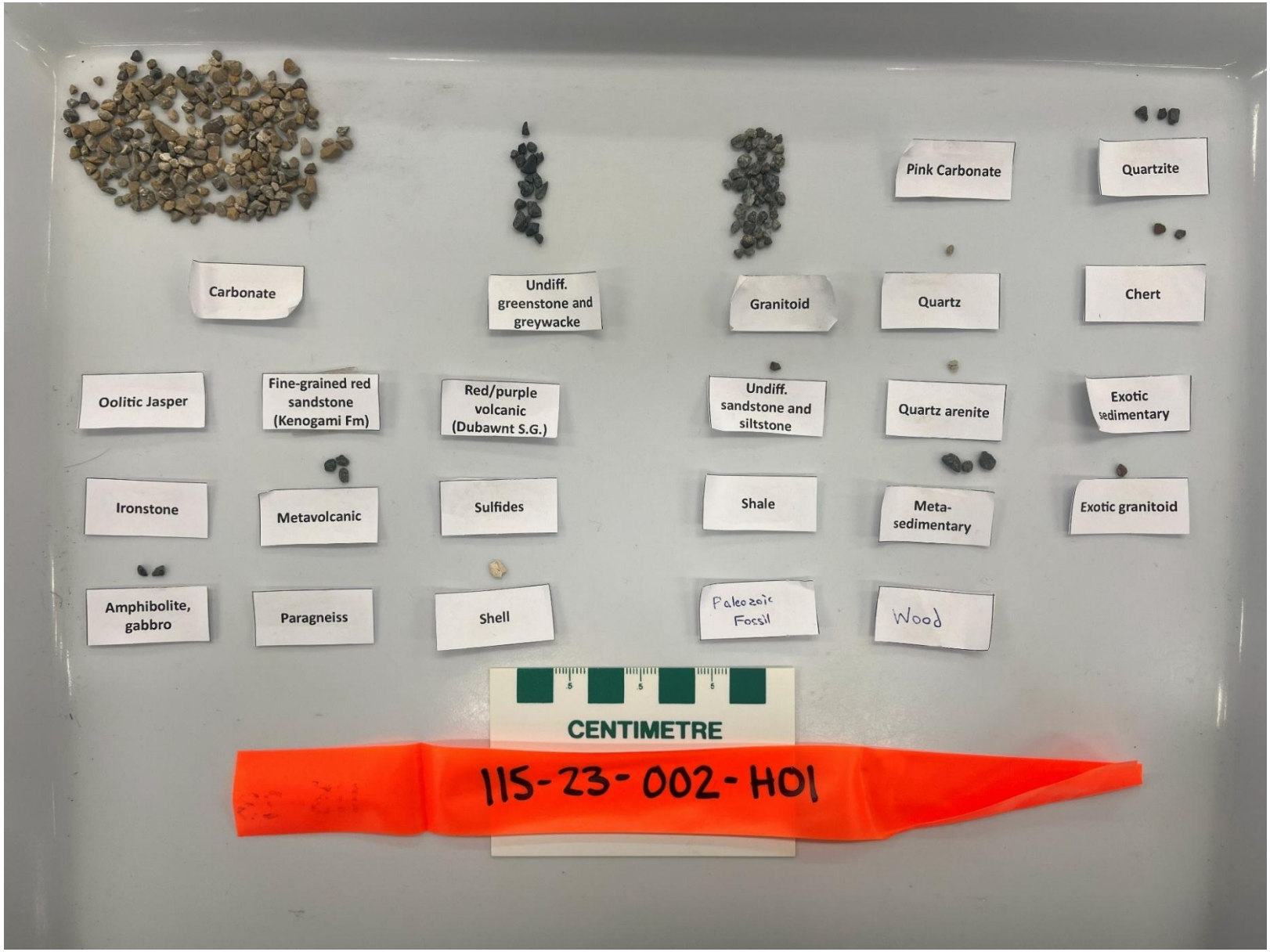

Carbonate
Undiff. greenstone and greywacke
Granitoid
Pink Carbonate
Quartzite
Chert
Quartz
Oolitic Jasper
Fine-grained red sandstone (Kenogami Fm)
Red/purple volcanic (Dubawnt S.G.)
Undiff. sandstone and siltstone
Quartz arenite
Exotic sedimentary
Ironstone
Metavolcanic
Sulfides
Shale
Meta-sedimentary
Exotic granitoid
Amphibolite, gabbro
Paragneiss
Shell
Paleozoic Fossil
Wood
CENTIMETRE
115-23-002-D02

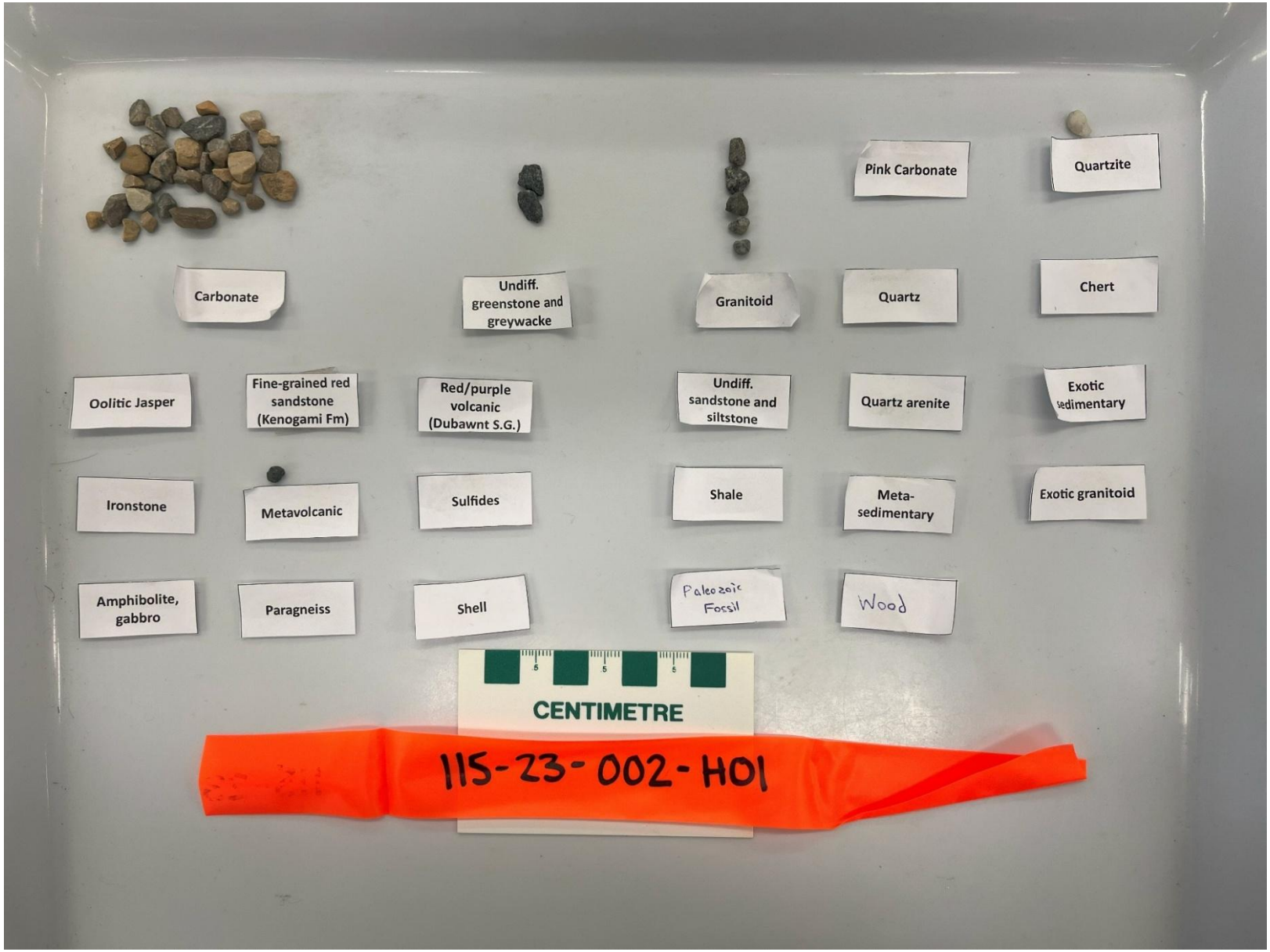

Carbonate
Undiff. greenstone and greywacke
Granitoid
Pink Carbonate
Quartzite
Quartz
Chert
Oolitic Jasper
Fine-grained red sandstone (Kenogami Fm)
Red/purple volcanic (Dubawnt S.G.)
Undiff. sandstone and siltstone
Quartz arenite
Exotic sedimentary
Ironstone
Metavolcanic
Sulfides
Shale
Meta-sedimentary
Exotic granitoid
Amphibolite, gabbro
Paragneiss
Shell
Paleozoic Fossil
Wood
CENTIMETRE
115-23-002-D03


Carbonate
Undiff. greenstone and greywacke
Granitoid
Pink Carbonate
Quartzite
Quartz
Chert
Oolitic Jasper
Fine-grained red sandstone (Kenogami Fm)
Red/purple volcanic (Dubawnt S.G.)
Undiff. sandstone and siltstone
Quartz arenite
Exotic sedimentary
Ironstone
Metavolcanic
Sulfides
Shale
Meta-sedimentary
Exotic granitoid
Amphibolite, gabbro
Paragneiss
Shell
Paleozoic Fossil
Wood
CENTIMETRE
115-23-002-D03

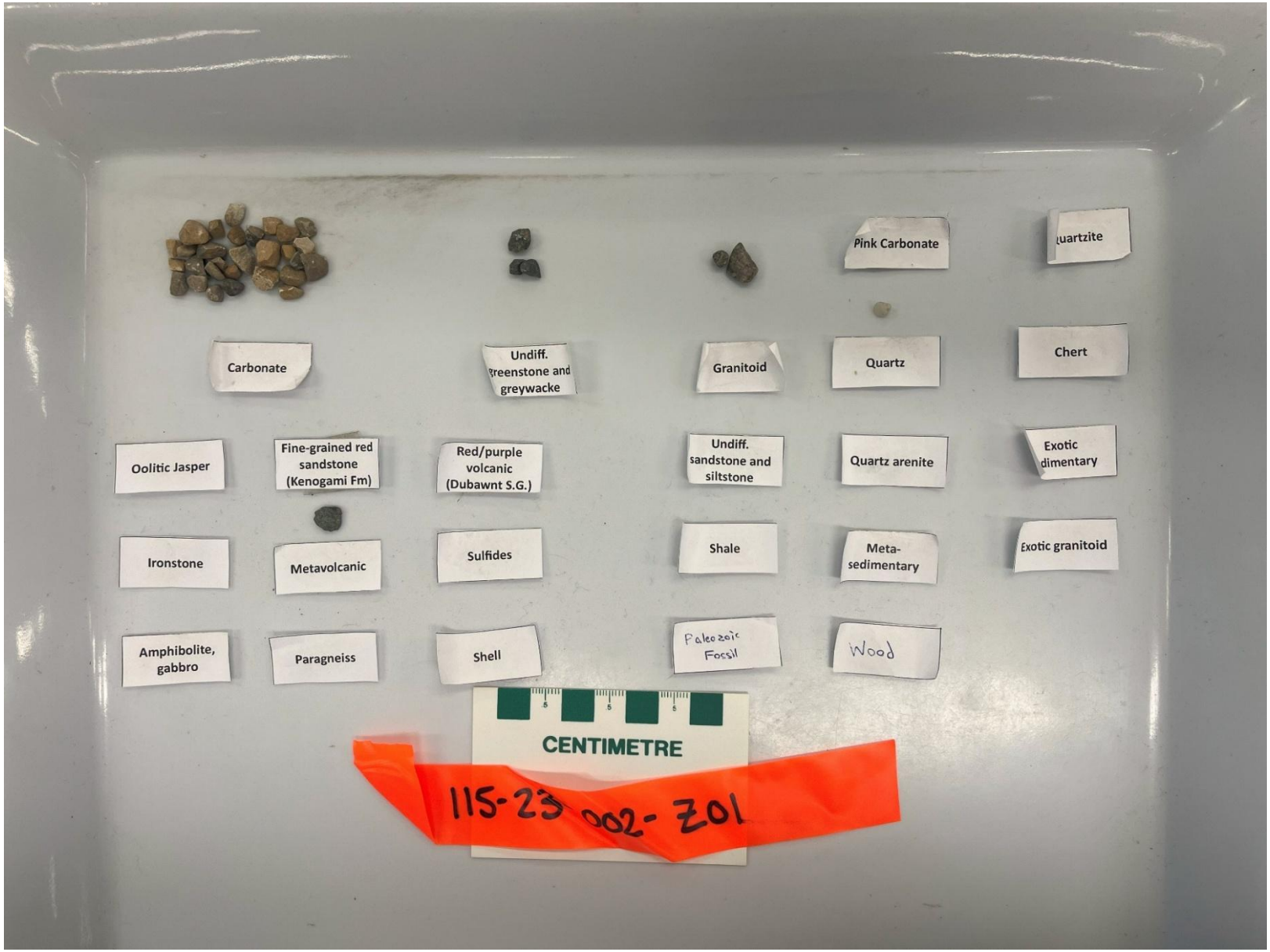

Carbonate
Undiff. greenstone and greywacke
Granitoid
Pink Carbonate
Quartzite
Quartz
Chert
Oolitic Jasper
Fine-grained red sandstone (Kenogami Fm)
Red/purple volcanic (Dubawnt S.G.)
Undiff. sandstone and siltstone
Quartz arenite
Exotic sedimentary
Ironstone
Metavolcanic
Sulfides
Shale
Meta-sedimentary
Exotic granitoid
MGS:Gauthier
115-23-002-D04
2.0-4.0 mm
Amphibolite, gabbro
Paragneiss
Shell
Paleozoic Fossil
Wood
CENTIMETRE


Carbonate
Undiff. greenstone and greywacke
Granitoid
Pink Carbonate
Oolitic Jasper
Fine-grained red sandstone (Kenogami Fm)
Red/purple volcanic (Dubawnt S.G.)
Quartz
Quartzite
Chert
Ironstone
Metavolcanic
Sulfides
Undiff. sandstone and siltstone
Quartz arenite
Exotic sedimentary
MGS:Gauthier
115-23-002-D04
4.0-8.0 mm
Amphibolite, gabbro
Paragneiss
Shell
Shale
Meta-sedimentary
Exotic granitoid
CENTIMETRE


Carbonate
Undiff. greenstone and greywacke
Granitoid
Pink Carbonate
Quartzite
Quartz
Chert
Oolitic Jasper
Fine-grained red sandstone (Kenogami Fm)
Red/purple volcanic (Dubawnt S.G.)
Undiff. sandstone and siltstone
Quartz arenite
Exotic sedimentary
Ironstone
Metavolcanic
Sulfides
Shale
Meta-sedimentary
Exotic granitoid
Amphibolite, gabbro
Paragneiss
Shell
Paleozoic Fossil
Wood
CENTIMETRE
115-23-002-H01


Carbonate
Undiff. greenstone and greywacke
Granitoid
Pink Carbonate
Quartzite
Quartz
Chert
Oolitic Jasper
Fine-grained red sandstone (Kenogami Fm)
Red/purple volcanic (Dubawnt S.G.)
Undiff. sandstone and siltstone
Quartz arenite
Exotic sedimentary
Ironstone
Metavolcanic
Sulfides
Shale
Meta-sedimentary
Exotic granitoid
Amphibolite, gabbro
Paragneiss
Shell
Paleozoic Fossil
Wood
CENTIMETRE
115-23-002-H01


Carbonate
Undiff. greenstone and greywacke
Granitoid
Pink Carbonate
Quartzite
Quartz
Chert
Oolitic Jasper
Fine-grained red sandstone (Kenogami Fm)
Red/purple volcanic (Dubawnt S.G.)
Undiff. sandstone and siltstone
Quartz arenite
Exotic sedimentary
Ironstone
Metavolcanic
Sulfides
Shale
Meta-sedimentary
Exotic granitoid
Amphibolite, gabbro
Paragneiss
Shell
Paleozoic Fossil
Wood
CENTIMETRE
115-23-002-Z01


Pink Carbonate
Quartzite
Carbonate
Undiff. Greenstone and greywacke
Granitoid
Quartz
Chert
Oolitic Jasper
Fine-grained red sandstone (Kenogami Fm)
Red/purple volcanic (Dubawnt S.G.)
Undiff. sandstone and siltstone
Quartz arenite
Exotic dimentary
Ironstone
Metavolcanic
Sulfides
Shale
Meta-sedimentary
Exotic granitoid
Amphibolite, gabbro
Paragneiss
Shell
Paleozoic Fossil
Wood
CENTIMETRE
115-23 002-Z01

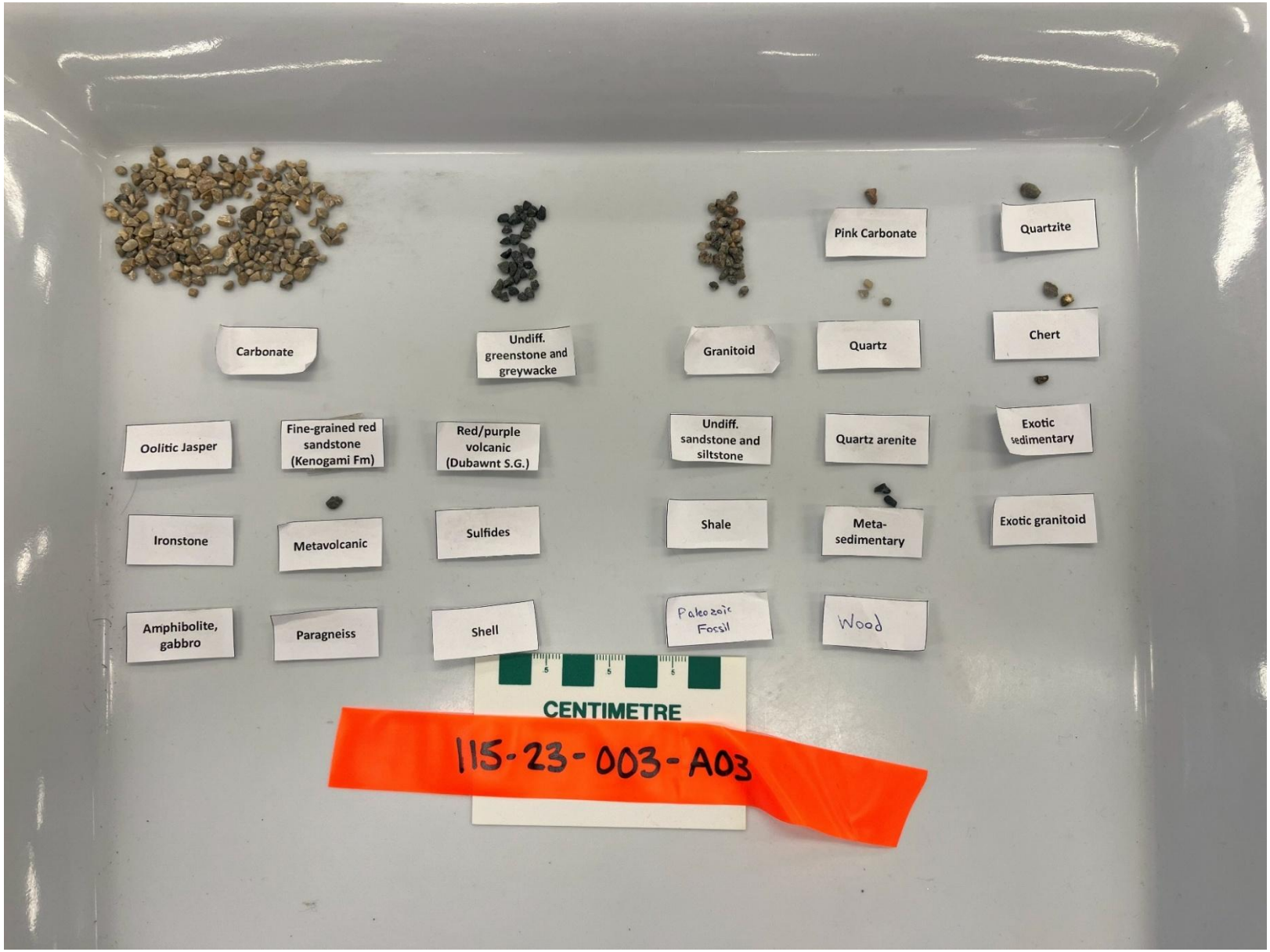
115-23-003


Carbonate
Undiff. greenstone and greywacke
Granitoid
Pink Carbonate
Quartzite
Quartz
Chert
Oolitic Jasper
Fine-grained red sandstone (Kenogami Fm)
Red/purple volcanic (Dubawnt S.G.)
Undiff. sandstone and siltstone
Quartz arenite
Exotic sedimentary
Ironstone
Metavolcanic
Sulfides
Shale
Meta-sedimentary
Exotic granitoid
Amphibolite, gabbro
Paragneiss
Shell
Paleozoic Fossil
Wood
CENTIMETRE
115-23-003-A01


Carbonate
Undiff. greenstone and greywacke
Granitoid
Pink Carbonate
Quartzite
Quartz
Chert
Oolitic Jasper
Fine-grained red sandstone (Kenogami Fm)
Red/purple volcanic (Dubawnt S.G.)
Undiff. sandstone and siltstone
Quartz arenite
Exotic sedimentary
Ironstone
Metavolcanic
Sulfides
Shale
Meta-sedimentary
Exotic granitoid
Amphibolite, gabbro
Paragneiss
Shell
Paleozoic Fossil
Wood
CENTIMETRE
115-23-003-A01


Carbonate
Undiff. greenstone and greywacke
Granitoid
Pink Carbonate
Quartzite
Quartz
Chert
Oolitic Jasper
Fine-grained red sandstone (Kenogami Fm)
Red/purple volcanic (Dubawnt S.G.)
Undiff. sandstone and siltstone
Quartz arenite
Exotic sedimentary
Ironstone
Metavolcanic
Sulfides
Shale
Meta-sedimentary
Exotic granitoid
MGS:Gauthier
115-23-003-A02
2.0-4.0 mm
Amphibolite, gabbro
Paragneiss
Shell
Paleozoic Fossil
Wood
CENTIMETRE


Carbonate
Undiff. greenstone and greywacke
Granitoid
Pink Carbonate
Oolitic Jasper
Fine-grained red sandstone (Kenogami Fm)
Red/purple volcanic (Dubawnt S.G.)
Quartz
Quartzite
Chert
Ironstone
Metavolcanic
Sulfides
Undiff. sandstone and siltstone
Quartz arenite
Exotic sedimentary
MGS:Gauthier
115-23-003-A02
4.0-8.0 mm
Amphibolite, gabbro
Paragneiss
Shell
Shale
Meta-sedimentary
Exotic granitoid
Paleozoic Fossil
CENTIMETRE


Carbonate
Undiff. greenstone and greywacke
Granitoid
Pink Carbonate
Quartzite
Quartz
Chert
Oolitic Jasper
Fine-grained red sandstone (Kenogami Fm)
Red/purple volcanic (Dubawnt S.G.)
Undiff. sandstone and siltstone
Quartz arenite
Exotic sedimentary
Ironstone
Metavolcanic
Sulfides
Shale
Meta-sedimentary
Exotic granitoid
Amphibolite, gabbro
Paragneiss
Shell
Paleozoic Fossil
Wood
CENTIMETRE
115-23-003-A03


Carbonate
Undiff. greenstone and greywacke
Granitoid
Pink Carbonate
Quartzite
Quartz
Chert
Oolitic Jasper
Fine-grained red sandstone (Kenogami Fm)
Red/purple volcanic (Dubawnt S.G.)
Undiff. sandstone and siltstone
Quartz arenite
Exotic sedimentary
Ironstone
Metavolcanic
Sulfides
Shale
Meta-sedimentary
Exotic granitoid
Amphibolite, gabbro
Paragneiss
Shell
Paleozoic Fossil
Wood
CENTIMETRE
115-23-003-A03


Carbonate
Undiff. greenstone and greywacke
Granitoid
Pink Carbonate
Quartzite
Quartz
Chert
Oolitic Jasper
Fine-grained red sandstone (Kenogami Fm)
Red/purple volcanic (Dubawnt S.G.)
Undiff. sandstone and siltstone
Quartz arenite
Exotic sedimentary
Ironstone
Metavolcanic
Sulfides
Shale
Meta-sedimentary
Exotic granitoid
MGS:Gauthier
115-23-003-B01
2.0-4.0 mm
Amphibolite, gabbro
Paragneiss
Shell
Paleozoic Fossil
Wood
CENTIMETRE


Carbonate
Undiff. greenstone and greywacke
Granitoid
Pink Carbonate
Oolitic Jasper
Fine-grained red sandstone (Kenogami Fm)
Red/purple volcanic (Dubawnt S.G.)
Quartz
Quartzite
Chert
Ironstone
Metavolcanic
Sulfides
Undiff. sandstone and siltstone
Quartz arenite
Exotic sedimentary
MGS:Gauthier
115-23-003-B01
4.0-8.0 mm
Amphibolite, gabbro
Paragneiss
Shell
Shale
Meta-sedimentary
Exotic granitoid
Paleozoic Fossil
CENTIMETRE


Carbonate
Undiff. greenstone and greywacke
Granitoid
Pink Carbonate
Quartzite
Quartz
Chert
Oolitic Jasper
Fine-grained red sandstone (Kenogami Fm)
Red/purple volcanic (Dubawnt S.G.)
Undiff. sandstone and siltstone
Quartz arenite
Exotic sedimentary
Ironstone
Metavolcanic
Sulfides
MGS:Gauthier
115-23-003-B02
2.0-4.0 mm
Shale
Meta-sedimentary
Exotic granitoid
Amphibolite, gabbro
Paragneiss
Shell
Paleozoic Fossil
Wood
CENTIMETRE


Carbonate
Undiff. greenstone and greywacke
Granitoid
Pink Carbonate
Oolitic Jasper
Fine-grained red sandstone (Kenogami Fm)
Red/purple volcanic (Dubawnt S.G.)
Quartz
Quartzite
Chert
Ironstone
Metavolcanic
Sulfides
Undiff. sandstone and siltstone
Quartz arenite
Exotic sedimentary
MGS:Gauthier
115-23-003-B02
4.0-8.0 mm
Amphibolite, gabbro
Paragneiss
Shell
Shale
Meta-sedimentary
Exotic granitoid
CENTIMETRE
Paleozoic Fossil


Carbonate
Undiff. greenstone and greywacke
Granitoid
Pink Carbonate
Quartzite
Chert
Quartz
Oolitic Jasper
Fine-grained red sandstone (Kenogami Fm)
Red/purple volcanic (Dubawnt S.G.)
Undiff. sandstone and siltstone
Quartz arenite
Exotic sedimentary
Ironstone
Metavolcanic
Sulfides
Shale
Meta-sedimentary
Exotic granitoid
MGS:Gauthier
115-23-003-D01
2.0-4.0 mm
Amphibolite, gabbro
Paragneiss
Shell
Paleozoic Fossil
Wood
CENTIMETRE


Carbonate
Undiff. greenstone and greywacke
Granitoid
Pink Carbonate
Oolitic Jasper
Fine-grained red sandstone (Kenogami Fm)
Red/purple volcanic (Dubawnt S.G.)
Quartz
Quartzite
Chert
Ironstone
Metavolcanic
Sulfides
Undiff. sandstone and siltstone
Quartz arenite
Exotic sedimentary
MGS:Gauthier
115-23-003-D01
4.0-8.0 mm
Amphibolite, gabbro
Paragneiss
Shell
Shale
Meta-sedimentary
Exotic granitoid
CENTIMETRE
Paleozoic Fossil

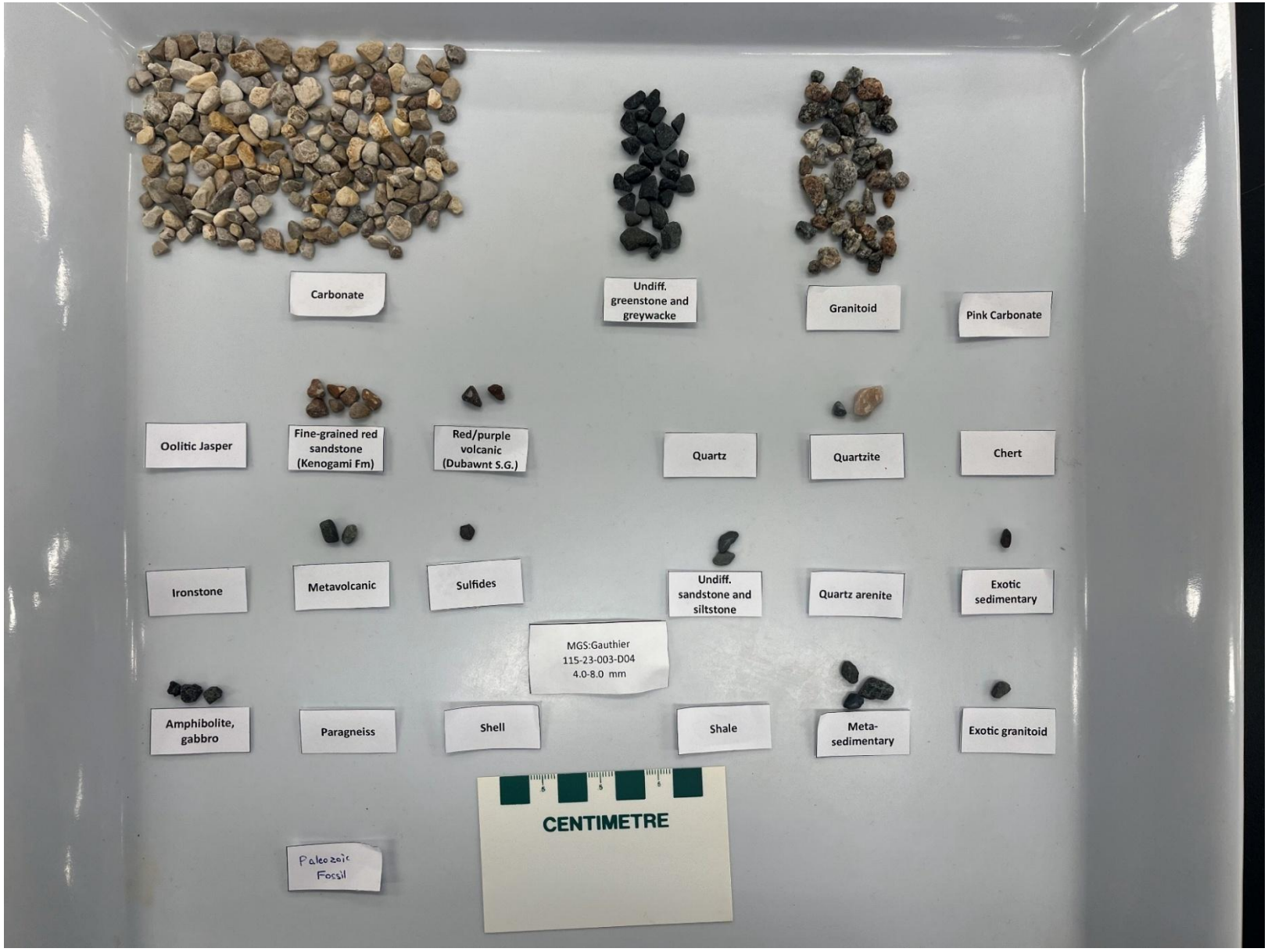

Carbonate
Undiff. greenstone and greywacke
Granitoid
Pink Carbonate
Quartzite
Quartz
Chert
Oolitic Jasper
Fine-grained red sandstone (Kenogami Fm)
Red/purple volcanic (Dubawnt S.G.)
Undiff. sandstone and siltstone
Quartz arenite
Exotic sedimentary
Ironstone
Metavolcanic
Sulfides
Shale
Meta-sedimentary
Exotic granitoid
Amphibolite, gabbro
Paragneiss
Shell
Paleozoic Fossil
Wood
CENTIMETRE
115-23-003-D02


Carbonate
Undiff. greenstone and greywacke
Granitoid
Pink Carbonate
Quartzite
Quartz
Chert
Oolitic Jasper
Fine-grained red sandstone (Kenogami Fm)
Red/purple volcanic (Dubawnt S.G.)
Undiff. sandstone and siltstone
Quartz arenite
Exotic sedimentary
Ironstone
Metavolcanic
Sulfides
Shale
Meta-sedimentary
Exotic granitoid
Amphibolite, gabbro
Paragneiss
Shell
Paleozoic Fossil
Wood
CENTIMETRE
115-23-003-D02


Carbonate
Undiff. greenstone and greywacke
Granitoid
Pink Carbonate
Quartzite
Quartz
Chert
Oolitic Jasper
Fine-grained red sandstone (Kenogami Fm)
Red/purple volcanic (Dubawnt S.G.)
Undiff. sandstone and siltstone
Quartz arenite
Exotic sedimentary
Ironstone
Metavolcanic
Sulfides
Shale
Meta-sedimentary
Exotic granitoid
Amphibolite, gabbro
Paragneiss
Shell
Paleozoic Fossil
Wood
CENTIMETRE
115-23-003-D03


Carbonate
Undiff. greenstone and greywacke
Granitoid
Pink Carbonate
Quartzite
Quartz
Chert
Oolitic Jasper
Fine-grained red sandstone (Kenogami Fm)
Red/purple volcanic (Dubawnt S.G.)
Undiff. sandstone and siltstone
Quartz arenite
Exotic sedimentary
Ironstone
Metavolcanic
Sulfides
Shale
Meta-sedimentary
Exotic granitoid
Amphibolite, gabbro
Paragneiss
Shell
Paleozoic Fossil
Wood
CENTIMETRE
115-23-003-D03


Carbonate
Undiff. greenstone and greywacke
Granitoid
Pink Carbonate
Quartzite
Quartz
Chert
Oolitic Jasper
Fine-grained red sandstone (Kenogami Fm)
Red/purple volcanic (Dubawnt S.G.)
Undiff. sandstone and siltstone
Quartz arenite
Exotic sedimentary
Ironstone
Metavolcanic
Sulfides
Shale
Meta-sedimentary
Exotic granitoid
MGS:Gauthier
115-23-003-D04
2.0-4.0 mm
Amphibolite, gabbro
Paragneiss
Shell
Paleozoic Fossil
Wood
CENTIMETRE


Carbonate
Undiff. greenstone and greywacke
Granitoid
Pink Carbonate
Oolitic Jasper
Fine-grained red sandstone (Kenogami Fm)
Red/purple volcanic (Dubawnt S.G.)
Quartz
Quartzite
Chert
Ironstone
Metavolcanic
Sulfides
Undiff. sandstone and siltstone
Quartz arenite
Exotic sedimentary
MGS:Gauthier
115-23-003-D04
4.0-8.0 mm
Amphibolite, gabbro
Paragneiss
Shell
Shale
Meta-sedimentary
Exotic granitoid
CENTIMETRE
Paleozoic Fossil


Carbonate
Undiff. greenstone and greywacke
Granitoid
Pink Carbonate
Quartzite
Quartz
Chert
Oolitic Jasper
Fine-grained red sandstone (Kenogami Fm)
Red/purple volcanic (Dubawnt S.G.)
Undiff. sandstone and siltstone
Quartz arenite
Exotic sedimentary
Ironstone
Metavolcanic
Sulfides
Shale
Meta-sedimentary
Exotic granitoid
Amphibolite, gabbro
Paragneiss
Shell
Paleozoic Fossil
Wood
CENTIMETRE
115-23-003-L01


Carbonate
Undiff. greenstone and greywacke
Granitoid
Pink Carbonate
Quartzite
Quartz
Chert
Oolitic Jasper
Fine-grained red sandstone (Kenogami Fm)
Red/purple volcanic (Dubawnt S.G.)
Undiff. sandstone and siltstone
Quartz arenite
Exotic sedimentary
Ironstone
Metavolcanic
Sulfides
Shale
Meta-sedimentary
Exotic granitoid
Amphibolite, gabbro
Paragneiss
Shell
Paleozoic Fossil
Wood
CENTIMETRE
115-23-003-L01

115-23-004


Carbonate
Undiff. greenstone and greywacke
Granitoid
Pink Carbonate
Quartzite
Quartz
Chert
Oolitic Jasper
Fine-grained red sandstone (Kenogami Fm)
Red/purple volcanic (Dubawnt S.G.)
Undiff. sandstone and siltstone
Quartz arenite
Exotic sedimentary
Ironstone
Metavolcanic
Sulfides
Shale
Meta-sedimentary
Exotic granitoid
Amphibolite, gabbro
Paragneiss
Shell
Paleozoic Fossil
Wood
CENTIMETRE
115-23-004-B01


Carbonate
Undiff. greenstone and greywacke
Granitoid
Pink Carbonate
Quartzite
Quartz
Chert
Oolitic Jasper
Fine-grained red sandstone (Kenogami Fm)
Red/purple volcanic (Dubawnt S.G.)
Undiff. sandstone and siltstone
Quartz arenite
Exotic sedimentary
Ironstone
Metavolcanic
Sulfides
Shale
Meta-sedimentary
Exotic granitoid
Amphibolite, gabbro
Paragneiss
Shell
Paleozoic Fossil
Wood
CENTIMETRE
115-23-004-B01

115-23-005


Carbonate
Undiff. greenstone and greywacke
Granitoid
Pink Carbonate
Quartzite
Quartz
Chert
Oolitic Jasper
Fine-grained red sandstone (Kenogami Fm)
Red/purple volcanic (Dubawnt S.G.)
Undiff. sandstone and siltstone
Quartz arenite
Exotic sedimentary
Ironstone
Metavolcanic
Sulfides
Shale
Meta-sedimentary
Exotic granitoid
MGS:Gauthier
115-23-005-B01
2.0-4.0 mm
Amphibolite, gabbro
Paragneiss
Shell
Paleozoic Fossil
Wood
CENTIMETRE

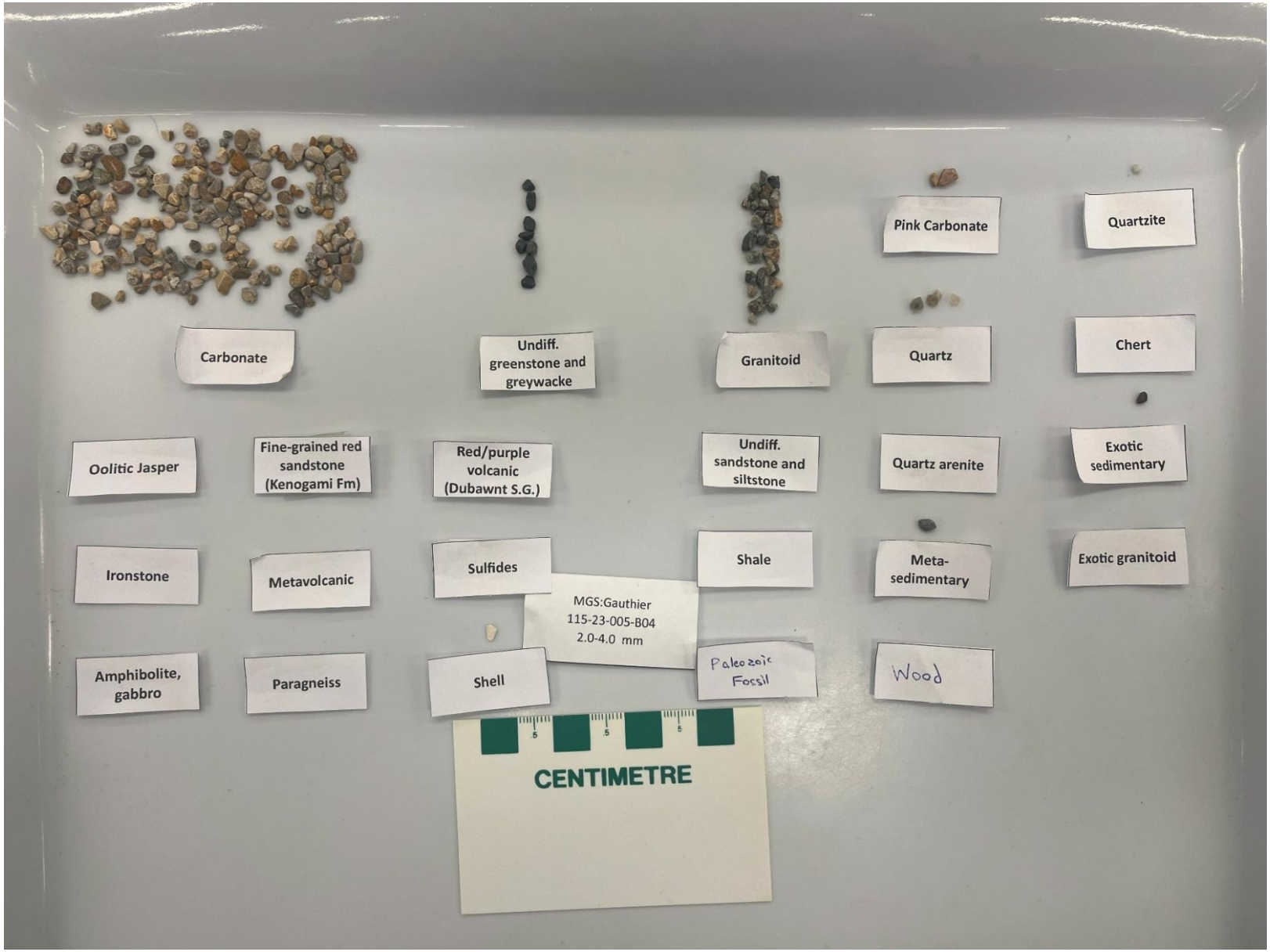

Carbonate
Undiff. greenstone and greywacke
Granitoid
Pink Carbonate
Oolitic Jasper
Fine-grained red sandstone (Kenogami Fm)
Red/purple volcanic (Dubawnt S.G.)
Quartz
Quartzite
Chert
Ironstone
Metavolcanic
Sulfides
Undiff. sandstone and siltstone
Quartz arenite
Exotic sedimentary
MGS:Gauthier
115-23-005-B01
4.0-8.0 mm
Amphibolite, gabbro
Paragneiss
Shell
Shale
Meta-sedimentary
Exotic granitoid
Paleozoic Fossil
CENTIMETRE

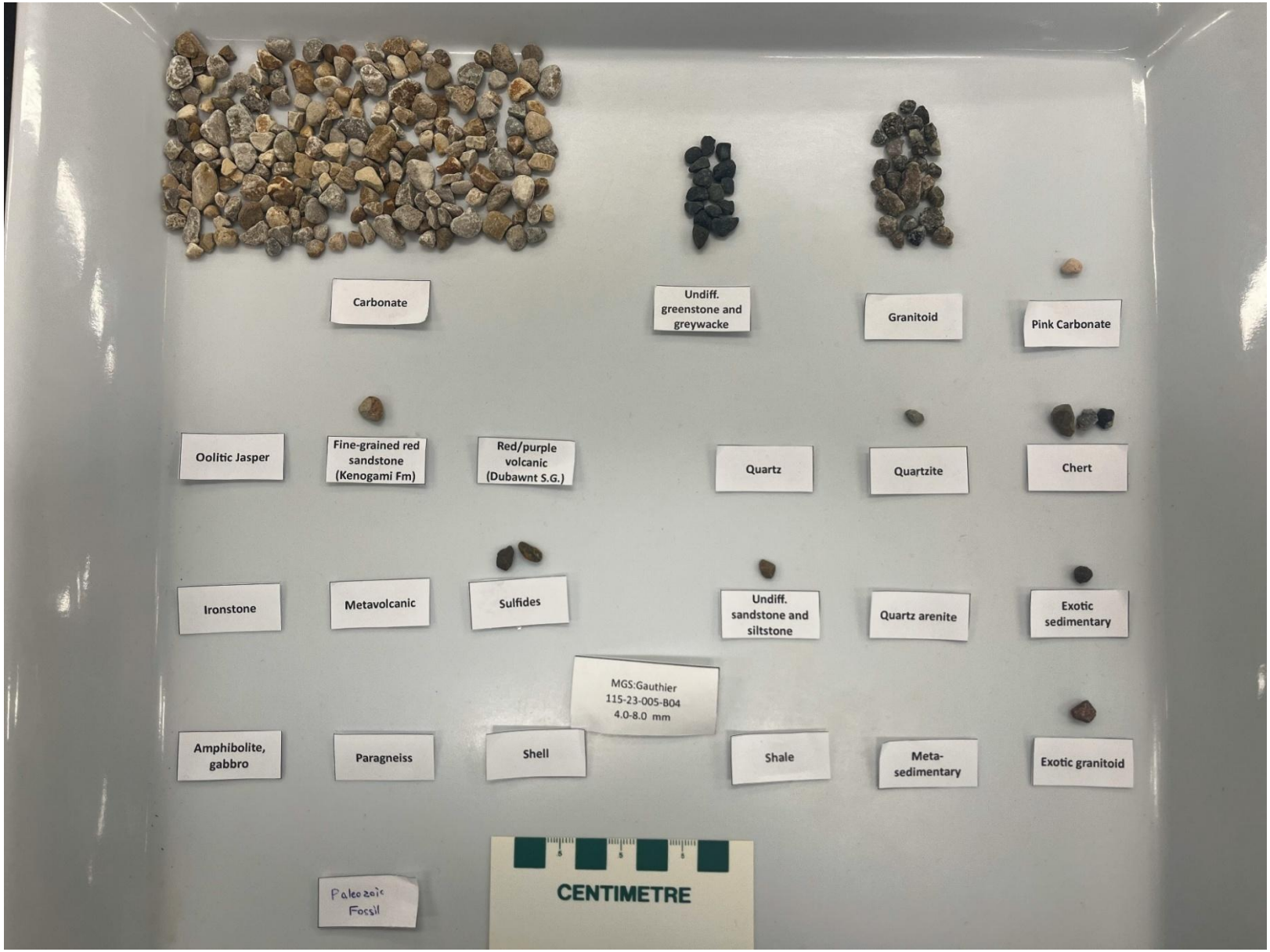

Carbonate
Undiff. greenstone and greywacke
Granitoid
Pink Carbonate
Quartzite
Quartz
Chert
Oolitic Jasper
Fine-grained red sandstone (Kenogami Fm)
Red/purple volcanic (Dubawnt S.G.)
Undiff. sandstone and siltstone
Quartz arenite
Exotic sedimentary
Ironstone
Metavolcanic
Sulfides
Shale
Meta-sedimentary
Exotic granitoid
Amphibolite, gabbro
Paragneiss
Shell
Paleozoic Fossil
Wood
CENTIMETRE
115-23-005-B02


Carbonate
Undiff. greenstone and greywacke
Granitoid
Pink Carbonate
uartzite
Quartz
Chert
Oolitic Jasper
Fine-grained red sandstone (Kenogami Fm)
Red/purple volcanic (Dubawnt S.G.)
Undiff. sandstone and siltstone
Quartz arenite
Exotic dimentary
Ironstone
Metavolcanic
Sulfides
Shale
Meta-sedimentary
Exotic granitoid
Amphibolite, gabbro
Paragneiss
Shell
Paleozoic Fossil
Wood
CENTIMETRE
115-23-005-B02


Carbonate
Undiff. greenstone and greywacke
Granitoid
Pink Carbonate
Quartzite
Quartz
Chert
Oolitic Jasper
Fine-grained red sandstone (Kenogami Fm)
Red/purple volcanic (Dubawnt S.G.)
Undiff. sandstone and siltstone
Quartz arenite
Exotic sedimentary
Ironstone
Metavolcanic
Sulfides
Shale
Meta-sedimentary
Exotic granitoid
Amphibolite, gabbro
Paragneiss
Shell
Paleozoic Fossil
Wood
CENTIMETRE
115-23-005-B03


Carbonate
Undiff. greenstone and greywacke
Granitoid
Pink Carbonate
Quartzite
Quartz
Chert
Oolitic Jasper
Fine-grained red sandstone (Kenogami Fm)
Red/purple volcanic (Dubawnt S.G.)
Undiff. sandstone and siltstone
Quartz arenite
Exotic sedimentary
Ironstone
Metavolcanic
Sulfides
Shale
Meta-sedimentary
Exotic granitoid
Amphibolite, gabbro
Paragneiss
Shell
Paleozoic Fossil
Wood
CENTIMETRE
115-23-005-B03

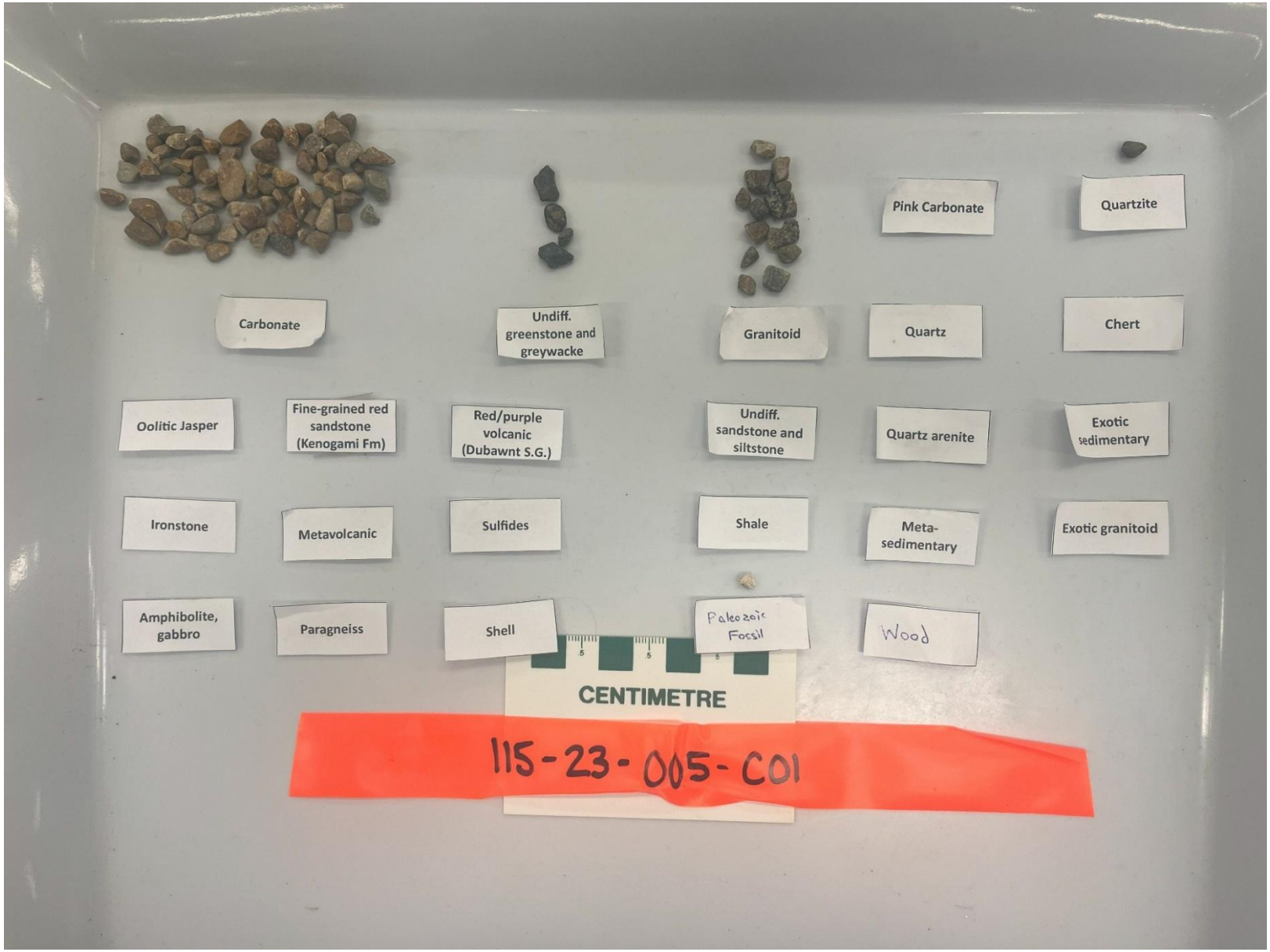

Carbonate
Undiff. greenstone and greywacke
Granitoid
Pink Carbonate
Quartzite
Quartz
Chert
Oolitic Jasper
Fine-grained red sandstone (Kenogami Fm)
Red/purple volcanic (Dubawnt S.G.)
Undiff. sandstone and siltstone
Quartz arenite
Exotic sedimentary
Ironstone
Metavolcanic
Sulfides
Shale
Meta-sedimentary
Exotic granitoid
MGS:Gauthier
115-23-005-B04
2.0-4.0 mm
Amphibolite, gabbro
Paragneiss
Shell
Paleozoic Fossil
Wood
CENTIMETRE


Carbonate
Undiff. greenstone and greywacke
Granitoid
Pink Carbonate
Oolitic Jasper
Fine-grained red sandstone (Kenogami Fm)
Red/purple volcanic (Dubawnt S.G.)
Quartz
Quartzite
Chert
Ironstone
Metavolcanic
Sulfides
Undiff. sandstone and siltstone
Quartz arenite
Exotic sedimentary
MGS:Gauthier
115-23-005-B04
4.0-8.0 mm
Amphibolite, gabbro
Paragneiss
Shell
Shale
Meta-sedimentary
Exotic granitoid
Paleozoic Fossil
CENTIMETRE

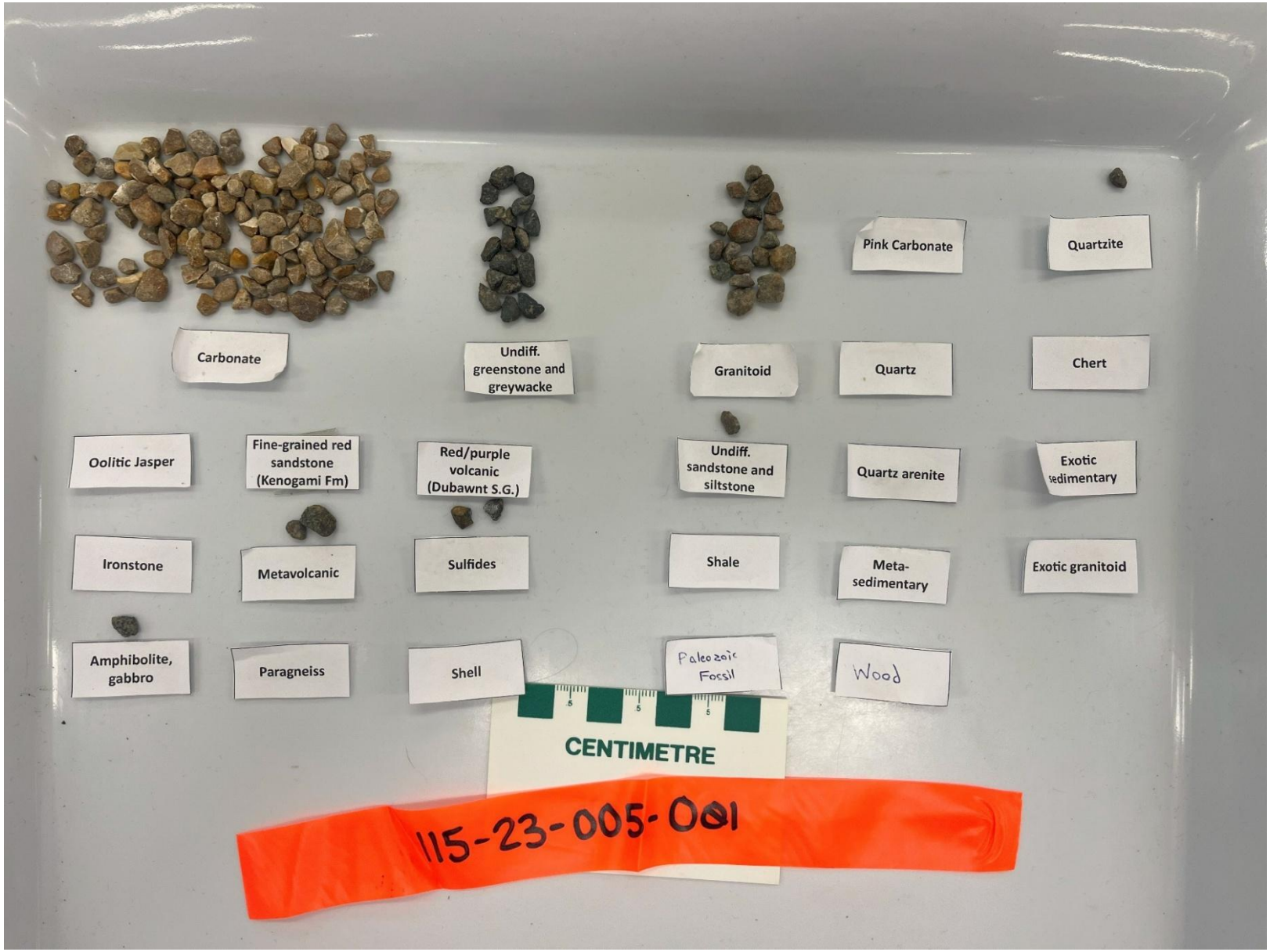

Carbonate
Undiff. greenstone and greywacke
Granitoid
Pink Carbonate
Quartzite
Quartz
Chert
Oolitic Jasper
Fine-grained red sandstone (Kenogami Fm)
Red/purple volcanic (Dubawnt S.G.)
Undiff. sandstone and siltstone
Quartz arenite
Exotic sedimentary
Ironstone
Metavolcanic
Sulfides
Shale
Meta-sedimentary
Exotic granitoid
Amphibolite, gabbro
Paragneiss
Shell
Paleozoic Fossil
Wood
CENTIMETRE
115-23-005-B05


Carbonate
Undiff. greenstone and greywacke
Granitoid
Pink Carbonate
Quartzite
Quartz
Chert
Oolitic Jasper
Fine-grained red sandstone (Kenogami Fm)
Red/purple volcanic (Dubawnt S.G.)
Undiff. sandstone and siltstone
Quartz arenite
Exotic sedimentary
Ironstone
Metavolcanic
Sulfides
Shale
Meta-sedimentary
Exotic granitoid
Amphibolite, gabbro
Paragneiss
Shell
Paleozoic Fossil
Wood
CENTIMETRE
115-23-005-B05

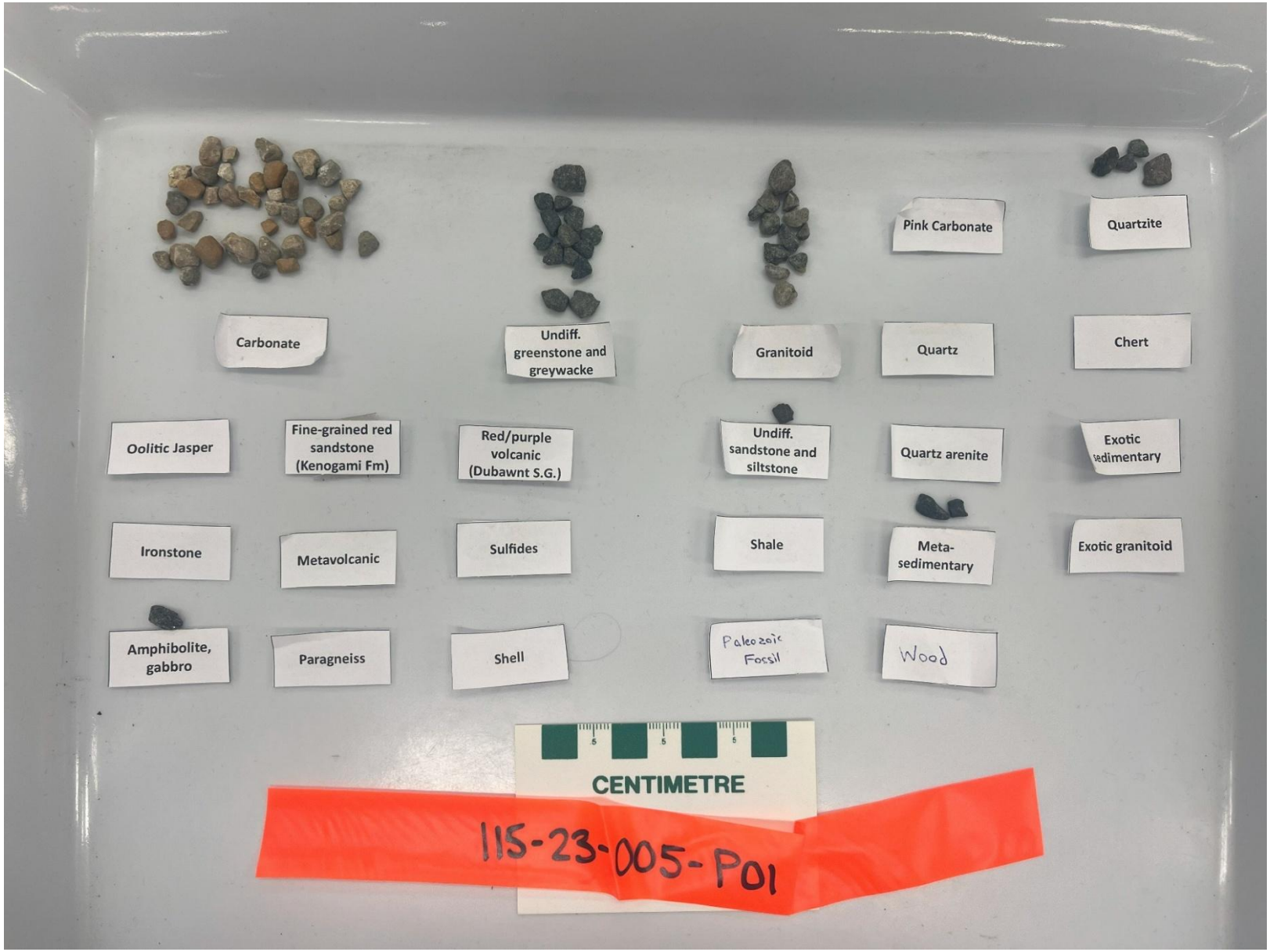

Carbonate
Undiff. greenstone and greywacke
Granitoid
Pink Carbonate
Quartzite
Quartz
Chert
Oolitic Jasper
Fine-grained red sandstone (Kenogami Fm)
Red/purple volcanic (Dubawnt S.G.)
Undiff. sandstone and siltstone
Quartz arenite
Exotic sedimentary
Ironstone
Metavolcanic
Sulfides
Shale
Meta-sedimentary
Exotic granitoid
Amphibolite, gabbro
Paragneiss
Shell
Paleozoic Fossil
Wood
CENTIMETRE
115-23-005-C01


Carbonate
Undiff. greenstone and greywacke
Granitoid
Pink Carbonate
Quartzite
Quartz
Chert
Oolitic Jasper
Fine-grained red sandstone (Kenogami Fm)
Red/purple volcanic (Dubawnt S.G.)
Undiff. sandstone and siltstone
Quartz arenite
Exotic sedimentary
Ironstone
Metavolcanic
Sulfides
Shale
Meta-sedimentary
Exotic granitoid
Amphibolite, gabbro
Paragneiss
Shell
Paleozoic Fossil
Wood
CENTIMETRE
115-23-005-C01

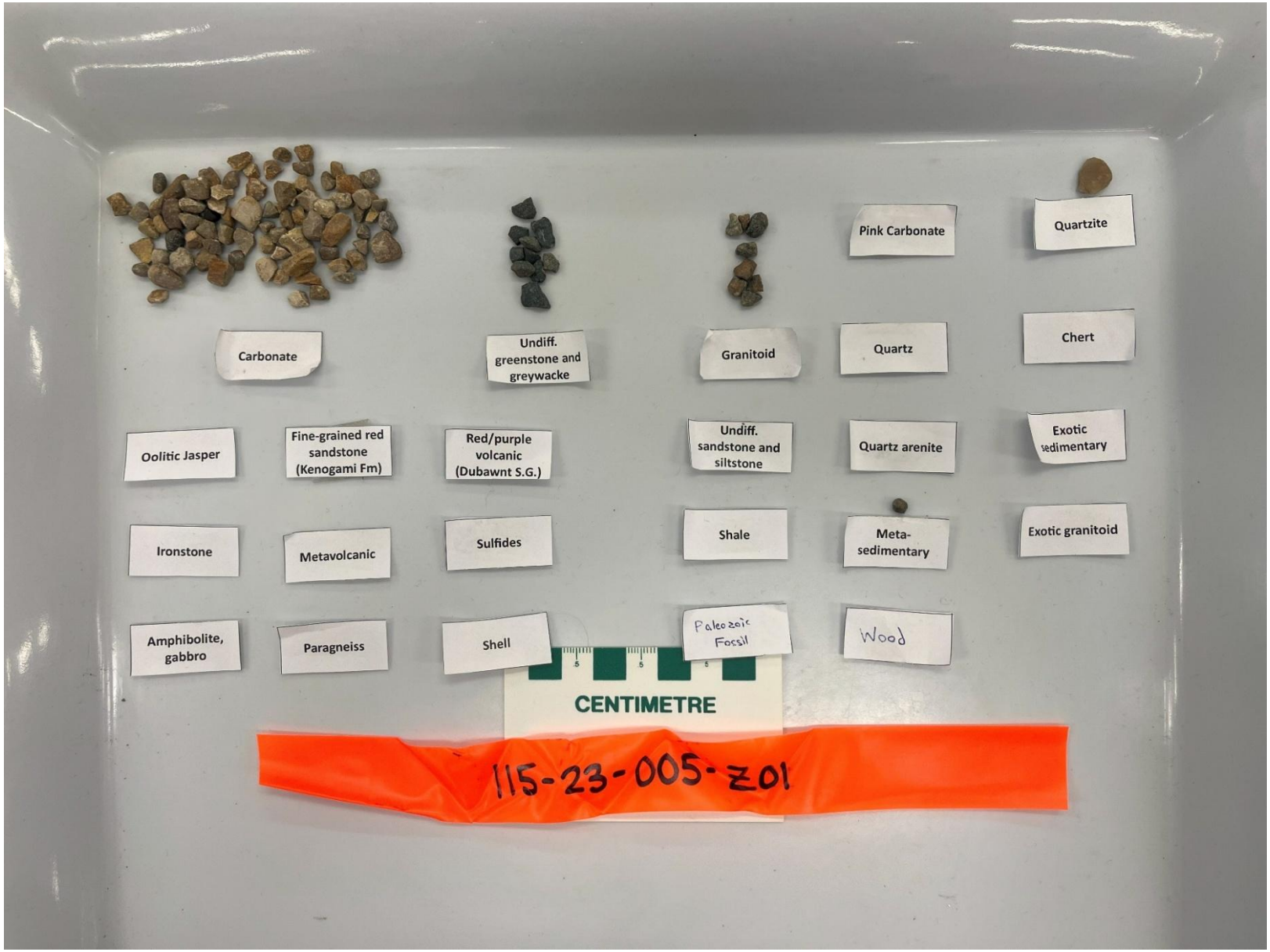

Carbonate
Undiff. greenstone and greywacke
Granitoid
Pink Carbonate
Quartzite
Quartz
Chert
Oolitic Jasper
Fine-grained red sandstone (Kenogami Fm)
Red/purple volcanic (Dubawnt S.G.)
Undiff. sandstone and siltstone
Quartz arenite
Exotic sedimentary
Ironstone
Metavolcanic
Sulfides
Shale
Meta-sedimentary
Exotic granitoid
Amphibolite, gabbro
Paragneiss
Shell
Paleozoic Fossil
Wood
CENTIMETRE
115-23-005-001


Carbonate
Undiff. greenstone and greywacke
Granitoid
Pink Carbonate
Quartzite
Quartz
Chert
Oolitic Jasper
Fine-grained red sandstone (Kenogami Fm)
Red/purple volcanic (Dubawnt S.G.)
Undiff. sandstone and siltstone
Quartz arenite
Exotic sedimentary
Ironstone
Metavolcanic
Sulfides
Shale
Meta-sedimentary
Exotic granitoid
Amphibolite, gabbro
Paragneiss
Shell
Paleozoic Fossil
Wood
CENTIMETRE
115-23-005-001

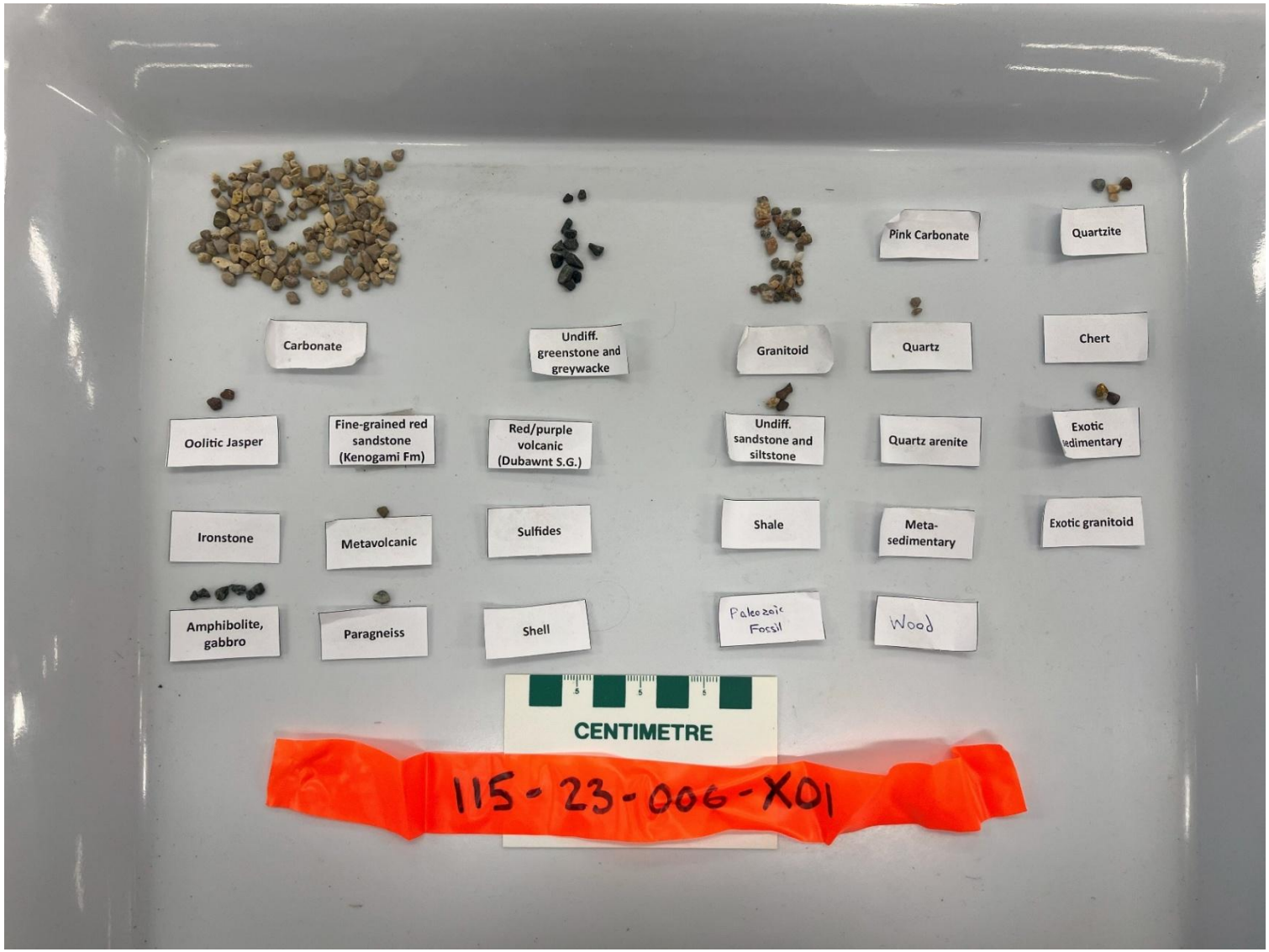

Carbonate
Undiff. greenstone and greywacke
Granitoid
Pink Carbonate
Quartzite
Quartz
Chert
Oolitic Jasper
Fine-grained red sandstone (Kenogami Fm)
Red/purple volcanic (Dubawnt S.G.)
Undiff. sandstone and siltstone
Quartz arenite
Exotic sedimentary
Ironstone
Metavolcanic
Sulfides
Shale
Meta-sedimentary
Exotic granitoid
Amphibolite, gabbro
Paragneiss
Shell
Paleozoic Fossil
Wood
CENTIMETRE
115-23-005-P01


Carbonate
Undiff. greenstone and greywacke
Granitoid
Pink Carbonate
Quartzite
Quartz
Chert
Oolitic Jasper
Fine-grained red sandstone (Kenogami Fm)
Red/purple volcanic (Dubawnt S.G.)
Undiff. sandstone and siltstone
Quartz arenite
Exotic sedimentary
Ironstone
Metavolcanic
Sulfides
Shale
Meta-sedimentary
Exotic granitoid
Amphibolite, gabbro
Paragneiss
Shell
Paleozoic Fossil
Wood
CENTIMETRE
115-23-005-P01

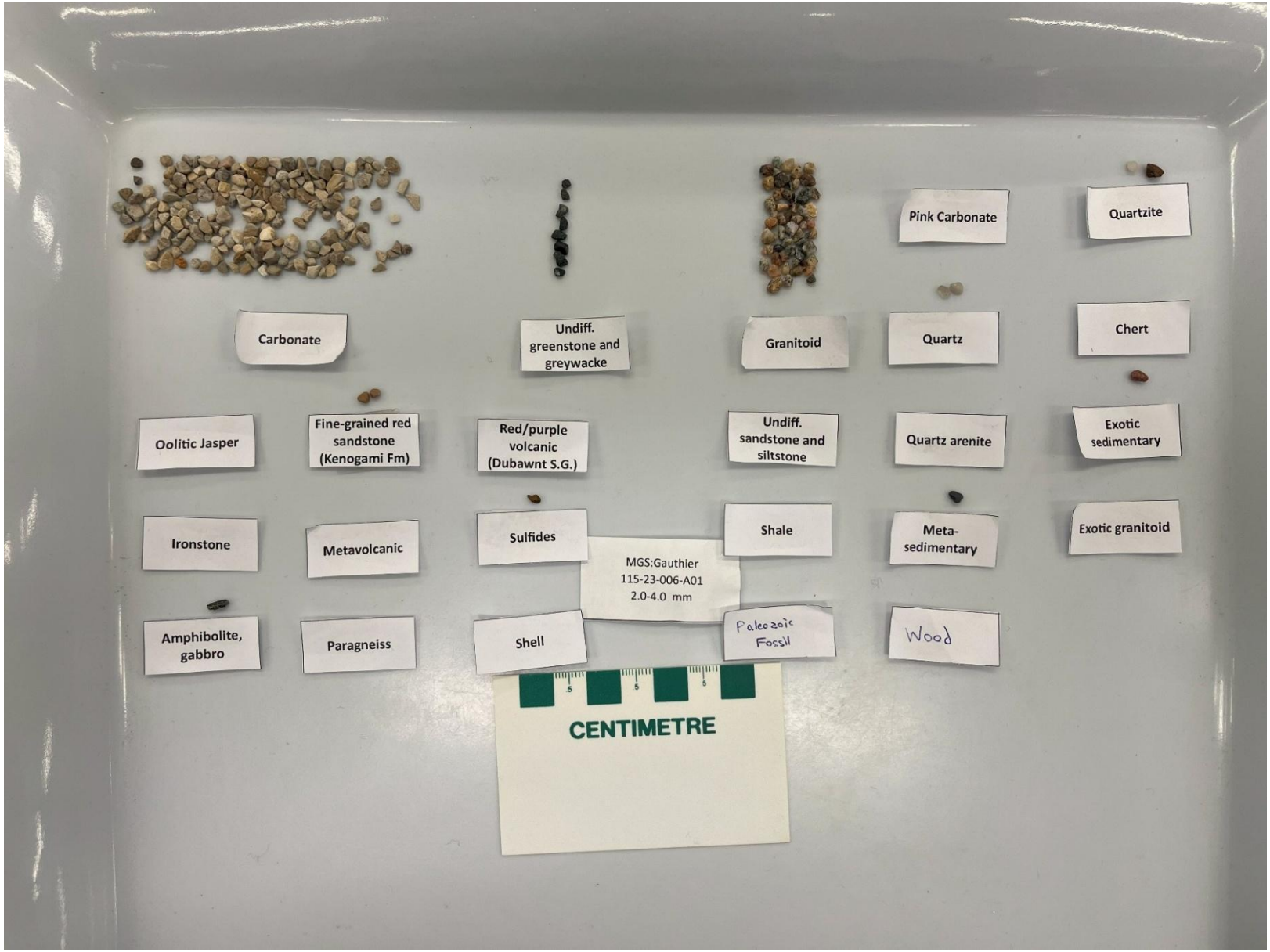

Carbonate
Undiff. greenstone and greywacke
Granitoid
Pink Carbonate
Quartzite
Quartz
Chert
Oolitic Jasper
Fine-grained red sandstone (Kenogami Fm)
Red/purple volcanic (Dubawnt S.G.)
Undiff. sandstone and siltstone
Quartz arenite
Exotic sedimentary
Ironstone
Metavolcanic
Sulfides
Shale
Meta-sedimentary
Exotic granitoid
Amphibolite, gabbro
Paragneiss
Shell
Paleozoic Fossil
Wood
CENTIMETRE
115-23-005-Z01


Carbonate
Undiff. greenstone and greywacke
Granitoid
Pink Carbonate
Quartzite
Quartz
Chert
Oolitic Jasper
Fine-grained red sandstone (Kenogami Fm)
Red/purple volcanic (Dubawnt S.G.)
Undiff. sandstone and siltstone
Quartz arenite
Exotic sedimentary
Ironstone
Metavolcanic
Sulfides
Shale
Meta-sedimentary
Exotic granitoid
Amphibolite, gabbro
Paragneiss
Shell
Paleozoic Fossil
Wood
CENTIMETRE
115-23-005-Z01

115-23-006


Carbonate
Undiff. greenstone and greywacke
Granitoid
Pink Carbonate
Quartzite
Quartz
Chert
Oolitic Jasper
Fine-grained red sandstone (Kenogami Fm)
Red/purple volcanic (Dubawnt S.G.)
Undiff. sandstone and siltstone
Quartz arenite
Exotic sedimentary
Ironstone
Metavolcanic
Sulfides
Shale
Meta-sedimentary
Exotic granitoid
Amphibolite, gabbro
Paragneiss
Shell
Paleozoic Fossil
Wood
CENTIMETRE
115-23-006-X01


Carbonate
Undiff. greenstone and greywacke
Granitoid
Pink Carbonate
Quartzite
Quartz
Chert
Undiff. sandstone and siltstone
Quartz arenite
Exotic sedimentary
Oolitic Jasper
Fine-grained red sandstone (Kenogami Fm)
Red/purple volcanic (Dubawnt S.G.)
Shale
Meta-sedimentary
Exotic granitoid
Ironstone
Metavolcanic
Sulfides
Amphibolite, gabbro
Paragneiss
Shell
Paleozoic Fossil
Wood
CENTIMETRE
115-23-006-X01


Carbonate
Undiff. greenstone and greywacke
Granitoid
Pink Carbonate
Quartzite
Quartz
Chert
Oolitic Jasper
Fine-grained red sandstone (Kenogami Fm)
Red/purple volcanic (Dubawnt S.G.)
Undiff. sandstone and siltstone
Quartz arenite
Exotic sedimentary
Ironstone
Metavolcanic
Sulfides
Shale
Meta-sedimentary
Exotic granitoid
MGS:Gauthier
115-23-006-A01
2.0-4.0 mm
Amphibolite, gabbro
Paragneiss
Shell
Paleozoic Fossil
Wood
CENTIMETRE


Carbonate
Undiff. greenstone and greywacke
Granitoid
Pink Carbonate
Oolitic Jasper
Fine-grained red sandstone (Kenogami Fm)
Red/purple volcanic (Dubawnt S.G.)
Quartz
Quartzite
Chert
Ironstone
Metavolcanic
Sulfides
Undiff. sandstone and siltstone
Quartz arenite
Exotic sedimentary
MGS:Gauthier
115-23-006-A01
4.0-8.0 mm
Amphibolite, gabbro
Paragneiss
Shell
Shale
Meta-sedimentary
Exotic granitoid
Paleozoic Fossil
CENTIMETRE


Carbonate
Undiff. greenstone and greywacke
Granitoid
Pink Carbonate
Quartzite
Quartz
Chert
Oolitic Jasper
Fine-grained red sandstone (Kenogami Fm)
Red/purple volcanic (Dubawnt S.G.)
Undiff. sandstone and siltstone
Quartz arenite
Exotic sedimentary
Ironstone
Metavolcanic
Sulfides
Shale
Meta-sedimentary
Exotic granitoid
Amphibolite, gabbro
Paragneiss
Shell
Paleozoic Fossil
Wood
CENTIMETRE
115-23-006-B01


Carbonate
Undiff. greenstone and greywacke
Granitoid
Pink Carbonate
Quartzite
Quartz
Chert
Oolitic Jasper
Fine-grained red sandstone (Kenogami Fm)
Red/purple volcanic (Dubawnt S.G.)
Undiff. sandstone and siltstone
Quartz arenite
Exotic sedimentary
Ironstone
Metavolcanic
Sulfides
Shale
Meta-sedimentary
Exotic granitoid
Amphibolite, gabbro
Paragneiss
Shell
Paleozoic Fossil
Wood
CENTIMETRE
115-23-006-B01

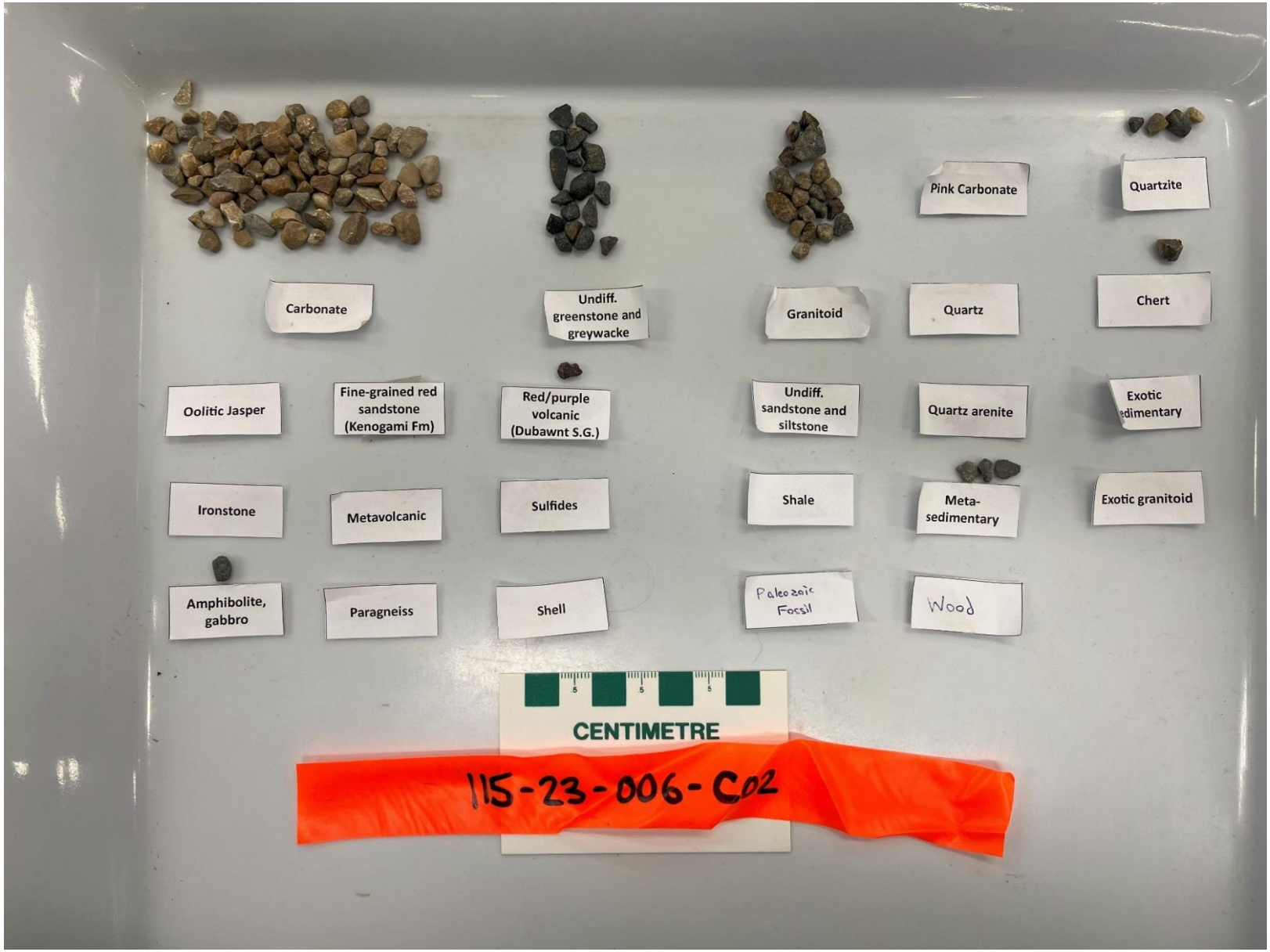

Carbonate
Undiff. greenstone and greywacke
Granitoid
Pink Carbonate
Quartzite
Quartz
Chert
Oolitic Jasper
Fine-grained red sandstone (Kenogami Fm)
Red/purple volcanic (Dubawnt S.G.)
Undiff. sandstone and siltstone
Quartz arenite
Exotic sedimentary
Ironstone
Metavolcanic
Sulfides
Shale
Meta-sedimentary
Exotic granitoid
MGS:Gauthier
115-23-006-B02
2.0-4.0 mm
Amphibolite, gabbro
Paragneiss
Shell
Paleozoic Fossil
Wood
CENTIMETRE


CARB
UGG
GR
P-Carb
Qalitic Jasper
Ken
Qvtzwt
Qtz
Qtzite
Chert
Ironstone
Volc
Sulfides
USS
Qtz arr
Ex Sed
Arrgln/gwb
P. Gneiss
Shell
115-23-006-B02
4.0-8.0 mm
Shale
Metased
ex. GR

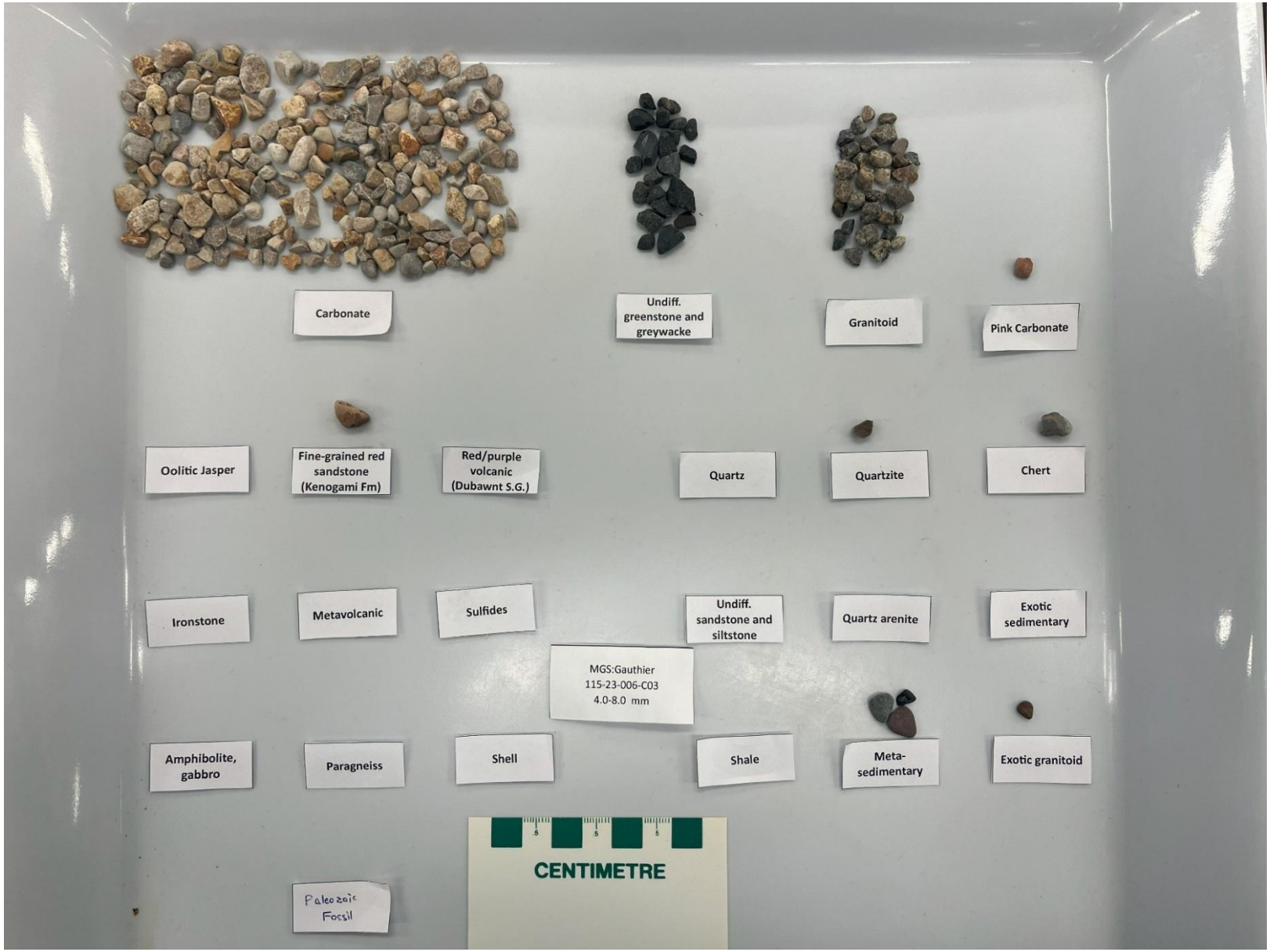

Carbonate
Undiff. greenstone and greywacke
Granitoid
Pink Carbonate
Quartzite
Quartz
Chert
Oolitic Jasper
Fine-grained red sandstone (Kenogami Fm)
Red/purple volcanic (Dubawnt S.G.)
Undiff. sandstone and siltstone
Quartz arenite
Exotic sedimentary
Ironstone
Metavolcanic
Sulfides
Shale
Meta-sedimentary
Exotic granitoid
MGS:Gauthier
115-23-006-C01
2.0-4.0 mm
Amphibolite, gabbro
Paragneiss
Shell
Paleozoic Fossil
Wood
CENTIMETRE


Carbonate
Undiff. greenstone and greywacke
Granitoid
Pink Carbonate
Oolitic Jasper
Fine-grained red sandstone (Kenogami Fm)
Red/purple volcanic (Dubawnt S.G.)
Quartz
Quartzite
Chert
Ironstone
Metavolcanic
Sulfides
Undiff. sandstone and siltstone
Quartz arenite
Exotic sedimentary
MGS:Gauthier
115-23-006-C01
4.0-8.0 mm
Amphibolite, gabbro
Paragneiss
Shell
Shale
Meta-sedimentary
Exotic granitoid
Paleozoic Fossil
CENTIMETRE


Carbonate
Undiff. greenstone and greywacke
Granitoid
Pink Carbonate
Quartz
Quartzite
Chert
Oolitic Jasper
Fine-grained red sandstone (Kenogami Fm)
Red/purple volcanic (Dubawnt S.G.)
Undiff. sandstone and siltstone
Quartz arenite
Exotic sedimentary
Ironstone
Metavolcanic
Sulfides
Shale
Meta-sedimentary
Exotic granitoid
Amphibolite, gabbro
Paragneiss
Shell
Paleozoic Fossil
Wood
CENTIMETRE
115-23-006-C02


Carbonate
Undiff. greenstone and greywacke
Granitoid
Pink Carbonate
Quartzite
Quartz
Chert
Oolitic Jasper
Fine-grained red sandstone (Kenogami Fm)
Red/purple volcanic (Dubawnt S.G.)
Undiff. sandstone and siltstone
Quartz arenite
Exotic sedimentary
Ironstone
Metavolcanic
Sulfides
Shale
Meta-sedimentary
Exotic granitoid
Amphibolite, gabbro
Paragneiss
Shell
Paleozoic Fossil
Wood
CENTIMETRE
115-23-006-C02

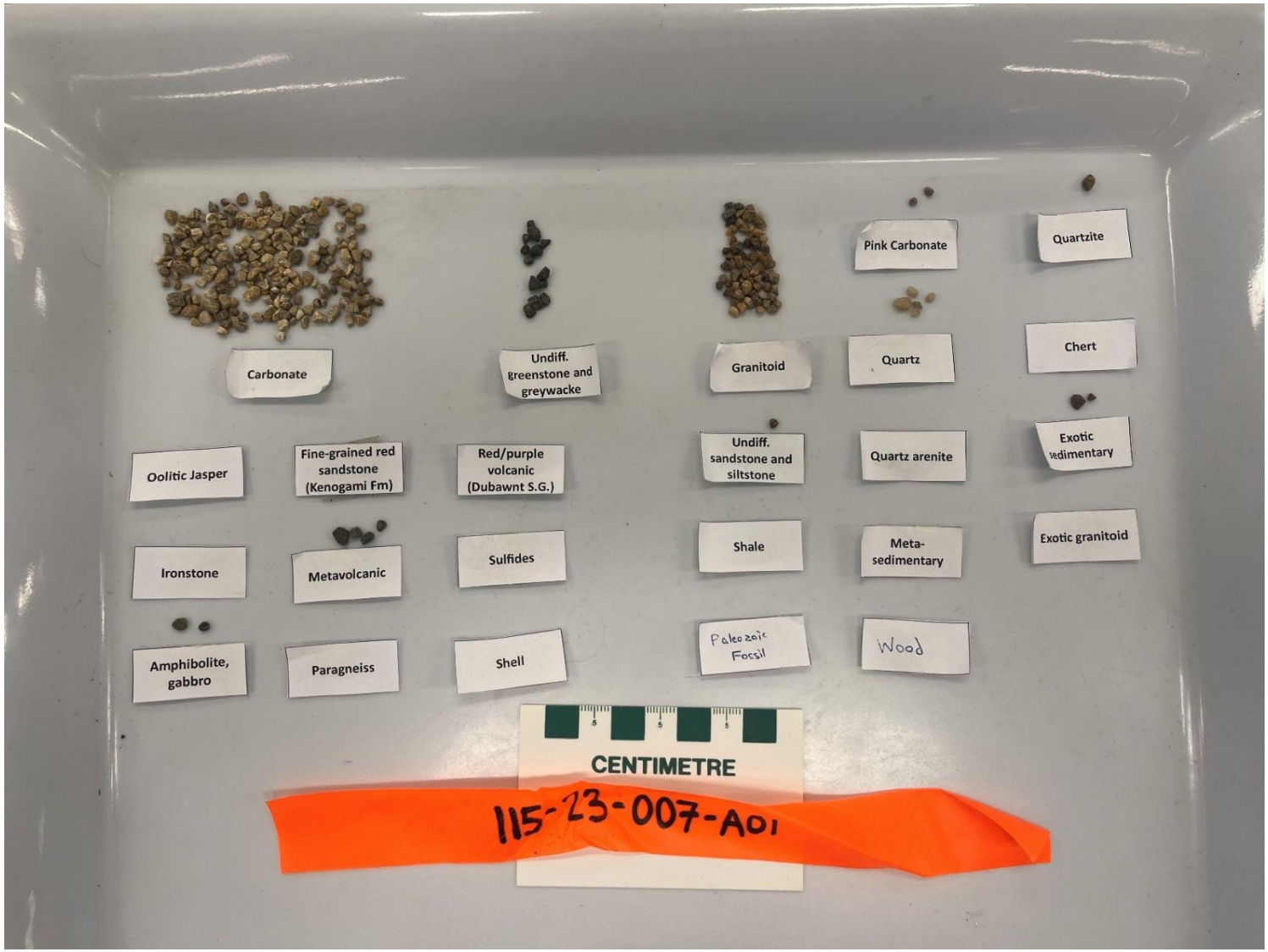

Carbonate
Undiff. greenstone and greywacke
Granitoid
Pink Carbonate
Quartzite
Quartz
Chert
Oolitic Jasper
Fine-grained red sandstone (Kenogami Fm)
Red/purple volcanic (Dubawnt S.G.)
Undiff. sandstone and siltstone
Quartz arenite
Exotic sedimentary
Ironstone
Metavolcanic
Sulfides
Shale
Meta-sedimentary
Exotic granitoid
MGS:Gauthier
115-23-006-C03
2.0-4.0 mm
Amphibolite, gabbro
Paragneiss
Shell
Paleozoic Fossil
Wood
CENTIMETRE


Carbonate
Undiff. greenstone and greywacke
Granitoid
Pink Carbonate
Oolitic Jasper
Fine-grained red sandstone (Kenogami Fm)
Red/purple volcanic (Dubawnt S.G.)
Quartz
Quartzite
Chert
Ironstone
Metavolcanic
Sulfides
Undiff. sandstone and siltstone
Quartz arenite
Exotic sedimentary
MGS:Gauthier
115-23-006-C03
4.0-8.0 mm
Amphibolite, gabbro
Paragneiss
Shell
Shale
Meta-sedimentary
Exotic granitoid
CENTIMETRE
Paleozoic Fossil

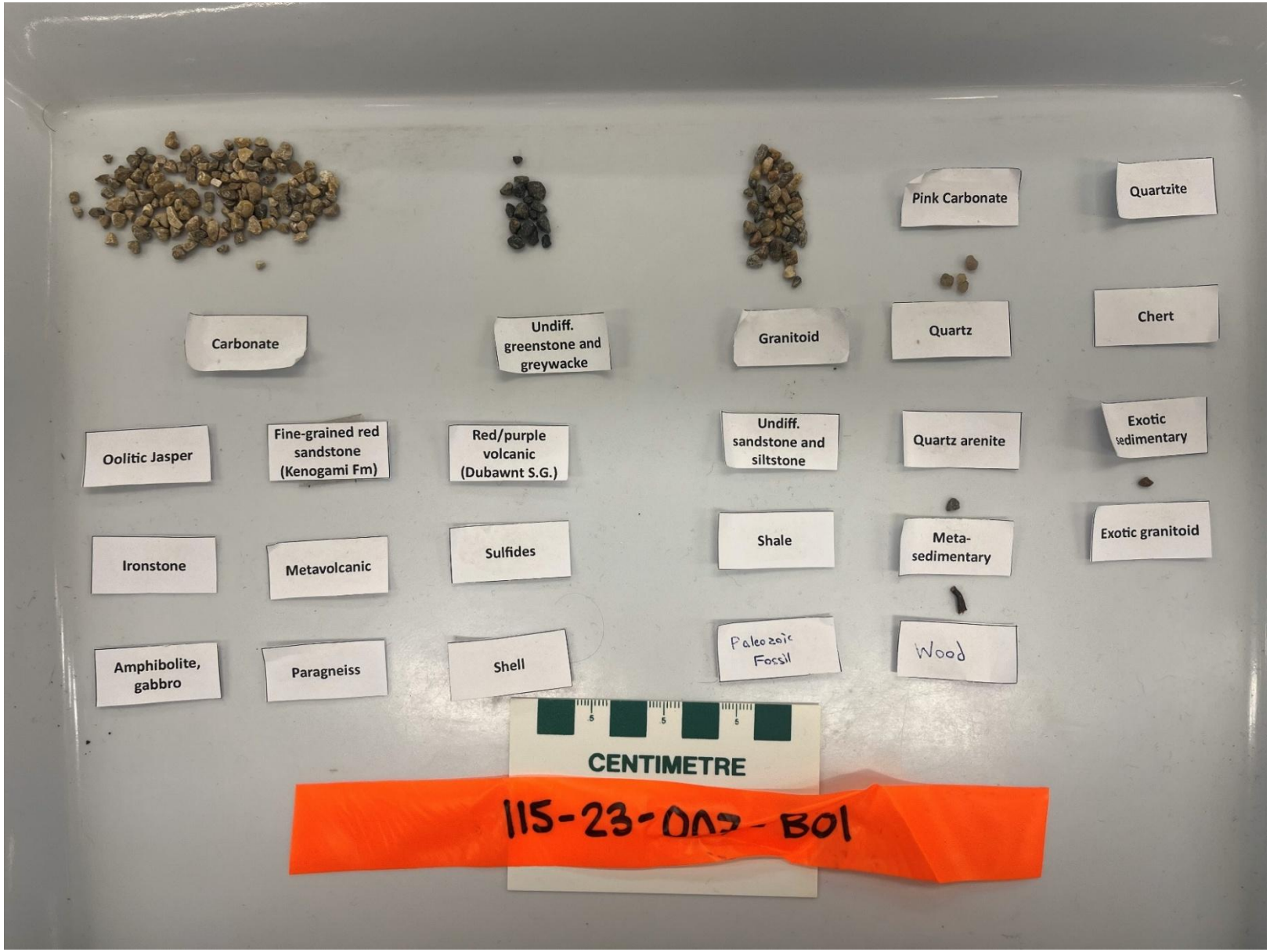

Carbonate
Undiff. greenstone and greywacke
Granitoid
Pink Carbonate
Quartzite
Chert
Quartz
Oolitic Jasper
Fine-grained red sandstone (Kenogami Fm)
Red/purple volcanic (Dubawnt S.G.)
Undiff. sandstone and siltstone
Quartz arenite
Exotic sedimentary
Ironstone
Metavolcanic
Sulfides
Shale
Meta-sedimentary
Exotic granitoid
MGS:Gauthier
115-23-006-D01
2.0-4.0 mm
Amphibolite, gabbro
Paragneiss
Shell
Paleozoic Fossil
Wood
CENTIMETRE

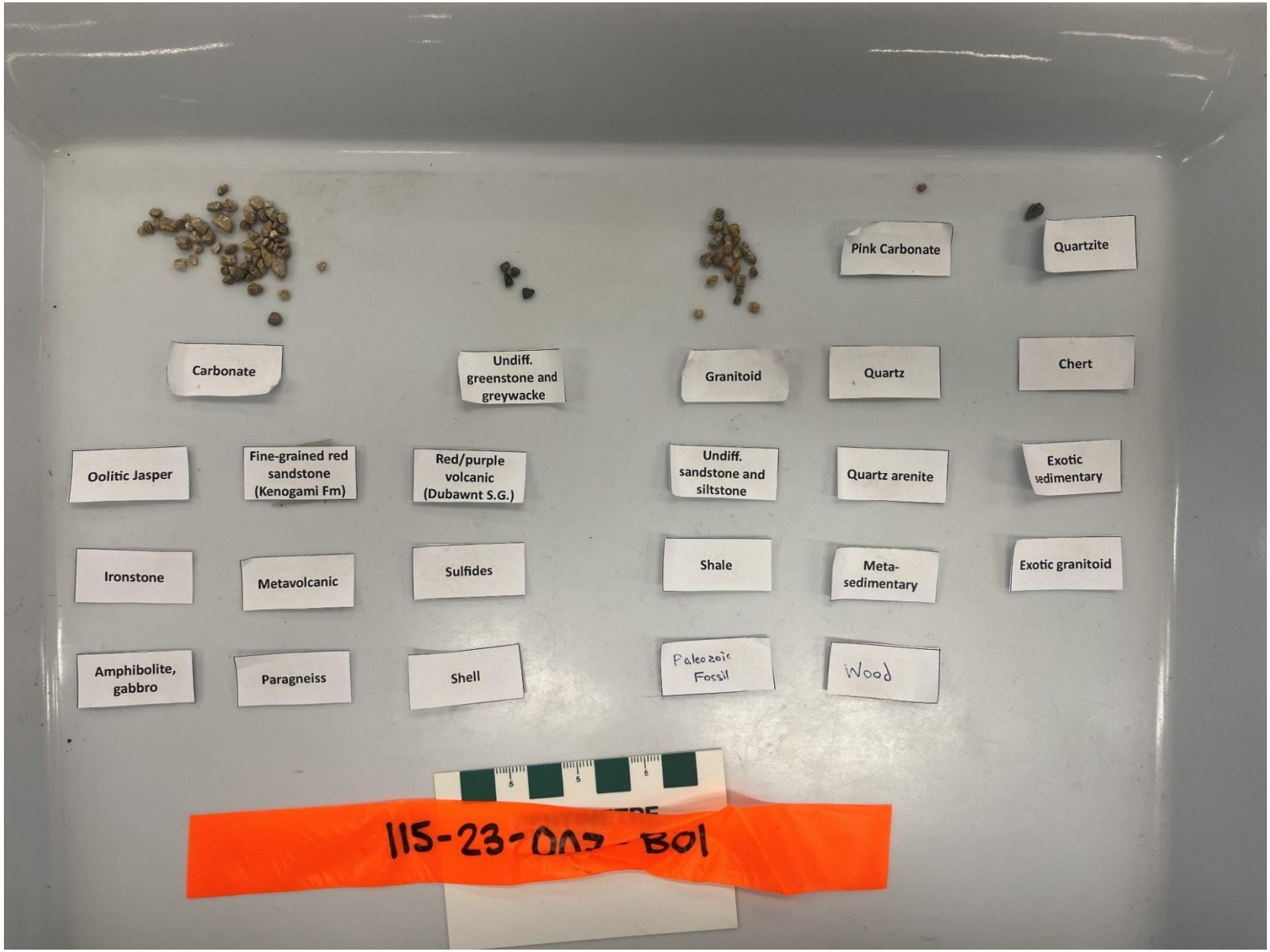

Carbonate
Undiff. greenstone and greywacke
Granitoid
Pink Carbonate
Oolitic Jasper
Fine-grained red sandstone (Kenogami Fm)
Red/purple volcanic (Dubawnt S.G.)
Quartz
Quartzite
Chert
Ironstone
Metavolcanic
Sulfides
Undiff. sandstone and siltstone
Quartz arenite
Exotic sedimentary
MGS:Gauthier
115-23-006-D01
4.0-8.0 mm
Amphibolite, gabbro
Paragneiss
Shell
Shale
Meta-sedimentary
Exotic granitoid
CENTIMETRE
Paleozoic Fossil

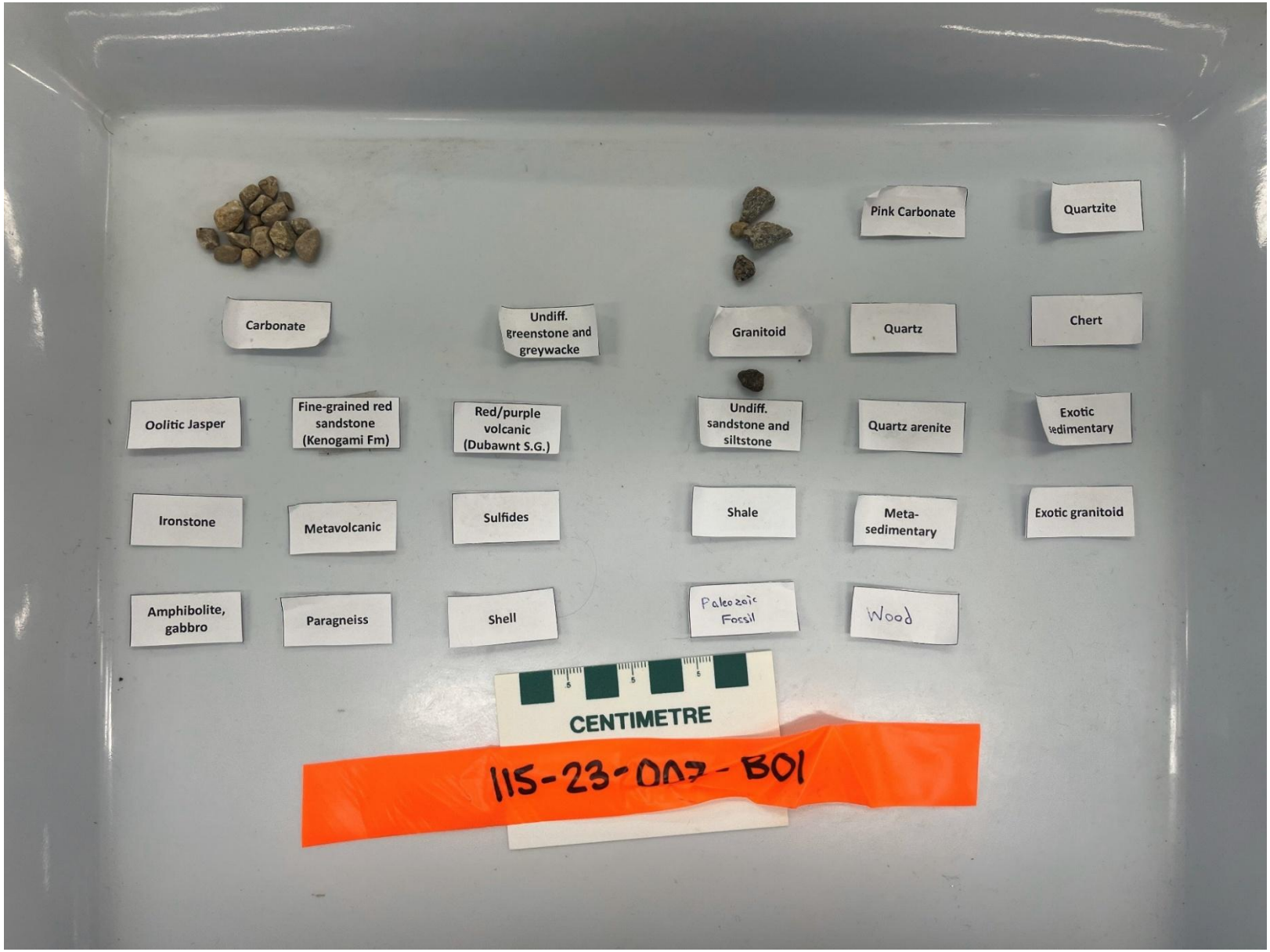
115-23-007


Carbonate
Undiff. greenstone and greywacke
Granitoid
Pink Carbonate
Quartzite
Quartz
Chert
Oolitic Jasper
Fine-grained red sandstone (Kenogami Fm)
Red/purple volcanic (Dubawnt S.G.)
Undiff. sandstone and siltstone
Quartz arenite
Exotic sedimentary
Ironstone
Metavolcanic
Sulfides
Shale
Meta-sedimentary
Exotic granitoid
Amphibolite, gabbro
Paragneiss
Shell
Paleozoic Fossil
Wood
CENTIMETRE
115-23-007-A01


Carbonate
Undiff. greenstone and greywacke
Granitoid
Pink Carbonate
Quartzite
Quartz
Chert
Oolitic Jasper
Fine-grained red sandstone (Kenogami Fm)
Red/purple volcanic (Dubawnt S.G.)
Undiff. sandstone and siltstone
Quartz arenite
Exotic sedimentary
Ironstone
Metavolcanic
Sulfides
Shale
Meta-sedimentary
Exotic granitoid
Amphibolite, gabbro
Paragneiss
Shell
Paleozoic Fossil
Wood
CENTIMETRE
115-23-007-A01


Carbonate
Undiff. greenstone and greywacke
Granitoid
Pink Carbonate
Quartzite
Quartz
Chert
Oolitic Jasper
Fine-grained red sandstone (Kenogami Fm)
Red/purple volcanic (Dubawnt S.G.)
Undiff. sandstone and siltstone
Quartz arenite
Exotic sedimentary
Ironstone
Metavolcanic
Sulfides
Shale
Meta-sedimentary
Exotic granitoid
Amphibolite, gabbro
Paragneiss
Shell
Paleozoic Fossil
Wood
CENTIMETRE
115-23-007-B01


Carbonate
Undiff. greenstone and greywacke
Granitoid
Pink Carbonate
Quartzite
Quartz
Chert
Oolitic Jasper
Fine-grained red sandstone (Kenogami Fm)
Red/purple volcanic (Dubawnt S.G.)
Undiff. sandstone and siltstone
Quartz arenite
Exotic sedimentary
Ironstone
Metavolcanic
Sulfides
Shale
Meta-sedimentary
Exotic granitoid
Amphibolite, gabbro
Paragneiss
Shell
Paleozoic Fossil
Wood
115-23-003-B01


Carbonate
Undiff. greenstone and greywacke
Granitoid
Pink Carbonate
Quartzite
Quartz
Chert
Oolitic Jasper
Fine-grained red sandstone (Kenogami Fm)
Red/purple volcanic (Dubawnt S.G.)
Undiff. sandstone and siltstone
Quartz arenite
Exotic sedimentary
Ironstone
Metavolcanic
Sulfides
Shale
Meta-sedimentary
Exotic granitoid
Amphibolite, gabbro
Paragneiss
Shell
Paleozoic Fossil
Wood
CENTIMETRE
115-23-007-B01

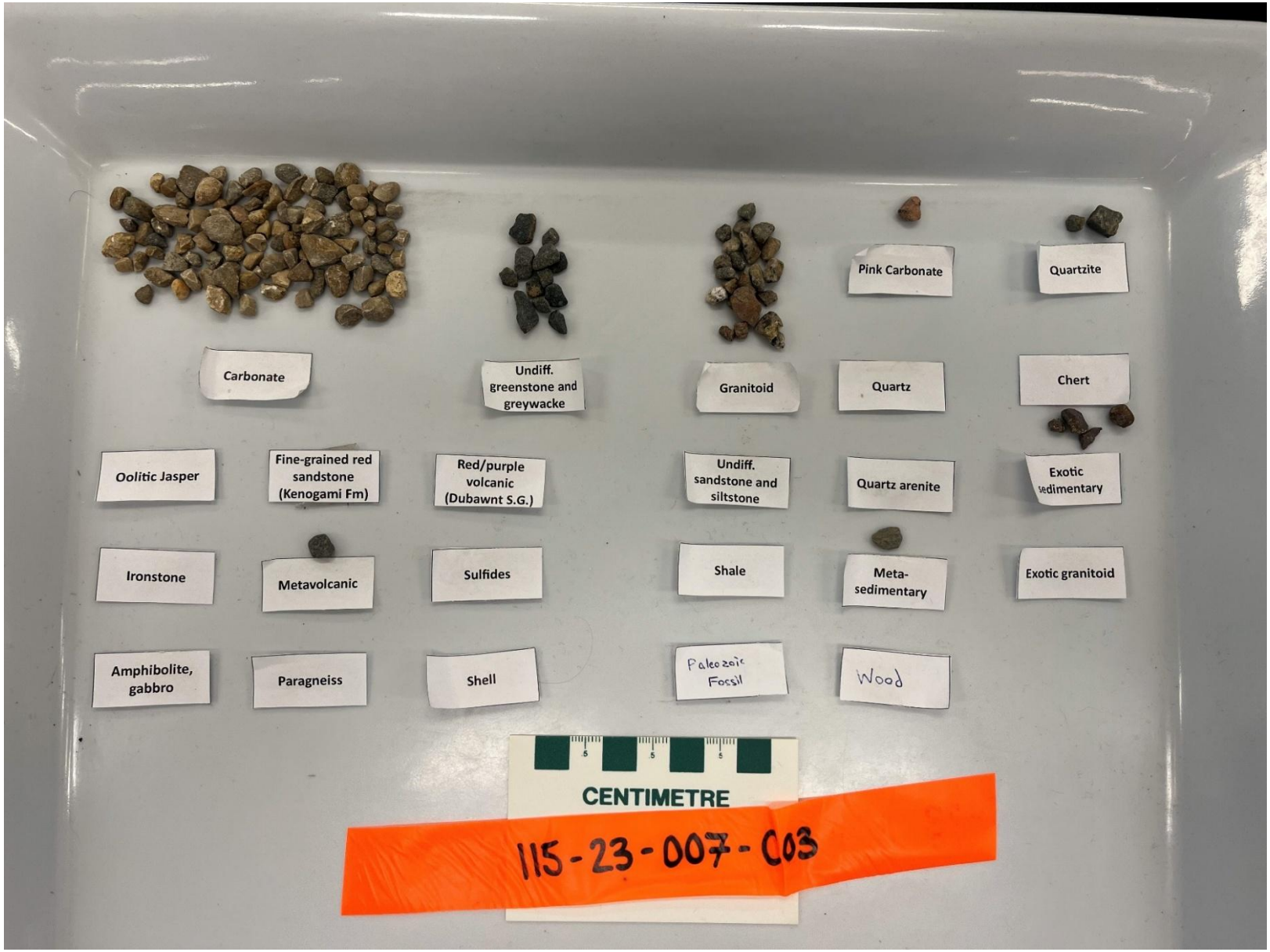

Carbonate
Undiff. greenstone and greywacke
Granitoid
Pink Carbonate
Quartzite
Quartz
Chert
Oolitic Jasper
Fine-grained red sandstone (Kenogami Fm)
Red/purple volcanic (Dubawnt S.G.)
Undiff. sandstone and siltstone
Quartz arenite
Exotic sedimentary
Ironstone
Metavolcanic
Sulfides
Shale
Meta-sedimentary
Exotic granitoid
MGS:Gauthier
115-23-007-B02
2.0-4.0 mm
Amphibolite, gabbro
Paragneiss
Shell
Paleozoic Fossil
Wood
CENTIMETRE


Carbonate
Undiff. greenstone and greywacke
Granitoid
Pink Carbonate
Oolitic Jasper
Fine-grained red sandstone (Kenogami Fm)
Red/purple volcanic (Dubawnt S.G.)
Quartz
Quartzite
Chert
Ironstone
Metavolcanic
Sulfides
Undiff. sandstone and siltstone
Quartz arenite
Exotic sedimentary
MGS:Gauthier
115-23-007-B02
4.0-8.0 mm
Amphibolite, gabbro
Paragneiss
Shell
Shale
Meta-sedimentary
Exotic granitoid
Paleozoic Fossil
CENTIMETRE


Carbonate
Undiff. greenstone and greywacke
Granitoid
Pink Carbonate
Quartzite
Quartz
Chert
Oolitic Jasper
Fine-grained red sandstone (Kenogami Fm)
Red/purple volcanic (Dubawnt S.G.)
Undiff. sandstone and siltstone
Quartz arenite
Exotic sedimentary
Ironstone
Metavolcanic
Sulfides
Shale
Meta-sedimentary
Exotic granitoid
MGS:Gauthier
115-23-007-C01
2.0-4.0 mm
Amphibolite, gabbro
Paragneiss
Shell
Paleozoic Fossil
Wood
CENTIMETRE

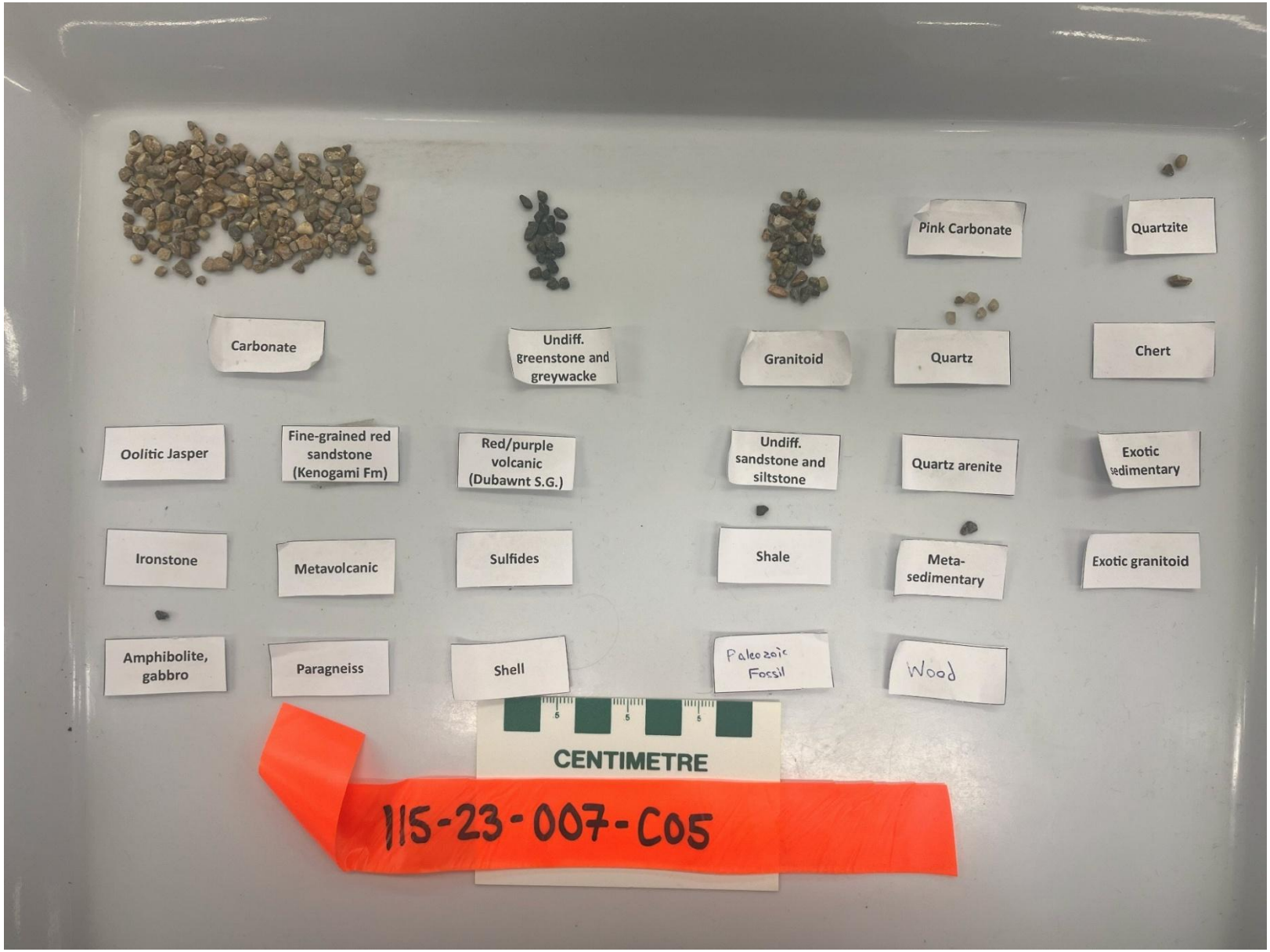

Carbonate
Undiff. greenstone and greywacke
Granitoid
Pink Carbonate
Oolitic Jasper
Fine-grained red sandstone (Kenogami Fm)
Red/purple volcanic (Dubawnt S.G.)
Quartz
Quartzite
Chert
Ironstone
Metavolcanic
Sulfides
Undiff. sandstone and siltstone
Quartz arenite
Exotic sedimentary
MGS:Gauthier
115-23-007-C01
4.0-8.0 mm
Amphibolite, gabbro
Paragneiss
Shell
Shale
Meta-sedimentary
Exotic granitoid
Paleozoic Fossil
CENTIMETRE


Carbonate
Undiff. greenstone and greywacke
Granitoid
Pink Carbonate
Quartzite
Quartz
Chert
Oolitic Jasper
Fine-grained red sandstone (Kenogami Fm)
Red/purple volcanic (Dubawnt S.G.)
Undiff. sandstone and siltstone
Quartz arenite
Exotic sedimentary
Ironstone
Metavolcanic
Sulfides
Shale
Meta-sedimentary
Exotic granitoid
Amphibolite, gabbro
Paragneiss
Shell
Paleozoic Fossil
Wood
CENTIMETRE
115-23-007-C03


Carbonate
Undiff. greenstone and greywacke
Granitoid
Pink Carbonate
Quartzite
Quartz
Chert
Oolitic Jasper
Fine-grained red sandstone (Kenogami Fm)
Red/purple volcanic (Dubawnt S.G.)
Undiff. sandstone and siltstone
Quartz arenite
Exotic sedimentary
Ironstone
Metavolcanic
Sulfides
Shale
Meta-sedimentary
Exotic granitoid
Amphibolite, gabbro
Paragneiss
Shell
Paleozoic Fossil
Wood
CENTIMETRE
115-23-007-C03


Carbonate
Undiff. greenstone and greywacke
Granitoid
Pink Carbonate
Quartzite
Quartz
Chert
Oolitic Jasper
Fine-grained red sandstone (Kenogami Fm)
Red/purple volcanic (Dubawnt S.G.)
Undiff. sandstone and siltstone
Quartz arenite
Exotic sedimentary
Ironstone
Metavolcanic
Sulfides
Shale
Meta-sedimentary
Exotic granitoid
MGS:Gauthier
115-23-007-C04
2.0-4.0 mm
Amphibolite, gabbro
Paragneiss
Shell
Paleozoic Fossil
Wood
CENTIMETRE

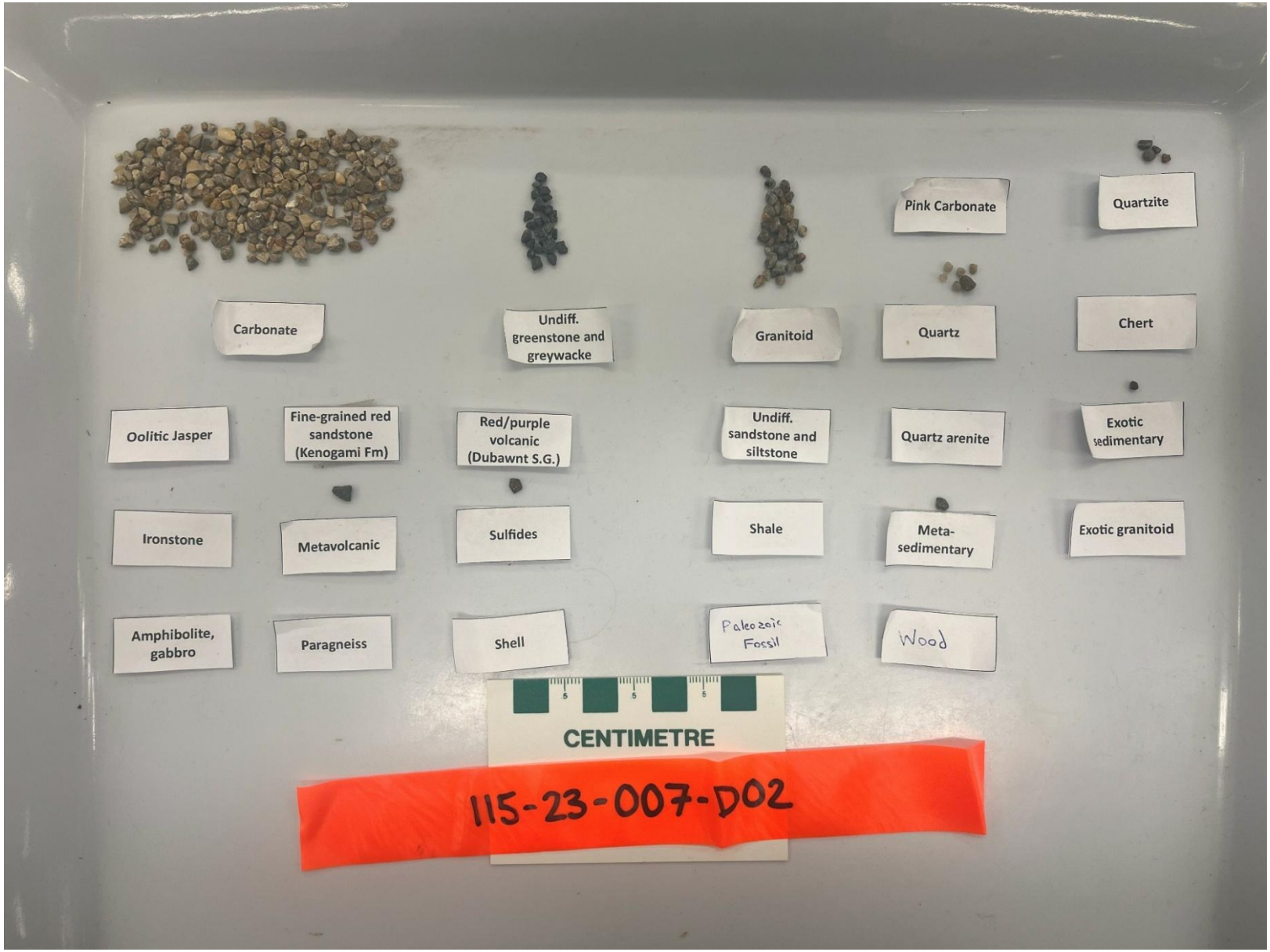

Carbonate
Undiff. greenstone and greywacke
Granitoid
Pink Carbonate
Oolitic Jasper
Fine-grained red sandstone (Kenogami Fm)
Red/purple volcanic (Dubawnt S.G.)
Quartz
Quartzite
Chert
Ironstone
Metavolcanic
Sulfides
Undiff. sandstone and siltstone
Quartz arenite
Exotic sedimentary
MGS:Gauthier
115-23-007-C04
4.0-8.0 mm
Amphibolite, gabbro
Paragneiss
Shell
Shale
Meta-sedimentary
Exotic granitoid
Paleozoic Fossil
CENTIMETRE


Carbonate
Undiff. greenstone and greywacke
Granitoid
Pink Carbonate
Quartzite
Quartz
Chert
Oolitic Jasper
Fine-grained red sandstone (Kenogami Fm)
Red/purple volcanic (Dubawnt S.G.)
Undiff. sandstone and siltstone
Quartz arenite
Exotic sedimentary
Ironstone
Metavolcanic
Sulfides
Shale
Meta-sedimentary
Exotic granitoid
Amphibolite, gabbro
Paragneiss
Shell
Paleozoic Fossil
Wood
CENTIMETRE
115-23-007-C05

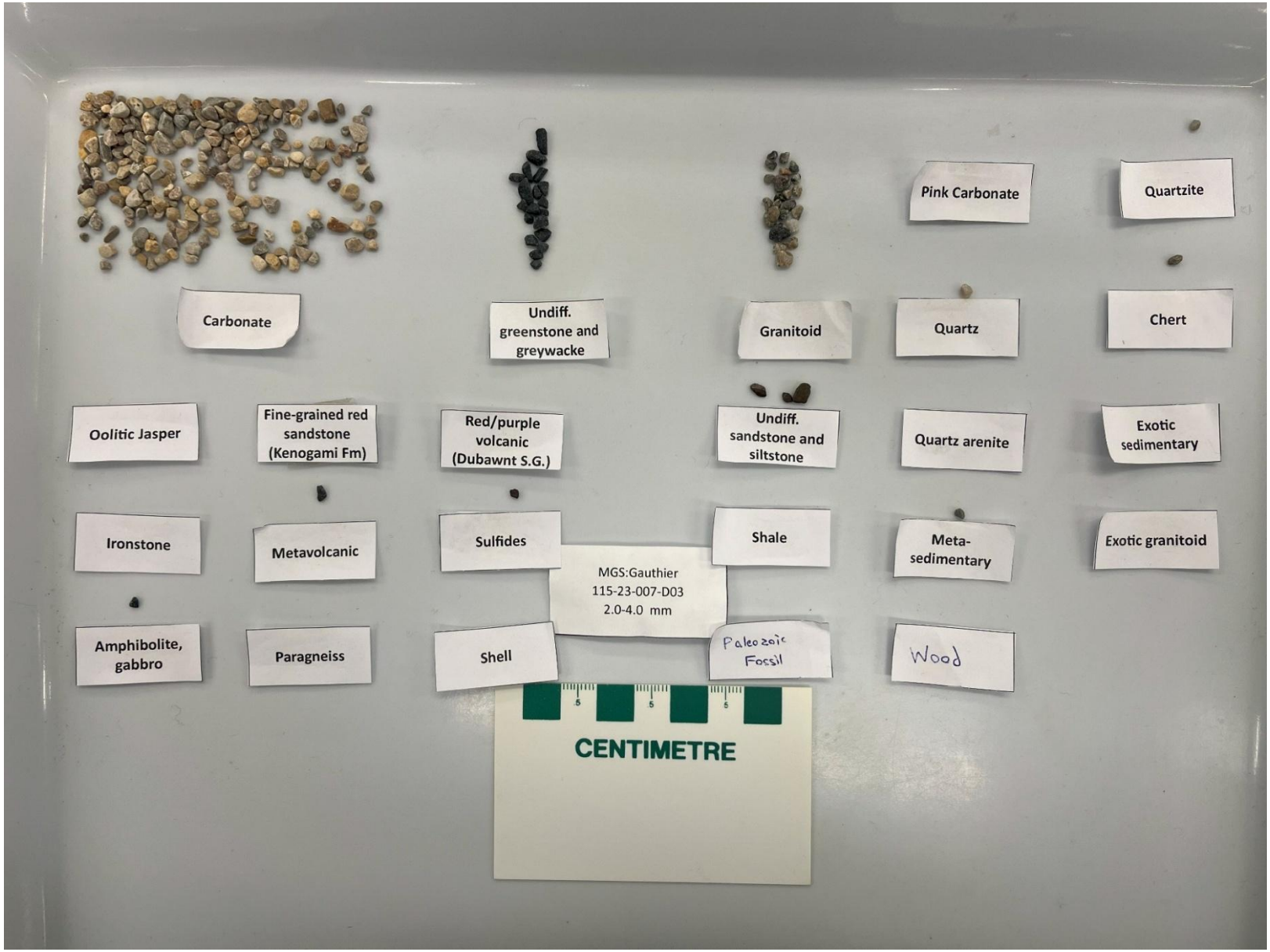

Carbonate
Undiff. greenstone and greywacke
Granitoid
Pink Carbonate
Quartzite
Quartz
Chert
Oolitic Jasper
Fine-grained red sandstone (Kenogami Fm)
Red/purple volcanic (Dubawnt S.G.)
Undiff. sandstone and siltstone
Quartz arenite
Exotic sedimentary
Ironstone
Metavolcanic
Sulfides
Shale
Meta-sedimentary
Exotic granitoid
Amphibolite, gabbro
Paragneiss
Shell
Paleozoic Fossil
Wood
CENTIMETRE
115-23-007-C05


Carbonate
Undiff. greenstone and greywacke
Granitoid
Pink Carbonate
Quartzite
Quartz
Chert
Oolitic Jasper
Fine-grained red sandstone (Kenogami Fm)
Red/purple volcanic (Dubawnt S.G.)
Undiff. sandstone and siltstone
Quartz arenite
Exotic sedimentary
Ironstone
Metavolcanic
Sulfides
Shale
Meta-sedimentary
Exotic granitoid
MGS:Gauthier
115-23-007-D01
2.0-4.0 mm
Amphibolite, gabbro
Paragneiss
Shell
Paleozoic Fossil
Wood
CENTIMETRE


Carbonate
Undiff. greenstone and greywacke
Granitoid
Pink Carbonate
Oolitic Jasper
Fine-grained red sandstone (Kenogami Fm)
Red/purple volcanic (Dubawnt S.G.)
Quartz
Quartzite
Chert
Ironstone
Metavolcanic
Sulfides
Undiff. sandstone and siltstone
Quartz arenite
Exotic sedimentary
MGS:Gauthier
115-23-007-D01
4.0-8.0 mm
Amphibolite, gabbro
Paragneiss
Shell
Shale
Meta-sedimentary
Exotic granitoid
Paleozoic Fossil
CENTIMETRE

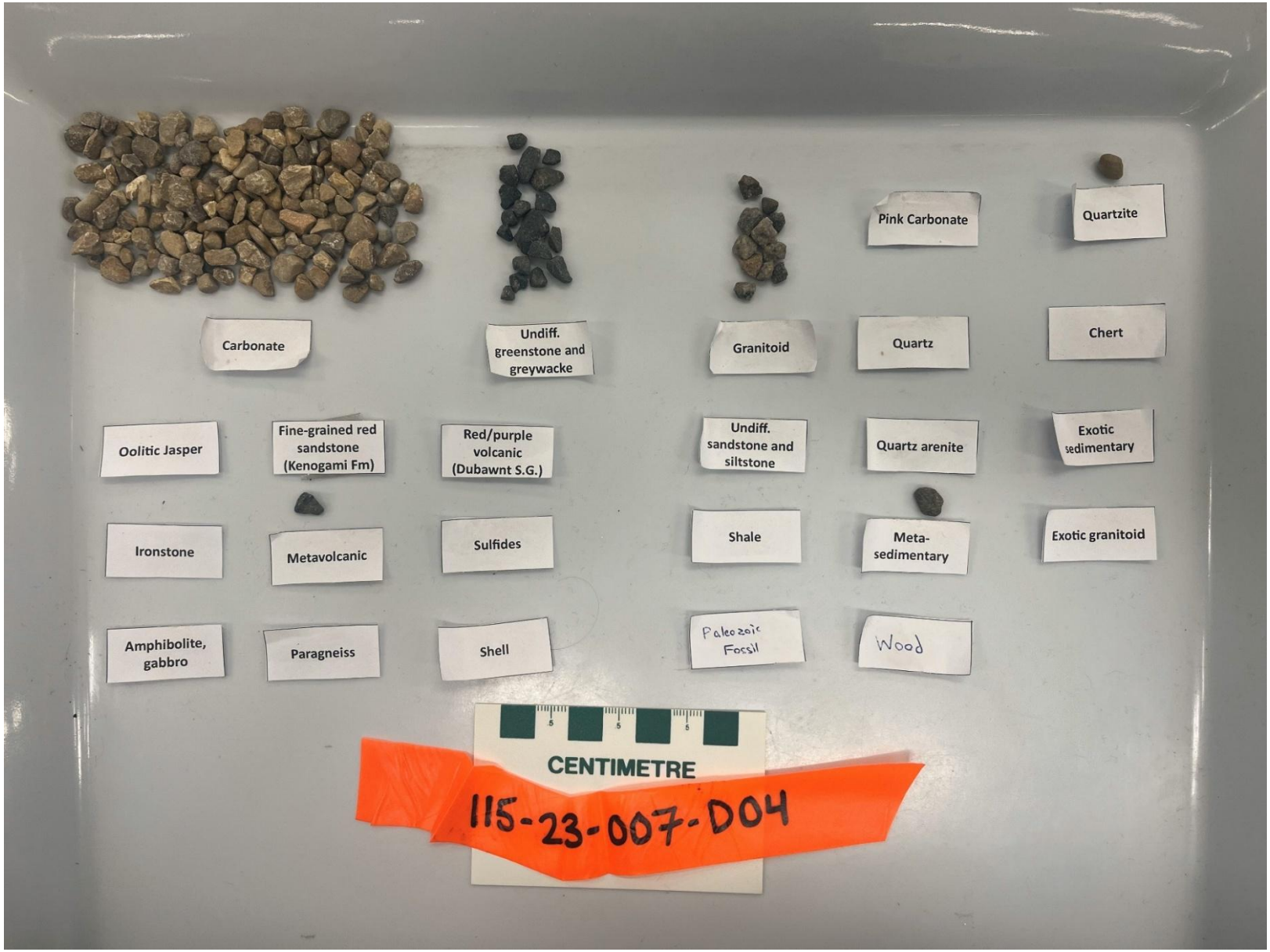

Carbonate
Undiff. greenstone and greywacke
Granitoid
Pink Carbonate
Quartzite
Quartz
Chert
Oolitic Jasper
Fine-grained red sandstone (Kenogami Fm)
Red/purple volcanic (Dubawnt S.G.)
Undiff. sandstone and siltstone
Quartz arenite
Exotic sedimentary
Ironstone
Metavolcanic
Sulfides
Shale
Meta-sedimentary
Exotic granitoid
Amphibolite, gabbro
Paragneiss
Shell
Paleozoic Fossil
Wood
CENTIMETRE
115-23-007-D02


Carbonate
Undiff. greenstone and greywacke
Granitoid
Pink Carbonate
Quartzite
Quartz
Chert
Oolitic Jasper
Fine-grained red sandstone (Kenogami Fm)
Red/purple volcanic (Dubawnt S.G.)
Undiff. sandstone and siltstone
Quartz arenite
Exotic sedimentary
Ironstone
Metavolcanic
Sulfides
Shale
Meta-sedimentary
Exotic granitoid
Amphibolite, gabbro
Paragneiss
Shell
Paleozoic Fossil
Wood
CENTIMETRE
115-23-007-D02


Carbonate
Undiff. greenstone and greywacke
Granitoid
Pink Carbonate
Quartzite
Quartz
Chert
Oolitic Jasper
Fine-grained red sandstone (Kenogami Fm)
Red/purple volcanic (Dubawnt S.G.)
Undiff. sandstone and siltstone
Quartz arenite
Exotic sedimentary
Ironstone
Metavolcanic
Sulfides
Shale
Meta-sedimentary
Exotic granitoid
MGS:Gauthier
115-23-007-D03
2.0-4.0 mm
Amphibolite, gabbro
Paragneiss
Shell
Paleozoic Fossil
Wood
CENTIMETRE


Carbonate
Undiff. greenstone and greywacke
Granitoid
Pink Carbonate
Oolitic Jasper
Fine-grained red sandstone (Kenogami Fm)
Red/purple volcanic (Dubawnt S.G.)
Quartz
Quartzite
Chert
Ironstone
Metavolcanic
Sulfides
Undiff. sandstone and siltstone
Quartz arenite
Exotic sedimentary
MGS:Gauthier
115-23-007-D03
4.0-8.0 mm
Amphibolite, gabbro
Paragneiss
Shell
Shale
Meta-sedimentary
Exotic granitoid
Paleozoic Fossil
CENTIMETRE


Carbonate
Undiff. greenstone and greywacke
Granitoid
Pink Carbonate
Quartzite
Quartz
Chert
Oolitic Jasper
Fine-grained red sandstone (Kenogami Fm)
Red/purple volcanic (Dubawnt S.G.)
Undiff. sandstone and siltstone
Quartz arenite
Exotic sedimentary
Ironstone
Metavolcanic
Sulfides
Shale
Meta-sedimentary
Exotic granitoid
Amphibolite, gabbro
Paragneiss
Shell
Paleozoic Fossil
Wood
CENTIMETRE
115-23-007-D04


Carbonate
Undiff. greenstone and greywacke
Granitoid
Pink Carbonate
Quartzite
Quartz
Chert
Oolitic Jasper
Fine-grained red sandstone (Kenogami Fm)
Red/purple volcanic (Dubawnt S.G.)
Undiff. sandstone and siltstone
Quartz arenite
Exotic sedimentary
Ironstone
Metavolcanic
Sulfides
Shale
Meta-sedimentary
Exotic granitoid
Amphibolite, gabbro
Paragneiss
Shell
Paleozoic Fossil
Wood
CENTIMETRE
115-23-007-D04


Carbonate
Undiff. greenstone and greywacke
Granitoid
Pink Carbonate
Quartzite
Quartz
Chert
Oolitic Jasper
Fine-grained red sandstone (Kenogami Fm)
Red/purple volcanic (Dubawnt S.G.)
Undiff. sandstone and siltstone
Quartz arenite
Exotic sedimentary
Ironstone
Metavolcanic
Sulfides
Shale
Meta-sedimentary
Exotic granitoid
Amphibolite, gabbro
Paragneiss
Shell
Paleozoic Fossil
Wood
CENTIMETRE
115-23-007-D05

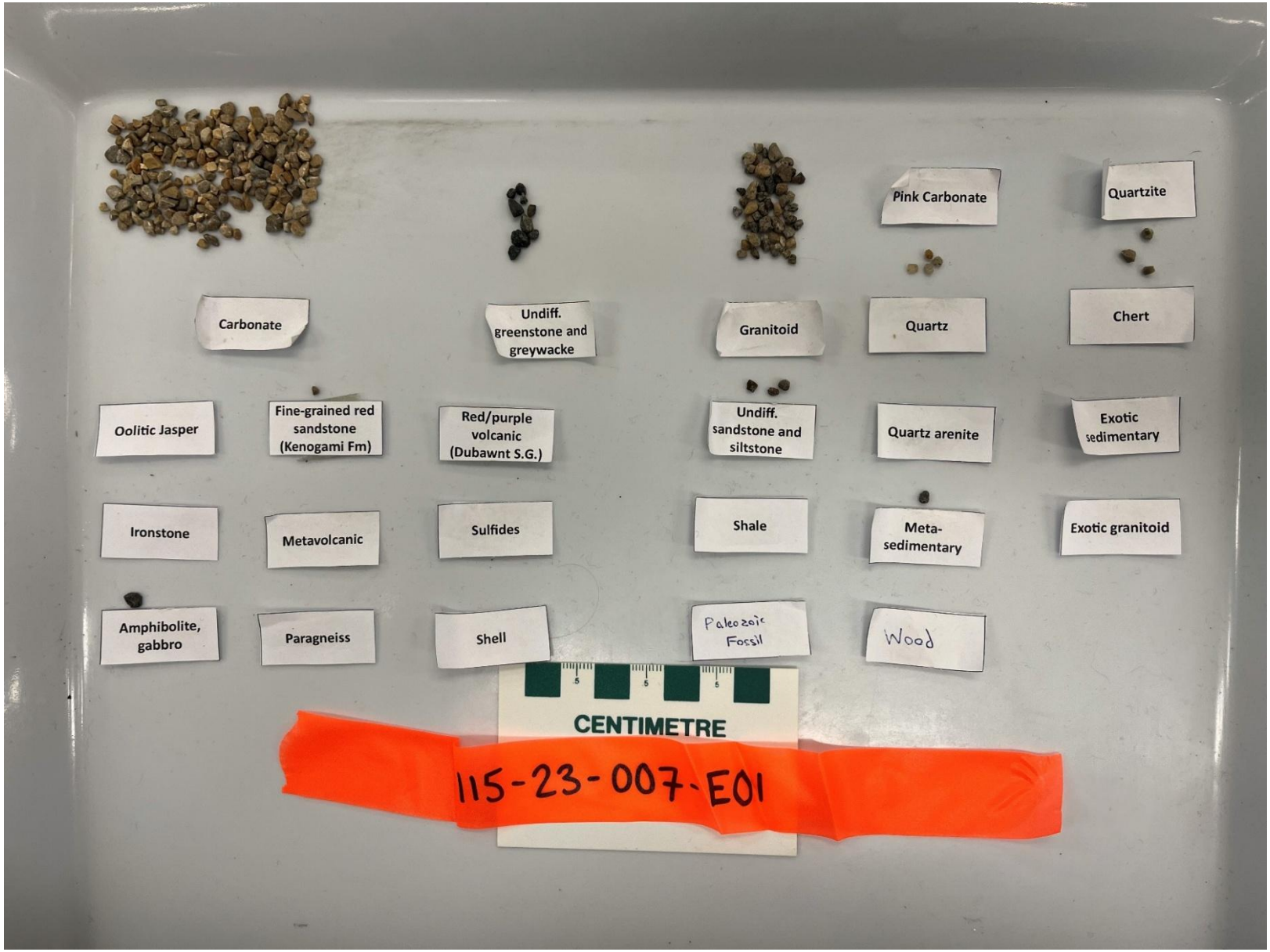

Carbonate
Undiff. greenstone and greywacke
Granitoid
Pink Carbonate
Quartzite
Quartz
Chert
Oolitic Jasper
Fine-grained red sandstone (Kenogami Fm)
Red/purple volcanic (Dubawnt S.G.)
Undiff. sandstone and siltstone
Quartz arenite
Exotic sedimentary
Ironstone
Metavolcanic
Sulfides
Shale
Meta-sedimentary
Exotic granitoid
Amphibolite, gabbro
Paragneiss
Shell
Paleozoic Fossil
Wood
CENTIMETRE
115-23-007-D05

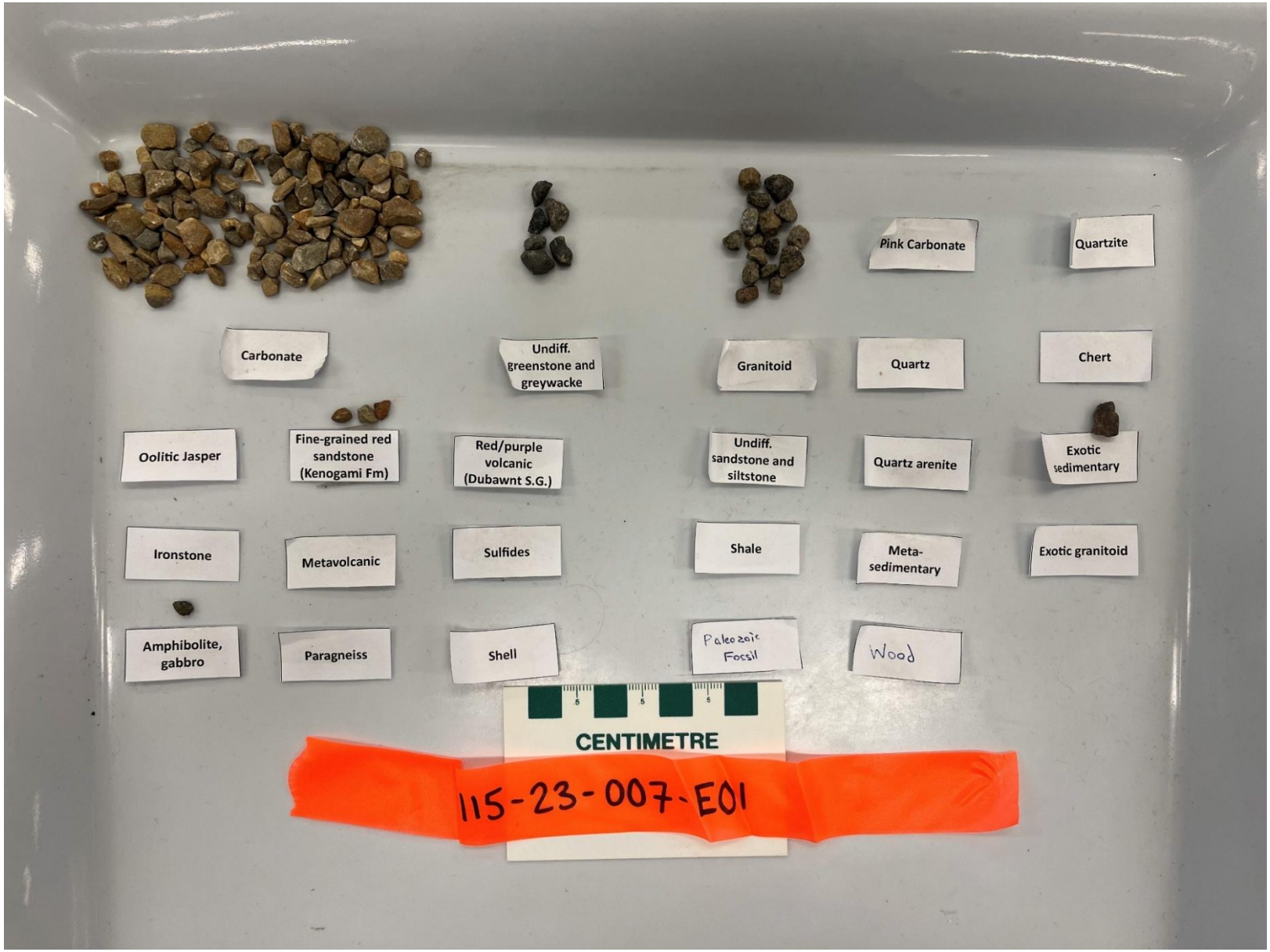

Carbonate
Undiff. greenstone and greywacke
Granitoid
Pink Carbonate
Quartzite
Quartz
Chert
Oolitic Jasper
Fine-grained red sandstone (Kenogami Fm)
Red/purple volcanic (Dubawnt S.G.)
Undiff. sandstone and siltstone
Quartz arenite
Exotic sedimentary
Ironstone
Metavolcanic
Sulfides
Shale
Meta-sedimentary
Exotic granitoid
Amphibolite, gabbro
Paragneiss
Shell
Paleozoic Fossil
Wood
CENTIMETRE
115-23-007-D06

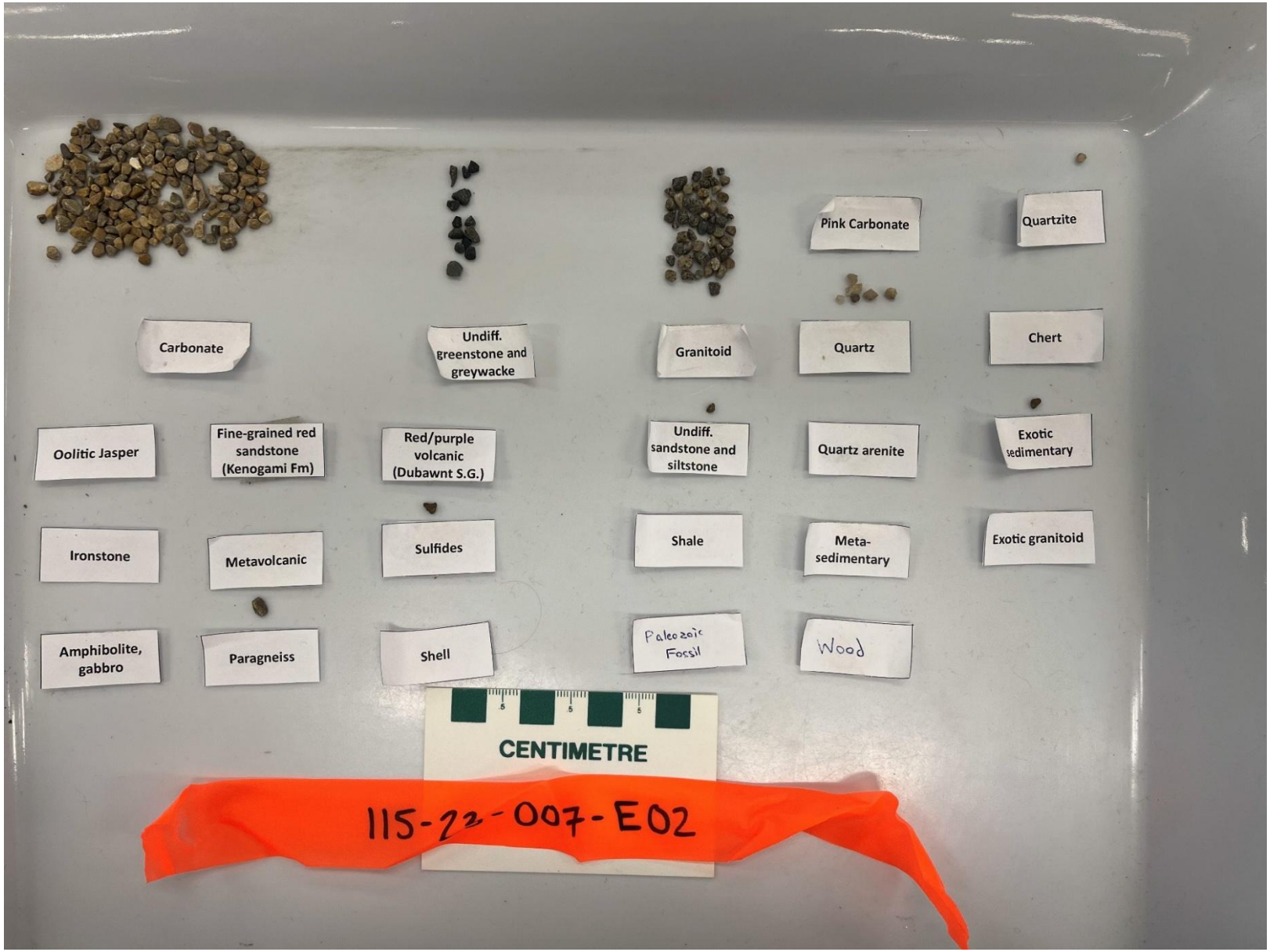

Carbonate
Undiff. greenstone and greywacke
Granitoid
Pink Carbonate
Quartzite
Quartz
Chert
Oolitic Jasper
Fine-grained red sandstone (Kenogami Fm)
Red/purple volcanic (Dubawnt S.G.)
Undiff. sandstone and siltstone
Quartz arenite
Exotic sedimentary
Ironstone
Metavolcanic
Sulfides
Shale
Meta-sedimentary
Exotic granitoid
Amphibolite, gabbro
Paragneiss
Shell
Paleozoic Fossil
Wood
CENTIMETRE
115-23-007-D06


Carbonate
Undiff. greenstone and greywacke
Granitoid
Pink Carbonate
Quartzite
Quartz
Chert
Oolitic Jasper
Fine-grained red sandstone (Kenogami Fm)
Red/purple volcanic (Dubawnt S.G.)
Undiff. sandstone and siltstone
Quartz arenite
Exotic sedimentary
Ironstone
Metavolcanic
Sulfides
Shale
Meta-sedimentary
Exotic granitoid
Amphibolite, gabbro
Paragneiss
Shell
Paleozoic Fossil
Wood
CENTIMETRE
115-23-007-D07

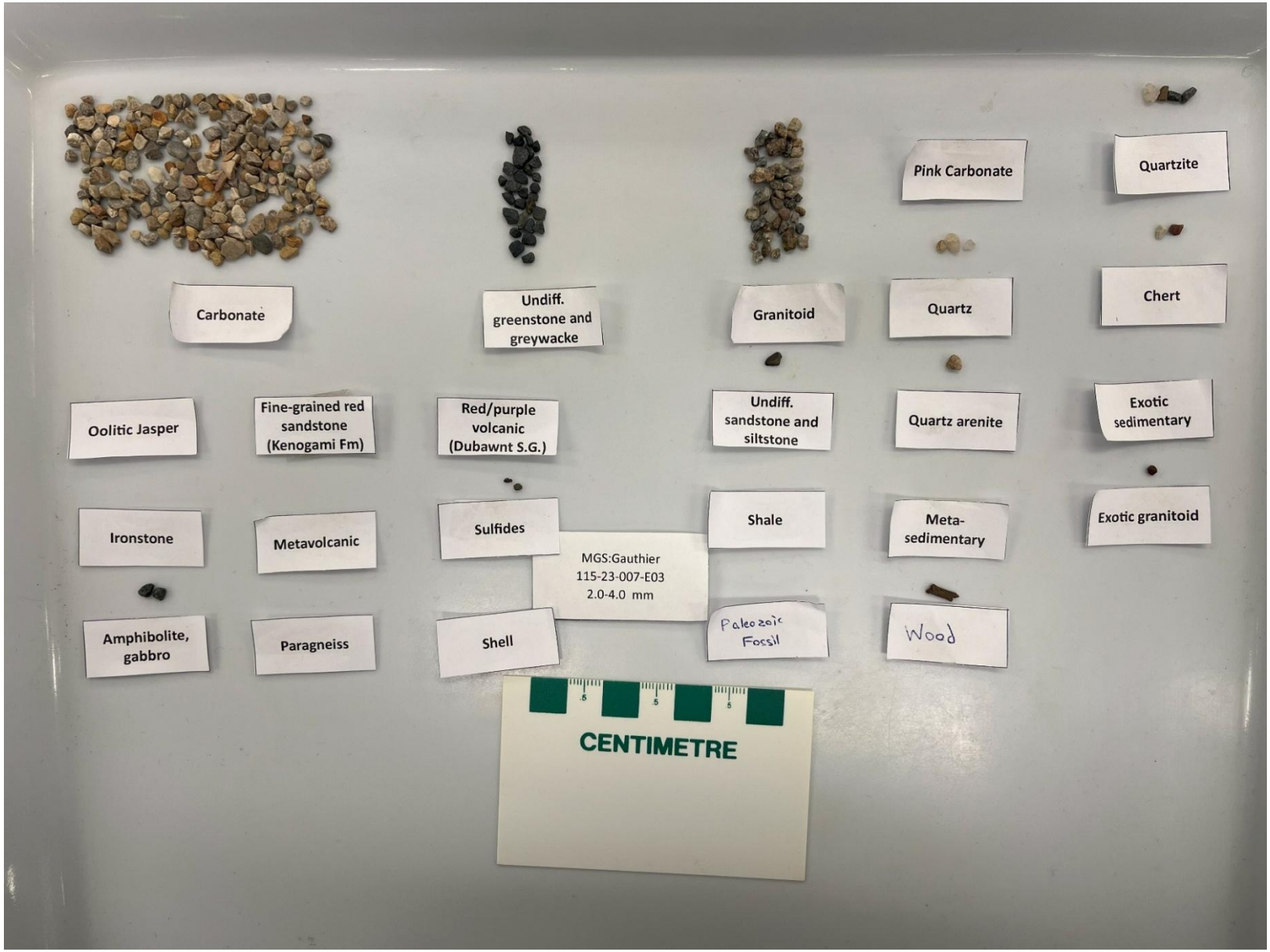

Carbonate
Undiff. greenstone and greywacke
Granitoid
Pink Carbonate
Quartzite
Quartz
Chert
Oolitic Jasper
Fine-grained red sandstone (Kenogami Fm)
Red/purple volcanic (Dubawnt S.G.)
Undiff. sandstone and siltstone
Quartz arenite
Exotic sedimentary
Ironstone
Metavolcanic
Sulfides
Shale
Meta-sedimentary
Exotic granitoid
Amphibolite, gabbro
Paragneiss
Shell
Paleozoic Fossil
Wood
CENTIMETRE
115-23-007-D07


Carbonate
Undiff. greenstone and greywacke
Granitoid
Pink Carbonate
Quartzite
Quartz
Chert
Oolitic Jasper
Fine-grained red sandstone (Kenogami Fm)
Red/purple volcanic (Dubawnt S.G.)
Undiff. sandstone and siltstone
Quartz arenite
Exotic sedimentary
Ironstone
Metavolcanic
Sulfides
Shale
Meta-sedimentary
Exotic granitoid
Amphibolite, gabbro
Paragneiss
Shell
Paleozoic Fossil
Wood
CENTIMETRE
115-23-007-E01


Pink Carbonate
Quartzite
Carbonate
Undiff. greenstone and greywacke
Granitoid
Quartz
Chert
Oolitic Jasper
Fine-grained red sandstone (Kenogami Fm)
Red/purple volcanic (Dubawnt S.G.)
Undiff. sandstone and siltstone
Quartz arenite
Exotic sedimentary
Ironstone
Metavolcanic
Sulfides
Shale
Meta-sedimentary
Exotic granitoid
Amphibolite, gabbro
Paragneiss
Shell
Paleozoic Fossil
Wood
CENTIMETRE
115-23-007-E01


Carbonate
Undiff. greenstone and greywacke
Granitoid
Pink Carbonate
Quartzite
Quartz
Chert
Oolitic Jasper
Fine-grained red sandstone (Kenogami Fm)
Red/purple volcanic (Dubawnt S.G.)
Undiff. sandstone and siltstone
Quartz arenite
Exotic sedimentary
Ironstone
Metavolcanic
Sulfides
Shale
Meta-sedimentary
Exotic granitoid
Amphibolite, gabbro
Paragneiss
Shell
Paleozoic Fossil
Wood
CENTIMETRE
115-22-007-E02


Carbonate
Undiff. greenstone and greywacke
Granitoid
Pink Carbonate
Quartzite
Quartz
Chert
Oolitic Jasper
Fine-grained red sandstone (Kenogami Fm)
Red/purple volcanic (Dubawnt S.G.)
Undiff. sandstone and siltstone
Quartz arenite
Exotic sedimentary
Ironstone
Metavolcanic
Sulfides
Shale
Meta-sedimentary
Exotic granitoid
Amphibolite, gabbro
Paragneiss
Shell
Paleozoic Fossil
Wood
CENTIMETRE
115-22-007-E02


Carbonate
Undiff. greenstone and greywacke
Granitoid
Pink Carbonate
Quartzite
Chert
Quartz
Oolitic Jasper
Fine-grained red sandstone (Kenogami Fm)
Red/purple volcanic (Dubawnt S.G.)
Undiff. sandstone and siltstone
Quartz arenite
Exotic sedimentary
Ironstone
Metavolcanic
Sulfides
Shale
Meta-sedimentary
Exotic granitoid
MGS:Gauthier
115-23-007-E03
2.0-4.0 mm
Amphibolite, gabbro
Paragneiss
Shell
Paleozoic Fossil
Wood
CENTIMETRE


Carbonate
Undiff. greenstone and greywacke
Granitoid
Pink Carbonate
Oolitic Jasper
Fine-grained red sandstone (Kenogami Fm)
Red/purple volcanic (Dubawnt S.G.)
Quartz
Quartzite
Chert
Ironstone
Metavolcanic
Sulfides
Undiff. sandstone and siltstone
Quartz arenite
Exotic sedimentary
MGS:Gauthier
115-23-007-E03
4.0-8.0 mm
Amphibolite, gabbro
Paragneiss
Shell
Shale
Meta-sedimentary
Exotic granitoid
Paleozoic Fossil
CENTIMETRE

Note: Clast counts of the 4-8 mm size fraction are displayed on paper, while clast counts of the 2-4 mm size fraction are within Petri dishes.






115-23-007-GRAV2
gran
magnetite-bearing iron stone
iron stone
or perhaps brown siltstone
metavolc.
chert
mafic int.
int. int.
UGG
Meta. sed.


115-23-007-GRAV2
UGG
fossil
chert
metavolc.
qtz
meta sed.
iron st.

115-23-008

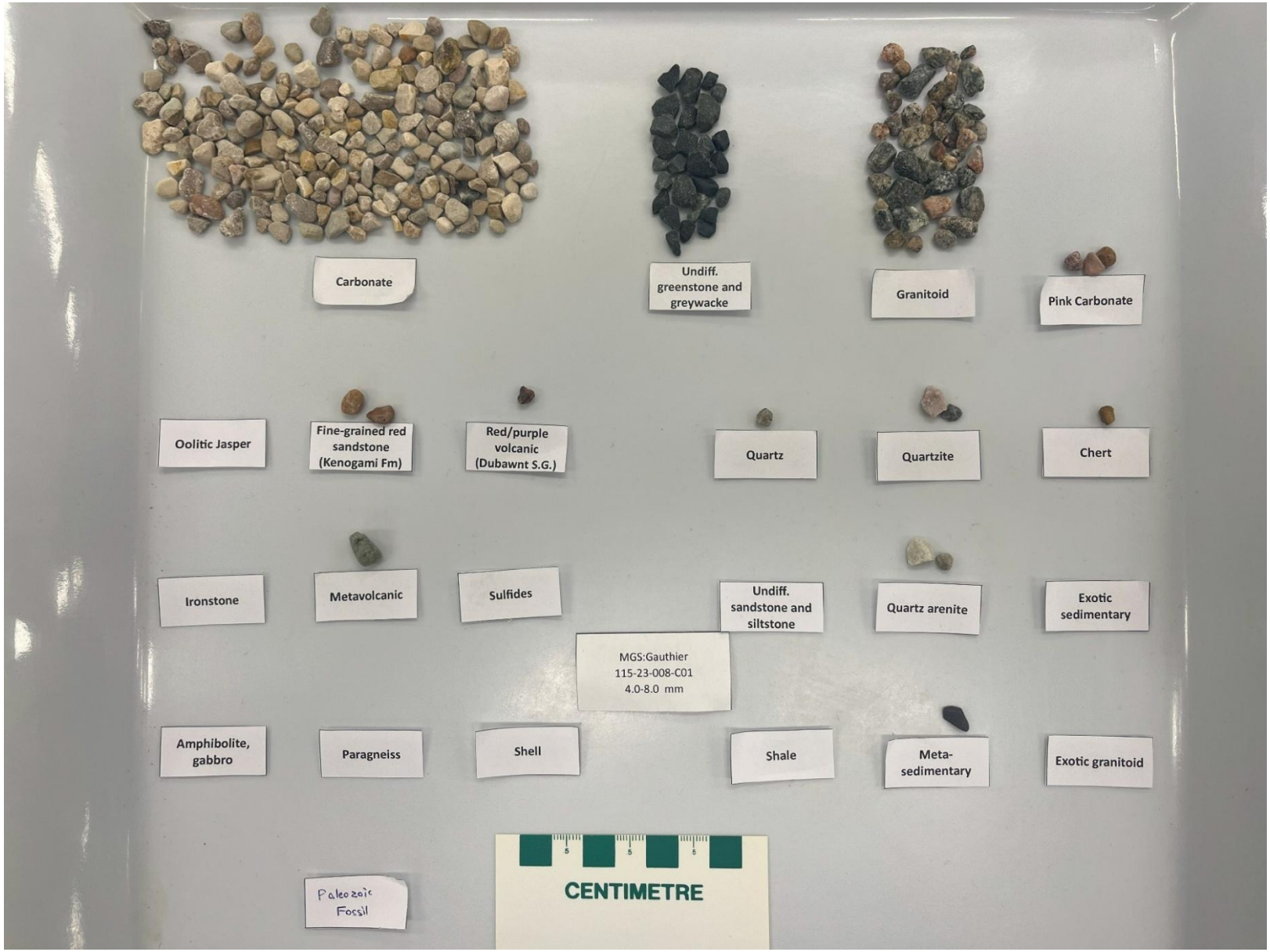

Carbonate
Undiff. greenstone and greywacke
Granitoid
Pink Carbonate
Quartzite
Quartz
Chert
Oolitic Jasper
Fine-grained red sandstone (Kenogami Fm)
Red/purple volcanic (Dubawnt S.G.)
Undiff. sandstone and siltstone
Quartz arenite
Exotic sedimentary
Ironstone
Metavolcanic
Sulfides
Shale
Meta-sedimentary
Exotic granitoid
Amphibolite, gabbro
Paragneiss
Shell
Paleozoic Fossil
Wood
CENTIMETRE
115-23-008-A01


Carbonate
Undiff. greenstone and greywacke
Granitoid
Pink Carbonate
Quartzite
Quartz
Chert
Oolitic Jasper
Fine-grained red sandstone (Kenogami Fm)
Red/purple volcanic (Dubawnt S.G.)
Undiff. sandstone and siltstone
Quartz arenite
Exotic sedimentary
Ironstone
Metavolcanic
Sulfides
Shale
Meta-sedimentary
Exotic granitoid
Amphibolite, gabbro
Paragneiss
Shell
Paleozoic Fossil
Wood
CENTIMETRE
115-23-008-A01

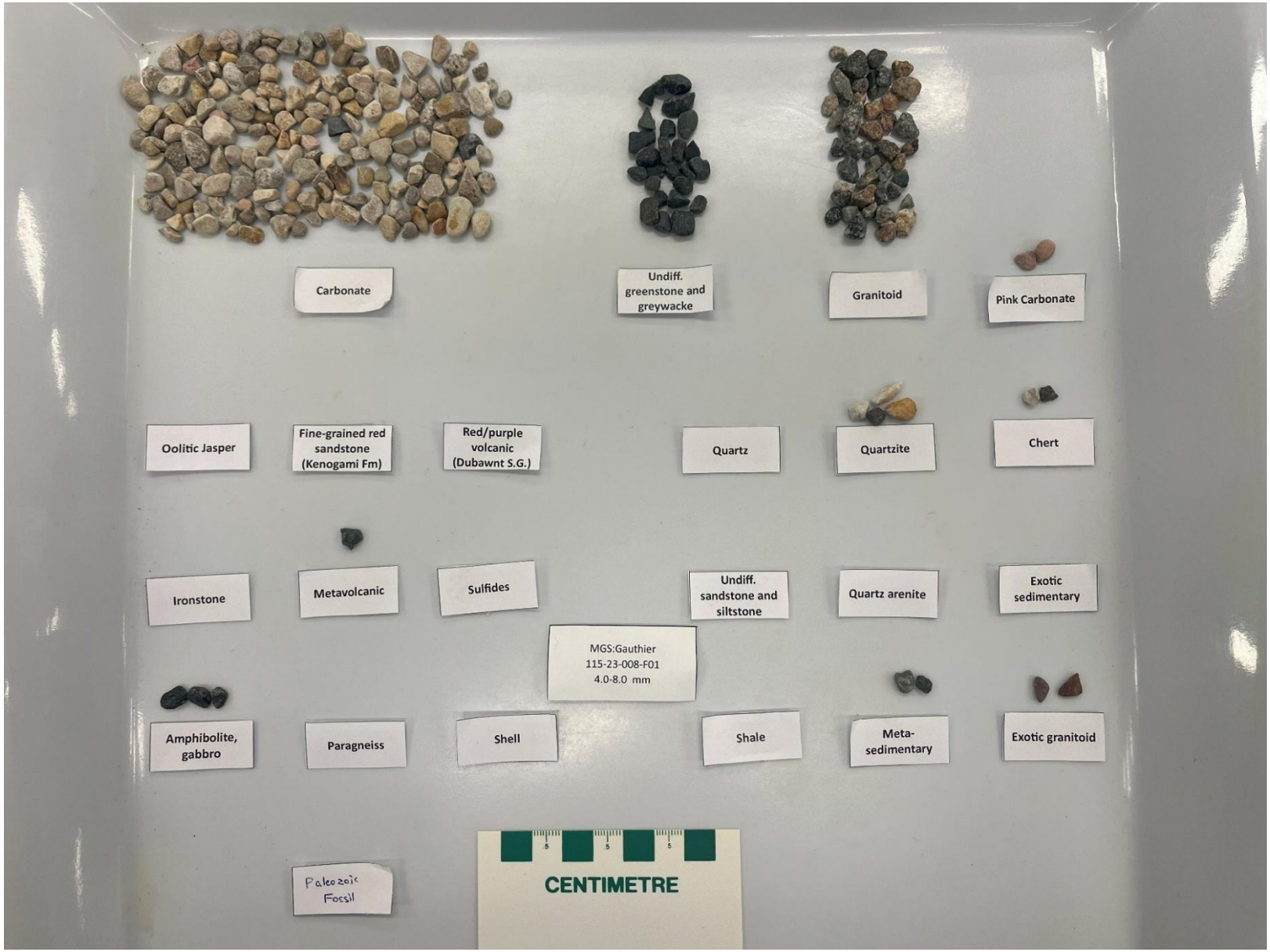

Carbonate
Undiff. greenstone and greywacke
Granitoid
Pink Carbonate
Quartzite
Quartz
Chert
Oolitic Jasper
Fine-grained red sandstone (Kenogami Fm)
Red/purple volcanic (Dubawnt S.G.)
Undiff. sandstone and siltstone
Quartz arenite
Exotic sedimentary
Ironstone
Metavolcanic
Sulfides
Shale
Meta-sedimentary
Exotic granitoid
MGS:Gauthier
115-23-008-B01
2.0-4.0 mm
Amphibolite, gabbro
Paragneiss
Shell
Paleozoic Fossil
Wood
CENTIMETRE


Carbonate
Undiff. greenstone and greywacke
Granitoid
Pink Carbonate
Oolitic Jasper
Fine-grained red sandstone (Kenogami Fm)
Red/purple volcanic (Dubawnt S.G.)
Quartz
Quartzite
Chert
Ironstone
Metavolcanic
Sulfides
Undiff. sandstone and siltstone
Quartz arenite
Exotic sedimentary
MGS:Gauthier
115-23-008-B01
4.0-8.0 mm
Amphibolite, gabbro
Paragneiss
Shell
Shale
Meta-sedimentary
Exotic granitoid
Paleozoic Fossil
CENTIMETRE


Carbonate
Undiff. greenstone and greywacke
Granitoid
Pink Carbonate
Quartzite
Quartz
Chert
Oolitic Jasper
Fine-grained red sandstone (Kenogami Fm)
Red/purple volcanic (Dubawnt S.G.)
Undiff. sandstone and siltstone
Quartz arenite
Exotic sedimentary
Ironstone
Metavolcanic
Sulfides
Shale
Meta-sedimentary
Exotic granitoid
MGS:Gauthier
115-23-008-C01
2.0-4.0 mm
Amphibolite, gabbro
Paragneiss
Shell
Paleozoic Fossil
Wood
CENTIMETRE


Carbonate
Undiff. greenstone and greywacke
Granitoid
Pink Carbonate
Oolitic Jasper
Fine-grained red sandstone (Kenogami Fm)
Red/purple volcanic (Dubawnt S.G.)
Quartz
Quartzite
Chert
Ironstone
Metavolcanic
Sulfides
Undiff. sandstone and siltstone
Quartz arenite
Exotic sedimentary
MGS:Gauthier
115-23-008-C01
4.0-8.0 mm
Amphibolite, gabbro
Paragneiss
Shell
Shale
Meta-sedimentary
Exotic granitoid
Paleozoic Fossil
CENTIMETRE

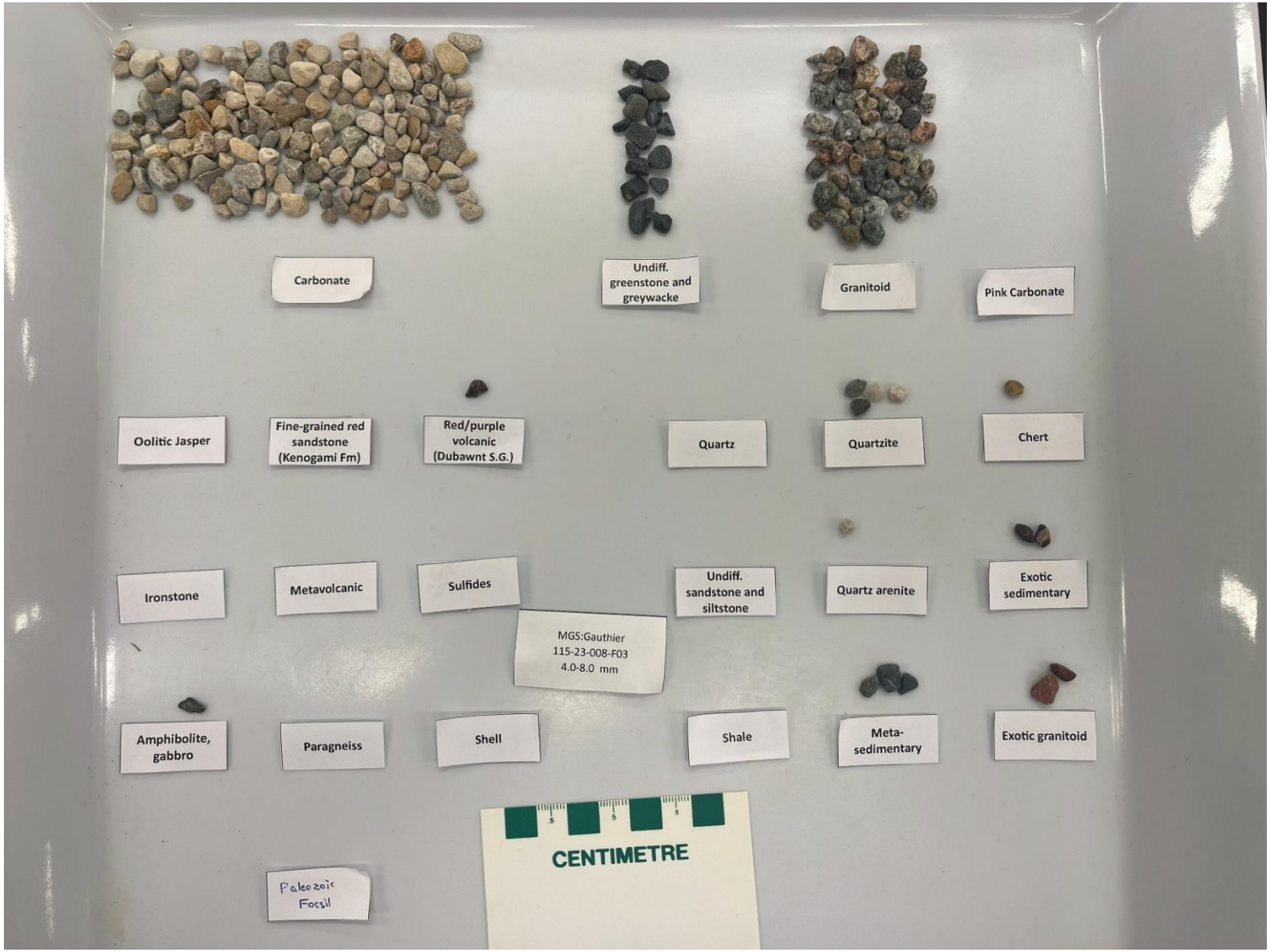

Carbonate
Undiff. greenstone and greywacke
Granitoid
Pink Carbonate
Quartzite
Quartz
Chert
Oolitic Jasper
Fine-grained red sandstone (Kenogami Fm)
Red/purple volcanic (Dubawnt S.G.)
Undiff. sandstone and siltstone
Quartz arenite
Exotic sedimentary
Ironstone
Metavolcanic
Sulfides
Shale
Meta-sedimentary
Exotic granitoid
MGS:Gauthier
115-23-008-F01
2.0-4.0 mm
Amphibolite, gabbro
Paragneiss
Shell
Paleozoic Fossil
Wood
CENTIMETRE

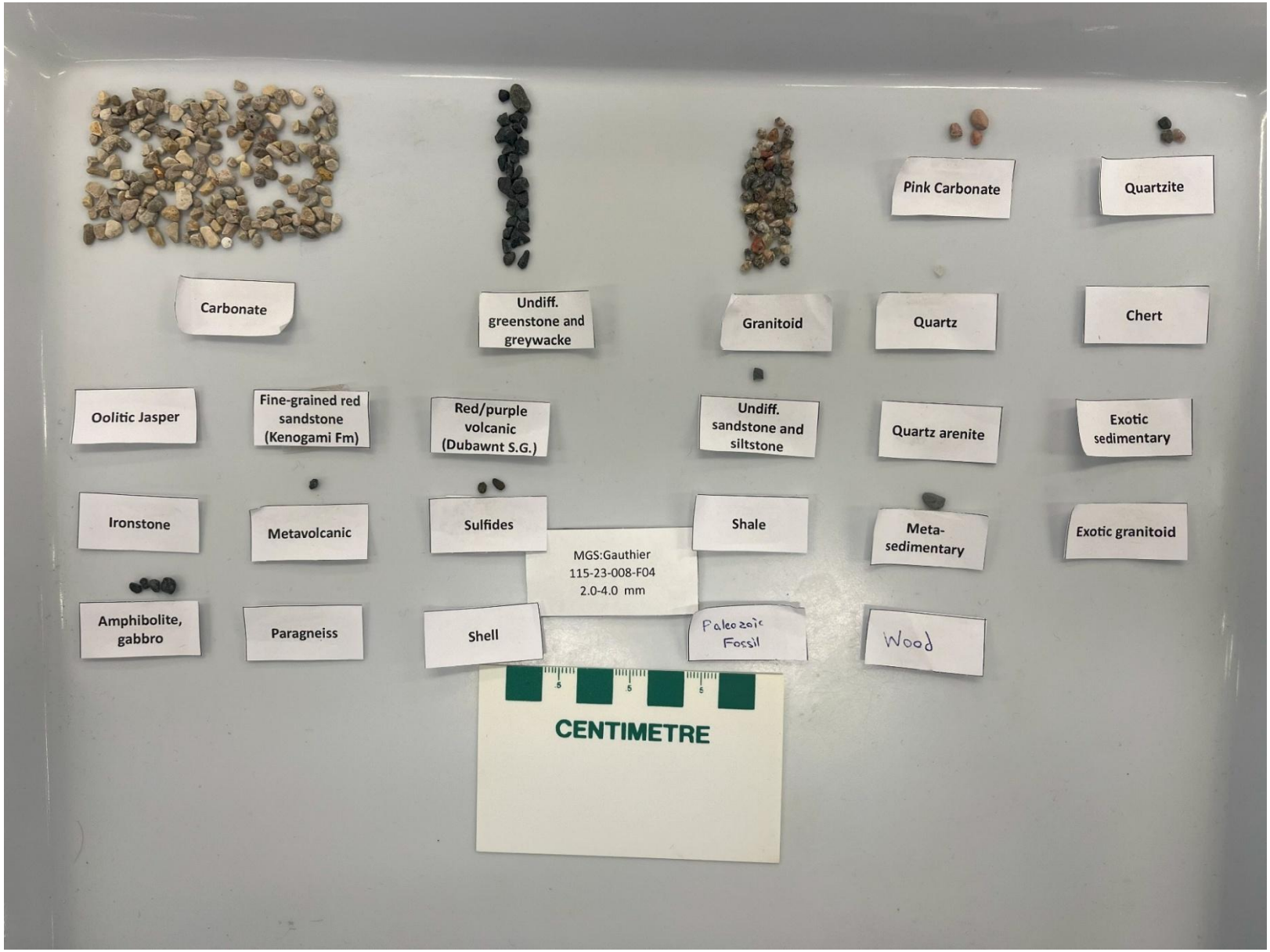

Carbonate
Undiff. greenstone and greywacke
Granitoid
Pink Carbonate
Oolitic Jasper
Fine-grained red sandstone (Kenogami Fm)
Red/purple volcanic (Dubawnt S.G.)
Quartz
Quartzite
Chert
Ironstone
Metavolcanic
Sulfides
Undiff. sandstone and siltstone
Quartz arenite
Exotic sedimentary
MGS:Gauthier
115-23-008-F01
4.0-8.0 mm
Amphibolite, gabbro
Paragneiss
Shell
Shale
Meta-sedimentary
Exotic granitoid
Paleozoic Fossil
CENTIMETRE

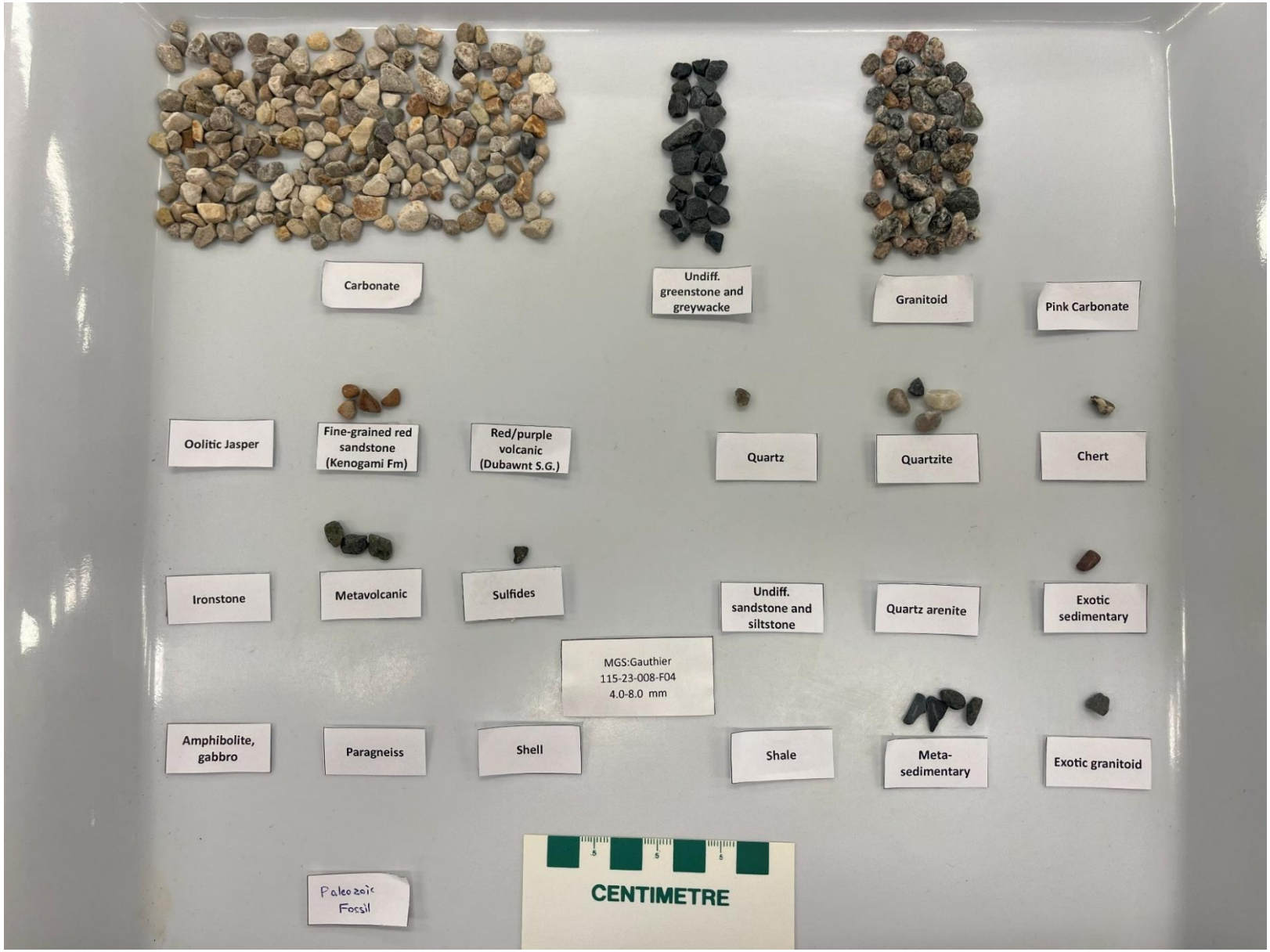

Carbonate
Undiff. greenstone and greywacke
Granitoid
Pink Carbonate
Quartzite
Quartz
Chert
Oolitic Jasper
Fine-grained red sandstone (Kenogami Fm)
Red/purple volcanic (Dubawnt S.G.)
Undiff. sandstone and siltstone
Quartz arenite
Exotic sedimentary
Ironstone
Metavolcanic
Sulfides
Shale
Meta-sedimentary
Exotic granitoid
Amphibolite, gabbro
Paragneiss
Shell
Paleozoic Fossil
Wood
CENTIMETRE
115-23-008-F02


Carbonate
Undiff. greenstone and greywacke
Granitoid
Pink Carbonate
Quartzite
Quartz
Chert
Oolitic Jasper
Fine-grained red sandstone (Kenogami Fm)
Red/purple volcanic (Dubawnt S.G.)
Undiff. sandstone and siltstone
Quartz arenite
Exotic sedimentary
Ironstone
Metavolcanic
Sulfides
Shale
Meta-sedimentary
Exotic granitoid
Amphibolite, gabbro
Paragneiss
Shell
Paleozoic Fossil
Wood
CENTIMETRE
115-23-008-F02

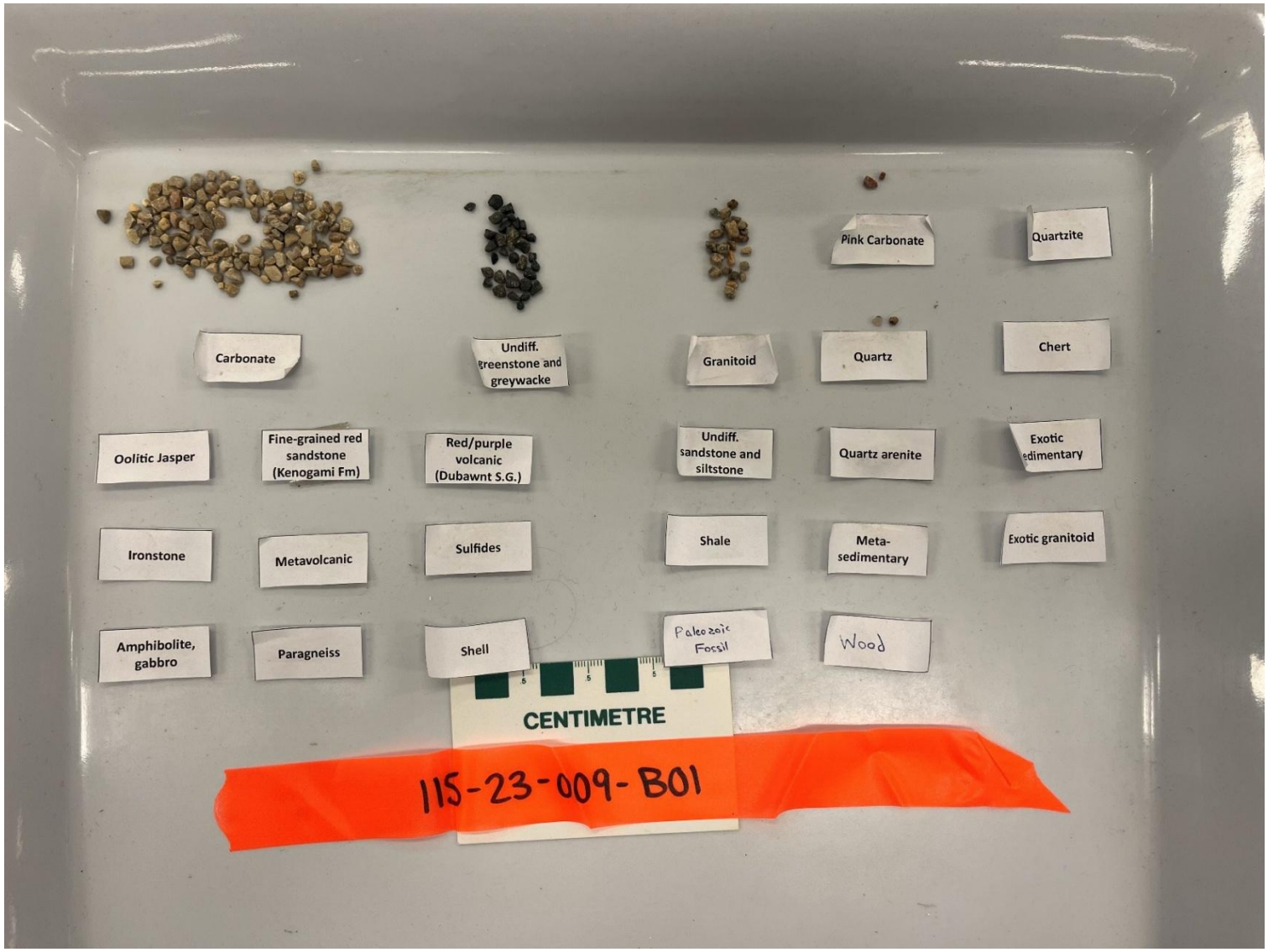

Carbonate
Undiff. greenstone and greywacke
Granitoid
Pink Carbonate
Quartzite
Quartz
Chert
Oolitic Jasper
Fine-grained red sandstone (Kenogami Fm)
Red/purple volcanic (Dubawnt S.G.)
Undiff. sandstone and siltstone
Quartz arenite
Exotic sedimentary
Ironstone
Metavolcanic
Sulfides
Shale
Meta-sedimentary
Exotic granitoid
MGS:Gauthier
115-23-008-F03
2.0-4.0 mm
Amphibolite, gabbro
Paragneiss
Shell
Paleozoic Fossil
Wood
CENTIMETRE


Carbonate
Undiff. greenstone and greywacke
Granitoid
Pink Carbonate
Oolitic Jasper
Fine-grained red sandstone (Kenogami Fm)
Red/purple volcanic (Dubawnt S.G.)
Quartz
Quartzite
Chert
Ironstone
Metavolcanic
Sulfides
Undiff. sandstone and siltstone
Quartz arenite
Exotic sedimentary
MGS:Gauthier
115-23-008-F03
4.0-8.0 mm
Amphibolite, gabbro
Paragneiss
Shell
Shale
Meta-sedimentary
Exotic granitoid
CENTIMETRE
Paleozoic Fossil


Carbonate
Undiff. greenstone and greywacke
Granitoid
Pink Carbonate
Quartzite
Quartz
Chert
Oolitic Jasper
Fine-grained red sandstone (Kenogami Fm)
Red/purple volcanic (Dubawnt S.G.)
Undiff. sandstone and siltstone
Quartz arenite
Exotic sedimentary
Ironstone
Metavolcanic
Sulfides
Shale
Meta-sedimentary
Exotic granitoid
MGS:Gauthier
115-23-008-F04
2.0-4.0 mm
Amphibolite, gabbro
Paragneiss
Shell
Paleozoic Fossil
Wood
CENTIMETRE


Carbonate
Undiff. greenstone and greywacke
Granitoid
Pink Carbonate
Oolitic Jasper
Fine-grained red sandstone (Kenogami Fm)
Red/purple volcanic (Dubawnt S.G.)
Quartz
Quartzite
Chert
Ironstone
Metavolcanic
Sulfides
Undiff. sandstone and siltstone
Quartz arenite
Exotic sedimentary
MGS:Gauthier
115-23-008-F04
4.0-8.0 mm
Amphibolite, gabbro
Paragneiss
Shell
Shale
Meta-sedimentary
Exotic granitoid
Paleozoic Fossil
CENTIMETRE

115-23-009


Carbonate
Undiff. greenstone and greywacke
Granitoid
Pink Carbonate
Quartzite
Quartz
Chert
Oolitic Jasper
Fine-grained red sandstone (Kenogami Fm)
Red/purple volcanic (Dubawnt S.G.)
Undiff. sandstone and siltstone
Quartz arenite
Exotic sedimentary
Ironstone
Metavolcanic
Sulfides
Shale
Meta-sedimentary
Exotic granitoid
Amphibolite, gabbro
Paragneiss
Shell
Paleozoic Fossil
Wood
CENTIMETRE
115-23-009-B01


Carbonate
Undiff. greenstone and greywacke
Granitoid
Pink Carbonate
Quartzite
Quartz
Chert
Oolitic Jasper
Fine-grained red sandstone (Kenogami Fm)
Red/purple volcanic (Dubawnt S.G.)
Undiff. sandstone and siltstone
Quartz arenite
Exotic sedimentary
Ironstone
Metavolcanic
Sulfides
Shale
Meta-sedimentary
Exotic granitoid
Amphibolite, gabbro
Paragneiss
Shell
Paleozoic Fossil
Wood
CENTIMETRE
115-23-009-B01

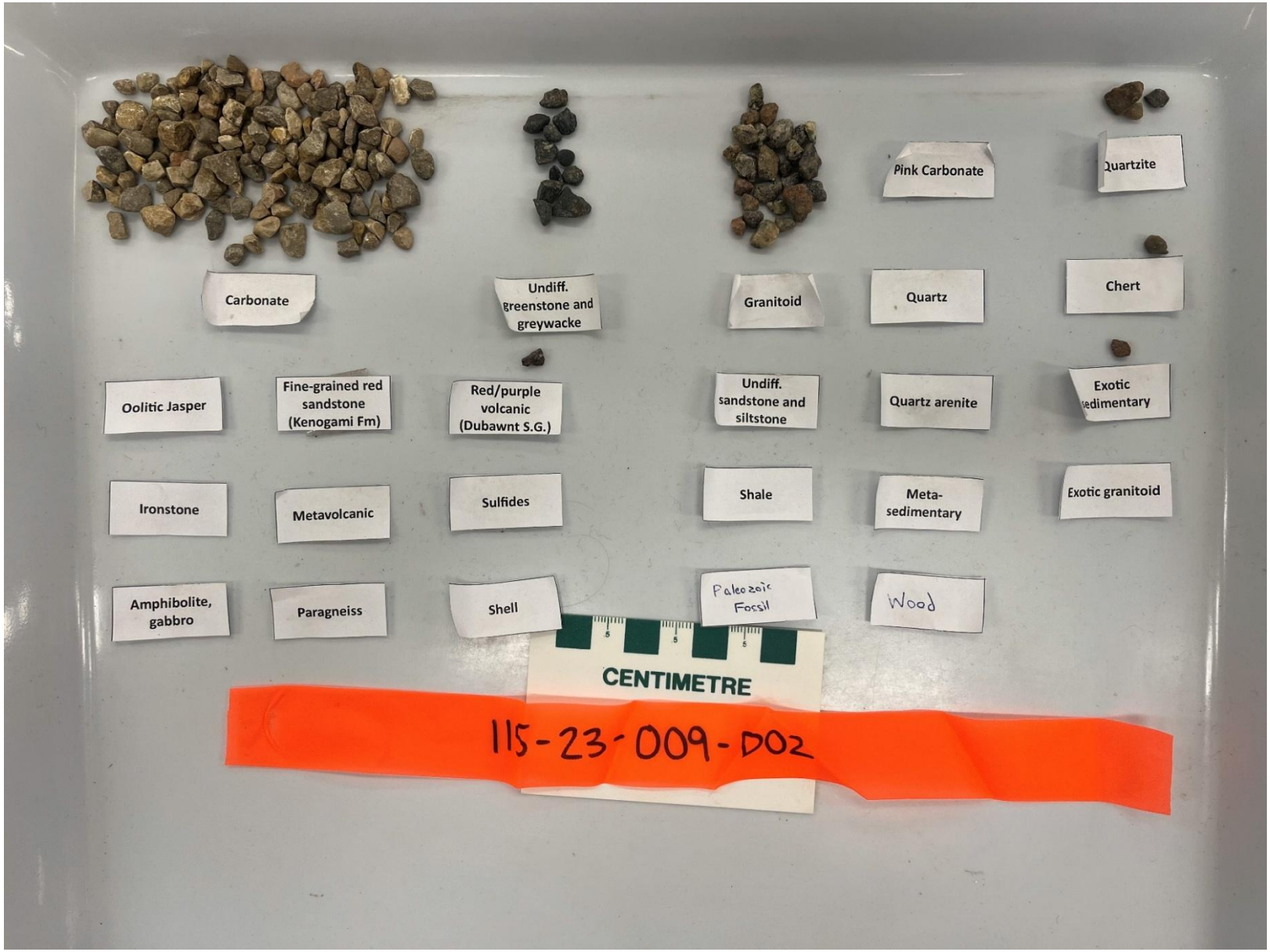

Carbonate
Undiff. greenstone and greywacke
Granitoid
Pink Carbonate
Quartzite
Quartz
Chert
Oolitic Jasper
Fine-grained red sandstone (Kenogami Fm)
Red/purple volcanic (Dubawnt S.G.)
Undiff. sandstone and siltstone
Quartz arenite
Exotic sedimentary
Ironstone
Metavolcanic
Sulfides
Shale
Meta-sedimentary
Exotic granitoid
Amphibolite, gabbro
Paragneiss
Shell
Paleozoic Fossil
Wood
CENTIMETRE
115-23-009-C01


Carbonate
Undiff. greenstone and greywacke
Granitoid
Pink Carbonate
Quartzite
Quartz
Chert
Oolitic Jasper
Fine-grained red sandstone (Kenogami Fm)
Red/purple volcanic (Dubawnt S.G.)
Undiff. sandstone and siltstone
Quartz arenite
Exotic sedimentary
Ironstone
Metavolcanic
Sulfides
Shale
Meta-sedimentary
Exotic granitoid
Amphibolite, gabbro
Paragneiss
Shell
Paleozoic Fossil
Wood
CENTIMETRE
115-23-009-C01


Carbonate
Undiff. Greenstone and greywacke
Granitoid
Pink Carbonate
Quartzite
Quartz
Chert
Oolitic Jasper
Fine-grained red sandstone (Kenogami Fm)
Red/purple volcanic (Dubawnt S.G.)
Undiff. sandstone and siltstone
Quartz arenite
Exotic sedimentary
Ironstone
Metavolcanic
Sulfides
Shale
Meta-sedimentary
Exotic granitoid
Amphibolite, gabbro
Paragneiss
Shell
Paleozoic Fossil
Wood
CENTIMETRE
115-23-009-D01


Carbonate
Undiff. Greenstone and greywacke
Granitoid
Pink Carbonate
Quartzite
Quartz
Chert
Oolitic Jasper
Fine-grained red sandstone (Kenogami Fm)
Red/purple volcanic (Dubawnt S.G.)
Undiff. sandstone and siltstone
Quartz arenite
Exotic sedimentary
Ironstone
Metavolcanic
Sulfides
Shale
Meta-sedimentary
Exotic granitoid
Amphibolite, gabbro
Paragneiss
Shell
Paleozoic Fossil
Wood
CENTIMETRE
115-23-009-D01


Carbonate
Undiff. greenstone and greywacke
Granitoid
Pink Carbonate
Quartzite
Quartz
Chert
Oolitic Jasper
Fine-grained red sandstone (Kenogami Fm)
Red/purple volcanic (Dubawnt S.G.)
Undiff. sandstone and siltstone
Quartz arenite
Exotic sedimentary
Ironstone
Metavolcanic
Sulfides
Shale
Meta-sedimentary
Exotic granitoid
Amphibolite, gabbro
Paragneiss
Shell
Paleozoic Fossil
Wood
CENTIMETRE
115-23-009-D02


Carbonate
Undiff. greenstone and greywacke
Granitoid
Pink Carbonate
Quartzite
Quartz
Chert
Oolitic Jasper
Fine-grained red sandstone (Kenogami Fm)
Red/purple volcanic (Dubawnt S.G.)
Undiff. sandstone and siltstone
Quartz arenite
Exotic sedimentary
Ironstone
Metavolcanic
Sulfides
Shale
Meta-sedimentary
Exotic granitoid
Amphibolite, gabbro
Paragneiss
Shell
Paleozoic Fossil
Wood
CENTIMETRE
115-23-009-D02


Carbonate
Undiff. Greenstone and greywacke
Granitoid
Pink Carbonate
Quartzite
Quartz
Chert
Oolitic Jasper
Fine-grained red sandstone (Kenogami Fm)
Red/purple volcanic (Dubawnt S.G.)
Undiff. sandstone and siltstone
Quartz arenite
Exotic sedimentary
Ironstone
Metavolcanic
Sulfides
Shale
Meta-sedimentary
Exotic granitoid
Amphibolite, gabbro
Paragneiss
Shell
Paleozoic Fossil
Wood
CENTIMETRE
115-23-009-N01


Carbonate
Undiff. greenstone and greywacke
Granitoid
Pink Carbonate
Quartzite
Quartz
Chert
Oolitic Jasper
Fine-grained red sandstone (Kenogami Fm)
Red/purple volcanic (Dubawnt S.G.)
Undiff. sandstone and siltstone
Quartz arenite
Exotic sedimentary
Ironstone
Metavolcanic
Sulfides
Shale
Meta-sedimentary
Exotic granitoid
Amphibolite, gabbro
Paragneiss
Shell
Paleozoic Fossil
Wood
CENTIMETRE
115-23-009-N01

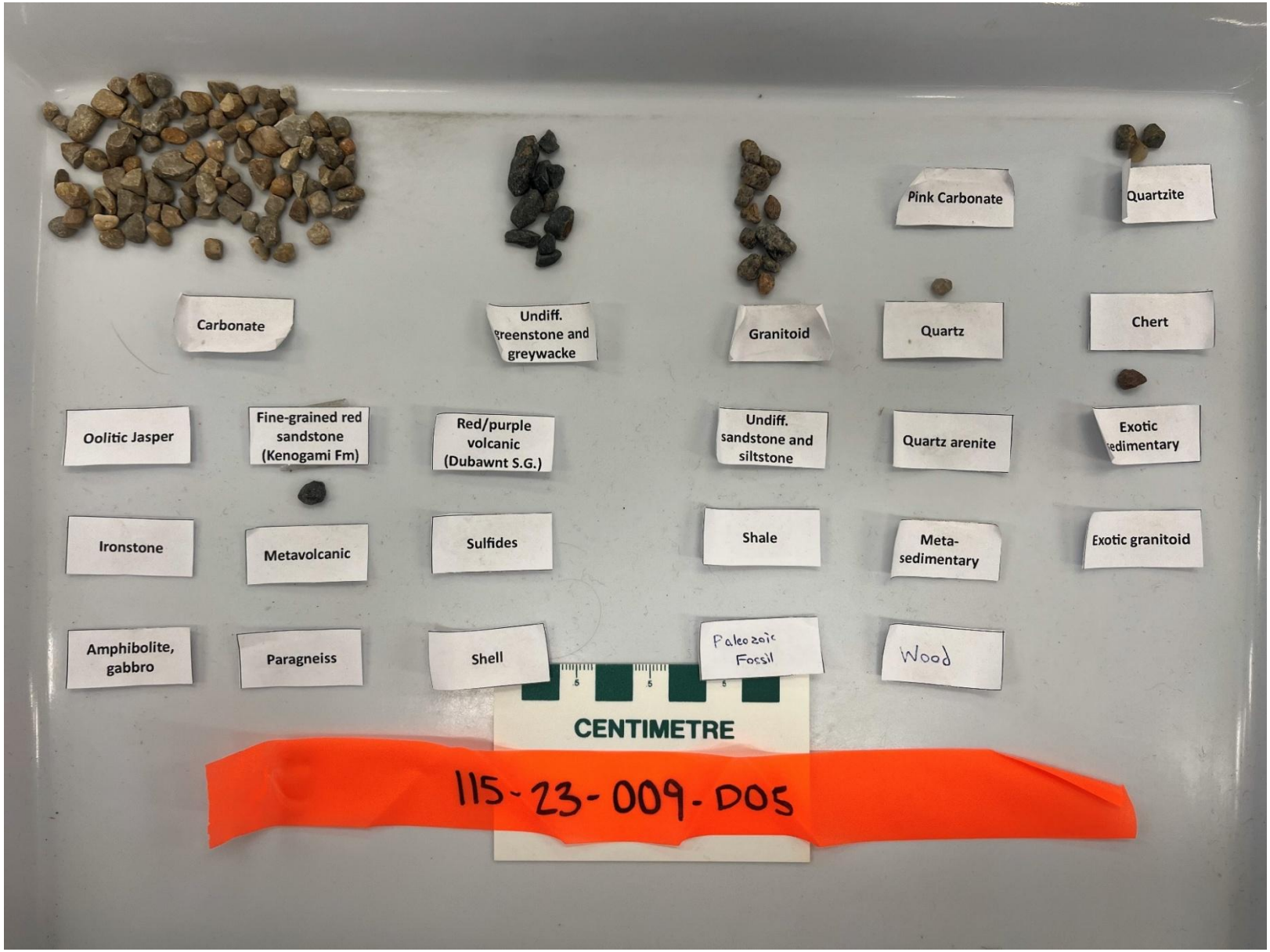

Carbonate
Undiff. greenstone and greywacke
Granitoid
Pink Carbonate
Quartzite
Quartz
Chert
Oolitic Jasper
Fine-grained red sandstone (Kenogami Fm)
Red/purple volcanic (Dubawnt S.G.)
Undiff. sandstone and siltstone
Quartz arenite
Exotic sedimentary
Ironstone
Metavolcanic
Sulfides
Shale
Meta-sedimentary
Exotic granitoid
Amphibolite, gabbro
Paragneiss
Shell
Paleozoic Fossil
Wood
CENTIMETRE
115-23-009-D03

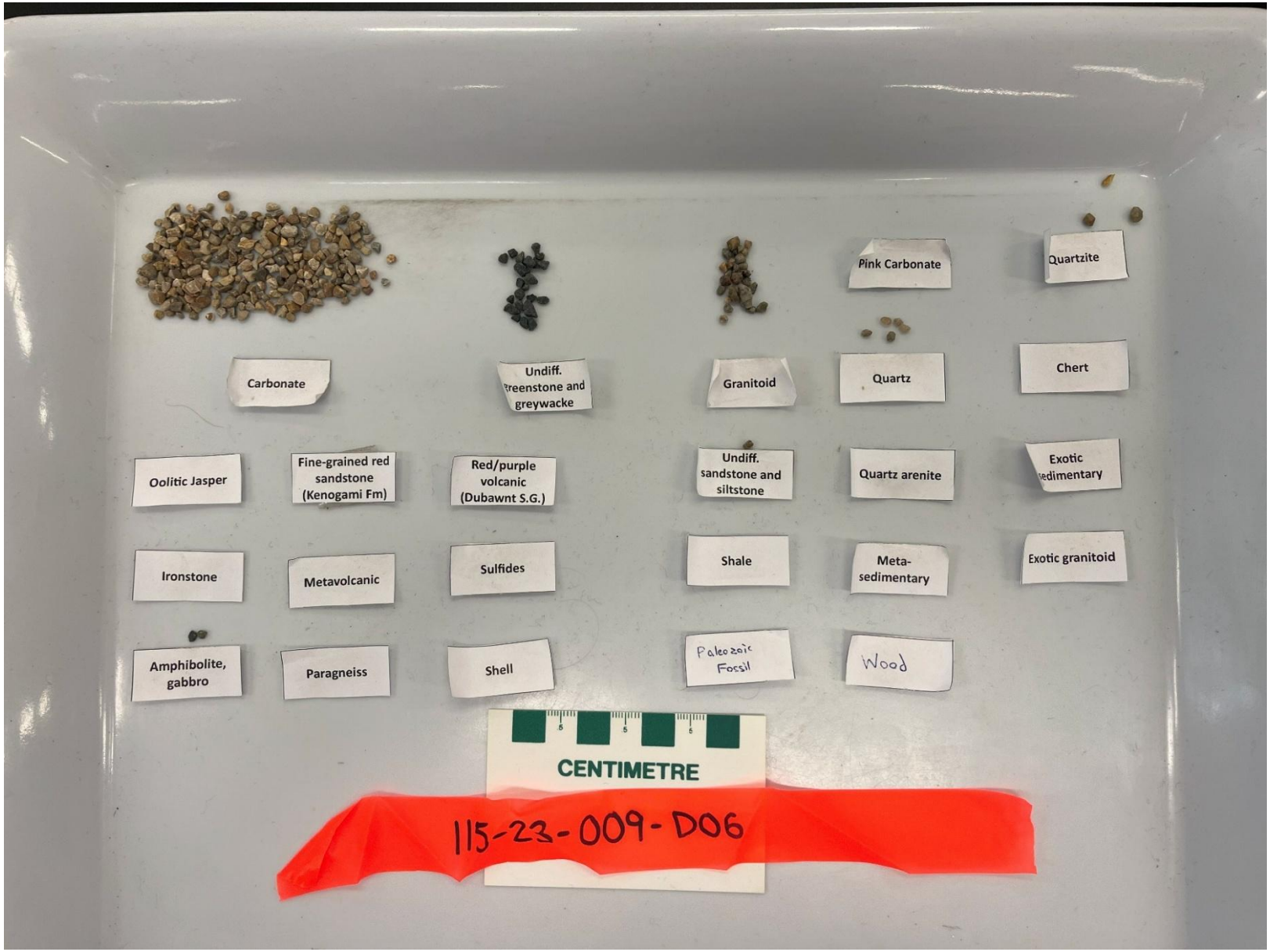

Carbonate
Undiff. greenstone and greywacke
Granitoid
Pink Carbonate
Quartzite
Quartz
Chert
Oolitic Jasper
Fine-grained red sandstone (Kenogami Fm)
Red/purple volcanic (Dubawnt S.G.)
Undiff. sandstone and siltstone
Quartz arenite
Exotic sedimentary
Ironstone
Metavolcanic
Sulfides
Shale
Meta-sedimentary
Exotic granitoid
Amphibolite, gabbro
Paragneiss
Shell
Paleozoic Fossil
Wood
CENTIMETRE
115-23-009-D03

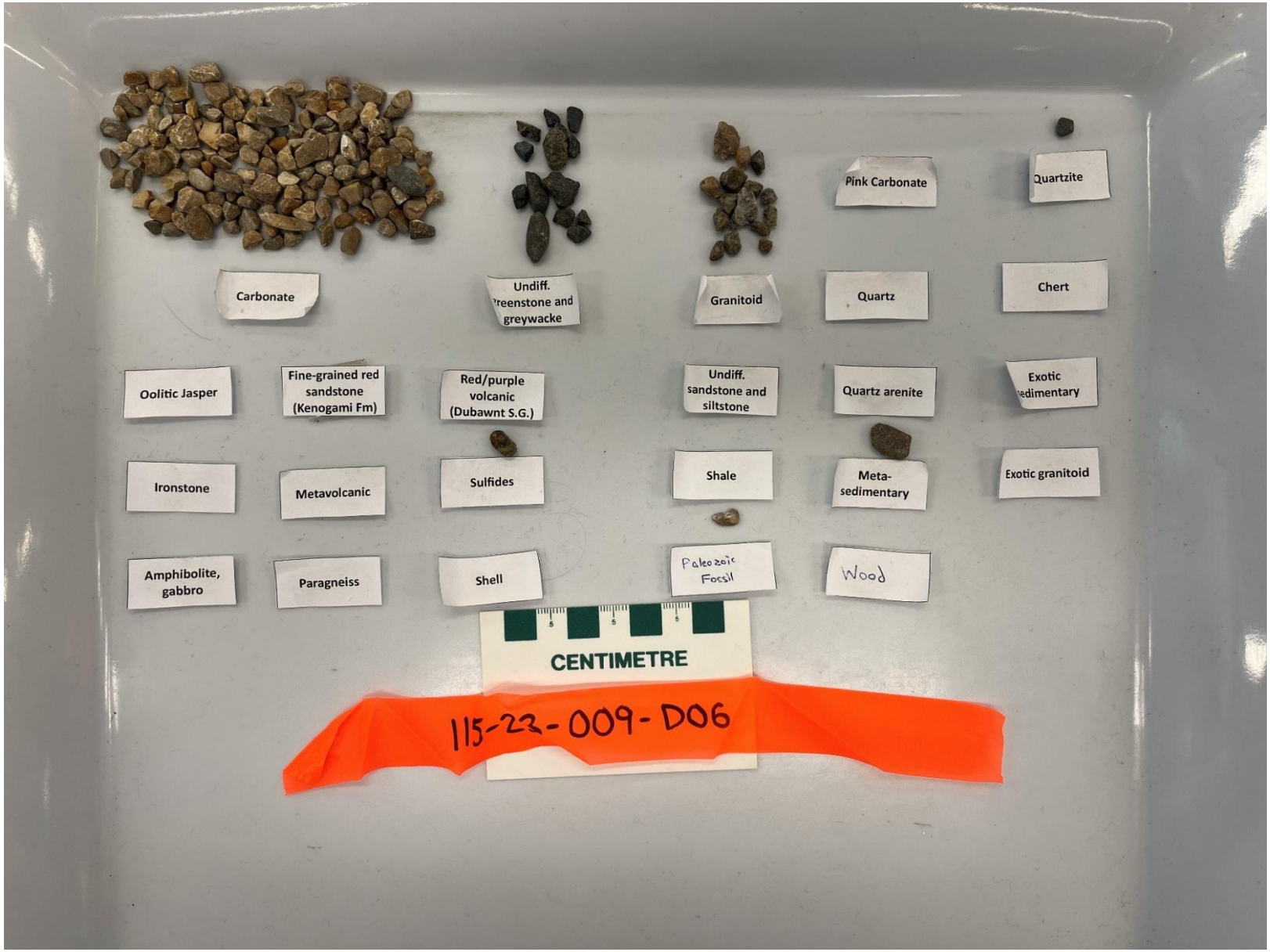

Carbonate
Undiff. greenstone and greywacke
Granitoid
Pink Carbonate
Quartzite
Quartz
Chert
Oolitic Jasper
Fine-grained red sandstone (Kenogami Fm)
Red/purple volcanic (Dubawnt S.G.)
Undiff. sandstone and siltstone
Quartz arenite
Exotic sedimentary
Ironstone
Metavolcanic
Sulfides
Shale
Meta-sedimentary
Exotic granitoid
Amphibolite, gabbro
Paragneiss
Shell
Paleozoic Fossil
Wood
CENTIMETRE
115-23-009-D04


Carbonate
Undiff. greenstone and greywacke
Granitoid
Pink Carbonate
Quartzite
Chert
Quartz
Oolitic Jasper
Fine-grained red sandstone (Kenogami Fm)
Red/purple volcanic (Dubawnt S.G.)
Undiff. sandstone and siltstone
Quartz arenite
Exotic sedimentary
Ironstone
Metavolcanic
Sulfides
Shale
Meta-sedimentary
Exotic granitoid
Amphibolite, gabbro
Paragneiss
Shell
Paleozoic Fossil
Wood
CENTIMETRE
115-23-009-D04


Carbonate
Undiff. reenstone and greywacke
Granitoid
Pink Carbonate
Quartzite
Quartz
Chert
Oolitic Jasper
Fine-grained red sandstone (Kenogami Fm)
Red/purple volcanic (Dubawnt S.G.)
Undiff. sandstone and siltstone
Quartz arenite
Exotic edimentary
Ironstone
Metavolcanic
Sulfides
Shale
Meta-sedimentary
Exotic granitoid
Amphibolite, gabbro
Paragneiss
Shell
Paleozoic Fossil
Wood
CENTIMETRE
115-23-009-D05


Carbonate
Undiff. greenstone and greywacke
Granitoid
Pink Carbonate
Quartzite
Quartz
Chert
Oolitic Jasper
Fine-grained red sandstone (Kenogami Fm)
Red/purple volcanic (Dubawnt S.G.)
Undiff. sandstone and siltstone
Quartz arenite
Exotic sedimentary
Ironstone
Metavolcanic
Sulfides
Shale
Meta-sedimentary
Exotic granitoid
Amphibolite, gabbro
Paragneiss
Shell
Paleozoic Fossil
Wood
CENTIMETRE
115-23-009-D05


Carbonate
Undiff. greenstone and greywacke
Granitoid
Pink Carbonate
Quartzite
Quartz
Chert
Oolitic Jasper
Fine-grained red sandstone (Kenogami Fm)
Red/purple volcanic (Dubawnt S.G.)
Undiff. sandstone and siltstone
Quartz arenite
Exotic sedimentary
Ironstone
Metavolcanic
Sulfides
Shale
Meta-sedimentary
Exotic granitoid
Amphibolite, gabbro
Paragneiss
Shell
Paleozoic Fossil
Wood
CENTIMETRE
115-23-009-D06

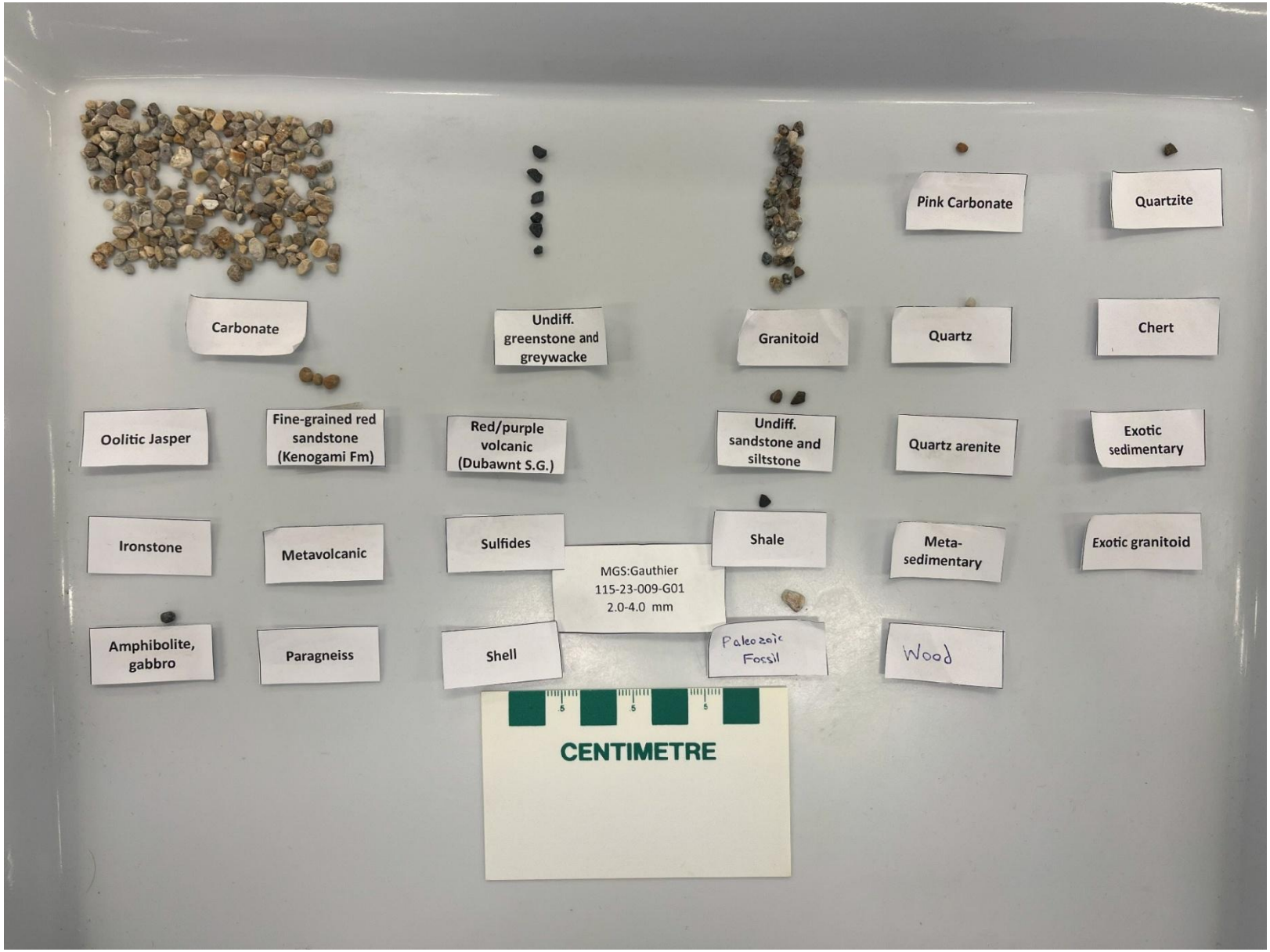

Carbonate
Undiff. greenstone and greywacke
Granitoid
Pink Carbonate
Quartzite
Quartz
Chert
Oolitic Jasper
Fine-grained red sandstone (Kenogami Fm)
Red/purple volcanic (Dubawnt S.G.)
Undiff. sandstone and siltstone
Quartz arenite
Exotic sedimentary
Ironstone
Metavolcanic
Sulfides
Shale
Meta-sedimentary
Exotic granitoid
Amphibolite, gabbro
Paragneiss
Shell
Paleozoic Fossil
Wood
CENTIMETRE
115-23-009-D06


Carbonate
Undiff. greenstone and greywacke
Granitoid
Pink Carbonate
Quartzite
Quartz
Chert
Oolitic Jasper
Fine-grained red sandstone (Kenogami Fm)
Red/purple volcanic (Dubawnt S.G.)
Undiff. sandstone and siltstone
Quartz arenite
Exotic sedimentary
Ironstone
Metavolcanic
Sulfides
Shale
Meta-sedimentary
Exotic granitoid
MGS:Gauthier
115-23-009-D07
2.0-4.0 mm
Amphibolite, gabbro
Paragneiss
Shell
Paleozoic Fossil
Wood
CENTIMETRE


Carbonate
Undiff. greenstone and greywacke
Granitoid
Pink Carbonate
Oolitic Jasper
Fine-grained red sandstone (Kenogami Fm)
Red/purple volcanic (Dubawnt S.G.)
Quartz
Quartzite
Chert
Ironstone
Metavolcanic
Sulfides
Undiff. sandstone and siltstone
Quartz arenite
Exotic sedimentary
MGS:Gauthier
115-23-009-D07
4.0-8.0 mm
Amphibolite, gabbro
Paragneiss
Shell
Shale
Meta-sedimentary
Exotic granitoid
Paleozoic Fossil
CENTIMETRE


Carbonate
Undiff. greenstone and greywacke
Granitoid
Pink Carbonate
Quartzite
Quartz
Chert
Oolitic Jasper
Fine-grained red sandstone (Kenogami Fm)
Red/purple volcanic (Dubawnt S.G.)
Undiff. sandstone and siltstone
Quartz arenite
Exotic sedimentary
Ironstone
Metavolcanic
Sulfides
Shale
Meta-sedimentary
Exotic granitoid
Amphibolite, gabbro
Paragneiss
Shell
Paleozoic Fossil
Wood
CENTIMETRE
115-23-009-E01


Carbonate
Undiff. greenstone and greywacke
Granitoid
Pink Carbonate
Quartzite
Quartz
Chert
Oolitic Jasper
Fine-grained red sandstone (Kenogami Fm)
Red/purple volcanic (Dubawnt S.G.)
Undiff. sandstone and siltstone
Quartz arenite
Exotic sedimentary
Ironstone
Metavolcanic
Sulfides
Shale
Meta-sedimentary
Exotic granitoid
Amphibolite, gabbro
Paragneiss
Shell
Paleozoic Fossil
Wood
CENTIMETRE
115-23-009-E01

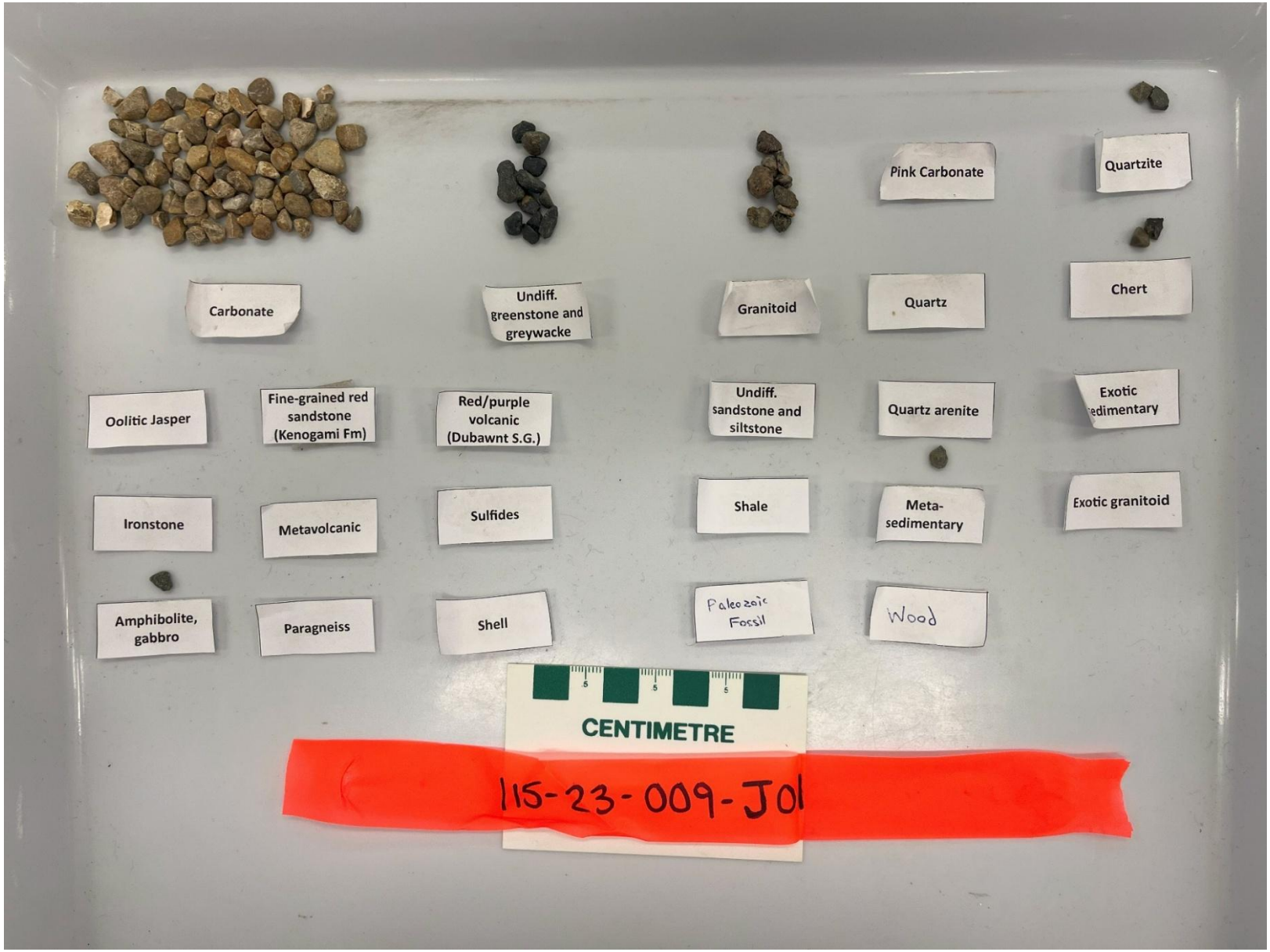

Carbonate
Undiff. greenstone and greywacke
Granitoid
Pink Carbonate
Quartzite
Quartz
Chert
Oolitic Jasper
Fine-grained red sandstone (Kenogami Fm)
Red/purple volcanic (Dubawnt S.G.)
Undiff. sandstone and siltstone
Quartz arenite
Exotic sedimentary
Ironstone
Metavolcanic
Sulfides
Shale
Meta-sedimentary
Exotic granitoid
MGS:Gauthier
115-23-009-G01
2.0-4.0 mm
Amphibolite, gabbro
Paragneiss
Shell
Paleozoic Fossil
Wood
CENTIMETRE


Carbonate
Undiff. greenstone and greywacke
Granitoid
Pink Carbonate
Oolitic Jasper
Fine-grained red sandstone (Kenogami Fm)
Red/purple volcanic (Dubawnt S.G.)
Quartz
Quartzite
Chert
Ironstone
Metavolcanic
Sulfides
Undiff. sandstone and siltstone
Quartz arenite
Exotic sedimentary
MGS:Gauthier
115-23-009-G01
4.0-8.0 mm
Amphibolite, gabbro
Paragneiss
Shell
Shale
Meta-sedimentary
Exotic granitoid
Paleozoic Fossil
CENTIMETRE

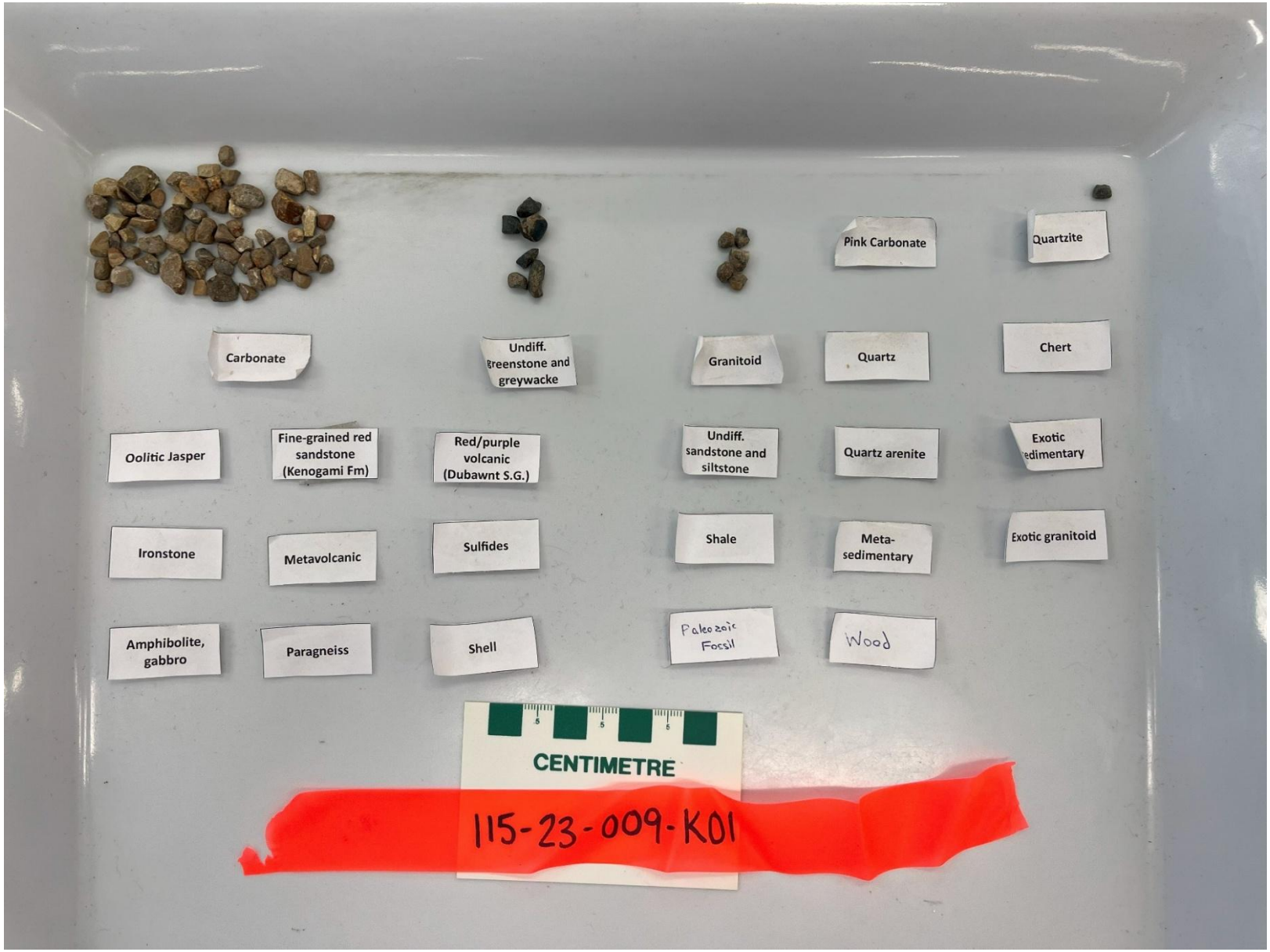

Carbonate
Undiff. greenstone and greywacke
Granitoid
Pink Carbonate
Quartz
uartzite
Chert
Oolitic Jasper
Fine-grained red sandstone (Kenogami Fm)
Red/purple volcanic (Dubawnt S.G.)
Undiff. sandstone and siltstone
Quartz arenite
Exotic dimentary
Ironstone
Metavolcanic
Sulfides
Shale
Meta-sedimentary
Exotic granitoid
Amphibolite, gabbro
Paragneiss
Shell
Paleozoic Fossil
Wood
CENTIMETRE
115-23-009-G02


Carbonate
Undiff. greenstone and greywacke
Granitoid
Pink Carbonate
Quartzite
Quartz
Chert
Oolitic Jasper
Fine-grained red sandstone (Kenogami Fm)
Red/purple volcanic (Dubawnt S.G.)
Undiff. sandstone and siltstone
Quartz arenite
Exotic sedimentary
Ironstone
Metavolcanic
Sulfides
Shale
Meta-sedimentary
Exotic granitoid
Amphibolite, gabbro
Paragneiss
Shell
Paleozoic Fossil
Wood
CENTIMETRE
15-23-009-G02


Carbonate
Undiff. greenstone and greywacke
Granitoid
Pink Carbonate
Quartzite
Quartz
Chert
Oolitic Jasper
Fine-grained red sandstone (Kenogami Fm)
Red/purple volcanic (Dubawnt S.G.)
Undiff. sandstone and siltstone
Quartz arenite
Exotic sedimentary
Ironstone
Metavolcanic
Sulfides
Shale
Meta-sedimentary
Exotic granitoid
Amphibolite, gabbro
Paragneiss
Shell
Paleozoic Fossil
Wood
CENTIMETRE
115-23-009-J01

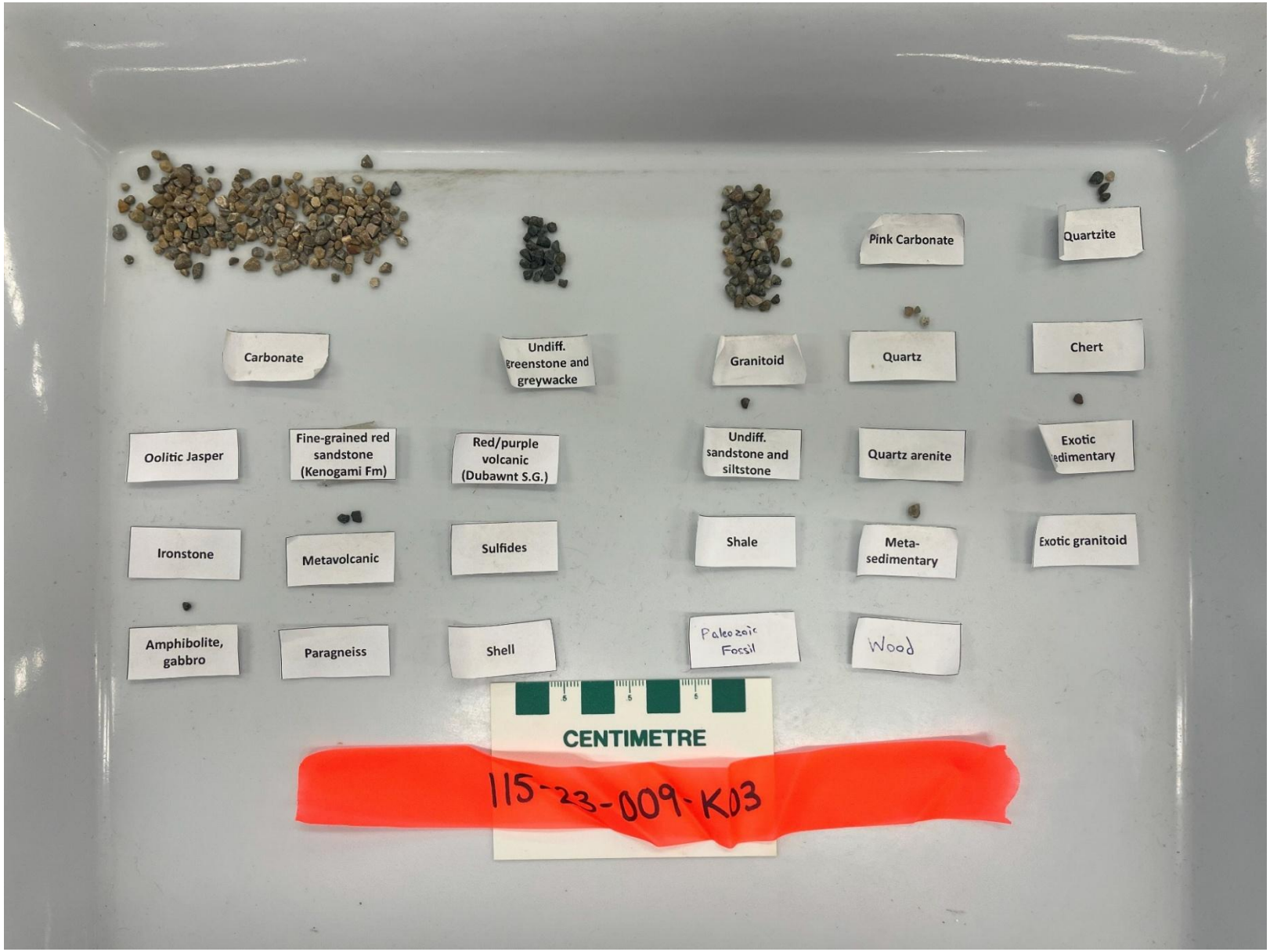

Carbonate
Undiff. greenstone and greywacke
Granitoid
Pink Carbonate
Quartzite
Quartz
Chert
Oolitic Jasper
Fine-grained red sandstone (Kenogami Fm)
Red/purple volcanic (Dubawnt S.G.)
Undiff. sandstone and siltstone
Quartz arenite
Exotic sedimentary
Ironstone
Metavolcanic
Sulfides
Shale
Meta-sedimentary
Exotic granitoid
Amphibolite, gabbro
Paragneiss
Shell
Paleozoic Fossil
Wood
CENTIMETRE
115-23-009-J01

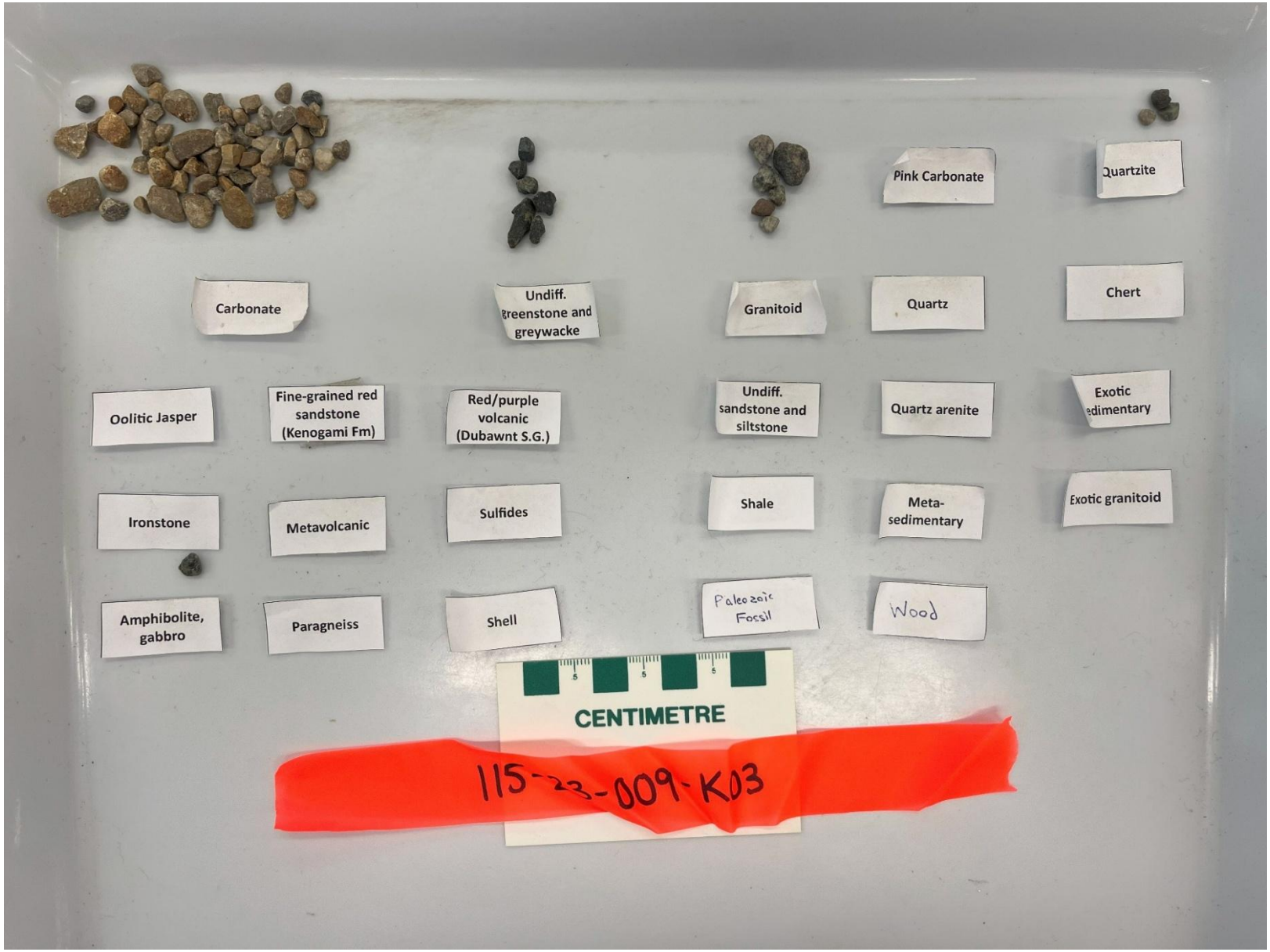

Carbonate
Undiff. greenstone and greywacke
Granitoid
Pink Carbonate
Quartzite
Quartz
Chert
Oolitic Jasper
Fine-grained red sandstone (Kenogami Fm)
Red/purple volcanic (Dubawnt S.G.)
Undiff. sandstone and siltstone
Quartz arenite
Exotic sedimentary
Ironstone
Metavolcanic
Sulfides
Shale
Meta-sedimentary
Exotic granitoid
Amphibolite, gabbro
Paragneiss
Shell
Paleozoic Fossil
Wood
CENTIMETRE
115-23-009-K01


Carbonate
Undiff. Greenstone and greywacke
Granitoid
Pink Carbonate
Quartzite
Quartz
Chert
Oolitic Jasper
Fine-grained red sandstone (Kenogami Fm)
Red/purple volcanic (Dubawnt S.G.)
Undiff. sandstone and siltstone
Quartz arenite
Exotic edimentary
Ironstone
Metavolcanic
Sulfides
Shale
Meta-sedimentary
Exotic granitoid
Amphibolite, gabbro
Paragneiss
Shell
Paleozoic Fossil
Wood
CENTIMETRE
115-23-009-K01


Carbonate
Undiff. greenstone and greywacke
Granitoid
Pink Carbonate
Quartzite
Quartz
Chert
Oolitic Jasper
Fine-grained red sandstone (Kenogami Fm)
Red/purple volcanic (Dubawnt S.G.)
Undiff. sandstone and siltstone
Quartz arenite
Exotic sedimentary
Ironstone
Metavolcanic
Sulfides
Shale
Meta-sedimentary
Exotic granitoid
MGS:Gauthier
115-23-009-K02
2.0-4.0 mm
Amphibolite, gabbro
Paragneiss
Shell
Paleozoic Fossil
Wood
CENTIMETRE


Carbonate
Undiff. greenstone and greywacke
Granitoid
Pink Carbonate
Oolitic Jasper
Fine-grained red sandstone (Kenogami Fm)
Red/purple volcanic (Dubawnt S.G.)
Quartz
Quartzite
Chert
Ironstone
Metavolcanic
Sulfides
Undiff. sandstone and siltstone
Quartz arenite
Exotic sedimentary
MGS:Gauthier
115-23-009-K02
4.0-8.0 mm
Amphibolite, gabbro
Paragneiss
Shell
Shale
Meta-sedimentary
Exotic granitoid
Paleozoic Fossil
CENTIMETRE


Carbonate
Undiff. Greenstone and greywacke
Granitoid
Pink Carbonate
Quartzite
Quartz
Chert
Oolitic Jasper
Fine-grained red sandstone (Kenogami Fm)
Red/purple volcanic (Dubawnt S.G.)
Undiff. sandstone and siltstone
Quartz arenite
Exotic sedimentary
Ironstone
Metavolcanic
Sulfides
Shale
Meta-sedimentary
Exotic granitoid
Amphibolite, gabbro
Paragneiss
Shell
Paleozoic Fossil
Wood
CENTIMETRE
115-23-009-K03

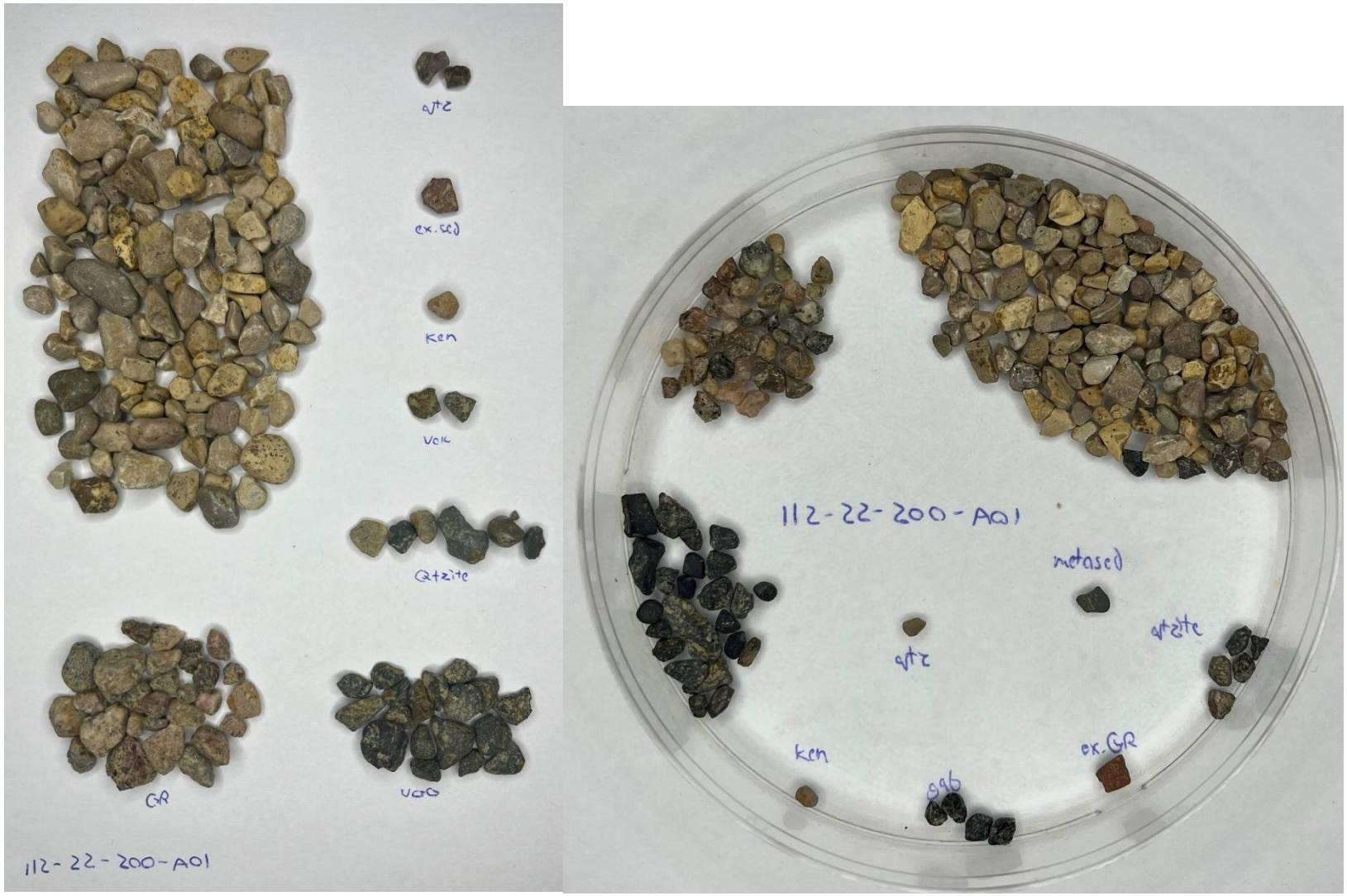

Carbonate
Undiff. Greenstone and greywacke
Granitoid
Pink Carbonate
Quartzite
Quartz
Chert
Oolitic Jasper
Fine-grained red sandstone (Kenogami Fm)
Red/purple volcanic (Dubawnt S.G.)
Undiff. sandstone and siltstone
Quartz arenite
Exotic edimentary
Ironstone
Metavolcanic
Sulfides
Shale
Meta-sedimentary
Exotic granitoid
Amphibolite, gabbro
Paragneiss
Shell
Paleozoic Fossil
Wood
CENTIMETRE
115-23-009-K03


Carbonate
Undiff. greenstone and greywacke
Granitoid
Pink Carbonate
Quartzite
Quartz
Chert
Oolitic Jasper
Fine-grained red sandstone (Kenogami Fm)
Red/purple volcanic (Dubawnt S.G.)
Undiff. sandstone and siltstone
Quartz arenite
Exotic sedimentary
Ironstone
Metavolcanic
Sulfides
Shale
Meta-sedimentary
Exotic granitoid
MGS:Gauthier
115-23-009-K04
2.0-4.0 mm
Amphibolite, gabbro
Paragneiss
Shell
Paleozoic Fossil
Wood
CENTIMETRE

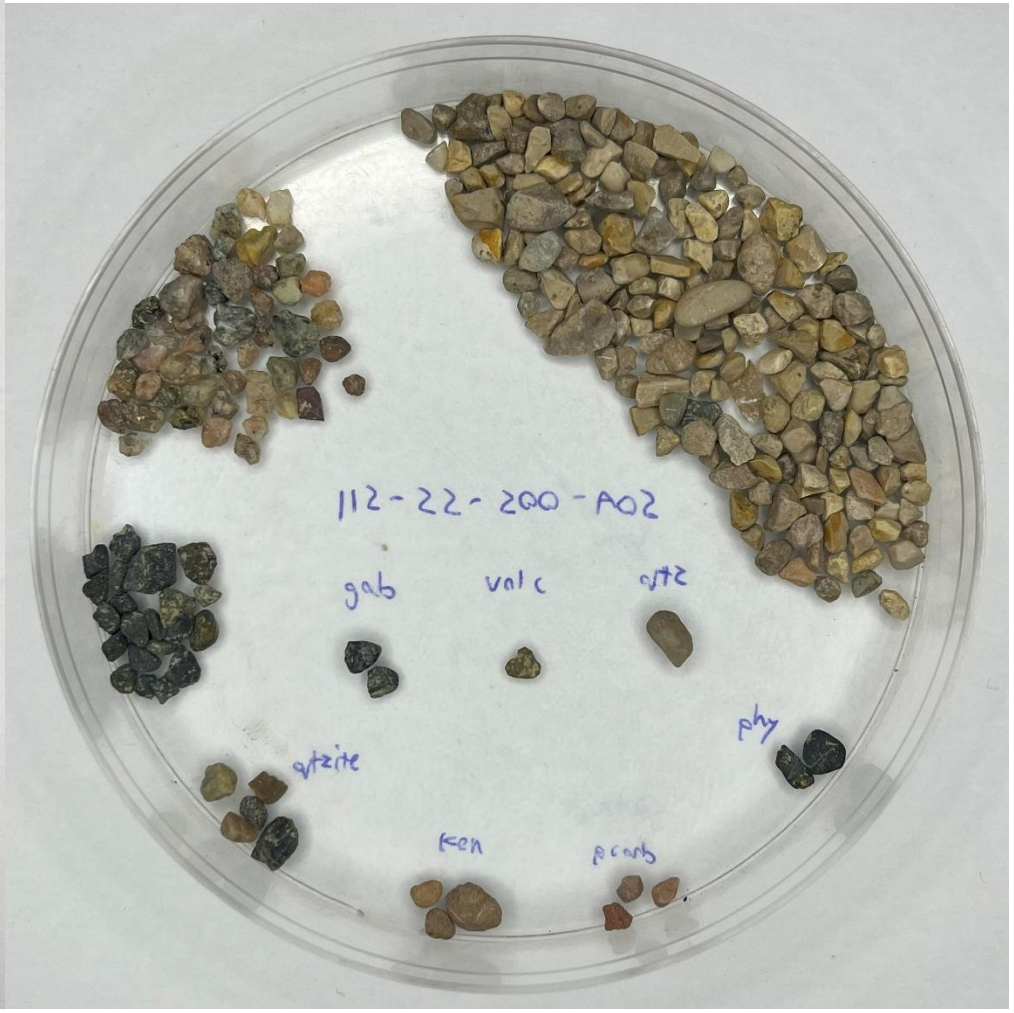

Carbonate
Undiff. greenstone and greywacke
Granitoid
Pink Carbonate
Oolitic Jasper
Fine-grained red sandstone (Kenogami Fm)
Red/purple volcanic (Dubawnt S.G.)
Quartz
Quartzite
Chert
Ironstone
Metavolcanic
Sulfides
Undiff. sandstone and siltstone
Quartz arenite
Exotic sedimentary
MGS:Gauthier
115-23-009-K04
4.0-8.0 mm
Amphibolite, gabbro
Paragneiss
Shell
Shale
Meta-sedimentary
Exotic granitoid
Paleozoic Fossil
CENTIMETRE
Wood

112-22-200

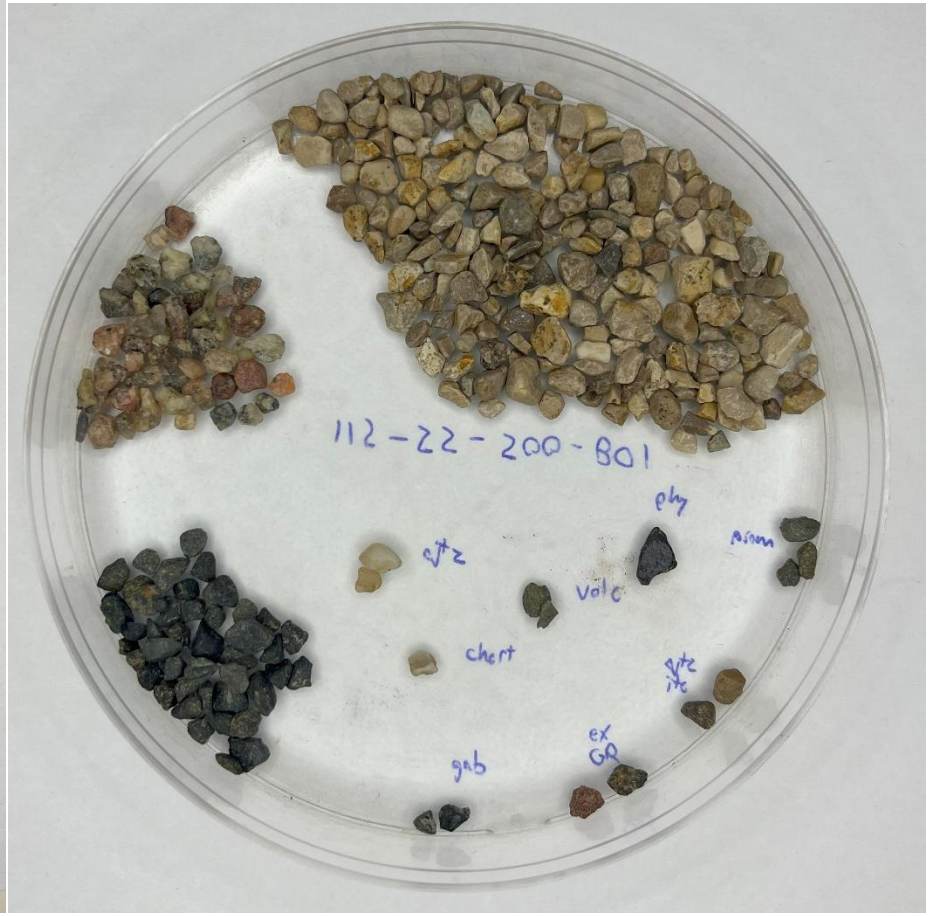
Note: Clast counts of the 4-8 mm size fraction are displayed on paper, while clast counts of the 2-4 mm size fraction are in Petri dishes.



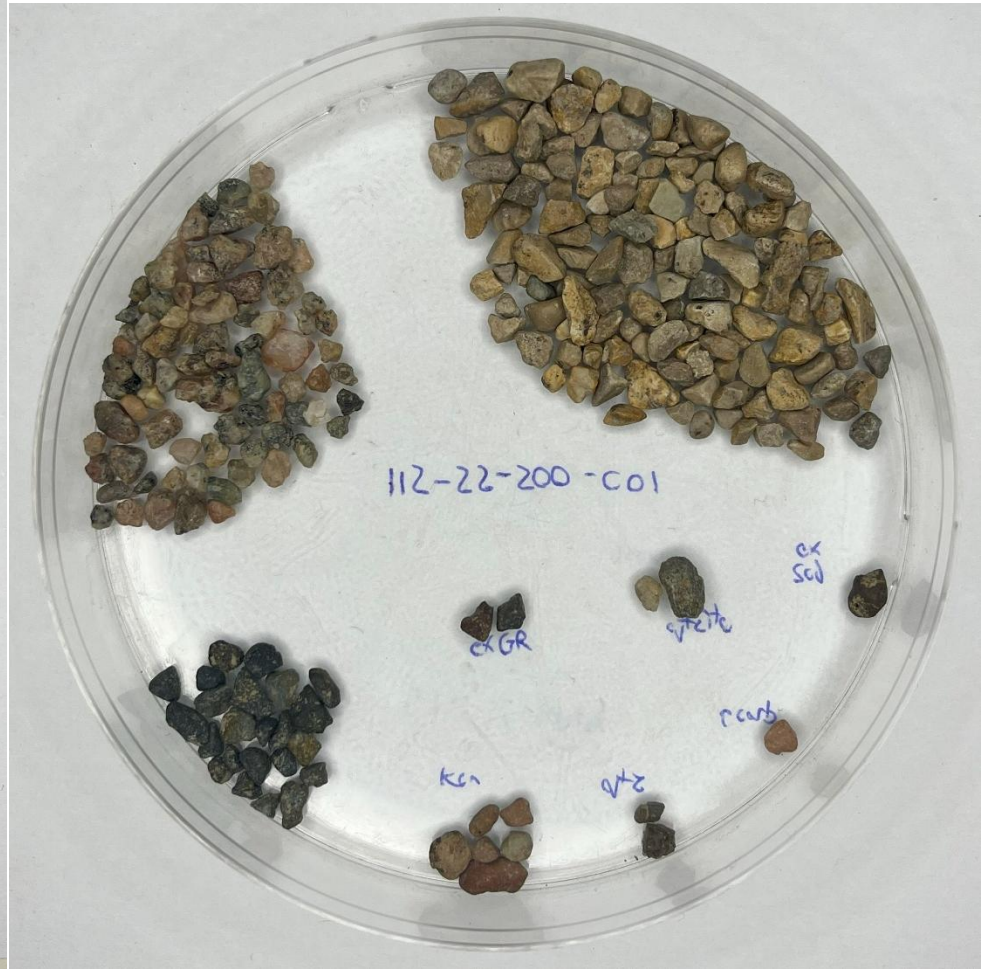

p carb
volc
qtzite
psam
GR
VGG
112-22-200-A02

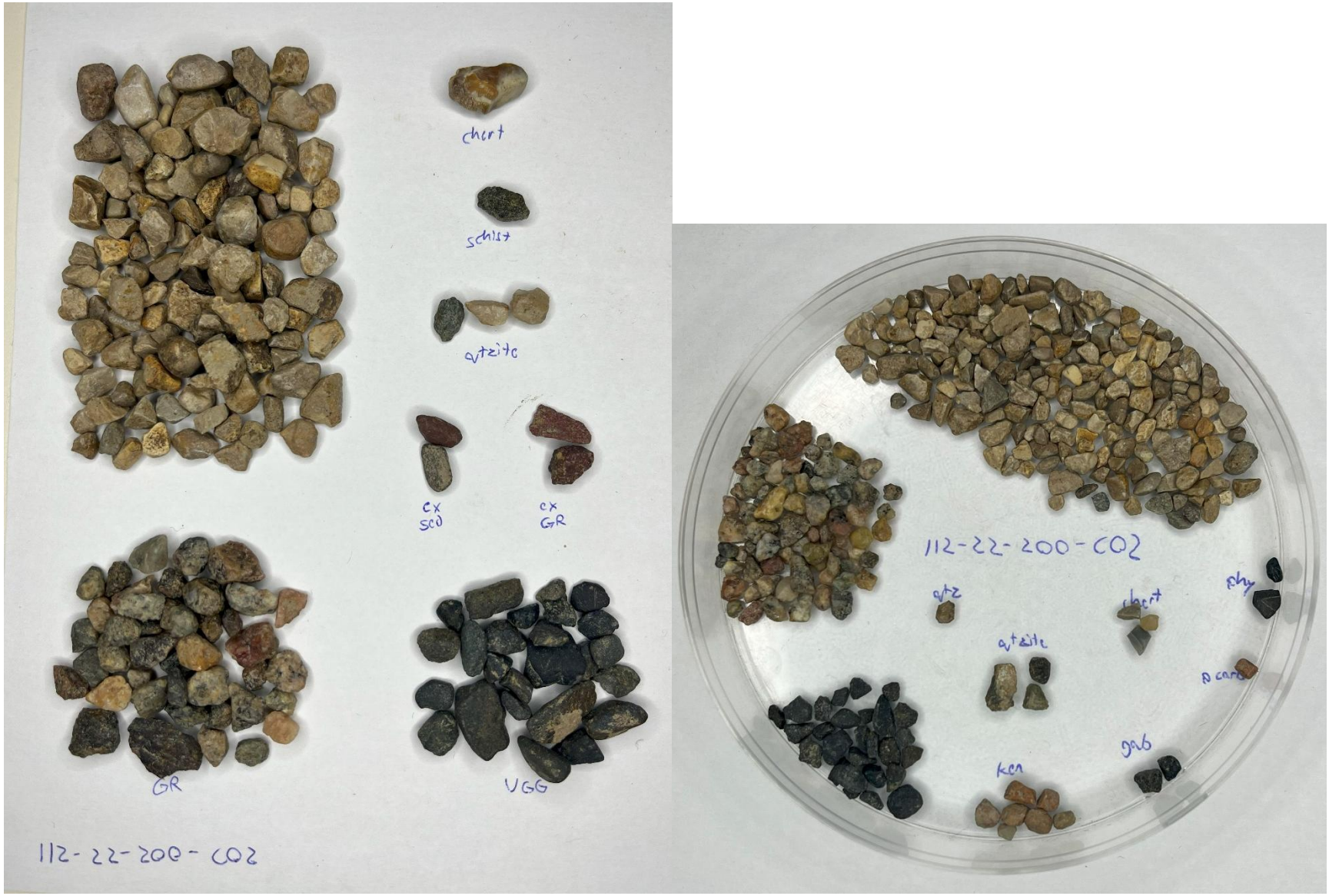

112-22-200-A02
gab
volc
qtz
phy
qtzite
ksp
p carb


phy
volc
112-22-200-B01

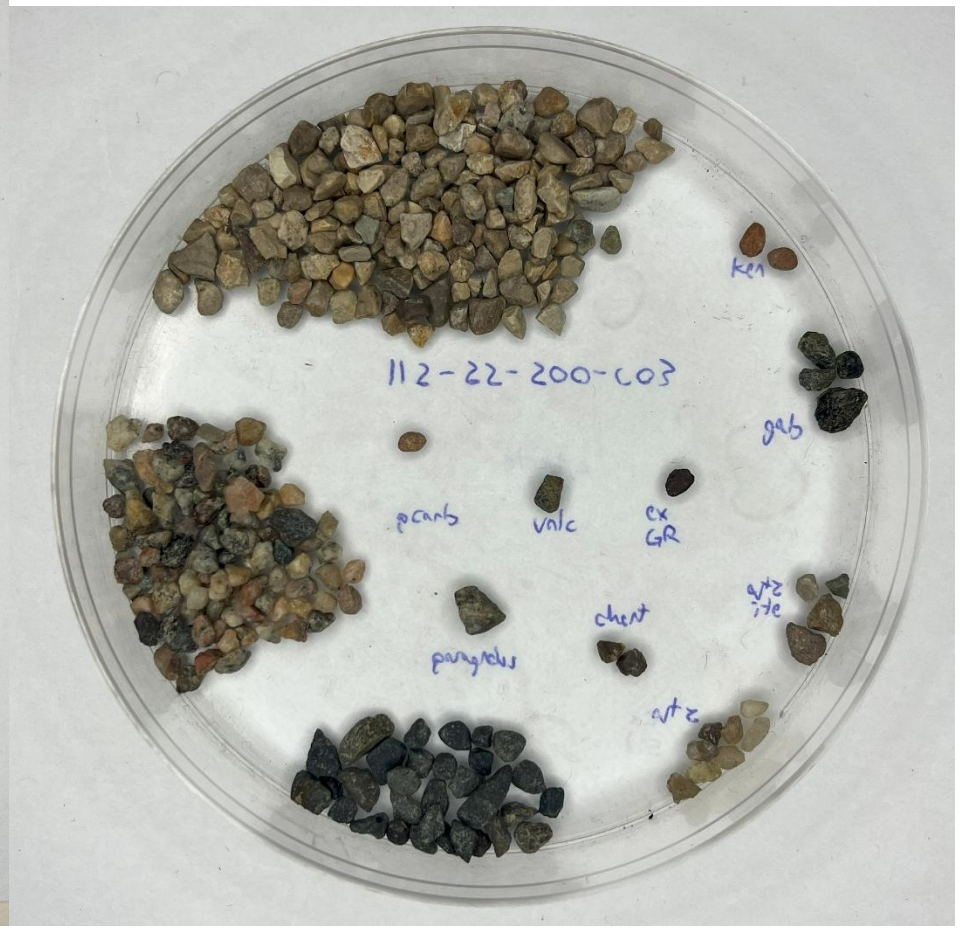

112-22-200-B01
phy
volc
chert
gab


ex GR
pcarb
psam
qtzite
GR
UGG
112-22-200-C01


112-22-200-C01
ex GR
qtzite
ex SCV
pcarb
qtz


chert
schist
qtzite
cx
SCD
cx
GR
GR
VGG
112-22-200-CO2
112-22-200-CO2
qtz
chert
phy
qtzite
gab
ker

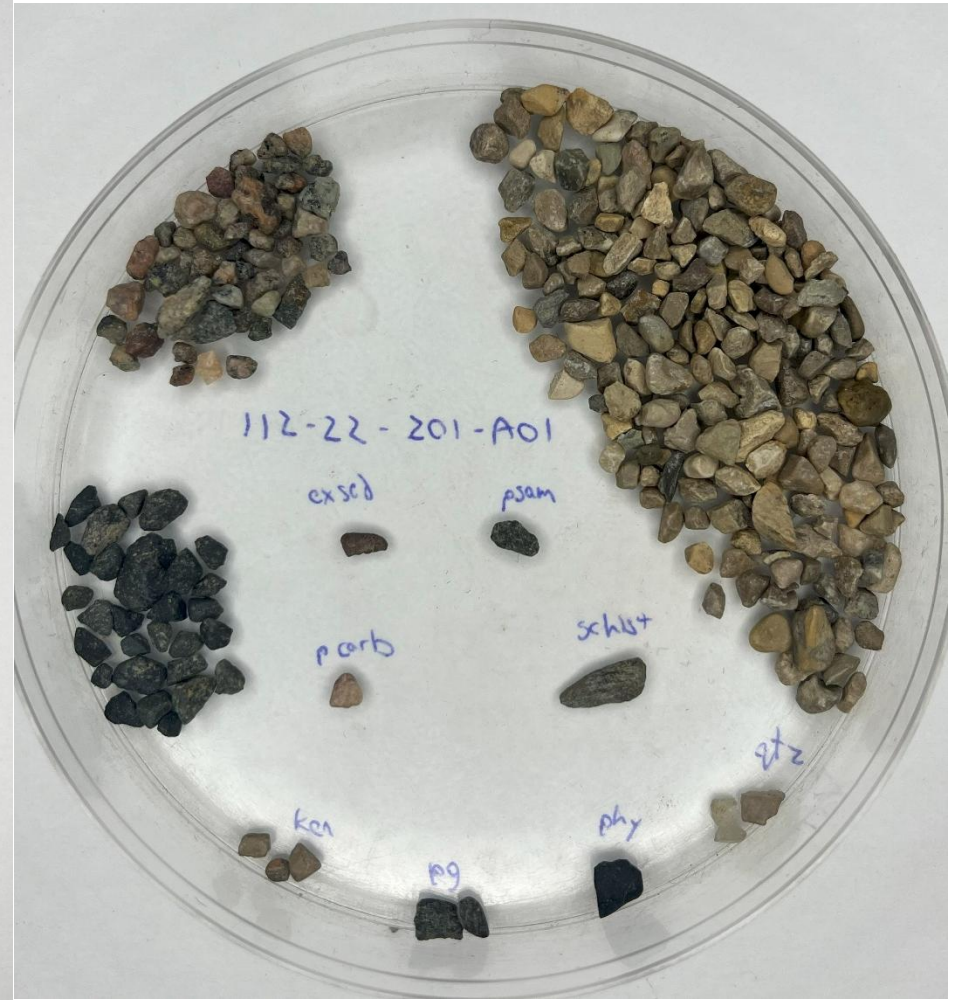

qtzite
ex GR
ken
gab
phy
GR
VGO
112-22-200-C03


112-22-200-C03
ken
gab
pcarb
volc
ex GR
qtz ite
chert
paragneiss
qtz

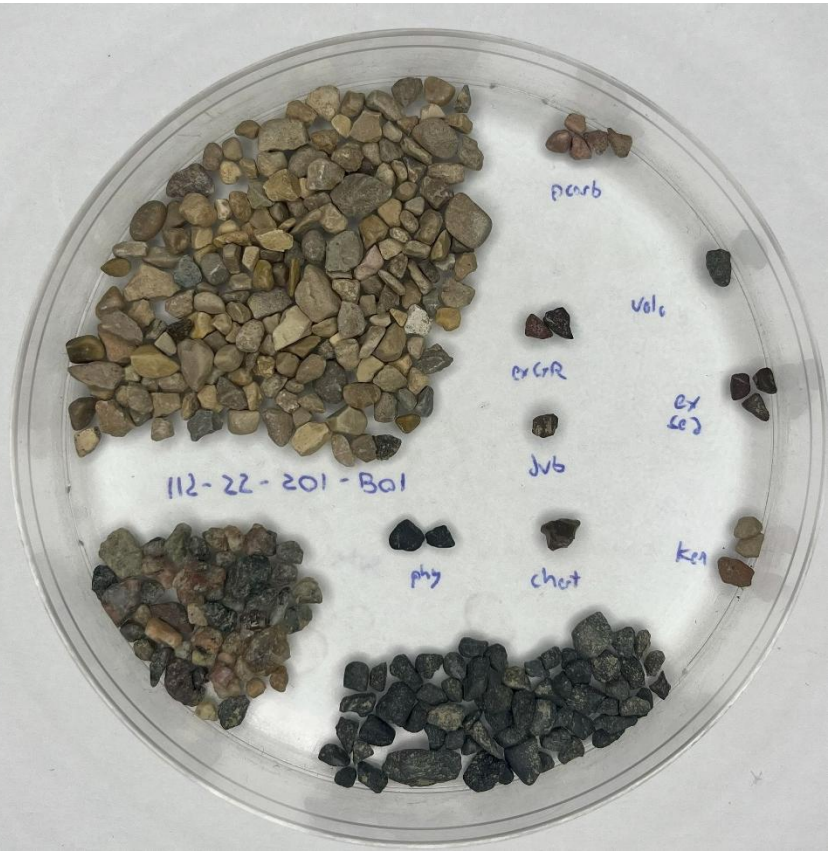
112-22-201

Note: Clast counts of the 4-8 mm size fraction are displayed on paper, while clast counts of the 2-4 mm size fraction are in Petri dishes.






pcarb
volc
USS
gytzll
psam
chert
ex sed
GR
UGG
phy
112-22-201-B01


pcarb
volc
ex GR
ex sed
JVb
112-22-201-B01
phy
chert

Appendix F – Radiocarbon dating

Table 1. Radiocarbon results for samples submitted to the Radiocarbon Laboratory at the University of Ottawa (errors are 1σ; reported ages are conventional).

Lab ID	Submitter ID	Material	14C yr BP	±	F14C	±	D14C ‰	±	Δ14C ‰	±
UOC-23328	115-23-003-R01	marine shell	7700	25	0.3838	0.0011	-616.20	1.09	-619.57	1.09
UOC-23329	115-23-006-R01	marine shell	7490	25	0.3937	0.0012	-606.26	1.21	-609.72	1.21
UOC-23330	115-23-006-R02	marine shell fragment	>47100 ϕ	--	<0.0028	--	<-997.2	--	<-997.2	--
UOC-26756	115-23-005-Ex2	wood; fragment from a log	>45500 ϕ	--	<0.0035	--	<-996.6	--	<-996.6	--

ϕNon-finite age - F14C less than limit of detection

Appendix G – Paleo-ice flow measurements

Table 1: Till-fabric measurements.

Section ID	Fabric site | Sample ID	Depth (m bgs)	A-axis dip direction (°)	A-axis dip (°)	A-axis length (cm)	B-axis length (cm)	C-axis length (cm)	A:B	Conducted by | Source publication
115-23-002	115-23-002-A01	4.50	14	55	16	10	7	1.6	N. Mesich
115-23-002	115-23-002-A01	4.50	192	5	20	12	7	1.7	N. Mesich
115-23-002	115-23-002-A01	4.50	139	14	19	13	7	1.5	N. Mesich
115-23-002	115-23-002-A01	4.50	30	46	15	9	7	1.7	N. Mesich
115-23-002	115-23-002-A01	4.50	1	9	30	19	10	1.6	N. Mesich
115-23-002	115-23-002-A01	4.50	217	12	19	9	6	2.1	N. Mesich
115-23-002	115-23-002-A01	4.50	189	12	18	12	9	1.5	N. Mesich
115-23-002	115-23-002-A01	4.50	35	2	14	7	5	2.0	N. Mesich
115-23-002	115-23-002-A01	4.50	25	3	11	7	4	1.6	N. Mesich
115-23-002	115-23-002-A01	4.50	34	24	9	6	5	1.5	N. Mesich
115-23-002	115-23-002-A01	4.50	11	21	12	7	4	1.7	N. Mesich
115-23-002	115-23-002-A01	4.50	264	14	21	7	4	3.0	N. Mesich
115-23-002	115-23-002-A01	4.50	36	13	12	6	6	2.0	N. Mesich
115-23-002	115-23-002-A01	4.50	55	30	10	4	4	2.5	N. Mesich
115-23-002	115-23-002-A01	4.50	175	30	20	13	7	1.5	N. Mesich
115-23-002	115-23-002-A01	4.50	197	19	10	6	3	1.7	N. Mesich
115-23-002	115-23-002-A01	4.50	213	9	12	8	5	1.5	N. Mesich
115-23-002	115-23-002-A01	4.50	61	26	13	7	2	1.9	N. Mesich
115-23-002	115-23-002-A01	4.50	68	23	26	18	10	1.4	N. Mesich
115-23-002	115-23-002-A01	4.50	18	6	23	13	8	1.8	N. Mesich
115-23-002	115-23-002-A01	4.50	46	27	25	14	9	1.8	N. Mesich
115-23-002	115-23-002-A01	4.50	27	38	18	12	7	1.5	N. Mesich
115-23-002	115-23-002-A01	4.50	163	50	16	10	2	1.6	N. Mesich

115-23-002	115-23-002-A01	4.50	357	0	17	10	6	1.7	N. Mesich
115-23-002	115-23-002-A01	4.50	66	18	15	10	5	1.5	N. Mesich
115-23-002	115-23-002-A01	4.50	75	36	13	7	7	1.9	N. Mesich
115-23-002	115-23-002-A01	4.50	44	24	22	10	6	2.2	N. Mesich
115-23-002	115-23-002-B02	6.50	120	4	45	18	15	2.5	M. Gauthier
115-23-002	115-23-002-B02	6.50	104	8	15	10	4	1.5	M. Gauthier
115-23-002	115-23-002-B02	6.50	258	20	8	5	2	1.6	M. Gauthier
115-23-002	115-23-002-B02	6.50	84	16	7	4	2	1.8	M. Gauthier
115-23-002	115-23-002-B02	6.50	118	16	11	6	4	1.8	M. Gauthier
115-23-002	115-23-002-B02	6.50	90	14	45	25	20	1.8	M. Gauthier
115-23-002	115-23-002-B02	6.50	80	16	16	9	4	1.8	M. Gauthier
115-23-002	115-23-002-B02	6.50	130	17	16	10	2	1.6	M. Gauthier
115-23-002	115-23-002-B02	6.50	134	22	30	20	6	1.5	M. Gauthier
115-23-002	115-23-002-B02	6.50	98	18	13	7	4	1.9	M. Gauthier
115-23-002	115-23-002-B02	6.50	115	16	26	12	6	2.2	M. Gauthier
115-23-002	115-23-002-B02	6.50	164	12	10	5	3	2.0	M. Gauthier
115-23-002	115-23-002-B02	6.50	54	8	15	10	5	1.5	M. Gauthier
115-23-002	115-23-002-B02	6.50	132	16	18	11	11	1.6	M. Gauthier
115-23-002	115-23-002-B02	6.50	130	28	15	8	4	1.9	M. Gauthier
115-23-002	115-23-002-B02	6.50	115	8	12	5	3	2.4	M. Gauthier
115-23-002	115-23-002-B02	6.50	115	28	22	10	4	2.2	M. Gauthier
115-23-002	115-23-002-B02	6.50	125	22	11	7	4	1.6	M. Gauthier
115-23-002	115-23-002-B02	6.50	138	20	7	4	2	1.8	M. Gauthier
115-23-002	115-23-002-B02	6.50	90	24	8	4	2	2.0	M. Gauthier
115-23-002	115-23-002-B02	6.50	149	28	17	9	5	1.9	M. Gauthier
115-23-002	115-23-002-B02	6.50	108	24	14	8	5	1.8	M. Gauthier
115-23-002	115-23-002-B02	6.50	145	30	18	12	7	1.5	M. Gauthier
115-23-002	115-23-002-B02	6.50	135	38	6	3	1	2.0	M. Gauthier

115-23-002	115-23-002-B02	6.50	94	6	10	4	2	2.5	M. Gauthier
115-23-002	115-23-002-B02	6.50	50	25	22	10	6	2.2	M. Gauthier
115-23-002	115-23-002-B02	6.50	252	18	26	10	10	2.6	M. Gauthier
115-23-002	115-23-002-B02	6.50	120	28	16	7	4	2.3	M. Gauthier
115-23-002	115-23-002-B02	6.50	60	12	12	6	3	2.0	M. Gauthier
115-23-002	115-23-002-B02	6.50	98	16	22	9	5	2.4	M. Gauthier
115-23-002	115-23-002-B03	9.00	108	20	6	3	1	2.0	M. Gauthier
115-23-002	115-23-002-B03	9.00	124	6	12	7	4	1.7	M. Gauthier
115-23-002	115-23-002-B03	9.00	4	8	12	6	3	2.0	M. Gauthier
115-23-002	115-23-002-B03	9.00	84	20	9	6	3	1.5	M. Gauthier
115-23-002	115-23-002-B03	9.00	98	12	8	5	2	1.6	M. Gauthier
115-23-002	115-23-002-B03	9.00	88	12	5	2	1	2.5	M. Gauthier
115-23-002	115-23-002-B03	9.00	140	8	6	4	4	1.5	M. Gauthier
115-23-002	115-23-002-B03	9.00	118	8	12	7	3	1.7	M. Gauthier
115-23-002	115-23-002-B03	9.00	112	12	8	4	2	2.0	M. Gauthier
115-23-002	115-23-002-B03	9.00	160	10	23	11	8	2.1	M. Gauthier
115-23-002	115-23-002-B03	9.00	55	32	9	4	3	2.3	M. Gauthier
115-23-002	115-23-002-B03	9.00	104	6	19	11	11	1.7	M. Gauthier
115-23-002	115-23-002-B03	9.00	140	10	11	5	3	2.2	M. Gauthier
115-23-002	115-23-002-B03	9.00	140	2	11	6	4	1.8	M. Gauthier
115-23-002	115-23-002-B03	9.00	142	10	12	6	2	2.0	M. Gauthier
115-23-002	115-23-002-B03	9.00	90	16	22	12	7	1.8	M. Gauthier
115-23-002	115-23-002-B03	9.00	94	14	19	12	7	1.6	M. Gauthier
115-23-002	115-23-002-B03	9.00	100	18	6	2	1	3.0	M. Gauthier
115-23-002	115-23-002-B03	9.00	118	18	65	35	35	1.9	M. Gauthier
115-23-002	115-23-002-B03	9.00	138	18	11	6	6	1.8	M. Gauthier
115-23-002	115-23-002-B03	9.00	320	16	8	3	1	2.7	M. Gauthier
115-23-002	115-23-002-B03	9.00	315	2	18	11	5	1.6	M. Gauthier

115-23-002	115-23-002-B03	9.00	115	2	15	8	4	1.9	M. Gauthier
115-23-002	115-23-002-B03	9.00	288	4	60	30	20	2.0	M. Gauthier
115-23-002	115-23-002-B03	9.00	85	8	8	4	2	2.0	M. Gauthier
115-23-002	115-23-002-B03	9.00	80	4	27	12	8	2.3	M. Gauthier
115-23-002	115-23-002-B03	9.00	134	36	10	6	3	1.7	M. Gauthier
115-23-002	115-23-002-B03	9.00	144	18	15	10	5	1.5	M. Gauthier
115-23-002	115-23-002-B03	9.00	102	18	17	8	4	2.1	M. Gauthier
115-23-002	115-23-002-B03	9.00	75	16	60	30	20	2.0	M. Gauthier
115-23-002	115-23-002-B03	9.00	122	14	17	9	5	1.9	M. Gauthier
115-23-002	115-23-002-C01	10.00	108	10	53	30	15	1.8	M. Ross
115-23-002	115-23-002-C01	10.00	290	22	21	13	10	1.6	M. Ross
115-23-002	115-23-002-C01	10.00	318	52	18	11	6	1.6	M. Ross
115-23-002	115-23-002-C01	10.00	75	41	25	20	13	1.3	M. Ross
115-23-002	115-23-002-C01	10.00	170	8	12	7	6	1.7	M. Ross
115-23-002	115-23-002-C01	10.00	98	16	8	4	3	2.0	M. Ross
115-23-002	115-23-002-C01	10.00	254	38	16	12	8	1.3	M. Ross
115-23-002	115-23-002-C01	10.00	75	34	20	12	8	1.7	M. Ross
115-23-002	115-23-002-C01	10.00	0	47	18	10	9	1.8	M. Ross
115-23-002	115-23-002-C01	10.00	195	15	10	6	3	1.7	M. Ross
115-23-002	115-23-002-C01	10.00	91	35	29	19	14	1.5	M. Ross
115-23-002	115-23-002-C01	10.00	351	37	18	12	9	1.5	M. Ross
115-23-002	115-23-002-C01	10.00	179	35	13	7	5	1.9	M. Ross
115-23-002	115-23-002-C01	10.00	307	28	8	6	4	1.3	M. Ross
115-23-002	115-23-002-C01	10.00	320	32	18	12	9	1.5	M. Ross
115-23-002	115-23-002-C01	10.00	342	12	10	6	5	1.7	M. Ross
115-23-002	115-23-002-C01	10.00	165	12	38	22	19	1.7	M. Ross
115-23-002	115-23-002-C01	10.00	338	36	15	9	6	1.7	M. Ross
115-23-002	115-23-002-C01	10.00	216	52	24	17	13	1.4	M. Ross

115-23-002	115-23-002-C01	10.00	186	25	13	6	4	2.2	M. Ross
115-23-002	115-23-002-C01	10.00	85	58	10	5	4	2.0	M. Ross
115-23-002	115-23-002-C01	10.00	115	6	20	11	6	1.8	M. Ross
115-23-002	115-23-002-C01	10.00	185	5	27	12	8	2.3	M. Ross
115-23-002	115-23-002-C01	10.00	150	26	21	12	10	1.8	M. Ross
115-23-002	115-23-002-C01	10.00	289	18	14	8	5	1.8	M. Ross
115-23-002	115-23-002-C01	10.00	145	28	15	9	5	1.7	M. Ross
115-23-002	115-23-002-C01	10.00	65	7	16	9	6	1.8	M. Ross
115-23-002	115-23-002-C01	10.00	40	12	33	23	17	1.4	M. Ross
115-23-002	115-23-002-C01	10.00	255	45	14	9	4	1.6	M. Ross
115-23-002	115-23-002-C01	10.00	36	8	23	14	12	1.6	M. Ross
115-23-002	115-23-002-C02	12.50	80	11	32	18	9	1.8	N. Mesich
115-23-002	115-23-002-C02	12.50	84	2	26	14	5	1.9	N. Mesich
115-23-002	115-23-002-C02	12.50	25	36	66	44	20	1.5	N. Mesich
115-23-002	115-23-002-C02	12.50	222	12	73	55	35	1.3	N. Mesich
115-23-002	115-23-002-C02	12.50	274	30	51	30	25	1.7	N. Mesich
115-23-002	115-23-002-C02	12.50	50	3	35	24	16	1.5	N. Mesich
115-23-002	115-23-002-C02	12.50	268	16	21	14	7	1.5	N. Mesich
115-23-002	115-23-002-C02	12.50	259	10	36	20	8	1.8	N. Mesich
115-23-002	115-23-002-C02	12.50	133	20	39	25	16	1.6	N. Mesich
115-23-002	115-23-002-C02	12.50	275	10	15	9	7	1.7	N. Mesich
115-23-002	115-23-002-C02	12.50	287	0	29	18	11	1.6	N. Mesich
115-23-002	115-23-002-C02	12.50	211	2	16	10	3	1.6	N. Mesich
115-23-002	115-23-002-C02	12.50	311	16	31	22	13	1.4	N. Mesich
115-23-002	115-23-002-C02	12.50	179	25	17	10	4	1.7	N. Mesich
115-23-002	115-23-002-C02	12.50	290	29	25	16	10	1.6	N. Mesich
115-23-002	115-23-002-C02	12.50	272	31	17	11	7	1.5	N. Mesich
115-23-002	115-23-002-C02	12.50	264	30	21	13	7	1.6	N. Mesich

115-23-002	115-23-002-C02	12.50	341	27	12	8	4	1.5	N. Mesich
115-23-002	115-23-002-C02	12.50	302	13	14	9	6	1.6	N. Mesich
115-23-002	115-23-002-C02	12.50	79	4	22	9	5	2.4	N. Mesich
115-23-002	115-23-002-C02	12.50	292	7	21	14	9	1.5	N. Mesich
115-23-002	115-23-002-C02	12.50	112	15	12	7	4	1.7	N. Mesich
115-23-002	115-23-002-C02	12.50	270	19	48	30	22	1.6	N. Mesich
115-23-002	115-23-002-C02	12.50	82	11	19	12	7	1.6	N. Mesich
115-23-002	115-23-002-C02	12.50	299	28	11	7	4	1.6	N. Mesich
115-23-002	115-23-002-C02	12.50	111	19	15	10	6	1.5	N. Mesich
115-23-002	115-23-002-C02	12.50	81	14	26	15	9	1.7	N. Mesich
115-23-002	115-23-002-C02	12.50	284	12	13	8	5	1.6	N. Mesich
115-23-002	115-23-002-C03	14.50	178	4	15	5	5	3.0	M. Gauthier
115-23-002	115-23-002-C03	14.50	168	8	16	10	5	1.6	M. Gauthier
115-23-002	115-23-002-C03	14.50	40	18	45	24	12	1.9	M. Gauthier
115-23-002	115-23-002-C03	14.50	48	8	33	17	11	1.9	M. Gauthier
115-23-002	115-23-002-C03	14.50	338	24	12	6	4	2.0	M. Gauthier
115-23-002	115-23-002-C03	14.50	42	12	38	16	12	2.4	M. Gauthier
115-23-002	115-23-002-C03	14.50	124	24	14	7	5	2.0	M. Gauthier
115-23-002	115-23-002-C03	14.50	324	20	20	8	4	2.5	M. Gauthier
115-23-002	115-23-002-C03	14.50	24	28	7	4	4	1.8	M. Gauthier
115-23-002	115-23-002-C03	14.50	30	20	15	10	8	1.5	M. Gauthier
115-23-002	115-23-002-C03	14.50	58	16	16	6	6	2.7	M. Gauthier
115-23-002	115-23-002-C03	14.50	2	8	10	6	4	1.7	M. Gauthier
115-23-002	115-23-002-C03	14.50	32	24	7	3	2	2.3	M. Gauthier
115-23-002	115-23-002-C03	14.50	64	8	11	5	3	2.2	M. Gauthier
115-23-002	115-23-002-C03	14.50	26	16	8	4	2	2.0	M. Gauthier
115-23-002	115-23-002-C03	14.50	36	16	12	7	4	1.7	M. Gauthier
115-23-002	115-23-002-C03	14.50	72	6	70	25	14	2.8	M. Gauthier

115-23-002	115-23-002-C03	14.50	52	6	31	6	4	5.2	M. Gauthier
115-23-002	115-23-002-C03	14.50	38	20	12	8	4	1.5	M. Gauthier
115-23-002	115-23-002-C03	14.50	36	6	6	3	3	2.0	M. Gauthier
115-23-002	115-23-002-C03	14.50	52	14	14	6	2	2.3	M. Gauthier
115-23-002	115-23-002-C03	14.50	34	8	6	3	3	2.0	M. Gauthier
115-23-002	115-23-002-C03	14.50	28	10	53	35	25	1.5	M. Gauthier
115-23-002	115-23-002-C03	14.50	66	24	22	11	5	2.0	M. Gauthier
115-23-002	115-23-002-C03	14.50	34	22	17	11	8	1.5	M. Gauthier
115-23-002	115-23-002-C03	14.50	95	14	21	12	5	1.8	M. Gauthier
115-23-002	115-23-002-C03	14.50	18	24	24	14	6	1.7	M. Gauthier
115-23-002	115-23-002-C03	14.50	46	16	25	13	8	1.9	M. Gauthier
115-23-002	115-23-002-C03	14.50	54	4	12	7	7	1.7	M. Gauthier
115-23-002	115-23-002-C03	14.50	14	22	15	6	4	2.5	M. Gauthier
115-23-002	115-23-002-C04	16.20	230	12	45	26	20	1.7	M. Ross
115-23-002	115-23-002-C04	16.20	288	28	68	40	26	1.7	M. Ross
115-23-002	115-23-002-C04	16.20	92	3	27	15	11	1.8	M. Ross
115-23-002	115-23-002-C04	16.20	65	4	25	16	9	1.6	M. Ross
115-23-002	115-23-002-C04	16.20	260	22	43	30	23	1.4	M. Ross
115-23-002	115-23-002-C04	16.20	164	14	25	16	9	1.6	M. Ross
115-23-002	115-23-002-C04	16.20	120	17	37	24	15	1.5	M. Ross
115-23-002	115-23-002-C04	16.20	80	4	25	20	12	1.3	M. Ross
115-23-002	115-23-002-C04	16.20	336	15	25	15	7	1.7	M. Ross
115-23-002	115-23-002-C04	16.20	46	11	30	18	11	1.7	M. Ross
115-23-002	115-23-002-C04	16.20	56	30	15	9	7	1.7	M. Ross
115-23-002	115-23-002-C04	16.20	110	17	15	8	4	1.9	M. Ross
115-23-002	115-23-002-C04	16.20	60	20	9	5	4	1.8	M. Ross
115-23-002	115-23-002-C04	16.20	210	41	68	48	32	1.4	M. Ross
115-23-002	115-23-002-C04	16.20	340	15	31	21	11	1.5	M. Ross

115-23-002	115-23-002-C04	16.20	94	10	17	10	8	1.7	M. Ross
115-23-002	115-23-002-C04	16.20	55	2	30	15	9	2.0	M. Ross
115-23-002	115-23-002-C04	16.20	16	8	26	16	10	1.6	M. Ross
115-23-002	115-23-002-C04	16.20	152	18	13	6	3	2.2	M. Ross
115-23-002	115-23-002-C04	16.20	210	20	18	12	6	1.5	M. Ross
115-23-002	115-23-002-C04	16.20	80	42	16	11	7	1.5	M. Ross
115-23-002	115-23-002-C04	16.20	106	34	30	19	10	1.6	M. Ross
115-23-002	115-23-002-C04	16.20	345	12	38	22	17	1.7	M. Ross
115-23-002	115-23-002-C04	16.20	22	3	42	25	15	1.7	M. Ross
115-23-002	115-23-002-C04	16.20	85	8	19	11	6	1.7	M. Ross
115-23-002	115-23-002-C04	16.20	86	18	14	10	7	1.4	M. Ross
115-23-002	115-23-002-C04	16.20	80	10	15	11	6	1.4	M. Ross
115-23-002	115-23-002-C04	16.20	215	14	25	16	6	1.6	M. Ross
115-23-002	115-23-002-C04	16.20	230	23	16	8	6	2.0	M. Ross
115-23-002	115-23-002-C04	16.20	145	15	40	24	13	1.7	M. Ross
115-23-002	115-23-002-C04	16.20	17	11	33	20	13	1.7	N. Mesich
115-23-002	115-23-002-C04	16.20	172	23	37	17	12	2.2	N. Mesich
115-23-002	115-23-002-C04	16.20	209	22	9	6	3	1.5	N. Mesich
115-23-002	115-23-002-C04	16.20	187	35	10	5	4	2.0	N. Mesich
115-23-002	115-23-002-C04	16.20	231	4	25	12	6	2.1	N. Mesich
115-23-002	115-23-002-C04	16.20	41	7	17	12	7	1.4	N. Mesich
115-23-002	115-23-002-C04	16.20	47	13	22	12	10	1.8	N. Mesich
115-23-002	115-23-002-C04	16.20	78	12	7	3	2	2.3	N. Mesich
115-23-002	115-23-002-C04	16.20	55	17	25	15	11	1.7	N. Mesich
115-23-002	115-23-002-C04	16.20	249	20	22	10	3	2.2	N. Mesich
115-23-002	115-23-002-C04	16.20	47	10	10	6	3	1.7	N. Mesich
115-23-002	115-23-002-C04	16.20	59	20	41	24	10	1.7	N. Mesich
115-23-002	115-23-002-C04	16.20	245	26	12	6	4	2.0	N. Mesich

115-23-002	115-23-002-C04	16.20	254	30	31	22	10	1.4	N. Mesich
115-23-002	115-23-002-C04	16.20	195	58	17	12	5	1.4	N. Mesich
115-23-002	115-23-002-C04	16.20	39	4	8	5	2	1.6	N. Mesich
115-23-002	115-23-002-C04	16.20	72	20	17	10	8	1.7	N. Mesich
115-23-002	115-23-002-C04	16.20	250	3	56	28	15	2.0	N. Mesich
115-23-002	115-23-002-C04	16.20	259	9	23	12	7	1.9	N. Mesich
115-23-002	115-23-002-C04	16.20	265	19	34	20	9	1.7	N. Mesich
115-23-002	115-23-002-D01	17.40	254	40	60	30	28	2.0	T. Hodder
115-23-002	115-23-002-D01	17.40	180	0	32	20	10	1.6	T. Hodder
115-23-002	115-23-002-D01	17.40	200	9	22	14	10	1.6	T. Hodder
115-23-002	115-23-002-D01	17.40	82	2	12	8	7	1.5	T. Hodder
115-23-002	115-23-002-D01	17.40	285	8	18	11	4	1.6	T. Hodder
115-23-002	115-23-002-D01	17.40	304	2	25	15	8	1.7	T. Hodder
115-23-002	115-23-002-D01	17.40	285	11	20	13	11	1.5	T. Hodder
115-23-002	115-23-002-D01	17.40	295	35	10	4	2	2.5	T. Hodder
115-23-002	115-23-002-D01	17.40	242	90	25	15	10	1.7	T. Hodder
115-23-002	115-23-002-D01	17.40	112	30	15	10	3	1.5	T. Hodder
115-23-002	115-23-002-D01	17.40	255	20	16	8	5	2.0	T. Hodder
115-23-002	115-23-002-D01	17.40	182	0	12	8	6	1.5	T. Hodder
115-23-002	115-23-002-D01	17.40	68	18	14	9	2	1.6	T. Hodder
115-23-002	115-23-002-D01	17.40	252	20	15	10	6	1.5	T. Hodder
115-23-002	115-23-002-D01	17.40	228	18	14	8	5	1.8	T. Hodder
115-23-002	115-23-002-D01	17.40	275	5	20	15	10	1.3	T. Hodder
115-23-002	115-23-002-D01	17.40	272	2	17	8	5	2.1	T. Hodder
115-23-002	115-23-002-D01	17.40	180	23	30	20	10	1.5	T. Hodder
115-23-002	115-23-002-D01	17.40	220	6	18	11	9	1.6	T. Hodder
115-23-002	115-23-002-D01	17.40	120	11	40	25	12	1.6	T. Hodder
115-23-002	115-23-002-D01	17.40	228	18	32	15	10	2.1	T. Hodder

115-23-002	115-23-002-D01	17.40	215	30	37	25	5	1.5	T. Hodder
115-23-002	115-23-002-D01	17.40	280	0	22	13	10	1.7	T. Hodder
115-23-002	115-23-002-D01	17.40	282	10	24	14	10	1.7	T. Hodder
115-23-002	115-23-002-D01	17.40	200	6	27	16	12	1.7	T. Hodder
115-23-002	115-23-002-D01	17.40	244	4	19	10	8	1.9	T. Hodder
115-23-002	115-23-002-D01	17.40	228	5	20	10	4	2.0	T. Hodder
115-23-002	115-23-002-D01	17.40	270	0	15	7	5	2.1	T. Hodder
115-23-002	115-23-002-D01	17.40	242	39	13	6	4	2.2	T. Hodder
115-23-002	115-23-002-D01	17.40	224	12	23	15	6	1.5	T. Hodder
115-23-002	115-23-002-D01	17.40	250	8	9	5	3	1.8	T. Hodder
115-23-002	115-23-002-D01	17.40	228	17	20	9	6	2.2	T. Hodder
115-23-002	115-23-002-D02	19.10	30	19	60	45	29	1.3	N. Mesich
115-23-002	115-23-002-D02	19.10	6	2	17	10	7	1.7	N. Mesich
115-23-002	115-23-002-D02	19.10	98	5	28	12	6	2.3	N. Mesich
115-23-002	115-23-002-D02	19.10	115	31	27	15	10	1.8	N. Mesich
115-23-002	115-23-002-D02	19.10	291	15	15	10	6	1.5	N. Mesich
115-23-002	115-23-002-D02	19.10	325	24	14	10	6	1.4	N. Mesich
115-23-002	115-23-002-D02	19.10	136	26	20	12	7	1.7	N. Mesich
115-23-002	115-23-002-D02	19.10	20	15	18	9	6	2.0	N. Mesich
115-23-002	115-23-002-D02	19.10	100	23	27	18	12	1.5	N. Mesich
115-23-002	115-23-002-D02	19.10	140	19	17	10	7	1.7	N. Mesich
115-23-002	115-23-002-D02	19.10	100	10	27	19	12	1.4	N. Mesich
115-23-002	115-23-002-D02	19.10	295	20	29	20	12	1.5	N. Mesich
115-23-002	115-23-002-D02	19.10	120	17	64	45	30	1.4	N. Mesich
115-23-002	115-23-002-D02	19.10	32	37	9	6	2	1.5	N. Mesich
115-23-002	115-23-002-D02	19.10	229	13	16	10	9	1.6	N. Mesich
115-23-002	115-23-002-D02	19.10	285	20	15	11	6	1.4	N. Mesich
115-23-002	115-23-002-D02	19.10	12	31	23	15	8	1.5	N. Mesich

115-23-002	115-23-002-D02	19.10	25	16	19	11	7	1.7	N. Mesich
115-23-002	115-23-002-D02	19.10	139	22	11	5	4	2.2	N. Mesich
115-23-002	115-23-002-D02	19.10	43	29	19	10	10	1.9	N. Mesich
115-23-002	115-23-002-D02	19.10	243	15	12	7	5	1.7	N. Mesich
115-23-002	115-23-002-D02	19.10	95	11	8	4	2	2.0	N. Mesich
115-23-002	115-23-002-D02	19.10	11	28	17	10	6	1.7	N. Mesich
115-23-002	115-23-002-D02	19.10	124	16	7	3	2	2.3	N. Mesich
115-23-002	115-23-002-D02	19.10	65	35	25	15	10	1.7	N. Mesich
115-23-002	115-23-002-D02	19.10	252	22	17	10	8	1.7	N. Mesich
115-23-002	115-23-002-D02	19.10	70	6	20	15	5	1.3	N. Mesich
115-23-002	115-23-002-D04	23.10	25	6	12	6	4	2.0	T. Hodder
115-23-002	115-23-002-D04	23.10	40	34	27	14	10	1.9	T. Hodder
115-23-002	115-23-002-D04	23.10	85	30	12	8	6	1.5	T. Hodder
115-23-002	115-23-002-D04	23.10	22	29	15	6	5	2.5	T. Hodder
115-23-002	115-23-002-D04	23.10	15	35	17	9	7	1.9	T. Hodder
115-23-002	115-23-002-D04	23.10	60	30	14	7	4	2.0	T. Hodder
115-23-002	115-23-002-D04	23.10	62	58	14	8	5	1.8	T. Hodder
115-23-002	115-23-002-D04	23.10	24	35	10	5	2	2.0	T. Hodder
115-23-002	115-23-002-D04	23.10	352	10	48	24	15	2.0	T. Hodder
115-23-002	115-23-002-D04	23.10	35	55	21	11	9	1.9	T. Hodder
115-23-002	115-23-002-D04	23.10	20	12	16	9	6	1.8	T. Hodder
115-23-002	115-23-002-D04	23.10	198	16	15	10	5	1.5	T. Hodder
115-23-002	115-23-002-D04	23.10	49	50	25	13	8	1.9	T. Hodder
115-23-002	115-23-002-D04	23.10	40	33	13	7	6	1.9	T. Hodder
115-23-002	115-23-002-D04	23.10	202	40	10	6	2	1.7	T. Hodder
115-23-002	115-23-002-D04	23.10	59	19	9	5	1	1.8	T. Hodder
115-23-002	115-23-002-D04	23.10	70	32	26	16	10	1.6	T. Hodder
115-23-002	115-23-002-D04	23.10	38	20	10	5	3	2.0	T. Hodder

115-23-002	115-23-002-D04	23.10	62	38	13	9	6	1.4	T. Hodder
115-23-002	115-23-002-D04	23.10	66	25	19	11	11	1.7	T. Hodder
115-23-002	115-23-002-D04	23.10	32	24	11	7	4	1.6	T. Hodder
115-23-002	115-23-002-D04	23.10	28	32	10	6	4	1.7	T. Hodder
115-23-002	115-23-002-D04	23.10	47	10	15	8	6	1.9	T. Hodder
115-23-002	115-23-002-D04	23.10	58	25	18	10	8	1.8	T. Hodder
115-23-002	115-23-002-D04	23.10	40	26	13	8	6	1.6	T. Hodder
115-23-002	115-23-002-D04	23.10	36	25	10	7	5	1.4	T. Hodder
115-23-002	115-23-002-D04	23.10	74	18	20	10	5	2.0	T. Hodder
115-23-002	115-23-002-D04	23.10	47	26	18	11	9	1.6	T. Hodder
115-23-002	115-23-002-D04	23.10	40	11	14	9	3	1.6	T. Hodder
115-23-002	115-23-002-D04	23.10	64	22	14	8	5	1.8	T. Hodder
115-23-003	115-23-003-A02	25.25	159	22	20	11	6	1.8	M. Gauthier
115-23-003	115-23-003-A02	25.25	108	24	22	14	8	1.6	M. Gauthier
115-23-003	115-23-003-A02	25.25	112	18	21	8	8	2.6	M. Gauthier
115-23-003	115-23-003-A02	25.25	146	8	9	6	3	1.5	M. Gauthier
115-23-003	115-23-003-A02	25.25	171	18	24	13	6	1.8	M. Gauthier
115-23-003	115-23-003-A02	25.25	348	2	70	31	24	2.3	M. Gauthier
115-23-003	115-23-003-A02	25.25	318	4	30	16	6	1.9	M. Gauthier
115-23-003	115-23-003-A02	25.25	126	4	18	10	6	1.8	M. Gauthier
115-23-003	115-23-003-A02	25.25	308	8	32	20	6	1.6	M. Gauthier
115-23-003	115-23-003-A02	25.25	114	10	24	8	6	3.0	M. Gauthier
115-23-003	115-23-003-A02	25.25	114	8	22	11	4	2.0	M. Gauthier
115-23-003	115-23-003-A02	25.25	342	14	12	6	4	2.0	M. Gauthier
115-23-003	115-23-003-A02	25.25	136	8	18	12	6	1.5	M. Gauthier
115-23-003	115-23-003-A02	25.25	327	8	15	10	6	1.5	M. Gauthier
115-23-003	115-23-003-A02	25.25	78	54	12	6	3	2.0	M. Gauthier
115-23-003	115-23-003-A02	25.25	115	8	22	9	6	2.4	M. Gauthier

115-23-003	115-23-003-A02	25.25	90	8	28	15	8	1.9	M. Gauthier
115-23-003	115-23-003-A02	25.25	164	12	15	12	7	1.3	M. Gauthier
115-23-003	115-23-003-A02	25.25	120	18	25	15	7	1.7	M. Gauthier
115-23-003	115-23-003-A02	25.25	116	16	17	7	3	2.4	M. Gauthier
115-23-003	115-23-003-A02	25.25	172	12	25	12	12	2.1	M. Gauthier
115-23-003	115-23-003-A02	25.25	168	24	30	12	4	2.5	M. Gauthier
115-23-003	115-23-003-A02	25.25	80	16	20	11	5	1.8	M. Gauthier
115-23-003	115-23-003-A02	25.25	128	38	21	12	7	1.8	M. Gauthier
115-23-003	115-23-003-A02	25.25	124	22	16	10	6	1.6	M. Gauthier
115-23-003	115-23-003-A02	25.25	348	20	22	14	7	1.6	M. Gauthier
115-23-003	115-23-003-A02	25.25	125	12	8	4	2	2.0	M. Gauthier
115-23-003	115-23-003-A02	25.25	309	16	36	20	17	1.8	M. Gauthier
115-23-003	115-23-003-A02	25.25	114	4	12	6	3	2.0	M. Gauthier
115-23-003	115-23-003-A02	25.25	162	20	15	7	6	2.1	M. Gauthier
115-23-003	115-23-003-A02	25.25	104	12	20	12	5	1.7	M. Gauthier
115-23-003	115-23-003-A02	25.25	155	20	16.5	11	4	1.5	M. Gauthier
115-23-003	115-23-003-B01	22.85	25	48	27	18	17	1.5	M. Ross
115-23-003	115-23-003-B01	22.85	242	4	26	21	16	1.2	M. Ross
115-23-003	115-23-003-B01	22.85	125	54	26	19	11	1.4	M. Ross
115-23-003	115-23-003-B01	22.85	135	9	30	24	19	1.3	M. Ross
115-23-003	115-23-003-B01	22.85	102	29	20	13	9	1.5	M. Ross
115-23-003	115-23-003-B01	22.85	160	19	28	16	14	1.8	M. Ross
115-23-003	115-23-003-B01	22.85	144	14	10	5	4	2.0	M. Ross
115-23-003	115-23-003-B01	22.85	150	6	21	11	9	1.9	M. Ross
115-23-003	115-23-003-B01	22.85	165	38	22	12	8	1.8	M. Ross
115-23-003	115-23-003-B01	22.85	312	5	28	20	12	1.4	M. Ross
115-23-003	115-23-003-B01	22.85	136	9	12	8	5	1.5	M. Ross
115-23-003	115-23-003-B01	22.85	72	19	23	8	6	2.9	M. Ross

115-23-003	115-23-003-B01	22.85	89	29	11	7	3	1.6	M. Ross
115-23-003	115-23-003-B01	22.85	145	17	10	6	4	1.7	M. Ross
115-23-003	115-23-003-B01	22.85	164	16	8	5	4	1.6	M. Ross
115-23-003	115-23-003-B01	22.85	149	17	19	12	7	1.6	M. Ross
115-23-003	115-23-003-B01	22.85	222	31	18	13	10	1.4	M. Ross
115-23-003	115-23-003-B01	22.85	88	14	15	11	5	1.4	M. Ross
115-23-003	115-23-003-B01	22.85	62	11	15	9	7	1.7	M. Ross
115-23-003	115-23-003-B01	22.85	206	10	17	11	10	1.5	M. Ross
115-23-003	115-23-003-B01	22.85	20	18	17	10	7	1.7	M. Ross
115-23-003	115-23-003-B01	22.85	132	24	29	23	10	1.3	M. Ross
115-23-003	115-23-003-B01	22.85	157	29	11	7	5	1.6	M. Ross
115-23-003	115-23-003-B01	22.85	166	27	12	7	6	1.7	M. Ross
115-23-003	115-23-003-B01	22.85	143	40	19	9	7	2.1	M. Ross
115-23-003	115-23-003-B01	22.85	132	28	20	14	6	1.4	M. Ross
115-23-003	115-23-003-B01	22.85	137	11	15	10	7	1.5	M. Ross
115-23-003	115-23-003-B01	22.85	300	2	15	12	6	1.3	M. Ross
115-23-003	115-23-003-B01	22.85	88	8	9	6	4	1.5	M. Ross
115-23-003	115-23-003-B01	22.85	134	2	17	11	7	1.5	M. Ross
115-23-003	115-23-003-B01	22.85	138	31	9	6	3	1.5	M. Ross
115-23-003	115-23-003-B01	22.85	260	32	16	11	10	1.5	M. Ross
115-23-003	115-23-003-B01	22.85	144	28	29	21	14	1.4	M. Ross
115-23-003	115-23-003-B01	22.85	128	11	16	13	10	1.2	M. Ross
115-23-003	115-23-003-B02	19.85	128	4	12	6	4	2.0	M. Gauthier
115-23-003	115-23-003-B02	19.85	266	20	12	8	4	1.5	M. Gauthier
115-23-003	115-23-003-B02	19.85	58	18	13	8	3	1.6	M. Gauthier
115-23-003	115-23-003-B02	19.85	90	12	9	5	5	1.8	M. Gauthier
115-23-003	115-23-003-B02	19.85	94	4	12	8	5	1.5	M. Gauthier
115-23-003	115-23-003-B02	19.85	108	4	14	8	3	1.8	M. Gauthier

115-23-003	115-23-003-B02	19.85	89	6	12	6	4	2.0	M. Gauthier
115-23-003	115-23-003-B02	19.85	132	22	9	4	3	2.3	M. Gauthier
115-23-003	115-23-003-B02	19.85	84	14	17	8	6	2.1	M. Gauthier
115-23-003	115-23-003-B02	19.85	108	6	18	10	6	1.8	M. Gauthier
115-23-003	115-23-003-B02	19.85	345	8	22	12	8	1.8	M. Gauthier
115-23-003	115-23-003-B02	19.85	106	4	17	7	6	2.4	M. Gauthier
115-23-003	115-23-003-B02	19.85	102	12	14	7	4	2.0	M. Gauthier
115-23-003	115-23-003-B02	19.85	152	10	24	12	8	2.0	M. Gauthier
115-23-003	115-23-003-B02	19.85	130	8	14	9	5	1.6	M. Gauthier
115-23-003	115-23-003-B02	19.85	164	24	16	10	6	1.6	M. Gauthier
115-23-003	115-23-003-B02	19.85	264	24	19	5	3	3.8	M. Gauthier
115-23-003	115-23-003-B02	19.85	262	45	12	7	2	1.7	M. Gauthier
115-23-003	115-23-003-B02	19.85	252	22	25	12	12	2.1	M. Gauthier
115-23-003	115-23-003-B02	19.85	110	10	13	8	5	1.6	M. Gauthier
115-23-003	115-23-003-B02	19.85	112	16	16	4	4	4.0	M. Gauthier
115-23-003	115-23-003-B02	19.85	290	20	15	8	7	1.9	M. Gauthier
115-23-003	115-23-003-B02	19.85	208	14	12	7	6	1.7	M. Gauthier
115-23-003	115-23-003-B02	19.85	90	4	8	4	2	2.0	M. Gauthier
115-23-003	115-23-003-B02	19.85	100	24	12	8	8	1.5	M. Gauthier
115-23-003	115-23-003-B02	19.85	76	8	16	10	6	1.6	M. Gauthier
115-23-003	115-23-003-B02	19.85	265	8	17	9	9	1.9	M. Gauthier
115-23-003	115-23-003-B02	19.85	96	12	6	4	2	1.5	M. Gauthier
115-23-003	115-23-003-D01	14.85	41	13	14	8	7	1.8	N. Mesich
115-23-003	115-23-003-D01	14.85	296	35	23	14	10	1.6	N. Mesich
115-23-003	115-23-003-D01	14.85	89	14	19	12	7	1.6	N. Mesich
115-23-003	115-23-003-D01	14.85	114	16	26	14	10	1.9	N. Mesich
115-23-003	115-23-003-D01	14.85	284	5	21	14	6	1.5	N. Mesich
115-23-003	115-23-003-D01	14.85	236	10	28	18	10	1.6	N. Mesich

115-23-003	115-23-003-D01	14.85	238	0	10	6	2	1.7	N. Mesich
115-23-003	115-23-003-D01	14.85	312	17	13	6	3	2.2	N. Mesich
115-23-003	115-23-003-D01	14.85	217	31	19	12	6	1.6	N. Mesich
115-23-003	115-23-003-D01	14.85	205	25	12	8	5	1.5	N. Mesich
115-23-003	115-23-003-D01	14.85	26	3	13	9	6	1.4	N. Mesich
115-23-003	115-23-003-D01	14.85	23	14	10	6	3	1.7	N. Mesich
115-23-003	115-23-003-D01	14.85	315	34	32	20	10	1.6	N. Mesich
115-23-003	115-23-003-D01	14.85	107	9	10	6	4	1.7	N. Mesich
115-23-003	115-23-003-D01	14.85	120	15	17	11	6	1.5	N. Mesich
115-23-003	115-23-003-D01	14.85	30	49	14	9	4	1.6	N. Mesich
115-23-003	115-23-003-D01	14.85	322	14	10	6	4	1.7	N. Mesich
115-23-003	115-23-003-D01	14.85	182	22	9	5	2	1.8	N. Mesich
115-23-003	115-23-003-D01	14.85	15	14	8	5	3	1.6	N. Mesich
115-23-003	115-23-003-D01	14.85	202	25	12	7	2	1.7	N. Mesich
115-23-003	115-23-003-D01	14.85	76	11	9	6	4	1.5	N. Mesich
115-23-003	115-23-003-D01	14.85	353	21	16	5	5	3.2	N. Mesich
115-23-003	115-23-003-D01	14.85	248	1	18	12	7	1.5	N. Mesich
115-23-003	115-23-003-D01	14.85	311	20	10	7	4	1.4	N. Mesich
115-23-003	115-23-003-D01	14.85	301	21	12	5	2	2.4	N. Mesich
115-23-003	115-23-003-D01	14.85	47	30	20	8	4	2.5	N. Mesich
115-23-003	115-23-003-D01	14.85	18	11	13	8	6	1.6	N. Mesich
115-23-003	115-23-003-D01	14.85	25	20	12	8	5	1.5	N. Mesich
115-23-003	115-23-003-D01	14.85	326	27	17	9	6	1.9	N. Mesich
115-23-003	115-23-003-L01	3.30	84	16	21	14	9	1.5	M. Gauthier
115-23-003	115-23-003-L01	3.30	85	10	17	10	6	1.7	M. Gauthier
115-23-003	115-23-003-L01	3.30	235	4	16	11	4	1.5	M. Gauthier
115-23-003	115-23-003-L01	3.30	235	8	16	10	5	1.6	M. Gauthier
115-23-003	115-23-003-L01	3.30	104	2	17	11	5	1.5	M. Gauthier

115-23-003	115-23-003-L01	3.30	90	20	11	6	6	1.8	M. Gauthier
115-23-003	115-23-003-L01	3.30	70	14	27	15	9	1.8	M. Gauthier
115-23-003	115-23-003-L01	3.30	70	8	15	10	5	1.5	M. Gauthier
115-23-003	115-23-003-L01	3.30	88	2	24	11	11	2.2	M. Gauthier
115-23-003	115-23-003-L01	3.30	52	4	15	8	4	1.9	M. Gauthier
115-23-003	115-23-003-L01	3.30	88	4	18	11	4	1.6	M. Gauthier
115-23-003	115-23-003-L01	3.30	316	6	9	5	5	1.8	M. Gauthier
115-23-003	115-23-003-L01	3.30	60	6	17	9	5	1.9	M. Gauthier
115-23-003	115-23-003-L01	3.30	84	20	18	10	5	1.8	M. Gauthier
115-23-003	115-23-003-L01	3.30	72	20	16	8	5	2.0	M. Gauthier
115-23-003	115-23-003-L01	3.30	230	4	18	7	5	2.6	M. Gauthier
115-23-003	115-23-003-L01	3.30	230	24	11	7	3	1.6	M. Gauthier
115-23-003	115-23-003-L01	3.30	228	40	34	19	14	1.8	M. Gauthier
115-23-003	115-23-003-L01	3.30	70	6	24	14	5	1.7	M. Gauthier
115-23-003	115-23-003-L01	3.30	88	16	28	16	11	1.8	M. Gauthier
115-23-003	115-23-003-L01	3.30	50	12	22	12	8	1.8	M. Gauthier
115-23-003	115-23-003-L01	3.30	56	40	18	5	2	3.6	M. Gauthier
115-23-003	115-23-003-L01	3.30	74	18	14	12	6	1.2	M. Gauthier
115-23-003	115-23-003-L01	3.30	252	28	34	20	10	1.7	M. Gauthier
115-23-003	115-23-003-L01	3.30	56	22	9	5	1	1.8	M. Gauthier
115-23-003	115-23-003-L01	3.30	240	24	15	10	5	1.5	M. Gauthier
115-23-003	115-23-003-L01	3.30	210	50	10	5	1	2.0	M. Gauthier
115-23-003	115-23-003-L01	3.30	85	4	17	8	2	2.1	M. Gauthier
115-23-003	115-23-003-L01	3.30	95	10	18	8	5	2.3	M. Gauthier
115-23-003	115-23-003-L01	3.30	62	2	23	12	4	1.9	M. Gauthier
115-23-004	115-23-004-B01	25.30	26	20	131	92	45	1.4	N. Mesich
115-23-004	115-23-004-B01	25.30	15	11	10	6	4	1.7	N. Mesich
115-23-004	115-23-004-B01	25.30	192	21	12	8	5	1.5	N. Mesich

115-23-004	115-23-004-B01	25.30	248	4	12	5	4	2.4	N. Mesich
115-23-004	115-23-004-B01	25.30	356	47	6	4	2	1.5	N. Mesich
115-23-004	115-23-004-B01	25.30	153	25	9	6	4	1.5	N. Mesich
115-23-004	115-23-004-B01	25.30	46	47	26	20	10	1.3	N. Mesich
115-23-004	115-23-004-B01	25.30	12	20	62	30	17	2.1	N. Mesich
115-23-004	115-23-004-B01	25.30	25	6	36	21	15	1.7	N. Mesich
115-23-004	115-23-004-B01	25.30	112	3	12	8	4	1.5	N. Mesich
115-23-004	115-23-004-B01	25.30	179	33	9	6	4	1.5	N. Mesich
115-23-004	115-23-004-B01	25.30	255	9	16	12	5	1.3	N. Mesich
115-23-004	115-23-004-B01	25.30	336	22	19	13	7	1.5	N. Mesich
115-23-004	115-23-004-B01	25.30	32	0	21	15	7	1.4	N. Mesich
115-23-004	115-23-004-B01	25.30	169	22	35	21	17	1.7	N. Mesich
115-23-004	115-23-004-B01	25.30	346	26	17	11	6	1.5	N. Mesich
115-23-004	115-23-004-B01	25.30	213	6	10	7	4	1.4	N. Mesich
115-23-004	115-23-004-B01	25.30	216	3	35	26	16	1.3	N. Mesich
115-23-004	115-23-004-B01	25.30	314	10	12	8	5	1.5	N. Mesich
115-23-004	115-23-004-B01	25.30	98	5	11	7	3	1.6	N. Mesich
115-23-004	115-23-004-B01	25.30	34	45	29	18	15	1.6	N. Mesich
115-23-004	115-23-004-B01	25.30	264	5	13	9	6	1.4	N. Mesich
115-23-004	115-23-004-B01	25.30	10	3	57	40	17	1.4	N. Mesich
115-23-004	115-23-004-B01	25.30	50	5	18	12	6	1.5	N. Mesich
115-23-004	115-23-004-B01	25.30	355	34	23	11	8	2.1	N. Mesich
115-23-004	115-23-004-B01	25.30	356	29	17	11	6	1.5	N. Mesich
115-23-004	115-23-004-B01	25.30	347	28	16	11	7	1.5	N. Mesich
115-23-004	115-23-004-B01	25.30	5	21	32	14	9	2.3	N. Mesich
115-23-004	115-23-004-B01	25.30	4	29	17	11	8	1.5	N. Mesich
115-23-005	115-23-005-B01	3.60	310	14	14	6	4	2.3	J. Hathaway
115-23-005	115-23-005-B01	3.60	342	20	15	7	6	2.1	J. Hathaway

115-23-005	115-23-005-B01	3.60	0	20	13	7	5	1.9	J. Hathaway
115-23-005	115-23-005-B01	3.60	38	10	15	7	4	2.1	J. Hathaway
115-23-005	115-23-005-B01	3.60	90	0	18	7	4	2.6	J. Hathaway
115-23-005	115-23-005-B01	3.60	234	10	12	6	5	2.0	J. Hathaway
115-23-005	115-23-005-B01	3.60	250	2	20	10	8	2.0	J. Hathaway
115-23-005	115-23-005-B01	3.60	330	11	10	5	4	2.0	J. Hathaway
115-23-005	115-23-005-B01	3.60	300	4	20	10	2	2.0	J. Hathaway
115-23-005	115-23-005-B01	3.60	328	18	12	7	5	1.7	J. Hathaway
115-23-005	115-23-005-B01	3.60	298	22	16	6	4	2.7	J. Hathaway
115-23-005	115-23-005-B01	3.60	320	60	17	9	6	1.9	J. Hathaway
115-23-005	115-23-005-B01	3.60	2	15	12	6	4	2.0	J. Hathaway
115-23-005	115-23-005-B01	3.60	290	2	20	12	6	1.7	J. Hathaway
115-23-005	115-23-005-B01	3.60	240	10	10	6	2	1.7	J. Hathaway
115-23-005	115-23-005-B01	3.60	304	60	22	13	8	1.7	J. Hathaway
115-23-005	115-23-005-B01	3.60	20	2	17	8	4	2.1	J. Hathaway
115-23-005	115-23-005-B01	3.60	292	18	10	5	4	2.0	J. Hathaway
115-23-005	115-23-005-B01	3.60	348	17	10	6	3	1.7	J. Hathaway
115-23-005	115-23-005-B01	3.60	45	2	10	6	4	1.7	J. Hathaway
115-23-005	115-23-005-B01	3.60	340	1	18	10	7	1.8	J. Hathaway
115-23-005	115-23-005-B01	3.60	88	20	17	9	7	1.9	J. Hathaway
115-23-005	115-23-005-B01	3.60	18	4	13	8	5	1.6	J. Hathaway
115-23-005	115-23-005-B01	3.60	312	12	24	13	9	1.8	J. Hathaway
115-23-005	115-23-005-B01	3.60	60	10	13	7	4	1.9	J. Hathaway
115-23-005	115-23-005-B01	3.60	318	32	32	20	12	1.6	J. Hathaway
115-23-005	115-23-005-B01	3.60	351	25	9	6	2	1.5	J. Hathaway
115-23-005	115-23-005-B01	3.60	298	18	16	10	7	1.6	J. Hathaway
115-23-005	115-23-005-B01	3.60	319	22	11	6	5	1.8	J. Hathaway
115-23-005	115-23-005-B01	3.60	327	34	23	15	8	1.5	J. Hathaway

115-23-005	115-23-005-B01	3.60	306	20	12	9	3	1.3	J. Hathaway
115-23-005	115-23-005-B01	3.60	306	2	16	9	4	1.8	J. Hathaway
115-23-005	115-23-005-B01	3.60	328	10	12	8	6	1.5	J. Hathaway
115-23-005	115-23-005-B04	9.10	42	17	12	6	2	2.0	N. Mesich
115-23-005	115-23-005-B04	9.10	26	12	11	7	4	1.6	N. Mesich
115-23-005	115-23-005-B04	9.10	211	3	15	10	4	1.5	N. Mesich
115-23-005	115-23-005-B04	9.10	25	22	8	5	3	1.6	N. Mesich
115-23-005	115-23-005-B04	9.10	192	10	9	6	3	1.5	N. Mesich
115-23-005	115-23-005-B04	9.10	188	11	14	10	6	1.4	N. Mesich
115-23-005	115-23-005-B04	9.10	31	36	11	7	3	1.6	N. Mesich
115-23-005	115-23-005-B04	9.10	1	14	12	8	4	1.5	N. Mesich
115-23-005	115-23-005-B04	9.10	6	14	16	10	4	1.6	N. Mesich
115-23-005	115-23-005-B04	9.10	194	19	14	9	5	1.6	N. Mesich
115-23-005	115-23-005-B04	9.10	203	10	11	7	4	1.6	N. Mesich
115-23-005	115-23-005-B04	9.10	15	23	11	8	5	1.4	N. Mesich
115-23-005	115-23-005-B04	9.10	34	17	17	12	7	1.4	N. Mesich
115-23-005	115-23-005-B04	9.10	204	8	17	11	6	1.5	N. Mesich
115-23-005	115-23-005-B04	9.10	218	5	15	9	3	1.7	N. Mesich
115-23-005	115-23-005-B04	9.10	339	11	30	15	10	2.0	N. Mesich
115-23-005	115-23-005-B04	9.10	225	17	15	11	11	1.4	N. Mesich
115-23-005	115-23-005-B04	9.10	9	23	12	7	5	1.7	N. Mesich
115-23-005	115-23-005-B04	9.10	6	20	21	15	9	1.4	N. Mesich
115-23-005	115-23-005-B04	9.10	11	26	17	10	8	1.7	N. Mesich
115-23-005	115-23-005-B04	9.10	0	20	13	7	3	1.9	N. Mesich
115-23-005	115-23-005-B04	9.10	32	11	10	5	2	2.0	N. Mesich
115-23-005	115-23-005-B04	9.10	35	25	28	16	12	1.8	N. Mesich
115-23-005	115-23-005-B04	9.10	45	27	22	16	9	1.4	N. Mesich
115-23-005	115-23-005-B04	9.10	29	19	14	7	5	2.0	N. Mesich

115-23-005	115-23-005-B04	9.10	42	18	8	4	2	2.0	N. Mesich
115-23-005	115-23-005-Z01	13.30	2	8	14	6	4	2.3	M. Gauthier
115-23-005	115-23-005-Z01	13.30	348	2	10	6	2	1.7	M. Gauthier
115-23-005	115-23-005-Z01	13.30	194	22	12	5	2	2.4	M. Gauthier
115-23-005	115-23-005-Z01	13.30	188	2	21	12	7	1.8	M. Gauthier
115-23-005	115-23-005-Z01	13.30	6	12	16	7	3	2.3	M. Gauthier
115-23-005	115-23-005-Z01	13.30	356	24	8	5	2	1.6	M. Gauthier
115-23-005	115-23-005-Z01	13.30	355	55	12	6	3	2.0	M. Gauthier
115-23-005	115-23-005-Z01	13.30	16	30	13	4	4	3.3	M. Gauthier
115-23-005	115-23-005-Z01	13.30	2	4	8	4	2	2.0	M. Gauthier
115-23-005	115-23-005-Z01	13.30	166	32	8	5	3	1.6	M. Gauthier
115-23-005	115-23-005-Z01	13.30	309	22	8	5	4	1.6	M. Gauthier
115-23-005	115-23-005-Z01	13.30	178	2	20	12	12	1.7	M. Gauthier
115-23-005	115-23-005-Z01	13.30	358	9	12	6	5	2.0	M. Gauthier
115-23-005	115-23-005-Z01	13.30	190	32	12	7	6	1.7	M. Gauthier
115-23-005	115-23-005-Z01	13.30	0	16	16	8	5	2.0	M. Gauthier
115-23-005	115-23-005-Z01	13.30	34	46	11	6	4	1.8	M. Gauthier
115-23-005	115-23-005-Z01	13.30	330	16	38	20	12	1.9	M. Gauthier
115-23-005	115-23-005-Z01	13.30	138	40	12	8	6	1.5	M. Gauthier
115-23-005	115-23-005-Z01	13.30	140	8	11	5	3	2.2	M. Gauthier
115-23-005	115-23-005-Z01	13.30	359	6	7	4	4	1.8	M. Gauthier
115-23-005	115-23-005-Z01	13.30	360	4	8	4	2	2.0	M. Gauthier
115-23-005	115-23-005-Z01	13.30	6	38	18	9	6	2.0	M. Gauthier
115-23-005	115-23-005-Z01	13.30	112	11	9	5	3	1.8	M. Gauthier
115-23-005	115-23-005-Z01	13.30	8	14	21	15	7	1.4	M. Gauthier
115-23-005	115-23-005-Z01	13.30	310	12	12	7	7	1.7	M. Gauthier
115-23-005	115-23-005-Z01	13.30	38	18	25	12	11	2.1	M. Gauthier
115-23-005	115-23-005-Z01	13.30	128	5	22	9	9	2.4	M. Gauthier

115-23-005	115-23-005-Z01	13.30	2	22	16	10	6	1.6	M. Gauthier
115-23-005	115-23-005-Z01	13.30	132	8	11	6	3	1.8	M. Gauthier
115-23-005	115-23-005-Z01	13.30	322	14	14	9	3	1.6	M. Gauthier
115-23-005	115-23-005-Z01	13.30	145	15	14	8	5	1.8	M. Gauthier
115-23-005	115-23-005-Z01	13.30	145	14	37	18	10	2.1	M. Gauthier
115-23-005	115-23-005-T01	17.50	107	20	20	11	6	1.8	T. Hodder
115-23-005	115-23-005-T01	17.50	110	14	24	16	10	1.5	T. Hodder
115-23-005	115-23-005-T01	17.50	85	27	16	10	8	1.6	T. Hodder
115-23-005	115-23-005-T01	17.50	277	2	25	15	3	1.7	T. Hodder
115-23-005	115-23-005-T01	17.50	110	20	11	5	3	2.2	T. Hodder
115-23-005	115-23-005-T01	17.50	299	16	14	9	2	1.6	T. Hodder
115-23-005	115-23-005-T01	17.50	125	4	11	6	4	1.8	T. Hodder
115-23-005	115-23-005-T01	17.50	312	28	10	4	2	2.5	T. Hodder
115-23-005	115-23-005-T01	17.50	90	25	13	7	4	1.9	T. Hodder
115-23-005	115-23-005-T01	17.50	295	30	12	8	5	1.5	T. Hodder
115-23-005	115-23-005-T01	17.50	277	23	19	12	8	1.6	T. Hodder
115-23-005	115-23-005-T01	17.50	278	11	15	8	5	1.9	T. Hodder
115-23-005	115-23-005-T01	17.50	92	36	13	8	4	1.6	T. Hodder
115-23-005	115-23-005-T01	17.50	292	24	15	9	5	1.7	T. Hodder
115-23-005	115-23-005-T01	17.50	324	9	15	9	7	1.7	T. Hodder
115-23-005	115-23-005-T01	17.50	175	18	28	13	5	2.2	T. Hodder
115-23-005	115-23-005-T01	17.50	322	10	18	11	3	1.6	T. Hodder
115-23-005	115-23-005-T01	17.50	332	11	18	10	5	1.8	T. Hodder
115-23-005	115-23-005-T01	17.50	325	16	25	11	5	2.3	T. Hodder
115-23-005	115-23-005-T01	17.50	270	22	11	6	4	1.8	T. Hodder
115-23-005	115-23-005-T01	17.50	158	7	15	10	2	1.5	T. Hodder
115-23-005	115-23-005-T01	17.50	335	15	17	9	5	1.9	T. Hodder
115-23-005	115-23-005-T01	17.50	314	10	14	8	5	1.8	T. Hodder

115-23-005	115-23-005-T01	17.50	317	69	6	4	2	1.5	T. Hodder
115-23-005	115-23-005-T01	17.50	326	33	13	8	2	1.6	T. Hodder
115-23-005	115-23-005-T01	17.50	297	25	15	10	3	1.5	T. Hodder
115-23-005	115-23-005-T01	17.50	312	14	17	10	5	1.7	T. Hodder
115-23-005	115-23-005-T01	17.50	295	42	8	5	3	1.6	T. Hodder
115-23-005	115-23-005-O01	15.05	346	2	16	8	5	2.0	M. Gauthier
115-23-005	115-23-005-O01	15.05	4	4	9	6	4	1.5	M. Gauthier
115-23-005	115-23-005-O01	15.05	142	4	10	5	3	2.0	M. Gauthier
115-23-005	115-23-005-O01	15.05	342	20	44	25	15	1.8	M. Gauthier
115-23-005	115-23-005-O01	15.05	230	20	43	25	20	1.7	M. Gauthier
115-23-005	115-23-005-O01	15.05	96	16	17	8	6	2.1	M. Gauthier
115-23-005	115-23-005-O01	15.05	292	4	13	8	3	1.6	M. Gauthier
115-23-005	115-23-005-O01	15.05	115	8	12	6	4	2.0	M. Gauthier
115-23-005	115-23-005-O01	15.05	118	6	50	32	30	1.6	M. Gauthier
115-23-005	115-23-005-O01	15.05	230	26	22	12	5	1.8	M. Gauthier
115-23-005	115-23-005-O01	15.05	276	8	32	15	10	2.1	M. Gauthier
115-23-005	115-23-005-O01	15.05	294	14	9	5	2	1.8	M. Gauthier
115-23-005	115-23-005-O01	15.05	158	2	11	3	2	3.7	M. Gauthier
115-23-005	115-23-005-O01	15.05	145	6	11	3	1	3.7	M. Gauthier
115-23-005	115-23-005-O01	15.05	75	24	17	8	4	2.1	M. Gauthier
115-23-005	115-23-005-O01	15.05	124	22	16	9	4	1.8	M. Gauthier
115-23-005	115-23-005-O01	15.05	32	6	135	65	27	2.1	M. Gauthier
115-23-005	115-23-005-O01	15.05	136	14	43	15	13	2.9	M. Gauthier
115-23-005	115-23-005-O01	15.05	134	22	15	10	6	1.5	M. Gauthier
115-23-005	115-23-005-O01	15.05	114	24	16	8	4	2.0	M. Gauthier
115-23-005	115-23-005-O01	15.05	168	30	13	8	3	1.6	M. Gauthier
115-23-005	115-23-005-O01	15.05	125	16	12	7	4	1.7	M. Gauthier
115-23-005	115-23-005-O01	15.05	146	15	18	8	5	2.3	M. Gauthier

115-23-005	115-23-005-O01	15.05	178	8	15	8	6	1.9	M. Gauthier
115-23-005	115-23-005-O01	15.05	326	6	19	9	7	2.1	M. Gauthier
115-23-005	115-23-005-O01	15.05	194	22	16	8	4	2.0	M. Gauthier
115-23-005	115-23-005-O01	15.05	105	20	55	32	12	1.7	M. Gauthier
115-23-005	115-23-005-O01	15.05	172	20	21	12	7	1.8	M. Gauthier
115-23-005	115-23-005-O01	15.05	140	12	15	6	5	2.5	M. Gauthier
115-23-005	115-23-005-O01	15.05	104	14	31	15	12	2.1	M. Gauthier
115-23-005	115-23-005-O01	15.05	170	24	25	11	6	2.3	M. Gauthier
115-23-005	115-23-005-O01	15.05	290	6	30	11	6	2.7	M. Gauthier
115-23-006	115-23-006-A01	4.75	165	8	41	15	15	2.7	M. Gauthier
115-23-006	115-23-006-A01	4.75	6	14	38	22	12	1.7	M. Gauthier
115-23-006	115-23-006-A01	4.75	350	14	20	12	9	1.7	M. Gauthier
115-23-006	115-23-006-A01	4.75	194	24	15	10	4	1.5	M. Gauthier
115-23-006	115-23-006-A01	4.75	218	14	54	25	20	2.2	M. Gauthier
115-23-006	115-23-006-A01	4.75	176	32	13	8	4	1.6	M. Gauthier
115-23-006	115-23-006-A01	4.75	158	6	30	16	12	1.9	M. Gauthier
115-23-006	115-23-006-A01	4.75	170	12	23	12	7	1.9	M. Gauthier
115-23-006	115-23-006-A01	4.75	198	2	22	12	6	1.8	M. Gauthier
115-23-006	115-23-006-A01	4.75	218	4	24	13	13	1.8	M. Gauthier
115-23-006	115-23-006-A01	4.75	175	8	33	20	15	1.7	M. Gauthier
115-23-006	115-23-006-A01	4.75	342	4	10	6	4	1.7	M. Gauthier
115-23-006	115-23-006-A01	4.75	164	6	18	12	6	1.5	M. Gauthier
115-23-006	115-23-006-A01	4.75	178	6	28	15	10	1.9	M. Gauthier
115-23-006	115-23-006-A01	4.75	202	4	11	6	4	1.8	M. Gauthier
115-23-006	115-23-006-A01	4.75	168	4	16	8	6	2.0	M. Gauthier
115-23-006	115-23-006-A01	4.75	198	4	26	12	12	2.2	M. Gauthier
115-23-006	115-23-006-A01	4.75	162	2	21	11	8	1.9	M. Gauthier
115-23-006	115-23-006-A01	4.75	184	8	26	12	12	2.2	M. Gauthier

115-23-006	115-23-006-A01	4.75	218	4	24	12	11	2.0	M. Gauthier
115-23-006	115-23-006-A01	4.75	352	8	23	13	9	1.8	M. Gauthier
115-23-006	115-23-006-A01	4.75	326	6	15	10	2	1.5	M. Gauthier
115-23-006	115-23-006-A01	4.75	158	8	16	8	8	2.0	M. Gauthier
115-23-006	115-23-006-A01	4.75	188	6	25	14	7	1.8	M. Gauthier
115-23-006	115-23-006-A01	4.75	356	8	16	9	5	1.8	M. Gauthier
115-23-006	115-23-006-A01	4.75	26	4	35	16	10	2.2	M. Gauthier
115-23-006	115-23-006-A01	4.75	200	10	38	16	10	2.4	M. Gauthier
115-23-006	115-23-006-A01	4.75	185	10	15	10	4	1.5	M. Gauthier
115-23-006	115-23-006-B01	5.25	130	17	104	62	34	1.7	N. Mesich
115-23-006	115-23-006-B01	5.25	213	38	64	42	20	1.5	N. Mesich
115-23-006	115-23-006-B01	5.25	44	34	18	12	7	1.5	N. Mesich
115-23-006	115-23-006-B01	5.25	37	10	10	7	3	1.4	N. Mesich
115-23-006	115-23-006-B01	5.25	63	19	10	6	4	1.7	N. Mesich
115-23-006	115-23-006-B01	5.25	225	4	14	9	4	1.6	N. Mesich
115-23-006	115-23-006-B01	5.25	15	21	15	10	5	1.5	N. Mesich
115-23-006	115-23-006-B01	5.25	220	19	19	12	6	1.6	N. Mesich
115-23-006	115-23-006-B01	5.25	54	5	11	7	3	1.6	N. Mesich
115-23-006	115-23-006-B01	5.25	52	7	9	5	3	1.8	N. Mesich
115-23-006	115-23-006-B01	5.25	25	16	18	10	7	1.8	N. Mesich
115-23-006	115-23-006-B01	5.25	163	36	22	15	6	1.5	N. Mesich
115-23-006	115-23-006-B01	5.25	205	24	11	7	4	1.6	N. Mesich
115-23-006	115-23-006-B01	5.25	222	20	17	11	6	1.5	N. Mesich
115-23-006	115-23-006-B01	5.25	201	3	21	12	10	1.8	N. Mesich
115-23-006	115-23-006-B01	5.25	61	13	14	8	3	1.8	N. Mesich
115-23-006	115-23-006-B01	5.25	72	11	20	14	7	1.4	N. Mesich
115-23-006	115-23-006-B01	5.25	25	4	21	15	6	1.4	N. Mesich
115-23-006	115-23-006-B01	5.25	209	24	15	10	6	1.5	N. Mesich

115-23-006	115-23-006-B01	5.25	240	9	22	16	7	1.4	N. Mesich
115-23-006	115-23-006-B01	5.25	10	10	25	14	8	1.8	N. Mesich
115-23-006	115-23-006-B01	5.25	268	14	16	10	4	1.6	N. Mesich
115-23-006	115-23-006-B01	5.25	217	21	37	25	15	1.5	N. Mesich
115-23-006	115-23-006-B01	5.25	197	34	12	7	3	1.7	N. Mesich
115-23-006	115-23-006-B01	5.25	212	11	18	12	6	1.5	N. Mesich
115-23-006	115-23-006-B01	5.25	197	12	21	13	9	1.6	N. Mesich
115-23-006	115-23-006-B01	5.25	225	17	9	6	3	1.5	N. Mesich
115-23-006	115-23-006-C01	8.45	128	14	8	4	1	2.0	M. Gauthier
115-23-006	115-23-006-C01	8.45	140	12	8	5	2	1.6	M. Gauthier
115-23-006	115-23-006-C01	8.45	140	16	18	11	5	1.6	M. Gauthier
115-23-006	115-23-006-C01	8.45	274	2	9	6	3	1.5	M. Gauthier
115-23-006	115-23-006-C01	8.45	172	16	12	7	4	1.7	M. Gauthier
115-23-006	115-23-006-C01	8.45	142	24	8	5	2	1.6	M. Gauthier
115-23-006	115-23-006-C01	8.45	322	10	35	17	17	2.1	M. Gauthier
115-23-006	115-23-006-C01	8.45	270	20	38	16	4	2.4	M. Gauthier
115-23-006	115-23-006-C01	8.45	264	26	22	12	12	1.8	M. Gauthier
115-23-006	115-23-006-C01	8.45	115	14	12	7	4	1.7	M. Gauthier
115-23-006	115-23-006-C01	8.45	88	4	17	7	5	2.4	M. Gauthier
115-23-006	115-23-006-C01	8.45	330	22	10	6	3	1.7	M. Gauthier
115-23-006	115-23-006-C01	8.45	144	4	6	2	2	3.0	M. Gauthier
115-23-006	115-23-006-C01	8.45	50	2	11	7	2	1.6	M. Gauthier
115-23-006	115-23-006-C01	8.45	116	2	11	6	4	1.8	M. Gauthier
115-23-006	115-23-006-C01	8.45	128	4	11	6	6	1.8	M. Gauthier
115-23-006	115-23-006-C01	8.45	38	20	22	7	2	3.1	M. Gauthier
115-23-006	115-23-006-C01	8.45	95	6	15	7	7	2.1	M. Gauthier
115-23-006	115-23-006-C01	8.45	316	6	14	7	5	2.0	M. Gauthier
115-23-006	115-23-006-C01	8.45	138	24	14	6	4	2.3	M. Gauthier

115-23-006	115-23-006-C01	8.45	256	22	11	8	5	1.4	M. Gauthier
115-23-006	115-23-006-C01	8.45	102	34	22	12	10	1.8	M. Gauthier
115-23-006	115-23-006-C01	8.45	232	20	15	9	3	1.7	M. Gauthier
115-23-006	115-23-006-C01	8.45	138	20	15	7	5	2.1	M. Gauthier
115-23-006	115-23-006-C01	8.45	295	8	23	12	6	1.9	M. Gauthier
115-23-006	115-23-006-C01	8.45	80	6	16	10	5	1.6	M. Gauthier
115-23-006	115-23-006-C01	8.45	322	20	10	5	3	2.0	M. Gauthier
115-23-006	115-23-006-C01	8.45	292	8	20	11	5	1.8	M. Gauthier
115-23-006	115-23-006-C01	8.45	48	16	30	13	13	2.3	M. Gauthier
115-23-006	115-23-006-C01	8.45	112	30	15	6	6	2.5	M. Gauthier
115-23-006	115-23-006-C01	8.45	38	10	17	8	4	2.1	M. Gauthier
115-23-006	115-23-006-C02	11.55	166	8	20	9	9	2.2	M. Gauthier
115-23-006	115-23-006-C02	11.55	358	24	20	11	4	1.8	M. Gauthier
115-23-006	115-23-006-C02	11.55	28	32	45	23	12	2.0	M. Gauthier
115-23-006	115-23-006-C02	11.55	155	6	21	12	12	1.8	M. Gauthier
115-23-006	115-23-006-C02	11.55	241	8	9	5	3	1.8	M. Gauthier
115-23-006	115-23-006-C02	11.55	45	40	17	11	5	1.5	M. Gauthier
115-23-006	115-23-006-C02	11.55	236	2	19	10	4	1.9	M. Gauthier
115-23-006	115-23-006-C02	11.55	342	28	33	21	12	1.6	M. Gauthier
115-23-006	115-23-006-C02	11.55	18	2	14	8	6	1.8	M. Gauthier
115-23-006	115-23-006-C02	11.55	318	52	12	4	2	3.0	M. Gauthier
115-23-006	115-23-006-C02	11.55	322	44	15	10	4	1.5	M. Gauthier
115-23-006	115-23-006-C02	11.55	340	4	10	4	2	2.5	M. Gauthier
115-23-006	115-23-006-C02	11.55	356	8	12	3	1	4.0	M. Gauthier
115-23-006	115-23-006-C02	11.55	136	10	16	8	7	2.0	M. Gauthier
115-23-006	115-23-006-C02	11.55	105	24	10	6	4	1.7	M. Gauthier
115-23-006	115-23-006-C02	11.55	302	4	11	5	3	2.2	M. Gauthier
115-23-006	115-23-006-C02	11.55	124	22	13	8	5	1.6	M. Gauthier

115-23-006	115-23-006-C02	11.55	145	16	20	13	9	1.5	M. Gauthier
115-23-006	115-23-006-C02	11.55	166	16	16	9	6	1.8	M. Gauthier
115-23-006	115-23-006-C02	11.55	142	2	8	4	2	2.0	M. Gauthier
115-23-006	115-23-006-C02	11.55	62	4	21	12	4	1.8	M. Gauthier
115-23-006	115-23-006-C02	11.55	266	2	16	10	5	1.6	M. Gauthier
115-23-006	115-23-006-C02	11.55	290	16	13	7	4	1.9	M. Gauthier
115-23-006	115-23-006-C02	11.55	126	14	8	4	4	2.0	M. Gauthier
115-23-006	115-23-006-C02	11.55	130	30	12	4	2	3.0	M. Gauthier
115-23-006	115-23-006-C02	11.55	82	2	20	11	6	1.8	M. Gauthier
115-23-006	115-23-006-C02	11.55	319	4	20	10	8	2.0	M. Gauthier
115-23-006	115-23-006-C02	11.55	125	38	30	16	11	1.9	M. Gauthier
115-23-006	115-23-006-C02	11.55	130	26	12	7	4	1.7	M. Gauthier
115-23-006	115-23-006-C02	11.55	122	6	15	6	3	2.5	M. Gauthier
115-23-006	115-23-006-C02	11.55	326	12	19	10	3	1.9	M. Gauthier
115-23-006	115-23-006-C02	11.55	342	26	10	6	2	1.7	M. Gauthier
115-23-006	115-23-006-C02	11.55	126	4	11	6	3	1.8	M. Gauthier
115-23-006	115-23-006-C02	11.55	336	2	17	9	3	1.9	M. Gauthier
115-23-006	115-23-006-C03	15.35	88	10	40	26	13	1.5	N. Mesich
115-23-006	115-23-006-C03	15.35	115	19	23	17	8	1.4	N. Mesich
115-23-006	115-23-006-C03	15.35	348	38	16	11	6	1.5	N. Mesich
115-23-006	115-23-006-C03	15.35	121	37	14	6	4	2.3	N. Mesich
115-23-006	115-23-006-C03	15.35	230	2	24	13	8	1.8	N. Mesich
115-23-006	115-23-006-C03	15.35	100	15	11	5	3	2.2	N. Mesich
115-23-006	115-23-006-C03	15.35	114	8	17	11	8	1.5	N. Mesich
115-23-006	115-23-006-C03	15.35	113	11	16	12	7	1.3	N. Mesich
115-23-006	115-23-006-C03	15.35	8	8	30	21	10	1.4	N. Mesich
115-23-006	115-23-006-C03	15.35	79	21	32	22	6	1.5	N. Mesich
115-23-006	115-23-006-C03	15.35	237	15	9	5	2	1.8	N. Mesich

115-23-006	115-23-006-C03	15.35	107	14	14	8	6	1.8	N. Mesich
115-23-006	115-23-006-C03	15.35	100	23	12	6	3	2.0	N. Mesich
115-23-006	115-23-006-C03	15.35	331	22	19	11	8	1.7	N. Mesich
115-23-006	115-23-006-C03	15.35	270	25	14	8	3	1.8	N. Mesich
115-23-006	115-23-006-C03	15.35	105	11	10	7	3	1.4	N. Mesich
115-23-006	115-23-006-C03	15.35	64	55	12	8	3	1.5	N. Mesich
115-23-006	115-23-006-C03	15.35	265	32	14	8	4	1.8	N. Mesich
115-23-006	115-23-006-C03	15.35	101	3	11	7	4	1.6	N. Mesich
115-23-006	115-23-006-C03	15.35	106	16	11	8	3	1.4	N. Mesich
115-23-006	115-23-006-C03	15.35	230	3	9	5	3	1.8	N. Mesich
115-23-006	115-23-006-C03	15.35	237	13	26	15	10	1.7	N. Mesich
115-23-006	115-23-006-C03	15.35	12	8	15	10	4	1.5	N. Mesich
115-23-006	115-23-006-C03	15.35	76	19	9	6	2	1.5	N. Mesich
115-23-006	115-23-006-C03	15.35	233	15	10	6	3	1.7	N. Mesich
115-23-006	115-23-006-C03	15.35	17	1	13	8	4	1.6	N. Mesich
115-23-006	115-23-006-C03	15.35	207	9	10	7	4	1.4	N. Mesich
115-23-006	115-23-006-C03	15.35	99	12	16	11	5	1.5	N. Mesich
115-23-006	115-23-006-C03	15.35	281	4	15	10	6	1.5	N. Mesich
115-23-007	115-23-007-A01	0.70	172	3	11	8	3	1.4	N. Mesich
115-23-007	115-23-007-A01	0.70	52	7	14	10	6	1.4	N. Mesich
115-23-007	115-23-007-A01	0.70	310	5	19	8	4	2.4	N. Mesich
115-23-007	115-23-007-A01	0.70	153	24	9	6	4	1.5	N. Mesich
115-23-007	115-23-007-A01	0.70	304	8	10	6	3	1.7	N. Mesich
115-23-007	115-23-007-A01	0.70	82	20	12	8	6	1.5	N. Mesich
115-23-007	115-23-007-A01	0.70	307	12	15	10	6	1.5	N. Mesich
115-23-007	115-23-007-A01	0.70	313	6	20	13	8	1.5	N. Mesich
115-23-007	115-23-007-A01	0.70	94	19	16	11	7	1.5	N. Mesich
115-23-007	115-23-007-A01	0.70	247	14	32	20	13	1.6	N. Mesich

115-23-007	115-23-007-A01	0.70	304	2	14	10	5	1.4	N. Mesich
115-23-007	115-23-007-A01	0.70	197	29	18	12	4	1.5	N. Mesich
115-23-007	115-23-007-A01	0.70	140	13	11	6	3	1.8	N. Mesich
115-23-007	115-23-007-A01	0.70	251	39	28	16	15	1.8	N. Mesich
115-23-007	115-23-007-A01	0.70	351	9	21	12	10	1.8	N. Mesich
115-23-007	115-23-007-A01	0.70	324	8	19	12	3	1.6	N. Mesich
115-23-007	115-23-007-A01	0.70	321	14	9	5	3	1.8	N. Mesich
115-23-007	115-23-007-A01	0.70	322	10	11	8	5	1.4	N. Mesich
115-23-007	115-23-007-A01	0.70	146	5	11	8	6	1.4	N. Mesich
115-23-007	115-23-007-A01	0.70	161	18	17	11	6	1.5	N. Mesich
115-23-007	115-23-007-A01	0.70	244	16	12	7	4	1.7	N. Mesich
115-23-007	115-23-007-A01	0.70	5	7	12	7	5	1.7	N. Mesich
115-23-007	115-23-007-A01	0.70	346	1	12	8	6	1.5	N. Mesich
115-23-007	115-23-007-A01	0.70	172	16	16	11	8	1.5	N. Mesich
115-23-007	115-23-007-A01	0.70	348	2	10	7	3	1.4	N. Mesich
115-23-007	115-23-007-A01	0.70	127	4	17	11	7	1.5	N. Mesich
115-23-007	115-23-007-A01	0.70	229	5	7	4	2	1.8	N. Mesich
115-23-007	115-23-007-B02	3.00	254	10	31	12	10	2.6	N. Mesich
115-23-007	115-23-007-B02	3.00	287	18	9	6	3	1.5	N. Mesich
115-23-007	115-23-007-B02	3.00	292	20	10	6	4	1.7	N. Mesich
115-23-007	115-23-007-B02	3.00	165	3	17	10	5	1.7	N. Mesich
115-23-007	115-23-007-B02	3.00	272	5	8	6	3	1.3	N. Mesich
115-23-007	115-23-007-B02	3.00	202	7	36	23	12	1.6	N. Mesich
115-23-007	115-23-007-B02	3.00	65	12	10	7	4	1.4	N. Mesich
115-23-007	115-23-007-B02	3.00	266	6	19	8	6	2.4	N. Mesich
115-23-007	115-23-007-B02	3.00	176	4	26	17	12	1.5	N. Mesich
115-23-007	115-23-007-B02	3.00	105	4	13	6	4	2.2	N. Mesich
115-23-007	115-23-007-B02	3.00	220	10	30	17	11	1.8	N. Mesich

115-23-007	115-23-007-B02	3.00	272	19	14	9	6	1.6	N. Mesich
115-23-007	115-23-007-B02	3.00	73	10	21	14	7	1.5	N. Mesich
115-23-007	115-23-007-B02	3.00	269	22	10	7	4	1.4	N. Mesich
115-23-007	115-23-007-B02	3.00	273	6	11	7	5	1.6	N. Mesich
115-23-007	115-23-007-B02	3.00	95	46	24	16	9	1.5	N. Mesich
115-23-007	115-23-007-B02	3.00	282	14	18	12	9	1.5	N. Mesich
115-23-007	115-23-007-B02	3.00	85	24	25	15	9	1.7	N. Mesich
115-23-007	115-23-007-B02	3.00	35	31	17	12	8	1.4	N. Mesich
115-23-007	115-23-007-B02	3.00	240	15	17	9	6	1.9	N. Mesich
115-23-007	115-23-007-B02	3.00	64	10	11	7	5	1.6	N. Mesich
115-23-007	115-23-007-B02	3.00	90	25	13	9	6	1.4	N. Mesich
115-23-007	115-23-007-B02	3.00	244	12	32	22	13	1.5	N. Mesich
115-23-007	115-23-007-B02	3.00	249	27	12	8	6	1.5	N. Mesich
115-23-007	115-23-007-B02	3.00	18	32	13	7	5	1.9	N. Mesich
115-23-007	115-23-007-B02	3.00	271	13	12	7	4	1.7	N. Mesich
115-23-007	115-23-007-B02	3.00	69	9	12	8	5	1.5	N. Mesich
115-23-007	115-23-007-B02	3.00	79	3	13	8	8	1.6	N. Mesich
115-23-007	115-23-007-B02	3.00	242	24	21	12	9	1.8	N. Mesich
115-23-007	115-23-007-B02	3.00	19	36	26	18	12	1.4	N. Mesich
115-23-007	115-23-007-C01	4.55	116	30	14	7	4	2.0	T. Hodder
115-23-007	115-23-007-C01	4.55	114	26	17	9	8	1.9	T. Hodder
115-23-007	115-23-007-C01	4.55	113	14	9	5	4	1.8	T. Hodder
115-23-007	115-23-007-C01	4.55	56	29	24	14	12	1.7	T. Hodder
115-23-007	115-23-007-C01	4.55	174	28	14	8	5	1.8	T. Hodder
115-23-007	115-23-007-C01	4.55	84	20	12	8	6	1.5	T. Hodder
115-23-007	115-23-007-C01	4.55	135	20	10	5	3	2.0	T. Hodder
115-23-007	115-23-007-C01	4.55	130	25	11	7	5	1.6	T. Hodder
115-23-007	115-23-007-C01	4.55	160	24	11	7	6	1.6	T. Hodder

115-23-007	115-23-007-C01	4.55	129	24	46	22	18	2.1	T. Hodder
115-23-007	115-23-007-C01	4.55	168	30	22	12	10	1.8	T. Hodder
115-23-007	115-23-007-C01	4.55	160	24	17	11	6	1.5	T. Hodder
115-23-007	115-23-007-C01	4.55	150	12	9	5	4	1.8	T. Hodder
115-23-007	115-23-007-C01	4.55	146	29	15	9	6	1.7	T. Hodder
115-23-007	115-23-007-C01	4.55	90	21	12	7	5	1.7	T. Hodder
115-23-007	115-23-007-C01	4.55	96	7	10	6	3	1.7	T. Hodder
115-23-007	115-23-007-C01	4.55	131	1	13	9	7	1.4	T. Hodder
115-23-007	115-23-007-C01	4.55	146	8	10	6	5	1.7	T. Hodder
115-23-007	115-23-007-C01	4.55	145	19	16	9	8	1.8	T. Hodder
115-23-007	115-23-007-C01	4.55	101	11	13	8	6	1.6	T. Hodder
115-23-007	115-23-007-C01	4.55	94	10	24	16	11	1.5	T. Hodder
115-23-007	115-23-007-C01	4.55	93	1	13	6	4	2.2	T. Hodder
115-23-007	115-23-007-C01	4.55	95	38	9	6	3	1.5	T. Hodder
115-23-007	115-23-007-C01	4.55	98	17	8	4	3	2.0	T. Hodder
115-23-007	115-23-007-C01	4.55	149	3	22	10	7	2.2	T. Hodder
115-23-007	115-23-007-C01	4.55	150	22	28	18	14	1.6	T. Hodder
115-23-007	115-23-007-C01	4.55	126	8	11	6	5	1.8	T. Hodder
115-23-007	115-23-007-C01	4.55	120	27	19	12	5	1.6	T. Hodder
115-23-007	115-23-007-C01	4.55	105	34	25	15	10	1.7	T. Hodder
115-23-007	115-23-007-C01	4.55	100	15	39	20	15	2.0	T. Hodder
115-23-007	115-23-007-C01	4.55	140	9	130	50	45	2.6	T. Hodder
115-23-007	115-23-007-C04	13.55	64	39	17	10	5	1.7	T. Hodder
115-23-007	115-23-007-C04	13.55	46	10	26	16	10	1.6	T. Hodder
115-23-007	115-23-007-C04	13.55	60	4	11	8	4	1.4	T. Hodder
115-23-007	115-23-007-C04	13.55	75	25	27	15	6	1.8	T. Hodder
115-23-007	115-23-007-C04	13.55	126	3	17	11	8	1.5	T. Hodder
115-23-007	115-23-007-C04	13.55	132	11	25	14	12	1.8	T. Hodder

115-23-007	115-23-007-C04	13.55	128	50	26	15	13	1.7	T. Hodder
115-23-007	115-23-007-C04	13.55	159	57	28	13	7	2.2	T. Hodder
115-23-007	115-23-007-C04	13.55	173	1	18	10	9	1.8	T. Hodder
115-23-007	115-23-007-C04	13.55	174	6	14	9	6	1.6	T. Hodder
115-23-007	115-23-007-C04	13.55	262	1	20	11	9	1.8	T. Hodder
115-23-007	115-23-007-C04	13.55	261	8	10	7	4	1.4	T. Hodder
115-23-007	115-23-007-C04	13.55	150	16	8	3	2	2.7	T. Hodder
115-23-007	115-23-007-C04	13.55	178	23	10	5	4	2.0	T. Hodder
115-23-007	115-23-007-C04	13.55	100	1	29	17	10	1.7	T. Hodder
115-23-007	115-23-007-C04	13.55	140	28	23	16	9	1.4	T. Hodder
115-23-007	115-23-007-C04	13.55	135	34	12	8	3	1.5	T. Hodder
115-23-007	115-23-007-C04	13.55	208	29	19	9	4	2.1	T. Hodder
115-23-007	115-23-007-C04	13.55	178	19	15	9	5	1.7	T. Hodder
115-23-007	115-23-007-C04	13.55	209	14	37	25	15	1.5	T. Hodder
115-23-007	115-23-007-C04	13.55	184	4	19	10	3	1.9	T. Hodder
115-23-007	115-23-007-C04	13.55	181	1	17	9	5	1.9	T. Hodder
115-23-007	115-23-007-C04	13.55	200	27	11	8	5	1.4	T. Hodder
115-23-007	115-23-007-C04	13.55	178	19	16	10	8	1.6	T. Hodder
115-23-007	115-23-007-C04	13.55	64	34	15	10	3	1.5	M. Gauthier
115-23-007	115-23-007-C04	13.55	142	14	9	5	2	1.8	M. Gauthier
115-23-007	115-23-007-C04	13.55	82	22	10	5	3	2.0	M. Gauthier
115-23-007	115-23-007-C04	13.55	325	18	9	5	5	1.8	M. Gauthier
115-23-007	115-23-007-C04	13.55	135	38	8	4	3	2.0	M. Gauthier
115-23-007	115-23-007-C04	13.55	150	18	9	4	4	2.3	M. Gauthier
115-23-007	115-23-007-C04	13.55	164	30	21	13	7	1.6	M. Gauthier
115-23-007	115-23-007-C04	13.55	182	22	13	8	5	1.6	M. Gauthier
115-23-007	115-23-007-C04	13.55	165	4	18	11	6	1.6	M. Gauthier
115-23-007	115-23-007-C04	13.55	336	8	7	4	2	1.8	M. Gauthier

115-23-007	115-23-007-C04	13.55	195	6	7	4	2	1.8	M. Gauthier
115-23-007	115-23-007-C04	13.55	196	12	12	7	7	1.7	M. Gauthier
115-23-007	115-23-007-C04	13.55	176	14	42	13	8	3.2	M. Gauthier
115-23-007	115-23-007-C04	13.55	198	16	14	7	5	2.0	M. Gauthier
115-23-007	115-23-007-C04	13.55	196	8	9	5	3	1.8	M. Gauthier
115-23-007	115-23-007-C04	13.55	222	16	7	4	3	1.8	M. Gauthier
115-23-007	115-23-007-C04	13.55	192	25	8	5	2	1.6	M. Gauthier
115-23-007	115-23-007-C04	13.55	168	24	22	10	10	2.2	M. Gauthier
115-23-007	115-23-007-C04	13.55	198	24	11	6	3	1.8	M. Gauthier
115-23-007	115-23-007-C04	13.55	215	16	13	7	5	1.9	M. Gauthier
115-23-007	115-23-007-C05	15.55	94	43	43	24	20	1.8	N. Mesich
115-23-007	115-23-007-C05	15.55	227	29	17	10	7	1.7	N. Mesich
115-23-007	115-23-007-C05	15.55	260	12	17	8	7	2.1	N. Mesich
115-23-007	115-23-007-C05	15.55	78	27	14	7	5	2.0	N. Mesich
115-23-007	115-23-007-C05	15.55	79	5	14	10	5	1.4	N. Mesich
115-23-007	115-23-007-C05	15.55	44	10	12	8	7	1.5	N. Mesich
115-23-007	115-23-007-C05	15.55	101	19	13	8	6	1.6	N. Mesich
115-23-007	115-23-007-C05	15.55	151	19	13	9	6	1.4	N. Mesich
115-23-007	115-23-007-C05	15.55	67	22	8	6	3	1.3	N. Mesich
115-23-007	115-23-007-C05	15.55	102	16	13	8	5	1.6	N. Mesich
115-23-007	115-23-007-C05	15.55	257	16	16	6	3	2.7	N. Mesich
115-23-007	115-23-007-C05	15.55	259	26	20	12	7	1.7	N. Mesich
115-23-007	115-23-007-C05	15.55	95	34	8	5	3	1.6	N. Mesich
115-23-007	115-23-007-C05	15.55	255	9	11	4	3	2.8	N. Mesich
115-23-007	115-23-007-C05	15.55	83	2	9	4	3	2.3	N. Mesich
115-23-007	115-23-007-C05	15.55	103	3	11	6	4	1.8	N. Mesich
115-23-007	115-23-007-C05	15.55	285	21	13	9	5	1.4	N. Mesich
115-23-007	115-23-007-C05	15.55	104	15	18	11	8	1.6	N. Mesich

115-23-007	115-23-007-C05	15.55	106	17	14	8	5	1.8	N. Mesich
115-23-007	115-23-007-C05	15.55	93	8	21	14	10	1.5	N. Mesich
115-23-007	115-23-007-C05	15.55	102	3	12	7	6	1.7	N. Mesich
115-23-007	115-23-007-C05	15.55	106	25	13	8	5	1.6	N. Mesich
115-23-007	115-23-007-C05	15.55	82	0	15	10	7	1.5	N. Mesich
115-23-007	115-23-007-C05	15.55	243	11	13	7	6	1.9	N. Mesich
115-23-007	115-23-007-C05	15.55	92	1	12	8	3	1.5	N. Mesich
115-23-007	115-23-007-C05	15.55	76	14	18	8	5	2.3	N. Mesich
115-23-007	115-23-007-C05	15.55	65	7	9	4	2	2.3	N. Mesich
115-23-007	115-23-007-C05	15.55	104	34	15	9	4	1.7	N. Mesich
115-23-007	115-23-007-C05	15.55	100	11	8	5	3	1.6	N. Mesich
115-23-007	115-23-007-C05	15.55	102	25	17	7	7	2.4	N. Mesich
115-23-007	115-23-007-D01	17.95	60	8	11	6	2	1.8	T. Hodder
115-23-007	115-23-007-D01	17.95	140	28	16	10	6	1.6	T. Hodder
115-23-007	115-23-007-D01	17.95	268	38	14	7	5	2.0	T. Hodder
115-23-007	115-23-007-D01	17.95	311	34	16	10	3	1.6	T. Hodder
115-23-007	115-23-007-D01	17.95	28	10	11	5	4	2.2	T. Hodder
115-23-007	115-23-007-D01	17.95	228	5	15	10	7	1.5	T. Hodder
115-23-007	115-23-007-D01	17.95	102	25	16	10	7	1.6	T. Hodder
115-23-007	115-23-007-D01	17.95	115	24	25	15	7	1.7	T. Hodder
115-23-007	115-23-007-D01	17.95	24	33	20	11	8	1.8	T. Hodder
115-23-007	115-23-007-D01	17.95	8	14	16	10	5	1.6	T. Hodder
115-23-007	115-23-007-D01	17.95	34	7	17	11	8	1.5	T. Hodder
115-23-007	115-23-007-D01	17.95	234	45	12	8	6	1.5	T. Hodder
115-23-007	115-23-007-D01	17.95	236	25	14	8	5	1.8	T. Hodder
115-23-007	115-23-007-D01	17.95	262	15	25	13	7	1.9	T. Hodder
115-23-007	115-23-007-D01	17.95	52	7	21	7	7	3.0	T. Hodder
115-23-007	115-23-007-D01	17.95	72	38	13	8	4	1.6	T. Hodder

115-23-007	115-23-007-D01	17.95	245	33	40	27	18	1.5	T. Hodder
115-23-007	115-23-007-D01	17.95	42	30	22	14	10	1.6	T. Hodder
115-23-007	115-23-007-D01	17.95	225	5	25	15	5	1.7	T. Hodder
115-23-007	115-23-007-D01	17.95	250	15	57	36	20	1.6	T. Hodder
115-23-007	115-23-007-D01	17.95	70	23	35	12	10	2.9	T. Hodder
115-23-007	115-23-007-D01	17.95	45	30	20	13	8	1.5	T. Hodder
115-23-007	115-23-007-D01	17.95	232	14	21	13	7	1.6	T. Hodder
115-23-007	115-23-007-D01	17.95	33	27	18	9	7	2.0	T. Hodder
115-23-007	115-23-007-D01	17.95	62	12	23	11	7	2.1	T. Hodder
115-23-007	115-23-007-D01	17.95	27	28	25	13	10	1.9	T. Hodder
115-23-007	115-23-007-D01	17.95	57	24	16	10	8	1.6	T. Hodder
115-23-007	115-23-007-D01	17.95	257	10	35	20	14	1.8	T. Hodder
115-23-007	115-23-007-D01	17.95	254	30	20	13	5	1.5	T. Hodder
115-23-007	115-23-007-D01	17.95	254	20	18	12	6	1.5	T. Hodder
115-23-007	115-23-007-D03	23.15	355	18	28	15	8	1.9	N. Mesich
115-23-007	115-23-007-D03	23.15	324	19	11	6	4	1.8	N. Mesich
115-23-007	115-23-007-D03	23.15	160	11	20	14	8	1.4	N. Mesich
115-23-007	115-23-007-D03	23.15	146	22	11	8	4	1.4	N. Mesich
115-23-007	115-23-007-D03	23.15	136	2	37	24	11	1.5	N. Mesich
115-23-007	115-23-007-D03	23.15	316	2	10	7	3	1.4	N. Mesich
115-23-007	115-23-007-D03	23.15	339	21	11	7	5	1.6	N. Mesich
115-23-007	115-23-007-D03	23.15	313	47	20	12	9	1.7	N. Mesich
115-23-007	115-23-007-D03	23.15	154	22	15	10	6	1.5	N. Mesich
115-23-007	115-23-007-D03	23.15	153	41	9	6	3	1.5	N. Mesich
115-23-007	115-23-007-D03	23.15	350	12	28	15	10	1.9	N. Mesich
115-23-007	115-23-007-D03	23.15	174	49	11	7	3	1.6	N. Mesich
115-23-007	115-23-007-D03	23.15	142	16	19	13	7	1.5	N. Mesich
115-23-007	115-23-007-D03	23.15	151	20	9	6	4	1.5	N. Mesich

115-23-007	115-23-007-D03	23.15	154	8	7	4	2	1.8	N. Mesich
115-23-007	115-23-007-D03	23.15	191	48	20	13	8	1.5	N. Mesich
115-23-007	115-23-007-D03	23.15	124	17	13	7	6	1.9	N. Mesich
115-23-007	115-23-007-D03	23.15	299	5	9	6	4	1.5	N. Mesich
115-23-007	115-23-007-D03	23.15	303	41	12	8	5	1.5	N. Mesich
115-23-007	115-23-007-D03	23.15	311	19	25	14	9	1.8	N. Mesich
115-23-007	115-23-007-D03	23.15	300	25	17	10	7	1.7	N. Mesich
115-23-007	115-23-007-D03	23.15	131	14	13	8	5	1.6	N. Mesich
115-23-007	115-23-007-D03	23.15	159	23	18	11	6	1.6	N. Mesich
115-23-007	115-23-007-D03	23.15	146	9	8	5	3	1.6	N. Mesich
115-23-007	115-23-007-D03	23.15	136	6	11	7	5	1.6	N. Mesich
115-23-007	115-23-007-D03	23.15	152	22	12	8	2	1.5	N. Mesich
115-23-007	115-23-007-D03	23.15	320	12	24	15	11	1.6	N. Mesich
115-23-007	115-23-007-D03	23.15	337	21	17	10	6	1.7	N. Mesich
115-23-007	115-23-007-D05	29.15	60	10	40	22	10.00	1.8	M. Gauthier
115-23-007	115-23-007-D05	29.15	288	10	9	3	1.00	3.0	M. Gauthier
115-23-007	115-23-007-D05	29.15	162	14	12	7	4.00	1.7	M. Gauthier
115-23-007	115-23-007-D05	29.15	158	14	25	13	11.00	1.9	M. Gauthier
115-23-007	115-23-007-D05	29.15	294	2	18	11	5.00	1.6	M. Gauthier
115-23-007	115-23-007-D05	29.15	160	16	12	6	4.00	2.0	M. Gauthier
115-23-007	115-23-007-D05	29.15	152	14	16	11	7.00	1.5	M. Gauthier
115-23-007	115-23-007-D05	29.15	235	6	23	13	7.00	1.8	M. Gauthier
115-23-007	115-23-007-D05	29.15	172	4	20	11	7.00	1.8	M. Gauthier
115-23-007	115-23-007-D05	29.15	84	10	16	11	4.00	1.5	M. Gauthier
115-23-007	115-23-007-D05	29.15	184	8	14	8	2.00	1.8	M. Gauthier
115-23-007	115-23-007-D05	29.15	198	22	65	35	12.00	1.9	M. Gauthier
115-23-007	115-23-007-D05	29.15	326	32	16	10	7.00	1.6	M. Gauthier
115-23-007	115-23-007-D05	29.15	128	14	15	8	2.00	1.9	M. Gauthier

115-23-007	115-23-007-D05	29.15	106	12	32	14	10.00	2.3	M. Gauthier
115-23-007	115-23-007-D05	29.15	24	12	18	10	4.00	1.8	M. Gauthier
115-23-007	115-23-007-D05	29.15	94	8	9	5	2.00	1.8	M. Gauthier
115-23-007	115-23-007-D05	29.15	142	12	10	6	2.00	1.7	M. Gauthier
115-23-007	115-23-007-D05	29.15	116	20	10	4	2.00	2.5	M. Gauthier
115-23-007	115-23-007-D05	29.15	80	4	20	11	8.00	1.8	M. Gauthier
115-23-007	115-23-007-D05	29.15	68	4	15	10	5.00	1.5	M. Gauthier
115-23-007	115-23-007-D05	29.15	138	10	12	5	3.00	2.4	M. Gauthier
115-23-007	115-23-007-D05	29.15	140	16	12	6	5.00	2.0	M. Gauthier
115-23-007	115-23-007-D05	29.15	122	15	14	8	5.00	1.8	M. Gauthier
115-23-007	115-23-007-D05	29.15	184	6	13	8	2.00	1.6	M. Gauthier
115-23-007	115-23-007-D05	29.15	48	20	43	25	9.00	1.7	M. Gauthier
115-23-007	115-23-007-D05	29.15	354	22	13	7	4.00	1.9	M. Gauthier
115-23-007	115-23-007-D05	29.15	300	16	15	5	4.00	3.0	M. Gauthier
115-23-007	115-23-007-D05	29.15	315	22	13	5	2.00	2.6	M. Gauthier
115-23-007	115-23-007-D05	29.15	309	6	15	9	5.00	1.7	M. Gauthier
115-23-007	115-23-007-D05	29.15	288	8	40	17	7.00	2.4	M. Gauthier
115-23-007	115-23-007-D05	29.15	170	4	15	8	3.00	1.9	M. Gauthier
115-23-007	115-23-007-D05	29.15	200	8	37	17	11.00	2.2	M. Gauthier
115-23-007	115-23-007-D05	29.15	18	6	18	10	5.00	1.8	M. Gauthier
115-23-007	115-23-007-D05	29.15	345	10	21	14	3.00	1.5	M. Gauthier
115-23-007	115-23-007-D05	29.15	80	22	14	7	4.00	2.0	M. Gauthier
115-23-007	115-23-007-D05	29.15	40	20	22	11	4.00	2.0	M. Gauthier
115-23-007	115-23-007-D05	29.15	234	2	26	11	8.00	2.4	M. Gauthier
115-23-007	115-23-007-D05	29.15	290	10	45	25	10.00	1.8	M. Gauthier
115-23-007	115-23-007-D05	29.15	94	16	18	11	4.00	1.6	M. Gauthier
115-23-007	115-23-007-D07	34.15	334	25	25	13	12	1.9	T. Hodder
115-23-007	115-23-007-D07	34.15	140	22	15	10	4	1.5	T. Hodder

115-23-007	115-23-007-D07	34.15	148	14	17	11	8	1.5	T. Hodder
115-23-007	115-23-007-D07	34.15	133	10	10	6	6	1.7	T. Hodder
115-23-007	115-23-007-D07	34.15	220	2	20	12	8	1.7	T. Hodder
115-23-007	115-23-007-D07	34.15	218	10	32	20	12	1.6	T. Hodder
115-23-007	115-23-007-D07	34.15	260	14	22	13	18	1.7	T. Hodder
115-23-007	115-23-007-D07	34.15	151	21	27	18	12	1.5	T. Hodder
115-23-007	115-23-007-D07	34.15	328	27	14	7	6	2.0	T. Hodder
115-23-007	115-23-007-D07	34.15	54	25	16	9	5	1.8	T. Hodder
115-23-007	115-23-007-D07	34.15	253	15	14	7	5	2.0	T. Hodder
115-23-007	115-23-007-D07	34.15	208	8	31	20	8	1.6	T. Hodder
115-23-007	115-23-007-D07	34.15	230	6	13	8	4	1.6	T. Hodder
115-23-007	115-23-007-D07	34.15	150	7	10	6	4	1.7	T. Hodder
115-23-007	115-23-007-D07	34.15	235	6	21	12	8	1.8	T. Hodder
115-23-007	115-23-007-D07	34.15	274	5	11	7	4	1.6	T. Hodder
115-23-007	115-23-007-D07	34.15	112	16	19	11	7	1.7	T. Hodder
115-23-007	115-23-007-D07	34.15	178	22	22	14	8	1.6	T. Hodder
115-23-007	115-23-007-D07	34.15	244	8	15	8	6	1.9	T. Hodder
115-23-007	115-23-007-D07	34.15	178	40	10	4	3	2.5	T. Hodder
115-23-007	115-23-007-D07	34.15	224	32	12	6	5	2.0	T. Hodder
115-23-007	115-23-007-D07	34.15	117	30	20	12	6	1.7	T. Hodder
115-23-007	115-23-007-D07	34.15	80	41	8	5	3	1.6	T. Hodder
115-23-007	115-23-007-D07	34.15	82	5	11	6	4	1.8	T. Hodder
115-23-007	115-23-007-D07	34.15	164	18	25	13	10	1.9	T. Hodder
115-23-007	115-23-007-D07	34.15	220	15	20	11	5	1.8	T. Hodder
115-23-007	115-23-007-D07	34.15	133	27	11	7	4	1.6	T. Hodder
115-23-007	115-23-007-D07	34.15	225	19	11	7	4	1.6	T. Hodder
115-23-007	115-23-007-D07	34.15	138	30	30	16	10	1.9	T. Hodder
115-23-007	115-23-007-D07	34.15	90	3	13	8	5	1.6	T. Hodder

115-23-007	115-23-007-D08	31.80	72.00	22	20	12	10	1.7	T. Hodder
115-23-007	115-23-007-D08	31.80	250.00	4	30	19	12	1.6	T. Hodder
115-23-007	115-23-007-D08	31.80	115.00	12	18	7	6	2.6	T. Hodder
115-23-007	115-23-007-D08	31.80	320.00	4	16	10	7	1.6	T. Hodder
115-23-007	115-23-007-D08	31.80	205.00	15	40	18	16	2.2	T. Hodder
115-23-007	115-23-007-D08	31.80	102.00	20	16	10	8	1.6	T. Hodder
115-23-007	115-23-007-D08	31.80	280.00	14	30	18	12	1.7	T. Hodder
115-23-007	115-23-007-D08	31.80	85.00	15	20	10	6	2.0	T. Hodder
115-23-007	115-23-007-D08	31.80	91.00	7	16	10	5	1.6	T. Hodder
115-23-007	115-23-007-D08	31.80	175.00	25	11	7	2	1.6	T. Hodder
115-23-007	115-23-007-D08	31.80	50.00	25	12	6	4	2.0	T. Hodder
115-23-007	115-23-007-D08	31.80	328.00	10	25	15	10	1.7	T. Hodder
115-23-007	115-23-007-D08	31.80	25.00	15	12	7	5	1.7	T. Hodder
115-23-007	115-23-007-D08	31.80	150.00	22	26	14	10	1.9	T. Hodder
115-23-007	115-23-007-D08	31.80	118.00	39	11	5	4	2.2	T. Hodder
115-23-007	115-23-007-D08	31.80	135.00	18	14	8	6	1.8	T. Hodder
115-23-007	115-23-007-D08	31.80	103.00	11	13	7	6	1.9	T. Hodder
115-23-007	115-23-007-D08	31.80	118.00	28	22	13	8	1.7	T. Hodder
115-23-007	115-23-007-D08	31.80	155.00	15	50	25	10	2.0	T. Hodder
115-23-007	115-23-007-D08	31.80	305.00	35	20	12	10	1.7	T. Hodder
115-23-007	115-23-007-D08	31.80	158.00	15	12	6	4	2.0	T. Hodder
115-23-007	115-23-007-D08	31.80	333.00	30	25	13	4	1.9	T. Hodder
115-23-007	115-23-007-D08	31.80	90.00	30	12	4	3	3.0	T. Hodder
115-23-007	115-23-007-D08	31.80	90.00	8	24	15	8	1.6	T. Hodder
115-23-007	115-23-007-D08	31.80	148.00	35	12	8	3	1.5	T. Hodder
115-23-007	115-23-007-D08	31.80	154.00	13	37	20	19	1.9	T. Hodder
115-23-007	115-23-007-D08	31.80	285.00	4	20	11	6	1.8	T. Hodder
115-23-007	115-23-007-D08	31.80	115.00	4	20	12	9	1.7	T. Hodder

115-23-007	115-23-007-D08	31.80	116.00	20	25	15	3	1.7	T. Hodder
115-23-007	115-23-007-D08	31.80	128.00	27	19	9	8	2.1	T. Hodder
115-23-007	115-23-007-D08	31.80	115.00	7	27	16	4	1.7	T. Hodder
115-23-007	115-23-007-D08	31.80	115.00	3	27	17	9	1.6	T. Hodder
115-23-007	115-23-007-D08	31.80	110.00	32	27	15	9	1.8	T. Hodder
115-23-007	115-23-007-D08	31.80	94.00	12	23	14	5	1.6	T. Hodder
115-23-007	115-23-007-D08	31.80	140.00	20	45	30	10	1.5	T. Hodder
115-23-007	115-23-007-E01	35.65	214	8	12	7	4	1.7	M. Gauthier
115-23-007	115-23-007-E01	35.65	352	2	15	6	3	2.5	M. Gauthier
115-23-007	115-23-007-E01	35.65	356	2	11	6	3	1.8	M. Gauthier
115-23-007	115-23-007-E01	35.65	30	24	19	10	9	1.9	M. Gauthier
115-23-007	115-23-007-E01	35.65	38	22	11	5	5	2.2	M. Gauthier
115-23-007	115-23-007-E01	35.65	222	6	35	16	15	2.2	M. Gauthier
115-23-007	115-23-007-E01	35.65	342	18	23	13	7	1.8	M. Gauthier
115-23-007	115-23-007-E01	35.65	224	8	16	7	5	2.3	M. Gauthier
115-23-007	115-23-007-E01	35.65	46	14	17	7	3	2.4	M. Gauthier
115-23-007	115-23-007-E01	35.65	18	3	23	15	4	1.5	M. Gauthier
115-23-007	115-23-007-E01	35.65	96	16	13	8	2	1.6	M. Gauthier
115-23-007	115-23-007-E01	35.65	46	6	17	11	9	1.5	M. Gauthier
115-23-007	115-23-007-E01	35.65	38	12	13	8	4	1.6	M. Gauthier
115-23-007	115-23-007-E01	35.65	92	6	17	10	3	1.7	M. Gauthier
115-23-007	115-23-007-E01	35.65	220	10	25	15	11	1.7	M. Gauthier
115-23-007	115-23-007-E01	35.65	220	2	17	7	5	2.4	M. Gauthier
115-23-007	115-23-007-E01	35.65	240	4	31	15	7	2.1	M. Gauthier
115-23-007	115-23-007-E01	35.65	240	30	15	8	4	1.9	M. Gauthier
115-23-007	115-23-007-E01	35.65	32	18	12	7	4	1.7	M. Gauthier
115-23-007	115-23-007-E01	35.65	40	8	10	5	3	2.0	M. Gauthier
115-23-007	115-23-007-E01	35.65	28	4	13	5	3	2.6	M. Gauthier

115-23-007	115-23-007-E01	35.65	50	20	31	15	15	2.1	M. Gauthier
115-23-007	115-23-007-E01	35.65	356	6	17	10	6	1.7	M. Gauthier
115-23-007	115-23-007-E01	35.65	7	10	12	6	4	2.0	M. Gauthier
115-23-007	115-23-007-E01	35.65	160	6	13	7	5	1.9	M. Gauthier
115-23-007	115-23-007-E01	35.65	342	2	10	3	1	3.3	M. Gauthier
115-23-007	115-23-007-E01	35.65	346	12	16	7	4	2.3	M. Gauthier
115-23-007	115-23-007-E01	35.65	184	4	16	9	7	1.8	M. Gauthier
115-23-007	115-23-007-E01	35.65	344	4	26	12	8	2.2	M. Gauthier
115-23-007	115-23-007-E01	35.65	166	24	12	6	4	2.0	M. Gauthier
115-23-007	115-23-007-E03	40.65	58	4	55	30	20	1.8	M. Gauthier
115-23-007	115-23-007-E03	40.65	358	26	27	12	10	2.3	M. Gauthier
115-23-007	115-23-007-E03	40.65	248	4	22	10	6	2.2	M. Gauthier
115-23-007	115-23-007-E03	40.65	235	8	23	11	6	2.1	M. Gauthier
115-23-007	115-23-007-E03	40.65	32	4	13	7	4	1.9	M. Gauthier
115-23-007	115-23-007-E03	40.65	50	6	52	33	22	1.6	M. Gauthier
115-23-007	115-23-007-E03	40.65	50	16	23	15	8	1.5	M. Gauthier
115-23-007	115-23-007-E03	40.65	76	2	22	10	7	2.2	M. Gauthier
115-23-007	115-23-007-E03	40.65	225	2	25	10	6	2.5	M. Gauthier
115-23-007	115-23-007-E03	40.65	36	32	33	17	17	1.9	M. Gauthier
115-23-007	115-23-007-E03	40.65	176	0	18	11	6	1.6	M. Gauthier
115-23-007	115-23-007-E03	40.65	346	8	18	11	6	1.6	M. Gauthier
115-23-007	115-23-007-E03	40.65	230	12	26	11	4	2.4	M. Gauthier
115-23-007	115-23-007-E03	40.65	166	8	12	6	4	2.0	M. Gauthier
115-23-007	115-23-007-E03	40.65	210	18	27	16	11	1.7	M. Gauthier
115-23-007	115-23-007-E03	40.65	31	6	24	12	12	2.0	M. Gauthier
115-23-007	115-23-007-E03	40.65	56	4	12	6	2	2.0	M. Gauthier
115-23-007	115-23-007-E03	40.65	225	2	12	8	4	1.5	M. Gauthier
115-23-007	115-23-007-E03	40.65	42	20	13	8	6.00	1.6	M. Gauthier

115-23-007	115-23-007-E03	40.65	208	22	14	9	5.00	1.6	M. Gauthier
115-23-007	115-23-007-E03	40.65	65	4	12	6	4.00	2.0	M. Gauthier
115-23-007	115-23-007-E03	40.65	44	10	8	4	2.00	2.0	M. Gauthier
115-23-007	115-23-007-E03	40.65	46	14	25	13	8.00	1.9	M. Gauthier
115-23-007	115-23-007-E03	40.65	55	6	11	6	3.00	1.8	M. Gauthier
115-23-007	115-23-007-E03	40.65	45	28	9	4	2.00	2.3	M. Gauthier
115-23-007	115-23-007-E03	40.65	58	36	8	4	2.00	2.0	M. Gauthier
115-23-007	115-23-007-E03	40.65	52	12	45	17	10.00	2.6	M. Gauthier
115-23-007	115-23-007-E03	40.65	26	23	47	22	12.00	2.1	M. Gauthier
115-23-007	115-23-007-E03	40.65	54	20	30	15	10.00	2.0	M. Gauthier
115-23-007	115-23-007-E03	40.65	38	28	18	10	6.00	1.8	M. Gauthier
115-23-008	115-23-008-A01	1.15	186	14	45	30	12	1.5	T. Hodder
115-23-008	115-23-008-A01	1.15	28	3	25	13	8	1.9	T. Hodder
115-23-008	115-23-008-A01	1.15	0	10	32	20	10	1.6	T. Hodder
115-23-008	115-23-008-A01	1.15	29	5	20	13	8	1.5	T. Hodder
115-23-008	115-23-008-A01	1.15	0	42	28	14	6	2.0	T. Hodder
115-23-008	115-23-008-A01	1.15	200	24	15	9	4	1.7	T. Hodder
115-23-008	115-23-008-A01	1.15	65	20	28	17	8	1.6	T. Hodder
115-23-008	115-23-008-A01	1.15	18	3	15	9	6	1.7	T. Hodder
115-23-008	115-23-008-A01	1.15	207	24	12	7	2	1.7	T. Hodder
115-23-008	115-23-008-A01	1.15	25	7	36	24	8	1.5	T. Hodder
115-23-008	115-23-008-A01	1.15	30	12	22	12	10	1.8	T. Hodder
115-23-008	115-23-008-A01	1.15	35	28	22	14	11	1.6	T. Hodder
115-23-008	115-23-008-A01	1.15	209	35	12	6	5	2.0	T. Hodder
115-23-008	115-23-008-A01	1.15	31	5	35	17	10	2.1	T. Hodder
115-23-008	115-23-008-A01	1.15	226	8	25	15	6	1.7	T. Hodder
115-23-008	115-23-008-A01	1.15	38	13	15	9	5	1.7	T. Hodder
115-23-008	115-23-008-A01	1.15	39	5	16	10	6	1.6	T. Hodder

115-23-008	115-23-008-A01	1.15	34	5	46	24	8	1.9	T. Hodder
115-23-008	115-23-008-A01	1.15	17	32	16	10	6	1.6	T. Hodder
115-23-008	115-23-008-A01	1.15	12	12	23	12	11	1.9	T. Hodder
115-23-008	115-23-008-A01	1.15	16	10	36	21	19	1.7	T. Hodder
115-23-008	115-23-008-A01	1.15	90	30	18	11	6	1.6	T. Hodder
115-23-008	115-23-008-A01	1.15	235	20	30	17	5	1.8	T. Hodder
115-23-008	115-23-008-A01	1.15	35	23	18	12	8	1.5	T. Hodder
115-23-008	115-23-008-A01	1.15	221	21	20	13	7	1.5	T. Hodder
115-23-008	115-23-008-A01	1.15	230	22	17	10	8	1.7	T. Hodder
115-23-008	115-23-008-A01	1.15	25	26	16	10	9	1.6	T. Hodder
115-23-008	115-23-008-A01	1.15	45	15	13	8	5	1.6	T. Hodder
115-23-008	115-23-008-A01	1.15	54	15	20	12	7	1.7	T. Hodder
115-23-008	115-23-008-A01	1.15	37	12	16	10	8	1.6	T. Hodder
115-23-008	115-23-008-A01	1.15	22	25	45	25	22	1.8	T. Hodder
115-23-008	115-23-008-B01	2.30	350	16	32	12	8	2.7	M. Gauthier
115-23-008	115-23-008-B01	2.30	168	12	12	6	3	2.0	M. Gauthier
115-23-008	115-23-008-B01	2.30	26	14	16	10	4	1.6	M. Gauthier
115-23-008	115-23-008-B01	2.30	258	18	32	20	12	1.6	M. Gauthier
115-23-008	115-23-008-B01	2.30	342	25	35	22	12	1.6	M. Gauthier
115-23-008	115-23-008-B01	2.30	182	12	40	22	9	1.8	M. Gauthier
115-23-008	115-23-008-B01	2.30	352	12	13	7	4	1.9	M. Gauthier
115-23-008	115-23-008-B01	2.30	4	26	37	20	12	1.9	M. Gauthier
115-23-008	115-23-008-B01	2.30	10	10	16	8	4	2.0	M. Gauthier
115-23-008	115-23-008-B01	2.30	10	38	17	10	5	1.7	M. Gauthier
115-23-008	115-23-008-B01	2.30	136	10	12	6	2	2.0	M. Gauthier
115-23-008	115-23-008-B01	2.30	330	16	15	6	6	2.5	M. Gauthier
115-23-008	115-23-008-B01	2.30	342	4	36	8	4	4.5	M. Gauthier
115-23-008	115-23-008-B01	2.30	158	38	6	2	1	3.0	M. Gauthier

115-23-008	115-23-008-B01	2.30	350	20	22	15	7	1.5	M. Gauthier
115-23-008	115-23-008-B01	2.30	22	2	24	13	6	1.8	M. Gauthier
115-23-008	115-23-008-B01	2.30	135	12	8	5	3	1.6	M. Gauthier
115-23-008	115-23-008-B01	2.30	12	24	12	7	4	1.7	M. Gauthier
115-23-008	115-23-008-B01	2.30	338	10	23	15	10	1.5	M. Gauthier
115-23-008	115-23-008-B01	2.30	353	12	23	13	7	1.8	M. Gauthier
115-23-008	115-23-008-B01	2.30	356	26	15	10	4	1.5	M. Gauthier
115-23-008	115-23-008-B01	2.30	340	8	45	23	17	2.0	M. Gauthier
115-23-008	115-23-008-B01	2.30	130	4	13	6	6	2.2	M. Gauthier
115-23-008	115-23-008-B01	2.30	64	4	36	22	10	1.6	M. Gauthier
115-23-008	115-23-008-B01	2.30	64	8	32	15	6	2.1	M. Gauthier
115-23-008	115-23-008-B01	2.30	58	32	22	10	8	2.2	M. Gauthier
115-23-008	115-23-008-B01	2.30	346	8	11	6	3	1.8	M. Gauthier
115-23-008	115-23-008-B01	2.30	216	6	30	15	8	2.0	M. Gauthier
115-23-008	115-23-008-B01	2.30	22	36	34	21	12	1.6	M. Gauthier
115-23-008	115-23-008-B01	2.30	355	10	13	8	6	1.6	M. Gauthier
115-23-008	115-23-008-C01	3.40	33	35	16	8	5	2.0	T. Hodder
115-23-008	115-23-008-C01	3.40	25	27	30	20	19	1.5	T. Hodder
115-23-008	115-23-008-C01	3.40	43	15	38	25	12	1.5	T. Hodder
115-23-008	115-23-008-C01	3.40	28	2	10	6	3	1.7	T. Hodder
115-23-008	115-23-008-C01	3.40	84	20	10	6	4	1.7	T. Hodder
115-23-008	115-23-008-C01	3.40	210	33	11	6	4	1.8	T. Hodder
115-23-008	115-23-008-C01	3.40	268	6	18	12	12	1.5	T. Hodder
115-23-008	115-23-008-C01	3.40	52	20	16	10	7	1.6	T. Hodder
115-23-008	115-23-008-C01	3.40	70	22	23	13	6	1.8	T. Hodder
115-23-008	115-23-008-C01	3.40	60	15	17	11	5	1.5	T. Hodder
115-23-008	115-23-008-C01	3.40	265	1	20	12	10	1.7	T. Hodder
115-23-008	115-23-008-C01	3.40	212	11	45	30	22	1.5	T. Hodder

115-23-008	115-23-008-C01	3.40	42	20	12	8	3	1.5	T. Hodder
115-23-008	115-23-008-C01	3.40	63	42	20	11	8	1.8	T. Hodder
115-23-008	115-23-008-C01	3.40	10	33	13	8	6	1.6	T. Hodder
115-23-008	115-23-008-C01	3.40	35	24	20	12	10	1.7	T. Hodder
115-23-008	115-23-008-C01	3.40	70	35	19	9	2	2.1	T. Hodder
115-23-008	115-23-008-C01	3.40	215	12	12	8	6	1.5	T. Hodder
115-23-008	115-23-008-C01	3.40	55	28	10	6	4	1.7	T. Hodder
115-23-008	115-23-008-C01	3.40	42	20	14	9	5	1.6	T. Hodder
115-23-008	115-23-008-C01	3.40	285	16	12	8	4	1.5	T. Hodder
115-23-008	115-23-008-C01	3.40	40	10	15	10	6	1.5	T. Hodder
115-23-008	115-23-008-C01	3.40	35	37	25	15	8	1.7	T. Hodder
115-23-008	115-23-008-C01	3.40	5	22	10	6	3	1.7	T. Hodder
115-23-008	115-23-008-C01	3.40	215	29	15	8	6	1.9	T. Hodder
115-23-008	115-23-008-C01	3.40	40	31	20	13	6	1.5	T. Hodder
115-23-008	115-23-008-C01	3.40	40	40	22	13	6	1.7	T. Hodder
115-23-008	115-23-008-C01	3.40	54	38	10	5	3	2.0	T. Hodder
115-23-008	115-23-008-C01	3.40	48	26	15	7	4	2.1	T. Hodder
115-23-008	115-23-008-C01	3.40	205	18	12	8	6	1.5	T. Hodder
115-23-008	115-23-008-F01	5.50	344	16	18	10	6	1.8	M. Gauthier
115-23-008	115-23-008-F01	5.50	204	18	17	11	5	1.5	M. Gauthier
115-23-008	115-23-008-F01	5.50	212	4	15	9	4	1.7	M. Gauthier
115-23-008	115-23-008-F01	5.50	188	18	10	5	2	2.0	M. Gauthier
115-23-008	115-23-008-F01	5.50	334	16	24	11	8	2.2	M. Gauthier
115-23-008	115-23-008-F01	5.50	336	20	9	6	4	1.5	M. Gauthier
115-23-008	115-23-008-F01	5.50	208	16	8	5	2	1.6	M. Gauthier
115-23-008	115-23-008-F01	5.50	24	8	30	16	8	1.9	M. Gauthier
115-23-008	115-23-008-F01	5.50	346	40	14	9	3	1.6	M. Gauthier
115-23-008	115-23-008-F01	5.50	192	4	9	5	3	1.8	M. Gauthier

115-23-008	115-23-008-F01	5.50	215	14	12	5	3	2.4	M. Gauthier
115-23-008	115-23-008-F01	5.50	196	18	13	7	2	1.9	M. Gauthier
115-23-008	115-23-008-F01	5.50	181	4	12	4	2	3.0	M. Gauthier
115-23-008	115-23-008-F01	5.50	192	4	45	20	8	2.3	M. Gauthier
115-23-008	115-23-008-F01	5.50	165	28	25	12	8	2.1	M. Gauthier
115-23-008	115-23-008-F01	5.50	338	24	21	10	6	2.1	M. Gauthier
115-23-008	115-23-008-F01	5.50	180	2	12	6	3	2.0	M. Gauthier
115-23-008	115-23-008-F01	5.50	164	2	14	6	4	2.3	M. Gauthier
115-23-008	115-23-008-F01	5.50	28	4	9	6	2	1.5	M. Gauthier
115-23-008	115-23-008-F01	5.50	352	14	7	4	2	1.8	M. Gauthier
115-23-008	115-23-008-F01	5.50	345	18	12	8	3	1.5	M. Gauthier
115-23-008	115-23-008-F01	5.50	184	12	20	10	6	2.0	M. Gauthier
115-23-008	115-23-008-F01	5.50	160	12	10	5	3	2.0	M. Gauthier
115-23-008	115-23-008-F01	5.50	28	6	12	7	4	1.7	M. Gauthier
115-23-008	115-23-008-F01	5.50	32	38	7	4	4	1.8	M. Gauthier
115-23-008	115-23-008-F01	5.50	32	20	8	5	2	1.6	M. Gauthier
115-23-008	115-23-008-F01	5.50	165	4	22	11	7	2.0	M. Gauthier
115-23-008	115-23-008-F01	5.50	25	22	15	10	6	1.5	M. Gauthier
115-23-008	115-23-008-F01	5.50	4	32	36	20	10	1.8	M. Gauthier
115-23-008	115-23-008-F01	5.50	204	40	9	5	3	1.8	M. Gauthier
115-23-008	115-23-008-F03	11.50	355	35	30	18	7	1.7	T. Hodder
115-23-008	115-23-008-F03	11.50	135	20	21	13	10	1.6	T. Hodder
115-23-008	115-23-008-F03	11.50	150	15	16	9	8	1.8	T. Hodder
115-23-008	115-23-008-F03	11.50	45	10	12	8	2	1.5	T. Hodder
115-23-008	115-23-008-F03	11.50	320	24	20	12	8	1.7	T. Hodder
115-23-008	115-23-008-F03	11.50	218	25	30	16	10	1.9	T. Hodder
115-23-008	115-23-008-F03	11.50	275	28	16	10	6	1.6	T. Hodder
115-23-008	115-23-008-F03	11.50	70	26	10	5	4	2.0	T. Hodder

115-23-008	115-23-008-F03	11.50	35	2	16	10	6	1.6	T. Hodder
115-23-008	115-23-008-F03	11.50	150	48	21	12	10	1.8	T. Hodder
115-23-008	115-23-008-F03	11.50	340	18	15	8	5	1.9	T. Hodder
115-23-008	115-23-008-F03	11.50	345	12	17	11	7	1.5	T. Hodder
115-23-008	115-23-008-F03	11.50	225	2	15	10	2	1.5	T. Hodder
115-23-008	115-23-008-F03	11.50	180	5	35	20	12	1.8	T. Hodder
115-23-008	115-23-008-F03	11.50	285	20	15	10	9	1.5	T. Hodder
115-23-008	115-23-008-F03	11.50	90	24	10	6	4	1.7	T. Hodder
115-23-008	115-23-008-F03	11.50	305	15	17	8	6	2.1	T. Hodder
115-23-008	115-23-008-F03	11.50	290	13	15	10	6	1.5	T. Hodder
115-23-008	115-23-008-F03	11.50	310	9	11	8	2	1.4	T. Hodder
115-23-008	115-23-008-F03	11.50	285	27	10	6	3	1.7	T. Hodder
115-23-008	115-23-008-F03	11.50	280	14	12	8	5	1.5	T. Hodder
115-23-008	115-23-008-F03	11.50	330	12	12	8	5	1.5	T. Hodder
115-23-008	115-23-008-F03	11.50	235	12	10	6	4	1.7	T. Hodder
115-23-008	115-23-008-F03	11.50	325	18	30	18	17	1.7	T. Hodder
115-23-008	115-23-008-F03	11.50	145	44	14	8	4	1.8	T. Hodder
115-23-008	115-23-008-F04	15.15	104	36	18	10	6	1.8	M. Gauthier
115-23-008	115-23-008-F04	15.15	94	14	13	6	3	2.2	M. Gauthier
115-23-008	115-23-008-F04	15.15	262	4	11	5	3	2.2	M. Gauthier
115-23-008	115-23-008-F04	15.15	240	4	28	15	10	1.9	M. Gauthier
115-23-008	115-23-008-F04	15.15	28	42	11	6	3	1.8	M. Gauthier
115-23-008	115-23-008-F04	15.15	90	16	12	7	6	1.7	M. Gauthier
115-23-008	115-23-008-F04	15.15	26	36	17	11	6	1.5	M. Gauthier
115-23-008	115-23-008-F04	15.15	282	6	17	10	7	1.7	M. Gauthier
115-23-008	115-23-008-F04	15.15	352	35	10	5	3	2.0	M. Gauthier
115-23-008	115-23-008-F04	15.15	80	4	9	6	2	1.5	M. Gauthier
115-23-008	115-23-008-F04	15.15	115	22	20	11	7	1.8	M. Gauthier

115-23-008	115-23-008-F04	15.15	255	16	15	10	6	1.5	M. Gauthier
115-23-008	115-23-008-F04	15.15	108	4	11	5	5	2.2	M. Gauthier
115-23-008	115-23-008-F04	15.15	288	6	8	4	2	2.0	M. Gauthier
115-23-008	115-23-008-F04	15.15	158	20	24	10	10	2.4	M. Gauthier
115-23-008	115-23-008-F04	15.15	108	22	11	5	3	2.2	M. Gauthier
115-23-008	115-23-008-F04	15.15	110	32	24	14	10	1.7	M. Gauthier
115-23-008	115-23-008-F04	15.15	122	12	18	7	5	2.6	M. Gauthier
115-23-008	115-23-008-F04	15.15	260	8	21	11	8	1.9	M. Gauthier
115-23-008	115-23-008-F04	15.15	268	10	11	6	2	1.8	M. Gauthier
115-23-008	115-23-008-F04	15.15	70	6	17	6	6	2.8	M. Gauthier
115-23-008	115-23-008-F04	15.15	238	22	9	5	3	1.8	M. Gauthier
115-23-008	115-23-008-F04	15.15	154	6	12	6	5	2.0	M. Gauthier
115-23-008	115-23-008-F04	15.15	322	14	17	11	7	1.5	M. Gauthier
115-23-008	115-23-008-F04	15.15	56	20	17	10	2	1.7	M. Gauthier
115-23-008	115-23-008-F04	15.15	296	20	17	11	5	1.5	M. Gauthier
115-23-008	115-23-008-F04	15.15	252	14	65	35	20	1.9	M. Gauthier
115-23-008	115-23-008-F04	15.15	248	36	21	10	4	2.1	M. Gauthier
115-23-009	115-23-009-B01	3.00	105	10	14	9	6	1.6	N. Mesich
115-23-009	115-23-009-B01	3.00	75	12	22	12	9	1.8	N. Mesich
115-23-009	115-23-009-B01	3.00	217	21	11	7	5	1.6	N. Mesich
115-23-009	115-23-009-B01	3.00	24	2	12	8	5	1.5	N. Mesich
115-23-009	115-23-009-B01	3.00	223	20	24	13	9	1.8	N. Mesich
115-23-009	115-23-009-B01	3.00	184	30	12	8	6	1.5	N. Mesich
115-23-009	115-23-009-B01	3.00	209	4	8	5	3	1.6	N. Mesich
115-23-009	115-23-009-B01	3.00	241	5	16	10	3	1.6	N. Mesich
115-23-009	115-23-009-B01	3.00	287	28	19	13	9	1.5	N. Mesich
115-23-009	115-23-009-B01	3.00	285	5	42	27	18	1.6	N. Mesich
115-23-009	115-23-009-B01	3.00	81	16	11	7	4	1.6	N. Mesich

115-23-009	115-23-009-B01	3.00	219	20	31	21	12	1.5	N. Mesich
115-23-009	115-23-009-B01	3.00	224	7	19	13	7	1.5	N. Mesich
115-23-009	115-23-009-B01	3.00	221	5	10	6	3	1.7	N. Mesich
115-23-009	115-23-009-B01	3.00	215	20	20	10	7	2.0	N. Mesich
115-23-009	115-23-009-B01	3.00	205	22	34	22	20	1.5	N. Mesich
115-23-009	115-23-009-B01	3.00	52	13	27	16	8	1.7	N. Mesich
115-23-009	115-23-009-B01	3.00	64	10	22	13	9	1.7	N. Mesich
115-23-009	115-23-009-B01	3.00	208	15	31	15	10	2.1	N. Mesich
115-23-009	115-23-009-B01	3.00	238	8	25	16	8	1.6	N. Mesich
115-23-009	115-23-009-B01	3.00	65	20	40	21	10	1.9	N. Mesich
115-23-009	115-23-009-B01	3.00	222	42	21	13	8	1.6	N. Mesich
115-23-009	115-23-009-B01	3.00	62	11	26	17	7	1.5	N. Mesich
115-23-009	115-23-009-B01	3.00	240	23	90	56	39	1.6	N. Mesich
115-23-009	115-23-009-B01	3.00	57	18	17	10	7	1.7	N. Mesich
115-23-009	115-23-009-B01	3.00	30	8	23	15	11	1.5	N. Mesich
115-23-009	115-23-009-B01	3.00	21	15	13	8	4	1.6	N. Mesich
115-23-009	115-23-009-C01	4.50	237	36	24	11	6	2.2	N. Mesich
115-23-009	115-23-009-C01	4.50	256	2	19	13	10	1.5	N. Mesich
115-23-009	115-23-009-C01	4.50	219	11	10	6	3	1.7	N. Mesich
115-23-009	115-23-009-C01	4.50	255	4	24	12	9	2.0	N. Mesich
115-23-009	115-23-009-C01	4.50	209	0	53	35	13	1.5	N. Mesich
115-23-009	115-23-009-C01	4.50	222	18	60	33	24	1.8	N. Mesich
115-23-009	115-23-009-C01	4.50	209	29	11	7	4	1.6	N. Mesich
115-23-009	115-23-009-C01	4.50	254	35	40	28	12	1.4	N. Mesich
115-23-009	115-23-009-C01	4.50	211	5	19	12	7	1.6	N. Mesich
115-23-009	115-23-009-C01	4.50	70	32	63	42	28	1.5	N. Mesich
115-23-009	115-23-009-C01	4.50	231	7	12	7	3	1.7	N. Mesich
115-23-009	115-23-009-C01	4.50	214	35	13	8	6	1.6	N. Mesich

115-23-009	115-23-009-C01	4.50	255	21	16	9	6	1.8	N. Mesich
115-23-009	115-23-009-C01	4.50	9	22	14	9	6	1.6	N. Mesich
115-23-009	115-23-009-C01	4.50	175	17	37	17	15	2.2	N. Mesich
115-23-009	115-23-009-C01	4.50	104	22	16	9	7	1.8	N. Mesich
115-23-009	115-23-009-C01	4.50	260	6	15	8	3	1.9	N. Mesich
115-23-009	115-23-009-C01	4.50	231	34	10	6	4	1.7	N. Mesich
115-23-009	115-23-009-C01	4.50	190	14	28	15	7	1.9	N. Mesich
115-23-009	115-23-009-C01	4.50	237	25	9	5	3	1.8	N. Mesich
115-23-009	115-23-009-C01	4.50	109	10	12	7	5	1.7	N. Mesich
115-23-009	115-23-009-C01	4.50	232	22	11	7	3	1.6	N. Mesich
115-23-009	115-23-009-C01	4.50	242	27	17	12	7	1.4	N. Mesich
115-23-009	115-23-009-C01	4.50	259	21	17	10	6	1.7	N. Mesich
115-23-009	115-23-009-C01	4.50	25	10	33	17	14	1.9	N. Mesich
115-23-009	115-23-009-C01	4.50	262	9	50	31	20	1.6	N. Mesich
115-23-009	115-23-009-C01	4.50	235	44	24	15	9	1.6	N. Mesich
115-23-009	115-23-009-C01	7.00	225	10	46	32	20	1.4	N. Mesich
115-23-009	115-23-009-C01	7.00	234	45	14	9	6	1.6	N. Mesich
115-23-009	115-23-009-D01	7.00	258	0	106	77	40	1.4	N. Mesich
115-23-009	115-23-009-D01	7.00	263	2	13	8	5	1.6	N. Mesich
115-23-009	115-23-009-D01	7.00	244	11	18	9	5	2.0	N. Mesich
115-23-009	115-23-009-D01	7.00	234	21	19	9	7	2.1	N. Mesich
115-23-009	115-23-009-D01	7.00	240	7	9	6	2	1.5	N. Mesich
115-23-009	115-23-009-D01	7.00	200	14	21	14	6	1.5	N. Mesich
115-23-009	115-23-009-D01	7.00	49	3	44	30	13	1.5	N. Mesich
115-23-009	115-23-009-D01	7.00	249	10	23	15	10	1.5	N. Mesich
115-23-009	115-23-009-D01	7.00	236	31	17	10	7	1.7	N. Mesich
115-23-009	115-23-009-D01	7.00	237	12	14	10	6	1.4	N. Mesich
115-23-009	115-23-009-D01	7.00	201	4	20	12	10	1.7	N. Mesich

115-23-009	115-23-009-D01	7.00	285	15	17	10	6	1.7	N. Mesich
115-23-009	115-23-009-D01	7.00	245	8	19	9	6	2.1	N. Mesich
115-23-009	115-23-009-D01	7.00	235	16	11	7	5	1.6	N. Mesich
115-23-009	115-23-009-D01	7.00	181	13	15	10	4	1.5	N. Mesich
115-23-009	115-23-009-D01	7.00	220	6	29	19	11	1.5	N. Mesich
115-23-009	115-23-009-D01	7.00	251	7	17	12	8	1.4	N. Mesich
115-23-009	115-23-009-D01	7.00	253	10	11	7	5	1.6	N. Mesich
115-23-009	115-23-009-D01	7.00	240	29	13	9	7	1.4	N. Mesich
115-23-009	115-23-009-D01	7.00	283	9	12	7	5	1.7	N. Mesich
115-23-009	115-23-009-D01	7.00	213	4	12	8	5	1.5	N. Mesich
115-23-009	115-23-009-D01	7.00	200	24	10	7	3	1.4	N. Mesich
115-23-009	115-23-009-D01	7.00	243	22	12	7	4	1.7	N. Mesich
115-23-009	115-23-009-D01	7.00	221	16	26	13	8	2.0	N. Mesich
115-23-009	115-23-009-D01	7.00	261	13	12	7	4	1.7	N. Mesich
115-23-009	115-23-009-D03	13.00	136	2	11	6	4	1.8	M. Gauthier
115-23-009	115-23-009-D03	13.00	165	4	11	5	3	2.2	M. Gauthier
115-23-009	115-23-009-D03	13.00	142	2	6	3	2	2.0	M. Gauthier
115-23-009	115-23-009-D03	13.00	145	12	11	5	2	2.2	M. Gauthier
115-23-009	115-23-009-D03	13.00	348	8	40	18	11	2.2	M. Gauthier
115-23-009	115-23-009-D03	13.00	145	8	40	18	18	2.2	M. Gauthier
115-23-009	115-23-009-D03	13.00	315	18	26	13	8	2.0	M. Gauthier
115-23-009	115-23-009-D03	13.00	348	4	13	8	5	1.6	M. Gauthier
115-23-009	115-23-009-D03	13.00	328	6	15	8	6	1.9	M. Gauthier
115-23-009	115-23-009-D03	13.00	294	2	18	10	4	1.8	M. Gauthier
115-23-009	115-23-009-D03	13.00	330	4	17	10	5	1.7	M. Gauthier
115-23-009	115-23-009-D03	13.00	132	0	15	5	3	3.0	M. Gauthier
115-23-009	115-23-009-D03	13.00	132	6	10	5	2	2.0	M. Gauthier
115-23-009	115-23-009-D03	13.00	296	12	38	20	12	1.9	M. Gauthier

115-23-009	115-23-009-D03	13.00	286	2	10	5	4	2.0	M. Gauthier
115-23-009	115-23-009-D03	13.00	272	20	8	4	2	2.0	M. Gauthier
115-23-009	115-23-009-D03	13.00	314	4	8	4	2	2.0	M. Gauthier
115-23-009	115-23-009-D03	13.00	90	8	7	2	1	3.5	M. Gauthier
115-23-009	115-23-009-D03	13.00	110	4	8	5	4	1.6	M. Gauthier
115-23-009	115-23-009-D03	13.00	292	8	9	4	2	2.3	M. Gauthier
115-23-009	115-23-009-D03	13.00	30	35	25	10	7	2.5	M. Gauthier
115-23-009	115-23-009-D03	13.00	295	16	6	3	2	2.0	M. Gauthier
115-23-009	115-23-009-D03	13.00	302	12	7	3	2	2.3	M. Gauthier
115-23-009	115-23-009-D03	13.00	90	6	17	6	4	2.8	M. Gauthier
115-23-009	115-23-009-D03	13.00	298	6	6	4	3	1.5	M. Gauthier
115-23-009	115-23-009-D05	19.00	360	20	13	8	5	1.6	M. Gauthier
115-23-009	115-23-009-D05	19.00	236	12	10	5	4	2.0	M. Gauthier
115-23-009	115-23-009-D05	19.00	328	18	17	9	6	1.9	M. Gauthier
115-23-009	115-23-009-D05	19.00	178	22	8	4	2	2.0	M. Gauthier
115-23-009	115-23-009-D05	19.00	230	22	13	6	4	2.2	M. Gauthier
115-23-009	115-23-009-D05	19.00	162	16	10	4	1	2.5	M. Gauthier
115-23-009	115-23-009-D05	19.00	150	2	10	5	3	2.0	M. Gauthier
115-23-009	115-23-009-D05	19.00	182	4	12	6	2	2.0	M. Gauthier
115-23-009	115-23-009-D05	19.00	215	6	10	5	3	2.0	M. Gauthier
115-23-009	115-23-009-D05	19.00	135	4	12	5	3	2.4	M. Gauthier
115-23-009	115-23-009-D05	19.00	342	6	10	5	3	2.0	M. Gauthier
115-23-009	115-23-009-D05	19.00	167	2	20	11	8	1.8	M. Gauthier
115-23-009	115-23-009-D05	19.00	75	26	8	4	3	2.0	M. Gauthier
115-23-009	115-23-009-D05	19.00	230	44	11	5	3	2.2	M. Gauthier
115-23-009	115-23-009-D05	19.00	238	22	20	10	5	2.0	M. Gauthier
115-23-009	115-23-009-D05	19.00	7	4	15	6	4	2.5	M. Gauthier
115-23-009	115-23-009-D05	19.00	226	15	17	8	4	2.1	M. Gauthier

115-23-009	115-23-009-D05	19.00	42	26	19	10	4	1.9	M. Gauthier
115-23-009	115-23-009-D05	19.00	184	16	8	4	3	2.0	M. Gauthier
115-23-009	115-23-009-D05	19.00	188	14	38	16	10	2.4	M. Gauthier
115-23-009	115-23-009-D05	19.00	170	25	33	12	12	2.8	M. Gauthier
115-23-009	115-23-009-D05	19.00	195	14	7	4	2	1.8	M. Gauthier
115-23-009	115-23-009-D05	19.00	12	12	11	6	4	1.8	M. Gauthier
115-23-009	115-23-009-D05	19.00	302	22	10	6	4	1.7	M. Gauthier
115-23-009	115-23-009-D05	19.00	334	22	48	23	12	2.1	M. Gauthier
115-23-009	115-23-009-D05	19.00	320	11	25	12	6	2.1	M. Gauthier
115-23-009	115-23-009-D05	19.00	340	20	11	5	3	2.2	M. Gauthier
115-23-009	115-23-009-D05	19.00	352	26	16	10	7	1.6	M. Gauthier
115-23-009	115-23-009-D05	19.00	346	34	11	7	7	1.6	M. Gauthier
115-23-009	115-23-009-D05	19.00	332	22	12	6	4	2.0	M. Gauthier
115-23-009	115-23-009-D07	22.80	276	6	100	50	35	2.0	M. Gauthier
115-23-009	115-23-009-D07	22.80	150	20	22	11	6	2.0	M. Gauthier
115-23-009	115-23-009-D07	22.80	240	8	95	50	35	1.9	M. Gauthier
115-23-009	115-23-009-D07	22.80	358	4	30	19	4	1.6	M. Gauthier
115-23-009	115-23-009-D07	22.80	208	20	17	8	4	2.1	M. Gauthier
115-23-009	115-23-009-D07	22.80	152	38	16	11	6	1.5	M. Gauthier
115-23-009	115-23-009-D07	22.80	96	20	20	10	6	2.0	M. Gauthier
115-23-009	115-23-009-D07	22.80	158	20	13	6	4	2.2	M. Gauthier
115-23-009	115-23-009-D07	22.80	168	14	13	6	4	2.2	M. Gauthier
115-23-009	115-23-009-D07	22.80	278	20	6	3	2	2.0	M. Gauthier
115-23-009	115-23-009-D07	22.80	142	10	16	8	4	2.0	M. Gauthier
115-23-009	115-23-009-D07	22.80	258	22	30	13	10	2.3	M. Gauthier
115-23-009	115-23-009-D07	22.80	126	14	38	20	10	1.9	M. Gauthier
115-23-009	115-23-009-D07	22.80	258	18	36	25	23	1.4	M. Gauthier
115-23-009	115-23-009-D07	22.80	50	4	14	9	6	1.6	M. Gauthier

115-23-009	115-23-009-D07	22.80	152	2	15	7	5	2.1	M. Gauthier
115-23-009	115-23-009-D07	22.80	332	6	19	11	7	1.7	M. Gauthier
115-23-009	115-23-009-D07	22.80	148	4	28	15	5	1.9	M. Gauthier
115-23-009	115-23-009-D07	22.80	168	6	18	12	6	1.5	M. Gauthier
115-23-009	115-23-009-D07	22.80	108	24	12	7	4	1.7	M. Gauthier
115-23-009	115-23-009-D07	22.80	110	6	10	5	2	2.0	M. Gauthier
115-23-009	115-23-009-D07	22.80	146	2	12	6	2	2.0	M. Gauthier
115-23-009	115-23-009-D07	22.80	182	16	7	4	2	1.8	M. Gauthier
115-23-009	115-23-009-D07	22.80	310	6	37	20	15	1.9	M. Gauthier
115-23-009	115-23-009-D07	22.80	258	6	17	10	4	1.7	M. Gauthier
115-23-009	115-23-009-D07	22.80	170	4	17	10	2	1.7	M. Gauthier
115-23-009	115-23-009-D07	22.80	52	2	13	6	5	2.2	M. Gauthier
115-23-009	115-23-009-D07	22.80	148	28	22	11	6	2.0	M. Gauthier
115-23-009	115-23-009-D07	22.80	156	20	24	13	7	1.8	M. Gauthier
115-23-009	115-23-009-D07	22.80	146	26	11	6	4	1.8	M. Gauthier
115-23-009	115-23-009-D07	22.80	155	8	10	5	2	2.0	M. Gauthier
115-23-009	115-23-009-D07	22.80	322	16	16	7	6	2.3	M. Gauthier
115-23-009	115-23-009-D07	22.80	136	10	10	5	2	2.0	M. Gauthier
115-23-009	115-23-009-D07	22.80	328	20	10	4	2	2.5	M. Gauthier
115-23-009	115-23-009-D07	22.80	82	4	18	10	6	1.8	M. Gauthier
115-23-009	115-23-009-E01	25.10	322	40	26	14	8	1.9	M. Gauthier
115-23-009	115-23-009-E01	25.10	182	6	20	11	10	1.8	M. Gauthier
115-23-009	115-23-009-E01	25.10	225	8	12	10	6	1.2	M. Gauthier
115-23-009	115-23-009-E01	25.10	230	7	15	8	4	1.9	M. Gauthier
115-23-009	115-23-009-E01	25.10	240	2	16	8	4	2.0	M. Gauthier
115-23-009	115-23-009-E01	25.10	270	4	16	10	5	1.6	M. Gauthier
115-23-009	115-23-009-E01	25.10	160	30	10	3	3	3.3	M. Gauthier
115-23-009	115-23-009-E01	25.10	164	30	24	15	5	1.6	M. Gauthier

115-23-009	115-23-009-E01	25.10	62	12	22	11	5	2.0	M. Gauthier
115-23-009	115-23-009-E01	25.10	90	8	12	6	4	2.0	M. Gauthier
115-23-009	115-23-009-E01	25.10	108	8	9	5	2	1.8	M. Gauthier
115-23-009	115-23-009-E01	25.10	200	6	110	60	32	1.8	M. Gauthier
115-23-009	115-23-009-E01	25.10	260	4	21	13	6	1.6	M. Gauthier
115-23-009	115-23-009-E01	25.10	250	18	50	25	12	2.0	M. Gauthier
115-23-009	115-23-009-E01	25.10	16	4	60	25	8	2.4	M. Gauthier
115-23-009	115-23-009-E01	25.10	175	12	12	6	2	2.0	M. Gauthier
115-23-009	115-23-009-E01	25.10	138	18	9	4	2	2.3	M. Gauthier
115-23-009	115-23-009-E01	25.10	48	6	12	6	4	2.0	M. Gauthier
115-23-009	115-23-009-E01	25.10	172	26	17	10	4	1.7	M. Gauthier
115-23-009	115-23-009-E01	25.10	90	2	40	20	15	2.0	M. Gauthier
115-23-009	115-23-009-E01	25.10	126	8	20	12	5	1.7	M. Gauthier
115-23-009	115-23-009-E01	25.10	250	10	14	8	4	1.8	M. Gauthier
115-23-009	115-23-009-E01	25.10	234	22	55	37	8	1.5	M. Gauthier
115-23-009	115-23-009-E01	25.10	138	14	17	10	2	1.7	M. Gauthier
115-23-009	115-23-009-E01	25.10	105	28	7	4	1	1.8	M. Gauthier
115-23-009	115-23-009-G01	26.95	247	7	35	20	7	1.8	T. Hodder
115-23-009	115-23-009-G01	26.95	33	10	11	7	4	1.6	T. Hodder
115-23-009	115-23-009-G01	26.95	205	2	25	12	10	2.1	T. Hodder
115-23-009	115-23-009-G01	26.95	52	10	15	10	7	1.5	T. Hodder
115-23-009	115-23-009-G01	26.95	28	30	24	15	10	1.6	T. Hodder
115-23-009	115-23-009-G01	26.95	35	38	27	15	8	1.8	T. Hodder
115-23-009	115-23-009-G01	26.95	64	22	25	16	10	1.6	T. Hodder
115-23-009	115-23-009-G01	26.95	258	20	7	3	2	2.3	T. Hodder
115-23-009	115-23-009-G01	26.95	225	10	15	10	7	1.5	T. Hodder
115-23-009	115-23-009-G01	26.95	215	23	13	6	4	2.2	T. Hodder
115-23-009	115-23-009-G01	26.95	190	10	17	9	6	1.9	T. Hodder

115-23-009	115-23-009-G01	26.95	216	8	22	12	11	1.8	T. Hodder
115-23-009	115-23-009-G01	26.95	228	9	11	5	3	2.2	T. Hodder
115-23-009	115-23-009-G01	26.95	212	8	17	10	6	1.7	T. Hodder
115-23-009	115-23-009-G01	26.95	216	5	25	15	12	1.7	T. Hodder
115-23-009	115-23-009-G01	26.95	219	5	25	15	7	1.7	T. Hodder
115-23-009	115-23-009-G01	26.95	60	2	22	14	10	1.6	T. Hodder
115-23-009	115-23-009-G01	26.95	208	12	15	10	4	1.5	T. Hodder
115-23-009	115-23-009-G01	26.95	38	2	11	7	4	1.6	T. Hodder
115-23-009	115-23-009-G01	26.95	188	10	33	10	5	3.3	T. Hodder
115-23-009	115-23-009-G01	26.95	25	11	35	22	14	1.6	T. Hodder
115-23-009	115-23-009-G01	26.95	250	7	33	18	15	1.8	T. Hodder
115-23-009	115-23-009-G01	26.95	220	5	10	6	5	1.7	T. Hodder
115-23-009	115-23-009-G01	26.95	20	9	14	9	3	1.6	T. Hodder
115-23-009	115-23-009-G01	26.95	225	15	18	11	9	1.6	T. Hodder
115-23-009	115-23-009-G01	26.95	60	4	17	11	6	1.5	T. Hodder
115-23-009	115-23-009-G01	26.95	240	17	10	6	4	1.7	T. Hodder
115-23-009	115-23-009-G01	26.95	45	26	60	40	15	1.5	T. Hodder
115-23-009	115-23-009-G01	26.95	60	5	15	8	5	1.9	T. Hodder
115-23-009	115-23-009-G01	26.95	215	10	12	8	4	1.5	T. Hodder
115-23-009	115-23-009-J01	32.45	50	2	14	8	6	1.8	M. Gauthier
115-23-009	115-23-009-J01	32.45	68	14	36	24	6	1.5	M. Gauthier
115-23-009	115-23-009-J01	32.45	252	8	35	20	12	1.8	M. Gauthier
115-23-009	115-23-009-J01	32.45	96	4	9	6	3	1.5	M. Gauthier
115-23-009	115-23-009-J01	32.45	82	22	12	8	2	1.5	M. Gauthier
115-23-009	115-23-009-J01	32.45	84	4	17	10	4	1.7	M. Gauthier
115-23-009	115-23-009-J01	32.45	130	16	17	9	5	1.9	M. Gauthier
115-23-009	115-23-009-J01	32.45	258	12	28	18	12	1.6	M. Gauthier
115-23-009	115-23-009-J01	32.45	268	26	18	12	8	1.5	M. Gauthier

115-23-009	115-23-009-J01	32.45	274	22	8	5	3	1.6	M. Gauthier
115-23-009	115-23-009-J01	32.45	52	16	9	6	2	1.5	M. Gauthier
115-23-009	115-23-009-J01	32.45	262	14	20	10	10	2.0	M. Gauthier
115-23-009	115-23-009-J01	32.45	275	30	13	6	5	2.2	M. Gauthier
115-23-009	115-23-009-J01	32.45	255	6	16	7	5	2.3	M. Gauthier
115-23-009	115-23-009-J01	32.45	350	22	52	20	15	2.6	M. Gauthier
115-23-009	115-23-009-J01	32.45	110	6	11	6	3	1.8	M. Gauthier
115-23-009	115-23-009-J01	32.45	275	34	11	6	4	1.8	M. Gauthier
115-23-009	115-23-009-J01	32.45	84	32	11	6	5	1.8	M. Gauthier
115-23-009	115-23-009-J01	32.45	115	8	12	7	3	1.7	M. Gauthier
115-23-009	115-23-009-J01	32.45	250	20	11	5	3	2.2	M. Gauthier
115-23-009	115-23-009-J01	32.45	86	45	9	6	2	1.5	M. Gauthier
115-23-009	115-23-009-J01	32.45	266	40	7	3	2	2.3	M. Gauthier
115-23-009	115-23-009-J01	32.45	72	10	10	5	5	2.0	M. Gauthier
115-23-009	115-23-009-J01	32.45	66	9	15	8	6	1.9	M. Gauthier
115-23-009	115-23-009-J01	32.45	264	8	8	3	1	2.7	M. Gauthier
115-23-009	115-23-009-J01	32.45	64	10	11	7	4	1.6	M. Gauthier
115-23-009	115-23-009-K02	37.30	220	37	13	8	4	1.6	T. Hodder
115-23-009	115-23-009-K02	37.30	152	12	10	6	5	1.7	T. Hodder
115-23-009	115-23-009-K02	37.30	44	18	22	14	10	1.6	T. Hodder
115-23-009	115-23-009-K02	37.30	240	10	12	4	3	3.0	T. Hodder
115-23-009	115-23-009-K02	37.30	270	7	22	13	8	1.7	T. Hodder
115-23-009	115-23-009-K02	37.30	245	1	21	13	11	1.6	T. Hodder
115-23-009	115-23-009-K02	37.30	47	17	12	8	3	1.5	T. Hodder
115-23-009	115-23-009-K02	37.30	235	24	10	6	2	1.7	T. Hodder
115-23-009	115-23-009-K02	37.30	25	20	13	7	5	1.9	T. Hodder
115-23-009	115-23-009-K02	37.30	58	2	10	6	5	1.7	T. Hodder
115-23-009	115-23-009-K02	37.30	235	35	23	10	8	2.3	T. Hodder

115-23-009	115-23-009-K02	37.30	220	32	9	6	2	1.5	T. Hodder
115-23-009	115-23-009-K02	37.30	260	20	12	7	4	1.7	T. Hodder
115-23-009	115-23-009-K02	37.30	210	22	13	5	4	2.6	T. Hodder
115-23-009	115-23-009-K02	37.30	223	12	13	8	6	1.6	T. Hodder
115-23-009	115-23-009-K02	37.30	245	25	16	10	7	1.6	T. Hodder
115-23-009	115-23-009-K02	37.30	262	4	8	3	2	2.7	T. Hodder
115-23-009	115-23-009-K02	37.30	234	15	16	10	5	1.6	T. Hodder
115-23-009	115-23-009-K02	37.30	76	5	17	8	6	2.1	T. Hodder
115-23-009	115-23-009-K02	37.30	33	4	13	8	4	1.6	T. Hodder
115-23-009	115-23-009-K02	37.30	208	6	15	10	8	1.5	T. Hodder
115-23-009	115-23-009-K02	37.30	236	22	7	4	3	1.8	T. Hodder
115-23-009	115-23-009-K02	37.30	240	18	17	9	8	1.9	T. Hodder
115-23-009	115-23-009-K02	37.30	222	23	25	16	7	1.6	T. Hodder
115-23-009	115-23-009-K02	37.30	221	7	38	25	17	1.5	T. Hodder
115-23-009	115-23-009-K02	37.30	88	7	19	7	5	2.7	T. Hodder
115-23-009	115-23-009-K02	37.30	251	15	27	15	12	1.8	T. Hodder
115-23-009	115-23-009-K02	37.30	214	24	8	5	2	1.6	T. Hodder
115-23-009	115-23-009-K02	37.30	210	22	15	8	5	1.9	T. Hodder
115-23-009	115-23-009-K02	37.30	247	34	17	10	9	1.7	T. Hodder
115-23-009	115-23-009-K04	43.35	179	39	88	56	39	1.6	N. Mesich
115-23-009	115-23-009-K04	43.35	186	30	10	6	3	1.7	N. Mesich
115-23-009	115-23-009-K04	43.35	126	11	18	10	5	1.8	N. Mesich
115-23-009	115-23-009-K04	43.35	352	46	32	20	15	1.6	N. Mesich
115-23-009	115-23-009-K04	43.35	209	19	15	10	6	1.5	N. Mesich
115-23-009	115-23-009-K04	43.35	166	17	18	12	7	1.5	N. Mesich
115-23-009	115-23-009-K04	43.35	225	55	10	5	1	2.0	N. Mesich
115-23-009	115-23-009-K04	43.35	41	52	18	13	8	1.4	N. Mesich
115-23-009	115-23-009-K04	43.35	124	13	17	8	5	2.1	N. Mesich

115-23-009	115-23-009-K04	43.35	149	39	20	11	10	1.8	N. Mesich
115-23-009	115-23-009-K04	43.35	330	4	16	11	7	1.5	N. Mesich
115-23-009	115-23-009-K04	43.35	64	6	20	14	9	1.4	N. Mesich
115-23-009	115-23-009-K04	43.35	101	19	7	5	3	1.4	N. Mesich
115-23-009	115-23-009-K04	43.35	171	18	10	6	4	1.7	N. Mesich
115-23-009	115-23-009-K04	43.35	347	30	17	10	8	1.7	N. Mesich
115-23-009	115-23-009-K04	43.35	232	20	18	12	8	1.5	T. Hodder
115-23-009	115-23-009-K04	43.35	275	22	15	10	7	1.5	T. Hodder
115-23-009	115-23-009-K04	43.35	270	23	9	5	3	1.8	T. Hodder
115-23-009	115-23-009-K04	43.35	295	18	13	10	6	1.3	T. Hodder
115-23-009	115-23-009-K04	43.35	262	17	13	9	7	1.4	T. Hodder
115-23-009	115-23-009-K04	43.35	275	24	17	7	6	2.4	T. Hodder
115-23-009	115-23-009-K04	43.35	305	4	22	15	8	1.5	T. Hodder
115-23-009	115-23-009-K04	43.35	311	22	37	24	16	1.5	T. Hodder
115-23-009	115-23-009-K04	43.35	305	12	21	14	11	1.5	T. Hodder
115-23-009	115-23-009-K04	43.35	282	24	13	7	5	1.9	T. Hodder
115-23-009	115-23-009-K04	43.35	294	41	17	11	9	1.5	T. Hodder
115-23-009	115-23-009-K04	43.35	282	19	14	9	4	1.6	T. Hodder
115-23-009	115-23-009-K04	43.35	80	15	14	9	6	1.6	T. Hodder
115-23-009	115-23-009-K04	43.35	168	18	13	8	5	1.6	M. Gauthier
115-23-009	115-23-009-K04	43.35	162	30	35	20	8	1.8	M. Gauthier
115-23-009	115-23-009-K04	43.35	158	24	12	6	2	2.0	M. Gauthier
115-23-009	115-23-009-K04	43.35	294	4	24	14	4	1.7	M. Gauthier
115-23-009	115-23-009-K04	43.35	7	8	20	10	6	2.0	M. Gauthier
115-23-009	115-23-009-K04	43.35	120	44	21	12	7	1.8	M. Gauthier
115-23-009	115-23-009-K04	43.35	302	10	6	4	2	1.5	M. Gauthier
115-23-009	115-23-009-K04	43.35	297	12	10	5	3	2.0	M. Gauthier
115-23-009	115-23-009-K04	43.35	294	6	17	11	4	1.5	M. Gauthier

115-23-009	115-23-009-K04	43.35	285	18	7	2	1	3.5	M. Gauthier
115-23-009	115-23-009-K04	43.35	295	8	10	5	3	2.0	M. Gauthier
115-23-009	115-23-009-K04	43.35	296	8	7	4	2	1.8	M. Gauthier
112-19-629	112-19-629-A01	15.1	145	17	20	10	3	2.0	Hodder and Gauthier (2022)
112-19-629	112-19-629-A01	15.1	205	33	25	15	5	1.7	Hodder and Gauthier (2022)
112-19-629	112-19-629-A01	15.1	15	24	25	12	8	2.1	Hodder and Gauthier (2022)
112-19-629	112-19-629-A01	15.1	110	3	10	5	4	2.0	Hodder and Gauthier (2022)
112-19-629	112-19-629-A01	15.1	150	22	12	7	4	1.7	Hodder and Gauthier (2022)
112-19-629	112-19-629-A01	15.1	165	24	20	8	7	2.5	Hodder and Gauthier (2022)
112-19-629	112-19-629-A01	15.1	335	33	16	10	5	1.6	Hodder and Gauthier (2022)
112-19-629	112-19-629-A01	15.1	148	28	20	11	7	1.8	Hodder and Gauthier (2022)
112-19-629	112-19-629-A01	15.1	172	18	21	14	6	1.5	Hodder and Gauthier (2022)
112-19-629	112-19-629-A01	15.1	145	20	40	25	11	1.6	Hodder and Gauthier (2022)
112-19-629	112-19-629-A01	15.1	112	5	20	10	8	2.0	Hodder and Gauthier (2022)
112-19-629	112-19-629-A01	15.1	130	6	15	10	5	1.5	Hodder and Gauthier (2022)
112-19-629	112-19-629-A01	15.1	140	5	21	14	9	1.5	Hodder and Gauthier (2022)
112-19-629	112-19-629-A01	15.1	120	15	30	20	12	1.5	Hodder and Gauthier (2022)
112-19-629	112-19-629-A01	15.1	131	10	15	8	5	1.9	Hodder and Gauthier (2022)
112-19-629	112-19-629-A01	15.1	315	5	30	13	10	2.3	Hodder and Gauthier (2022)
112-19-629	112-19-629-A01	15.1	110	10	10	5	4	2.0	Hodder and Gauthier (2022)
112-19-629	112-19-629-A01	15.1	128	37	18	12	2	1.5	Hodder and Gauthier (2022)
112-19-629	112-19-629-A01	15.1	122	30	16	8	6	2.0	Hodder and Gauthier (2022)
112-19-629	112-19-629-A01	15.1	15	5	28	16	10	1.8	Hodder and Gauthier (2022)
112-19-629	112-19-629-A01	15.1	180	16	11	6	4	1.8	Hodder and Gauthier (2022)
112-19-629	112-19-629-A01	15.1	318	16	22	11	6	2.0	Hodder and Gauthier (2022)
112-19-629	112-19-629-A01	15.1	142	10	8	4	2	2.0	Hodder and Gauthier (2022)
112-19-629	112-19-629-A01	15.1	252	11	18	10	4	1.8	Hodder and Gauthier (2022)
112-19-629	112-19-629-A01	15.1	104	4	8	5	5	1.6	Hodder and Gauthier (2022)

112-19-629	112-19-629-A01	15.1	120	2	17	7	6	2.4	Hodder and Gauthier (2022)
112-19-629	112-19-629-A01	15.1	168	10	20	9	6	2.2	Hodder and Gauthier (2022)
112-19-629	112-19-629-A01	15.1	152	14	32	12	8	2.7	Hodder and Gauthier (2022)
112-19-629	112-19-629-A01	15.1	242	4	15	8	2	1.9	Hodder and Gauthier (2022)
112-19-629	112-19-629-A01	15.1	270	6	8	3	3	2.7	Hodder and Gauthier (2022)
112-19-629	112-19-629-A01	15.1	200	22	26	14	12	1.9	Hodder and Gauthier (2022)
112-19-629	112-19-629-A01	15.1	80	22	14	7	3	2.0	Hodder and Gauthier (2022)
112-19-629	112-19-629-A01	15.1	300	6	55	25	14	2.2	Hodder and Gauthier (2022)
112-19-629	112-19-629-A01	15.1	302	20	8	5	2	1.6	Hodder and Gauthier (2022)
112-19-629	112-19-629-A01	15.1	230	16	37	18	10	2.1	Hodder and Gauthier (2022)
112-19-629	112-19-629-A01	15.1	222	14	62	35	8	1.8	Hodder and Gauthier (2022)
112-19-629	112-19-629-A01	15.1	240	16	17	10	7	1.7	Hodder and Gauthier (2022)
112-19-629	112-19-629-A01	15.1	280	24	17	9	6	1.9	Hodder and Gauthier (2022)
112-19-629	112-19-629-C01	18.0	58	22	14	6	4	2.3	Hodder and Gauthier (2022)
112-19-629	112-19-629-C01	18.0	62	2	17	6	5	2.8	Hodder and Gauthier (2022)
112-19-629	112-19-629-C01	18.0	238	30	6	3	3	2.0	Hodder and Gauthier (2022)
112-19-629	112-19-629-C01	18.0	208	2	7	3	2	2.3	Hodder and Gauthier (2022)
112-19-629	112-19-629-C01	18.0	232	18	15	7	5	2.1	Hodder and Gauthier (2022)
112-19-629	112-19-629-C01	18.0	45	24	14	8	4	1.8	Hodder and Gauthier (2022)
112-19-629	112-19-629-C01	18.0	255	32	13	6	5	2.2	Hodder and Gauthier (2022)
112-19-629	112-19-629-C01	18.0	85	12	12	5	3	2.4	Hodder and Gauthier (2022)
112-19-629	112-19-629-C01	18.0	238	5	6	3	2	2.0	Hodder and Gauthier (2022)
112-19-629	112-19-629-C01	18.0	228	42	13	6	6	2.2	Hodder and Gauthier (2022)
112-19-629	112-19-629-C01	18.0	222	2	21	6	4	3.5	Hodder and Gauthier (2022)
112-19-629	112-19-629-C01	18.0	212	28	4	2	1	2.0	Hodder and Gauthier (2022)
112-19-629	112-19-629-C01	18.0	208	30	6	2	2	3.0	Hodder and Gauthier (2022)
112-19-629	112-19-629-C01	18.0	212	8	18	6	3	3.0	Hodder and Gauthier (2022)
112-19-629	112-19-629-C01	18.0	212	8	12	6	5	2.0	Hodder and Gauthier (2022)

112-19-629	112-19-629-C01	18.0	242	8	17	11	3	1.5	Hodder and Gauthier (2022)
112-19-629	112-19-629-C01	18.0	220	10	8	4	3	2.0	Hodder and Gauthier (2022)
112-19-629	112-19-629-C01	18.0	0	50	9	5	3	1.8	Hodder and Gauthier (2022)
112-19-629	112-19-629-C01	18.0	218	16	12	6	2	2.0	Hodder and Gauthier (2022)
112-19-629	112-19-629-C01	18.0	216	8	30	20	8	1.5	Hodder and Gauthier (2022)
112-19-629	112-19-629-C01	18.0	38	16	35	20	10	1.8	Hodder and Gauthier (2022)
112-19-629	112-19-629-C01	18.0	222	28	15	8	6	1.9	Hodder and Gauthier (2022)
112-19-629	112-19-629-C01	18.0	28	42	10	6	2	1.7	Hodder and Gauthier (2022)
112-19-629	112-19-629-C01	18.0	208	16	11	6	4	1.8	Hodder and Gauthier (2022)
112-19-629	112-19-629-C01	18.0	216	6	14	8	6	1.8	Hodder and Gauthier (2022)
112-19-629	112-19-629-C01	18.0	196	20	31	15	14	2.1	Hodder and Gauthier (2022)
112-19-629	112-19-629-C01	18.0	208	14	10	6	2	1.7	Hodder and Gauthier (2022)
112-19-629	112-19-629-C01	18.0	208	36	5	2	2	2.5	Hodder and Gauthier (2022)
112-19-629	112-19-629-C01	18.0	2	44	14	8	6	1.8	Hodder and Gauthier (2022)
112-19-629	112-19-629-C01	18.0	196	18	8	4	4	2.0	Hodder and Gauthier (2022)
112-22-200	112-22-200-A01	0.9	235	2	12	8	4	1.5	Hodder and Gauthier (2022)
112-22-200	112-22-200-A01	0.9	240	14	33	20	10	1.7	Hodder and Gauthier (2022)
112-22-200	112-22-200-A01	0.9	295	12	20	13	8	1.5	Hodder and Gauthier (2022)
112-22-200	112-22-200-A01	0.9	245	9	14	6	2	2.3	Hodder and Gauthier (2022)
112-22-200	112-22-200-A01	0.9	195	10	14	8	3	1.8	Hodder and Gauthier (2022)
112-22-200	112-22-200-A01	0.9	65	22	43	20	16	2.2	Hodder and Gauthier (2022)
112-22-200	112-22-200-A01	0.9	106	2	12	6	4	2.0	Hodder and Gauthier (2022)
112-22-200	112-22-200-A01	0.9	133	2	20	12	4	1.7	Hodder and Gauthier (2022)
112-22-200	112-22-200-A01	0.9	280	5	15	8	5	1.9	Hodder and Gauthier (2022)
112-22-200	112-22-200-A01	0.9	304	32	25	15	10	1.7	Hodder and Gauthier (2022)
112-22-200	112-22-200-A01	0.9	266	5	15	10	6	1.5	Hodder and Gauthier (2022)
112-22-200	112-22-200-A01	0.9	250	4	35	20	18	1.8	Hodder and Gauthier (2022)
112-22-200	112-22-200-A01	0.9	138	16	16	7	3	2.3	Hodder and Gauthier (2022)

112-22-200	112-22-200-A01	0.9	142	22	12	6	2	2.0	Hodder and Gauthier (2022)
112-22-200	112-22-200-A01	0.9	277	14	11	6	5	1.8	Hodder and Gauthier (2022)
112-22-200	112-22-200-A01	0.9	115	26	12	6	5	2.0	Hodder and Gauthier (2022)
112-22-200	112-22-200-A01	0.9	330	10	16	8	5	2.0	Hodder and Gauthier (2022)
112-22-200	112-22-200-A01	0.9	115	0	13	8	3	1.6	Hodder and Gauthier (2022)
112-22-200	112-22-200-A01	0.9	275	13	17	10	4	1.7	Hodder and Gauthier (2022)
112-22-200	112-22-200-A01	0.9	66	3	17	10	9	1.7	Hodder and Gauthier (2022)
112-22-200	112-22-200-A01	0.9	270	6	23	15	9	1.5	Hodder and Gauthier (2022)
112-22-200	112-22-200-A01	0.9	115	17	10	6	4	1.7	Hodder and Gauthier (2022)
112-22-200	112-22-200-A01	0.9	75	24	12	6	3	2.0	Hodder and Gauthier (2022)
112-22-200	112-22-200-A01	0.9	270	12	16	7	5	2.3	Hodder and Gauthier (2022)
112-22-200	112-22-200-A01	0.9	81	4	18	12	6	1.5	Hodder and Gauthier (2022)
112-22-200	112-22-200-A01	0.9	281	14	14	9	4	1.6	Hodder and Gauthier (2022)
112-22-200	112-22-200-A01	0.9	145	22	10	5	4	2.0	Hodder and Gauthier (2022)
112-22-200	112-22-200-A01	0.9	278	1	19	10	5	1.9	Hodder and Gauthier (2022)
112-22-200	112-22-200-A01	0.9	103	35	20	10	6	2.0	Hodder and Gauthier (2022)
112-22-200	112-22-200-A01	0.9	289	5	14	7	6	2.0	Hodder and Gauthier (2022)
112-22-200	112-22-200-B01	2.5	105	20	21	14	10	1.5	Hodder and Gauthier (2022)
112-22-200	112-22-200-B01	2.5	95	12	15	8	5	1.9	Hodder and Gauthier (2022)
112-22-200	112-22-200-B01	2.5	135	10	18	12	8	1.5	Hodder and Gauthier (2022)
112-22-200	112-22-200-B01	2.5	98	28	11	6	4	1.8	Hodder and Gauthier (2022)
112-22-200	112-22-200-B01	2.5	111	7	20	13	8	1.5	Hodder and Gauthier (2022)
112-22-200	112-22-200-B01	2.5	82	14	11	5	4	2.2	Hodder and Gauthier (2022)
112-22-200	112-22-200-B01	2.5	296	10	13	7	5	1.9	Hodder and Gauthier (2022)
112-22-200	112-22-200-B01	2.5	80	10	15	10	5	1.5	Hodder and Gauthier (2022)
112-22-200	112-22-200-B01	2.5	274	2	20	12	5	1.7	Hodder and Gauthier (2022)
112-22-200	112-22-200-B01	2.5	58	12	35	22	11	1.6	Hodder and Gauthier (2022)
112-22-200	112-22-200-B01	2.5	95	15	19	11	10	1.7	Hodder and Gauthier (2022)

112-22-200	112-22-200-B01	2.5	75	14	33	20	16	1.7	Hodder and Gauthier (2022)
112-22-200	112-22-200-B01	2.5	118	14	14	6	5	2.3	Hodder and Gauthier (2022)
112-22-200	112-22-200-B01	2.5	95	15	17	10	5	1.7	Hodder and Gauthier (2022)
112-22-200	112-22-200-B01	2.5	315	22	18	12	6	1.5	Hodder and Gauthier (2022)
112-22-200	112-22-200-B01	2.5	135	22	16	10	2	1.6	Hodder and Gauthier (2022)
112-22-200	112-22-200-B01	2.5	82	26	20	12	8	1.7	Hodder and Gauthier (2022)
112-22-200	112-22-200-B01	2.5	125	20	21	14	9	1.5	Hodder and Gauthier (2022)
112-22-200	112-22-200-B01	2.5	94	3	21	9	5	2.3	Hodder and Gauthier (2022)
112-22-200	112-22-200-B01	2.5	216	20	17	10	5	1.7	Hodder and Gauthier (2022)
112-22-200	112-22-200-B01	2.5	68	30	15	10	5	1.5	Hodder and Gauthier (2022)
112-22-200	112-22-200-B01	2.5	272	36	33	20	8	1.7	Hodder and Gauthier (2022)
112-22-200	112-22-200-B01	2.5	135	12	40	25	20	1.6	Hodder and Gauthier (2022)
112-22-200	112-22-200-B01	2.5	106	2	26	15	8	1.7	Hodder and Gauthier (2022)
112-22-200	112-22-200-B01	2.5	85	30	11	5	5	2.2	Hodder and Gauthier (2022)
112-22-200	112-22-200-B01	2.5	115	22	33	20	14	1.7	Hodder and Gauthier (2022)
112-22-200	112-22-200-B01	2.5	130	5	30	20	12	1.5	Hodder and Gauthier (2022)
112-22-200	112-22-200-B01	2.5	78	10	35	17	12	2.1	Hodder and Gauthier (2022)
112-22-200	112-22-200-B01	2.5	75	3	23	11	10	2.1	Hodder and Gauthier (2022)
112-22-200	112-22-200-B01	2.5	110	22	42	25	15	1.7	Hodder and Gauthier (2022)
112-22-200	112-22-200-C01	4.2	225	8	14	7	2	2.0	Hodder and Gauthier (2022)
112-22-200	112-22-200-C01	4.2	170	14	14	8	6	1.8	Hodder and Gauthier (2022)
112-22-200	112-22-200-C01	4.2	68	17	7	4	2	1.8	Hodder and Gauthier (2022)
112-22-200	112-22-200-C01	4.2	72	8	17	8	7	2.1	Hodder and Gauthier (2022)
112-22-200	112-22-200-C01	4.2	84	14	17	10	4	1.7	Hodder and Gauthier (2022)
112-22-200	112-22-200-C01	4.2	81	25	9	5	2	1.8	Hodder and Gauthier (2022)
112-22-200	112-22-200-C01	4.2	54	14	25	9	7	2.8	Hodder and Gauthier (2022)
112-22-200	112-22-200-C01	4.2	58	24	40	22	8	1.8	Hodder and Gauthier (2022)
112-22-200	112-22-200-C01	4.2	302	36	20	11	6	1.8	Hodder and Gauthier (2022)

112-22-200	112-22-200-C01	4.2	88	4	13	6	6	2.2	Hodder and Gauthier (2022)
112-22-200	112-22-200-C01	4.2	202	20	21	14	7	1.5	Hodder and Gauthier (2022)
112-22-200	112-22-200-C01	4.2	246	12	22	11	11	2.0	Hodder and Gauthier (2022)
112-22-200	112-22-200-C01	4.2	2	32	19	11	4	1.7	Hodder and Gauthier (2022)
112-22-200	112-22-200-C01	4.2	239	6	8	2	2	4.0	Hodder and Gauthier (2022)
112-22-200	112-22-200-C01	4.2	258	8	14	6	6	2.3	Hodder and Gauthier (2022)
112-22-200	112-22-200-C01	4.2	62	22	14	8	6	1.8	Hodder and Gauthier (2022)
112-22-200	112-22-200-C01	4.2	192	35	12	5	5	2.4	Hodder and Gauthier (2022)
112-22-200	112-22-200-C01	4.2	196	12	8	4	4	2.0	Hodder and Gauthier (2022)
112-22-200	112-22-200-C01	4.2	202	42	30	12	12	2.5	Hodder and Gauthier (2022)
112-22-200	112-22-200-C01	4.2	212	24	12	5	3	2.4	Hodder and Gauthier (2022)
112-22-200	112-22-200-C01	4.2	214	18	7	4	4	1.8	Hodder and Gauthier (2022)
112-22-200	112-22-200-C01	4.2	42	14	9	6	4	1.5	Hodder and Gauthier (2022)
112-22-200	112-22-200-C01	4.2	246	6	8	4	3	2.0	Hodder and Gauthier (2022)
112-22-200	112-22-200-C01	4.2	229	16	16	6	6	2.7	Hodder and Gauthier (2022)
112-22-200	112-22-200-C01	4.2	185	56	15	8	5	1.9	Hodder and Gauthier (2022)
112-22-200	112-22-200-C01	4.2	208	26	15	6	4	2.5	Hodder and Gauthier (2022)
112-22-200	112-22-200-C01	4.2	180	26	15	10	5	1.5	Hodder and Gauthier (2022)
112-22-200	112-22-200-C01	4.2	75	8	14	7	7	2.0	Hodder and Gauthier (2022)
112-22-200	112-22-200-C01	4.2	189	46	20	11	6	1.8	Hodder and Gauthier (2022)
112-22-200	112-22-200-C01	4.2	205	42	16	10	3	1.6	Hodder and Gauthier (2022)
112-22-200	112-22-200-C01	4.2	212	20	10	6	4	1.7	Hodder and Gauthier (2022)
112-22-200	112-22-200-C01	4.2	190	22	27	15	13	1.8	Hodder and Gauthier (2022)
112-22-200	112-22-200-C01	4.2	38	17	14	6	3	2.3	Hodder and Gauthier (2022)
112-22-200	112-22-200-C01	4.2	210	15	12	6	4	2.0	Hodder and Gauthier (2022)
112-22-200	112-22-200-C01	4.2	208	18	31	16	7	1.9	Hodder and Gauthier (2022)
112-22-200	112-22-200-C02	7.2	204	6	27	16	10	1.7	Hodder and Gauthier (2022)
112-22-200	112-22-200-C02	7.2	220	6	40	24	10	1.7	Hodder and Gauthier (2022)

112-22-200	112-22-200-C02	7.2	208	22	22	12	8	1.8	Hodder and Gauthier (2022)
112-22-200	112-22-200-C02	7.2	180	18	12	6	4	2.0	Hodder and Gauthier (2022)
112-22-200	112-22-200-C02	7.2	200	4	12	7	6	1.7	Hodder and Gauthier (2022)
112-22-200	112-22-200-C02	7.2	48	2	17	11	8	1.5	Hodder and Gauthier (2022)
112-22-200	112-22-200-C02	7.2	98	24	14	8	4	1.8	Hodder and Gauthier (2022)
112-22-200	112-22-200-C02	7.2	15	32	14	6	6	2.3	Hodder and Gauthier (2022)
112-22-200	112-22-200-C02	7.2	14	20	11	6	4	1.8	Hodder and Gauthier (2022)
112-22-200	112-22-200-C02	7.2	26	12	13	6	4	2.2	Hodder and Gauthier (2022)
112-22-200	112-22-200-C02	7.2	35	8	20	10	10	2.0	Hodder and Gauthier (2022)
112-22-200	112-22-200-C02	7.2	154	22	20	12	6	1.7	Hodder and Gauthier (2022)
112-22-200	112-22-200-C02	7.2	2	24	35	15	15	2.3	Hodder and Gauthier (2022)
112-22-200	112-22-200-C02	7.2	16	16	37	15	12	2.5	Hodder and Gauthier (2022)
112-22-200	112-22-200-C02	7.2	205	22	17	7	5	2.4	Hodder and Gauthier (2022)
112-22-200	112-22-200-C02	7.2	345	30	35	22	12	1.6	Hodder and Gauthier (2022)
112-22-200	112-22-200-C02	7.2	238	4	23	12	8	1.9	Hodder and Gauthier (2022)
112-22-200	112-22-200-C02	7.2	345	6	8	4	3	2.0	Hodder and Gauthier (2022)
112-22-200	112-22-200-C02	7.2	22	6	28	14	12	2.0	Hodder and Gauthier (2022)
112-22-200	112-22-200-C02	7.2	208	16	8	2	2	4.0	Hodder and Gauthier (2022)
112-22-200	112-22-200-C02	7.2	4	25	35	16	14	2.2	Hodder and Gauthier (2022)
112-22-200	112-22-200-C02	7.2	2	24	8	4	4	2.0	Hodder and Gauthier (2022)
112-22-200	112-22-200-C02	7.2	4	20	20	12	5	1.7	Hodder and Gauthier (2022)
112-22-200	112-22-200-C02	7.2	208	4	17	10	8	1.7	Hodder and Gauthier (2022)
112-22-200	112-22-200-C02	7.2	92	6	10	6	4	1.7	Hodder and Gauthier (2022)
112-22-200	112-22-200-C02	7.2	0	4	9	6	4	1.5	Hodder and Gauthier (2022)
112-22-200	112-22-200-C02	7.2	20	20	11	6	2	1.8	Hodder and Gauthier (2022)
112-22-200	112-22-200-C02	7.2	202	8	17	7	7	2.4	Hodder and Gauthier (2022)
112-22-200	112-22-200-C02	7.2	194	8	17	11	9	1.5	Hodder and Gauthier (2022)
112-22-200	112-22-200-C03	10.2	124	14	18	10	6	1.8	Hodder and Gauthier (2022)

112-22-200	112-22-200-C03	10.2	142	33	22	12	12	1.8	Hodder and Gauthier (2022)
112-22-200	112-22-200-C03	10.2	222	10	8	4	4	2.0	Hodder and Gauthier (2022)
112-22-200	112-22-200-C03	10.2	74	20	40	22	20	1.8	Hodder and Gauthier (2022)
112-22-200	112-22-200-C03	10.2	76	18	6	2	2	3.0	Hodder and Gauthier (2022)
112-22-200	112-22-200-C03	10.2	256	12	10	5	5	2.0	Hodder and Gauthier (2022)
112-22-200	112-22-200-C03	10.2	120	20	12	6	5	2.0	Hodder and Gauthier (2022)
112-22-200	112-22-200-C03	10.2	46	14	14	6	4	2.3	Hodder and Gauthier (2022)
112-22-200	112-22-200-C03	10.2	64	22	14	8	6	1.8	Hodder and Gauthier (2022)
112-22-200	112-22-200-C03	10.2	80	16	12	6	4	2.0	Hodder and Gauthier (2022)
112-22-200	112-22-200-C03	10.2	58	20	22	12	10	1.8	Hodder and Gauthier (2022)
112-22-200	112-22-200-C03	10.2	74	33	16	8	8	2.0	Hodder and Gauthier (2022)
112-22-200	112-22-200-C03	10.2	69	8	15	10	7	1.5	Hodder and Gauthier (2022)
112-22-200	112-22-200-C03	10.2	148	6	32	16	10	2.0	Hodder and Gauthier (2022)
112-22-200	112-22-200-C03	10.2	79	12	14	8	5	1.8	Hodder and Gauthier (2022)
112-22-200	112-22-200-C03	10.2	60	20	9	3	2	3.0	Hodder and Gauthier (2022)
112-22-200	112-22-200-C03	10.2	64	18	19	11	6	1.7	Hodder and Gauthier (2022)
112-22-200	112-22-200-C03	10.2	158	12	12	6	3	2.0	Hodder and Gauthier (2022)
112-22-200	112-22-200-C03	10.2	72	10	10	6	4	1.7	Hodder and Gauthier (2022)
112-22-200	112-22-200-C03	10.2	112	35	28	17	6	1.6	Hodder and Gauthier (2022)
112-22-200	112-22-200-C03	10.2	62	22	6	2	2	3.0	Hodder and Gauthier (2022)
112-22-200	112-22-200-C03	10.2	55	16	16	6	5	2.7	Hodder and Gauthier (2022)
112-22-200	112-22-200-C03	10.2	84	18	18	7	6	2.6	Hodder and Gauthier (2022)
112-22-200	112-22-200-C03	10.2	98	30	47	22	20	2.1	Hodder and Gauthier (2022)
112-22-200	112-22-200-C03	10.2	86	18	22	14	8	1.6	Hodder and Gauthier (2022)
112-22-200	112-22-200-C03	10.2	88	30	12	6	4	2.0	Hodder and Gauthier (2022)
112-22-200	112-22-200-C03	10.2	58	18	18	12	8	1.5	Hodder and Gauthier (2022)
112-22-200	112-22-200-C03	10.2	85	30	17	10	8	1.7	Hodder and Gauthier (2022)
112-22-200	112-22-200-C03	10.2	55	12	8	5	2	1.6	Hodder and Gauthier (2022)

112-22-200	112-22-200-C03	10.2	60	25	12	6	4	2.0	Hodder and Gauthier (2022)
112-22-201	112-22-201-A01	10.8	20	25	15	9	8	1.7	Hodder and Gauthier (2022)
112-22-201	112-22-201-A01	10.8	43	32	18	11	8	1.6	Hodder and Gauthier (2022)
112-22-201	112-22-201-A01	10.8	110	14	15	7	3	2.1	Hodder and Gauthier (2022)
112-22-201	112-22-201-A01	10.8	150	5	20	12	10	1.7	Hodder and Gauthier (2022)
112-22-201	112-22-201-A01	10.8	303	25	12	6	5	2.0	Hodder and Gauthier (2022)
112-22-201	112-22-201-A01	10.8	13	25	9	6	2	1.5	Hodder and Gauthier (2022)
112-22-201	112-22-201-A01	10.8	322	20	9	3	2	3.0	Hodder and Gauthier (2022)
112-22-201	112-22-201-A01	10.8	145	6	16	10	8	1.6	Hodder and Gauthier (2022)
112-22-201	112-22-201-A01	10.8	35	35	19	10	8	1.9	Hodder and Gauthier (2022)
112-22-201	112-22-201-A01	10.8	325	26	11	6	5	1.8	Hodder and Gauthier (2022)
112-22-201	112-22-201-A01	10.8	327	35	15	10	3	1.5	Hodder and Gauthier (2022)
112-22-201	112-22-201-A01	10.8	125	18	25	14	6	1.8	Hodder and Gauthier (2022)
112-22-201	112-22-201-A01	10.8	315	2	25	15	12	1.7	Hodder and Gauthier (2022)
112-22-201	112-22-201-A01	10.8	310	12	23	11	10	2.1	Hodder and Gauthier (2022)
112-22-201	112-22-201-A01	10.8	5	34	15	10	8	1.5	Hodder and Gauthier (2022)
112-22-201	112-22-201-A01	10.8	140	28	20	8	7	2.5	Hodder and Gauthier (2022)
112-22-201	112-22-201-A01	10.8	342	42	18	12	10	1.5	Hodder and Gauthier (2022)
112-22-201	112-22-201-A01	10.8	320	23	13	8	10	1.6	Hodder and Gauthier (2022)
112-22-201	112-22-201-A01	10.8	344	25	12	7	5	1.7	Hodder and Gauthier (2022)
112-22-201	112-22-201-A01	10.8	332	16	16	8	5	2.0	Hodder and Gauthier (2022)
112-22-201	112-22-201-A01	10.8	340	48	17	10	7	1.7	Hodder and Gauthier (2022)
112-22-201	112-22-201-A01	10.8	315	26	18	11	5	1.6	Hodder and Gauthier (2022)
112-22-201	112-22-201-A01	10.8	318	35	30	18	7	1.7	Hodder and Gauthier (2022)
112-22-201	112-22-201-A01	10.8	310	11	20	10	5	2.0	Hodder and Gauthier (2022)
112-22-201	112-22-201-A01	10.8	305	16	15	9	6	1.7	Hodder and Gauthier (2022)
112-22-201	112-22-201-A01	10.8	90	26	26	11	6	2.4	Hodder and Gauthier (2022)
112-22-201	112-22-201-A01	10.8	140	13	30	16	10	1.9	Hodder and Gauthier (2022)

112-22-201	112-22-201-A01	10.8	35	26	26	15	10	1.7	Hodder and Gauthier (2022)
112-22-201	112-22-201-A01	10.8	340	30	21	13	10	1.6	Hodder and Gauthier (2022)
112-22-201	112-22-201-A01	10.8	285	16	15	8	6	1.9	Hodder and Gauthier (2022)
112-22-201	112-22-201-A01	10.8	300	5	23	9	7	2.6	Hodder and Gauthier (2022)
112-22-201	112-22-201-A01	10.8	330	10	25	14	3	1.8	Hodder and Gauthier (2022)
112-22-201	112-22-201-B01	10.9	294	14	20	12	8	1.7	Hodder and Gauthier (2022)
112-22-201	112-22-201-B01	10.9	314	22	14	8	6	1.8	Hodder and Gauthier (2022)
112-22-201	112-22-201-B01	10.9	305	6	17	11	4	1.5	Hodder and Gauthier (2022)
112-22-201	112-22-201-B01	10.9	348	6	12	6	2	2.0	Hodder and Gauthier (2022)
112-22-201	112-22-201-B01	10.9	295	28	8	4	2	2.0	Hodder and Gauthier (2022)
112-22-201	112-22-201-B01	10.9	359	12	12	4	4	3.0	Hodder and Gauthier (2022)
112-22-201	112-22-201-B01	10.9	335	12	40	20	20	2.0	Hodder and Gauthier (2022)
112-22-201	112-22-201-B01	10.9	289	24	12	7	4	1.7	Hodder and Gauthier (2022)
112-22-201	112-22-201-B01	10.9	335	8	12	4	2	3.0	Hodder and Gauthier (2022)
112-22-201	112-22-201-B01	10.9	340	26	15	7	5	2.1	Hodder and Gauthier (2022)
112-22-201	112-22-201-B01	10.9	278	32	16	10	5	1.6	Hodder and Gauthier (2022)
112-22-201	112-22-201-B01	10.9	346	22	25	12	7	2.1	Hodder and Gauthier (2022)
112-22-201	112-22-201-B01	10.9	306	35	11	6	2	1.8	Hodder and Gauthier (2022)
112-22-201	112-22-201-B01	10.9	308	14	17	11	7	1.5	Hodder and Gauthier (2022)
112-22-201	112-22-201-B01	10.9	306	20	21	14	10	1.5	Hodder and Gauthier (2022)
112-22-201	112-22-201-B01	10.9	284	12	17	11	6	1.5	Hodder and Gauthier (2022)
112-22-201	112-22-201-B01	10.9	292	18	18	11	7	1.6	Hodder and Gauthier (2022)
112-22-201	112-22-201-B01	10.9	275	22	13	6	4	2.2	Hodder and Gauthier (2022)
112-22-201	112-22-201-B01	10.9	315	38	9	6	2	1.5	Hodder and Gauthier (2022)
112-22-201	112-22-201-B01	10.9	330	18	12	6	4	2.0	Hodder and Gauthier (2022)
112-22-201	112-22-201-B01	10.9	342	14	25	13	13	1.9	Hodder and Gauthier (2022)
112-22-201	112-22-201-B01	10.9	268	4	16	10	4	1.6	Hodder and Gauthier (2022)
112-22-201	112-22-201-B01	10.9	280	22	23	13	8	1.8	Hodder and Gauthier (2022)

112-22-201	112-22-201-B01	10.9	289	8	10	6	6	1.7	Hodder and Gauthier (2022)
112-22-201	112-22-201-B01	10.9	318	4	21	8	5	2.6	Hodder and Gauthier (2022)
112-22-201	112-22-201-B01	10.9	100	4	15	10	4	1.5	Hodder and Gauthier (2022)
112-22-201	112-22-201-B01	10.9	315	22	14	8	4	1.8	Hodder and Gauthier (2022)
112-22-201	112-22-201-B01	10.9	332	22	16	8	5	2.0	Hodder and Gauthier (2022)
112-22-201	112-22-201-B01	10.9	246	15	18	11	6	1.6	Hodder and Gauthier (2022)
112-22-201	112-22-201-B01	10.9	295	24	16	8	8	2.0	Hodder and Gauthier (2022)
112-19-629	W9765	15.1	332	36	-	-	-	-	Hodder et al. (2017)
112-19-629	W9765	15.1	50	5	-	-	-	-	Hodder et al. (2017)
112-19-629	W9765	15.1	330	15	-	-	-	-	Hodder et al. (2017)
112-19-629	W9765	15.1	104	21	-	-	-	-	Hodder et al. (2017)
112-19-629	W9765	15.1	21	6	-	-	-	-	Hodder et al. (2017)
112-19-629	W9765	15.1	63	19	-	-	-	-	Hodder et al. (2017)
112-19-629	W9765	15.1	12	21	-	-	-	-	Hodder et al. (2017)
112-19-629	W9765	15.1	350	26	-	-	-	-	Hodder et al. (2017)
112-19-629	W9765	15.1	3	2	-	-	-	-	Hodder et al. (2017)
112-19-629	W9765	15.1	18	16	-	-	-	-	Hodder et al. (2017)
112-19-629	W9765	15.1	188	7	-	-	-	-	Hodder et al. (2017)
112-19-629	W9765	15.1	337	1	-	-	-	-	Hodder et al. (2017)
112-19-629	W9765	15.1	110	16	-	-	-	-	Hodder et al. (2017)
112-19-629	W9765	15.1	120	13	-	-	-	-	Hodder et al. (2017)
112-19-629	W9765	15.1	3	9	-	-	-	-	Hodder et al. (2017)
112-19-629	W9765	15.1	356	4	-	-	-	-	Hodder et al. (2017)
112-19-629	W9765	15.1	325	6	-	-	-	-	Hodder et al. (2017)
112-19-629	W9765	15.1	162	10	-	-	-	-	Hodder et al. (2017)
112-19-629	W9765	15.1	166	10	-	-	-	-	Hodder et al. (2017)
112-19-629	W9765	15.1	244	9	-	-	-	-	Hodder et al. (2017)
112-19-629	W9765	15.1	10	1	-	-	-	-	Hodder et al. (2017)

112-19-629	W9765	15.1	312	38	-	-	-	-	Hodder et al. (2017)
112-19-629	W9765	15.1	11	10	-	-	-	-	Hodder et al. (2017)
112-19-629	W9765	15.1	294	4	-	-	-	-	Hodder et al. (2017)
112-19-629	W9765	15.1	310	15	-	-	-	-	Hodder et al. (2017)
112-19-629	W9765	15.1	13	10	-	-	-	-	Hodder et al. (2017)
112-19-629	W9765	15.1	143	8	-	-	-	-	Hodder et al. (2017)
112-19-629	W9765	15.1	129	11	-	-	-	-	Hodder et al. (2017)
112-19-629	W9765	15.1	167	12	-	-	-	-	Hodder et al. (2017)
112-19-629	W9765	15.1	5	7	-	-	-	-	Hodder et al. (2017)
112-19-629	W9769	21	120	8	-	-	-	-	Hodder et al. (2017)
112-19-629	W9769	21	297	18	-	-	-	-	Hodder et al. (2017)
112-19-629	W9769	21	353	6	-	-	-	-	Hodder et al. (2017)
112-19-629	W9769	21	297	15	-	-	-	-	Hodder et al. (2017)
112-19-629	W9769	21	101	20	-	-	-	-	Hodder et al. (2017)
112-19-629	W9769	21	110	9	-	-	-	-	Hodder et al. (2017)
112-19-629	W9769	21	141	10	-	-	-	-	Hodder et al. (2017)
112-19-629	W9769	21	305	16	-	-	-	-	Hodder et al. (2017)
112-19-629	W9769	21	357	23	-	-	-	-	Hodder et al. (2017)
112-19-629	W9769	21	171	1	-	-	-	-	Hodder et al. (2017)
112-19-629	W9769	21	104	21	-	-	-	-	Hodder et al. (2017)
112-19-629	W9769	21	116	9	-	-	-	-	Hodder et al. (2017)
112-19-629	W9769	21	340	19	-	-	-	-	Hodder et al. (2017)
112-19-629	W9769	21	160	2	-	-	-	-	Hodder et al. (2017)
112-19-629	W9769	21	91	7	-	-	-	-	Hodder et al. (2017)
112-19-629	W9769	21	109	25	-	-	-	-	Hodder et al. (2017)
112-19-629	W9769	21	212	28	-	-	-	-	Hodder et al. (2017)
112-19-629	W9769	21	310	26	-	-	-	-	Hodder et al. (2017)
112-19-629	W9769	21	267	18	-	-	-	-	Hodder et al. (2017)

112-19-629	W9769	21	36	26	-	-	-	-	Hodder et al. (2017)
112-19-629	W9769	21	330	14	-	-	-	-	Hodder et al. (2017)
112-19-629	W9769	21	45	22	-	-	-	-	Hodder et al. (2017)
112-19-629	W9769	21	344	15	-	-	-	-	Hodder et al. (2017)
112-19-629	W9769	21	327	10	-	-	-	-	Hodder et al. (2017)
112-19-629	W9769	21	322	41	-	-	-	-	Hodder et al. (2017)
112-19-629	W9769	21	74	22	-	-	-	-	Hodder et al. (2017)
112-19-629	W9769	21	316	1	-	-	-	-	Hodder et al. (2017)
112-19-629	W9769	21	312	18	-	-	-	-	Hodder et al. (2017)
112-19-629	W9769	21	5	2	-	-	-	-	Hodder et al. (2017)
112-19-629	W9769	21	226	7	-	-	-	-	Hodder et al. (2017)
112-19-629	W9771	23.5	220	27	-	-	-	-	Hodder et al. (2017)
112-19-629	W9771	23.5	355	1	-	-	-	-	Hodder et al. (2017)
112-19-629	W9771	23.5	201	25	-	-	-	-	Hodder et al. (2017)
112-19-629	W9771	23.5	332	37	-	-	-	-	Hodder et al. (2017)
112-19-629	W9771	23.5	352	2	-	-	-	-	Hodder et al. (2017)
112-19-629	W9771	23.5	333	40	-	-	-	-	Hodder et al. (2017)
112-19-629	W9771	23.5	351	25	-	-	-	-	Hodder et al. (2017)
112-19-629	W9771	23.5	109	10	-	-	-	-	Hodder et al. (2017)
112-19-629	W9771	23.5	303	22	-	-	-	-	Hodder et al. (2017)
112-19-629	W9771	23.5	340	16	-	-	-	-	Hodder et al. (2017)
112-19-629	W9771	23.5	326	11	-	-	-	-	Hodder et al. (2017)
112-19-629	W9771	23.5	256	3	-	-	-	-	Hodder et al. (2017)
112-19-629	W9771	23.5	333	22	-	-	-	-	Hodder et al. (2017)
112-19-629	W9771	23.5	243	40	-	-	-	-	Hodder et al. (2017)
112-19-629	W9771	23.5	311	22	-	-	-	-	Hodder et al. (2017)
112-19-629	W9771	23.5	268	1	-	-	-	-	Hodder et al. (2017)
112-19-629	W9771	23.5	15	21	-	-	-	-	Hodder et al. (2017)

112-19-629	W9771	23.5	297	25	-	-	-	-	Hodder et al. (2017)
112-19-629	W9771	23.5	162	18	-	-	-	-	Hodder et al. (2017)
112-19-629	W9771	23.5	122	25	-	-	-	-	Hodder et al. (2017)
112-19-629	W9771	23.5	148	18	-	-	-	-	Hodder et al. (2017)
112-19-629	W9771	23.5	141	33	-	-	-	-	Hodder et al. (2017)
112-19-629	W9771	23.5	291	9	-	-	-	-	Hodder et al. (2017)
112-19-629	W9771	23.5	338	9	-	-	-	-	Hodder et al. (2017)
112-19-629	W9771	23.5	92	11	-	-	-	-	Hodder et al. (2017)
112-19-629	W9771	23.5	329	10	-	-	-	-	Hodder et al. (2017)
112-19-629	W9771	23.5	2	1	-	-	-	-	Hodder et al. (2017)
112-19-629	W9771	23.5	47	32	-	-	-	-	Hodder et al. (2017)
112-19-629	W9771	23.5	348	37	-	-	-	-	Hodder et al. (2017)
112-19-629	W9771	23.5	311	19	-	-	-	-	Hodder et al. (2017)
112-19-628	112-19-628-B01	12.4	162	25	2	1	0.4	2.0	Hodder et al. (2024a)
112-19-628	112-19-628-B01	12.4	148	20	1.3	0.3	0.2	4.3	Hodder et al. (2024a)
112-19-628	112-19-628-B01	12.4	96	8	2.5	1.3	1.2	1.9	Hodder et al. (2024a)
112-19-628	112-19-628-B01	12.4	130	14	0.8	0.4	0.2	2.0	Hodder et al. (2024a)
112-19-628	112-19-628-B01	12.4	106	6	1.2	0.8	0.6	1.5	Hodder et al. (2024a)
112-19-628	112-19-628-B01	12.4	136	32	1.5	1	0.4	1.5	Hodder et al. (2024a)
112-19-628	112-19-628-B01	12.4	200	12	1	0.4	0.4	2.5	Hodder et al. (2024a)
112-19-628	112-19-628-B01	12.4	96	12	1	0.6	0.6	1.7	Hodder et al. (2024a)
112-19-628	112-19-628-B01	12.4	70	2	0.9	0.6	0.5	1.5	Hodder et al. (2024a)
112-19-628	112-19-628-B01	12.4	99	12	0.9	0.6	0.3	1.5	Hodder et al. (2024a)
112-19-628	112-19-628-B01	12.4	288	10	1.3	0.6	0.6	2.2	Hodder et al. (2024a)
112-19-628	112-19-628-B01	12.4	274	2	2	1.1	1	1.8	Hodder et al. (2024a)
112-19-628	112-19-628-B01	12.4	108	35	0.8	0.4	0.2	2.0	Hodder et al. (2024a)
112-19-628	112-19-628-B01	12.4	2	12	2.6	1.1	1	2.4	Hodder et al. (2024a)
112-19-628	112-19-628-B01	12.4	116	26	1.2	0.8	0.4	1.5	Hodder et al. (2024a)

112-19-628	112-19-628-B01	12.4	22	22	1.3	0.8	0.3	1.6	Hodder et al. (2024a)
112-19-628	112-19-628-B01	12.4	104	32	0.9	0.5	0.3	1.8	Hodder et al. (2024a)
112-19-628	112-19-628-B01	12.4	58	30	0.9	0.4	0.2	2.3	Hodder et al. (2024a)
112-19-628	112-19-628-B01	12.4	286	12	0.9	0.5	0.3	1.8	Hodder et al. (2024a)
112-19-628	112-19-628-B01	12.4	170	6	1	0.5	0.3	2.0	Hodder et al. (2024a)
112-19-628	112-19-628-B01	12.4	162	5	1	0.5	0.2	2.0	Hodder et al. (2024a)
112-19-628	112-19-628-B01	12.4	168	30	0.8	0.3	0.3	2.7	Hodder et al. (2024a)
112-19-628	112-19-628-B01	12.4	195	14	0.7	0.3	0.2	2.3	Hodder et al. (2024a)
112-19-628	112-19-628-B01	12.4	310	12	1.2	0.4	0.4	3.0	Hodder et al. (2024a)
112-19-628	112-19-628-B01	12.4	176	20	0.9	0.5	0.2	1.8	Hodder et al. (2024a)
112-19-628	112-19-628-B01	12.4	218	28	3	1	1	3.0	Hodder et al. (2024a)
112-19-628	112-19-628-B01	12.4	265	8	0.8	0.2	0.2	4.0	Hodder et al. (2024a)
112-19-628	112-19-628-B01	12.4	127	32	0.6	0.3	0.2	2.0	Hodder et al. (2024a)
112-19-628	112-19-628-B01	12.4	150	35	1.2	0.7	0.7	1.7	Hodder et al. (2024a)
112-19-628	112-19-628-B01	12.4	86	15	3	2	1	1.5	Hodder et al. (2024a)
112-19-628	112-19-628-B01	12.4	92	48	0.9	0.2	0.2	4.5	Hodder et al. (2024a)
112-19-628	112-19-628-B01	12.4	110	28	1.2	0.4	0.4	3.0	Hodder et al. (2024a)
112-19-628	112-19-628-B01	12.4	268	10	1.1	0.6	0.3	1.8	Hodder et al. (2024a)
112-19-628	112-19-628-B01	12.4	262	8	0.8	0.4	0.4	2.0	Hodder et al. (2024a)
112-19-628	112-19-628-B01	12.4	55	20	1	0.4	0.2	2.5	Hodder et al. (2024a)
112-19-628	112-19-628-D01	3.0	25	2	1.1	0.6	0.5	1.8	Hodder et al. (2024a)
112-19-628	112-19-628-D01	3.0	224	14	0.9	0.5	0.2	1.8	Hodder et al. (2024a)
112-19-628	112-19-628-D01	3.0	44	40	1.2	0.8	0.6	1.5	Hodder et al. (2024a)
112-19-628	112-19-628-D01	3.0	219	12	2	1.1	1.1	1.8	Hodder et al. (2024a)
112-19-628	112-19-628-D01	3.0	262	26	1	0.6	0.3	1.7	Hodder et al. (2024a)
112-19-628	112-19-628-D01	3.0	318	16	1.2	0.8	0.6	1.5	Hodder et al. (2024a)
112-19-628	112-19-628-D01	3.0	46	20	3.2	2.1	1.8	1.5	Hodder et al. (2024a)
112-19-628	112-19-628-D01	3.0	214	4	1.1	0.6	0.2	1.8	Hodder et al. (2024a)

112-19-628	112-19-628-D01	3.0	35	14	1.3	0.7	0.3	1.9	Hodder et al. (2024a)
112-19-628	112-19-628-D01	3.0	355	8	1.4	0.8	0.8	1.8	Hodder et al. (2024a)
112-19-628	112-19-628-D01	3.0	70	28	2	1	1	2.0	Hodder et al. (2024a)
112-19-628	112-19-628-D01	3.0	164	14	0.8	0.4	0.4	2.0	Hodder et al. (2024a)
112-19-628	112-19-628-D01	3.0	239	18	2.8	1.6	1	1.8	Hodder et al. (2024a)
112-19-628	112-19-628-D01	3.0	214	26	1.8	0.9	0.8	2.0	Hodder et al. (2024a)
112-19-628	112-19-628-D01	3.0	99	18	2.1	0.9	0.4	2.3	Hodder et al. (2024a)
112-19-628	112-19-628-D01	3.0	248	12	2.4	1.2	0.4	2.0	Hodder et al. (2024a)
112-19-628	112-19-628-D01	3.0	218	22	0.8	0.4	0.3	2.0	Hodder et al. (2024a)
112-19-628	112-19-628-D01	3.0	252	6	0.8	0.4	0.2	2.0	Hodder et al. (2024a)
112-19-628	112-19-628-D01	3.0	232	8	1	0.5	0.3	2.0	Hodder et al. (2024a)
112-19-628	112-19-628-D01	3.0	95	4	2	0.9	0.4	2.2	Hodder et al. (2024a)
112-19-628	112-19-628-D01	3.0	59	22	0.6	0.3	0.1	2.0	Hodder et al. (2024a)
112-19-628	112-19-628-D01	3.0	58	10	1.2	0.6	0.4	2.0	Hodder et al. (2024a)
112-19-628	112-19-628-D01	3.0	35	22	1.3	0.7	0.5	1.9	Hodder et al. (2024a)
112-19-628	112-19-628-D01	3.0	192	6	1.3	0.7	0.5	1.9	Hodder et al. (2024a)
112-19-628	112-19-628-D01	3.0	5	10	3	1.8	1.6	1.7	Hodder et al. (2024a)
112-19-628	112-19-628-D01	3.0	262	22	0.8	0.4	0.4	2.0	Hodder et al. (2024a)
112-19-628	112-19-628-D01	3.0	269	6	2.4	1.2	0.1	2.0	Hodder et al. (2024a)
112-19-628	112-19-628-D01	3.0	234	6	1.2	0.8	0.6	1.5	Hodder et al. (2024a)
112-19-628	112-19-628-D01	3.0	37	32	1.4	0.9	0.4	1.6	Hodder et al. (2024a)
112-19-628	112-19-628-D01	3.0	232	22	1.8	1.2	0.9	1.5	Hodder et al. (2024a)

Table 2: Lodged boulder measurements.

Section ID	Closest till sample	Depth (m bgs)	Azimuth (°)	Comments	Data source
115-23-002	115-23-002-C04	16.2	45–50	3-4 boulders all have a-axis of 45-50°, one with parallel striations, ~168°	This study
115-23-003	115-23-003-A01	26.4	156	Few at 196°	This study
115-23-005	115-23-005-B05	12.6	220	Boulder pavement; large granitic boulder (~0.8 m length x 0.3 m width x 0.4 m thick); parallel grooves on upper surface of boulder that are parallel to a-axis of the boulder; excellent indicator	This study
115-23-005	115-23-005-B05	12.6	175	Boulder pavement; large granitic boulder (~1.0 m length x 1.0 m width x 0.6 m thick); upper flat surface is well polished with parallel striations and grooves; excellent ice-flow indicator	This study
115-23-006	115-23-006-B02	9.0	235	A-axis and grooves align, excellent ice-flow indicator	This study
115-23-009	115-23-009-G02	29.0	175	-	This study
112-19-628	112-19-628-D02	14.0	235	Lodged cobble; 0.24 x 0.14 x 0.10 m dimensions; small grooves on flat upper surface of cobble	Hodder et al. (2024a)
112-19-628	112-19-628-D04	16.5	230	Lodged cobble; parallel striae on flat upper surface indicate 230°	Hodder et al. (2024a)

Table 3: Till-fabric ice-flow indicator statistics and interpretations.

Section ID	Sample ID	Depth (m bgs)	Data source	Number of clasts observed	Modality[1]	V_1 azimuth (°)	V_1 dip (°)	S_1	S_2	S_3	Interpreted ice-flow (°)	Interpreted ice-flow (direction)
115-23-002	115-23-002-A01	4.50	This study	26	SU	29	12	0.7	0.2	0.1	209	SSW
115-23-002	115-23-002-B02	6.50	This study	30	SU	110	19	0.8	0.2	0.0	110-290	WNW-ESE
115-23-002	115-23-002-B03	8.00	This study	31	SU	115	12	0.8	0.2	0.0	115-295	WNW-ESE
115-23-002	115-23-002-C01	10.00	This study	25	SB	329	1	0.5	0.3	0.2	-	-
115-23-002	115-23-002-C02	12.50	This study	26	SU	275	7	0.7	0.2	0.1	275	W
115-23-002	115-23-002-C03	14.50	This study	30	SU	37	15	0.8	0.2	0.0	216	SW
115-23-002	115-23-002-C04	16.20	This study	42	SU	56	3	0.6	0.3	0.1	236	SW
115-23-002	115-23-002-D01	17.40	This study	31	SU	250	12	0.6	0.3	0.1	250	WSW
115-23-002	115-23-002-D02	19.10	This study	21	SB	83	15	0.5	0.4	0.1	-	-
115-23-002	115-23-002-D04	23.10	This study	28	SU	43	27	0.8	0.1	0.1	223	SW
115-23-003	115-23-003-A02	25.25	This study	31	SU	132	11	0.8	0.2	0.1	312	NW
115-23-003	115-23-003-B01	22.85	This study	23	SU	142	21	0.6	0.3	0.1	322	NW
115-23-003	115-23-003-B02	19.85	This study	28	SU	101	4	0.8	0.2	0.1	281	WNW
115-23-003	115-23-003-D01	14.85	This study	27	SB	45	6	0.5	0.4	0.1	-	-
115-23-003	115-23-003-L01	3.30	This study	29	U	71	4	0.8	0.1	0.1	251	WSW
115-23-004	115-23-004-B01	25.30	This study	21	SU	360	16	0.7	0.2	0.1	180	S
115-23-005	115-23-005-B01	3.60	This study	32	SU	321	19	0.6	0.3	0.1	321	NW
115-23-005	115-23-005-B04	9.10	This study	20	SU	21	11	0.9	0.1	0.1	201	SSW
115-23-005	115-23-005-Z01	13.30	This study	31	SU	136	10	0.7	0.3	0.1	348-168	NNW-SSE
115-23-005	115-23-005-T01	17.50	This study	28	SU	303	10	0.7	0.2	0.1	303-123	WNW-ESE
115-23-005	115-23-005-O01	15.05	This study	32	SU	348	6	0.7	0.2	0.1	136-316	NW-SE
115-23-006	115-23-006-A01	4.75	This study	28	SU	181	5	0.9	0.1	0.0	181	S
115-23-006	115-23-006-B01	5.25	This study	23	SU	215	8	0.8	0.2	0.1	215	SW
115-23-006	115-23-006-C01	8.45	This study	30	SU	118	5	0.7	0.3	0.1	118-298	WNW-ESE
115-23-006	115-23-006-C02	11.55	This study	34	SU	140	1	0.6	0.3	0.1	140-320	NW-SE

115-23-006	115-23-006-C03	15.35	This study	23	SU	83	5	0.6	0.2	0.1	263	W
115-23-007	115-23-007-A01	0.70	This study	21	SU	142	2	0.6	0.3	0.1	142-322	NW-SE
115-23-007	115-23-007-B02	3.00	This study	24	SU	258	5	0.7	0.2	0.1	258	WSW
115-23-007	115-23-007-C01	4.55	This study	30	SU	123	21	0.8	0.2	0.0	123-303	WNW-ESE
115-23-007	115-23-007-C04	13.55	This study	40	SU	176	17	0.7	0.3	0.1	176	S
115-23-007	115-23-007-C05	15.55	This study	26	U	88	9	0.8	0.1	0.0	268	W
115-23-007	115-23-007-D01	17.95	This study	30	SU	57	3	0.7	0.2	0.1	237	SW
115-23-007	115-23-007-D03	23.15	This study	25	U	146	2	0.8	0.2	0.1	326	NW
115-23-007	115-23-007-D05	29.15	This study	40	SU	134	4	0.6	0.4	0.1	314	NW
115-23-007	115-23-007-D07	34.15	This study	30	SB	79	1	0.5	0.4	0.1	-	-
115-23-007	115-23-007-D08	31.80	This study	35	SU	118	14	0.7	0.2	0.1	298	WNW
115-23-007	115-23-007-E01	35.65	This study	30	SU	24	4	0.7	0.2	0.0	204	SSW
115-23-007	115-23-007-E03	40.65	This study	30	SU	43	9	0.8	0.1	0.1	223	SW
115-23-008	115-23-008-A01	1.15	This study	31	U	32	7	0.8	0.1	0.1	212	SW
115-23-008	115-23-008-B01	2.30	This study	30	SU	356	11	0.7	0.2	0.1	176	S
115-23-008	115-23-008-C01	3.40	This study	30	U	46	18	0.8	0.1	0.1	226	SW
115-23-008	115-23-008-F01	5.50	This study	30	SU	6	2	0.8	0.1	0.1	186	S
115-23-008	115-23-008-F03	11.50	This study	24	SU	311	8	0.5	0.3	0.1	131-311	NW-SE
115-23-008	115-23-008-F04	15.15	This study	28	SU	93	4	0.7	0.2	0.1	272	W
115-23-009	115-23-009-B01	3.00	This study	27	SU	229	5	0.8	0.2	0.1	229	SW
115-23-009	115-23-009-C01	4.50	This study	26	SU	232	16	0.7	0.2	0.1	232	SW
115-23-009	115-23-009-D01	7.00	This study	20	SU	237	13	0.8	0.2	0.0	237	SW
115-23-009	115-23-009-D03	13.00	This study	25	SU	309	3	0.8	0.2	0.0	309-129	NW-SE
115-23-009	115-23-009-D05	19.00	This study	30	SU	357	2	0.7	0.3	0.1	357-177	NNW-SSE
115-23-009	115-23-009-D07	22.80	This study	34	SU	143	9	0.7	0.3	0.1	323	NW
115-23-009	115-23-009-E01	25.10	This study	24	SU	255	1	0.5	0.4	0.1	-	-
115-23-009	115-23-009-G01	26.95	This study	30	SU	222	1	0.9	0.1	0.1	222	SW
115-23-009	115-23-009-J01	32.45	This study	26	SU	262	2	0.8	0.1	0.1	262	W

115-23-009	115-23-009-K02	37.30	This study	30	SU	233	13	0.8	0.1	0.1	233	SW
115-23-009	115-23-009-K04	43.35	This study	35	SU	307	5	0.6	0.3	0.1	307	NW
112-19-629	W9765	15.1	Hodder et al. (2017)	30	SU	348	6	0.7	0.3	0.1	348	NNW
112-19-629	112-19-629-A01	15.1	Hodder and Gauthier (2022)	38	SU	133	8	0.6	0.3	0.1	313	NW
112-19-629	112-19-629-C01	18	Hodder and Gauthier (2022)	30	SU	220	9	0.8	0.1	0.1	220	SW
112-19-629	W9769	21	Hodder et al. (2017)	30	SU	314	6	0.6	0.3	0.1	314	NW
112-19-629	W9771	23.5	Hodder et al. (2017)	30	SU	327	11	0.6	0.3	0.1	327	NNW
112-22-200	112-22-200-A01	0.9	Hodder and Gauthier (2022)	30	SU	99	1	0.7	0.2	0.1	279	W
112-22-200	112-22-200-B01	2.5	Hodder and Gauthier (2022)	30	SU	100	12	0.8	0.1	0.1	280	W
112-22-200	112-22-200-C01	4.2	Hodder and Gauthier (2022)	35	SU	223	10	0.7	0.2	0.1	223	SW
112-22-200	112-22-200-C02	7.2	Hodder and Gauthier (2022)	29	SU	18	5	0.8	0.1	0.1	198	SSW
112-22-200	112-22-200-C03	10.2	Hodder and Gauthier (2022)	30	SU	76	20	0.8	0.2	0	256	WSW
112-22-201	112-22-201-A01	10.8	Hodder and Gauthier (2022)	32	SU	325	18	0.7	0.2	0.1	325-145	NW-SE
112-22-201	112-22-201-B01	10.9	Hodder and Gauthier (2022)	30	SU	307	19	0.8	0.2	0	307	NW
112-19-628	112-19-628-B01	3	Hodder et al. (2024a)	35	SU	112	16	0.6	0.3	0.1	282	W
112-19-628	112-19-628-D01	12.4	Hodder et al. (2024a)	30	SU	229	0	0.7	0.2	0.1	229	SW

Abbreviations: SB, spread bimodal; SU, spread unimodal; U, unimodal.

[1]As defined by Hicock et al. (1996)

Appendix H – Stratigraphic columns for 2019 and 2022 sections

Sections 112-19-628 and 112-19-629

The full stratigraphic log and associated photographs for sections 112-19-628 and 112-19-629 can be found in Appendix 2 of OF2024-1, available for download from the Manitoba Geological Survey website (https://gov.mb.ca/iem/info/libmin/2024pubs.html; last accessed 2025-06-05). Specifically, in the OF2024-1.zip/Appendices/OF2024-1_Appendix 2 folder, OF2024-1_Figure 40__112-19-628.pdf and OF2024-1_Figure 41__112-19-629.pdf can be found.

Section 112-22-200

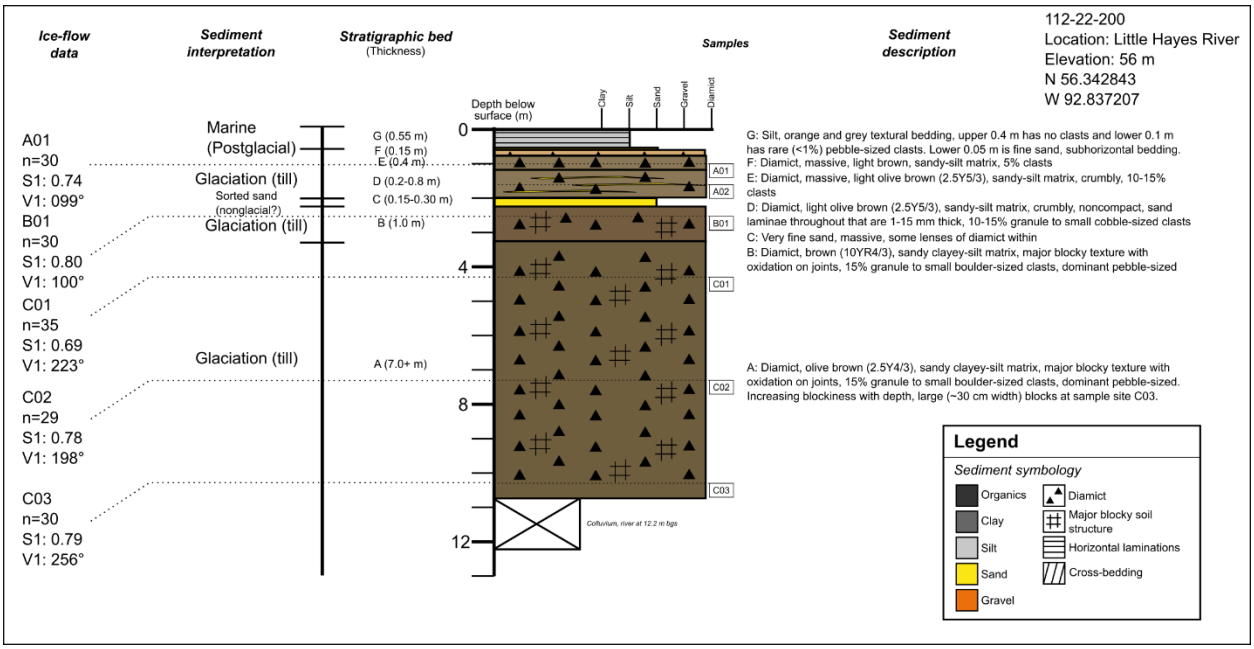


Figure 1: Stratigraphic column for Section 112-22-200.

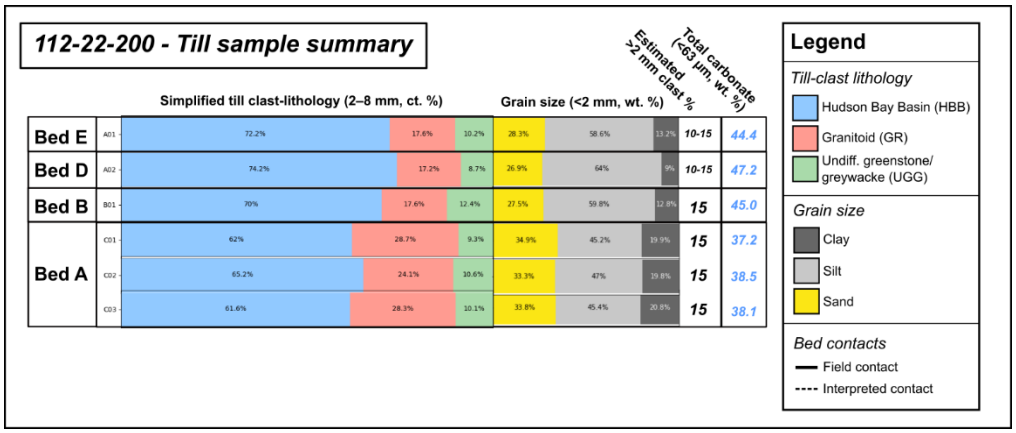


Figure 2: Till sample summary for Section 112-22-200.

Section 112-22-201

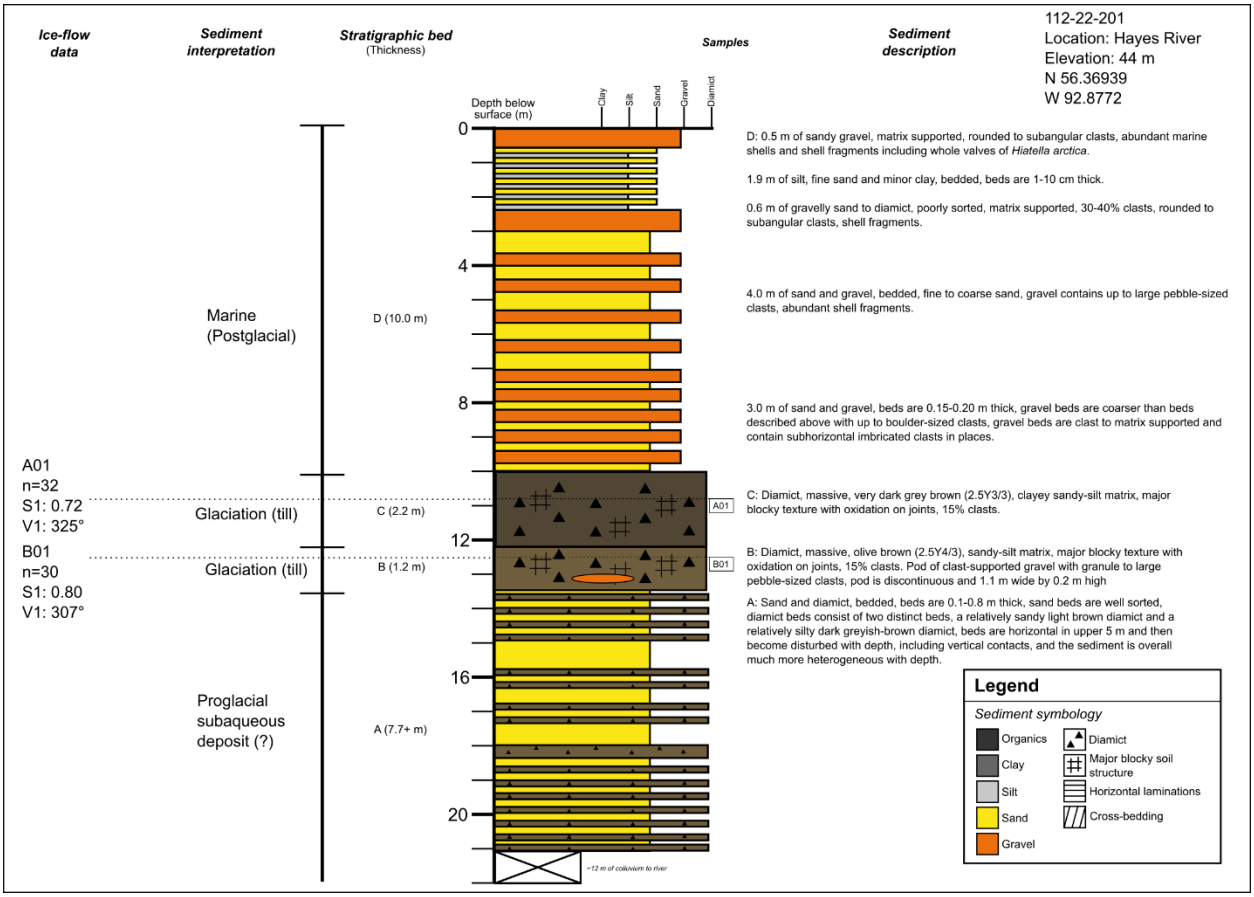


Figure 3: Stratigraphic column for Section 112-22-201.

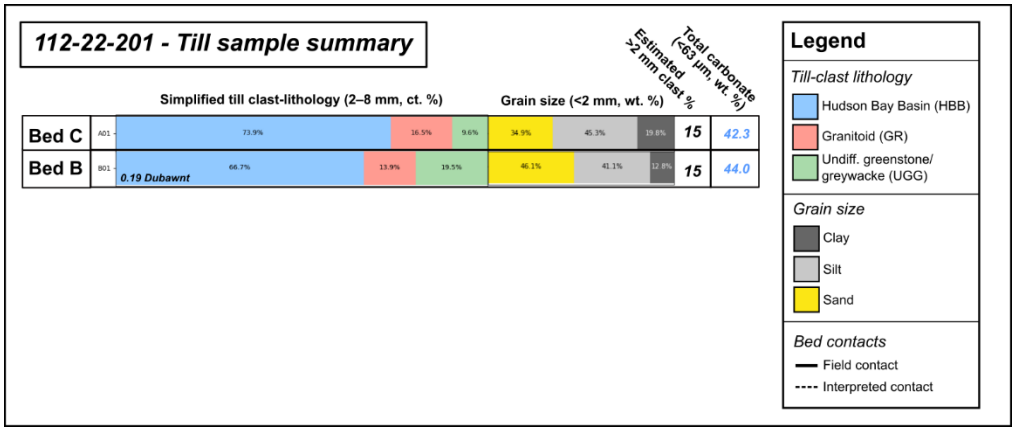


Figure 4: Till sample summary for Section 112-22-201.

Appendix I – Till composition analysis

Clast-lithology clustering

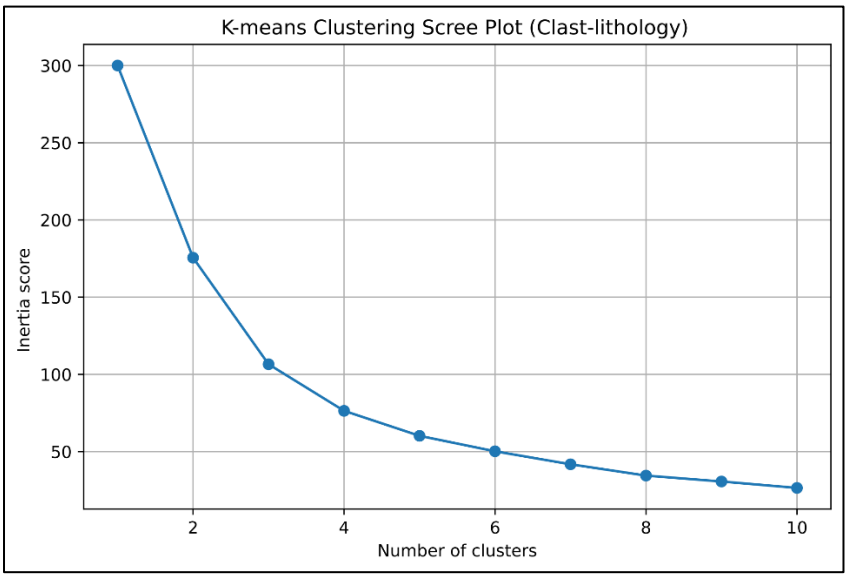


Figure 1: Scree plot for k-means clustering of preprocessed clast-lithology proportions data (inertia is a measure of explained variance). The elbow method did not indicate a clear optimal number of clusters on the scree plot, but instead a range of possibilities (k = 3 to 5), from which 5 was chosen as ideal.

Till-matrix geochemistry

QA/QC

QA/QC assessments (see Appendix D) were conducted on elemental proportions determined from lithium metaborate fusion digestion. Elements excluded from multivariate analysis due to uncertain QA/QC results are shown below in Table 1. This led to an initial set of 21 elements retained for multivariate exploration (Al, Ba, Ca, Co, Cr, Cu, Er, Eu, Fe, Ga, Gd, K, Mg, Na, Nd, Pb, Sm, Sr, Th, Ti, V, Y, Yb, and Zn).

Table 1: Elements excluded from multivariate analysis based on QA/QC issues. Abbreviations: RSD, relative standard deviation; RD, relative difference; BDL, below detection limit.

Issue	Metric	Elements Affected
Low analytical precision	>20% variation in duplicates	As, Bi, Be, Ge, Hf, Ho, Lu, Ni, Pr, Sn, Tm, W
High relative standard deviation (poor measurement reproducibility)	%RSD >10%,	As, Be, Cs, Dy, Ge, Hg, Lu, Sn, Tb, Tm, U
High relative difference, (poor accuracy in replicate measurements)	%RD >±10%	Be, Ce, Dy, La, Rb, Ta, Zr
Frequent values below detection limit (poor statistical reliability)	BDL in >10% of samples	Ag, Bi, Cd, Mo, Se, Te, W
Low analytical resolution	≤10 unique values	Ag, Bi, Cd, Mn, Mo, Nb, P, Sb, Sc, Te

Initial element data reduction

Elements considered:

Major elements: Al, Ca, Fe, K, Mg, Mn, Na, P, Si, Ti

Trace elements: Th

Mn and P have low analytical resolution (see Figure 2).

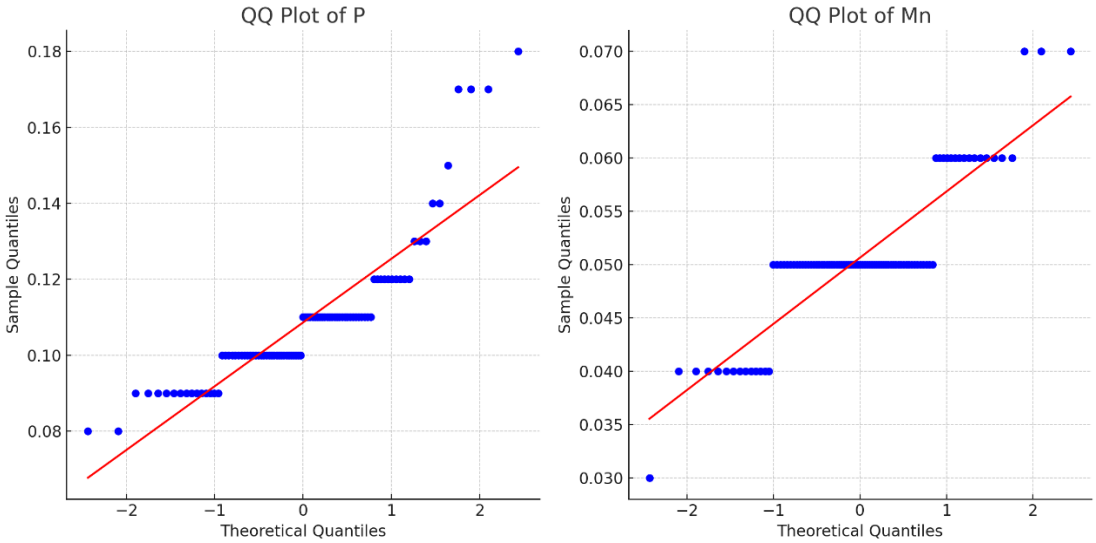


Figure 2: QQ plots of P and Mn, displaying poor analytical resolution (quantization).

Remaining elements (final element assemblage): Al, Ca, Fe, K, Mg, Na, Si, Ti, Th

Pre-processing

First, any censored values were imputed using half of the lower limit of detection. Then, a centered log ratio transformation was applied, and data was standardized.

Principal component analysis

After running PCA on the compiled dataset (from the 2022 and 2023 field seasons), the optimal number of principal components was determined to be 2 based on the 'elbow' method (Figure 3), where two PCs explain 77.2% of the variance of the data (Table 2).

Table 2: Principal components and their explained variance for the major element assemblage.

Principal component	Explained variance (%)
1	59.41
2	17.79
3	11.31
4	5.04
5	4.44

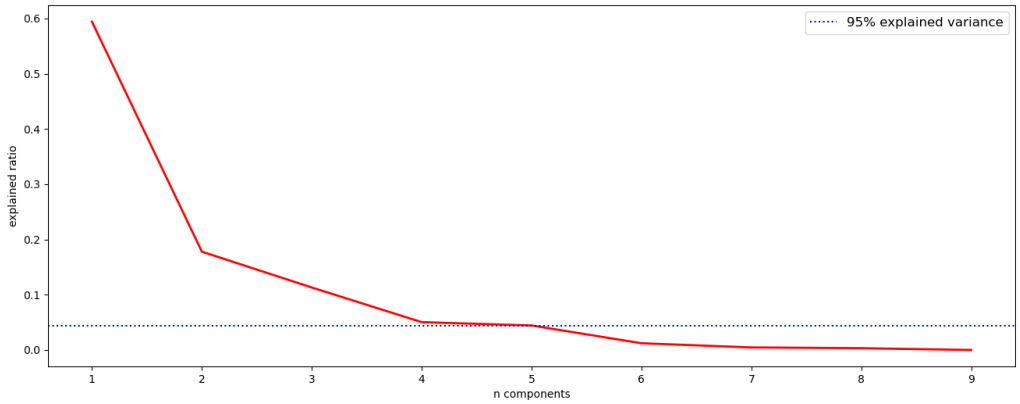


Figure 3: Scree plot to determine the optimal number of PCs for the major element assemblage.

Appendix J – Till unit data

Table 1: Color, texture, total carbonate, clast composition, PC2 score, and clast fabric for till units. All statistical data are shown as [range (average, st. dev)].

Stratigraphic unit	1t	2t	3t	5t	6t	8t	9t	10t
Number of samples	1	3	1	5	8	4	15	7
Colour	very dark grey brown	very dark grey brown	dark grey brown	**very dark grey (40%)** **very dark grey brown (40%)** dark grey (20%)	**dark grey brown (62%)** very dark grey brown (38%)	dark grey brown (50%) olive brown (50%)	**dark grey brown (47%)** olive brown (27%) very dark grey brown (13%) dark olive brown (7%) grey brown (7%)	**olive brown (86%)** very dark grey brown (14.3%)
Sand wt%	29.5	23.00–24.20 (23.73, 0.64)	24.9	13.10–29.10 (17.30, 6.74)	24.00–31.80 (28.19, 2.84)	28.80–34.50 (31.80, 2.33)	21.00–40.60 (29.91, 4.40)	28.70–34.90 (30.74, 1.98)
Silt wt%	48.1	47.60–48.60 (48.20, 0.53)	53.1	37.00–49.20 (40.66, 5.17)	48.20–49.60 (48.98, 0.47)	51.20–55.00 (53.15, 1.61)	48.40–63.50 (52.77, 3.92)	43.10–53.00 (48.31, 3.07)
Clay wt%	22.4	27.40–28.60 (28.07, 0.61)	22	21.80–49.90 (42.08, 11.62)	19.40–27.00 (22.82, 2.91)	12.80–16.90 (15.05, 1.86)	10.50–24.60 (17.32, 4.39)	17.00–24.20 (20.97, 2.54)
Total carbonate wt%	47.05	37.59–41.14 (38.90, 1.95)	35.79	23.36–42.18 (29.17, 7.58)	35.29–47.61 (41.79, 4.34)	45.64–48.41 (47.27, 1.19)	31.80–50.32 (44.89, 5.83)	35.86–47.74 (41.67, 4.34)
HBB clasts ct%	70.8	73.10–79.60 (76.33, 3.25)	75.3	62.40–80.10 (75.58, 7.43)	75.20–86.70 (81.17, 4.02)	78.30–80.40 (79.40, 1.16)	77.70–85.40 (81.03, 2.67)	77.40–84.50 (82.06, 2.49)
GR clasts ct%	11.6	14.10–20.20 (17.00, 3.06)	16.3	14.70–16.70 (15.62, 0.91)	10.20–18.20 (14.11, 2.83)	6.50–8.70 (7.80, 0.96)	7.40–15.80 (9.89, 2.53)	7.60–13.50 (10.59, 2.08)
UGG clasts ct%	17.6	6.40–7.00 (6.73, 0.31)	8.4	5.10–22.10 (8.82, 7.43)	2.50–9.70 (4.70, 2.15)	10.90–14.10 (12.82, 1.36)	4.00–14.80 (9.08, 3.08)	4.40–11.00 (7.37, 2.31)
PC2 score	0.61	-0.46–-0.13 (-0.27, 0.17)	0.9	0.82	-0.50–1.51 (0.67, 0.63)	0.92–1.64 (1.30, 0.32)	-0.83–1.71 (1.14, 0.68)	-0.37–1.35 (0.68, 0.80)
Interpreted till-fabric direction (°)	NW (307)	SW (233)	W (262)	S (175–180)	SSW–WSW (204–250)	SW (216–236)	WNW–NNW (298–336)	W–WNW (263–295)

Stratigraphic unit	11t	13t	14t	15t	16t	18t	20t
Number of samples	6	4	5	15	12	2	12
Colour	**dark grey brown (50%)** dark grey (17%) reddish brown (17%) very dark grey brown (17%)	**olive brown (50%)** dark grey brown (25%) dark olive brown (25%)	**dark grey brown (80%)** dark olive brown (20%)	**dark grey brown (33%)** very dark grey brown (27%) dark olive brown (20%) olive brown (13%) dark grey (7%)	**olive brown (50%)** dark grey brown (33%) brown (17%)	brown (50%) light yellow brown (50%)	**light olive brown (33%)** olive brown (17%) brown (17%) dark grey brown (8%) dark yellow brown (8%) light yellow brown (8%) yellow brown (8%)
Sand wt%	14.60–37.00 (24.97, 7.34)	28.50–33.80 (31.22, 2.31)	24.00–29.40 (27.00, 2.01)	26.90–46.10 (30.39, 4.76)	25.40–34.90 (29.09, 2.72)	27.50–36.00 (31.75, 6.01)	21.70–50.70 (33.69, 8.05)
Silt wt%	43.00–78.20 (57.85, 11.56)	45.40–49.90 (47.08, 1.96)	45.80–50.20 (47.74, 1.87)	41.10–50.50 (47.24, 2.22)	45.20–55.10 (49.59, 2.81)	56.50–59.80 (58.15, 2.33)	43.70–64.00 (51.64, 6.22)
Clay wt%	7.20–25.80 (17.18, 6.22)	20.80–23.60 (22.20, 1.51)	23.20–30.20 (25.26, 2.89)	12.80–25.20 (22.35, 3.06)	18.80–24.40 (21.32, 1.69)	7.40–12.80 (10.10, 3.82)	3.50–27.40 (14.68, 7.28)
Total carbonate wt%	30.04–43.61 (38.29, 5.25)	35.88–42.11 (38.87, 2.60)	35.74–45.05 (41.40, 3.46)	34.82–44.01 (40.06, 2.55)	37.20–44.68 (40.88, 2.37)	44.98–46.04 (45.51, 0.75)	37.48–49.11 (43.15, 3.65)
HBB clasts ct%	75.10–83.90 (79.48, 3.62)	61.60–76.10 (69.05, 6.25)	75.30–84.50 (80.60, 3.86)	61.10–81.80 (72.40, 6.00)	62.00–78.70 (71.05, 5.07)	70.00–73.10 (71.55, 2.19)	67.00–78.40 (73.11, 3.08)
GR clasts ct%	10.00–20.50 (14.50, 4.03)	15.50–28.30 (20.93, 5.36)	10.00–15.90 (13.56, 2.71)	11.10–25.70 (17.28, 4.12)	11.30–28.70 (18.42, 4.80)	17.60–17.80 (17.70, 0.14)	9.10–23.10 (16.97, 3.99)
UGG clasts ct%	3.50–10.10 (6.03, 2.29)	8.40–12.80 (10.05, 1.97)	4.50–8.80 (5.82, 1.71)	5.90–25.50 (10.33, 5.33)	5.90–23.10 (10.52, 4.73)	9.10–12.40 (10.75, 2.33)	3.40–17.80 (9.92, 4.79)
PC2 score	0.71	-2.81–-0.21 (-1.71, 1.10)	-0.12–1.04 (0.45, 0.50)	-2.49–1.10 (-0.53, 1.21)	-3.52–0.80 (-1.24, 1.32)	-2.01–-0.41 (-1.21, 1.13)	-2.15–0.48 (-0.60, 0.88)
Interpreted till-fabric direction (°)	SW (229–238)	WSW–W (256–272)	S–SSW (176–201)	WNW–NW (292–325) or ESE–SE (118–145)	S–SW (186–237)	SW–W (226–280)	Variable